Sulfonamide Supported Catalysts for the Ring Opening Polymerisation of Cyclic Esters

Andrew Douglas Schwarz



Thesis submitted to the University of Oxford for the degree of
Doctor of Philosophy, March 2010.

The work described in this Thesis was carried out in the Chemistry Research Laboratory, University of Oxford from October 2006 to March 2010 under the supervision of Professor Philip Mountford. All work is my own unless stated to the contrary, and has not previously been submitted for any degree at this or any other university.

Andrew Douglas Schwarz

March 2010

Abstract

Andrew Douglas Schwarz Hilary 2010

Linacre College D.Phil. Thesis

This Thesis describes the synthesis and characterisation of sulfonamide supported titanium, zirconium and aluminium complexes and their use as ring opening polymerisation catalysts for ε-caprolactone and *rac*-lactide.

Chapter 1 introduces polyester use, development and characterisation in general. Metal catalysed ring opening polymerisation of cyclic esters is considered in a literature review of the field. Titanium, zirconium and aluminium complexes supported by polydentate sulfonamide ligands are also discussed.

Chapter 2 describes the synthesis and characterisation of new sulfonamide supported titanium amide, isopropoxide and zirconium isopropoxide complexes. Their application as catalysts for the ring opening polymerisation of ε-caprolactone and *rac*-lactide is discussed and compared with known zirconium isopropoxide complexes supported by bis(phenolate) amine ligands.

Chapter 3 describes the synthesis and characterisation of C_s symmetric titanium amide and alkoxide complexes supported by dianionic, tri- and tetradentate sulfonamide ligands. Zirconium alkyl and amide complexes supported by C_3-symmetric trianionic 'tren' type ligands bearing three different sulfonamide groups are also presented. The application of these complexes for the ring opening polymerisation of ε-caprolactone and *rac*-lactide is described and compared with the complexes presented in Chapter 2.

Chapter 4 provides an overview of the synthesis and characterisation of aluminium alkoxide and alkyl complexes supported by dianionic, tri- and tetradentate sulfonamide ligands. Solution state behaviour and solid state structures are presented and discussed. An assessment of these complexes for the ring opening polymerisation of *rac*-lactide is presented.

Chapter 5 presents full experimental procedures and characterisation data for the new complexes reported.

CD Appendix contains .cif files for all new crystallographically characterised complexes described, and additional polymerisation graphs.

Contents

	Declaration	i
	Abstract	ii
	Contents	iii
	Acknowledgements	vi
	Abbreviations	vii
	Notes	x
Chapter One – Introduction		1
1.1	Outline	2
1.2	Historical background to polyester development	2
1.3	Biodegradable and biorenewable polyesters	3
1.4	Polymer Description	4
1.5	ROP mechanism	5
1.5.1	Coordination-insertion polymerisation	5
1.5.2	Transesterification side reactions	6
1.5.3	Living polymerisation	8
1.5.4	Immortal polymerisation	10
1.6	Polymer Characterisation	11
1.6.1	NMR spectroscopy	12
1.6.2	MALDI-ToF MS	13
1.6.3	Gel Permeation Chromatography	13
1.7	Stereocontrol of *rac*-lactide polymerisation	14
1.7.1	Stereoisomers of lactide	14
1.7.2	Tacticity of polyesters	15
1.7.3	Characterisation of polymer chain stereosequences by NMR	16
1.8	Literature review	18
1.8.1	Catalysts employed in industry	19
1.8.2	Cyclopentadienyl ligand	21
1.8.3	O-donor ligands	22
1.8.4	N-donor ligands	23
1.8.5	Bi- and Tridentate N,O-donor ligands	25
1.8.6	Tetradentate N,O-donor ligands	28
1.8.7	Tetradentate N,O-donor ligands - salen and salan supported complexes	30

1.8.8 Tetradentate C3 symmetric O,N donor ligands 34
1.8.9 Summary 36
1.9 Novel sulfonamide ancillary ligands for ROP catalysts 36
1.10 Aims and Outlook 38
1.11 References 38

Chapter Two – Sulfonamide-Supported Group 4 Catalysts for the Ring-Opening Polymerization of ε-Caprolactone and *rac*-Lactide 50

2.1 Overview 51
2.2 Introduction to Group 4 ROP 51
2.3 Aims 54
2.4 Synthesis of protio-ligand precursors 54
2.5 Synthesis of titanium and zirconium amide and isopropoxide complexes 56
2.6 Solid state structures 60
2.7 Polymerisation studies: ROP of ε-caprolactone 69
2.8 Polymerisation studies: ROP of *rac*-lactide 75
2.9 Summary and Conclusions 80
2.10 References 81

Chapter Three – Ligand variation in Sulfonamide-Supported Group 4 ROP Catalysts 85

3.1 Overview 86
3.2 Introduction 86
3.3 Aims 88
3.4 Synthesis of protio-ligand precursors 89
3.5 Synthesis of titanium amide and isopropoxide complexes 95
3.6 Solid state structures of titanium complexes **12**, **17**, **18** and **19** 99
3.7 Synthesis of zirconium complexes supported by C_3 symmetric sulfonamide ligands 106
3.8 Solid state structure of zirconium complexes **20**, **21**, **23** and **24** 112
3.9 Polymerisation studies: ROP of ε-caprolactone 122
3.9.1 Polymerisation studies: ROP of ε-caprolactone, titanium catalysts 124
3.9.2 Polymerisation studies: ROP of ε-caprolactone, zirconium catalysts 127
3.10 Polymerisation studies: ROP of *rac*-lactide 130

3.11	Summary and Conclusion	134
3.12	References	135
Chapter Four – Sulfonamide-Supported Aluminum Catalysts for the Ring-Opening Polymerization of *rac*-Lactide		139
4.1	Overview	140
4.2	Introduction	140
4.3	Aims	143
4.4	Synthesis of protio-ligand precursors	144
4.5	Synthesis of aluminium alkyl complexes	144
4.6	Solid state structures of aluminium alkyl complexes **27**, **29 - 31**	146
4.7	Synthesis of aluminium alkoxide complexes	150
4.8	Synthesis of aluminium chloride complexes	153
4.9	Synthesis of aluminium sulfonamide complexes bearing ethoxy amine ligand	155
4.10	Synthesis of aluminium sulfonamide complexes bearing 2-*N*,*N*-dimethylaminoethoxide ligand	160
4.11	Polymerisation studies: solution ROP of *rac*-LA	161
4.12	Polymerisation studies: ROP of *rac*-LA under solvent-free (melt) conditions	170
4.13	Summary and Conclusions	171
4.14	References	172
Chapter Five – Experimental details and characterising data		177
5.1	General methods and instrumentation	178
5.2	Literature preparations	179
5.3	Experimental details and characterisation data for Chapter Two	179
5.4	Experimental details and characterisation data for Chapter Three	182
5.5	Experimental details and characterisation data for Chapter Four	192
5.6	Polymerisation procedures for Chapters 2, 3 and 4	201
5.7	X-ray data collection and processing parameters for Chapter 2	204
5.8	X-ray data collection and processing parameters for Chapter 3	207
5.9	X-ray data collection and processing parameters for Chapter 4	211
5.10	References	214

Acknowledgements

Firstly, I would like to thank my supervisor Professor Philip Mountford for his help and support throughout the course of my studies. I would also like to express my appreciation to him for suggesting that I worked on this excellent project which has provided many interesting challenges and ultimately proved to be highly successful, in terms of my development as a chemist.

I would like to thank the people who have contributed to the sulfonamide project; including Katherine Herbert, Nigel Yong (Part 2's), Christina Manu (summer student) and Zengyong Chu (visiting academic). My deepest gratitude must go to everyone I have worked with in the Mountford group for providing a great place to work, and banter to get me through the dark months of negative results that are inevitable in any research project. Special mention must go to Dr Hellen Dyer who helped me through my first months in Oxford to get the project off the ground; and to (the soon to be Dr) Alex Heath who's always provided stimulating chemistry chats and been a great laugh, especially at the many Chemistry nights out.

I'd also like to thank Colin Sparrow and Dr Nick Rees, for help with mass spectroscopy and NMR. Dr Amber L. Thompson and Dr David J. Watkin also deserve my warmest appreciation for teaching me everything I know about X-ray crystallography and always being friendly and interested in my terrible crystals.

I'd like to thank Rebecca who, as always, has been fantastic help and has kept me going though the slog of writing up with many doses of Welsh cakes and chocolate chip muffins. Finally, I must thank my family who have been brilliant throughout all my time at university and have provided me with all the help and support I could ever need!

Abbreviations

General

Å	Ångstrom
av.	average
ca.	*circa*, about
calcd	calculated
º	degrees
ºC	degrees Celsius
d	day(s)
g	gram(s)
GPC	gel permeation chromatography
h	hour(s)
K	Kelvin
k_i	rate constant of initiation
k_p	rate constant of propagation
min	minute(s)
s	second(s)
rt	room temperature

Chemical

$Al(O^iPr)_3$	aluminium tris(isopropoxide)
Ar	aryl group
Bn	benzyl
Cp	C_5H_5
Cp*	C_5Me_5
Cy	cyclohexyl
D-lactide	(*R*,*R*)-cis-3,6-dimethyl-1,4-dioxane-2,5-dione
E	generic chalcogen atom
Et	ethyl
^{i}Bu	*iso*-butyl
ICI	Imperial Chemical Industries
^{i}Pr	*iso*-propyl
^{i}PrOH	isopropyl alcohol
$\kappa^2(N,O)$	sulfonamide binding through nitrogen and oxygen

L	a supporting ligand (set)
L-lactide	(*S*,*S*)-cis-3,6-dimethyl-1,4-dioxane-2,5-dione
Me	methyl
Mes	2,4,6-$C_6H_2Me_3$
meso- isomers	(*R*,*S*)-cis-3,6-dimethyl-1,4-dioxane-2,5-dione
M_n	number average molecular weight
M_p	peak molecular weight
M-OR	metal alkoxide
Ms	Mesyl (SO_2Me)
M_w	weight average molecular weight
^nBu	*n*-butyl
PDI	poly dispersity index
PET or PETE	polyethylene terephthalate
Ph	phenyl
P_m	probability of *meso*- linkages
poly(LA)	poly(lactic acid)
poly(ε-CL)	poly(ε-caprolactone)
P_r	probability of racemic linkages
p-Tol	4-C_6H_4Me
py	pyridine
pz	pyrazolyl
R	generic aryl or alkyl
rac-lactide	a racemic mixture of *D*- and *L*-lactide
ROP	ring opening polymerisation
$Sn(Oct)_2$	Tin octanoate
^tBu	*tert*-butyl
TArF	$SO_2(3,5\text{-}C_6H_3(CF_3)_2)$
THF	tetrahydrofuran
Ts	Tosyl (SO_2Tol)
X	Generic halide

Mass Spectrometry

EI	electron impact
FI	field ionisation

m/*z*	mass to charge ratio
MS	mass spectrometry
MALDI-ToF MS	matrix-assisted laser desorption/ionization - time of flight mass spectroscopy

Nuclear Magnetic Resonance Spectroscopy

^{13}C-{^{1}H}	proton-decoupled ^{13}C
app.	apparent
br	broad
COSY	correlation spectroscopy
d	doublet
HETCOR	heteronuclear correlation
HMBC	heteronuclear multiple bond correlation
HMQC	heteronuclear single quantum correlation
i	*ipso*
J	coupling constant
m	*meta*
m	multiplet
NMR	nuclear magnetic resonance
nOe	nuclear Overhauser effect
o	*ortho*
p	*para*
ppm	parts per million
q	quartet
ROESY	rotating-frame nuclear Overhauser Effect spectroscopy
s	singlet
sept	septet
t	triplet
VT	variable temperature
δ	chemical shift in ppm

Infrared Spectroscopy

br	broad
FT-IR	fourier transform infrared red
IR	infrared red

m	medium
s	strong
w	weak
ν	frequency

Notes

Literature compounds described in this Thesis are numbered **1.x**, **2.x**, **3.x**, **4.x** according to the Chapter in which they first occur. The new compounds described in this Thesis are numbered **1** – **43**. MALDI-ToF mass spectroscopy was performed by Colin Sparrow, and elemental analysis were performed by Stephen Boyer at London Metropolitan University.

Chapter One

Introduction

1.1 Outline

In this Chapter, polyesters will be discussed in general along with some desirable properties and the analytical tools employed to characterise them. Metal catalysed ring opening polymerisation (ROP) of cyclic esters is introduced, and a general literature review provided with an emphasis on those complexes of Group 4 and Group 13 elements which have been applied to ROP. Titanium, zirconium and aluminium complexes supported by polydentate sulfonamide ligands will also be introduced, which are the subject of the work reported here.

1.2 Historical background to polyester development

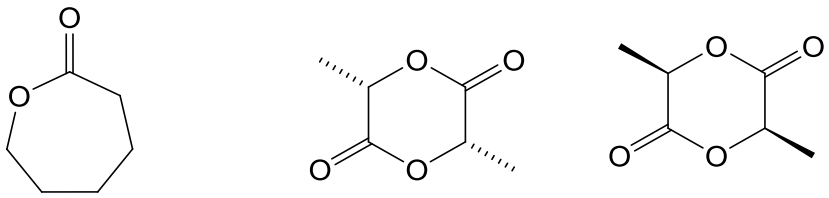
The first truly synthetic polymer was discovered in 1909 by Leo Baekeland and was synthesised from phenol and formaldehyde. Marketed as Bakelite it was used mainly as casings of home appliances such as radios, telephones and door handles. Nylon (a generic designation for a family of synthetic polyamides) was first discovered in the 1920s, but was only extensively exploited during the Second World War as a replacement for Asian silk and hemp in the manufacturing of parachutes. After the war, polymer chemistry progressed rapidly owing to low oil prices and an intense research effort, with plastic becoming common place in people's homes and lives through the introduction of products such as Tupperware. The worldwide production of plastics has soared over the last 60 years growing from 1.3 million tons in 1950 to *ca*. 230 million tons in 2008.[1,2] Polyesters are a particular class of plastics which contain repeating ester linkages, the first example of which was pioneered in the late 1920's by W. H. Carothers.[3] He found that fibres could be created by the polycondensation of diols with dicarboxylic acids. However, this discovery came at a similar time to Nylon, and so the newly synthesised polyester took a back seat until two British scientists, John Rex Whinfield and James Tennant Dickson, employees of the Calico Printer's Association of Manchester, patented "polyethylene terephthalate" (commonly known as PET or PETE) in 1941 which was manufactured by ICI and subsequently DuPont.[4] Polyesters eventually became popular as a textile fibre that would remain wrinkle-free upon washing and wearing.

Challenges in the field of plastics have changed markedly since the early days of their synthesis due to the increasing oil price and the need to make polymers for which the

degradation properties have been evaluated. Modern plastics need to be synthesised with minimum environmental impact but they also have to retain the desired levels of performance and longevity.

1.3 Biodegradable and biorenewable polyesters

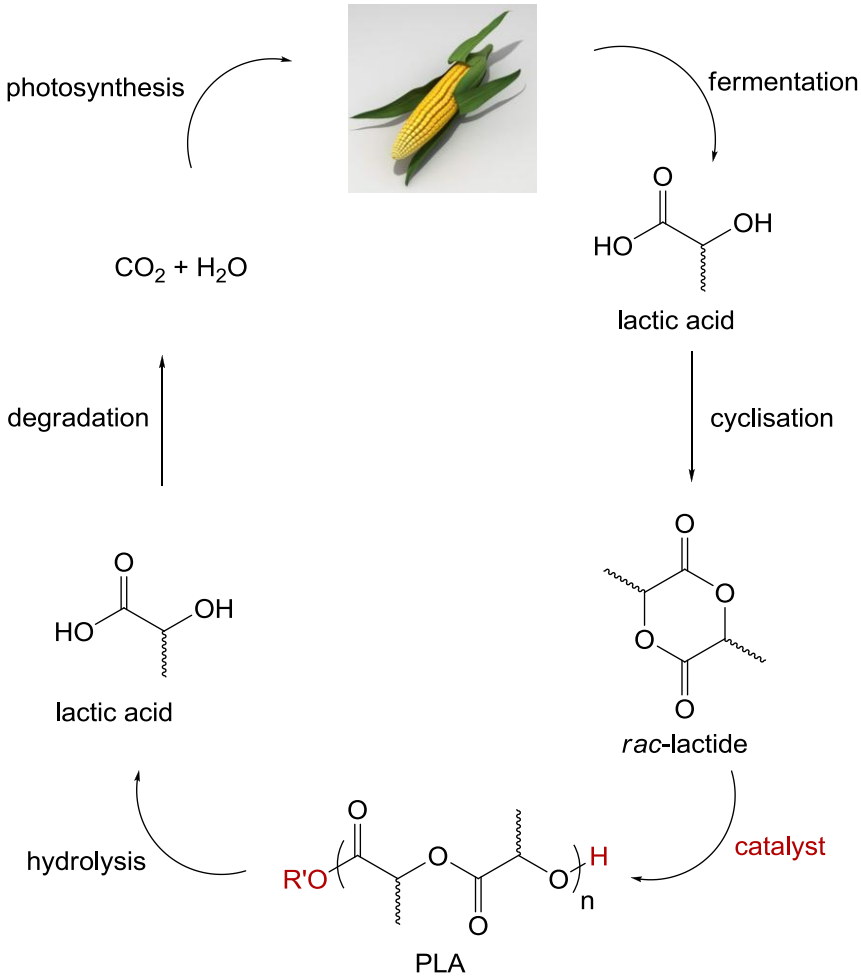
A significant new class of polyesters are those based upon poly(lactic acid) (poly(LA)) and poly(ε-caprolactone) (poly(ε-CL)). Traditionally, these polymers were synthesised utilising high-temperature polycondensation reactions of the appropriate α-hydroxy acids, but this step growth method is accompanied by poor chain length control and low molecular weights, severely limiting their use.[4] Therefore, these polymers are generally synthesised from the ring opening polymerisation (ROP) of the cyclic esters ε-caprolactone or lactide. Interest is especially focused upon poly(LA) which is derived from 100 % renewable resources including corn and sugar beet, because it can replace oil-based materials as well as having many biomedical applications, such as in drug delivery agents or degradable implants. [5-13]



ε - caprolactone *rac* - lactide

Materials such as poly(LA) degrade into compounds that are readily metabolised by microorganisms to give environmentally benign side products, a process which is illustrated in Figure 1.1. It is important to note that although poly(ε-CL) shares poly(LA)'s biocompatibility it is not obtained from renewable resources being prepared industrially by Baeyer-Villiger oxidation of cyclohexanone with peracetic acid.[14] Otherwise the process, which is highlighted in Figure 1.1 has the potential to be carbon-neutral. However, with current agricultural technology being based predominantly on large scale industrial farming which utilises energy generation that is not carbon-neutral, major advances in fertiliser synthesis and energy generation need to be realised before poly(LA) can be considered a carbon neutral polymer.

Figure 1.1. Life cycle of poly(LA).



1.4 Polymer description

Polymers rarely contain one uniform length species and so are described by an average molecular weight, calculated as a number or weight average, alongside a measure of the distribution of the molecular weights, the poly dispersity index (PDI).

The number average molecular weight (M_n) is given by Equation 1.1 (where N_i is the number of molecules having a molar mass M_i).

$$M_n = \frac{\sum N_i . M_i}{\sum N_i} \qquad \textbf{Equation 1.1}$$

The weight average molecular weight, M_w, is given by Equation 1.2 (where W_i is the total mass of polymer *(N_i* x *M_i)* having molar mass M_i).

$$M_w = \frac{\sum W_i . M_i}{\sum W_i} \qquad \textbf{Equation 1.2}$$

The poly dispersity index, PDI, is given by Equation 1.3.

$$PDI = \frac{M_w}{M_n} \qquad \textbf{Equation 1.3}$$

The bias of the weight average molecular weight towards higher molecular weight chains means that the PDI gives a convenient measure of the distribution of the chain lengths of a polymer sample. Polymers entirely consisting of the same length chains have the same value of M_n and M_w and therefore have a PDI of 1.0. However, once the polymer contains a normally distributed range of chain lengths, M_w is larger than M_n and its PDI is greater than 1.0. In practice, even extremely well controlled polymerisation reactions yield polymers with a PDI larger than 1.0, as a result of chain transfer, termination reactions, transesterification and slow initiation relative to propagation. Within the field of ROP a PDI of less than 1.2 is described as "narrow", that between 1.2 and 1.8 as "moderate" and anything above 1.8 as a "broad" distribution. Typically living polymerisation yields polymers with a narrow PDI (*ca*. less that 1.2). For the polyesters synthesised in this thesis and in the field of ROP in general, polymers are described in terms of M_n, and PDI with M_w generally being more relevant to poly-olefins.

1.5 ROP mechanism

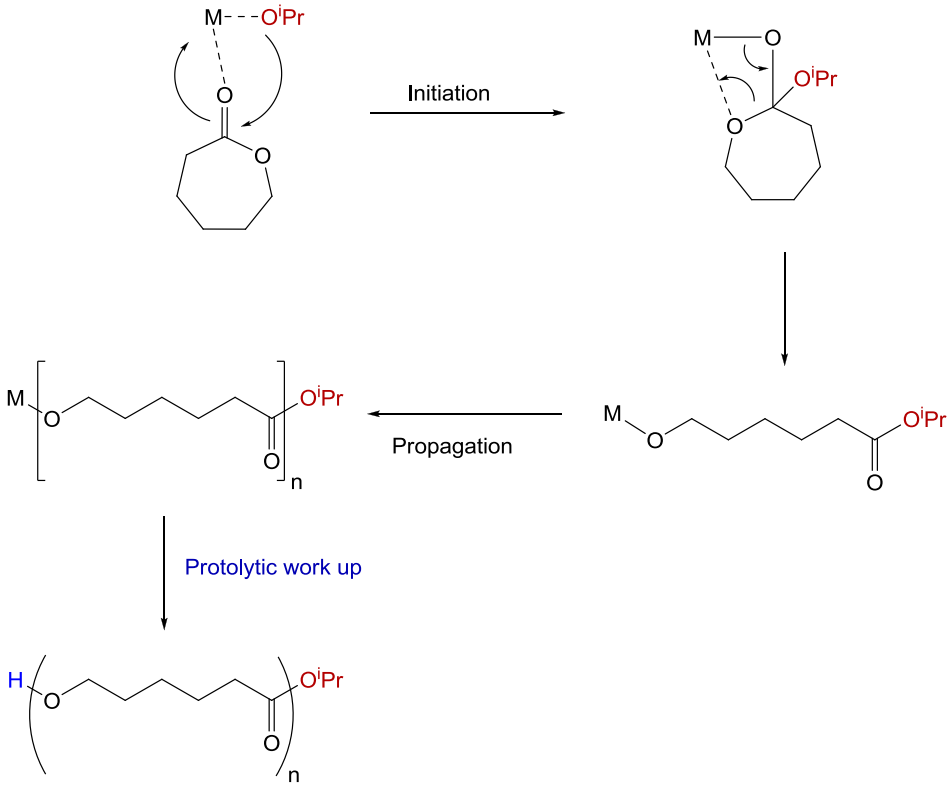
There are a wide variety of approaches to and pathways for the synthesis of poly(ε-CL) and poly(LA), which include coordination-insertion, cationic, anionic, organo-catalytic and enzymatic methods. These have been extensively reviewed in recent literature.[10,15-21] This Thesis will concentrate on coordination-insertion ROP for the synthesis of poly(ε-CL) and poly(LA).

1.5.1 Coordination-insertion polymerisation

Coordination-insertion polymerisation is the most extensively used polymerisation pathway to synthesise poly(LA) and poly(ε-CL), both industrially and in academia, and many examples will be presented throughout this Thesis. In general, there are three steps in this polymerisation mechanism. First, the exocyclic oxygen atom of the

monomer is coordinated to the metal fragment rendering the molecule more susceptible to nucleophilic attack. Secondly, acyl-oxygen scission takes place by insertion into the M-OR bond of the initiator. Finally, coordination of a further lactide monomer regenerates the propagating species.[22-31] Once all the monomer has been consumed the polymer is liberated from the metal centre by a protolytic work up (Figure 1.2). There are also limited examples known in which the ring breaks at the alkyl-oxygen bond, and as such the propagating species is a metal carboxylate.[32] However, none of the catalysts presented in this Thesis operate via this route (as is evidenced by MALDI-ToF MS and ^{1}H NMR spectroscopy), so these catalysts will not be discussed further.

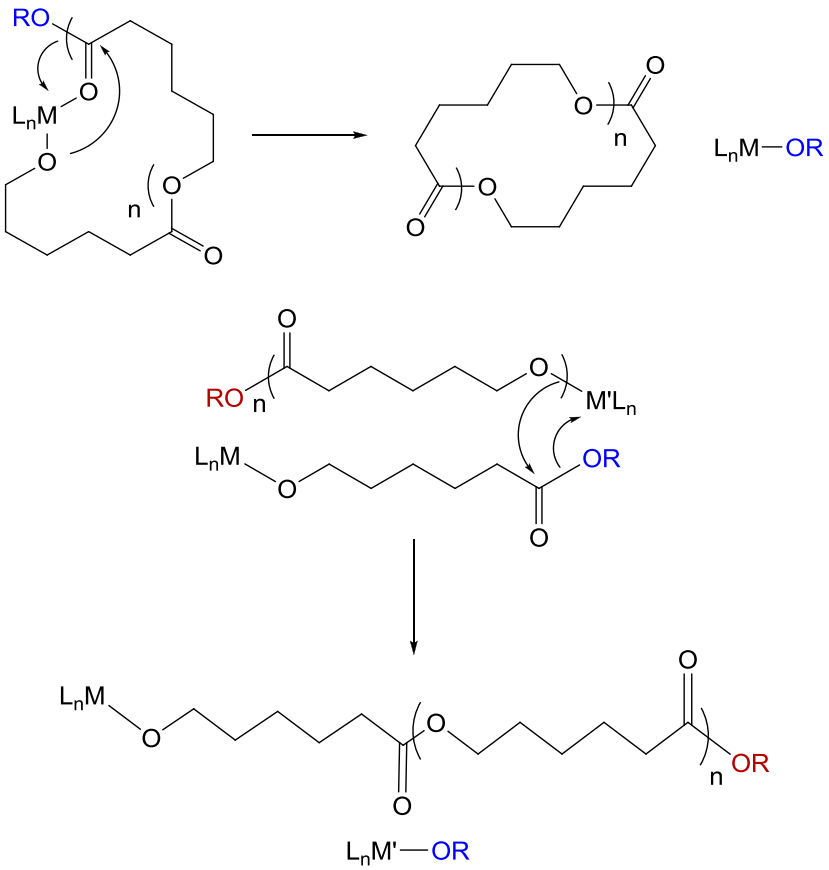
Figure 1.2. Coordination-insertion mechanism



1.5.2 Transesterification side reactions

The efficiency of a coordination-insertion polymerisation depends upon the ratio of the rate constants, k_p/k_i and the extent of intramolecular or intermolecular transesterification side reactions (Figure 1.3). Where k_p is the rate constant of propagation, and k_i is the rate constant of initiation.

Figure 1.3. Transesterification side reactions. Top: intramolecular 'backbiting'; bottom: intermolecular. OR = Propagating chain; n = number of ring opened monomer units.



In intramolecular transesterification reactions, the growing polymer chain coordinates to the metal centre leading to insertion and formation of cyclic structures alongside a shorter propagating species. Intramolecular transesterification is often called 'back-biting' and is evidenced by macrocyclic structures or shorter than expected polymer chains, Figure 1.3 (top).[27,33-35] Intermolecular transesterification reactions give chain redistribution, where a linear chain coordinates to a metal centre of a different propagating species, the ensuing insertion then gives a shorter and a longer linear chain. Transesterification reactions result in a broadening of the polymer PDI and poorer control of the polymer length.

The extent of transesterification side reactions depends markedly on the metal initiator employed. For example tin octanoate ($Sn(Oct)_2$) (used in the presence of an alcohol co-initiator) is much more active than $Al(O^iPr)_3$. Typically $Sn(Oct)_2$ polymerises

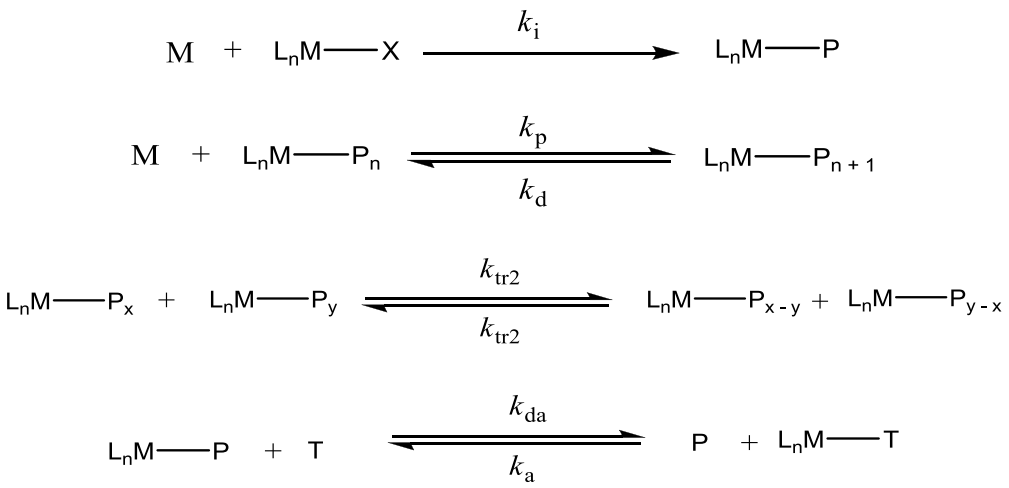
lactide in the bulk in a few hours rather than a few days for $Al(O^iPr)_3$. However, the resulting poly(LA) produced by Sn exhibits significantly higher PDI values, *ca*. 2 versus 1.5 or less.[36-39] In a similar study, Kricheldorf *et al*. established the following order for simple metal alkoxides in terms of polymerisation control: $Al(O^iPr)_3$ > $Zr(O^nPr)_4$ > $Ti(O^nBu)_4$ > Bu_3SnOMe > $Bu_2Sn(OMe)_2$.[27,35]

Post-polymerisation transesterification is associated with a slow continuous decrease in M_n and increasing PDI at high monomer conversion. Non-linear M_n versus conversion and M_n versus $[Monomer]_0$:$[Catalyst]_0$ relationships and/or poor agreement between experimental and calculated M_n values (with broad PDIs) are consistent with transesterification side reactions and slow initiation rates versus propagation rates during polymerisation.

1.5.3 Living polymerisation

Polymerisation reactions in which there is an absence of transesterification or other termination steps, and for where the initiation rate constant, k_i, is greater than or equal to the propagation rate constant, k_p, are defined as 'living' systems. Living polymerisations yield predictable molecular weights and narrow PDIs with no chain transfer or termination steps.

Figure 1.4. Kinetic treatment of the lactide polymerisation process[40]



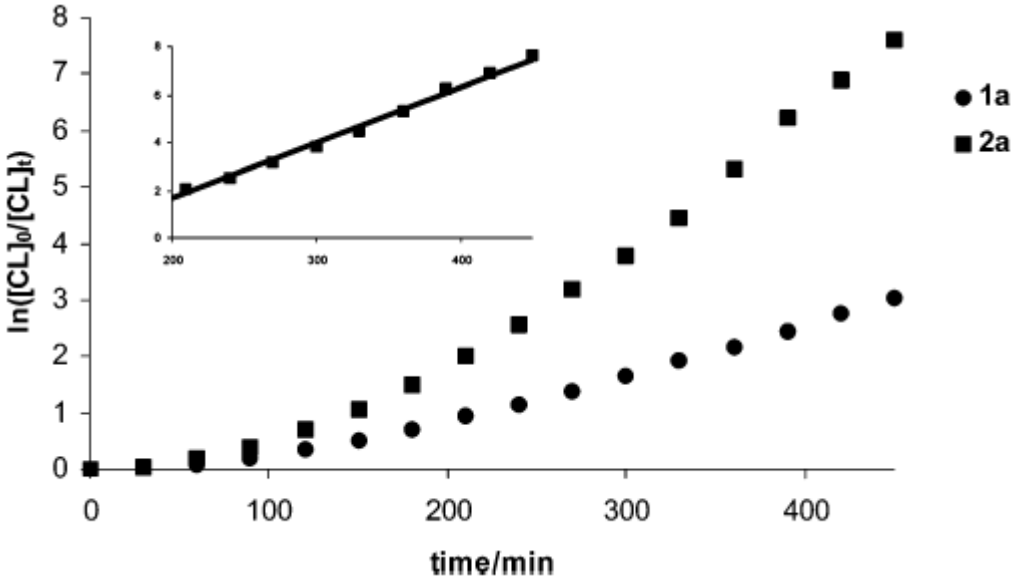
Key:

M	monomer
L_nM-P_n	propagating polymer chain (bound to a metal catalyst)

T	terminating agent such as a protic molecule
k_i	rate constant of initiation
k_p	rate constant of propagation
k_d	rate constant of depolymerisation
k_{tr2}	rate constant for bimolecular transfer to polymer with chain rupture (transesterification)
k_{da}	rate constant of temporary deactivation
k_a	rate constant of temporary activation

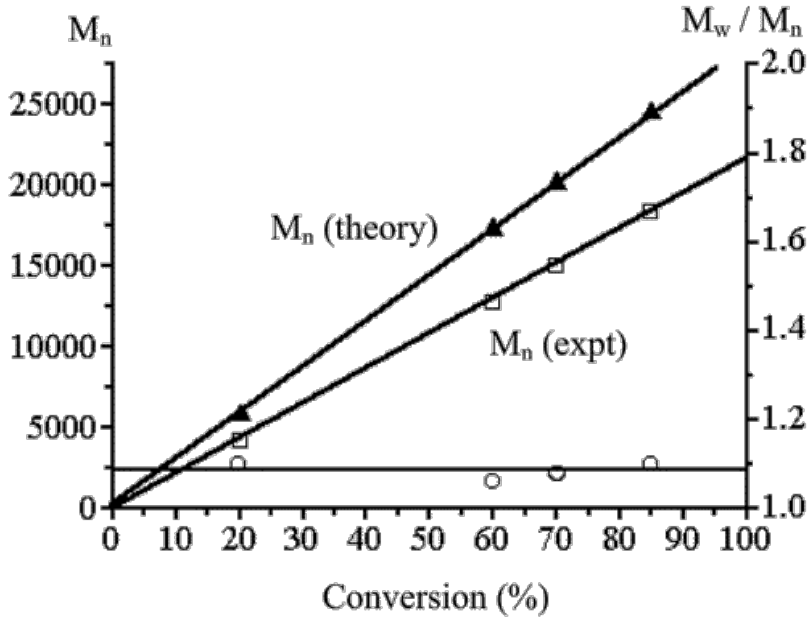
In a 'living' type system, after initiation, the rate constant k_p dominates giving a first order kinetic dependence on monomer concentration (Figure 1.5), and a linear relationship between M_n and monomer conversion (Figure 1.6). Cases have also been documented of initiation periods prior to a 'living' process where either aggregation process is present or there are limitations on the insertion into the metal initiator bond.[34,41,42]

Figure 1.5. Kinetics of ε-caprolactone polymerization initiated with $Zr(O^iPr)_2(O_2N_2)$ (**1.26**).[43]



Inset shows linear fit (r^2 = 0.9931) for the first-order region after initiation period for $Zr(O^iPr)_2(O_2N_2)$ (**1.26**).

Figure 1.6. Plot of M_n and PDI values (determined by GPC) *vs* conversion for Ti(O^{i}Pr)(N$_3$O) (**1.36**).[44]

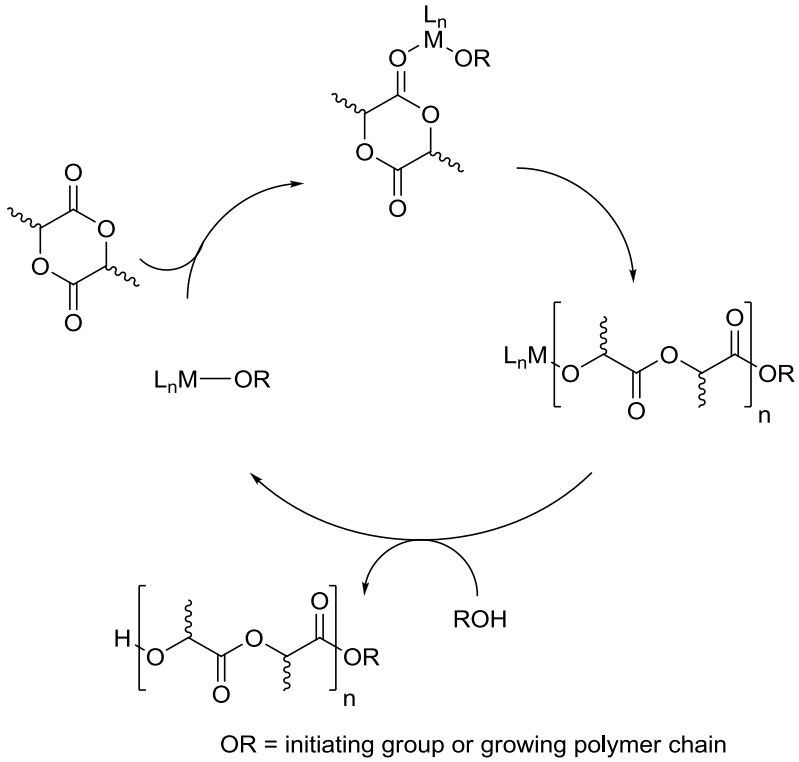


For highly active systems (80-100% conversion in under 2 min) and melt polymerisations (130 °C, solventless) reaction monitoring is not possible; living polymerisations can be evidenced by a linear increase in M_n as a function of $[Monomer]_0$:$[Catalyst]_0$ ratio. Polymerisations in which a linear dependency is not observed are a consequence of slow initiation, slow chain propagation, transesterification, chain transfer and termination reactions or catalyst decomposition.

1.5.4 Immortal polymerisation

A special case of living polymerisation is immortal polymerisation, in which the polymerisation proceeds in the presence of a chain transfer reaction. For the ROP of cyclic esters, chain transfer reagents can be an alcohol such as ^{i}PrOH. The alcohol chain transfer reagents are in rapid exchange with the 'living' polymer chain attached to the metal centre allowing the formation of multiple polymer chains per metal centre (Figure 1.7).

Figure 1.7. Schematic representation of immortal polymerisation



If the rate at which the alcohol initiators (or alcohol terminated oligomers and polymers) exchange is greater than the rate of propagation, k_p, the alcohols can act as chain transfer agents yielding polymers of uniform molecular weight. The M_n is then dependent upon the ratio of alcohol initiators to the monomer equivalents, enabling the production of large quantities of polymer with small amounts of catalyst. Productivity is optimised and polymers with functional end-groups can be prepared, which may then be employed as intermediates for macromolecular engineering applications.[45] Work within our group has shown that primary and secondary amines can initiate polymerisations in a similar manner, where an activated monomer mechanism generates alcohol terminated oligomers that take part in immortal polymerisation to generate heterotactically enriched poly(LA) with narrow PDIs.[46]

1.6 Polymer Characterisation

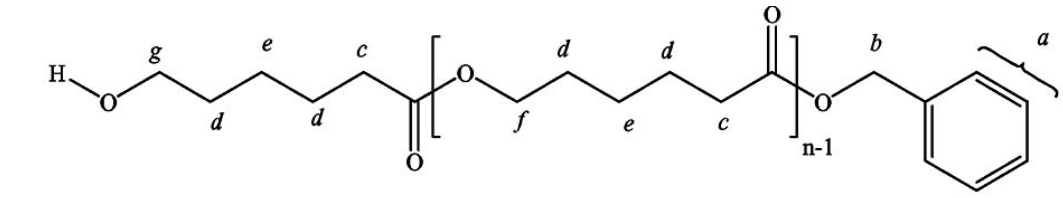
Polyesters such as poly(ε-CL) and poly(LA) can be characterised by a variety of methods that include: ^{1}H and ^{13}C NMR spectroscopy; matrix-assisted laser desorption/ionization - time of flight mass spectroscopy (MALDI-ToF MS); and gel

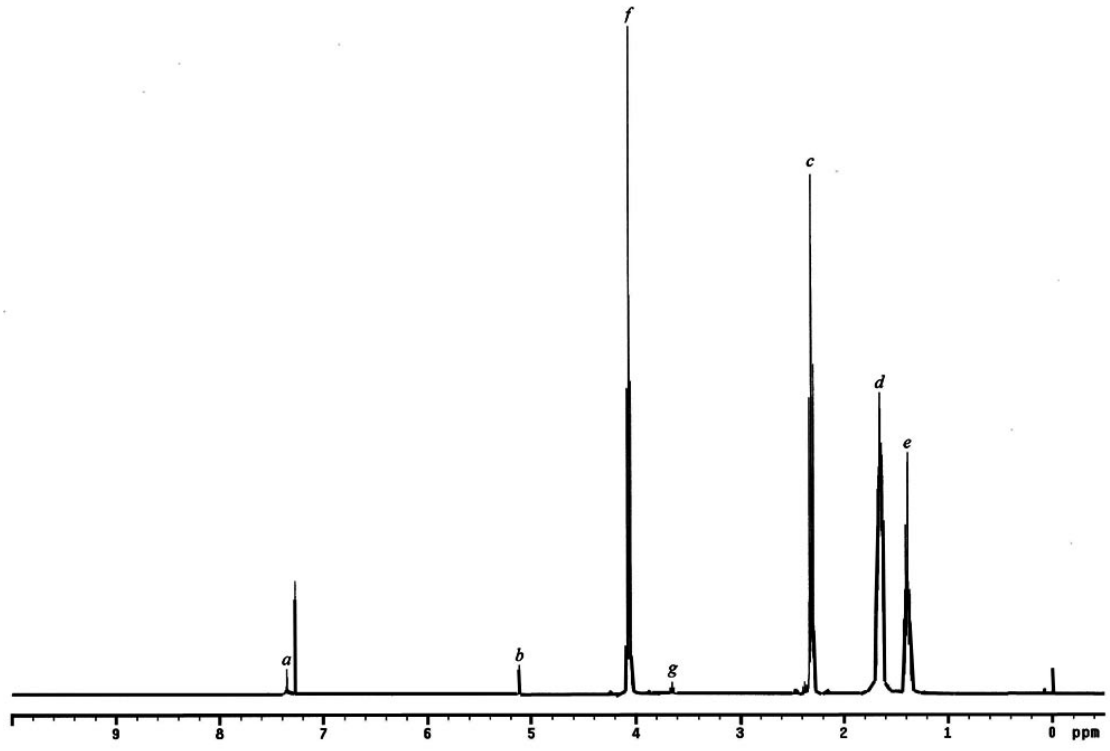
permeation chromatography (GPC, also referred to as size exclusion chromatography (SEC)).

1.6.1 NMR spectroscopy

^{1}H and ^{13}C NMR can be used to obtain information regarding polymer structures such as the end-group in a linear polymer. Additionally, M_n can be calculated by integration of end group resonances to those that correspond to the polymer backbone (Figure 1.8). However, this information can often prove unreliable as the polymer proton resonances can be 10^3 times more intense and so end groups are often unobservable. Another drawback is that NMR spectroscopy is unable to detect cyclic architectures because the backbone polymer resonances overlap with those of the linear polymer.[42,43,47] NMR spectroscopy is also used to determine polymer tacticity for poly(*rac*-LA), further details of which will be given in, Section 1.10.

Figure 1.8. Literature example of a ^{1}H NMR spectrum of poly(ε-CL).[48]





1.6.2 MALDI-ToF MS

MALDI-ToF MS can give insights into polymer structure and the possible side reactions taking place. Linear polymers and cyclic polymer architectures are easily characterised, and so are the end groups of linear polymers. This technique can also provide insights into possible side reactions during the polymerisation process; for instance, for poly(LA), peaks appearing 72.1 *m*/*z* apart can only be present due to transesterification side reactions. MALDI-ToF MS is, however, not quantitative due to the complex relationship between polymer structure, length and ionisation of the polyesters. Therefore the individual peaks in the MALDI-ToF MS spectrum cannot be integrated to give information regarding chain length and distribution.

1.6.3 Gel Permeation Chromatography

The most versatile and widely employed method is GPC analysis which generates data corresponding to number average molecular weight (M_n), weight average molecular weight (M_w) and the poly dispersity indices (PDI).

Polymer samples are dissolved in an organic solvent and passed though a styrene divinyl benzene copolymer column containing pores of various sizes. The polymers are separated according to their hydrodynamic radius. Smaller chains enter the pores and are retarded on their path down the column so have longer retention times. Longer chains pass though the column without having their path diverted so have shorter retention times.

The GPC instrument is calibrated against linear polystyrene samples of known molecular weight and narrow PDI. However, the hydrodynamic volume of polystyrene is very different to that of polyesters such as poly(LA) and poly(ε-CL) and so larger than expected M_n values are obtained when samples are analysed using this calibration method alone. A way to circumvent this is to apply a correction that relates the observed M_n to their true values. This universal calibration method is based on the hydrodynamic volume of a molecule in solution.[49] Separation on a GPC column is based upon the hydrodynamic volume of a given species; therefore it follows that molecules which elute at the same volume will have the same molecular size and hydrodynamic volume. Their absolute molecular weights can be defined by Equation 1.4 which relates the intrinsic viscosity at infinite dilution [η], and the molecular

weight M of the given species. Hydrodynamic volume and so polymer molecular weight is then proportional to the intrinsic viscosity.

$$[\eta] = K.M^{\alpha} \qquad \textbf{Equation 1.4}$$

The Mark-Houwink constants (K and α) are determined experimentally for each polymer type, by plotting log[η] *vs*. log(M) over the whole molecular weight range. The Mark-Houwink constants are only valid for the solvent and the temperature in which they are determined. They describe the polymer characteristics in solution, where α relates to the stiffness of the polymers, a value of 0 represents a hard sphere, 1 a semi-coil and 2 an absolute rigid rod. The M_n, M_w and M_p values reported in this Thesis are obtained by GPC analysis in THF at 30 °C, with the application of the appropriate corrections as previously determined for poly(ε-CL)[50] and poly(*rac*-LA)[51] after calibration against polystyrene standards. The drawbacks to this method of characterisation are that cyclic polymer architectures are not accurately described, and that literature examples often do not quote their polymer M_n after application of the appropriate corrections with the result that significantly higher than expected polymer lengths are observed (M_n (polystyrene) = ~0.58 M_n (polyester)).

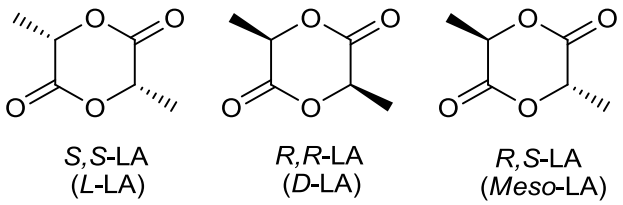
1.7 Stereocontrol of *rac*-lactide polymerisation

1.7.1 Stereoisomers of lactide

Poly(LA) of industrially relevant high molecular weight can be prepared by ring opening polymerisation of cyclic esters either utilising a coordination insertion or anionic mechanism.[40] Polymer molecular weight and PDI strongly influence bulk polymer properties but for poly(*rac*-LA) tacticity is also critical.

Lactide, the cyclic ester of lactic acid can exist as three stereoisomers, Figure 1.9. *L*-lactide is the naturally occurring isomer. The *D*- and *meso*- isomers and *rac*-lactide (a 1:1 racemic mixture of *D*- and *L*-lactide) are all derived by epimerisation and subsequent separation. *L*-lactide is therefore the cheapest form of lactide possible whereas *D*-lactide is the most expensive as it requires separation from the racemic mixture.

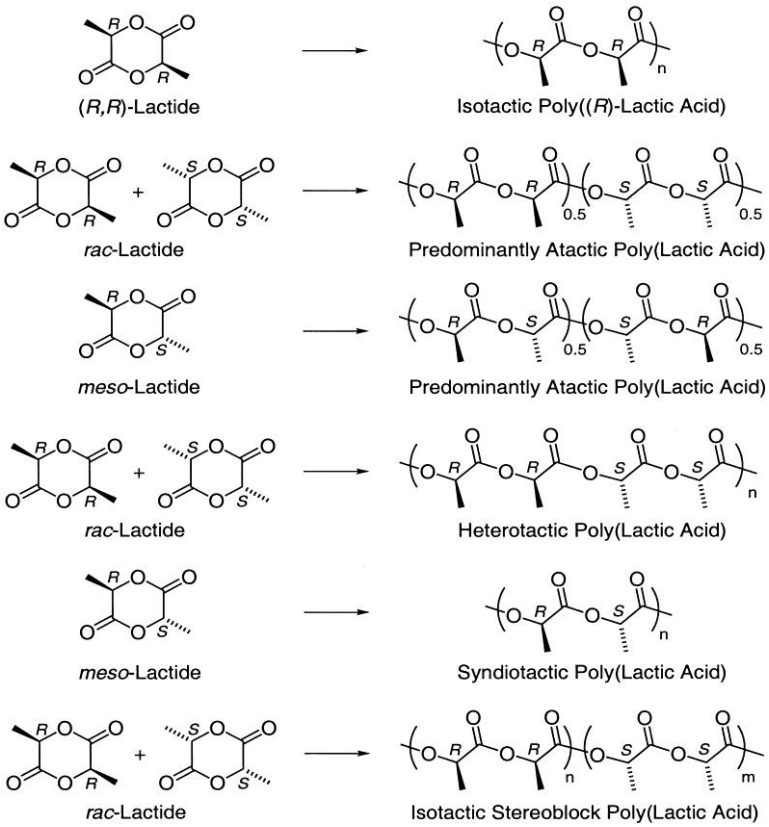
Figure 1.9 Stereoisomers of lactide[20]



1.7.2 Tacticity of polyesters

The two stereogenic centres in lactide allow the synthesis of polymers of different tacticity, which range from highly crystalline to totally amorphous. Atactic poly(LA) is amorphous and has a glass transition temperature (T_g) of around 55–60 °C, low tensile strength and a relatively rapid degradation. Semi-crystalline isotactic polymers prepared from *L*-lactide have melting temperatures (T_m) around 180 °C, higher tensile strength and much slower degredation.[52,53] Without any stereobias or epimerisation of the stereogenic centres, polymers prepared from *L*- or *D*-lactide will yield isotactic poly(LA), and *rac*-lactide or *meso*-lactide will yield predominately atactic poly(LA).

Figure 1.10 Lactide stereoisomers and poly(LA) microstructures.[54]



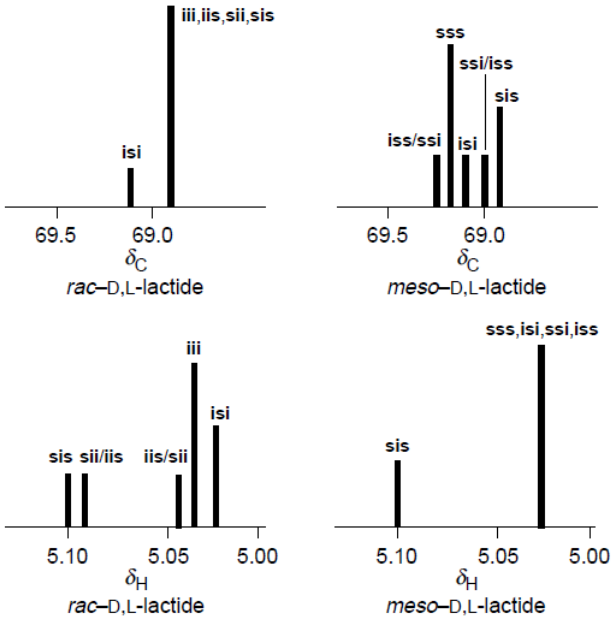
There are many different poly(LA) isomers possible upon application of the appropriate polymerisation pathway (Figure 1.10). These include isotactic, syndiotactic and heterotactic isomers. Interestingly, in addition to the microstructures described in Figure 1.10, polymer chains of different tacticity can interact to yield stereo complexes with enhanced properties, such as when independently synthesized poly(*L*-LA) and poly(*D*-LA) are mixed, the chains co-crystallize to form a stereo-complex with a melting point of up to 230 °C, which is 50 °C higher than that of poly(*L*-LA) and poly(*D*-LA) alone.[55]

The two strategies for the synthesis of stereo-regular poly(LA) from *rac*-lactide are chain-end control and enantiomorphic site control. Chain-end control is observed in achiral complexes where the stereogenic centre of the previously inserted monomer directs the chirality of the next monomer addition. Polymerisation utilising chain-end control typically accounts for the synthesis of hetereotactically enriched poly(LA) by achiral complexes[45,46,56-71], but isotactically enriched poly(LA) stereo-complexes have also been observed.[59,72-76] Enantiomorphic site control is evidenced when the chirality of the initiator is able to consistently differentiate between *D*- and *L*-lactide throughout the polymerisation. Utilising this mechanism it is possible to synthesise isotactically enriched (or isotactic block copolymer) poly(LA) from *rac*-lactide with a racemic catalyst,[77-82] stereo-gradient poly(LA) from a resolved catalyst and *rac*-lactide,[47,54,83,84] and syndiotactic poly(LA) from *meso*-lactide.[54,64] Enantiomorphic site control can either be enhanced or quenched by chain-end control, the specific influence of each mechanism is still in doubt.[81]

1.7.3 Characterisation of polymer chain stereosequences by NMR spectroscopy

Determination of polymer tacticity is obtained by analysis of homodecoupled ^{1}H and ^{13}C-$\{^{1}H\}$ NMR spectroscopy. Assignments were first proposed by Lillie and Schulz,[85] and Schindler and Harper[86] in the mid 1970s derived from models based on Bernoullian statistics, for single and pair wise addition of lactide repeating units in the growing chain. They established that the configurational structure of poly(LA) is determined by a pair addition mechanism and, assuming that epimerisation does not take place can be described by pair addition Bernoullian statistics. The theoretical intensity values for polymer mixes are displayed in Figure 1.11.

Figure 1.11. Schematic representation of the currently accepted assignments (CH) for poly(LA) at the tetrad level.[87]



HETCOR NMR spectroscopy has been employed upon homodecoupled ^{1}H and ^{13}C NMR to confirm the above assignments for the various poly(LA) stereosequences. In Figure 1.11, *i* refers to an isotactic linkage (two adjacent stereo centres of the same configuration, i.e. *S*,*S*), and *s* refers to a sydiotactic linkage (two adjacent stereo centres of opposing configuration, i.e. *R*,*S*). As shown in Figure 1.11, assignments are possible at the hexad level, which is the addition of 3 lactide units or six stereo centres in series. Values of tacticity are typically quoted as a probability where P_r is the probability of *racemic* linkages (heterotactic enrichment) and P_m is the probability of *meso* linkages (isotactic enrichment) with respect to those expected from Bernoullian statistics for random pair wise addition. Some stereo sequences are not possible though pair wise addition of (*S*,*S*) or (*R*,*R*) lactide units such as the *sss* sequence (in absolute terms (*S*,*R*,*S*,*R*,*S*,*R*)) this indicates transesterification or epimerisation reactions have occured.[60,88-93] However, in practice polymerisation reactions with a high propensity for transesterification side reaction have overlapping or poorly defined peaks in the homodecoupled ^{1}H or ^{13}C-{^{1}H} NMR, therefore MALDI-ToF MS is a more convenient technique to probe these side reactions. It should be noted that there is still some ambiguity regarding the actual assignments and research into better models is still ongoing.[87,90-92]

Figure 1.12. The methine resonances in the homonuclear decoupled ^{1}H NMR spectrum of poly(LA) illustrating isotactic block poly(LA) chains (a) and heterotactic poly(LA) chains (b).[63]

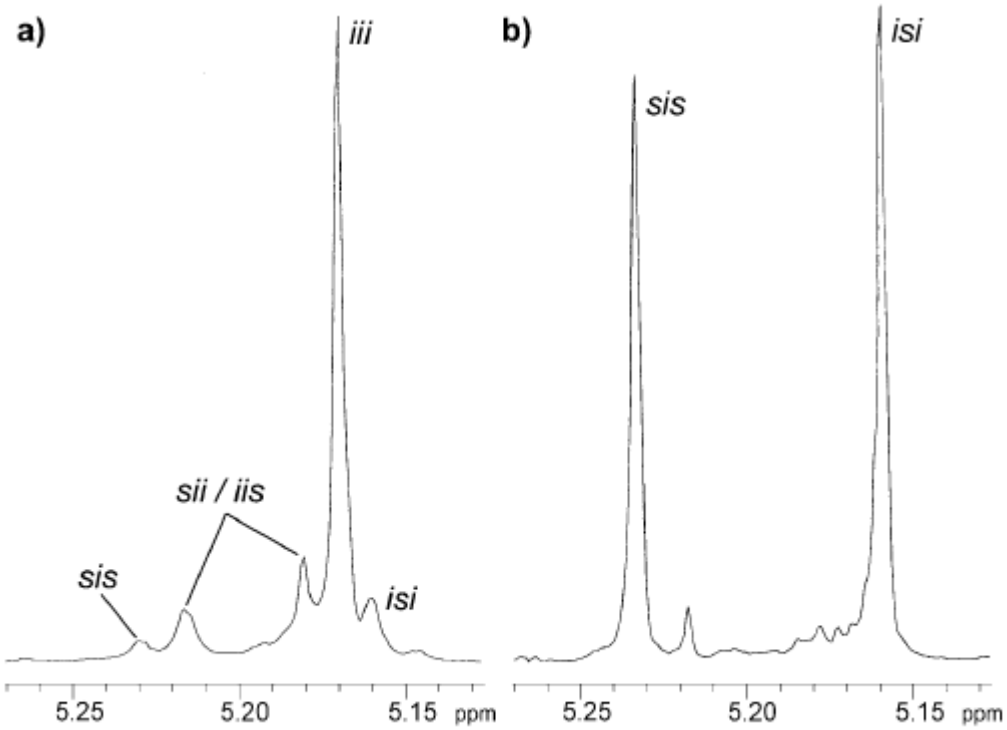
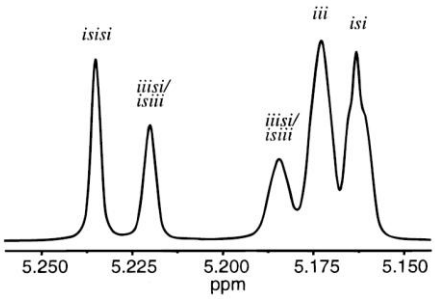


Figure 1.13. The methine resonances in the homonuclear decoupled ^{1}H NMR spectrum of poly(LA) illustrating atactic poly(LA) chains.[91]



Figures 1.12 and 1.13 show typical examples of homodecoupled ^{1}H NMR of isotactic, heterotactic and atactic polymers previously reported.

1.8 Literature review

Over the recent decade numerous efforts have been devoted to the synthesis of catalytic systems for the ROP of ε-caprolactone and lactide that would promote ROP under mild conditions with high efficiency and polymerisation control.[40] This section

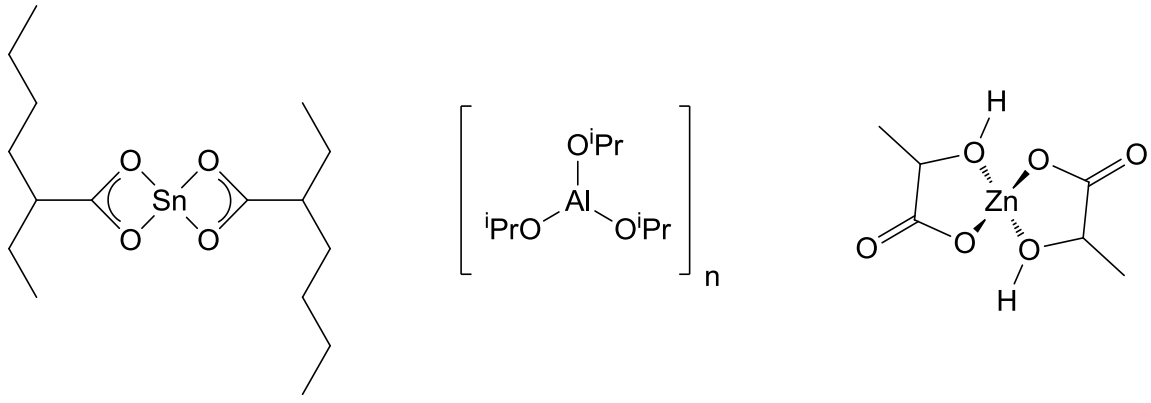
provides a selective overview of this exciting research field highlighting important achievements. Catalysts are presented according to the nature of the ancillary ligand(s) employed.

Metal-based catalysts for the ROP of cyclic esters are generally derived from Lewis acidic metals, feature one or more alkoxide functional (initiating) groups, and are supported by a polydentate ancillary ligand (set) which controls the catalyst nuclearity and coordination-insertion chain growth mechanism. It is an area of research that has been extensively reviewed recently and the reader is referred to these reviews for detailed accounts.[16,19-21] Catalyst systems can be based on many metals such as magnesium,[57,94-97] zinc,[57,60,64,95,97-99] calcium,[41,96,97,100] aluminum,[99,101-104] yttrium,[56,105,106] the lanthanides,[70,107-109] tin,[110] the Group 4 elements,[99,111-118] germanium,[71] indium,[58,119] iron[120,121], and bismuth.[122,123] Chapter 2 describes in further detail catalysts based upon the Group 4 metals, and Chapter 4 provides further details into aluminium based catalysts for ROP.

1.8.1 Catalysts employed in industry

Industrially, tin (II) 2-ethylhexanoate (stannous octanoate) with an alcohol co-initiator is the most commonly employed system. This is primarily due to its ease of handling, versatility, solubility in organic solvents (and in the bulk monomer under melt conditions), and crucially, FDA approval as a food additive in the USA.[13,15]

Figure 1.14. Stannous octanoate (left), aluminium isopropoxide (middle), zinc lactate (right).



$Sn(Oct)_2$ $Al(O^iPr)_3$ $Zn(Lact)_2$

It has been proposed that the $Sn(Oct)_2$ system acts through an activated monomer mechanism whereby a monomer bound to tin is ring opened by an alcohol co-initiator which then proceeds to propagate though a coordination insertion mechanism.[15,124,125] Although stannous octanoate has FDA approval as a food additive, its use in biomedical applications is restricted due to the retention of tin residues in the polymers, and the highly toxic nature of organo tin complexes.[125] It should be noted however that Sn(II) species are far less toxic than organometallic Sn(IV) complexes.[126] Alternative homoleptic initiators such as zinc lactate and aluminium tris(alkoxide) have therefore been developed.

At present zinc based catalysts, zinc metal, zinc octanoate, zinc stearate, zinc salicylate and zinc lactate are among the most common catalysts for poly(LA) synthesis for pharmaceutical and medicinal applications.[127-129] However, compared to tin catalysts, zinc based initiators are far less active and result in poorer control of polymer M_n and lower molecular weights.

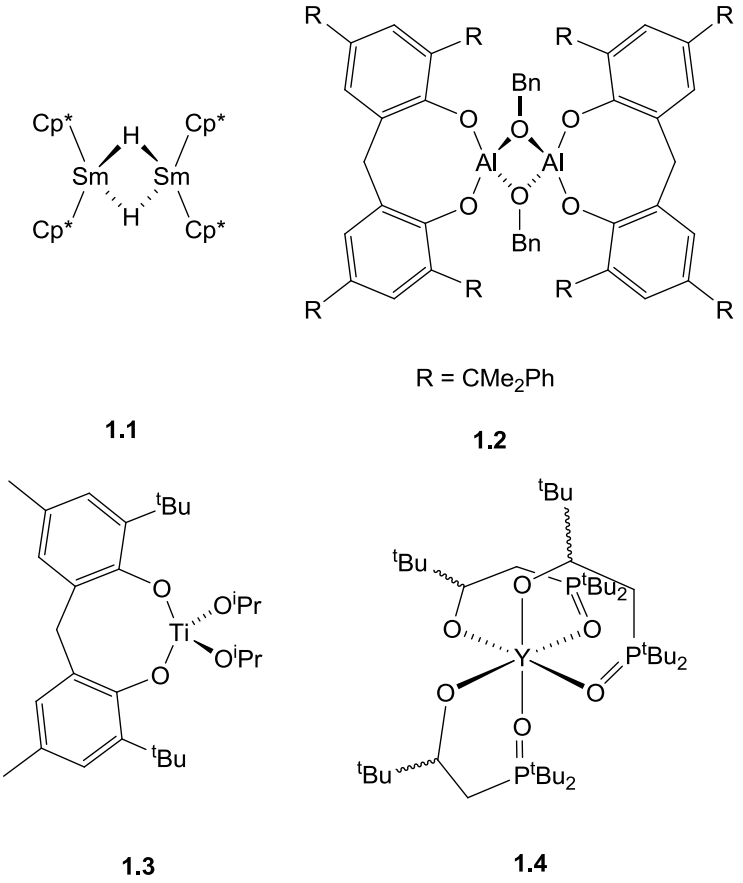
Although providing the most controlled polymerisations, aluminium alkoxide initiators, suffer from relatively slow propagation rates compared to tin for lactide polymerisation. The slower propagation towards lactide has been attributed to coordination of the nearest inserted carbonyl of the polymer chain to the metal centre, leading to formation of a stable 5-membered chelate, which hinders monomer uptake.[130] Aluminium alkoxides are, however, the industrial catalyst of choice for ε-caprolactone polymerisation due to the relative ease of polymerisation of this monomer. A potential solution to these issues is to employ non-toxic and highly active rare earth or less active but well controlled Group 4 alternatives for the ROP of cyclic esters.[131] Recent developments by Tolman and Hillmyer have employed indium chloride with benzyl alcohol and triethylamine co-initiators to yield heterotactically enriched (P_r = 0.95) poly(LA) of predictable M_n and narrow PDI, and, although no melt polymerisations were undertaken, the simplicity of this system seems ideal for industrial application.[58]

Recent academic research into initiators for ROP of cyclic esters has been aimed at producing well-defined single site catalysts, which have the potential to tune the reaction rate and selectivity through manipulation of inert ancillary ligand(s).

1.8.2 Cyclopentadienyl ligand

In classical organometallic chemistry there is no more exploited ligand class then those based upon cyclopentadieyl ligands. These ligands can themselves initiate ROP, and the complexes Cp^*_3Sm and $(\eta\text{-}C_5H_4R)_3Ln$ (R = Me or H, Ln = Y, Sm or Er) have been shown to initiate ε-caprolactone polymerisation in solution with modest control and broad PDIs (>2.1).[132-134] Yasuda reported the extremely efficient polymerisation of ε-CL with the hydride complex **1.1** (Figure 1.15) to yield high molecular weight polymer with narrow PDI (~1.1).[31] THF-stabilised methyl complexes bearing Cp* ligands were also found to be highly efficient for the ROP of ε-CL giving a linear increase of M_n with conversion which is indicative of a living type process.[31] Complexes of the type $(\eta^5\text{-}C_5R_5)TiCl_2(OMe)$ were also found to be initiators for the ROP of ε-CL in toluene solution.[135] The polymerisation rate and control were found to be highly dependent on the C_5R_5 ring substitution pattern. Catalysts containing $\eta^5\text{-}C_5H_3(SiMe_3)_2$ gave the highest activity. Overall the polymer produced was of moderate PDI (~1.5) but with reasonable agreement between calculated and observed M_n.[135] Other Group 4 half-sandwich compounds have also been investigated for the ROP of ε-CL. These catalysts generally feature modest control (PDI ~1.3), but allowed the synthesis of relatively high molecular weight polymers (M_n up to 60,000 g mol^{-1}).[136,137]

Figure 1.15 ROP catalysts employing Cp* and bidentate bis(phenolate) ligands.[31,99,138-143]



1.8.3 O-donor ligands

Bis(phenolates) have been evaluated as ancillary ligands for aluminium, zinc and titanium, Figure 1.15.[99,138-144] The aluminium and zinc species exhibit a dimeric structure with low activity, for example complex **1.2** reaches 81% completion of 50 equivalents of *L*-lactide after 48 h in refluxing toluene. It does however exhibit good control of the polymerisation reaction with close agreement between observed M_n and calculated M_n with narrow PDI (~1.1). Complex **1.3** polymerises 100 equivalents of ε-CL in 5 hours at RT in dichloromethane, with reasonable agreement beween M_n calculated and M_n observed by GPC and narrow PDI (~1.2). However no lactide polymerisation was reported.[143]

Arnold has reported homoleptic phosphine oxide-alkoxide rare earth complexes such as **1.4**, Figure 1.15. At low temperature (-18 °C) these are able to produce isotactically

enriched poly(LA) from *rac*-lactide with narrow to moderate PDIs (1.2 - 1.4) and P_r = 0.80.[145]

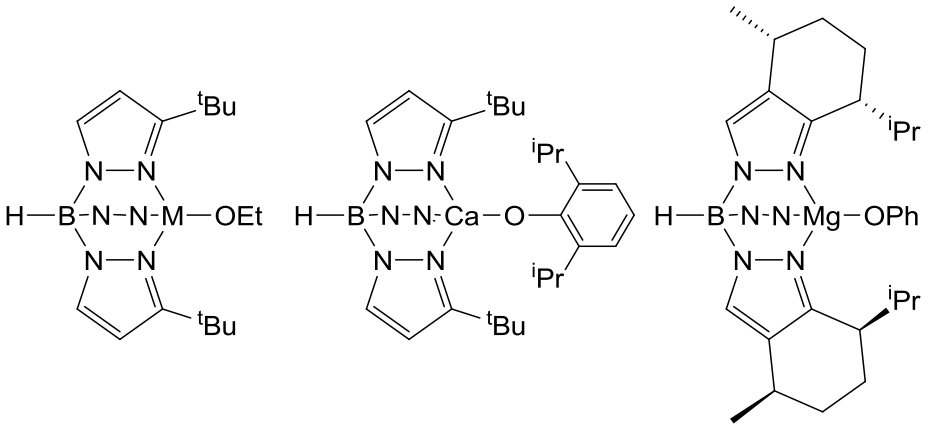
1.8.4 N-donor ligands

Nitrogen donor ligands have been employed for ROP with a view to controlling the aggregation phenomenon associated with oxygen containing ligands. It is also expected that the more sterically hindered N-donors would be inert with regards to ROP.[40]

Tris(pyrazolyl) borate (Tp^R) ligands

Tp^R ligands have been employed by Chisholm to produce magnesium, zinc and calcium alkoxide or aryloxides for the ROP of lactide. The calcium complex was found to be one of the most active species so far discovered, polymerising 100 equivalents in less than one minute in THF at room temperature.[65] The order of activity was postulated to depend on the polarity of the initiating metal oxygen bond in the order Ca > Mg > Zn. Interestingly, the reverse trend is observed for polymerisation control where calcium initiated poly(LA) yields moderate PDIs (~1.6) whereas that initiated by magnesium and zinc yield narrow PDIs (~1.2). This trade off between activity and control is a feature of ROP across the periodic table when employing the same ancillary ligands on different metals. Heterotactic enrichment is observed in complex **1.7** for the ROP of *rac*-lactide.[65,66] For complex **1.8** a moderate selectivity (~25%) to form syndiotactic poly(LA) was observed when polymerising *meso*-lactide at -40 °C in dichloromethane.

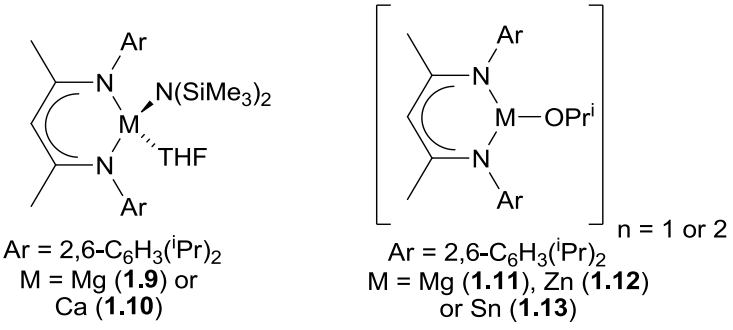
Figure 1.16. ROP catalysts employing tris(pyrazolyl) borate (Tp^R) ancillary ligands.[64-66]



β-Diiminate ligands

Coates and Chisholm investigated β-diiminate complexes of zinc and magnesium (Figure 1.17) and observed a similar trend in reactivities to bulky Tp ligands where magnesium was again found to be more active than zinc in lactide polymerisation (100 equivalents of *rac*-lactide to >95% conversion in 5 minutes for Mg and 80 minutes for Zn, at room temperature).[61] Good to moderate PDIs (1.1-1.5) and predictable M_n were observed for polymerisation reactions initiated with these catalysts.

Figure 1.17. ROP catalysts employing β-diiminate ancillary ligands.[57,61,66,146,147]



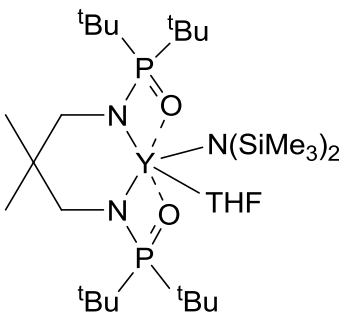
Strikingly excellent control of polymer tacticity was achieved with **1.12** where *L*-lactide was polymerised to yield isotactic poly(LA) without epimerization of the monomer, and *rac*-lactide to yield heterotactic poly(LA) (P_r = 0.94 at 0 °C), and *meso*-lactide to yield syndiotactic poly(LA) (P_r = 0.76 at 0 °C).[57] Calcium, tin and

iron(II) have also been evaluated but found to be less effective, with calcium exhibiting redistribution reactions to yield homoleptic alkoxide and β-diiminate complexes.[57,61,66,146,147] The slower reactivity of tin and iron is attributed to their comparative electronegativity. The tin example does, however, produce well controlled polymerisation results with >90% conversion of 100 equivalents being observed after 1.5 hours at 60 °C in toluene with good control of the M_n and narrow PDI (~1.2) and a small amount of heterotactic enrichment (P_r = ~65%).[147]

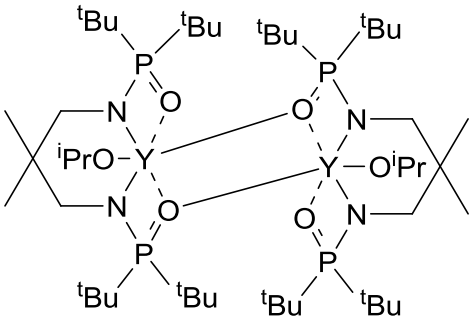
Bis(phosphinic)diamido ligands

A series of yttrium complexes supported by bis(phosphinic)-diamido ligands have been employed for the ROP of *rac*-lactide, **1.14** and **1.15** (Figure 1.18). Polymers of reasonable agreement between experimental and calculated M_n with moderate PDI (1.4-1.6) were formed.[148-150] Interestingly, it was found that there was a strong dependence on the reaction solvent with regard to the heterotacticity obtained with these catalysts. In THF, P_r values of 0.85 were achieved, whereas in dichloromethane the polymers had P_r values of 0.62. The authors' explanation postulates a highly effective monomer in THF but a dimer with little selectivity in dichloromethane.[151]

Figure 1.18. ROP catalysts employing bis(phosphinic)diamido ancillary ligands.[148-151]



1.14



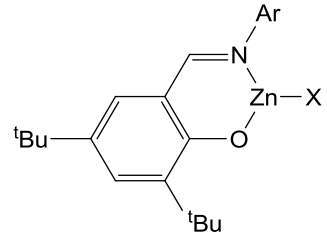
1.15

1.8.5 Bi- and Tridentate N,O-donor ligands

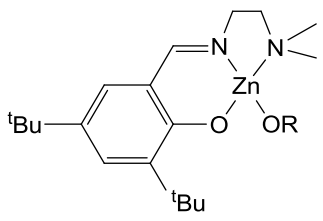
Bi- and tridentate N,O-donor ligands have been employed for the ROP of cyclic esters. Chisholm investigated the Schiff base complexes **1.16** and **1.17** (Figure 1.19) as alternatives to the spectacularly successful β-diiminates.[152] However, low reactivity was observed (4 hours for **1.16** and 72 hours for **1.17**) to polymerise 20 equivalents of *rac*-lactide at room temperature, with no stereoselectivity. Presumably the low

selectivity reflects the less sterically hindered metal centre when coordinated by the Schiff base ligands relative to its β-diiminate counterpart. Ligand redistribution reactions to form homoleptic $(L)_2Zn$ along with either $Zn\{N(SiMe_3)_2\}_2$ or $Zn(O\text{-}2,6\text{-}C_6H_3{}^tBu_2)_2$ compounds were observed upon heating of these complexes.[152]

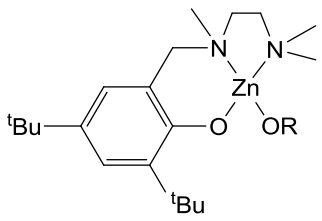
Figure 1.19. ROP catalysts employing bi- and tridentate N,O-donor ligands[152-155]



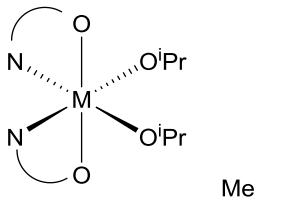
Ar = 2,6-$C_6H_3{}^iPr_2$
X = $N(SiMe_3)_2$ (**1.16**)
X = O-2,6-$C_6H_3{}^tBu_2$ (**1.17**)

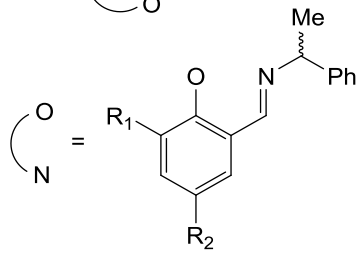


1.18

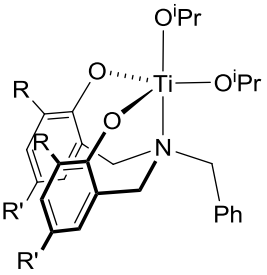


1.19

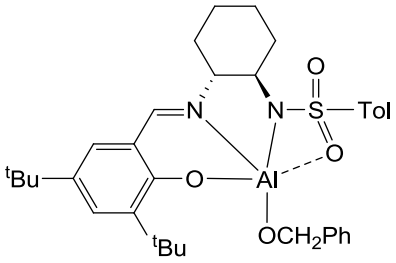




1.20



1.21



1.22

Complexes supported by Schiff bases containing a donor pendent arm have also been evaluated for ROP. Typical examples, **1.18** and **1.19**, are shown in Figure 1.19.[153,154] Lin reported the use of **1.18** as a catalyst for the ROP of *rac*-lactide polymerising 100 equivalents over 4 hours in dichloromethane at room temperature with good M_n control (7100 $gmol^{-1}$ GPC, 6700 $gmol^{-1}$ calculated) and narrow PDI (1.2). For low temperature polymerisations at -55 °C over one week, heterotactically enriched poly(LA) could be obtained (P_r = 91%). In a good example of the non-predictable nature of ROP complexes, **1.19** employed by Tolman and Hillmyer proved to be a much more active catalyst than **1.18**. Polymerisation of 1500 equivalents of *rac*-lactide to yield polymer with M_n of 130,000 $gmol^{-1}$ with narrow to moderate PDI (1.34) was

observed in just 18 minutes at room temperature in dichloromethane.[154] As expected for living polymerisations, the rate law for the reaction was determined to be -d[LA]/d*t* = k_p[(L)ZnOEt][LA].

Davidson has employed chiral Schiff base ancillary ligands to synthesise Group 4 isopropoxide catalysts **1.20** (Figure 1.19). The ligands gave only weak chiral induction with both Δ and Λ isomers of the 6-coordinate octahedral complexes being present in solution. However, zirconium catalysts were found to afford heterotactically enriched polylactide both in toluene solution (at 20 °C and 80 °C) and in the melt (P_r = 0.68 – 0.73), probably a result of chain-end control rather than enantiomorphic site control being imparted by the chiral catalysts. Solution polymerisations were generally found to be well-controlled, giving predictable molecular weights and narrow PDI (1.2) in toluene solution at 20 °C. In contrast, melt polymerisations were found to be somewhat less controlled giving PDIs in the range of 1.7-2.0 but retaining the heterotactic enrichment.[156] Davidson has also exploited tridentate bis(phenolate)-amine complexes such as **1.21** for the ROP of ε-caprolactone, observing a well controlled polymerisation over 24 hours at room temperature to give polymer of narrow PDI (~1.1 – 1.2) and predictable M_n.[42] Similar titanium isopropoxide complexes supported by dialkanolamine ligands have been employed by the group of Karlov for the ROP of ε-caprolactone.[157] These complexes were found to be moderately well controlled with good agreement between found and calculated M_n with narrow to moderate PDI (1.2-1.6).[157]

Tridentate bis(phenolate)-amine complexes have also been evaluated for aluminium for the ROP of ε-caprolactone. The reaction proceeds well to yield poly(ε-CL) of narrow PDI (1.1-1.2) with good agreement between calculated M_n and that determined by NMR and GPC (after the application of Mark-Houwink corrections).[158]

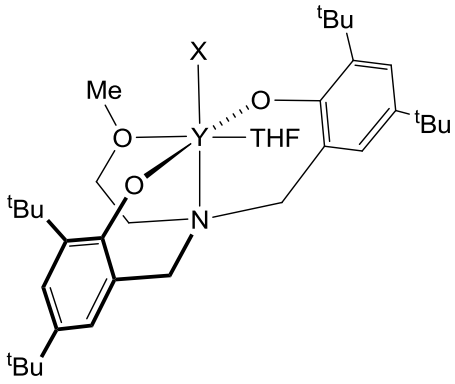
Wu has reported aluminium complexes supported by chiral tridentate Schiff base-sulfonamide complexes (**1.22**, Figure 1.19) and exploited them for the ROP of *L*-lactide. Compound **1.22** showed excellent control in the polymerisation of *L*-LA yielding isotactic polymers with narrow PDIs and close agreement between expected M_n values and those measured by GPC over 24 hours in refluxing toluene.[155] Somewhat disappointingly, no polymerisations of *rac*-, *meso*- or *D*-lactide were

reported so it is not possible to quantify any effects of the chiral backbone on the polymerisation.

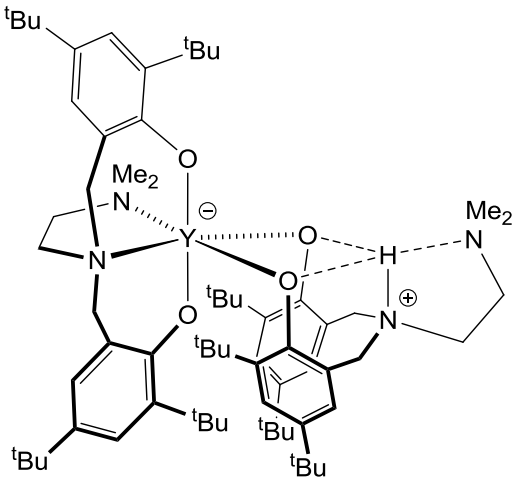
1.8.6 Tetradentate N,O-donor ligands

Metal complexes supported by polydentate phenoxy-amine ligands have been extensively exploited for the ROP of cyclic esters.[42,43,45,46,56,67-70,104,108,156,158-166] Important advances have been achieved with group 3 and the rare earth metals. Carpentier was the first to deploy group 3 alkyl and amide complexes supported by bis(phenolate)-amine ligands for the ROP of *rac*-lactide (e.g. **1.23** and **1.24**, Figure 1.20). Polymerisation of *rac*-lactide yielded hetereotactically-enriched poly(LA) (P_r = 0.80) with good agreement between calculated and found M_n and narrow to moderate PDI (1.25-1.35) for up to 500 equivalents of monomer.[56]

Figure 1.20. Group 3 ROP catalysts employing Tetradentate N,O-Donor ligands.[46,56]



X = $N(SiHMe_2)_2$ (**1.23**)
or CH_2SiMe_3 (**1.24**)

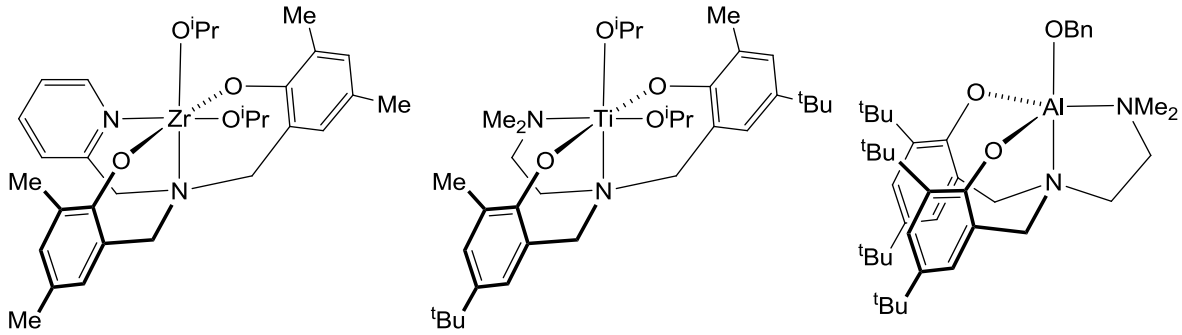


1.25

Structure-activity relationships and alternative initiators have been investigated by Carpentier, Cui, Okuda (on a similar system with a disulfide bridge) and within our group.[67-70] Carpentier later showed that this system would undergo immortal polymerisations in the presence of alcohol chain transfer reagents to yield heterotactically enriched poly(LA) of narrow PDI (1.1) and good control of M_n.[45] Work within our group showed that it was also possible to enter the immortal polymerisation cycle from zwitterionic complexes such as **1.25** (Figure 1.20), in the presence of amine or alcohol co-initiators.[46] It was found that alternative initiators

such as a borohydride group would furnish heterotactically enriched poly(LA) (P_r = 87) but with poorer control of the polymerisation process as is evidenced by moderate PDIs (~1.6).

Figure 1.21. Group 4 and 13 ROP catalysts employing tetradentate N,O-donor ligands.[43,159-163,166]



1.26 **1.27** **1.28**

Group 4 complexes bearing tetradentate bis(phenolate)-amine complexes have been employed for the ROP of lactide and ε-caprolactone by Bochmann, Davidson and Kol.[43,159,166] Davidson and Kol studied structure activity relationships within the Group 4 triad and found that zirconium catalysts bearing low sterically bulky ligands displayed the highest activity and control of all the species studied. Titanium catalysts were found to be poor, in that only highly strained systems were able to initiate the polymerisation. These results were explained as a consequence of monomer accessibility to the metal centre. Davidson looked at *rac*-lactide both in toluene solution and in the melt, and found atactic polymers were produced (P_r = 0.5). However, for ligands bearing a diamino ethane bridge between phenolate groups a small amount of isotactic enrichment was possible yielding polymer with good M_n control (10,700 g mol^{-1} (found) versus 9,150 g mol^{-1} (expected)) narrow PDI (1.17) and P_m = 0.75, over two hours in toluene at 110 °C.

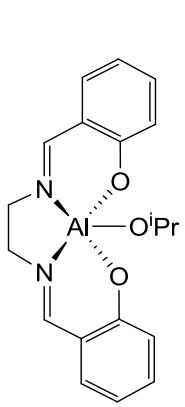
Bochmann reported the attempted polymerisation of ε-caprolactone with **1.27** but found that it was inactive over four hours in toluene at 60 °C. Interestingly, reduction of **1.27** with sodium amalgam yielded a highly active catalyst which would polymerise 200 equivalents of ε-caprolactone in two hours under similar conditions, although with broad PDIs (2.5).[166]

Group 13 complexes of polydentate bis(phenolate)-amine ligands (e.g., **1.28** Figure 1.21) have also been investigated for the ROP of both *rac*-LA and ε-caprolactone.[158,160-163] Complexes of this type are well-controlled but somewhat slow catalysts for the ROP of ε-caprolactone. For example, complex **1.28** polymerises 150 equivalents in toluene at 50 °C over 6 hours to 81% completion giving polymer with the expected M_n and narrow PDI (1.05). However, complexes such as these bearing bulky phenolate ligands were found to be inactive for lactide polymerisation.[162,163] Gibson observed that employing phenolate ligands bearing methyl substituents instead of *tert*-butyl yielded an active catalyst for *rac*-lactide. The polymerisation proceeds slowly reaching 91% conversion of 50 equivalents over 12 hours at 70 °C in toluene, but in a controlled fashion (PDI = 1.08) to give isotactically enriched poly(LA) (P_m = 0.73). Interesting, and at times contradictory, steric and electronic effects of ligand variation upon catalysis have been observed for these systems. A prime example is the system studied by Hillmyer and Tolman[162] (**1.28**, Figure 1.21) in which changing the *tert*-butyl substituent in the 5-position of the phenolate ring to bromine significantly decreases activity. This is in stark contrast to the corresponding salen ligands for which Gibson showed halide substituents on the phenolate ring *enhanced* activity (**1.33**, Figure 1.22).[104]

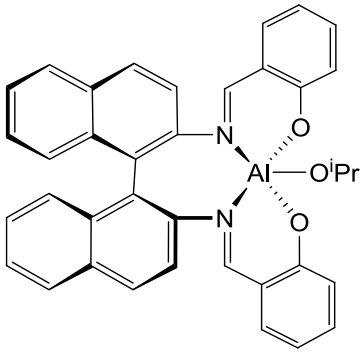
1.8.7 Tetradentate N,O-donor ligands - salen and salan supported complexes

Notable examples of aluminum-based catalysts are the salen[73-75,77,83,167-175] and salan[63] complexes with which highly isotactic stereo-block, syndiotactic or tapered isotactic block copolymers can be formed, depending on the stereoisomer of the LA and ligands employed (e.g., **1.29**–**1.33**, Figure 1.22).

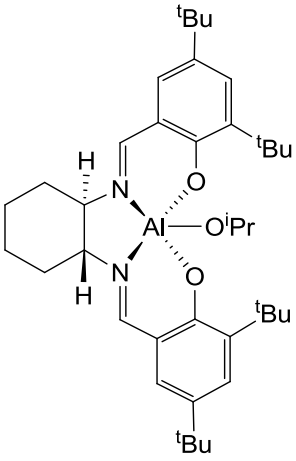
Figure 1.22. Examples of salen- and salan-supported aluminum catalysts for the ROP of cyclic esters.[63,73-75,77,83,167-176]



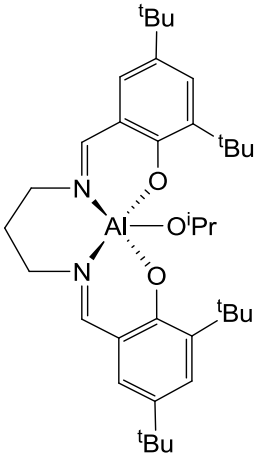
1.29



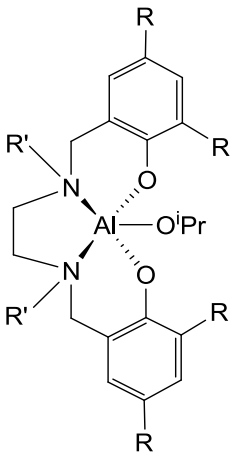
1.30



1.31



1.32



1.33

Spassky demonstrated the first stereo selective polymerisation of *rac*-lactide employing methoxide complexes bearing the *(R)*-stereoisomer of **1.30** (Figure 1.22). It was observed that the *D*-monomer is preferentially polymerised over the *L*-monomer to yield a stereo-gradient block polymer with a PDI of 1.10. It should be noted that, while this polymerisation is highly controlled, it is extremely slow only polymerising 75 equivalents of *rac*-lactide over 113 hours to 90% conversion. The first 50% of the monomer however, polymerises relatively quickly in around five hours due to the kinetic resolution of the isomers. Coates then applied the *(R)*-stereoisomer of complex **1.30** to the polymerisation of *meso*-lactide to produce highly syndiotactic enriched poly(LA) (P_m = 0.96). Interestingly, yttrium complexes investigated alongside the

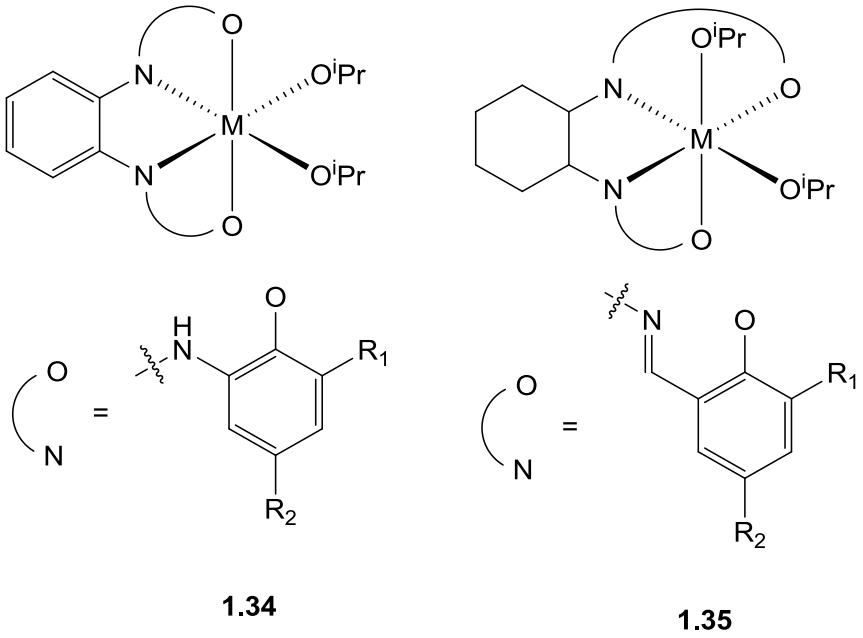
aluminium analogues gave totally atactic polymer.[168,176] Baker and Smith used a racemic mixture of **1.30** to polymerise *rac*-lactide to produce isotactically enriched poly(LA) (P_m > 0.90).[170] However, Coates observed that a polymer exchange mechanism between catalyst centres was in fact in operation so the polymer was best described as an isotactic stereo-block of approximately 11 monomer chains per block rather than two separate isotactically enriched poly(LA) chains as Baker and Smith suggested.[83] Similarly, polymerisation of *meso*-lactide with the *rac* form of the ligand did not produce the expected syndiotactic poly(LA) but produced heterotactically enriched poly(LA) (P_r = 0.80) again as postulated though a polymer exchange mechanism.[54]

Feijen employed Jacobsen's ligand with $Al(O^iPr)_3$ to form **1.31** (Figure 1.22) which proved to be a highly selective catalyst for lactide polymerisation. Strong stereo-induction was observed where the (*R*,*R*)-ligand polymerised *L*-lactide fourteen times faster than *D*-lactide. Utilising this stereo preference it was possible to synthesise polymers of predominantly *D*-lactide constitution by the kinetic resolution of *rac*-lactide at upto 50% conversion. Polymerisation of *rac*-lactide using the *rac*-ligand complex yields isotactic stereo-block polylactides with narrow PDI (<1.1) with predictable M_n and a P_m value of 0.92.[47,177] Chisholm and co-workers examined the stereoselective preferences of salen type systems by studying complex **1.31** with different chirality in the ring-opening event of *rac*-lactide. It was found that both the chirality of the ligand bound to the metal and the chirality of the end group of the growing chain, as well as the solvent, all play a complex and rather unpredictable role in the preference for the ring opening of *L*- or *D*-LA in a racemic mixture. This demonstrates the unknown nature of the stereo-inductive effects of chain-end control versus enantiomorphic site control,[81] (a further good example is provided by Gibson in achiral salan systems, see below).

Concurrently with the work of Spassky and Coates, achiral salen complexes have been studied as ROP catalyst for lactide. Exhaustive studies exploring structure-activity relationships by systematic ligand variation upon systems of the type **1.33** (Figure 1.22) were studied by the groups of Spassky, Gibson, Nomura, Chen and Jing. Generally, it was found that there was a trade off between activity and selectivity, where it was possible to prepare highly isotactic stereo-block poly(LA) (P_m = 0.98, T_m

= 210 °C) from *rac*-lactide with $^{t}BuMe_2Si$ substituents at the 3-position of the phenolate. However, hydrogen, methyl or chloro substitution was found to enhance activities depending on the backbone of the salen ligand employed. The backbone was also found to significantly affect activity and selectivity of the complexes.[74,75] Importantly, it was observed that it was possible to synthesise isotactically enriched stereo-block poly(LA) under industrially relevant melt conditions, polymerising 300 equivalents of *rac*-lactide at 130 °C in an hour to yield polymer with narrow PDI (1.1) and good control of M_n.[75] For the salan type systems **1.33** (Figure 1.22) Gibson showed it was possible to synthesise isotactically or heterotactically enriched poly(LA) depending on the phenolate substitution. The presence of hydrogen in the 4-postion yielded heterotactic polymer with P_r = 0.79, but with chloro substitution isotactically enriched stereo-block poly(LA) was synthesised (P_m = 0.96). The polymerisation reaction employing these complexes was generally well controlled yielding poly(LA) of narrow PDI (>1.1) and predictable M_n, polymerising 100 equivalents of *rac*-lactide within 21 hours at 70 °C in toluene solution.[63]

Figure 1.23. Salen and salophan complexes of the Group 4 metals. [80,178]



1.34 **1.35**

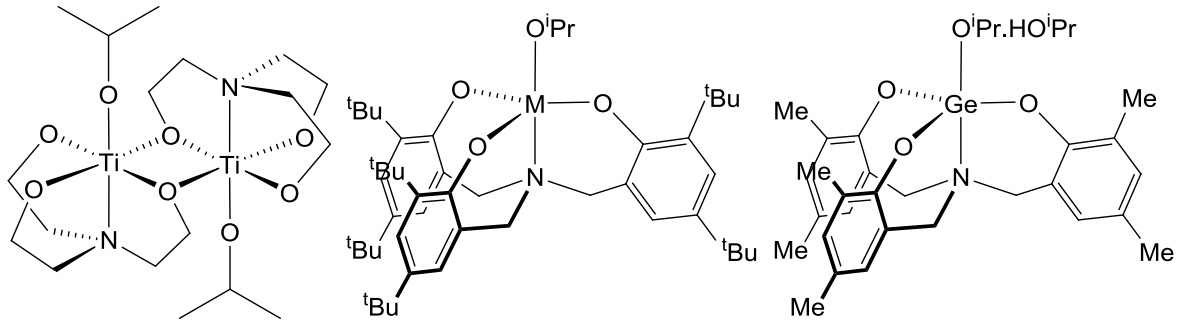
Salophan (a salan ligand with a phenylene backbone) and salen complexes have also been employed with the Group 4 metals, **1.34** and **1.35** (Figure 1.23). Gibson studied titanium isopropoxide complexes (**1.35**) supported by the same salen ligands as in complexes **1.29** and **1.31** (Figure 1.22). A generally well controlled polymerisation of

100 equivalents of *rac*-lactide was observed with 86% conversion after 8 hours in toluene at 70 °C, with good control of M_n and narrow PDI (1.2). In contrast to the aluminium systems, polymerisations produced atactic or slightly heterotactically enriched poly(LA) (P_r = 0.57). It was found that halide substitution decreased activity for the same systems in which it had enhanced activity in aluminium systems, further highlighting the difficult nature of structure activity relationships in the field of ROP.[80] Recent work by Kol has developed salophan ligands for Group 4 isopropoxides, **1.34** (Figure 1.23). Interestingly, these highly active titanium catalysts are able to polymerise 300 equivalents of *rac*-lactide in under one minute at 130 °C. This report is the only case of titanium being observed to provide the most active catalyst in the Group 4 triad for a given ancillary ligand.[178] Otherwise, the polymerisation shows moderate control with lower than expected M_n and moderate PDI (1.48), and a heterotactic bias (P_r = 87).

1.8.8 Tetradentate C_3 symmetric O,N-donor ligands

The first instances of heteroleptic titanium complexes for the ROP of lactide were reported by Verkade in 2002 for complex **1.36** (Figure 1.24). Complexes of this type were found to be only moderately active, typically requiring 15 hours to polymerise 300 equivalents of *rac*-lactide at 130 °C in the melt or 36 hours to polymerise 300 equivalents of *rac*-lactide at 70 °C to 70% completion in toluene. Solution polymerisations yield good agreement between M_n determined and that expected from conversion with a narrow PDI (1.1-1.2), although poor control is observed in the melt as evidenced by moderate to broad PDI (1.6-2.0) and a meagre correlation between the expected and observed M_n. Interestingly, employing $Ti(O^iPr)Cl_3$ for the ROP of *rac*-lactide was observed to yield slightly heterotactically enriched poly(LA) (P_r ~ 0.60), with moderate control (PDI = 1.3 – 1.4) in the melt and good control in toluene solution (PDI = 1.2).[179-181]

Figure 1.24. Group 4 and 13 ROP catalysts employing C_3 symetric N,O-donor ligands. [71,164,179-181]


O
N
O
O
Ti
O
O
Ti
O
O
O
N
O
O
O
M
O
tBu
tBu
tBu
tBu
tBu
N
O
O
O
Ge
O
Me
Me
Me
Me
Me
N
O
O
O

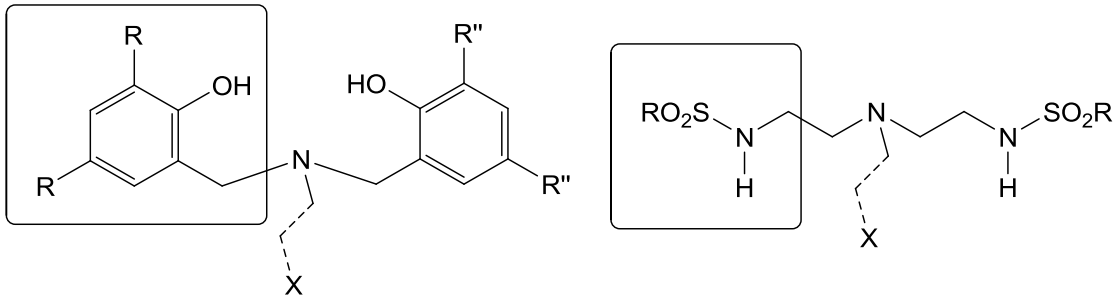
1.8.9 Summary

The above literature review highlights the extensive research already carried out in the field of ROP. It has been found that there is the general order of reactivity towards ROP for catalysts based on the following metals: rare earth and Group 3 complexes ~ calcium ~ magnesium > zinc > tin ~ zirconium and hafnium > titanium ~ aluminium.[27,40] Catalysts based on germanium, gallium, indium and bismuth have only recently been employed so their activities have not yet been fully explored. Undoubtedly the order of reactivity proposed above is highly subjective and application of the appropriate ancillary ligand has dramatic effects on the activities and selectivity of the resulting catalyst (Kol's discovery of highly active titanium complexes is a good example).[178] Trends in polymerisation control are even more difficult to elucidate with examples of excellent control having been seen for each of the metals given above. Therefore, the search for novel ancillary ligands which will afford high activity and good control is of tremendous importance.

1.9 Novel sulfonamide ancillary ligands for ROP catalysts

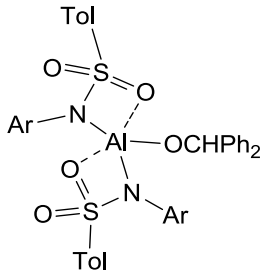
This thesis is directed towards the synthesis of novel ancillary ligands to support ROP catalysts for titanium, zirconium and aluminium. We speculated that polydentate sulfonamides (containing –N(R)SO_2R´ functional groups) could be useful in this regard. The electron-withdrawing SO_2R´ moieties reduce the normal basicity of anionic amide donors "NR_2" and might therefore allow them to act as phenolate mimics. Although N(R)SO_2R´ based ligands lack the steric control afforded by bulky ring-substituted phenolates OAr (e.g. **1.37-1.39** Figure 1.24), the well-established ability of sulfonamide ligands to adopt $\kappa^2(N,O)$ coordination modes[183-193] could confer additional stability on otherwise unsaturated metal centres. Sulfonamides in general are attractive synthetic targets due to their relatively simple preparation from the corresponding sulfonyl chlorides, a wide range of which are commercially available.

Figure 1.25. Analogy between sulfonamide and phenolate ligands.

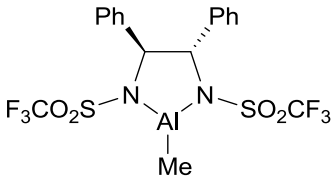


Outside of the work presented in this Thesis, there have been only two examples of sulfonamide-supported aluminum ROP catalysts, namely **1.41 (**Figure 1.25) and **1.22** (Figure 1.19)[194,195] and no examples of Group 4 sulfonamide compounds. Compound **1.41** gave poor control of the polymerisation process with a much lower than expected M_n and a moderately broad PDI under melt conditions after 10 h at 130 °C. In contrast, **1.22** showed excellent control in the polymerisation of *L*-LA yielding predominantly isotactic polymers with narrow PDIs and close agreement between expected M_n values and those measured by GPC, as described above, Section 1.8.5.[155]

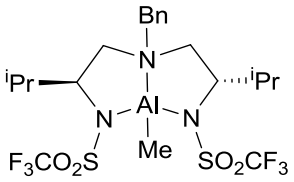
Figure 1.26. Sulfonamide supported complexes of aluminium[194-197] and the Group 4 metals.[185,190,191]



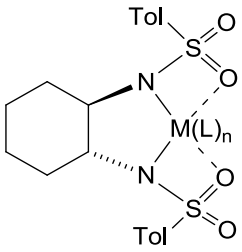
1.41



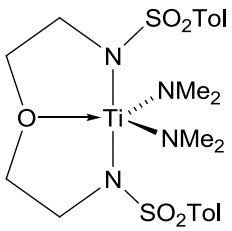
1.42



1.43



$M(L)_n$ = $Ti(O^iPr)_2$ **1.44** or
$Zr(NMe_2)_2(NHMe_2)$ **1.45**



1.46

In general a number of aluminum sulfonamide complexes have been reported (e.g. **1.42** and **1.43**, Figure 1.26) and employed for transformations such as the enantioselective catalytic Diels-Alder reactions,[196] asymmetric aldehyde cycloaddition reactions,[197,198] the Meerwein-Ponndorf-Verley reduction of carbonyl substrates,[199] the enantioselective [2+2] cycloaddition of trimethylsilylketene to aldehydes,[200] and the cyclopropanation of allylic alcohols.[201] A number of Group 4 (in particular titanium) complexes of cer tain bi- and tri-dentate bis(sulfonamide) ligands have also been reported over the past 10 years (Figure 1.26) and are effective for a variety of catalytic transformations such as synthesis of acetylenic alcohols,[202] enantioselective addition of diethyl zinc to benzaldehyde,[187,203] hydroamination of alkynes and allenes,[191] and Ziegler-Natta catalysis.[204]

1.10 Aims and Outlook

This thesis describes the synthesis, characterisation and ring opening polymerisation capability for ε-caprolactone and *rac*-lactide of titanium, zirconium and aluminium sulfonamide supported amide, alkyl, and alkoxide catalysts. The solution state behaviour will be discussed along with solid state structural determinations that have been undertaken to elucidate the structure and bonding of the complexes presented.

1.11 References

(1) East, A. J. *Encyclopedia of Polymer Science and Technology, Polyesters, Thermoplastic, 7* **2002**, *John Wiley and Sons*., 504-528.

(2) Production, W. P. *Plastics Europe*, *WG Market Research and Statistics*.

(3) Carothers, W. H.; Dorough, G. L.; Natta, F. J. v. *J. Am. Chem. Soc.* **1932**, *54*, 761-772.

(4) Gilding, D. K.; Reed, A. M. *Polymer* **1979**, *20*, 1459-1464.

(5) Emo, C.; Roberto, S. *Adv. Mater.* **1996**, *8*, 305-313.

(6) Uhrich, K. E.; Cannizzaro, S. M.; Langer, R. S.; Shakesheff, K. M. *Chem. Rev.* **1999**, *99*, 3181-3198.

(7) Drumright, R. E.; Gruber, P. R.; Henton, D. E. *Adv. Mater.* **2000**, *12*, 1841 - 1846.

(8) Yoshito, I.; Hideto, T. *Macromol. Rapid Commun.* **2000**, *21*, 117-132.

(9) Stefan, M. *Angew. Chem. Int. Ed.* **2004**, *43*, 1078-1085.

(10) Williams, C. K.; Hillmyer, M. A. *Polym. Rev.* **2008**, *48*, 1 - 10.

(11) Place, E. S.; George, J. H.; Williams, C. K.; Stevens, M. M. *Chem. Soc. Rev.* **2009**, *38*, 1139-1151.

(12) Vink, E. T. H.; Rábago, K. R.; Glassner, D. A.; Gruber, P. R. *Polym. Deg. Stab.* **2003**, *80*, 403-419.

(13) Drumright, R. E.; Gruber, P. R.; Henton, D. E. *Adv. Mater.* **2000**, *12*, 1841-1846.

(14) Raja, R.; Thomas, J. M. *Z. Anorg. Allg. Chem.* **2005**, *631*, 2942-2946.

(15) Albertsson, A.-C.; Varma, I. K. *Biomacromol.* **2003**, *4*, 1466-1486.

(16) Dechy-Cabaret, O.; Martin-Vaca, B.; Bourissou, D. *Chem. Rev.* **2004**, *104*, 6147-6176.

(17) Bourissou, D.; Martin-Vaca, B.; Dumitrescu, A.; Graullier, M.; Lacombe, F. *Macromolecules* **2005**, *38*, 9993-9998.

(18) Biela, T.; Kowalski, A.; Libiszowski, J.; Duda, A.; Penczek, S. *Macromol. Symp.* **2006**, *240*, 47-55.

(19) Kamber, N. E.; Jeong, W.; Waymouth, R. M.; Pratt, R. C.; Lohmeijer, B. G. G.; Hedrick, J. L. *Chem. Rev.* **2007**, *107*, 5813-5840.

(20) O'Keefe, B. J.; Hillmyer, M. A.; Tolman, W. B. *J. Chem. Soc., Dalton Trans.* **2001**, 2215-2224.

(21) Platel, R. H.; Hodgson, L. M.; Williams, C. K. *Polym. Rev.* **2008**, *48*, 11 - 63.

(22) Dubois, P.; Jacobs, C.; Jerome, R.; Teyssie, P. *Macromolecules* **1991**, *24*, 2266-2270.

(23) Dubois, P.; Jerome, R.; Teyssie, P. *Macromolecules* **1991**, *24*, 977-981.

(24) Barakat, I.; Dubois, P.; Jérôme, R.; Teyssié, P.; Goethals, E. *J. Polym. Sci., Part A: Polym. Chem.* **1994**, *32*, 2099-2110.

(25) Barakat, I.; Dubois, P.; Grandfils, C.; Jérôme, R. *J. Polym. Sci., Part A: Polym. Chem.* **1996**, *34*, 497-502.

(26) Barakat, I.; Dubois, P.; Grandfils, C.; Jérôme, R. *J. Polym. Sci., Part A: Polym. Chem.* **1999**, *37*, 2401-2411.

(27) Kricheldorf, H. R.; Berl, M.; Scharnagl, N. *Macromolecules* **1988**, *21*, 286-293.

(28) Ouhadi, T.; Stevens, C.; Teyssie, P. *Makromol. Chem. Suppl.* **1975**, *1*, 191.

(29) Hamitou, A.; Jerome, R.; Teyssié, P. *J. Polym. Sci., Polym. Chem.* **1977**, *15*, 1035-1041.

(30) Hamitou, A.; Ouhadi, T.; Jerome, R.; Teyssié, P. *J. Polym. Sci., Polym. Chem.* **1977**, *15*, 865-873.

(31) Yamashita, M.; Takemoto, Y.; Ihara, E.; Yasuda, H. *Macromolecules* **1996**, *29*, 1798-1806.

(32) Yasuda, T.; Aida, T.; Inoue, S. *Macromolecules* **1983**, *16*, 1792-1796.

(33) Spassky, N.; Simic, V.; Montaudo, M. S.; Hubert-Pfalzgraf, L. G. *Macromolecular Chemistry and Physics* **2000**, *201*, 2432-2440.

(34) Duda, A.; Penczek, S. *Macromolecules* **1995**, *28*, 5981-5992.

(35) Baran, J.; Duda, A.; Kowalski, A.; Szymanski, R.; Penczek, S. *Macromol. Rapid Commun.* **1997**, *18*, 325-333.

(36) Dubois, P.; Jerome, R.; Teyssie, P. *Makromol. Chem., Macromol. Symp.* **1991**, *42/43*, 103.

(37) Dubois, P.; Jerome, R.; Teyssie, P. *Polym. Bull.* **1989**, *22*, 475-482.

(38) Barakat, I.; Dubois, P.; Jérôme, R.; Teyssié, P. *J. Polym. Sci. Part A: Polym. Chem.* **1993**, *31*, 505-514.

(39) Eguiburu, J. L.; Fernandez Berridi, M. J.; San Román, J. *Polymer* **1995**, *36*, 173-179.

(40) Dubois, P.; Coulembier, O.; Raquez, J.-M. *Wiley-VCH* **2009**, Handbook of Ring-Opening Polymerisation.

(41) Zhong, Z.; Dijkstra, P. J.; Birg, C.; Westerhausen, M.; Feijen, J. *Macromolecules* **2001**, *34*, 3863-3868.

(42) Chmura, A. J.; Davidson, M. G.; Jones, M. D.; Lunn, M. D.; Mahon, M. F. *Dalton Trans*. **2006**, 887-889.

(43) Chmura, A. J.; Davidson, M. G.; Jones, M. D.; Lunn, M. D.; Mahon, M. F.; Johnson, A. F.; Khunkamchoo, P.; Roberts, S. L.; Wong, S. S. F. *Macromolecules* **2006**, *39*, 7250-7257.

(44) Kim, Y.; Jnaneshwara, G. K.; Verkade, J. G. *Inorg*. *Chem*. **2003**, *42*, 1437-1447.

(45) Amgoune, A.; Thomas, C. M.; Carpentier, J.-F. *Macromol*. *Rapid Commun*. **2007**, *28*, 693-697.

(46) Clark, L.; Cushion, M. G.; Dyer, H. E.; Schwarz, A. D.; Duchateau, R.; Mountford, P. *Chem*. *Commun*. **2010**, *46*, 273-275.

(47) Zhong, Z.; Dijkstra, P. J.; Feijen, J. *J*. *Am*. *Chem*. *Soc*. **2003**, *125*, 11291-11298.

(48) Chen, C.-T.; Han-Jade; Ming-Tsz, W.; Chi-An, C.; Peng, H. K.-F. *E*. *J*. *Inorg*. *Chem*. **2009**, *2009*, 2129-2135.

(49) Rudin, A.; Hoegy, H., L. W. *J*. *Polym*. *Sci*. *Part A: Polym*. *Chem*. **1972**, *10*, 217-235.

(50) Save, M.; Schppacher, M.; Soum, A. *Macromol*. *Chem*. *Phys*. **2002**, *203*, 889.

(51) Dorgan, J. R.; Janzen, J.; Knauss, D. M.; Hait, S. B.; Limoges, B. R.; Hutchinson, M. H. *J*. *Polym*. *Sci*. *Part B: Polym*. *Phys*. **2005**, *43*, 3100-3111.

(52) Priya, S. G.; Jungvid, H.; Kumar, A. *Tissue Eng Part B: Rev* **2008**, *14*, 105-118.

(53) Slivniak, R.; Domb, A. J. *Biomacromol*. **2002**, *3*, 754-760.

(54) Ovitt, T. M.; Coates, G. W. *J*. *Am*. *Chem*. *Soc*. **2002**, *124*, 1316-1326.

(55) Ikada, Y.; Jamshidi, K.; Tsuji, H.; Hyon, S. H. *Macromolecules* **1987**, *20*, 904-906.

(56) Cai, C.-X.; Amgoune, A.; Lehmann, C. W.; Carpentier, J.-F. *Chem. Commun.* **2004**, 330-331.

(57) Chamberlain, B. M.; Cheng, M.; Moore, D. R.; Ovitt, T. M.; Lobkovsky, E. B.; Coates, G. W. *J. Am. Chem. Soc.* **2001**, *123*, 3229-3238.

(58) Pietrangelo, A.; Hillmyer, M. A.; Tolman, W. B. *Chem. Commun.* **2009**, 2736-2737.

(59) Jensen, T. R.; Breyfogle, L. E.; Hillmyer, M. A.; Tolman, W. B. *Chem. Commun.* **2004**, 2504-2505.

(60) Cheng, M.; Attygalle, A. B.; Lobkovsky, E. B.; Coates, G. W. *J. Am. Chem. Soc.* **1999**, *121*, 11583-11584.

(61) Chisholm, M. H.; Gallucci, J.; Phomphrai, K. *Inorg. Chem.* **2002**, *41*, 2785-2794.

(62) Chisholm, M. H.; Gallucci, J. C.; Phomphrai, K. *Inorg. Chem.* **2005**, *44*, 8004-8010.

(63) Hormnirun, P.; Marshall, E. L.; Gibson, V. C.; White, A. J. P.; Williams, D. J. *J. Am. Chem. Soc.* **2004**, *126*, 2688-2689.

(64) Chisholm, M. H.; Eilerts, N. W.; Huffman, J. C.; Iyer, S. S.; Pacold, M.; Phomphrai, K. *J. Am. Chem. Soc.* **2000**, *122*, 11845-11854.

(65) Chisholm, M. H.; Gallucci, J.; Phomphrai, K. *Chem. Commun.* **2003**, 48-49.

(66) Chisholm, M. H.; Gallucci, J. C.; Phomphrai, K. *Inorg. Chem.* **2004**, *43*, 6717-6725.

(67) Ma, H.; Spaniol, T. P.; Okuda, J. *Angew. Chem. Int. Ed.* **2006**, *45*, 7818-7821.

(68) Amgoune, A.; Thomas, C. M.; Roisnel, T.; Carpentier, J.-F. *Chem. Euro. J.* **2006**, *12*, 169-179.

(69) Liu, X.; Shang, X.; Tang, T.; Hu, N.; Pei, F.; Cui, D.; Chen, X.; Jing, X. *Organometallics* **2007**, *26*, 2747-2757.

(70) Bonnet, F.; Cowley, A. R.; Mountford, P. *Inorg. Chem.* **2005**, *44*, 9046-9055.

(71) Chmura, A. J.; Chuck, C. J.; Davidson, M. G.; Jones, M. D.; Lunn, M. D.; Bull, S. D.; Mahon, M. F. *Angew. Chem. Int. Ed.* **2007**, *46*, 2280-2283.

(72) Nomura, N.; Ishii, R.; Akakura, M.; Aoi, K. *J. Am. Chem. Soc.* **2002**, *124*, 5938-5939.

(73) Tang, Z.; Chen, X.; Pang, X.; Yang, Y.; Zhang, X.; Jing, X. *Biomacromol*. **2004**, *5*, 965-970.

(74) Du, H. Z.; Pang, X.; Yu, H. Y.; Zhuang, X. L.; Chen, X. S.; Cui, D. M.; Wang, X. H.; Jing, X. B. *Macromolecules* **2007**, *40*, 1904-1913.

(75) Nomura, N.; Ishii, R.; Yamamoto, Y.; Kondo, T. *Chem*. *Eur*. *J*. **2007**, *13*, 4433-4451.

(76) Dove, A. P.; Li, H.; Pratt, R. C.; Lohmeijer, B. G. G.; Culkin, D. A.; Waymouth, R. M.; Hedrick, J. L. *Chem*. *Commun*. **2006**, 2881-2883.

(77) Wisniewski, M.; Borgne, A. L.; Spassky, N. *Macromol*. *Chem*. *Phys*. **1997**, *198*, 1227-1238.

(78) Bhaw-Luximon, A.; Jhurry, D.; Spassky, N. *Polymer Bulletin* **2000**, *44*, 31-38.

(79) Jhurry, D.; Bhaw-Luximon, A.; Spassky, N. *Macromol*. *Symp*. **2001**, *175*, 67-80.

(80) Gregson, C. K. A.; Blackmore, I. J.; Gibson, V. C.; Long, N. J.; Marshall, E. L.; White, A. J. P. *Dalton Trans*. **2006**, 3134-3140.

(81) Chisholm, M. H.; Patmore, N. J.; Zhou, Z. *Chem*. *Commun*. **2005**, 127-129.

(82) Cameron, P. A.; Jhurry, D.; Gibson, V. C.; White, A. J. P.; Williams, D. J.; Williams, S. *Macromol*. *Rapid Commun*. **1999**, *20*, 616-618.

(83) Ovitt, T. M.; Coates, G. W. *J*. *Polym*. *Sci*. *Part A: Polym*. *Chem*. **2000**, *38*, 4686-4692.

(84) Majerska, K.; Duda, A. *J*. *Am*. *Chem*. *Soc*. **2004**, *126*, 1026.

(85) Lillie, E.; Schulz, R. C. *Mackromol*. *Chem*. **1975**, *176*, 1901.

(86) Schindler, A.; Harper, D. *J*. *Polym*. *Sci*.*: Polym*. *Lett*. **1976**, *14*, 729-734.

(87) Chisholm, M. H.; Iyer, S. S.; Matison, M. E. *Chem*. *Commun*. **1997**, 1999-2000.

(88) Kasperczyk, J. E. *Macromolecules* **1995**, *28*, 3937-3939.

(89) Kricheldorf, H. R.; Boettcher, C.; Tönnes, K.-U. *Polymer* **1992**, *33*, 2817-2824.

(90) Kasperczyk, J. E. *Polymer* **1999**, *40*, 5455-5458.

(91) Thakur, K. A. M.; Kean, R. T.; Zell, M. T.; Padden, B. E.; Munson, E. J. *Chem*. *Comm*. **1998**, 1913 - 1914.

(92) Chisholm, M. H.; Iyer, S. S.; McCollum, D. G.; Pagel, M.; Werner-Zwanziger, U. *Macromolecules* **1999**, *32*, 963-973.

(93) Thakur, K. A. M.; Kean, R. T.; Hall, E. S.; Kolstad, J. J.; Lindgren, T. A.; Doscotch, M. A.; Siepmann, J. I.; Munson, E. J. *Macromolecules* **1997**, *30*, 2422-2428.

(94) Chisholm, M. H.; Eilerts, N. W. *Chem*. *Commun*. **1996**, 853-854.

(95) Chisholm, M. H.; Huffman, J. C.; Phomphrai, K. *J*. *Chem*. *Soc*., *Dalton Trans*. **2001**, 222-224.

(96) Wheaton, C. A.; Hayes, P. G.; Ireland, B. J. *Dalton Trans*. **2009**, 4832-4846.

(97) Poirier, V.; Roisnel, T.; Carpentier, J.-F.; Sarazin, Y. *Dalton Trans*. **2009**, 9820-9827.

(98) Wheaton, C. A.; Ireland, B. J.; Hayes, P. G. *Organometallics* **2009**, *28*, 1282-1285.

(99) Chisholm, M. H.; Lin, C.-C.; Gallucci, J. C.; Ko, B.-T. *Dalton Trans*. **2003**, 406-412.

(100) Antelmann, B.; Chisholm, M. H.; Iyer, S. S.; Huffman, J. C.; Navarro-Llobet, D.; Pagel, M.; Simonsick, W. J.; Zhong, W. *Macromolecules* **2001**, *34*, 3159-3175.

(101) Dubois, P.; Jerome, R.; Teyssie, P. *Macromol*. **1991**, *24*, 977-981.

(102) Kowalski, A.; Duda, A.; Penczek, S. *Macromolecules* **1998**, *31*, 2114-2122.

(103) Aida, T.; Inoue, S. *Acc*. *Chem*. *Res*. **1996**, *29*, 39-48.

(104) Paul A. Cameron; Jhurry, D.; Gibson, V. C.; White, A. J. P.; Williams, D. J.; Williams, S. *Macromol*. *Rapid Commun*. **1999**, *20*, 616-618.

(105) McLain, S. J.; Ford, T. M.; Drysdale, N. E. *Polym*. *Prepr*. *(Am*. *Chem*. *Soc*., *Div*. *Polym*. *Sci*.*)* **1992**, *33*, 463.

(106) Chamberlain, B. M.; Sun, Y.; Hagadorn, J. R.; Hemmesch, E. W.; Young, V. G.; Jr; Hillmyer, M. A.; Tolman, W. B. *Macromolecules* **1999**, *32*, 2400-2402.

(107) Giesbrecht, G. R.; Whitener, G. D.; Arnold, J. *J*. *Chem*. *Soc*., *Dalton Trans*. **2001**, 923-927.

(108) Dyer, H. E.; Huijser, S.; Schwarz, A. D.; Wang, C.; Duchateau, R.; Mountford, P. *Dalton Trans*. **2008**, 32-35.

(109) Ma, H.; Okuda, J. *Macromol*. **2005**, *38*, 2665-2673.

(110) Kricheldorf, H. R.; Kreiser-Saunders, I.; Boettcher, C. *Polymer* **1995**, *36*, 1253-1259.

(111) Kricheldorf, H. R.; Berl, M.; Scharnagl, N. *Macromol*. **1988**, *21*, 286-293.

(112) Kim, Y.; Jnaneshwara, G. K.; Verkade, J. G. *Inorg*. *Chem*. **2003**, *42*, 1437-1447.

(113) Thomas, D.; Arndt, P.; Peulecke, N.; Spannenberg, A.; Kempe, R.; Rosenthal, U. *E*. *J*. *Inorg*. *Chem*. **1998**, *1998*, 1351-1357.

(114) Dobrzynski, P.; Li, S.; Kasperczyk, J.; Bero, M.; Gasc, F.; Vert, M. *Biomacromol*. **2005**, *6*, 483-488.

(115) Mogstad, A.-L.; Waymouth, R. M. *Macromolecules* **1994**, *27*, 2313-2315.

(116) Miola Delaite, C.; Hamaide, T.; Spitz, R. *Macromol*. *Chem*. *Phys*. **1999**, *200*, 1771-1778.

(117) Hsieh, K. C.; Lee, W. Y.; Hsueh, L. F.; Lee, H. M.; Huang, J. H. *E*. *J*. *Inorg*. *Chem*. **2006**, 2306-2312.

(118) Zelikoff, A. L.; Kopilov, J.; Goldberg, I.; Coates, G. W.; Kol, M. *Chem*. *Comm*. **2009**, 6804-6806.

(119) Douglas, A F.; Patrick, B.; Mehrkhodavandi, P. *Angew*. *Chem*. *Int*. *Ed*. **2008**, *47*, 2290-2293.

(120) O'Keefe, B. J.; Monnier, S. M.; Hillmyer, M. A.; Tolman, W. B. *J*. *Am*. *Chem*. *Soc*. **2001**, *123*, 339-340.

(121) O'Keefe, B. J.; Breyfogle, L. E.; Hillmyer, M. A.; Tolman, W. B. *J*. *Am*. *Chem*. *Soc*. **2002**, *124*, 4384-4393.

(122) Kricheldorf, H. R.; Behnken, G.; Schwarz, G.; Kopf, J. *Macromolecules* **2008**, *41*, 4102-4107.

(123) Kricheldorf, H. R.; Behnken, G.; Schwarz, G.; Brockaert, J. A. *Macromol*. *Chem*. *Phys*. **2008**, *209*, 1586-1592.

(124) Ryner, M.; Stridsberg, K.; Albertsson, A.-C.; von Schenck, H.; Svensson, M. *Macromolecules* **2001**, *34*, 3877-3881.

(125) Schwach, G.; Coudane, J.; Engel, R.; Vert, M. *Polym*. *Bull*. **1996**, *37*, 771-776.

(126) Stjerndahl, A.; Wistrand, A. F.; Albertsson, A.-C. *Biomacromol* **2007**, *8*, 937-940.

(127) Schwach, G.; Coudane, J.; Engel, R.; Vert, M. *Polym*. *Bull*. **1994**, *32*, 617-623.

(128) Schwach, G.; Coudane, J.; Engel, R.; Vert, M. *Polym*. *Int*. **1998**, *46*, 177-182.

(129) Schwach, G.; Vert, M. *Int*. *J*. *Biol*. *Macromol*. **1999**, *25*, 283-291.

(130) Vanhoorne, P.; Dubois, P.; Jerome, R.; Teyssie, P. *Macromolecules* **1992**, *25*, 37-44.

(131) Martin, E.; Dubois, P.; Jerome, R. *Macromolecules* **2000**, *33*, 1530-1535.

(132) Evans, W. J.; Forrestal, K. J.; Ziller, J. W. *J. Am. Chem. Soc.* **1998**, *120*, 9273-9282.

(133) Hongmei, S.; Shuang, C.; Yingming, Y.; Qi, S.; Kaibei, Y. *Appl. Organomet. Chem.* **2006**, *20*, 310-314.

(134) Deng, X.; Yuan, M.; Li, X.; Xiong, C. *Eur. Polym. J.* **2000**, *36*, 1151-1156.

(135) Okuda, J.; Rushkin, I. L. *Macromolecules* **1993**, *26*, 5530-5532.

(136) Touris, A.; Kostakis, K.; Mourmouris, S.; Kotzabasakis, V.; Pitsikalis, M.; Hadjichristidis, N. *Macromolecules* **2008**, *41*, 2426-2438.

(137) Priftis, D.; Petzetakis, N.; Sakellariou, G.; Pitsikalis, M.; Baskaran, D.; Mays, J. W.; Hadjichristidis, N. *Macromolecules* **2009**, *42*, 3340-3346.

(138) Ko, B.-T.; Wu, C.-C.; Lin, C.-C. *Organometallics* **2000**, *19*, 1864-1869.

(139) Chisholm, M. H.; Navarro-Llobet, D.; Simonsick, W. J. *Macromolecules* **2001**, *34*, 8851-8857.

(140) Liu, Y.-C.; Ko, B.-T.; Lin, C.-C. *Macromolecules* **2001**, *34*, 6196-6201.

(141) Ko, B.-T.; Lin, C.-C. *J. Am. Chem. Soc.* **2001**, *123*, 7973-7977.

(142) Hsueh, M.-L.; Huang, B.-H.; Wu, J.; Lin, C.-C. *Macromolecules* **2005**, *38*, 9482-9487.

(143) Takeuchi, D.; Nakamura, T.; Aida, T. *Macromolecules* **2000**, *33*, 725-729.

(144) Pérez, Y.; del Hierro, I.; Sierra, I.; Gómez-Sal, P.; Fajardo, M.; Otero, A. *J. Organomet. Chem.* **2006**, *691*, 3053-3059.

(145) Arnold, P L.; Buffet, J. C.; Blaudeck, R P.; Sujecki, S.; Blake, A J.; Wilson, C. *Angew. Chem. Int. Ed.* **2008**, *47*, 6033-6036.

(146) Cheng, M.; Attygalle, A. B.; Lobkovsky, E. B.; Coates, G. W. *J. Am. Chem. Soc.* **1999**, *121*, 11583-11584.

(147) Dove, A. P.; Gibson, V. C.; Marshall, E. L.; Rzepa, H. S.; White, A. J. P.; Williams, D. J. *J. Am. Chem. Soc.* **2006**, *128*, 9834-9843.

(148) Hodgson, L. M.; Platel, R. H.; White, A. J. P.; Williams, C. K. *Macromolecules* **2008**, *41*, 8603-8607.

(149) Platel, R. H.; Hodgson, L. M.; White, A. J. P.; Williams, C. K. *Organometallics* **2007**, *26*, 4955-4963.

(150) Hodgson, L. M.; White, A. J. P.; Williams, C. K. *J. Polym. Sci. Part A: Polym. Chem.* **2006**, *44*, 6646-6651.

(151) Platel, R. H.; White, A. J. P.; Williams, C. K. *Chem. Commun.* **2009**, 4115-4117.

(152) Chisholm, M. H.; Gallucci, J. C.; Zhen, H.; Huffman, J. C. *Inorg. Chem.* **2001**, *40*, 5051-5054.

(153) Chen, H.-Y.; Tang, H.-Y.; Lin, C.-C. *Macromolecules* **2006**, *39*, 3745-3752.

(154) Williams, C. K.; Breyfogle, L. E.; Choi, S. K.; Nam, W.; Young, V. G.; Hillmyer, M. A.; Tolman, W. B. *J. Am. Chem. Soc.* **2003**, *125*, 11350-11359.

(155) Wu, J.; Pan, X.; Tang, N.; Lin, C.-C. *Eur. Polym. J.* **2007**, *43*, 5040-5046.

(156) Chmura, A. J.; Cousins, D. M.; Davidson, M. G.; Jones, M. D.; Lunn, M. D.; Mahon, M. F. *Dalton Trans.* **2008**, 1437-1443.

(157) Yulia, A. P.; Irina, V. V.; Sergei, V. K.; Kirill, V. Z.; Galina, S. Z.; Sergei, S. K. *J. Polym. Sci. Part A: Polym. Chem.* **2010**, *48*, 1230-1240.

(158) Chen, C.-T.; Huang, C.-A.; Huang, B.-H. *Macromolecules* **2004**, *37*, 7968-7973.

(159) Gendler, S.; Segal, S.; Goldberg, I.; Goldschmidt, Z.; Kol, M. *Inorg. Chem.* **2006**, *45*, 4783-4790.

(160) Johnson, A. L.; Davidson, M. G.; Perez, Y.; Jones, M. D.; Merle, N.; Raithby, P. R.; Richards, S. P. *Dalton Trans.* **2009**, 5551-5558.

(161) Tang, Z.; Gibson, V. C. *E. Polym. J.* **2007**, *43*, 150-155.

(162) Alcazar-Roman, L. M.; O'Keefe, B. J.; Hillmyer, M. A.; Tolman, W. B. *Dalton Trans.* **2003**, 3082-3087.

(163) Chen, C.-T.; Huang, C.-A.; Huang, B.-H. *Dalton Trans.* **2003**, 3799-3803.

(164) Chmura, A. J.; Davidson, M. G.; Frankis, C. J.; Jones, M. D.; Lunn, M. D. *Chem. Commun.* **2008**, 1293-1295.

(165) Castro, P. M.; Zhao, G.; Amgoune, A.; Thomas, C. M.; Carpentier, J.-F. *Chem. Commun.* **2006**, 4509-4511.

(166) Sarazin, Y.; Howard, R. H.; Hughes, D. L.; Humphrey, S. M.; Bochmann, M. *Dalton Trans.* **2006**, 340-350.

(167) Zhaohui, T.; Xuesi, C.; Yongkun, Y.; Xuan, P.; Jingru, S.; Xuefei, Z.; Xiabin, J. *J. Polym. Sci. Part A: Polym. Chem.* **2004**, *42*, 5974-5982.

(168) Spassky, N.; Wisniewski, M.; Pluta, C.; LeBorgne, A. *Macromol. Chem. Phys.* **1996**, *197*, 2627-2637.

(169) Ovitt, T. M.; Coates, G. W. *J. Am. Chem. Soc.* **2002**, *124*, 1316.

(170) Radano, C. P.; Baker, G. L.; Smith, M. R. *J. Am. Chem. Soc.* **2000**, *122*, 1552-1553.

(171) Zhong, Z. Y.; Dijkstra, P. J.; Feijen, J. *Angew. Chem., Int. Ed.* **2002**, *41*, 4510.

(172) Zhong, Z. Y.; Dijkstra, P. J.; Feijen, J. *J. Am. Chem. Soc.* **2003**, *125*, 11291.

(173) Nomura, N.; Ishii, R.; Akakura, M.; Aoi, K. *J. Am. Chem. Soc.* **2002**, *124*, 5938.

(174) Chisholm, M. H.; Gallucci, J. C.; Quisenberry, K. T.; Zhou, Z. *Inorg. Chem.* **2008**, *47*, 2613-2624.

(175) Jing, Y.; Qiaobo, L.; Yang, L.; Lin, J.; Qiang, F.; Amin, C. *J. Polym. Sci. Part A: Polym. Chem.* **2006**, *44*, 2045-2058.

(176) Ovitt, T. M.; Coates, G. W. *J. Am. Chem. Soc.* **1999**, *121*, 4072.

(177) Zhong, Z.; Dijkstra, P. J.; Feijen, J. *Angew. Chem. Int. Ed.* **2002**, *41*, 4510-4513.

(178) Zelikoff, A. L.; Kopilov, J.; Goldberg, I.; Coates, G. W.; Kol, M. *Chem. Commun.* **2009**, 6804-6806.

(179) Kim, Y.; Kapoor, P. N.; Verkade, J. G. *Inorg. Chem.* **2002**, *41*, 4834-4838.

(180) Kim, Y.; Verkade, J. G. *Organometallics* **2002**, *21*, 2395-2399.

(181) Kim, Y.; Verkade, J. G. *Macromol. Symp.* **2005**, *224*, 105-118.

(182) Whitelaw, E. L.; Jones, M. D.; Mahon, M. F.; Kociok-Kohn, G. *Dalton Trans* **2009**, 9020-9025.

(183) Armistead, L. T.; White, P. S.; Gagne, M. R. *Organometallics* **1998**, *17*, 216-220.

(184) Armistead, L. T.; White, P. S.; Gagne, M. R. *Organometallics* **1998**, *17*, 4232-4239.

(185) Pritchett, S.; Gantzel, P.; Walsh, P. J. *Organometallics* **1997**, *16*, 5130-5132.

(186) Pritchett, S.; Woodmansee, D. H.; Gantzel, P.; Walsh, P. J. *J. Am. Chem. Soc.* **1998**, *120*, 6423-6424.

(187) Pritchett, S.; Gantzel, P.; Walsh, P. J. *Organometallics* **1999**, *18*, 823-831.

(188) Lensink, C.; Gainsford, G. J.; Baxter, N. I. *Acta Cryst. Sec. C* **2001**, *57*, 366-367.

(189) Lensink, C.; Gainsford, G. J.; Baxter, N. I. *Acta Cryst. Sec. C* **2001**, *57*, 368-369.

(190) Hamura, S.; Oda, T.; Shimizu, Y.; Matsubara, K.; Nagashima, H. *J. Chem. Soc., Dalton Trans*. **2002**, 1521-1527.

(191) Ackermann, L.; Bergman, R. G.; Loy, R. N. *J. Am. Chem. Soc*. **2003**, *125*, 11956-11963.

(192) Costa, A. M.; García, C.; Carroll, P. J.; Walsh, P. J. *Tetrahedron* **2005**, *61*, 6442-6446.

(193) Massimiliano, F.; Fredrik, L.; Myriam Mba, B.; Patrick, R.; Marco, C.; Lutz, H. G.; Giulia, L.; Christina, M. *E. J. Inorg. Chem*. **2006**, 1032-1040.

(194) Zhao, J.; Song, H.; Cui, C. *Organometallics* **2007**, *26*, 1947-1954.

(195) Wu, J.; Pan, X.; Tang, N.; Lin, C.-C. *E. Polym. J*. **2007**, *43*, 5040-5046.

(196) Corey, E. J.; Sarshar, S.; Lee, D.-H. *J. Am. Chem. Soc*. **1994**, *116*, 12089-12090.

(197) Nelson, S. G.; Kim, B.-K.; Peelen, T. J. *J. Am. Chem. Soc*. **2000**, *122*, 9318-9319.

(198) Nelson, S. G.; Peelen, T. J.; Wan, Z. *J. Am. Chem. Soc*. **1999**, *121*, 9742-9743.

(199) Takashi, O.; Hayato, I.; Keiji, M. *Angew. Chem. Int. Ed*. **2001**, *40*, 3610-3612.

(200) Dymock, B. W.; Kocienski, P. J.; Pons, J. M. *Chem. Commun*. **1996**, 1053 - 1054.

(201) Imai, N.; Takahashi, H.; Kobayashi, S. *Chem, Lett*. **1994**, 177 - 180.

(202) Lütjens, H.; Nowotny, S.; Knochel, P. *Tetrahedron-Asymm*. **1995**, *6*, 2675-2678.

(203) Cheng, G.; Jun, Q.; Zhang, X.; Verdugo, D.; Larter, M. L.; Christie, R.; Kenney, P.; Walsh, P. J. *Tetrahedron* **1997**, *53*, 4145-4158.

(204) Padmanabhan, S.; Govindarajan, S. *J. Polym. Sci. Part A: Polym. Chem*. **2006**, *44*, 4006-4014.

Chapter Two

Sulfonamide-Supported Group 4 Catalysts for the Ring-Opening Polymerization of ε-Caprolactone and *rac*-Lactide

2.1 Overview

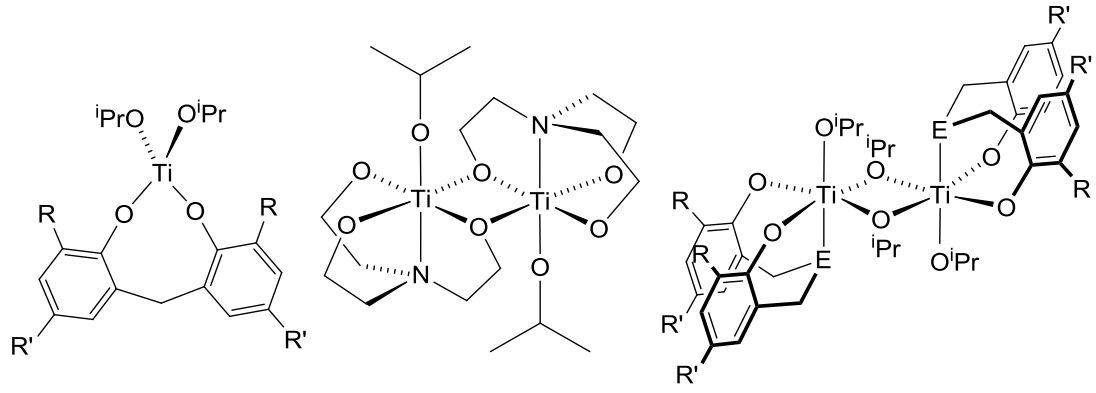
This Chapter will provide an introduction into Group 4 catalysed ROP. An overview of the synthesis and characterisation of Group 4 isopropoxide and amide complexes supported by sulfonamide ligands will be presented. Their solid state structures and solution behaviour will be discussed, in conjunction with their application to the ring opening polymerisation of cyclic esters. Comparison of the newly reported sulfonamide complexes and previously reported bis(phenolate) complexes will be undertaken within the context of the solid state structures and the ROP activity and selectivity observed. This work has recently been published.[1]

2.2 Introduction to Group 4 ROP

Amongst the transition metals, Group 4 complexes have exhibited very good control of the polymerisation process, featuring reasonably fast initiation and minimal side reactions (chain transfer). This leads to polymers of well-defined and predictable M_n, narrow PDIs, and (for *rac*-LA) heterotactic[2-4] or isotactic[5] enrichment. Early work with these metals was based around simple homoleptic metal alkoxides $M(OR)_4$ (R = alkyl; M = Ti or Zr),[3,6] which operate as ROP catalysts *via* a coordination-insertion mechanism. This work was further extended by the groups of Bounor-Legaré and Cassagnau who explored $Ti(OPh)_4$ and $Ti(O^nPr)_4$ for the bulk polymerisation of ε-caprolactone. It was observed that $Ti(O^nPr)_4$ initiated a more controlled polymerisation process, yielding a narrower PDI (1.9-2.0 versus 2.1-3.2).[6-8] Grafov employed $Ti\{N(SiMe_3)_2\}_4$ to the ROP of *rac*-lactide to give reasonable control of the polymerisation process. Polymerisation of 100 equivalents in toluene at 120 °C over 16 hours yielded polymers with good agreement between calculated M_n and that observed by ^{1}H NMR and GPC with moderate PDI (1.47). However, it was observed that use of $Ti(O^iPr)_4$ gave slightly higher conversion and similar M_n control but with narrow PDI (1.13).[9]

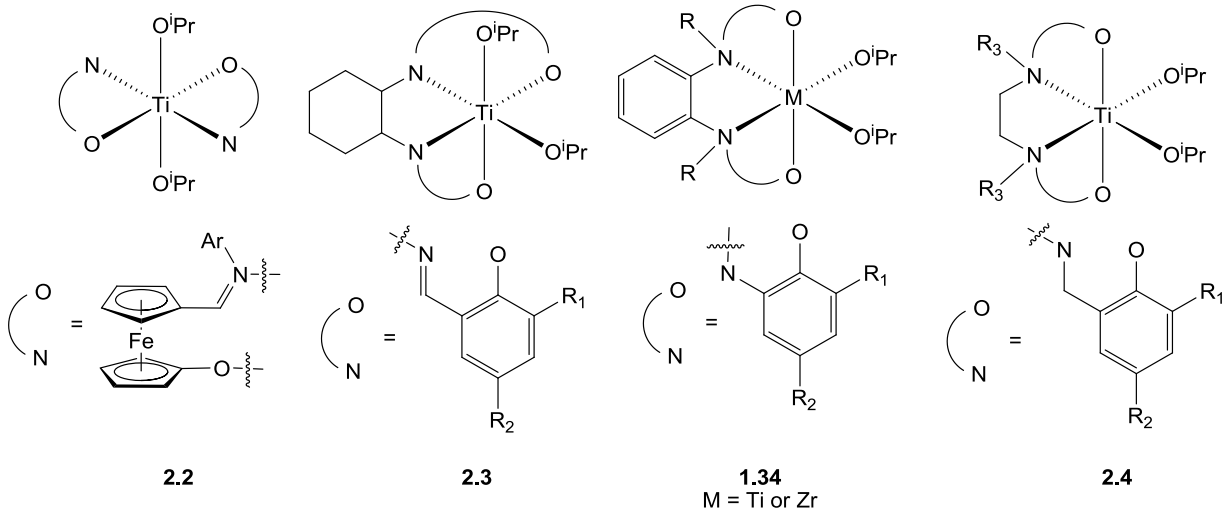
With the aim of producing well-defined single site catalysts, research groups began applying inert supporting ancillary ligands to metals with the aim of enhancing their catalytic activity and limiting adverse transesterification reactions. Aida employed bidentate bis(phenolate) ancillary ligands on titanium with isoproxide initiating groups, obtaining poly(ε-CL) with narrow PDI (*ca*. 1.2) (**1.3** in Figure 2.1).[10-12]

Figure 2.1. Early examples of Group 4 catalysts for the ROP of cyclic esters.[10,11,13-16]



Subsequent work by Verkade employed titanatranes of various structures featuring either bulky aryloxide or isopropoxide initiating groups in the first reported case of *rac*-lactide polymerisation by a heteroleptic titanium complex (**1.36** in Figure 2.1).[13-16] Concurrent with these developments, Harada reported bulky bidentate and tridentate phenolate complexes of titanium bearing isopropoxide and diethylamide initiating groups. These species demonstrated moderate activities and control for the polymerisation of ε-CL and LA in toluene at elevated temperatures (**2.1** in Figure 2.1).[17,18]

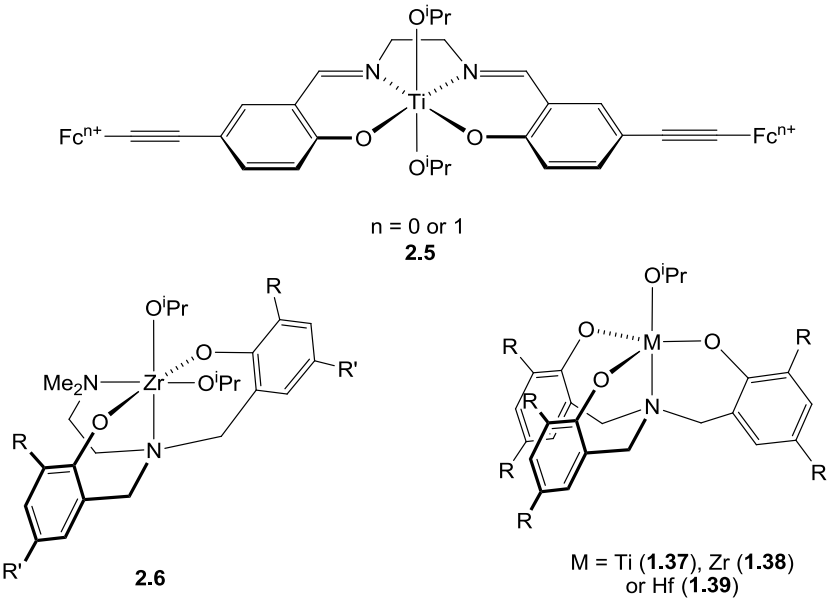
Figure 2.2. Group 4 salan, salen, and salophan catalysts for the ROP of cyclic esters.[2,19-22]



Gibson and Long were the first to employ salen ligands bound to titanium for the polymerisation of LA in toluene at 70 °C and obtained poly(LA) with narrow PDI (1.1 - 1.2) and good activity (e.g. 96% conversion after 6 h). However, where *rac*-LA was

employed, no significant control over polymer tacticity was obtained (**2.2** and **2.3**, Figure 2.2).[19,21] Kim has built upon this early work through systematic evaluation of salan type systems for titanium. Good polymerisation behaviour for *L*-lactide is observed with narrow PDI and good control of M_n at elevated temperatures in toluene.[22] As part of wider studies into bis(phenolate) ligands, Davidson and Kol observed that there was no appreciable difference between the polymerisation capabilities of salan-type systems as compared to other bis(phenolate) systems such as **2.4** (Figure 2.2), although modest isotactic enrichment was possible with the appropriate salan ancillary ligand.[2,5] Salophan complexes such as **1.34** (Figure 2.2) demonstrate remarkable activity, with titanium complexes found to be more active than zirconium in contrast to all other studies looking at the activities of the Group 4 triad for a given ligand.[2,5,20] Arnold and Dagorne have employed titanium complexes bearing alkoxide or phenolate with a linked N-heterocyclic carbine. Good conversions of lactide with narrow PDIs are observed; indicative of living behaviour.[23,24] Interestingly, upon employing complex **2.5** (Figure 2.3) it was possible to moderate catalyst activity by redox control of the ferrocenyl groups on the ligand periphery.[25]

Figure 2.3. Examples of Group 4 catalysts for the ROP of cyclic esters.[2,4,10,11,25,26]

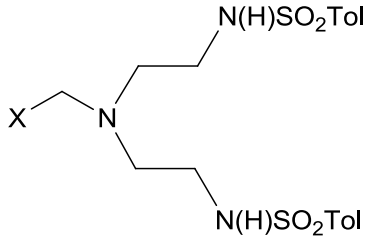


Significant advances have been achieved using tetradentate bis(phenolate)diamine and related ancillary ligands such as in **2.6** and **1.17**-**1.39** (Figure 2.3).[2,4,5,26-28] Good control has also been achieved for the ROP of *rac*-LA under industrially desirable melt conditions. C_3-symmetric zirconium tris(phenolate)amine isopropoxide

complexes of the type **1.38** (Figure 2.3) act as well-controlled single site catalysts, giving both narrow PDIs and highly heterotactically enriched poly(LA) from *rac*-lactide.[26]

2.3 Aims

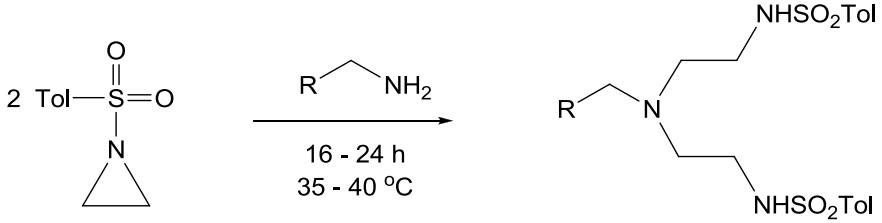
Reported in this Chapter are the syntheses and structures of a series of new titanium and zirconium complexes derived from the N_4-donor sulfonamide ligand $(2\text{-}NC_5H_4)CH_2N(CH_2CH_2NHSO_2Tol)_2$ (**2.7**, $H_2N_2^{Ts}N^{py}$) and the related N_3O-donor $MeOCH_2CH_2N(CH_2CH_2NHSO_2Tol)_2$ (**2.8**, $H_2N_2^{Ts}N^{OMe}$) together with their performance as ROP catalysts for ε-CL and *rac*-LA.



X = 2-NC_5H_4 (**2.7**) or
CH_2OMe (**2.8**)

2.4 Synthesis of protio-ligand precursors

The known[29,30] protio-ligands $H_2N_2^{Ts}N^{py}$ (**2.7**) and $H_2N_2^{Ts}N^{OMe}$ (**2.8**) were synthesised in high yield by ring opening reactions of N-tosyl aziridine with the appropriate amine, namely 2-$NC_5H_4CH_2NH_2$ or $MeOCH_2CH_2NH_2$, respectively (Equation 2.1).



R = 2-py (**2.7**) or
CH_2OMe (**2.8**)

Equation 2.1.[29,30]

Although the solid state structure of **2.7** has been previously described,[31] that of **2.8** has not been reported. Therefore, for comparison with its metal complexes described below, the X-ray structure of **2.8** was determined. The molecular structure is shown in Figure 2.4 and selected distances and angles are listed in Table 2.1.

Figure 2.4. Displacement ellipsoid plot of $H_2N_2{}^{Ts}N^{OMe}$ (**2.8**). C-bound H atoms are omitted for clarity, H(1) and H(2) are drawn as spheres of arbitrary radius and the ellipsoids are drawn at the 20% probability level.

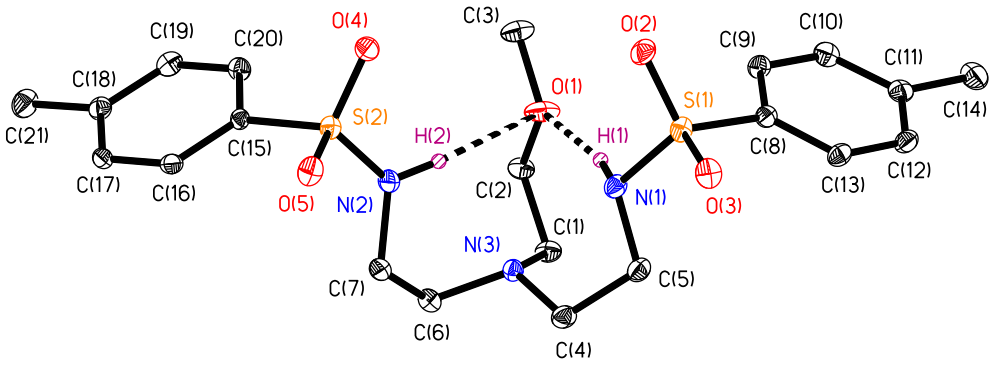
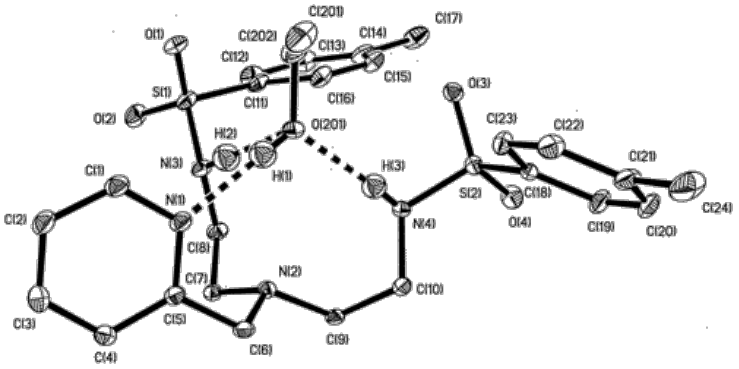


Table 2.1. Selected bond distances (Å) and angles (°) for $H_2N_2{}^{Ts}N^{OMe}$ (**2.8**).

N(1)-S(1)	1.618(2)	S(2)-O(5)	1.432(2)
N(2)-S(2)	1.602(2)	N(1)-H(1)	0.83(3)
S(1)-O(2)	1.433(2)	N(2)-H(2)	0.92(3)
S(1)-O(3)	1.432(2)	H(1)···O(1)	2.20(4)
S(2)-O(4)	1.434(2)	H(2)···O(1)	2.53(4)
N(1)-H(1)···O(1)	168(3)	S(1)-N(1)-H(1)	106(2)
N(2)-H(2)···O(1)	155(3)	H(1)-N(1)-C(5)	111(2)
C(3)-O(1)-C(2)	112.2(2)	S(2)-N(2)-C(7)	121.3(2)
C(3)-O(1)···H(1)	131.0(9)	S(2)-N(2)-H(2)	120(2)
C(3)-O(1)···H(2)	105.6(8)	H(2)-N(2)-C(7)	115(2)
S(1)-N(1)-C(5)	118.84(18)		

Molecules of $H_2N_2{}^{Ts}N^{OMe}$ (**2.8**) possess two intramolecular N-H···O hydrogen bonds between the two sulfonamide nitrogens and the OMe group oxygen atom. This pre-organises $H_2N_2{}^{Ts}N^{OMe}$ (**2.8**) into a geometry similar to that required to bind a metal centre. All bond lengths and angles for $H_2N_2{}^{Ts}N^{OMe}$ (**2.8**) lie within the expected ranges for compounds of this type.[32] Protio-ligand $H_2N_2{}^{Ts}N^{py}$ (**2.7**) also crystallised in a pre-organized manner, but in that case an EtOH molecule of crystallisation was incorporated into the ligand cavity through multiple H-bonding interactions (Figure 2.5).[29]

Figure 2.5. Displacement ellipsoid plot of $H_2N_2{}^{Ts}N^{py}$ (**2.7**).[29]



2.5 Synthesis of titanium and zirconium amide and isopropoxide complexes

Protonolysis reactions of **2.7** or **2.8** with 1 equivalent of $Ti(NMe_2)_4$ in benzene at ambient temperature gave the bis(dimethylamide) complexes $Ti(N_2{}^{Ts}N^{py})(NMe_2)_2$ (**1**) and $Ti(N_2{}^{Ts}N^{OMe})(NMe_2)_2$ (**2**) respectively, in 50-55% yield after recrystallisation (Scheme 2.1). When followed in CD_2Cl_2 on the NMR tube scale the yields were effectively quantitative and the expected $HNMe_2$ side product was observed. The solid state structures of both compounds have been determined (*vide infra*) and confirm those shown in Scheme 2.1. The solution NMR spectra at 303K for $Ti(N_2{}^{Ts}N^{py})(NMe_2)_2$ (**1**) or ambient temperature for $Ti(N_2{}^{Ts}N^{OMe})(NMe_2)_2$ (**2**) (Figure 2.6) are also consistent with the C_s symmetric solid state structures. However, cooling the NMR sample of $Ti(N_2{}^{Ts}N^{py})(NMe_2)_2$ (**1**) to ambient temperature or below led to considerable broadening of the resonances and then the appearance of multiple ligand environments (Figure 2.7). This suggests that several different isomers may exist in solution, perhaps involving C_1 and C_s symmetry (*cf*. certain bis(phenolate) complexes)[31] and/or additional intra- and/or inter-molecular coordination of the tosyl group oxygen atoms as discussed below and noted elsewhere (*cf*. Figure 2.12, compound $Zr(N_2{}^{Ts}N^{OMe})(O^iPr)_2$ (**6**)).[33-36]

Scheme 2.1. Synthesis of the new complexes **1** - **6**.

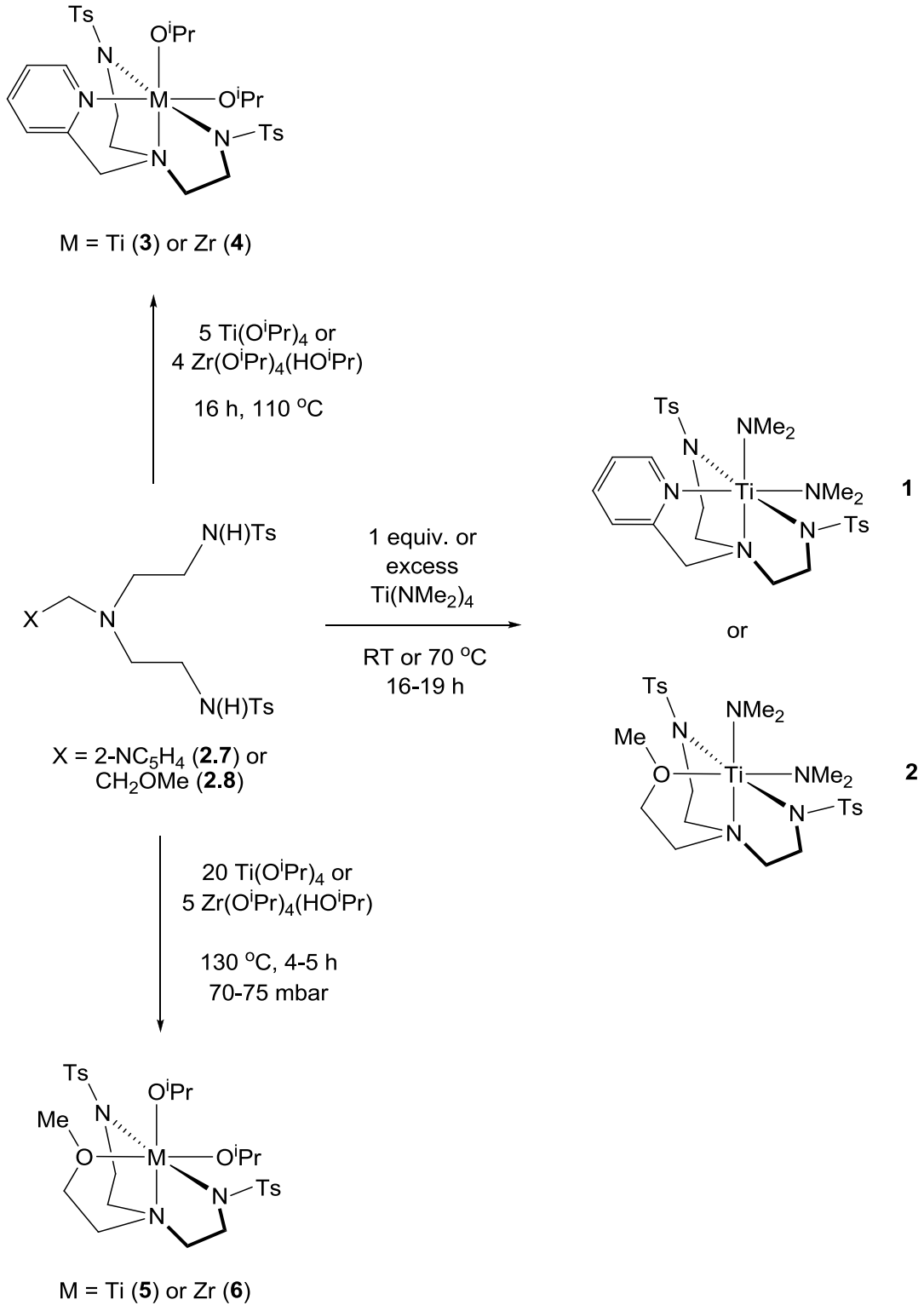


Figure 2.6. ^{1}H NMR spectrum (299.9 MHz) of **2** in CD_2Cl_2 at 298 K ('s' denotes residual protio-solvent).

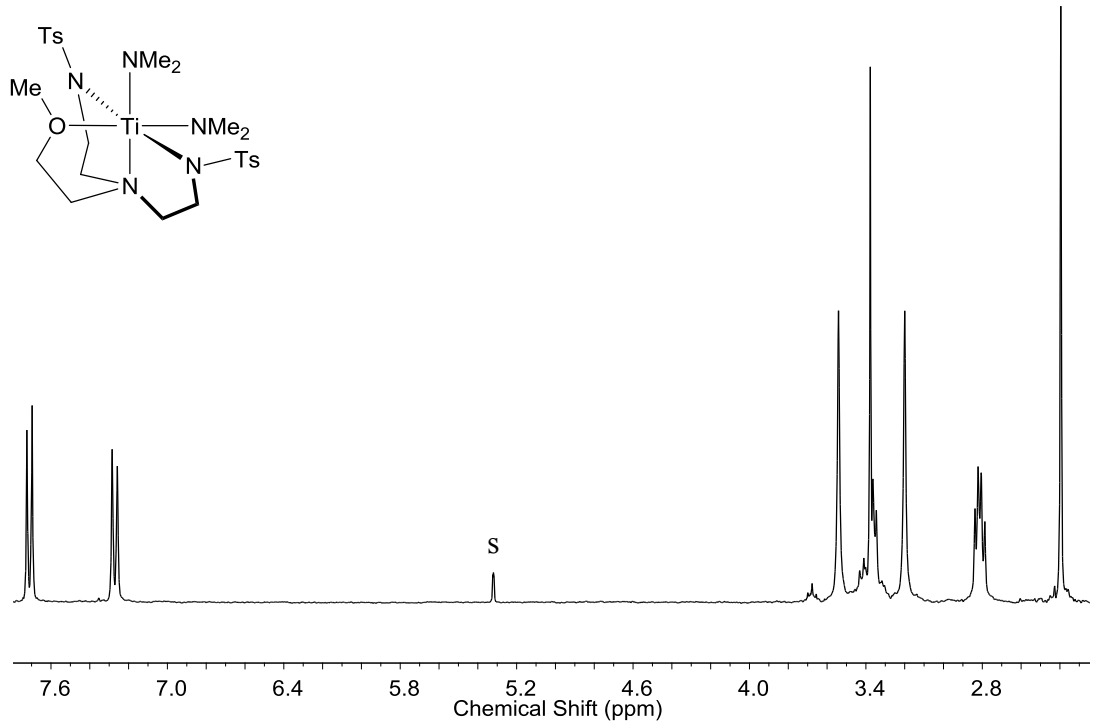
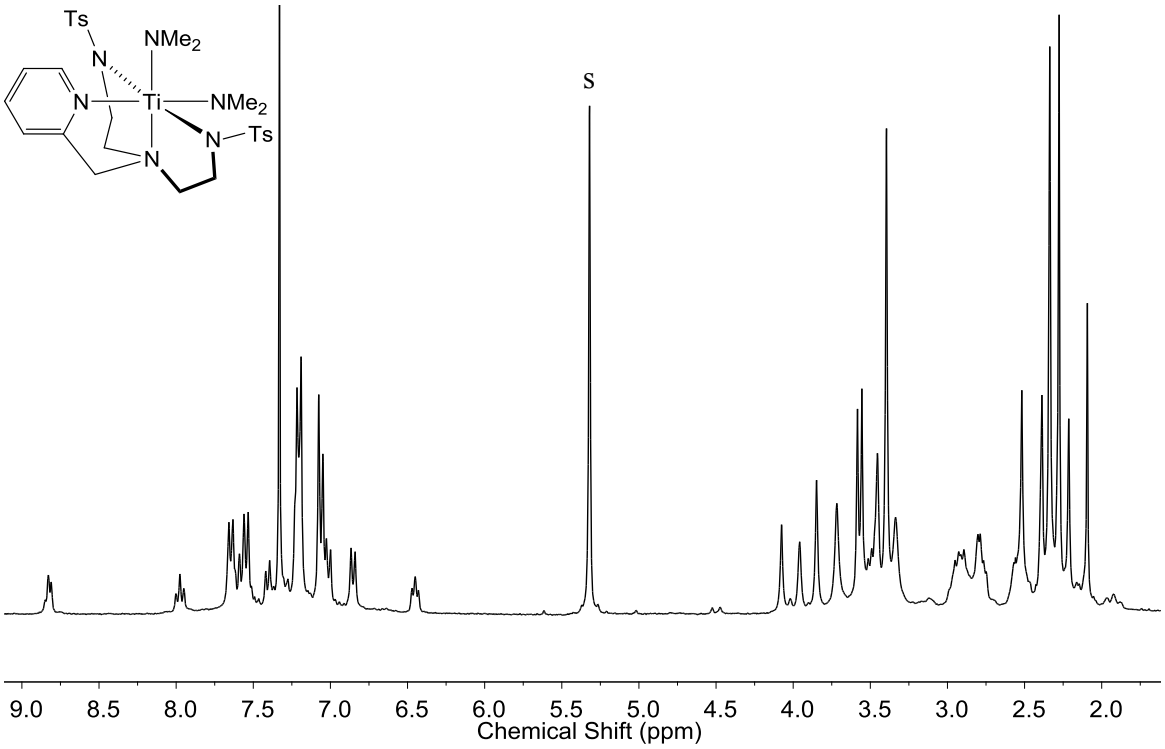


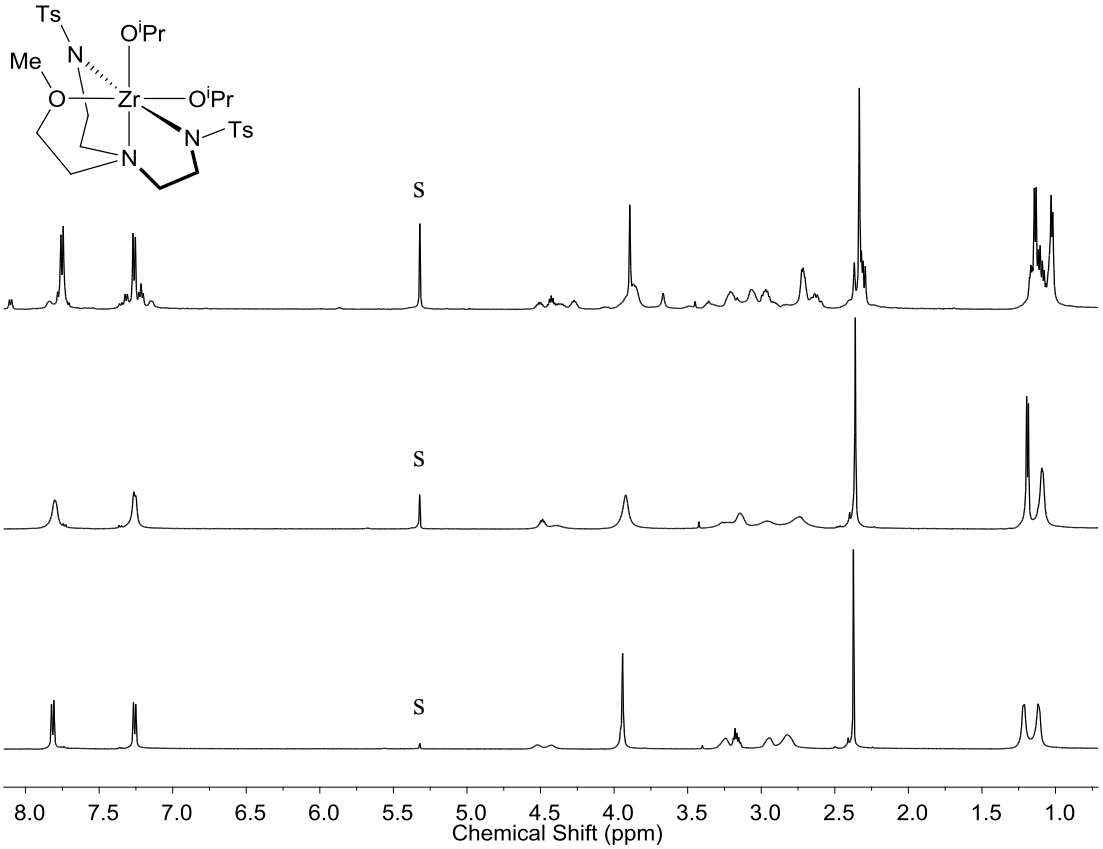
Figure 2.7. ^{1}H NMR spectrum (299.9 MHz) of **1** in CD_2Cl_2 at 213 K ('s' denotes residual protio-solvent).

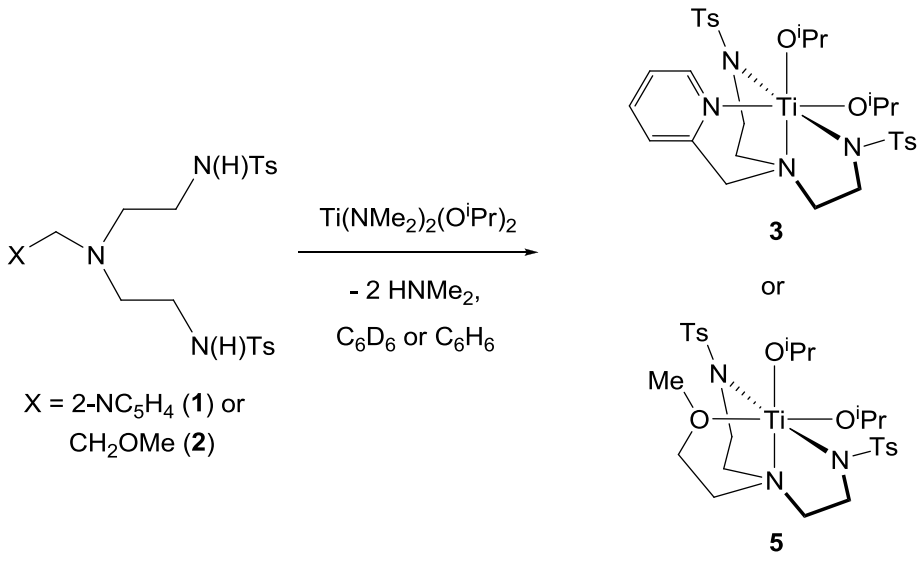


As described below, these bis(dimethylamide) compounds were poor catalysts for the ROP of ε-CL, and so effort was focussed on the bis(isopropoxide) homologues, $M(N_2^{Ts}N^{py})(O^iPr)_2$ (M = Ti (**3**) or Zr (**4**)) and $M(N_2^{Ts}N^{OMe})(O^iPr)_2$ (M = Ti (**5**) or Zr (**6**)) (Scheme 2.1). Attempted stoichiometric reaction of $H_2N_2^{Ts}N^{py}$ (**2.7**) with $Ti(O^iPr)_4$ did not proceed at any appreciable rate at ambient temperature, presumably reflecting the reduced basicity of isopropoxide compared to dimethylamide in the respective titanium starting materials. Nonetheless, heating $H_2N_2^{Ts}N^{py}$ (**2.7**) with an excess of $Ti(O^iPr)_4$ in toluene for 16 hours gave good yields of $Ti(N_2^{Ts}N^{py})(O^iPr)_2$ (**3**) after recrystallisation. The zirconium congener $Zr(N_2^{Ts}N^{py})(O^iPr)_2$ (**4**) was prepared in 42% recrystallised yield in an analogous fashion using an excess of $Zr(^iOPr)_4{\cdot}HO^iPr$. However, the L^{OMe}-substituted analogues $Ti(N_2^{Ts}N^{OMe})(O^iPr)_2$ (**5**) and $Zr(N_2^{Ts}N^{OMe})(O^iPr)_2$ (**6**) could not be obtained by the solution reaction of $H_2N_2^{Ts}N^{OMe}$, even when using large excesses of $Ti(O^iPr)_4$ or $Zr(^iOPr)_4{\cdot}HO^iPr$ and extended reaction times. This highlights the equilibrium nature of these alcohol-elimination reactions and the apparent need for a strong σ-donor to aid complexation to the metal. Compounds $Ti(N_2^{Ts}N^{OMe})(O^iPr)_2$ (**5**) and $Zr(N_2^{Ts}N^{OMe})(O^iPr)_2$ (**6**) were eventually prepared using melt conditions at 125-130 ^oC for 4 – 5 hours under a dynamic partial pressure to remove the eliminated ^{i}PrOH. Recrystallisation afforded the pure complexes in *ca*. 45% yield. As for $Ti(N_2^{Ts}N^{py})(NMe_2)_2$ (**1**), the NMR spectra of the zirconium complexes showed evidence of complex solution state dynamic behaviour (Figure 2.8).

The molecular structures of all four complexes **3** – **6** were therefore determined (*vide infra*) and again support the structures depicted in Scheme 2.1. As shown in Equation 2.2, $Ti(N_2^{Ts}N^{py})(O^iPr)_2$ (**3**) and $Ti(N_2^{Ts}N^{OMe})(O^iPr)_2$ (**5**) could also be prepared from $Ti(NMe_2)_2(O^iPr)_2$ and 1 equivalent of the respective protio-ligand. No evidence for the formation of the bis(dimethylamide) complexes **1** or **2** was found in either case. Compound **5** was isolated in 78% yield on the preparative scale after 2 hours reaction time. An NMR tube scale reaction showed quantitative formation of **3** for the corresponding reaction with $H_2N_2^{Ts}N^{py}$ (**2.7**).

Figure 2.8. ^{1}H NMR spectrum (299.9 MHz) of **6** in CD_2Cl_2 at 213 K (top), 263 K (middle) and 298 K (bottom) ('s' denotes residual protio-solvent).





Equation 2.2

2.6 Solid state structures

The X-ray structures of all six complexes **1** – **6** have been determined. First the four titanium compounds **1** – **3** and **5** will be discussed. The molecular structures are shown

in Figures 2.9 and 2.10 and selected distances and angles are listed in Tables 2.2 – 2.5. All four possess pseudo-octahedral titanium centres and approximately C_s molecular symmetry, consistent with the fast-exchange limiting NMR spectra discussed above. In general terms the metric parameters lie within the expected ranges to the types of linkages and functional groups present.[32] Unlike many of the previous titanium structures with bi- and tri-dentate bis(sulfonamide) ligands,[33-37] none of these structures contain additional Ti···O interactions to the tosyl substituents.

Figure 2.9. Top: displacement ellipsoid plot of $Ti(N_2{}^{Ts}N^{py})(NMe_2)_2$ (**1**). Bottom: displacement ellipsoid plot of $Ti(N_2{}^{Ts}N^{OMe})(NMe_2)_2$ (**2**) where atoms carrying the suffix 'A' are related to their counterparts by the symmetry operator $-x$, y, $-z+{}^3/_2$. Ellipsoids are drawn at the 20% probablility level. H atoms and benzene molecules of crystallisation and elements of disorder (for **2**) are omitted for clarity.

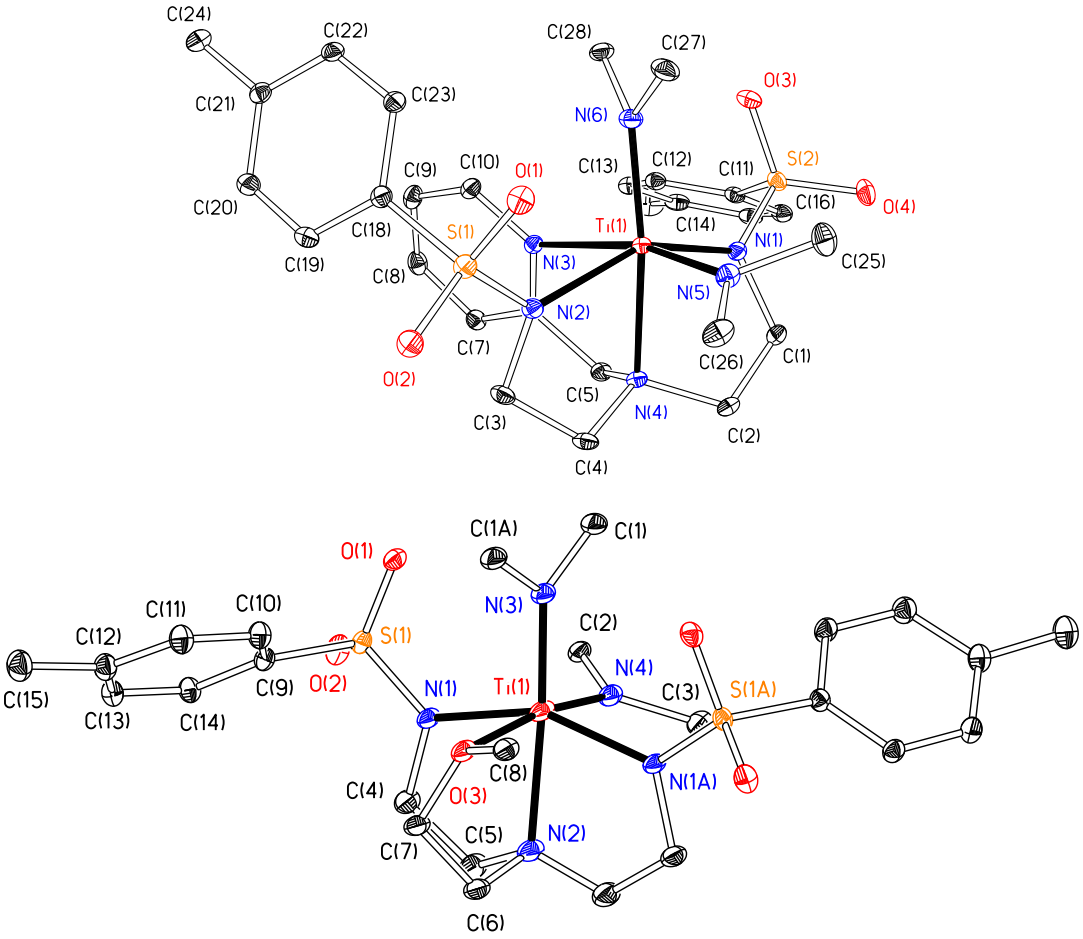


Table 2.2. Selected bond distances (Å) and angles (°) for $Ti(N_2{}^{Ts}N^{py})(NMe_2)_2$ (**1**).

Ti(1)-N(1)	2.129(2)	Ti(1)-N(6)	1.916(2)
Ti(1)-N(2)	2.099(2)	S(1)-O(1)	1.439(2)
Ti(1)-N(3)	2.369(2)	S(1)-O(2)	1.447(2)
Ti(1)-N(4)	2.282(2)	S(2)-O(3)	1.439(2)
Ti(1)-N(5)	1.912(2)	S(2)-O(4)	1.445(2)
Ti(1)-N(1)-S(2)	131.72(11)	Ti(1)-N(5)-C(25)	120.4(2)
Ti(1)-N(1)-C(1)	117.2(2)	Ti(1)-N(5)-C(26)	131.0(2)
S(2)-N(1)-C(1)	110.9(2)	C(25)-N(5)-C(26)	108.5(2)
Ti(1)-N(2)-S(1)	127.40(12)	Ti(1)-N(6)-C(27)	122.2(2)
Ti(1)-N(2)-C(3)	116.4(2)	Ti(1)-N(6)-C(28)	129.9(2)
S(1)-N(2)-C(3)	115.7(2)	C(27)-N(6)-C(28)	107.6(2)

Table 2.3. Selected bond distances (Å) and angles (°) for $Ti(N_2{}^{Ts}N^{OMe})(NMe_2)_2$ (**2**). Atoms carrying the suffix 'A' are related to their counterparts by the symmetry operator $-x, y, -z+{}^3/_2$.

Ti(1)-N(1)	2.096(4)	Ti(1)-O(3)	2.267(7)
Ti(1)-N(2)	2.201(7)	S(1)-O(1)	1.439(4)
Ti(1)-N(3)	1.898(6)	S(1)-O(2)	1.452(3)
Ti(1)-N(4)	1.981(7)		
Ti(1)-N(1)-S(1)	129.6(2)	Ti(1)-N(4)-C(2)	123.1(9)
Ti(1)-N(1)-C(4)	118.1(3)	Ti(1)-N(4)-C(3)	136.1(9)
S(1)-N(1)-C(4)	112.2(3)	C(2)-N(4)-C(3)	100.0(9)
Ti(1)-N(3)-C(1)	125.8(3)	Ti(1)-O(3)-C(8)	120.1(1)
C(1)-N(3)-C(1A)	108.4(6)		

Figure 2.10. Top: displacement ellipsoid plot of $Ti(N_2{}^{Ts}N^{py})(O^iPr)_2$ (**3**). Bottom: displacement ellipsoid plot of $Ti(N_2{}^{Ts}N^{OMe})(O^iPr)_2$ (**5**). Ellipsoids are drawn at the 20% probablility level and H atoms are omitted for clarity.

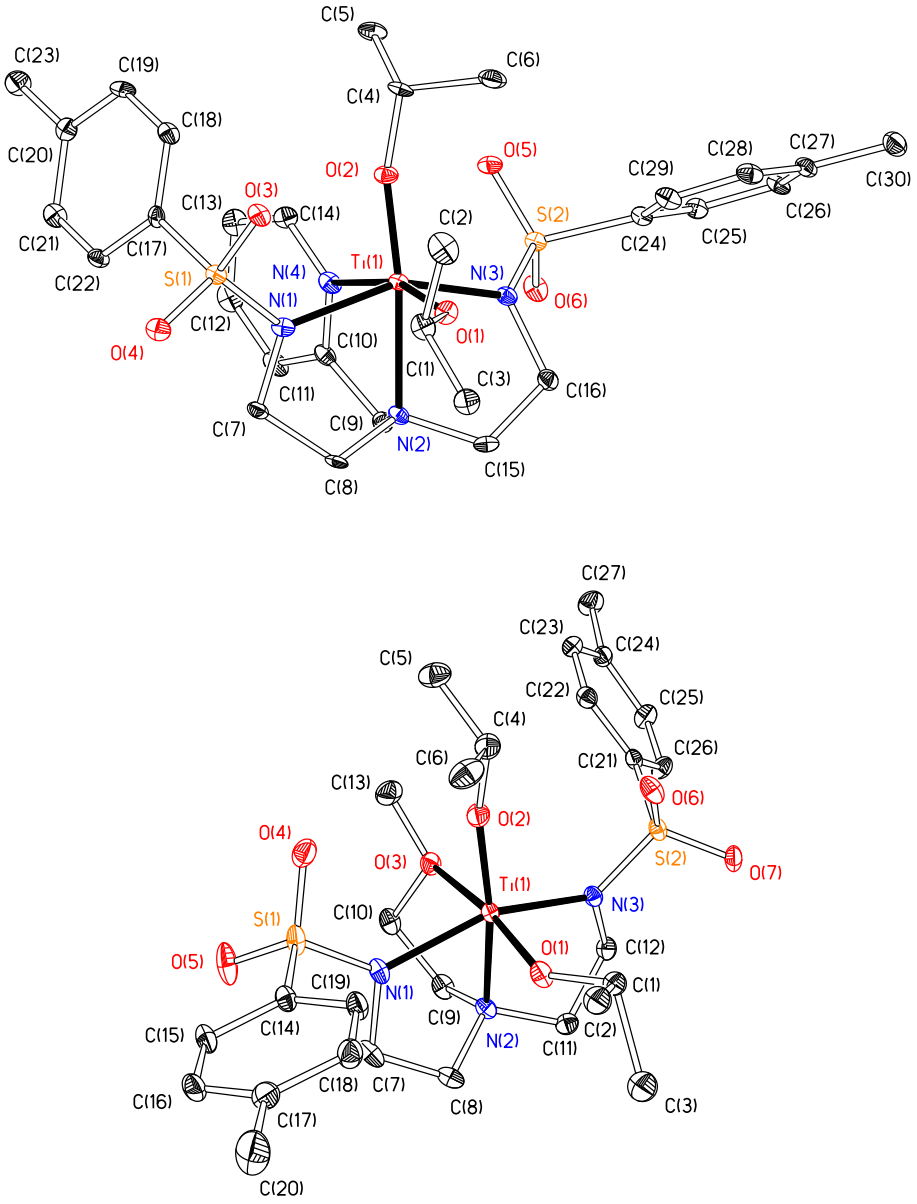


Table 2.4. Selected bond distances (Å) and angles (°) for $Ti(N_2{}^{Ts}N^{py})(O^iPr)_2$ (**3**).

Ti(1)-O(1)	1.810(4)	Ti(1)-N(4)	2.278(6)
Ti(1)-O(2)	1.741(4)	S(1)-O(3)	1.429(4)
Ti(1)-N(1)	2.098(5)	S(1)-O(4)	1.447(4)
Ti(1)-N(2)	2.264(5)	S(2)-O(5)	1.433(5)
Ti(1)-N(3)	2.069(5)	S(2)-O(6)	1.444(5)
Ti(1)-O(1)-C(1)	139.2(4)	S(1)-N(1)-C(7)	117.3(4)
Ti(1)-O(2)-C(4)	159.7(4)	Ti(1)-N(3)-S(2)	127.1(3)
Ti(1)-N(1)-S(1)	125.0(3)	Ti(1)-N(3)-C(16)	116.3(4)
Ti(1)-N(1)-C(7)	117.4(4)	S(2)-N(3)-C(16)	113.4(4)

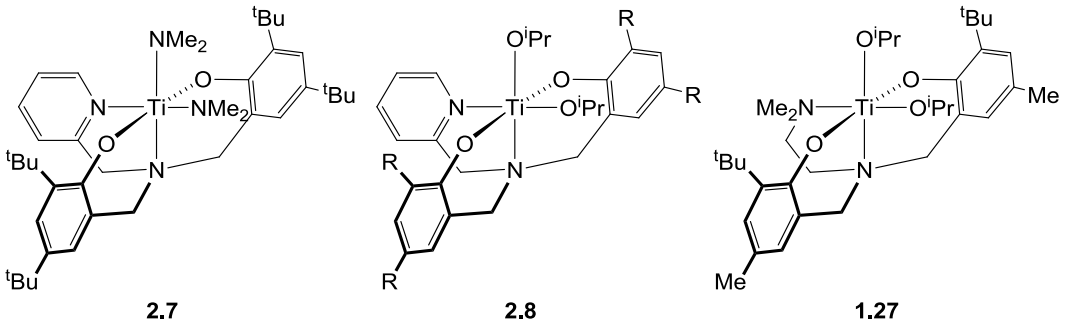
Table 2.5. Selected bond distances (Å) and angles (°) for $Ti(N_2{}^{Ts}N^{OMe})(O^iPr)_2$ (**5**).

Ti(1)-O(1)	1.792(2)	Ti(1)-N(3)	2.087(2)
Ti(1)-O(2)	1.753(2)	S(1)-O(4)	1.436(2)
Ti(1)-O(3)	2.327(2)	S(1)-O(5)	1.445(2)
Ti(1)-N(1)	2.091(2)	S(2)-O(6)	1.434(2)
Ti(1)-N(2)	2.277(2)	S(2)-O(7)	1.446(2)
Ti(1)-O(1)-C(1)	146.1(3)	S(1)-N(1)-C(7)	112.3(2)
Ti(1)-O(2)-C(4)	158.1(2)	Ti(1)-N(3)-S(2)	127.2(1)
Ti(1)-O(3)-C(13)	120.4(2)	Ti(1)-N(3)-C(12)	118.3(1)
Ti(1)-N(1)-S(1)	129.3(1)	S(2)-N(3)-C(12)	114.5(2)
Ti(1)-N(1)-C(7)	118.4(2)		

The average Ti-N_{Ts} distance in **1** – **3** and **5** (av. 2.096 Å, range 2.069(5) – 2.129(2) Å) is slightly longer than the values reported previously (av. 2.078 Å, range 2.039 – 2.119 Å). The average Ti-N_{Ts} distance of 2.108 Å in the bis(dimethylamide) complexes **1** and **2** is longer than in the bis(isopropoxide) homologues (av. 2.086 Å) consistent with the better donor ability of NMe_2 compared with that of O^iPr. Consistent with previous structural studies, the average Ti-NMe_2 distance of 1.909 Å in **1** and **2** is substantially shorter than the average Ti-N_{Ts} distance, due mainly to the electron-withdrawing

nature of the -SO_2Tol substituents. As in other poly(amide) early transition metal structures,[38,39] the various amide ligand substituents in **1** and **2** are arranged so as to maximize $2p_\pi$-$3d_\pi$ bonding interactions. Only one six-coordinate bis(phenolate)-diamine analogue of **1** and **2** has been structurally authenticated, namely Ti(O_2^{tBu}N^{py})(NMe_2)$_2$ (**2.7**).[40] The overall geometries of **1** and **2** are comparable with that of **2.7**, with the Ti-NMe_2 distances in **1** (1.912(2), 1.916(2) Å) being slightly shorter than in the bis(phenolate) analogue (1.927(3), 1.940(3) Å).

Figure 2.11. Phenolate complexes previously reported. [2,4,40]



Comparisons can be made between Ti(N_2^{Ts}N^{py})(O^iPr)$_2$ (**3**) and Ti(N_2^{Ts}N^{OMe})(O^iPr)$_2$ (**5**) and *ca*. 40 structurally characterised, six-coordinate bis(phenolate)-supported bis(isopropoxide) complexes in general,[32] including Ti(O_2^{R}N^{py})(O^iPr)$_2$ (**2.8**, R = Me or ^{t}Bu) and Ti(O_2^{R}N^{NMe2})(O^iPr)$_2$ (**1.27**) specifically.[2,4] The overall geometries are comparable, as are the Ti-O-^{i}Pr angles (literature range 127 – 168^o, av. 143^o; for **3** and **5** range 139.2(4) – 159.7(4)^o, av. 150^o). However, the Ti-O^{i}Pr distances are, as for the Ti-NMe_2 distances discussed above, shorter in the sulfonamide analogues with average values of 1.774 Å compared with a literature value of 1.804 Å (range 1.749 – 1.852 Å) in general and 1.813 Å (range 1.806 – 1.832 Å) for **2.8** and **1.27**.

Figure 2.12. Top: displacement ellipsoid plot of $Zr(N_2{}^{Ts}N^{py})(O^iPr)_2$ (**4**). Bottom: displacement ellipsoid plot of $Zr(N_2{}^{Ts}N^{OMe})(O^iPr)_2$ (**6**). Ellipsoids are drawn at the 20% probablility level and H atoms are omitted for clarity.

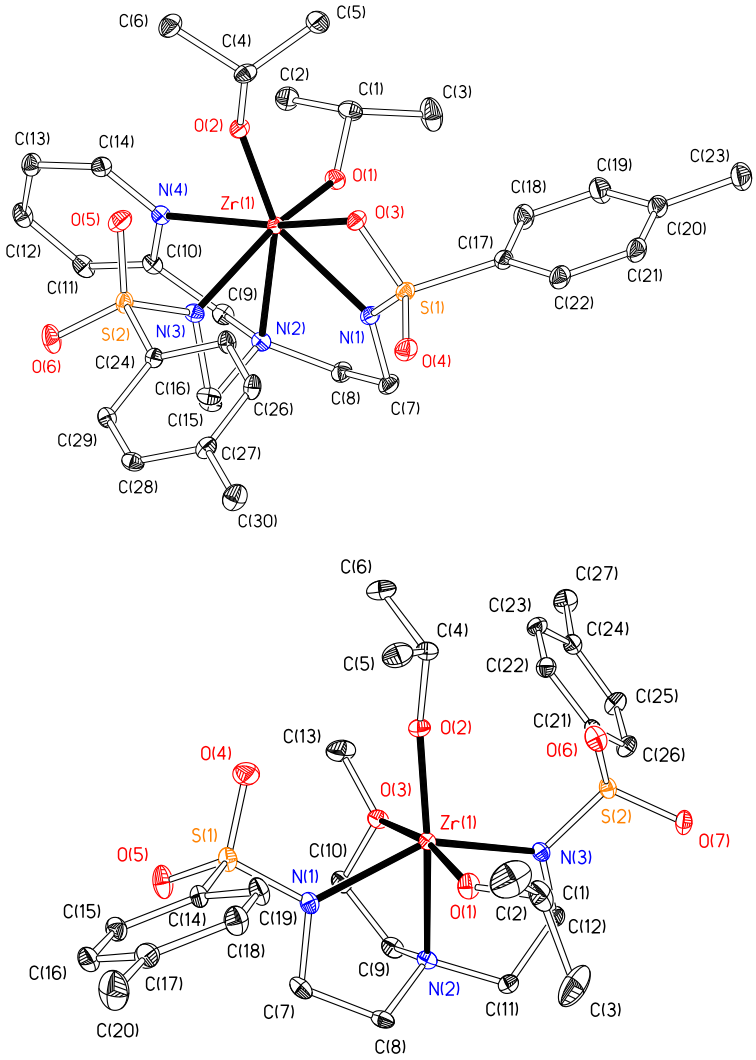


Table 2.6. Selected bond distances (Å) and angles (°) for $Zr(N_2{}^{Ts}N^{py})(O^iPr)_2$ (**4**).

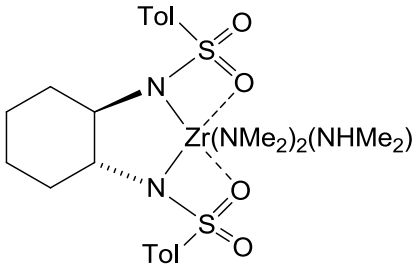
Zr(1)-O(1)	1.964(2)	Zr(1)-N(4)	2.388(2)
Zr(1)-O(2)	1.926(2)	S(1)-O(3)	1.488(2)
Zr(1)-O(3)	2.350(2)	S(1)-O(4)	1.437(2)
Zr(1)-N(1)	2.233(2)	S(2)-O(5)	1.435(2)
Zr(1)-N(2)	2.493(2)	S(2)-O(6)	1.454(2)
Zr(1)-N(3)	2.270(2)		
Zr(1)-O(1)-C(1)	145.8(2)	S(1)-N(1)-C(7)	128.2(2)
Zr(1)-O(2)-C(4)	148.1(2)	Zr(1)-N(3)-S(2)	132.5(1)
Zr(1)-O(3)-S(1)	99.3(1)	Zr(1)-N(3)-C(16)	113.5(1)
Zr(1)-N(1)-S(1)	102.18(10)	S(2)-N(3)-C(16)	114.0(2)
Zr(1)-N(1)-C(7)	129.3(2)		

Table 2.7. Selected bond distances (Å) and angles (°) for $Zr(N_2{}^{Ts}N^{OMe})(O^iPr)_2$ (**6**).

Zr(1)-O(1)	1.910(2)	Zr(1)-N(3)	2.216(2)
Zr(1)-O(2)	1.911(2)	S(1)-O(4)	1.440(3)
Zr(1)-O(3)	2.393(2)	S(1)-O(5)	1.441(2)
Zr(1)-N(1)	2.227(3)	S(2)-O(6)	1.439(2)
Zr(1)-N(2)	2.434(3)	S(2)-O(7)	1.444(2)
Zr(1)-O(1)-C(1)	148.4(3)	S(1)-N(1)-C(7)	115.1(2)
Zr(1)-O(2)-C(4)	155.3(2)	Zr(1)-N(3)-S(2)	122.2(2)
Zr(1)-O(3)-C(13)	120.3(2)	Zr(1)-N(3)-C(12)	121.1(2)
Zr(1)-N(1)-S(1)	123.56(15)	S(2)-N(3)-C(12)	116.7(2)
Zr(1)-N(1)-C(7)	121.33(19)		

The molecular structures of $Zr(N_2{}^{Ts}N^{py})(O^iPr)_2$ (**4**) and $Zr(N_2{}^{Ts}N^{OMe})(O^iPr)_2$ (**6**) are shown in Figure 2.12 and selected bond distances and angles are listed in Tables 2.6 and 2.7. Crystals of **6** are isomorphous with those of **5** and the molecular geometries are essentially identical. Five six-coordinate bis(phenolate)-supported analogues of **6** have been structurally characterised, including the zirconium congeners of **2.8** and

1.27 (Figure 2.11).[2,4] Their geometries are again all comparable to that of **6** but the Zr-O^{i}Pr bond lengths in the latter (1.910(2), 1.911(2) Å) are shorter than the bis(phenolate) examples (av. 1.943 Å, range 1.910 – 1.967 Å). This parallels the trends found in the titanium systems.



1.45

Only one monomeric zirconium sulfonamide compound has been structurally characterised previously, namely the seven-coordinate Zr{1,2-C_6H_{10}(NTs)$_2$}(NMe$_2$)$_2$(NHMe$_2$) (**1.45**) which posseses two κ^2(*N*,*O*) bound NTs groups. As mentioned, this κ^2(*N*,*O*) coordination mode of NSO_2R groups is very common for Group 4 and other electron-deficient metals. As can be seen from Figure 2.12, Zr($N_2^{Ts}N^{py}$)(O^{i}Pr)$_2$ (**4**) possesses one κ^2(*N*,*O*) bound NTs group giving an unsymmetrical seven-coordinate metal centre. This is in contrast to the C_s, six-coordinate geometry of its congener, **3** (presumably due to the smaller atomic radius of titanium), and also **6**. However, the complicated solution phase NMR spectra mentioned above for **3**, **5** and **6** imply that several more complicated geometries may be accessible in solution. The Zr-O^{i}Pr and Zr-N distances in **4** are all longer than the corresponding ones in **6** reflecting the higher coordination number of the former. The S(1)-O(3) distance for the bridging sulfonamide oxygen is 0.051(3) Å longer than the terminal S(1)-O(4) bond as expected.

Overall the geometries of **1** - **6** parallel those of the well-established bis(phenolate) complexes but with slightly shorter Ti-NMe$_2$ and M-O^{i}Pr distances and the potential in both the solid state and solution for additional stabilisation of the metal centers *via* M···O_{Ts} interactions.

2.7 Polymerisation studies: ROP of ε-caprolactone

A principal aim of this work was to evaluate the potential of sulfonamide-supported Group 4 complexes for the catalytic ROP of ε-CL and *rac*-LA. An initial study using the six compounds **1** - **6** was undertaken using ε-CL owing to the relative ease of its polymerisation due to the favourable release of 7-membered ring strain. Initial studies performed in THF gave extremely long reaction times and negligible conversions, presumably due to THF competition for coordination to the metal centre. Subsequent studies were performed in toluene at 100 °C, and under these conditions all the complexes were found to be active. The progress of each reaction was monitored by regular sampling and the results summarised in Table 2.8 correspond to when the polymerisations eventually reached 100% conversion. The molecular weights and PDIs were determined by gel permeation chromotography (GPC) using the appropriate Mark-Houwink corrections[41-43] and the yield refers to the amount of poly(ε-CL) isolated. The M_n(calcd) values are those expected for two polymer chains growing per metal centre (i.e. one chain per Ti-NMe_2 or M-O^{i}Pr bond in the starting complex) at 100% conversion of monomer.

The bis(dimethylamide) catalysts Ti($N_2^{Ts}N^R$)(NMe_2)$_2$ (**1** and **2**) were the slowest of the six evaluated. The GPC data are consistent with only one poly(ε-CL) chain forming per metal (M_n(calcd) = 11,420 g mol^{-1}) on average. This is consistent with the rate of initiation by the expected coordination-insertion mechanism[3] (insertion of ε-CL into Ti-NMe_2) being much slower than propagation (insertion of subsequent ε-CLs into the growing Ti-{O(CH_2)$_5$C(O)}$_n$$NMe_2$ chain). Analogous effects have been recorded elsewhere.[18] Although the observed and calculated M_n values for the poly(ε-CL) formed with **1** and **2** are in fairly good agreement for a living-type process, the broad PDIs of 1.91 and 1.60 show that there is poor control in terms of the distribution of molecular weights. Subsequent effort therefore focussed on the bis(isopropoxide) systems.

Table 2.8. Solution polymerisation of ε-CL by $Ti(N_2{}^{Ts}N^{py})(NMe_2)_2$ (**1**), $Ti(N_2{}^{Ts}N^{OMe})(NMe_2)_2$ (**2**), $Ti(N_2{}^{Ts}N^{py})(O^iPr)_2$ (**3**), $Zr(N_2{}^{Ts}N^{py})(O^iPr)_2$ (**4**), $Ti(N_2{}^{Ts}N^{OMe})(O^iPr)_2$ (**5**), and $Zr(N_2{}^{Ts}N^{OMe})(O^iPr)_2$ (**6**).[a]

Catalyst	Yield (%)[b]	Time (h)	M_n (GPC)[c]	M_n (calcd)[d]	M_w/M_n
$Ti(N_2{}^{Ts}N^{py})(NMe_2)_2$ (**1**)	97	12	12,990	5,710	1.91
$Ti(N_2{}^{Ts}N^{OMe})(NMe_2)_2$ (**2**)	95	22	14,260	5,710	1.60
$Ti(N_2{}^{Ts}N^{py})(O^iPr)_2$ (**3**)	93	9	5,720	5,710	1.80
$Ti(N_2{}^{Ts}N^{OMe})(O^iPr)_2$ (**5**)	87	1	6,390	5,710	1.39
$Zr(N_2{}^{Ts}N^{py})(O^iPr)_2$ (**4**)	91	1	5,180	5,710	1.19
$Zr(N_2{}^{Ts}N^{OMe})(O^iPr)_2$ (**6**)	93	1	7,770	5,710	1.18

[a] Conditions: [ε-CL]/[catalyst] = 100:1, 6.8 mL toluene at 100 °C. See Experimental section for other details. [b] Isolated yield at 100 % NMR conversion. [c] Molecular weights (g mol^{-1}) determined from GPC using the appropriate Mark-Houwink corrections. [d] Expected M_n (g mol^{-1}) for 2 chains growing per metal centre at 100% conversion. For one chain per metal centre the calculated value is 11,410 g mol^{-1}.

Changing from $Ti(N_2{}^{Ts}N^{R})(NMe_2)_2$ (**1** and **2**) to $Ti(N_2{}^{Ts}N^{R})(O^iPr)_2$ (**3** and **5**) gave a clear switch from *ca*. one to two poly(ε-CL) chains per metal centre and also (especially for **5**) a significant increase in activity. Interestingly, the Ti-NMe_2 catalysts are slower than the Ti-O^iPr ones for a given ligand; however it could be expected that they would have the same propagating species after initiation. It is well known that M-OR inserts more effectively than M-NMe_2 so once the $Ti(L)(NMe_2)_2$ initiates the propagating species is $Ti(L)(NMe_2)$(O-PCL) as is evidenced by only 1 chain propagating per metal centre. Whereas, for the $Ti(L)(O^iPr)_2$ initiators it is clear from the M_n results in Table 2.8 two chains propagate per metal centre. The rationale for the difference in propagation rates is then that the spectator Ti-NMe_2 group in $Ti(L)(NMe_2)$(O-PCL) is both bulkier than the two Ti-O-PCL groups in $Ti(L)(O\text{-}PLA)_2$ and also NMe_2 is a better donor, making pre-coordination of CL to Ti less favourable. The zirconium analogues **4** and **6** were, according to the primary screen in Table 2.8, at least as productive as **5**, also forming two chains per metal centre. In addition, the PDI values for these two catalysts indicated a better controlled polymerisation process than for any of the titanium systems. ^{1}H NMR and MALDI-ToF-MS analysis of all four poly(ε-CL)s showed one O^iPr end group per chain, consistent with a coordination-insertion mechanism (Figures 2.13 and 2.14).[3]

Figure 2.13. ^{1}H NMR spectrum of poly(ε-CL) synthesised using Zr($N_2^{Ts}N^{OMe}$)(O^iPr)$_2$ (**6**).

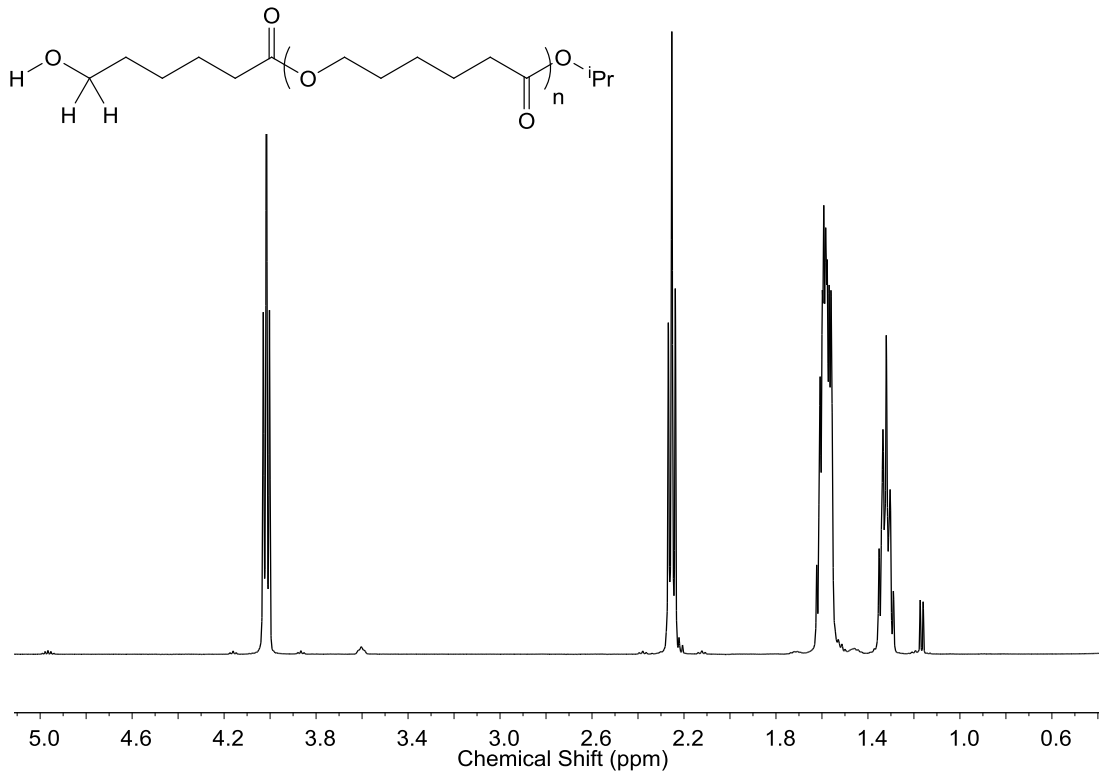
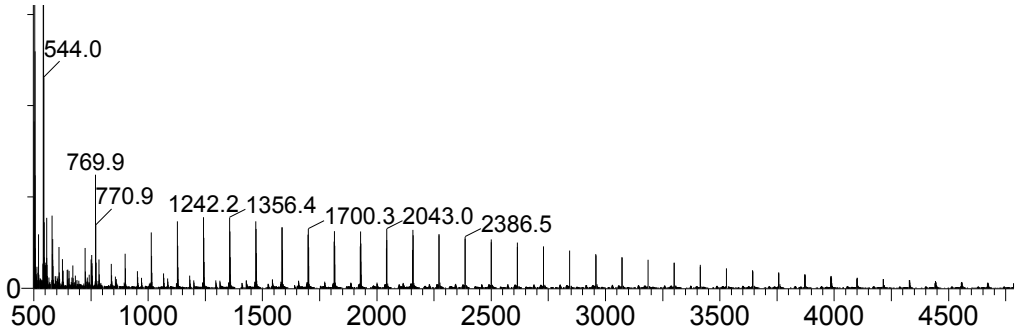


Figure 2.14. MALDI-ToF MS of poly(ε-CL) synthesised using Ti($N_2^{Ts}N^{OMe}$)(O^iPr)$_2$ (**5**). M_n by GPC analysis was 2030 g mol^{-1}.

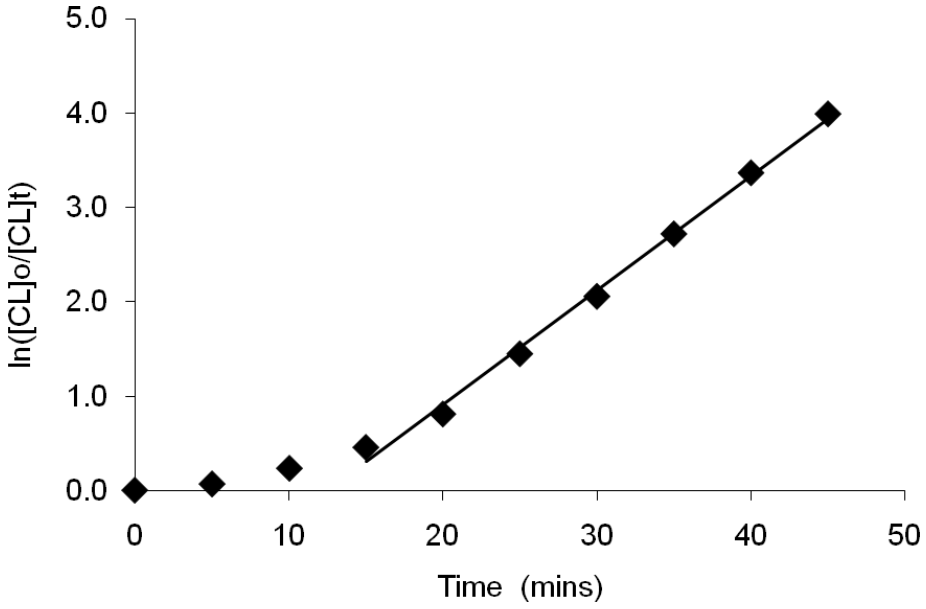


Further experiments were carried out with **3** – **6** to evaluate: the kinetic behaviour, the first order rates of propagation, and also how M_n increases with conversion. Representative plots are shown in Figures 2.15 and 2.16 for Zr($N_2^{Ts}N^{OMe}$)(O^iPr)$_2$ (**6**). Analogous plots for **3** – **5** are shown in the Appendix. First order propagation rate constants (k_p) obtained from the linear part of the log plots are given in Table 2.9. Catalysts **4** – **6** show a relatively short induction period of 5-10 minutes followed by a polymerisation process that is first order with respect to ε-CL concentration (Figure 2.15). Similar induction periods have been observed for main group and transition

metal isopropoxide catalysts.[4,44,45] The induction period for Ti($N_2^{Ts}N^{py}$)(O^iPr)$_2$ (**3**, see the Appendix) was substantially longer (*ca*. 60-70 minutes) than the other three. It is possible to analyse the initial non-linear portion of the first order rate plot to establish the rate constant for initiation k_i, in a similar manner to that already well established for metallocene based olefin polymerisation.[46] However, the limited amount of data and the time required to establish accurate values for k_i would preclude performing a substantial structural optimisation study. Additionally values of k_i would only be valid for solution based polymerisations and give little information regarding industrially relevant melt conditions which are performed under extremely different conditions. For these reasons a fuller kinetic treatment of the polymerisation data was not performed.

The k_p values (Table 2.9) show two main features. Firstly, as found for the corresponding bis(phenolate) systems,[2,4] the zirconium catalysts are faster than titanium for a given supporting ligand. Secondly, there is a pendant arm effect for both pairs of catalysts with the k_p values for L^{py} supported systems being less than for their L^{OMe} analogues (considerably so in the case of **3** and **5**). These effects can be interpreted in terms of easier access to the metal centre since Zr is larger than Ti and OMe is a more labile donor than pyridyl.

Figure 2.15. First order plot for ε-CL consumption using Zr($N_2^{Ts}N^{OMe}$)(O^iPr)$_2$ (**6**).[a]



[a] Conditions: [ε-CL_0]/[**6**] = 100:1, 6.8 mL toluene, 100 °C, 0.1 mL aliquots taken at the given intervals. See Experimental section for other details. Linear fit (r^2 = 0.995) shown is for the first order region after the induction period. See the Appendix for corresponding plots for **3**, **4** and **5**.

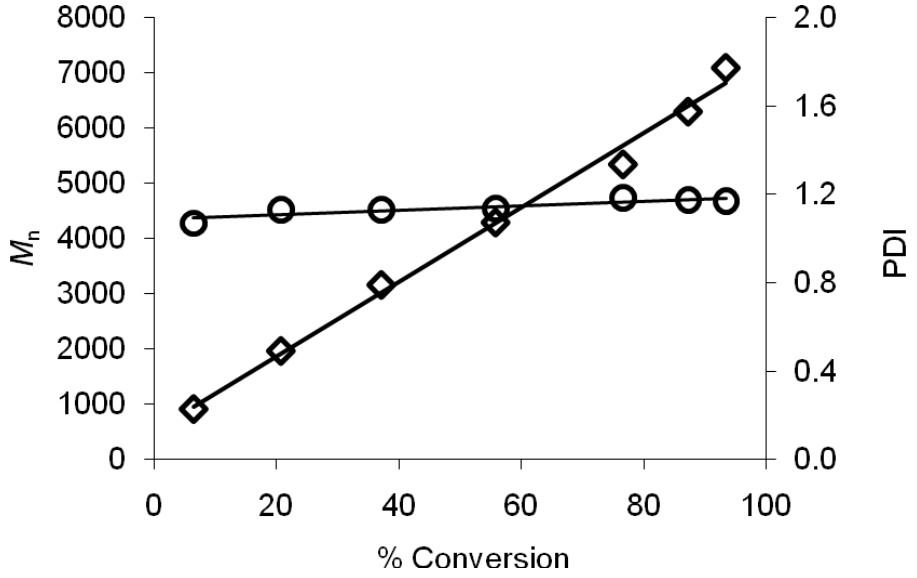
Table 2.9. First order propagation rate constant (k_p) for ε-CL polymerisation by $Ti(N_2^{Ts}N^{py})(O^iPr)_2$ (**3**), $Zr(N_2^{Ts}N^{py})(O^iPr)_2$ (**4**), $Ti(N_2^{Ts}N^{OMe})(O^iPr)_2$ (**5**), and $Zr(N_2^{Ts}N^{OMe})(O^iPr)_2$ (**6**).[a]

Catalyst	k_p (min^{-1})
$Ti(N_2^{Ts}N^{py})(O^iPr)_2$ (**3**)	0.0075(7)
$Ti(N_2^{Ts}N^{OMe})(O^iPr)_2$ (**5**)	0.065(3)
$Zr(N_2^{Ts}N^{py})(O^iPr)_2$ (**4**)	0.108(5)
$Zr(N_2^{Ts}N^{OMe})(O^iPr)_2$ (**6**)	0.121(4)

[a] Conditions: [ε-CL_0]/[Catalyst] = 100:1, 6.8 mL toluene, 100 °C.

Catalysts **4**, **5** and **6** gave reasonably linear plots of M_n *vs* % conversion (Figure 2.16 and the Appendix) with narrow PDIs (1.10 – 1.20 for **4** and **6**, somewhat broader for the less well-behaved **5**) which remained effectively constant throughout the process. The gradients of the M_n *vs* % conversion plots were 47(2), 64(4) and 67(3) g mol^{-1} (% conversion)$^{-1}$ (av. 59 g mol^{-1} (% conversion)$^{-1}$) which is close to that expected (57 g mol^{-1} (% conversion)$^{-1}$) for two poly(ε-CL) chains growing per metal centre. All of these data are consistent with these species acting as living catalysts for the ROP of ε-CL.

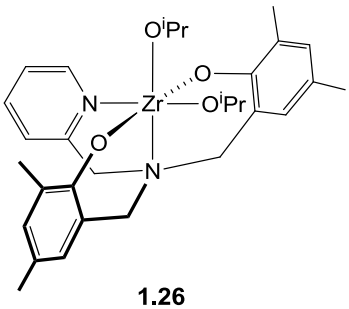
Figure 2.16. Plots of M_n and PDI (determined by GPC) *vs* conversion for the polymerisation of ε-CL using $Zr(N_2^{Ts}N^{OMe})(O^iPr)_2$ (**6**).[a]



[a] Conditions: [ε-CL_0]/[**6**] = 100:1, 6.8 mL toluene, 100 °C, 0.1 mL aliquots taken at the given intervals. Hollow diamonds correspond to M_n and hollow circles to PDI.

To make a proper comparison with previously reported bis(phenolate)amine systems Davidson's[5] ROP catalyst $Zr(O_2^{Me}N^{py})(O^iPr)_2$ (**1.26**) was evaluated under the same conditions as **3** – **6**. This had a slightly shorter induction period (5 minutes) and a k_p of 0.226(8) s^{-1}. The k_p for compound **1.26** is therefore twice that of the most comparable bis(sulfonamide) catalyst **4** (k_p = 0.108(5) s^{-1}). However, the corresponding sulfonamide demonstrated a more controlled polymerisation process with a M_n of 5,180 g mol^{-1} and a PDI of 1.19 compared to **1.26** which yielded poly(ε-CL) with a M_n of 8,000 g mol^{-1} and a PDI of 1.55, where the calculated value of M_n for 2 chains per metal centre is 5,710 g mol^{-1}.

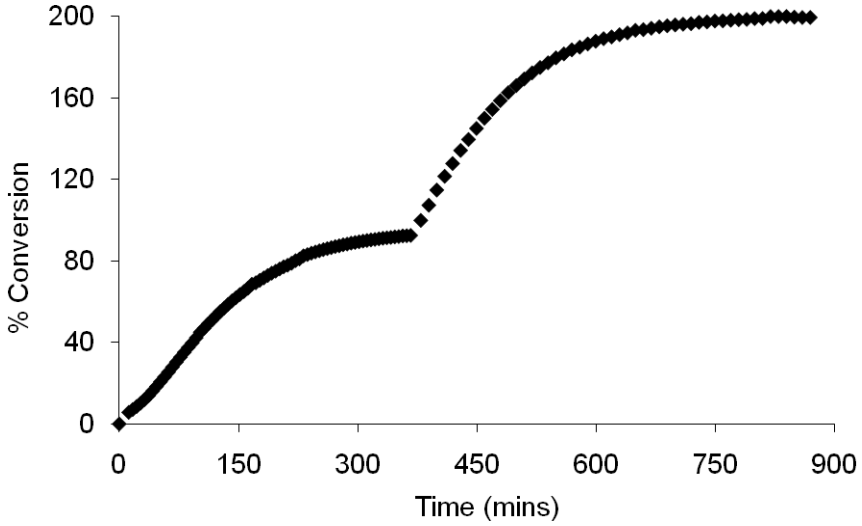
Figure 2.17. Davidson's ROP catalyst $Zr(O_2^{Me}N^{py})(O^iPr)_2$ (**1.26**).[5]



1.26

As a final probe of the living characteristics of the most active catalyst, **6**, polymerisation resumption experiments were undertaken in which 100 equivalents of ε-CL were polymerised on the NMR tube scale at 70 °C in C_6D_6. Once full conversion had been observed, a further 100 equivalents were added and the reaction once again monitored until completion (Figure 2.18). Consistent with Figure 2.17, the data in Figure 2.18 indicate a short induction period before becoming first order in monomer concentration (see the Appendix for the corresponding semi-logarithmic plots). Interestingly, the second 100 equivalents of monomer show minimal induction period, presumably because the active catalyst is fully formed after the initial polymerisation and is still "living". The k_p values for both parts of Figure 2.18 (i.e. the first and second portions of ε-CL) are identical at 0.009(1) min^{-1}. GPC analysis of the poly(ε-CL) showed a narrow PDI (1.19) and a M_n of 9,980 g mol^{-1}, which is in reasonable agreement with the M_n(calc) value of 11,410 g mol^{-1} for two chains per metal centre.

Figure 2.18. Plot of % conversion *vs* time for the polymerisation of two consecutive batches of ε-CL using $Zr(N_2{}^{Ts}N^{OMe})(O^iPr)_2$ (**6**).[a]



[a.] Conditions $[CL_0]/[\mathbf{6}] = 100:1$ followed by a further 100 equivalents. at $t = 400$ min., 0.75 mL C_6D_6, 70 °C.

2.8 Polymerisation studies: ROP of *rac*-lactide

The studies of the ROP of ε-CL showed $Zr(N_2{}^{Ts}N^{py})(O^iPr)_2$ (**4**) and $Zr(N_2{}^{Ts}N^{OMe})(O^iPr)_2$ (**6**) to be the best catalysts in terms of activity and polymerisation control. Studies were next extended to the more challenging monomer, *rac*-lactide. Preliminary experiments showed **6** to be significantly more active than **4**, but with otherwise similar ROP features (control of M_n, PDI), Table 2.10. Titanium complexes $Ti(N_2{}^{Ts}N^{py})(O^iPr)_2$ (**3**) and $Ti(N_2{}^{Ts}N^{OMe})(O^iPr)_2$ (**5**) were also shown to be active but with low reactivity, with only 70 – 90% conversion after 24 h in toluene at 70 °C, see Table 2.10. The activities are in agreement with the trends observed in the study with ε-caprolactone, namely that zirconium catalysts provide a more active system, and for a given metal the (L^{OMe}) complexes display a more active catalyst than (L^{py}). The titanium complexes show a much better controlled polymerisation process when compared to ε-caprolactone, yielding polymers of narrow PDIs (~1.2) compared with moderate to broad (1.4-1.8) for poly(ε-CL). The polymers are *ca*. 40% larger than expected for 2 chains propagating per metal centre but smaller than would be expected for one propagating chain. This is interpreted as instability of the pre-catalyst prior to activation and propagation of the polymer chain, giving a concentration of catalysts that is effectively less than expected. Similar behaviour of M_n was observed with

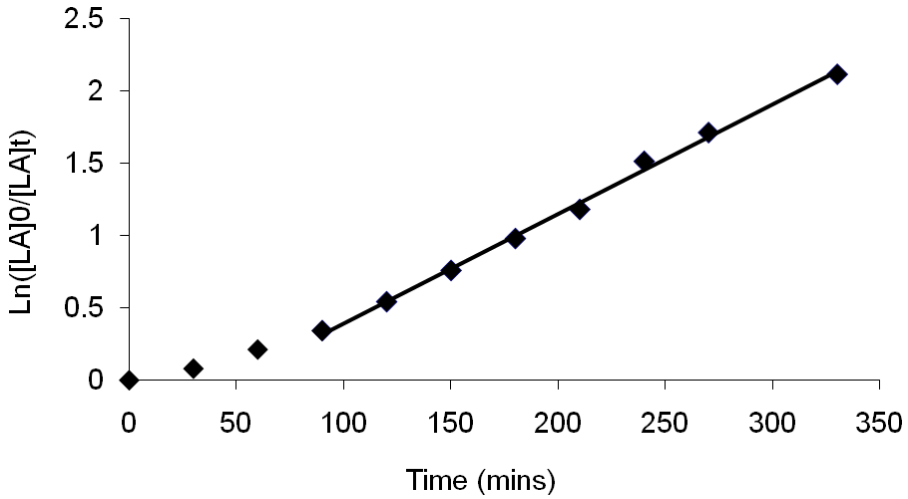
aluminium catalysts bearing related ligands, see Chapter 4. According to the selectively homonuclear decoupled ^{1}H NMR spectrum all polymers were observed to be predominantly atactic. Effort therefore was focussed on Zr($N_2^{Ts}N^{OMe}$)(O^iPr)$_2$ (**6**) for detailed studies. Solution polymerisations were performed in toluene at 70 °C until *ca*. 95% completion. As shown in Figure 2.19 the polymerisation follows first order consumption of *rac*-LA (k_p = 0.0076(2) min^{-1}) and there is again a noticeable induction period.[4,44,45]

Table 2.10. Solution polymerisation of *rac*-lactide by Ti($N_2^{Ts}N^{py}$)(O^iPr)$_2$ (**3**), Zr($N_2^{Ts}N^{py}$)(O^iPr)$_2$ (**4**), Ti($N_2^{Ts}N^{OMe}$)(O^iPr)$_2$ (**5**), and Zr($N_2^{Ts}N^{OMe}$)(O^iPr)$_2$ (**6**).[a]

Catalyst	Conversion (%)[b]	Time (h)	M_n (GPC)[c]	M_n (calcd)[d]	M_w/M_n
Ti($N_2^{Ts}N^{py}$)(O^iPr)$_2$ (**3**)	23	10	2,600	1,680	1.26
Ti($N_2^{Ts}N^{py}$)(O^iPr)$_2$ (**3**)	73	24	7,230	5,230	1.16
Ti($N_2^{Ts}N^{OMe}$)(O^iPr)$_2$ (**5**)	35	10	3,660	2,610	1.12
Ti($N_2^{Ts}N^{OMe}$)(O^iPr)$_2$ (**5**)	90	24	8,990	6,480	1.21
Zr($N_2^{Ts}N^{py}$)(O^iPr)$_2$ (**4**)	57	10	4,480	4,107	1.19
Zr($N_2^{Ts}N^{OMe}$)(O^iPr)$_2$ (**6**)	91	6	7,660	6,340	1.13

[a] Conditions: [rac-LA]/[catalyst] = 100:1, 6.0 mL toluene at 70 °C. See Experimental section for other details. [b] % conversion by ^{1}H NMR. [c] Molecular weights (g mol^{-1}) determined from GPC using the appropriate Mark-Houwink corrections. [d] Expected M_n (g mol^{-1}) for 2 chains growing per metal centre at the % conversion by ^{1}H NMR.

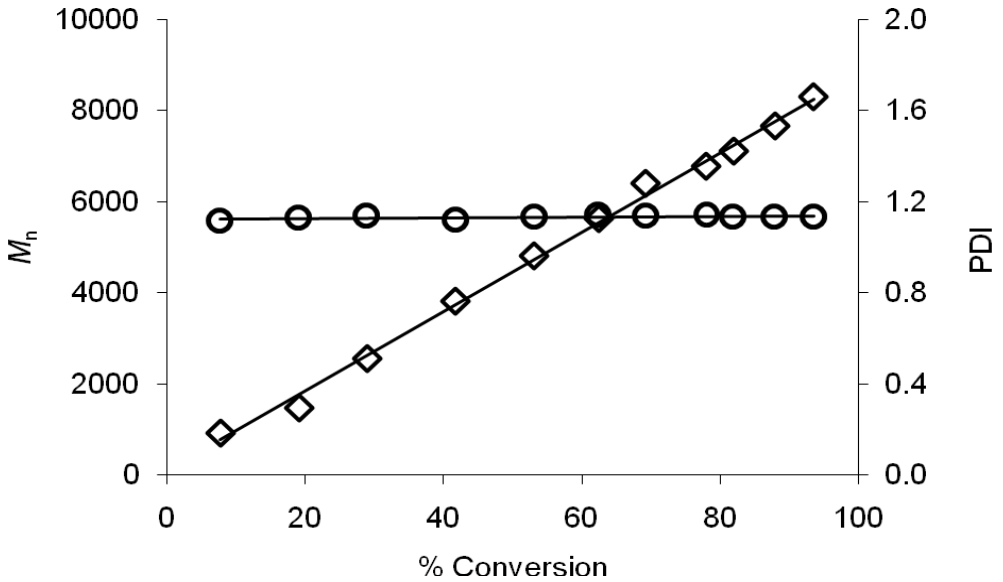
Figure 2.19. First order plot for *rac*-LA consumption using Zr($N_2^{Ts}N^{OMe}$)(O^iPr)$_2$ (**6**).[a]



[a] Conditions [*rac*-LA_0]/[**6**] = 100:1, 6 mL toluene, 70 °C, 0.1 mL aliquots taken at the given intervals. See Experimental section for other details. Linear fit (r^2 = 0.996) shown is for the first order region after the induction period.

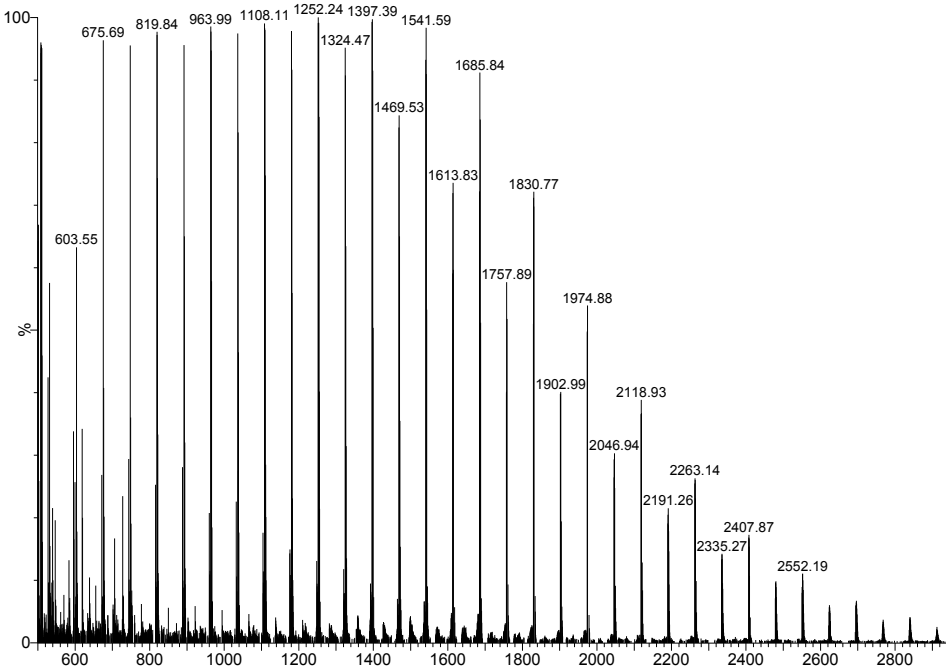
Figure 2.20 shows that M_n increases linearly with conversion in a living fashion. The final experimental M_n (94% conversion) of 8,290 g mol^{-1} at 8 hours is in good agreement with the expected value of 6,740 g mol^{-1} if two *rac*-LA chains were growing per metal centre. The gradient of the plot is 88(1) g mol^{-1} (% conversion)$^{-1}$ which compares favourably with the expected value (72 g mol^{-1} (% conversion)$^{-1}$). Figure 2.20 also shows that the PDIs remain very narrow and effectively constant between 1.12-1.14 throughout the process, consistent with a single site catalyst. The ^{1}H NMR and MALDI-ToF-MS spectra of the poly(*rac*-LA) show the expected single O^{i}Pr end group per chain, consistent with a coordination-insertion mechanism (Figure 2.21). Unfortunately, the selectively homonuclear decoupled ^{1}H NMR spectrum showed that the polymer was effectively atactic throughout the whole polymerisation (in accord with the behaviour of the corresponding bis(phenolate)amine-supported catalysts) and so under these conditions the bis(sulfonamide) supporting ligand is not able to significantly influence the enchainment preferences of *L*-LA and *D*-LA (chain end control). The separation between the *m*/z envelopes in the MALDI-TOF-MS (see Figure 2.21) was 72 g mol^{-1} which is half the molecular weight of a single lactidyl unit and therefore indicative of extensive intermolecular transesterification during the polymerisation process as is very often observed with metal-based catalysts.

Figure 2.20. Plots of M_n and PDI (determined by GPC) *vs* conversion for the solution polymerisation of *rac*-LA using Zr(N$_2$^{Ts}N^{OMe})(O^{i}Pr)$_2$ (**6**).[a]



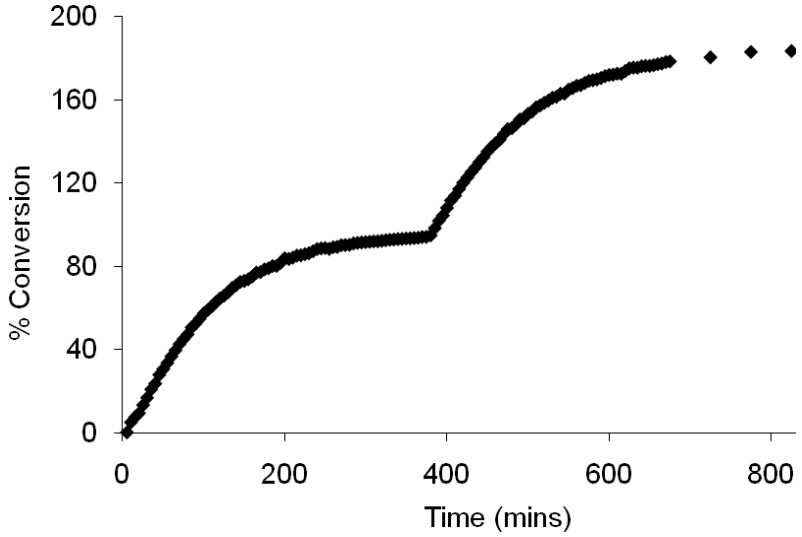
[a] Conditions: [*rac*-LA$_0$]/[**6**] = 100:1, 6.0 mL toluene, 70 °C, 0.1 mL aliquots taken at the given intervals. Hollow diamonds correspond to M_n and hollow circles to PDI.

Figure 2.21. MALDI-ToF MS of poly(rac-LA) synthesised using $Zr(N_2{}^{Ts}N^{OMe})(O^iPr)_2$ (**6**). M_n by GPC analysis was 1470 g mol^{-1}.



Again it was possible to conduct polymerisation resumption experiments similar to those undertaken for ε-caprolactone (Figure 2.18) to confirm the living nature of the polymerisation. A short induction period before becoming first order in monomer concentration (see the Appendix for the corresponding semi-logarithmic plots) is observed and again the second 100 equivalents of monomer show minimal induction period. The k_p values for both parts of Figure 2.22 (i.e. the first and second portions of *rac*-LA) are identical at 0.0002(1) min^{-1}.

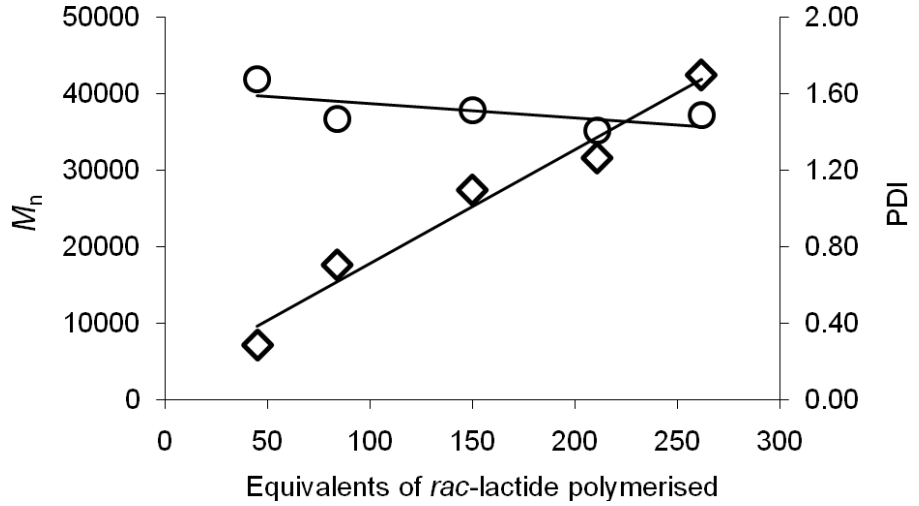
Figure 2.22. Plot of % conversion *vs* time for the polymerisation of two consecutive batches of *rac*-lactide using $Zr(N_2{}^{Ts}N^{OMe})(O^iPr)_2$ (**6**).[a]



[a.] Conditions $[LA_0]/[\mathbf{6}] = 100:1$ followed by a further 100 equivalents. at $t = 400$ min., 0.75 mL C_6D_6, 70 °C.

Polymerisation experiments were also undertaken under industrially relevant melt conditions to evaluate catalyst **6** (Figure 2.23).[47,48] Excellent conversions (*ca*. 90%) of between 50 and 300 starting equivalents of *rac*-LA in 30 minutes at 130 °C were obtained giving atactic, isopropoxy-terminated polymers with M_n values up to 42,430 g mol^{-1} (PDI = 1.49), starting with 300 equivalents of *rac*-LA. This value compares fairly well with an expected M_n of 37,690 g mol^{-1} for *one* chain per metal. The gradient of the M_n *vs* equivalents *rac*-LA polymerized plot (Figure 2.23) is 149(16) g mol^{-1} equiv^{-1} which is the same within error as the expected value of 144 for one chain per metal centre and consistent with a living catalyst. It is not clear why only one chain grows per metal centre in the melt compared to two per metal in solution. The polymers had broader PDIs than in the solution experiments (carried out at lower temperature) as expected. Again the poly(*rac*-LA) was predominantly atactic. Nonetheless, the activity of **6** under these conditions is superior to those of the aforementioned bis(phenolate) systems which gave up to 75 % conversion over somewhat longer reaction times (2 hours),[5] and is comparable to the tris(phenolate) systems of the type **1.38** in Figure 2.3 (50 or 95% conversion after 0.5 hours (M = Ti or Hf); 78% conversion after 0.1 h (M = Zr) for [*rac*-LA]:[**1.38**] = 300).[4,26]

Figure 2.23. Plots of M_n and PDI (determined by GPC) *vs* conversion for the melt polymerisation of various equivalents of *rac*-LA using $Zr(N_2^{Ts}N^{OMe})(O^iPr)_2$ (**6**).[a]



[a] Conditions: [*rac*-LA_0]/[**6**] = various values between 50:1 and 300:1, 130 °C, 30 minutes. See Experimental section for other details. Hollow diamonds correspond to M_n and hollow circles to PDI.

2.9 Summary and Conclusions

This Chapter has reported the first transition metal sulfonamide-supported catalysts for the ROP of ε-CL and *rac*-LA. The productivities of these new complexes are comparable to those of the well-established and thoroughly-explored bis(phenoxide) and related Group 4 analogues. The new bis(amide) complexes $Ti(N_2^{Ts}N^{py})(NMe_2)_2$ (**1**) or $Ti(N_2^{Ts}N^{OMe})(NMe_2)_2$ (**2**) were easily prepared under mild conditions due to the high basicity of the NMe_2 ligand, whereas the bis(isopropoxide) analogues $M(N_2^{Ts}N^{py})(O^iPr)_2$ and $M(N_2^{Ts}N^{OMe})(O^iPr)_2$ (**3 – 6**) required more forcing conditions when starting from the homoleptic precursors. Indeed, it is somewhat surprising that the sulfonamides $H_2N_2^{Ts}N^R$ (**2.7**, **2.8**) were able to displace ^{i}PrOH at all, and the reaction conditions required for their synthesis certainly testify to the equilibrium nature of the reactions. The amide complexes **1** and **2** were found to be poor catalysts for the ROP of ε-CL, and long reaction times and poor control were observed. This is attributed to the greater dissimilarity between the initiating group Ti-NMe_2 and the subsequent growing chain Ti-$\{O(CH_2)_5C(O)\}_nNMe_2$, as well as to the smaller radius of Ti compared with Zr. With respect to the Group 4 isopropoxide complexes, the ROP results for ε-CL and *rac*-LA were in agreement with literature precedent in that the zirconium homologues were more active than their titanium counterparts. Polymerisation rates were higher for the catalysts bearing an OMe donor (**5** and **6**)

compared to a pyridyl one. For the ROP of *rac*-lactide initial studies found similar trends in activity for **3**, **4**, **5** and **6** to the ε-caprolactone polymerisations, however all catalysts were observed to give a well controlled polymerisation under the conditions employed (PDI 1.1 – 1.2). The zirconium catalyst **6** was found to be an active and well-controlled catalyst for the living ROP of *rac*-LA both in solution and in the melt. All poly(LA)s formed were predominantly atactic.

2.10 References

(1) Schwarz, A. D.; Thompson, A. L.; Mountford, P. *Inorg*. *Chem*. 2009, *48*, 10442-10454.

(2) Gendler, S.; Segal, S.; Goldberg, I.; Goldschmidt, Z.; Kol, M. *Inorg*. *Chem*. 2006, *45*, 4783-4790.

(3) Kricheldorf, H. R.; Berl, M.; Scharnagl, N. *Macromol*. 1988, *21*, 286-293.

(4) Chmura, A. J.; Davidson, M. G.; Jones, M. D.; Lunn, M. D.; Mahon, M. F. *Dalton Trans*. 2006, 887-889.

(5) Chmura, A. J.; Davidson, M. G.; Jones, M. D.; Lunn, M. D.; Mahon, M. F.; Johnson, A. F.; Khunkamchoo, P.; Roberts, S. L.; Wong, S. S. F. *Macromol*. 2006, *39*, 7250-7257.

(6) Cayuela, J.; Bounor-Legare, V.; Cassagnau, P.; Michel, A. *Macromol*. 2006, *39*, 1338-1346.

(7) Gimenez, J.; Cassagnau, P.; Fulchiron, R.; Michel, A. *Macromol*. *Chem*. *Phys*. 2000, *201*, 479-490.

(8) Machado, A. V.; Bounor-Legare, V.; Gonçalves, N. D.; Melis, F.; Cassagnau, P.; Michel, A. *J*. *Appl*. *Polym*. *Sci*. 2008, *110*, 3480-3487.

(9) Grafov, A.; Vuorinen, S.; Repo, T.; Kemell, M.; Nieger, M.; Leskelä, M. *E*. *Polym*. *J*. 2008, *44*, 3797-3805.

(10) Takeuchi, D.; Nakamura, T.; Aida, T. *Macromol*. 2000, *33*, 725-729.

(11) Takeuchi, D.; Aida, T. *Macromol*. 2000, *33*, 4607-4609.

(12) Ejfler, J.; Kobylka, M.; Jerzykiewicz, L. B.; Sobota, P. *J*. *Mol*. *Catal*. *A: Chem*. 2006, *257*, 105-111.

(13) Kim, Y.; Verkade, J. G. *Organometallics* 2002, *21*, 2395-2399.

(14) Kim, Y.; Verkade, J. G. *Macromol*. *Rapid Commun*. 2002, *23*, 917-921.

(15) Kim, Y.; Jnaneshwara, G. K.; Verkade, J. G. *Inorg*. *Chem*. 2003, *42*, 1437-1447.

(16) Kim, Y.; Verkade, J. G. *Macromol*. *Symp*. 2005, *224*, 105-118.

(17) Takashima, Y.; Nakayama, Y.; Watanabe, K.; Itono, T.; Ueyama, N.; Nakamura, A.; Yasuda, H.; Harada, A.; Okuda, J. *Macromol*. 2002, *35*, 7538-7544.

(18) Takashima, Y.; Nakayama, Y.; Hirao, T.; Yasuda, H.; Harada, A. *J*. *Organomet*. *Chem*. 2004, *689*, 612-619.

(19) Gregson, C. K. A.; Blackmore, I. J.; Gibson, V. C.; Long, N. J.; Marshall, E. L.; White, A. J. P. *Dalton Trans*. 2006, 3134-3140.

(20) Zelikoff, A. L.; Kopilov, J.; Goldberg, I.; Coates, G. W.; Kol, M. *Chem*. *Commun*. 2009, 6804-6806.

(21) Atkinson, R. C. J.; Gerry, K.; Gibson, V. C.; Long, N. J.; Marshall, E. L.; West, L. J. *Organometallics* 2006, *26*, 316-320.

(22) Kim, S. H.; Lee, J.; Kim, D. J.; Moon, J. H.; Yoon, S.; Oh, H. J.; Do, Y.; Ko, Y. S.; Yim, J.-H.; Kim, Y. *Journal of Organometallic Chemistry* 2009, *694*, 3409-3417.

(23) Romain, C.; Brelot, L.; Bellemin-Laponnaz, S.; Dagorne, S. *Organometallics* 2010, 1191–1198.

(24) Patel, D.; Liddle, S. T.; Mungur, S. A.; Rodden, M.; Blake, A. J.; Arnold, P. L. *Chem*. *Commun*. 2006, 1124-1126.

(25) Gregson, C. K. A.; Gibson, V. C.; Long, N. J.; Marshall, E. L.; Oxford, P. J.; White, A. J. P. *J*. *Am*. *Chem*. *Soc*. 2006, *128*, 7410-7411.

(26) Chmura, A. J.; Davidson, M. G.; Frankis, C. J.; Jones, M. D.; Lunn, M. D. *Chem*. *Commun*. 2008, 1293-1295.

(27) Sarazin, Y.; Howard, R. H.; Hughes, D. L.; Humphrey, S. M.; Bochmann, M. *Dalton Trans*. 2006, 340-350.

(28) Chmura, A. J.; Cousins, D. M.; Davidson, M. G.; Jones, M. D.; Lunn, M. D.; Mahon, M. F. *Dalton Trans*. 2008, 1437-1443.

(29) Skinner, M. E. G.; Li, Y.; Mountford, P. *Inorg*. *Chem*. 2002, *41*, 1110-1119.

(30) Bailey, N. A.; Fenton, D. E.; Hellier, P. C.; Hempstead, P. D.; Casellatob, U.; Vigatob, P. A. *Dalton Trans*. 1992, 2809-2816.

(31) Toupance, T.; Dubberley, S. R.; Rees, N. H.; Tyrrell, B. R.; Mountford, P. *Organometallics* 2002, *21*, 1367-1382.

(32) Fletcher, D. A.; McMeeking, R. F.; Parkin, D. *J*. *Chem*. *Inf*. *Comput*. *Sci*. 1996, *36*, 746 (The United Kingdom Chemical Database Service).

(33) Pritchett, S.; Gantzel, P.; Walsh, P. J. *Organomet*. 1999, *18*, 823-831.

(34) Pritchett, S.; Woodmansee, D. H.; Gantzel, P.; Walsh, P. J. *J*. *Am*. *Chem*. *Soc*. 1998, *120*, 6423-6424.

(35) Pritchett, S.; Gantzel, P.; Walsh, P. J. *Organometallics* 1997, *16*, 5130-5132.

(36) Ackermann, L.; Bergman, R. G.; Loy, R. N. *J*. *Am*. *Chem*. *Soc*. 2003, *125*, 11956-11963.

(37) Costa, A. M.; García, C.; Carroll, P. J.; Walsh, P. J. *Tetrahedron* 2005, *61*, 6442-6446.

(38) Selby, J. D.; Manley, C. D.; Schwarz, A. D.; Clot, E.; Mountford, P. *Organometallics* 2008, *27*, 6479-6494.

(39) Ward, B. D.; Orde, G.; Clot, E.; Cowley, A. R.; Gade, L. H.; Mountford, P. *Organometallics* 2004, *23*, 4444-4461.

(40) Boyd, C. L.; Toupance, T.; Tyrrell, B. R.; Ward, B. D.; Wilson, C. R.; Cowley, A. R.; Mountford, P. *Organometallics* 2005, *24*, 309-330.

(41) Rudin, A.; Hoegy, H. L. W. *J*. *Polym*. *Sci*. *Part A: Polym*. *Chem*. 1972, *10*, 217-235.

(42) Barakat, I.; Ph, D.; Jérôme, R.; Ph, T. *J*. *Polym*. *Sci*. *Part A: Polym*. *Chem*. 1993, *31*, 505-514.

(43) Dorgan, J. R.; Janzen, J.; Knauss, D. M.; Hait, S. B.; Limoges, B. R.; Hutchinson, M. H. *J*. *Polym*. *Sci*. *Part B: Polym*. *Phys*. 2005, *43*, 3100-3111.

(44) Duda, A.; Penczek, S. *Macromol*. 1995, *28*, 5981-5992.

(45) Zhong, Z.; Dijkstra, P. J.; Birg, C.; Westerhausen, M.; Feijen, J. *Macromol*. 2001, *34*, 3863-3868.

(46) Song, F.; Cannon, R. D.; Bochmann, M. *J*. *Am*. *Chem*. *Soc*. 2003, *125*, 7641-7653.

(47) Vink, E. T. H.; Rábago, K. R.; Glassner, D. A.; Gruber, P. R. *Polym*. *Deg*. *Stab*. 2003, *80*, 403-419.

(48) Drumright, R. E.; Gruber, P. R.; Henton, D. E. *Adv*. *Mater*. 2000, *12*, 1841-1846.

Chapter Three

Ligand Variation in Sulfonamide-Supported Group 4 ROP Catalysts

3.1 Overview

Metal catalysed ROP was introduced in detail in Chapters 1 and 2. This Chapter provides an overview of the synthesis and characterisation of C_s symmetric titanium amide and alkoxide complexes supported by dianionic, tri- and tetradentate sulfonamide ligands. Zirconium alkyl and amide complexes supported by C_3-symmetric trianionic 'tren' type ligands bearing three different sulfonamide groups have also been investigated. Solution state behaviour and solid state structures will be presented and discussed. These complexes, alongside previously reported titanium isopropoxide species supported by sulfonamide ligands utilising a 1,2-cyclohexadiamine backbone and *in situ* generated zirconium isopropoxide complexes, have been synthesised and assessed for the ROP of ε-caprolactone and *rac*-lactide. Comparisons of the activity and selectivity of these catalysts will be made to the tetradentate bis(sulfonamide) complexes reported in Chapter 2.

3.2 Introduction

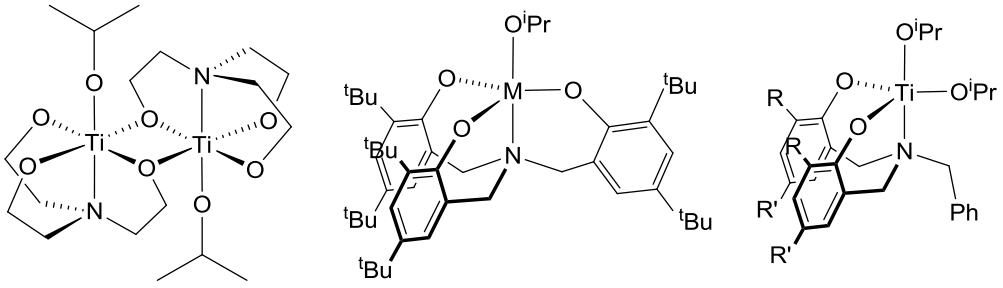
In Chapter 2 it was found that zirconium isopropoxide complexes supported by dianionic tetradentate sulfonamide ligands provided a stable platform for the ROP of *rac*-lactide and ε-caprolactone. Both the activity and control of these catalysts were found to be similar to the extensively exploited tetradentate bis(phenolate) amine ligands, but the ROP of *rac*-lactide did not provide any stereochemical bias.

Davidson, Aida, Okuda and Harada investigated titanium complexes of bi- and tridentate bis(phenolate) ligands for the ROP of ε-caprolactone and *L*-lactide.[1-4] Davidson found that polymerisation of ε-CL with **1.21** (Figure 3.1) gave a well controlled process yielding polymer of narrow PDI (~1.2) and predictable M_n.[1] The polymerisation was also much better controlled than with the analogous tetradentate bis(phenolate) amine complex bearing a pyridyl donor arm, which showed no activity under the same conditions.[5] Indeed, the only tetradentate bis(phenolate) amine complex found to be active gave a very poorly controlled polymerisation with broad PDI (2.60) and larger than expected M_n.[5] Titanium complexes bearing bi- and tridentate bis(phenolate) complexes with either CH_2 or chalcogen bridges were investigated for the ROP of ε-CL by Aida, Okuda and Harada. Good yields, narrow PDIs and close agreement with calculated M_n were achieved with these catalysts.[2-4,6]

Highly successful Group 4 ROP catalysts supported by C_3 symmetric alkyl or aryl

oxides have been developed by Verkade, Davidson and Kol.[7-11] Verkade was the first to employ titanatranes of various structures for the ROP of *rac*-lactide (**1.36** in Figure 3.1).[7-9,12] Polymerisations conducted under melt conditions (130 °C, 2 hours) gave polymers with moderate to broad PDIs (1.31-3.68) and poor control over M_n. In contrast, polymerisations conducted in toluene solution at 70 °C yielded an extremely well controlled polymerisation of *L*- and *rac*-lactide for complex **1.36**, with predictable M_n and narrow PDI. Polymerisations of *L*-lactide gave isotactic p(LA) as would be expected if no epimerisation of the lactide stereogenic centres was taking place. However, polymerisation of *rac*-lactide yielded only atactic polymers.[7-9,12-14] Kol then compared tetradentate bis(phenolate) amine complexes for titanium and zirconium to C_3 symmetric tris(phenolate) amine ligands. For titanium the tripodal complexes bearing chloride substituents provided a more active polymerisation of *L*-lactide giving 55% conversion under melt conditions in 22 hours. A marked difference was seen with zirconium, where the tripodal complexes were generally slower than their bis(phenolate) amine analogues. However, O^{t}Bu rather than O^{i}Pr initiators were employed for the tris(phenolate) amine complexes which would presumably provide a lower activity due to slower initiation into a bulkier M-OR bond.[11]

Figure 3.1. Group 4 ROP catalysts employing N,O-donor ligands. [1,9,10,12,14,15]



1.36 | M = Ti (**1.37**), Zr (**1.38**), or Hf (**1.39**) | **1.21**

Davidson synthesised **1.37**, **1.38** and **1.39** (Figure 3.1) which are the isopropoxide analogues of the *tert*-butoxide complexes Kol studied. The titanium complexes gave activities and control for the ROP of *rac*-lactide that were similar to those observed previously by Verkade and Kol, (30 minutes, 50% conversion, PDI = 1.39 and larger than expected M_n). In contrast, the zirconium and hafnium analogues gave an extremely well controlled polymerisation of *rac*-lactide with narrow PDI, predictable M_n, good heterotactic enrichment (P_r = 0.98), and high conversion after 30 minutes

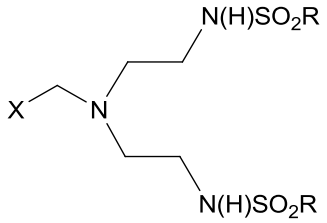
under melt conditions. Solution based polymerisations in toluene at room temperature gave similar results, although conversion was low (50% after 48 hours at room temperature).[10]

3.3 Aims

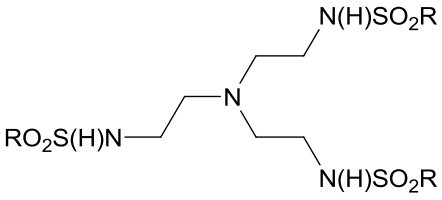
In the light of the success of these bi- and tridentate phenolate ligands, it was of interest to synthesise 4- and 5-coordinate titanium complexes supported by sulfonamide ligands to compare these with the previously described tetradentate sulfonamide complexes discussed in Chapter 2. Complexes bearing C_3 symmetric sulfonamide ligands analogous to the tris(phenolate) amine complexes were also of interest. Zirconium complexes were especially desirable since they have been shown to give the best control and activity for the ROP of *rac*-lactide, in both literature examples and with the complexes studied in Chapter 2.[10]

It was also reasoned that, by synthesising sulfonamide ligands with sterically less encumbering groups, such as mesyl (-SO_2Me) instead of tosyl (-SO_2Tol), would enhance the activity of the resulting catalysts. Therefore, the synthesis of tri- and tetradentate sulfonamide complexes bearing mesyl sulfone groups was also undertaken. The new tetradentate ligands were designed utilising a methoxy arm rather than a pyridyl because it had been found previously that this provided a more active and controlled catalyst (Chapter 2).

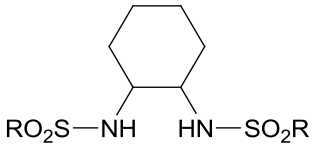
This Chapter reports the syntheses and structures of a series of new titanium complexes derived from the N_3-donor sulfonamides (Ph)$CH_2N(CH_2CH_2NHSO_2Tol)_2$ (**7**, $H_2N_2^{Ts}N^{Ph}$) and (Ph)$CH_2N(CH_2CH_2NHSO_2Me)_2$ (**8**, $H_2N_2^{Ms}N^{Ph}$) or the N_3O-donor sulfonamide (MeOCH_2)$CH_2N(CH_2CH_2NHSO_2Me)_2$ (**9**, $H_2N_2^{Ms}N^{OMe}$). New zirconium complexes based on N_4-donor C_3 symmetric ligands $N(CH_2CH_2NHSO_2Tol)_3$ (**3.1**, $H_3N_3^{Ts}N$), $N(CH_2CH_2NHSO_2Me)_3$ (**10**, $H_3N_3^{Ms}N$) and $N(CH_2CH_2NHSO_2C_6H_3(CF_3)_2)_3$ (**11**, $H_3N_3^{TArF}N$) were also synthesised. These, together with previously reported titanium isopropoxide complexes supported by 1,2-$C_6H_{10}(NHSO_2R)_2$ (R = Tol (**3.2**, $H_2CyN_2^{Ts}$) or Mes (**3.3**, $H_2CyN_2^{SO_2Mes}$)) ligands were investigated for their performance as ROP catalysts for ε-CL and *rac*-LA.



X = Ph, R = Tol (**7**)
or Me (**8**)
X = CH_2OMe, R = Me (**9**)



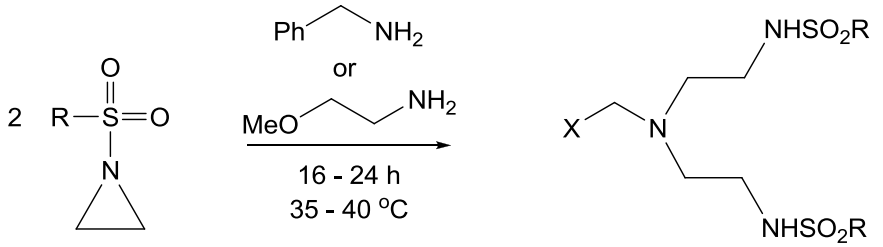
R = Tol (**3.1**), Me (**10**) or
$C_6H_3(CF_3)_2$ (**11**)



R = Tol (**3.2**) or
Mes (**3.3**)

3.4 Synthesis of protio-ligand precursors

The previously reported bidentate and tetradentate protio-ligands $H_3N_3{}^{Ts}N$ (**3.1**)[16] and $H_2CyN_2{}^{Ts}$ (**3.2**),[17] $H_2CyN_2{}^{SO_2Mes}$ (**3.3**),[18] were synthesised according to the literature methods. The new tridentate protio-ligands $PhCH_2N(CH_2CH_2NHSO_2R)_2$ (R = Tol (**7**, $H_2N_2{}^{Ts}N^{Ph}$) or Me (**8**, $H_2N_2{}^{Ms}N^{Ph}$)) and tetradentate protio-ligand $MeOCH_2CH_2N(CH_2CH_2NHSO_2Me)_2$ (**9**, $H_2N_2{}^{Ms}N^{OMe}$) were also synthesised. Utilising a similar synthetic route to that for $H_2N_2{}^{Ts}N^{py}$ (**2.7**) and $H_2N_2{}^{Ts}N^{OMe}$ (**2.8**) (Chapter 2), reaction of benzyl amine or $MeOCH_2CH_2NH_2$ with the appropriate *N*-sulfonyl aziridine gave good yields of **7**, **8** and **9** (Equation 3.1).

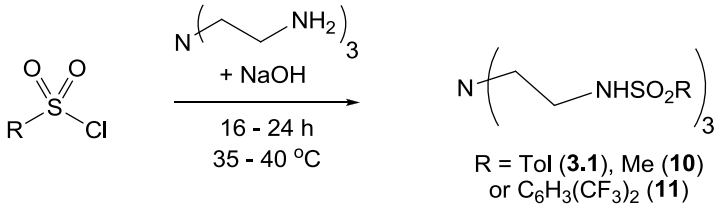


X = Ph, R = Tol (**7**) or Me (**8**)
X = $MeOCH_2$, R = Me (**9**)

Equation 3.1.

To assess structure-activity relationships in trianionic sulfonamide ligands with potential C_3 symmetry, the new ligands $N(CH_2CH_2NHSO_2Me)_3$ (**10**, $H_3N_3{}^{Ms}N$) and $N(CH_2CH_2NHSO_2C_6H_3(CF_3)_2)_3$ (**11**, $H_3N_3{}^{TArF}N$), were also synthesised. Similar syntheses to $H_2CyN_2{}^{Ts}$ (**3.2**),[17] $H_2CyN_2{}^{SO_2Mes}$ (**3.3**),[18] and $H_3N_3{}^{Ts}N$ (**3.1**)[16] were employed, where reaction of the appropriate sulfonyl chloride with tris(2-aminoethyl)amine or *trans*-1,2-cyclohexadiamine gave the desired products. Reactions with $SO_2Cl(3,5\text{-}C_6H_3(CF_3)_2)$ proceeded in high yield to give $H_3N_3{}^{TArF}N$ (**11**). However, reaction with SO_2ClMe only gave poor yields (18%) of $H_3N_3{}^{Ms}N$ (**10**).

The reaction was carried out in a biphasic solution of diethyl ether and water, and for protio-ligands $H_3N_3{}^{Ts}N$ (**3.1**) and $H_3N_3{}^{TArF}N$ (**11**) the product precipitated out of the ether layer in high yield following completion of the reaction to give analytically pure products after recrystallisation from methanol. $H_3N_3{}^{Ms}N$ (**10**) is however highly soluble even in basified water, making separation from the aqueous soluble side products extremely difficult. Analytically pure product was eventually obtained in low yield by recrystallisation from concentrated aqueous solution at room temperature.



Equation 3.2.

So as to make comparisons with their metal complexes (see below) and the previously reported **3.2**,[19,20] $H_2N_2{}^{Ts}N^{OMe}$ (**2.8**, Chapter 2),[21] and $H_2N_2{}^{Ts}N^{py}$ (**2.7**, Chapter 2),[22] the X-ray structures of **7**, **8**, **10** and **3.3** were determined. The molecular structures and selected distances and angles are given in, Figures 3.2, 3.3 and 3.4 and Tables 3.1, 3.2, 3.3 and 3.4.

Figure 3.2. Top: displacement ellipsoid plots of $H_2N_2{}^{Ts}N^{Ph}$ (**7**) and bottom: $H_2N_2{}^{Ms}N^{Ph}$ (**8**). C-bound H atoms omitted for clarity, N-bound H atoms are drawn as spheres of arbitrary radius. Ellipsoids are drawn at the 20% probability level.

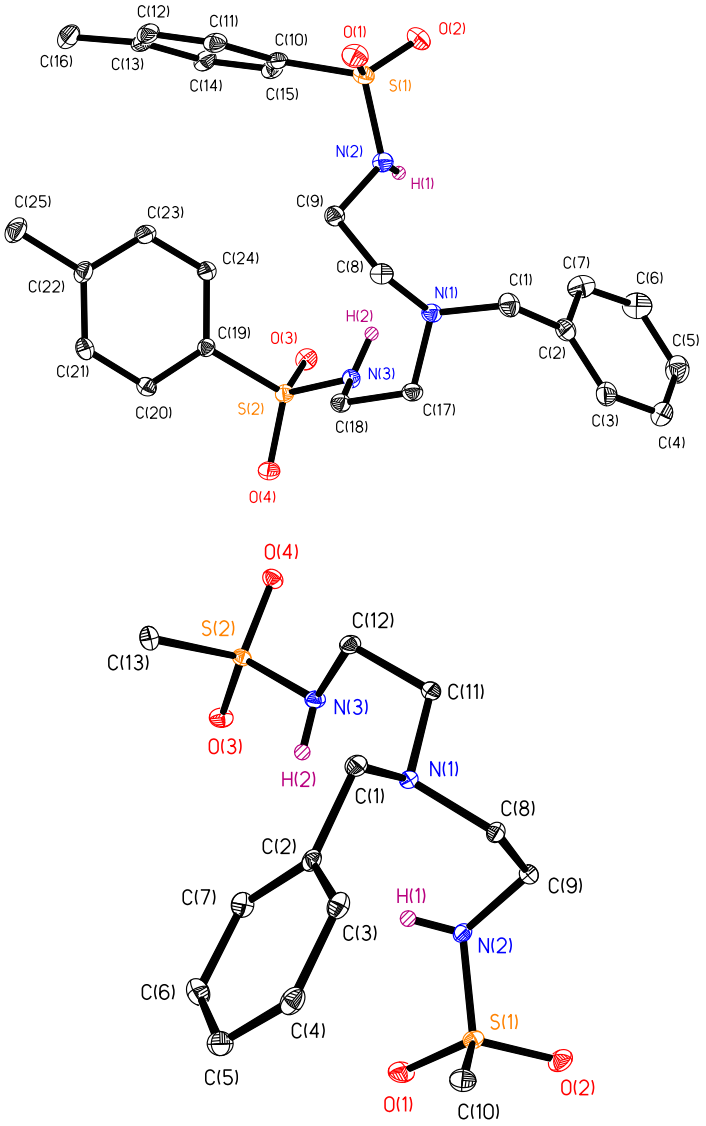


Table 3.1. Selected bond distances (Å) and angles (°) for $H_2N_2{}^{Ts}N^{Ph}$ (**7**).

N(1)-C(8)	1.479(2)	N(1)-C(1)	1.475(2)
N(1)-C(17)	1.475(2)	N(2)-S(1)	1.620(2)
N(3)-S(2)	1.622(2)	N(2)-H(1)	0.86(2)
N(3)-H(2)	0.90(2)	S(2)-O(4)	1.433(1)
S(1)-O(1)	1.433(1)	S(1)-O(2)	1.433(1)
S(2)-O(3)	1.447(1)	S(1)-C(10)	1.760(2)
S(2)-C(19)	1.765(2)		
C(1)-N(1)-C(8)	110.0(1)	S(1)-N(2)-H(1)	110.0(2)
C(1)-N(1)-C(17)	110.4(1)	C(9)-N(2)-H(1)	118.4(2)
C(8)-N(1)-C(17)	111.6(1)	C(19)-S(2)-N(3)	107.4(1)
S(2)-N(3)-H(2)	113.6(1)	C(18)-N(3)-H(2)	114.5(1)
C(9)-N(2)-S(1)	119.4(1)	C(10)-S(1)-N(2)	108.3(1)
C(19)-S(2)-N(3)	107.5(1)		

Table 3.2. Selected bond distances (Å) and angles (°) for $H_2N_2{}^{Ms}N^{Ph}$ (**8**).

N(1)-C(1)	1.479(2)	N(1)-C(8)	1.473(2)
N(1)-C(11)	1.470(2)	N(2)-S(1)	1.621(2)
N(2)-C(9)	1.471(2)	N(2)-H(1)	0.86(2)
N(3)-S(2)	1.628(2)	N(3)-C(12)	1.481(2)
N(3)-H(2)	0.86(3)	S(1)-O(1)	1.433(2)
S(1)-O(2)	1.428(2)	S(1)-C(10)	1.758(2)
S(2)-O(3)	1.440(1)	S(2)-O(4)	1.432(1)
S(2)-C(13)	1.757(2)		
C(1)-N(1)-C(8)	109.0(2)	C(1)-N(1)-C(11)	110.5(1)
C(8)-N(1)-C(11)	109.8(2)	S(1)-N(2)-C(9)	120.1(1)
S(2)-N(3)-C(12)	116.6(1)	N(2)-S(1)-C(10)	108.1(1)
N(3)-S(2)-C(13)	107.3(1)		

Figure 3.3. Displacement ellipsoid plots of $H_3N_3{}^{Ms}N$ (**10**), molecular structure (left), inter-molecular hydrogen bonding (symmetry operator, x ± 1, y, z) (right). C-bound H atoms omitted for clarity. H(1), H(2) and H(3) are drawn as spheres of arbitrary radius. Ellipsoids are drawn at the 25% probability level.

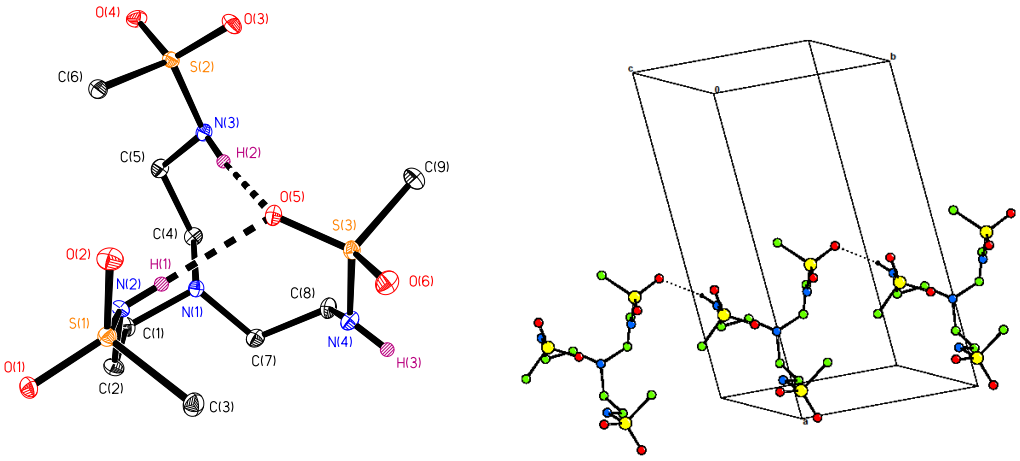


Table 3.3. Selected bond distances (Å) and angles (°) for $H_3N_3{}^{Ms}N$ (**10**).

N(2)-S(1)	1.611(2)	N(2)-H(1)	0.81(3)
N(3)-S(2)	1.619(2)	N(3)-H(2)	0.83(3)
N(4)-S(3)	1.613(2)	N(4)-H(3)	0.82(3)
O(1)-S(1)	1.4435(19)	O(1)-H(3)	2.23(4)
O(2)-S(1)	1.435(2)	O(3)-S(2)	1.439(2)
O(4)-S(2)	1.443(2)	O(5)-S(3)	1.441(2)
O(5)···H(1)	2.23(3)	O(5)···H(2)	2.17(3)
O(6)-S(3)	1.4288(19)	S(1)-C(3)	1.762(3)
S(2)-C(6)	1.757(3)	S(3)-C(9)	1.752(3)
C(1)-N(1)-C(4)	110.6(2)	C(1)-N(1)-C(7)	111.7(2)
C(4)-N(1)-C(7)	110.7(2)	S(1)-N(2)-C(2)	119.1(2)
S(1)-N(2)-H(1)	110.2(2)	C(2)-N(2)-H(1)	110.5(1)
S(2)-N(3)-C(5)	118.8(2)	S(2)-N(3)-H(2)	110(2)
C(5)-N(3)-H(2)	113(2)	S(3)-N(4)-C(8)	122.8(2)
S(3)-N(4)-H(3)	112(2)	C(8)-N(4)-H(3)	112(2)

The solid state molecular structures of **7** and **8** are comparable, and the geometries represent an arrangement which is reminiscent of that required to bind to a metal centre (in terms of N(1) lone pair and N-H bond orientations). Similar arrangements were found previously for $H_2N_2^{Ts}N^{OMe}$ (**2.8**, Chapter 2),[21] and $H_2N_2^{Ts}N^{py}$ (**2.7**, Chapter 2).[22] Unexpectedly, there is no intra- or inter-molecular hydrogen bonding present in either compound.

$H_3N_3^{Ms}N$ (**10**) displays a similar geometry to $H_2N_2^{Ts}N^{OMe}$ (**2.8**, Chapter 2), possessing two intra-molecular N-H···O hydrogen bonds between the two sulfonamides and one of the sulfone oxygens. The remaining sulfonamide takes part in inter-molecular N-H···O hydrogen bonding to the sulfone oxygen of another molecule giving a linear chain along the crystallographic *b* axis of the unit cell. In general terms, the bond lengths and angles lie within the expected ranges for compounds of these types.[23]

Figure 3.4. Displacement ellipsoid plots of $H_2CyN_2^{SO_2Mes}$ (**3.3**), molecular structure (left), inter-molecular hydrogen bonding (symmetry operator, x ± 1, y, z) (right). C-bound H atoms omitted for clarity. H(1) and H(2) are drawn as spheres of arbitrary radius. Ellipsoids are drawn at the 25% probability level.

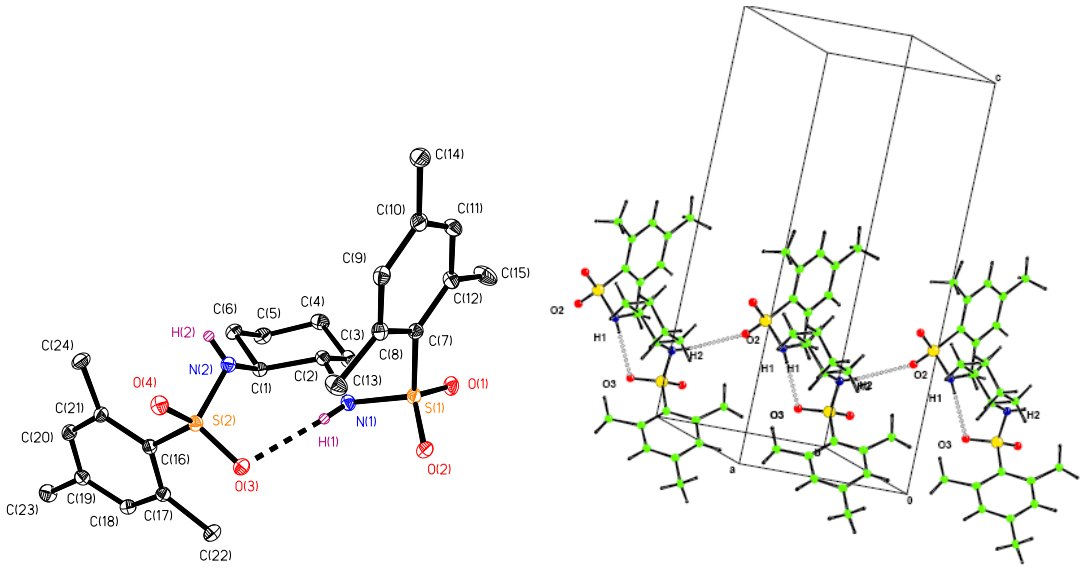


Table 3.4. Selected bond distances (Å) and angles (°) for $H_2CyN_2^{SO_2Mes}$ (**3.3**).

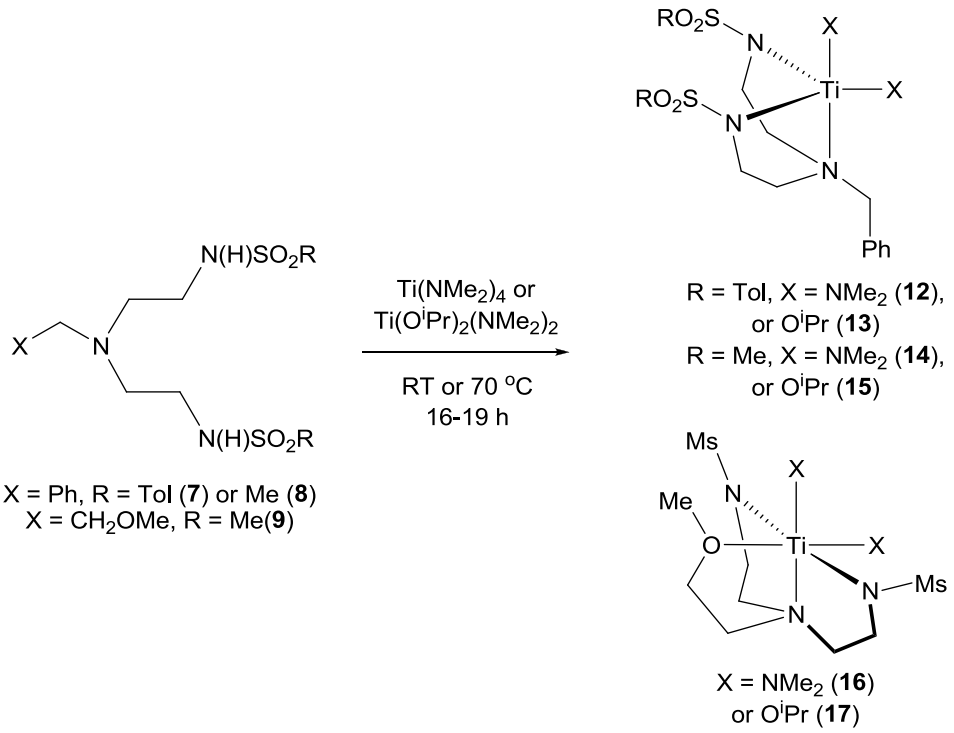
C(1)-N(2)	1.478(3)	C(2)-N(1)	1.483(3)
N(2)-S(2)	1.637(2)	N(1)-S(1)	1.628(2)
N(2)-H(2)	0.80(3)	N(1)-H(1)	0.84(3)
S(2)-O(3)	1.435(2)	S(1)-O(1)	1.432(2)
S(2)-O(4)	1.434(2)	S(1)-O(2)	1.442(2)
C(16)-S(2)	1.784(2)	C(7)-S(1)	1.787(2)
O(3)···H(1)	2.22(3)	H(2)···O(2A)	2.64(3)
C(2)-N(1)-S(1)	121.9(1)	C(2)-N(1)-H(1)	113.3(2)
S(1)-N(1)-H(1)	112.7(2)	C(1)-N(2)-S(2)	118.8(1)
C(1)-N(2)-H(2)	113(2)	S(2)-N(2)-H(2)	113(2)
N(2)-H(2)···O(2A)	169(3)	S(2)-O(3)···H(1)	105.4(7)
N(1)-H(1)···O(3)	157(3)		

The solid state structure of $H_2CyN_2^{SO_2Mes}$ (**3.3**) was also determined. The molecular structure possesses an intra-molecular N-H···O hydrogen bond between one sulfonamide and one of the sulfone oxygens. An inter-molecular N-H···O hydrogen bond between the remaining sulfonamide and a sulfone oxygen gives a linear chain of molecules throughout the crystal lattice (Figure 3.3). As for the other sulfonamide protio-ligands, the bond lengths and angles lie within the expected ranges for compounds of this type, Table 3.4.[23]

3.5 Synthesis of titanium amide and isopropoxide complexes

Protonolysis reactions of $Ti(NMe_2)_4$ with one equivalent of protio-ligands **7**, **8** and **9**, gave the corresponding titanium bis(dimethylamide) complexes $Ti(N_2^{Ts}N^{Ph})(NMe_2)_2$ (**12**), $Ti(N_2^{Ms}N^{Ph})(NMe_2)_2$ (**14**) and $Ti(N_2^{Ms}N^{OMe})(NMe_2)_2$ (**16**), respectively, in moderate to good yield (39 – 60%) after recrystallisation. When the reaction was followed in CD_2Cl_2 on the NMR tube scale the yields were effectively quantitative and the expected $HNMe_2$ side product was observed. Lower yields were observed in the case of the mesyl complexes (45 and 39%, **14** and **16** respectively) compared to the corresponding tosyl complexes (60 and 51%, **12** and **2** respectively) were a consequence of the formers high solubility in non-polar solvents such as hexane.

Scheme 3.1. Synthesis of the new complexes **12 - 17**.



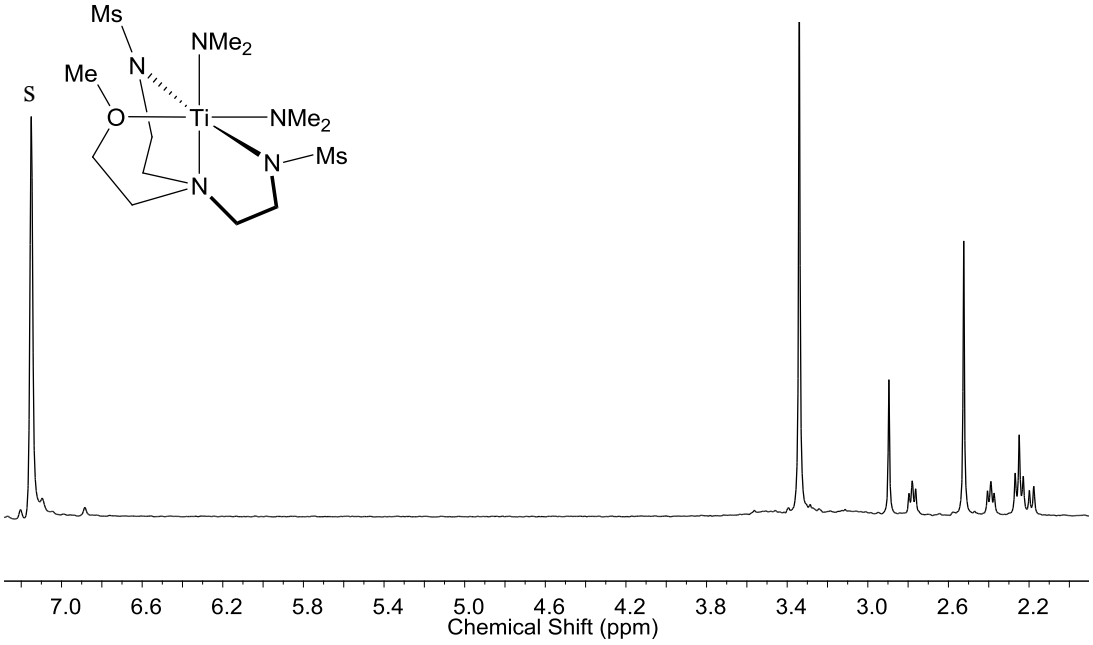
As shown in Scheme 3.1, Ti($N_2^{Ts}N^{Ph}$)(O^iPr)$_2$ (**13**), Ti($N_2^{Ms}N^{Ph}$)(O^iPr)$_2$ (**15**) and Ti($N_2^{Ms}N^{OMe}$)(O^iPr)$_2$ (**17**) could be prepared from Ti(NMe_2)$_2$(O^iPr)$_2$ and one equivalent of the respective protio-ligand. NMR scale investigations found quantitative formation of **13**, **15** or **17** and no evidence for the formation of the bis(dimethylamide) complexes **12**, **14** or **16**. On the preparative scale the complexes could be synthesised in 44 – 56% yield after 2 hours reaction time.

The solid state structures of Ti($N_2^{Ts}N^{Ph}$)(NMe_2)$_2$ (**12**) and Ti($N_2^{Ms}N^{OMe}$)(O^iPr)$_2$ (**17**) have been determined (*vide infra*) and confirm those proposed in Scheme 3.1. The ^{1}H NMR spectra of Ti($N_2^{Ms}N^{OMe}$)(NMe_2)$_2$ (**16**) and Ti($N_2^{Ms}N^{OMe}$)(O^iPr)$_2$ (**17**) at ambient temperature feature a singlet for the axial and equatorial NMe_2 or O^iPr groups consistent with exchange processes in solution (Figure 3.5), however the low temperature (253 K) are consistent with C_s symmetric octahedral complexes similar to Ti($N_2^{Ts}N^{OMe}$)(NMe_2)$_2$ (**2**) and Ti($N_2^{Ts}N^{OMe}$)(O^iPr)$_2$ (**5**) as seen in Chapter 2.

For Ti($N_2^{Ts}N^{Ph}$)(NMe_2)$_2$ (**12**), Ti($N_2^{Ms}N^{Ph}$)(NMe_2)$_2$ (**14**), Ti($N_2^{Ts}N^{Ph}$)(O^iPr)$_2$ (**13**) and Ti($N_2^{Ms}N^{Ph}$)(O^iPr)$_2$ (**15**) at 363 K equivalent environments are observed for the diastereotopic backbone protons in addition to a singlet for the axial and equatorial NMe_2 or O^iPr groups, indicative of rapid exchange on the NMR time scale. However, upon cooling the samples to 240 K in dichloromethane, four diastereotopic backbone

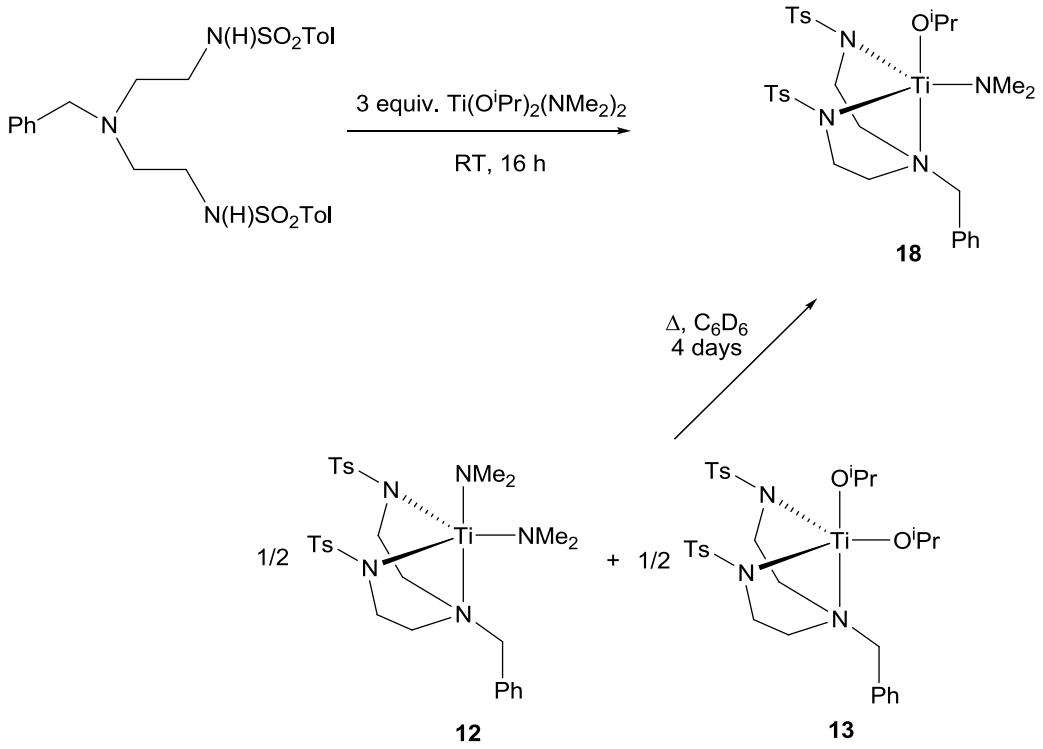
protons and inequivalent axial and equatorial NMe_2 environments are observed as would be expected for a C_s symmetric, approximately trigonal bipyramidal structure in solution consistent with the solid state structure for $Ti(N_2{}^{Ts}N^{Ph})(NMe_2)_2$ (**12**).

Figure 3.5. ^1H NMR spectrum (299.9 MHz) of **16** in C_6D_6 at 298 K. ('s' denotes residual protio-solvent).



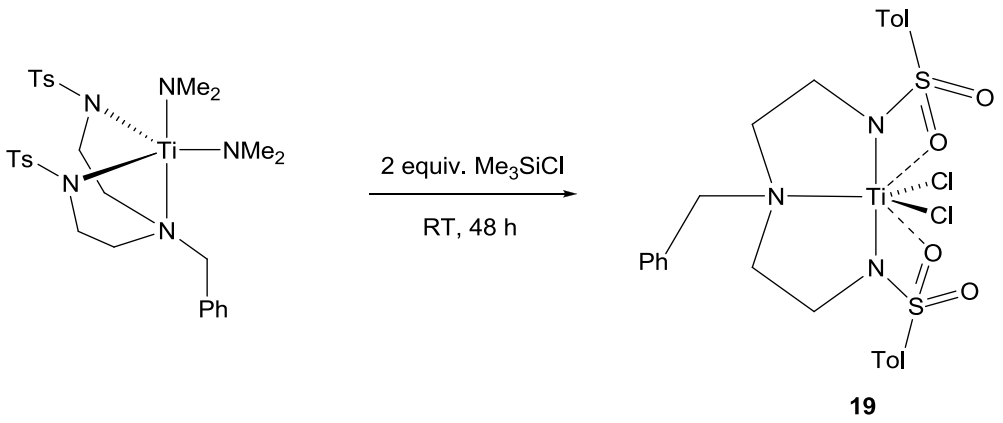
Reactions of $H_2N_2{}^{Ts}N^{Ph}$ (**7**) with various equivalents of $Ti(NMe_2)_2(O^iPr)_2$ were undertaken to probe possible redistribution reactions. As stated above, reaction with one equivalent yielded quantitative formation of $Ti(N_2{}^{Ts}N^{Ph})(O^iPr)_2$ (**13**). However, with three equivalents of $Ti(NMe_2)_2(O^iPr)_2$ it was possible to synthesise $Ti(N_2{}^{Ts}N^{Ph})(O^iPr)(NMe_2)$ (**18**). This is explained as the consequence of a presumed redistribution reaction of the initially formed $Ti(N_2{}^{Ts}N^{Ph})(O^iPr)_2$ with $Ti(NMe_2)_2(O^iPr)_2$ to give $Ti(N_2{}^{Ts}N^{Ph})(O^iPr)(NMe_2)$ (**18**) alongside $Ti(NMe_2)(O^iPr)_3$. It was also possible to synthesise **18** through the redistribution reaction for $Ti(N_2{}^{Ts}N^{Ph})(NMe_2)_2$ (**12**) and $Ti(N_2{}^{Ts}N^{Ph})(O^iPr)_2$ (**13**) on the NMR tube scale (Scheme 3.2) although this reaction is slow, requiring heating for 4 days at 353 K in benzene solution to achieve completion.

Scheme 3.2. Synthesis of $Ti(N_2{}^{Ts}N^{Ph})(O^iPr)(NMe_2)$ (**18**)



Complex $Ti(N_2{}^{Ts}N^{Ph})(O^iPr)(NMe_2)$ (**18**) was prepared on the preparative scale in 74% yield by reaction of $H_2N_2{}^{Ts}N^{Ph}$ (**9**) with three equivalents of $Ti(O^iPr)_2(NMe_2)_2$ for 16 hours at ambient temperature. The solid state structure was determined (Section 3.6) and confirmed the structure given in Scheme 3.2. The ambient temperature ^1H NMR spectrum is broad, indicative of exchange reactions also observed with the other complexes bearing this ligand (**12** and **13**). Cooling the samples to 240 K in CD_2Cl_2 gave four diastereotopic backbone proton resonances and equivalent tosyl substituents, as expected for a C_s symmetric approximately trigonal bipyramidal structure in solution and consistent with both the solid state structure and that given in Scheme 3.2.

It was also possible to synthesise $Ti(N_2{}^{Ts}N^{Ph})Cl_2$ (**19**) by reaction of two equivalents of Me_3SiCl with $Ti(N_2{}^{Ts}N^{Ph})(NMe_2)_2$ (**12**) at ambient temperature over 48 hours (Equation 3.3). The solid state structure has been determined and is consistent with the structure proposed in Equation 3.3. The NMR is consistent with the other species synthesised utilising this ligand (namely **12**, **13** and **18**) with the low temperature NMR (260 K) being indicative of a C_s symmetric species.



19

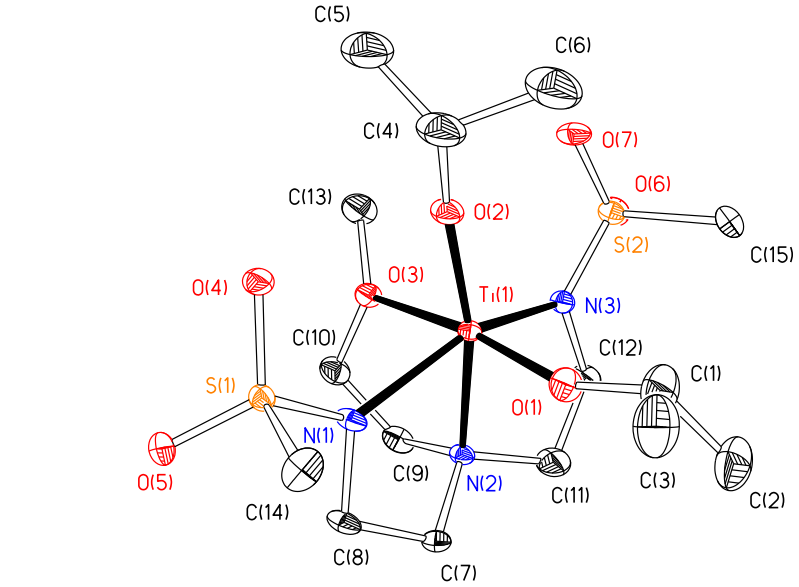
Equation 3.3.

To allow the comparison of 4-, 5- and 6-coordinate titanium sulfonamide complexes the known complexes Ti(CyN_2^{Ts})(O^iPr)$_2$ (**3.4**) and Ti($CyN_2^{SO_2Mes}$)(O^iPr)$_2$ (**3.5**) were synthesised. These complexes contain a (*rac*)-*trans*-cyclohexadiamine backbone and were synthesised according to literature methods in moderate to high yield.[24]

3.6 Solid state structures of titanium complexes 12, 17, 18 and 19

In total the X-ray structures of four titanium complexes, namely **12, 17, 18** and **19**, have been determined. The molecular structures are shown in Figure 3.6 and 3.7, selected distances and angles are listed in Tables 3.5 – 3.8.

Figure 3.6. Top: displacement ellipsoid plots of Ti($N_2^{Ms}N^{OMe}$)(O^iPr)$_2$ (**17**) and bottom: Ti($N_2^{Ts}N^{Ph}$)(NMe_2)$_2$ (**12**), C-bound H atoms omitted for clarity. Ellipsoids are drawn at the 20% probability level.



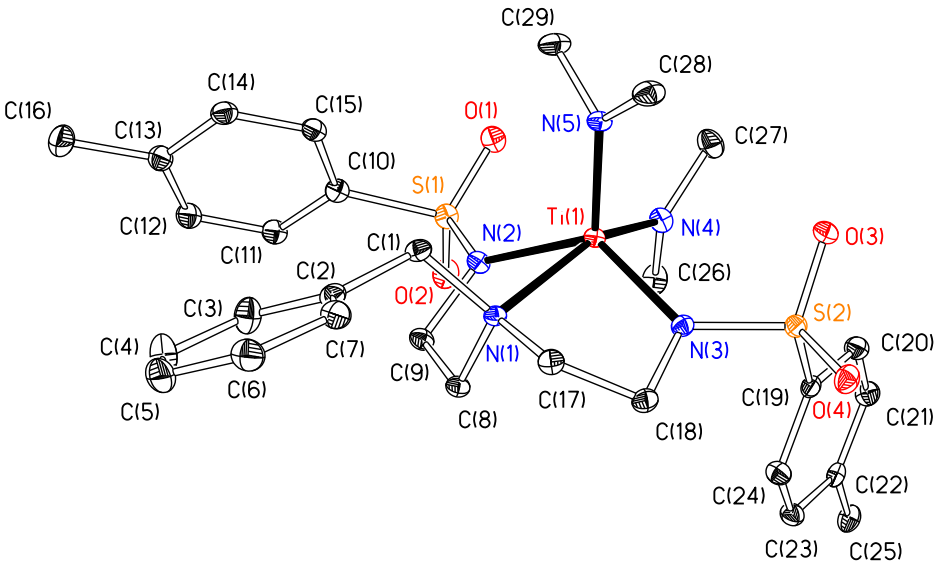


Figure 3.7. Top: displacement ellipsoid plots of Ti($N_2^{Ts}N^{Ph}$)(O^iPr)(NMe_2) (**18**) and bottom: Ti($N_2^{Ts}N^{Ph}$)Cl_2 (**19**), C-bound H atoms omitted for clarity. Ellipsoids are drawn at the 20% probability level.

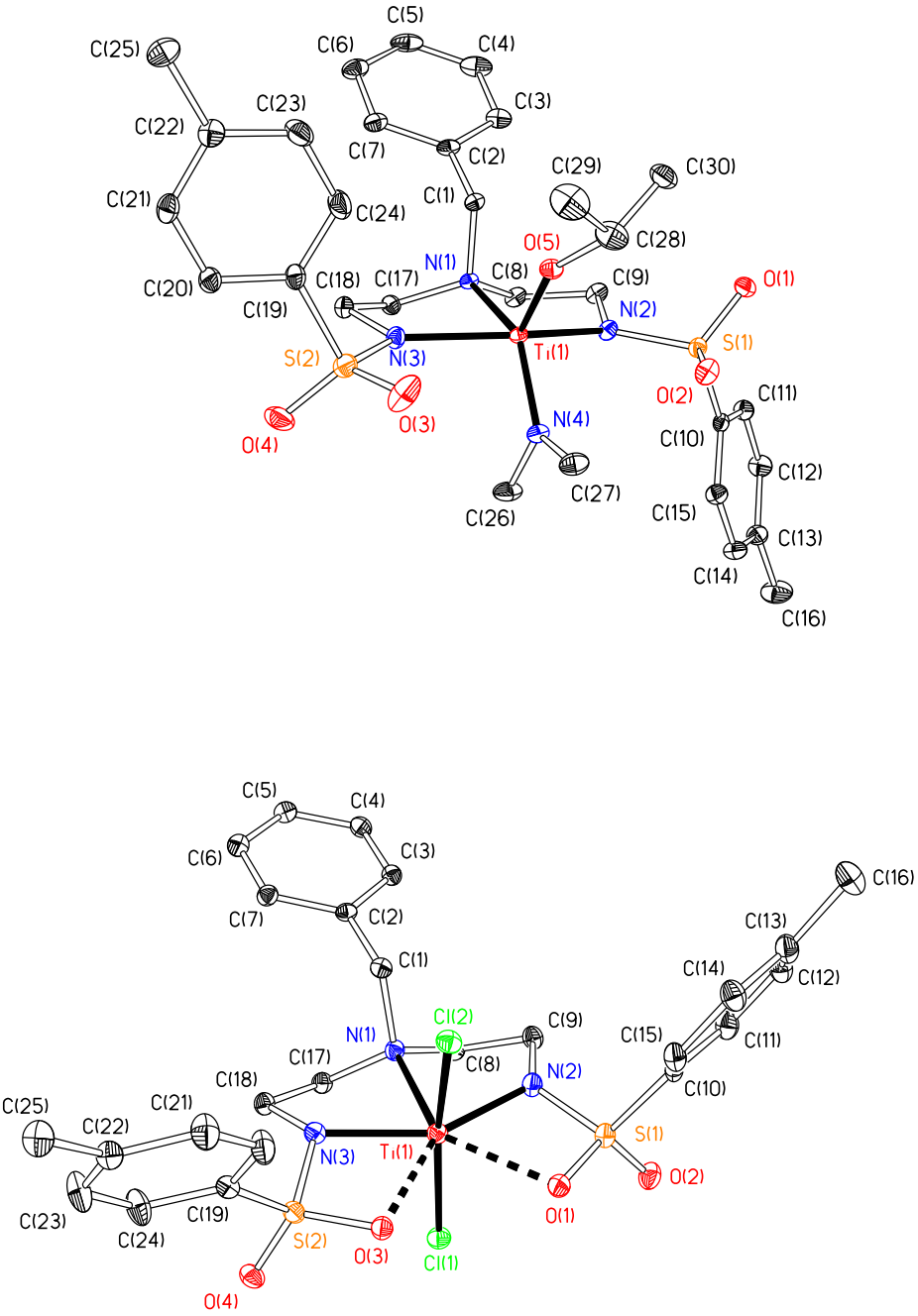


Table 3.5. Selected bond distances (Å) and angles (°) for $Ti(N_2{}^{Ms}N^{OMe})(O^iPr)_2$ (**17**).

Ti(1)-N(1)	2.103(5)	Ti(1)-N(2)	2.248(4)
Ti(1)-N(3)	2.096(5)	Ti(1)-O(1)	1.778(4)
Ti(1)-O(2)	1.762(4)	Ti(1)-O(3)	2.271(4)
N(1)-Ti(1)-N(2)	75.4(2)	N(1)-Ti(1)-N(3)	151.1(2)
N(2)-Ti(1)-N(3)	76.2(2)	N(1)-Ti(1)-O(1)	94.2(2)
N(2)-Ti(1)-O(1)	94.5(2)	N(3)-Ti(1)-O(1)	93.2(2)
N(1)-Ti(1)-O(2)	102.0(2)	N(2)-Ti(1)-O(2)	163.0(2)
N(3)-Ti(1)-O(2)	103.6(2)	O(1)-Ti(1)-O(2)	102.6(2)
N(1)-Ti(1)-O(3)	84.9(2)	N(2)-Ti(1)-O(3)	74.3(2)
N(3)-Ti(1)-O(3)	82.4(2)	O(1)-Ti(1)-O(3)	168.6(2)
O(2)-Ti(1)-O(3)	88.7(2)		

Table 3.6. Selected bond distances (Å) and angles (°) for $Ti(N_2{}^{Ts}N^{Ph})(NMe_2)_2$ (**12**).

Ti(1)-N(1)	2.278(2)	Ti(1)-N(2)	2.081(2)
Ti(1)-N(3)	2.041(2)	Ti(1)-N(4)	1.889(2)
Ti(1)-N(5)	1.878(2)	S(1)-O(1)	1.439(2)
S(1)-O(2)	1.441(2)	S(2)-O(3)	1.435(2)
S(2)-O(4)	1.444(2)		
N(1)-Ti(1)-N(2)	73.4(1)	N(1)-Ti(1)-N(3)	76.4(1)
N(2)-Ti(1)-N(3)	131.0(1)	N(1)-Ti(1)-N(4)	156.4(1)
N(2)-Ti(1)-N(4)	93.1(1)	N(3)-Ti(1)-N(4)	100.0(1)
N(1)-Ti(1)-N(5)	99.4(1)	N(2)-Ti(1)-N(5)	115.2(1)
N(3)-Ti(1)-N(5)	107.1(1)	N(4)-Ti(1)-N(5)	103.9(1)

Table 3.7. Selected bond distances (Å) and angles (°) for $Ti(N_2{}^{Ts}N^{Ph})(O^iPr)(NMe_2)$ (**18**).

Ti(1)-N(1)	2.267(2)	Ti(1)-N(2)	2.086(2)
Ti(1)-N(3)	2.073(2)	Ti(1)-N(4)	1.855(2)
Ti(1)-O(5)	1.766(2)	S(1)-O(1)	1.444(2)
S(1)-O(2)	1.4375(18)	S(2)-O(3)	1.440(2)
S(2)-O(4)	1.437(2)		
N(1)-Ti(1)-N(2)	74.1(1)	N(1)-Ti(1)-N(3)	73.9(1)
N(2)-Ti(1)-N(3)	144.9(1)	N(1)-Ti(1)-N(4)	139.5 (1)
N(2)-Ti(1)-N(4)	98.57(8)	N(3)-Ti(1)-N(4)	96.37(9)
N(1)-Ti(1)-O(5)	114.6(1)	N(2)-Ti(1)-O(5)	103.4(1)
N(3)-Ti(1)-O(5)	102.8(1)	N(4)-Ti(1)-O(5)	105.8(1)

Table 3.8. Selected bond distances (Å) and angles (°) for $Ti(N_2{}^{Ts}N^{Ph})Cl_2$ (**19**).

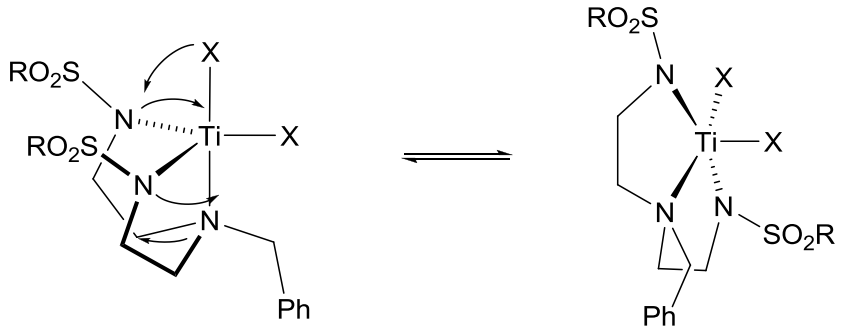
Ti(1)-N(1)	2.285(3)	Ti(1)-N(2)	1.994(3)
Ti(1)-N(3)	1.999(3)	Ti(1)-O(1)	2.231(2)
Ti(1)-O(3)	2.182(2)	Ti(1)-Cl(1)	2.379(1)
Ti(1)-Cl(2)	2.3228(11)	S(1)-O(1)	1.478(3)
S(1)-O(2)	1.432(3)	S(1)-C(10)	1.752(4)
S(2)-O(3)	1.484(2)	S(2)-O(4)	1.431(3)
S(2)-C(19)	1.758(4)		
N(1)-Ti(1)-N(2)	71.6(1)	N(1)-Ti(1)-N(3)	71.4(1)
N(2)-Ti(1)-N(3)	143.0(1)	N(1)-Ti(1)-Cl(1)	89.78(9)
N(2)-Ti(1)-Cl(1)	90.10(9)	N(3)-Ti(1)-Cl(1)	90.89(9)
O(1)-Ti(1)-Cl(1)	84.76(7)	O(3)-Ti(1)-Cl(1)	84.37(7)
N(1)-Ti(1)-Cl(2)	102.1(1)	N(2)-Ti(1)-Cl(2)	92.34(9)
N(3)-Ti(1)-Cl(2)	94.15(9)	Cl(1)-Ti(1)-Cl(2)	168.1(1)

$Ti(N_2{}^{Ms}N^{OMe})(O^iPr)_2$ (**17**) is isostructural with the tosyl analogue $Ti(N_2{}^{Ts}N^{OMe})(O^iPr)_2$ (**5**) and the zirconium homologue from Chapter 2, displaying a pseudo-octahedral complex with approximately C_s molecular symmetry and *trans* sulfonamide groups (Figure 3.6), consistent with the NMR spectrum discussed above. As observed with the tosyl analogue there is no sulfone oxygen to metal interaction, as had also been previously seen with complexes containing bi- and tri-dentate bis(sulfonamide) ligands.[20,24-27] The average Ti-N_{Ts} distance in **17** (av. 2.100 Å, 2.096(5) and 2.103(5) Å) is the same within error as in the octahedral titanium sulfonamide complexes structurally characterised in Chapter 2 (**1** – **3** and **5**) (av. 2.096 Å, range 2.069(5) – 2.129(2) Å). Indeed all the metric parameters of $Ti(N_2{}^{Ms}N^{OMe})(O^iPr)_2$ (**17**) are very similar to the tosyl analogue $Ti(N_2{}^{Ts}N^{OMe})(O^iPr)_2$ (**5**). For example, the average Ti-O^iPr distances for **17** and **5** are both 1.77 Å. Therefore, it is likely that any differences in the polymerisation capacity will be a consequence of reduced steric bulk associated with the mesyl groups rather than the tosyl groups.

The molecular structures of complexes $Ti(N_2{}^{Ts}N^{Ph})(NMe_2)_2$ (**12**), $Ti(N_2{}^{Ts}N^{Ph})(O^iPr)(NMe_2)$ (**18**) and $Ti(N_2{}^{Ts}N^{Ph})Cl_2$ (**19**), all bearing the same sulfonamide ligand, show an interesting progression from a highly distorted trigonal bipyramid to a 7-coordinate structure based on a pentagonal bipyramid, depending on the co-ligands employed (Figure 3.6 and 3.7). **12** and **18** possess very similar structures with a distorted trigonal bipyramidal titanium centre. The overall geometries are comparable, as are the angles around titanium (for **12** range 73.38(7) - 115.17(9), av. 96.1°; for **18** range 73.90(8) – 114.61(8)°, av. 96.2°). The titanium centre is significantly distorted away from an ideal trigonal bipyramidal geometry towards a square-based pyramid as is displayed by the similar bond angles of the four equatorial groups and the axial group (av. 106.4°, range 99.44(8) - 115.17(9)) and the angles between the equatorial groups (av. 85.71°, range 73.38(7) - 99.97(9)) for **12**. However, the angle between the two sulfonamide amides (130.98(8)° for **12** and 144.85(8)° for **18**) are closer to the 120° expected for a trigonal bipyramid rather than the 180° for a square based pyramid. It is evident from the ^{1}H NMR data that these species are extremely fluxional; it is therefore presumed that both trigonal bipyramidal and square based pyramidal structures are in equilibrium in solution. This would be expected for the first stages of Berry pseudo-rotation, although full interconversion between axial and equatorial groups would require inversion of the bound neutral amine, which is

not possible without breaking the bond, rearrangement and subsequent re-coordination (Figure 3.8).

Figure 3.8. Structural interconversions in 5-coordinate sulfonamide species.



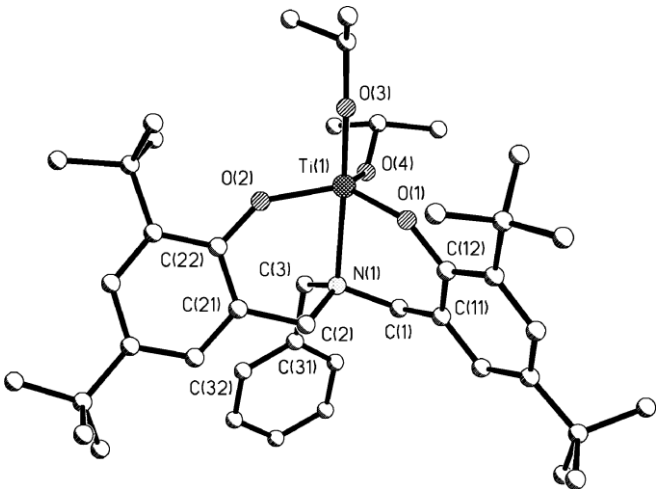
$Ti(N_2^{Ts}N^{Ph})Cl_2$ (**19**) possesses a seven-coordinate pseudo pentagonal bipyramidal titanium centre with the coordination of two $\kappa^2(N,O)$ bound sulfonamide groups completing the coordination sphere. A similar arrangement was observed in zirconium dimethylamide complexes supported by bidentate bis(sulfonamide) ligands (**1.45**, Figure 3.16) where the additional donor site is occupied by a $NHMe_2$ ligand.[25] The increased Lewis acidity of the titanium centre facillitated by the electronegative chloride ligands and the poorer π-donor ability, in conjunction with the smaller steric profile of chloride ligands when compared to dimethylamide donors in **12** presumably encourages $\kappa^2(N,O)$ sulfonamide bonding. As expected, the S-O distance for the bridging sulfonamide oxygen is on average 0.050 Å longer than the terminal S-O bond, a difference which is similar to that observed for $\kappa^2(N,O)$ sulfonamide bonding in $Zr(N_2^{Ts}N^{py})(O^iPr)_2$ (**4**, 0.051 Å). However, the fluxional solution phase NMR spectra mentioned above for **12**, **17** and **18** imply that several more complicated geometries may be accessible in solution containing $\kappa^2(N,O)$ sulfonamide bonding.

Complex $Ti(N_2^{Ts}N^{Ph})(NMe_2)_2$ (**12**) has a slightly shorter Ti-N_{Ts} bond length than $Ti(N_2^{Ts}N^{Ph})(O^iPr)(NMe_2)$ (**18**) (av. 2.061 vs. 2.080 Å, 2.041(2) and 2.081(2) Å for **12**; 2.086(2) and 2.073(2) Å for **18**), and as expected both of these 5-coordinate complexes feature slightly shorter Ti-N_{Ts} distances (av. 2.070 Å, range 2.041(2) – 2.086(2) Å) than the 6-coordinate octahedral titanium complexes investigated in Chapter 2 (av. 2.096 Å, range 2.069(5) – 2.129(2) Å). The Ti-N_{Ts} distances for the chloride complex $Ti(N_2^{Ts}N^{Ph})Cl_2$ (**19**) are shorter (av. 1.996 Å, 1.994(3) and 1.999(3) Å) than those observed for all other Group 4 sulfonamide complexes in this series.

For complex Ti($N_2^{Ts}N^{Ph}$)(O^iPr)(NMe_2) (**18**) the Ti-NMe_2 distance is shorter (1.855(2) Å) than in Ti($N_2^{Ts}N^{Ph}$)(NMe_2)$_2$ (**12**) (av. 1.883 Å, 1.877(2) and 1.889(2) Å), consistent with reduced competition for $2p_\pi$-$3d_\pi$ bonding interactions between NMe_2 and O^iPr ligands.

The most closely related five-coordinate bis(phenolate)-supported bis(isopropoxide) complex was reported by Davidson and is displayed in Figure 3.9.[1] This complex features a trigonal bipyramidal structure with *fac* coordination of the tridentate ligand. As had been observed for the 6-coordinate complexes, the Ti-O^iPr bond is slightly shorter in the case of the sulfonamide complex (1.766(2) Å) than in the phenolate complex (av. 1.790 Å, 1.781(1) and 1.800(1) Å).

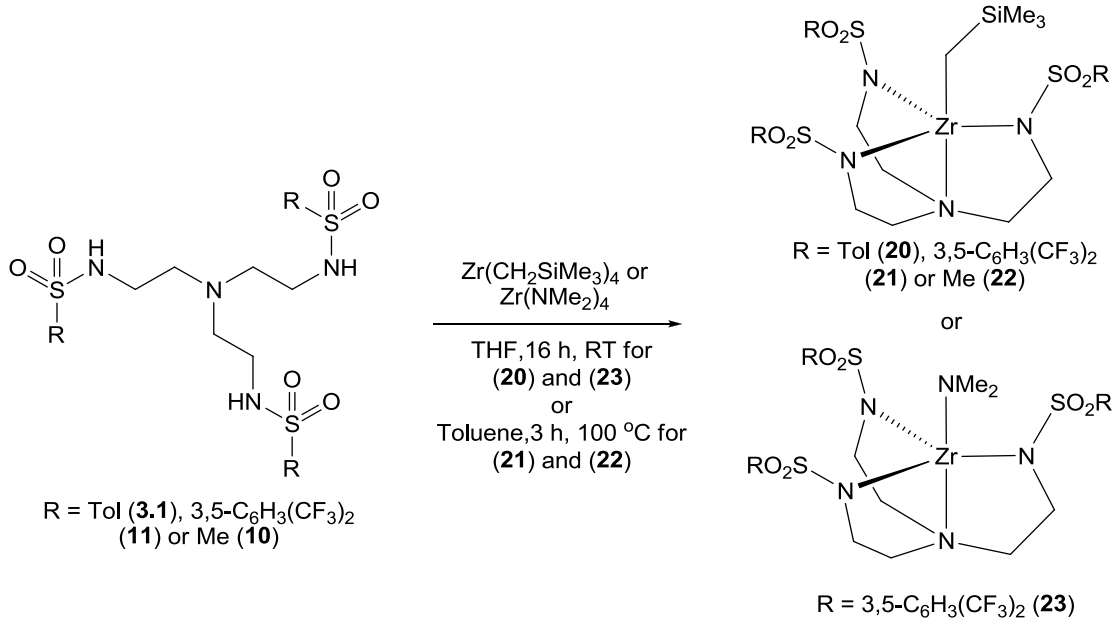
Figure 3.9. Previously reported five-coordinate bis(phenolate)-supported bis(isopropoxide) complex.[1]



3.7 Synthesis of zirconium complexes supported by C_3 symmetric sulfonamide ligands

No reaction was observed between Zr(O^iPr)$_4$.HO^iPr or Ti(O^iPr)$_4$ and the protio-ligands **3.1**, **10** and **11**, even when using large excesses of Ti(O^iPr)$_4$ or Zr(O^iPr)$_4$·HO^iPr and extended reaction times. The reaction did not proceed even under melt conditions and a dynamic vacuum as employed during the syntheses of Ti($N_2^{Ts}N^{OMe}$)(O^iPr)$_2$ (**5**) and Zr($N_2^{Ts}N^{OMe}$)(O^iPr)$_2$ (**6**) (Chapter 2). Reaction of the tris(sulfonamide) protio-ligands **3.1**, **10** and **11** with Ti(NMe_2)$_4$ led to complicated product mixtures from which no single product could be identified, so instead reactions were attempted with the zirconium amide (Zr(NMe_2)$_4$) and zirconium alkyl (Zr(CH_2SiMe_3)$_4$) starting materials.

Scheme 3.3. Synthesis of the new complexes **20** - **23**.



Protonolysis reaction between one equivalent of $Zr(CH_2SiMe_3)_4$ and the tris(sulfonamide) protio-ligands **3.1**, **10** and **11**, gave the corresponding zirconium alkyl complexes $Zr(N_3^{Ts}N)(CH_2SiMe_3)$ (**20**), $Zr(N_3^{TArF}N)(CH_2SiMe_3)$ (**21**) and $Zr(N_3^{Ms}N)(CH_2SiMe_3)$ (**22**), respectively, in good to excellent yield (60 – 89%) after recrystallisation. When followed in C_6D_6 on the NMR tube scale the yields were effectively quantitative and the expected $SiMe_4$ side product was observed.

Likewise, reaction of one equivalent of $Zr(NMe_2)_4$ with $H_3N_3^{TArF}N$ (**11**), gave the corresponding zirconium amide complex $Zr(N_3^{TArF}N)(NMe_2)$ (**23**), in excellent yield (82%) after recrystallisation. Reaction of tris(sulfonamide) protio-ligands **3.1**, **10** and **11** with $Zr(NMe_2)_4$ on the NMR tube scale in CD_2Cl_2 showed the formation of products and the expected $HNMe_2$ side product. However, scale up of the reactions met with difficulties associated with simultaneous synthesis of oxo-bridged dimers from adventitious water present in the solvent. The highly sensitive nature of these amides is further highlighted in Equation 3.4, where washing the initially formed amide with hexane, pentane or diethyl ether yielded the oxo-bridged dimer **24**. All solution NMR samples of pure $Zr(N_3^{TArF}N)(NMe_2)$ (**23**) (recrystallised, X-ray structure and accurate elemental analysis) were contaminated by the oxo species from reaction with residual H_2O present in solution, despite the samples being prepared in a nitrogen atmosphere glove box and the NMR solvent being rigorously dried and distilled (see Chapter 5 for further details). Different concentrations of

$Zr(N_3^{TArF}N)(NMe_2)$ (**23**) produced different concentrations of the oxo-dimer, as expected for reaction with residual H_2O in the solvent, for example dissolving 10 mg in 0.20 ml of C_6D_6 gave *ca*. 5% of the oxo species (Figure 3.10). If this mixture was then diluted further by taking 0.01 ml of the solution and dissolving in 0.20 ml of fresh C_6D_6 effectively quantitative formation of $\{Zr(N_3^{TArF}N)\}_2(\mu\text{-O})$ (**24**) was observed (Figure 3.11). Bulk synthesis of $\{Zr(N_3^{TArF}N)\}_2(\mu\text{-O})$ (**24**) was performed by washing $Zr(N_3^{TArF}N)(NMe_2)$ (**23**) with diethyl ether at room temperature, Equation 3.4. No other compound synthesised in this Thesis undergoes reactions with trace water present in the reaction solvent.

Figure 3.10. ^{1}H NMR spectrum (299.9 MHz) of $Zr(N_3^{TArF}N)(NMe_2)$ (**23**) featuring contamination with $\{Zr(N_3^{TArF}N)\}_2(\mu\text{-O})$ (**24**) (denoted as *) in C_6D_6 at 298 K. ('s' denotes residual protio-solvent).

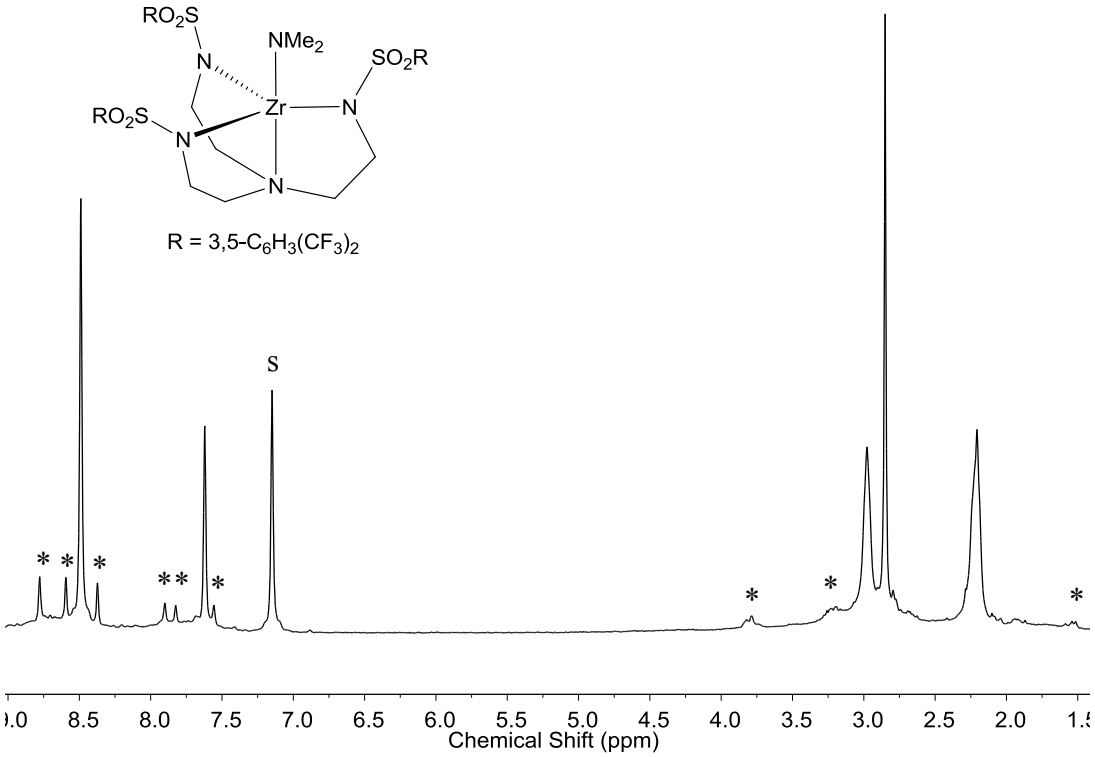
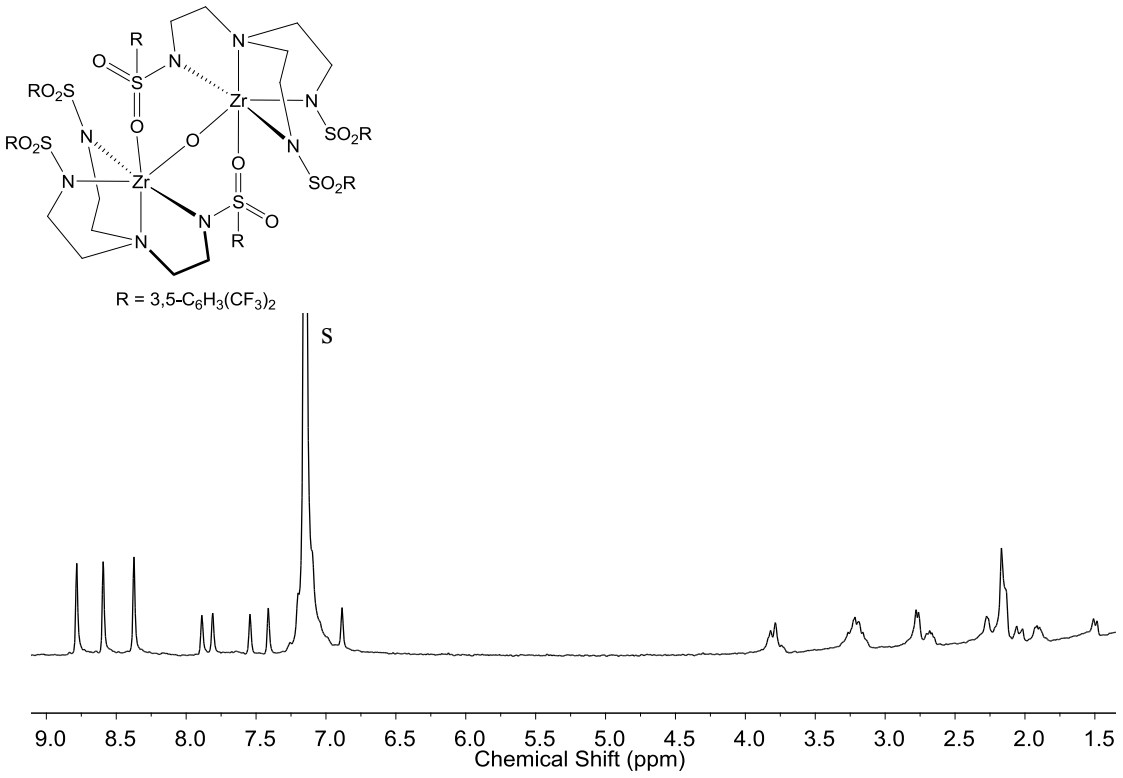
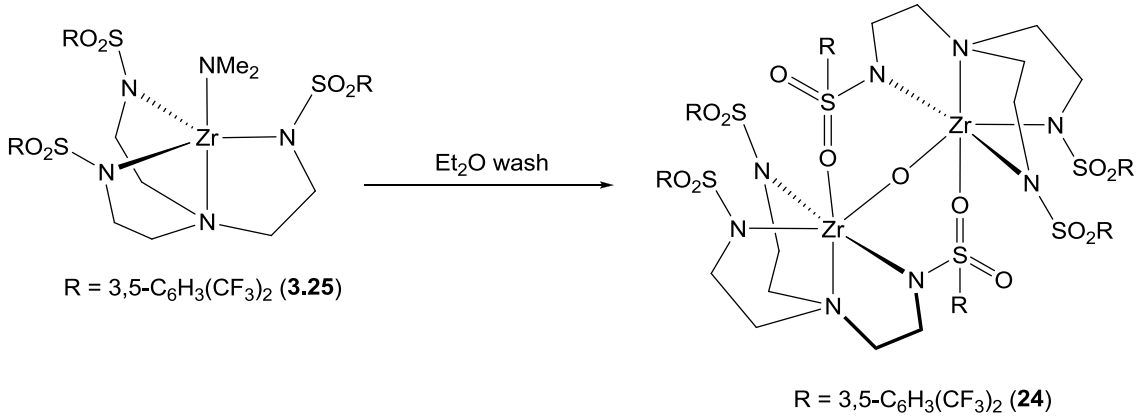


Figure 3.11. ^{1}H NMR spectrum (299.9 MHz) of {Zr($N_3^{TArF}N$)}$_2$(μ-O) (**24**) (denoted as *) in C_6D_6 at 298 K ('s' denotes residual protio-solvent).



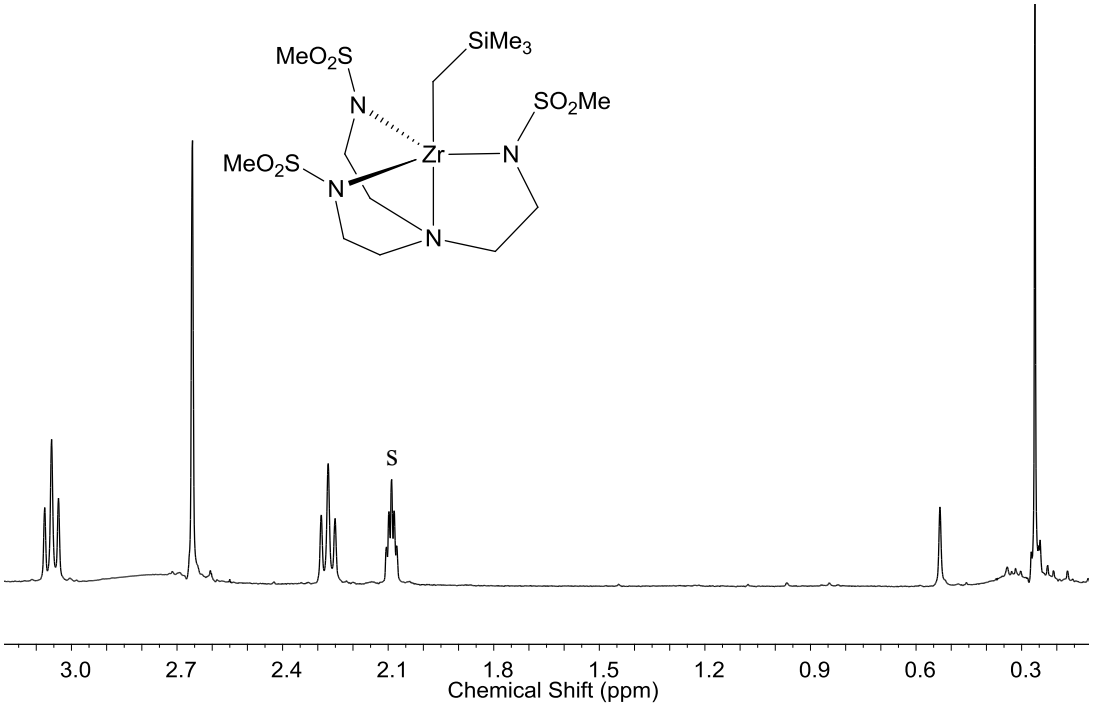


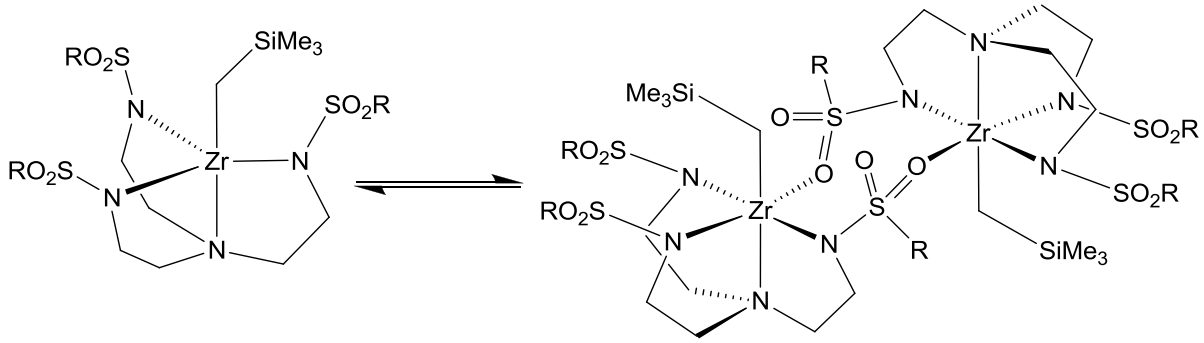
Equation 3.4.

The solid state structures of the alkyl complexes **20** and **21** as well as the amide complex **23** and the oxo-bridged dimer **24** have been determined. The alkyl complexes feature a dimeric structure whereas the amide is monomeric in the solid state, but all the structures feature multiple sulfone oxygen to zirconium interactions (either bridging or $\kappa^2(N,O)$ bound) which are likely to be highly fluxional in solution. Indeed the NMR spectra of the zirconium complexes **20** - **23** showed evidence of complex solution state dynamic behaviour implying that complicated geometries may be accessible in solution here as well. However, the high temperature NMR is indicative

of a time averaged C_3 symmetric species in solution (Figure 3.12) consistent with the structure proposed in Scheme 3.3. The low temperature NMR spectra of all the complexes **20** - **22** are indicative of highly complicated structures accessible in solution, such as dimer formation as is observed in the solid state structures of **20** and **21** (Equation 3.5).

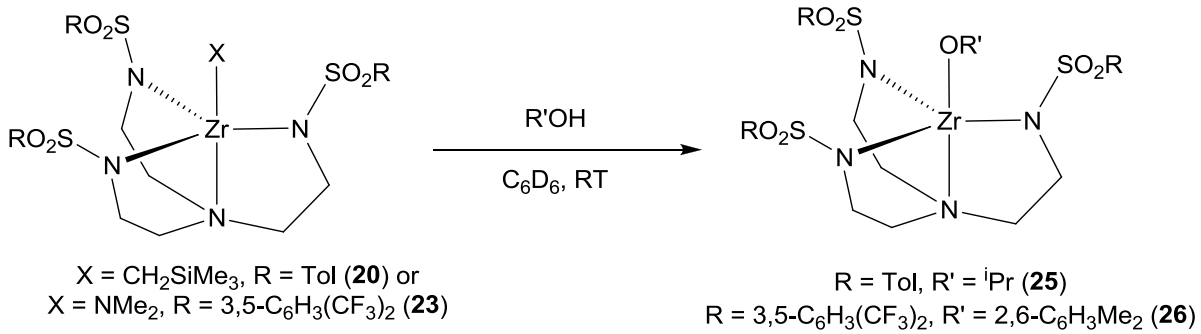
Figure 3.12. ^{1}H NMR spectrum (299.9 MHz) of **22** in d_8-toluene at 363 K. ('s' denotes residual protio-solvent).





Equation 3.5.

In contrast to the dynamic behaviour observed in the alkyl and amide complexes **20** - **23** the oxo-bridged dimer displays a NMR spectrum consistent with the structure proposed in Equation 3.4. The dimeric nature of the species in solution is confirmed by the inequivalent sulfonamide groups where three distinct resonances are observed in both the ^{1}H and ^{19}F NMR spectra (Equation 3.4).



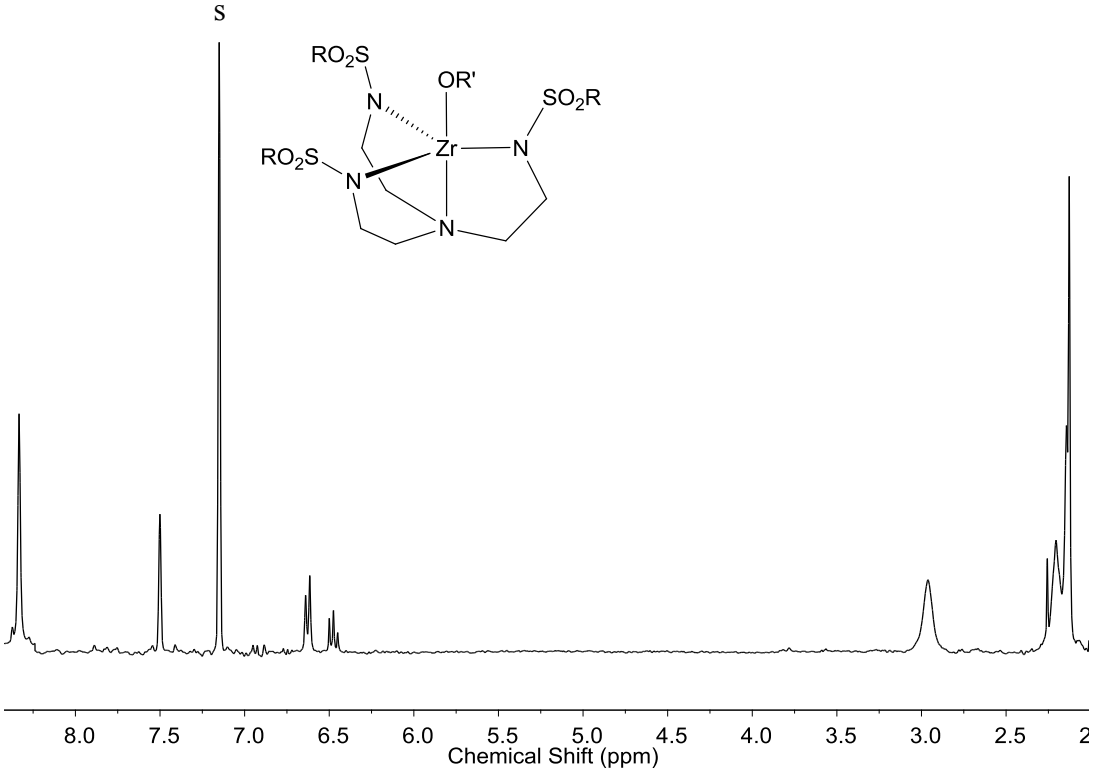
X = CH_2SiMe_3, R = Tol (**20**) or
X = NMe_2, R = 3,5-$C_6H_3(CF_3)_2$ (**23**)

R = Tol, R' = ^{i}Pr (**25**)
R = 3,5-$C_6H_3(CF_3)_2$, R' = 2,6-$C_6H_3Me_2$ (**26**)

Equation 3.6.

As described below in Section 3.9 and 3.10, the dimethylamide and alkyl compounds are relatively poor catalysts for the ROP of ε-CL and *rac*-lactide, so effort was focussed on the synthesis of alkoxide derivatives. For complexes supported by dianionic sulfonamide ligands of the type $H_2N_2^{SO_2R}N^X$ investigated in Chapters 2, 3 and 4 it was found that reaction of alkyl or amide complexes with alcohols such as HO^{i}Pr yielded competitive protonation of the sulfonamide ligand to give the homoleptic metal alkoxide and protio-ligand. However, for Zr(N_3^{Ts}N)(CH_2SiMe_3) (**20**), reaction with ^{i}PrOH on the NMR scale in C_6D_6 quantitatively yields the corresponding alkoxide species Zr(N_3^{Ts}N)(O^{i}Pr) (**25**). Likewise, reaction of one equivalent of ArOH with Zr(N_3^{TArF}N)(NMe_2) (**23**) on the NMR scale in C_6D_6 gave the aryloxide species Zr(N_3^{TArF}N)(OAr) (Ar = 2,6-$C_6H_3Me_2$) (**26**, Figure 3.13). Larger scale synthesis of these species proved troublesome because of oxo-bridged dimer contamination from adventitious water present in solution. Therefore, compounds utilised in ROP experiments were generated *in situ* prior to the polymerisation reactions.

Figure 3.13. ^{1}H NMR spectrum (299.9 MHz) of **26** in C_6D_6 at 298 K. ('s' denotes residual protio-solvent). R = 3,5-$C_6H_3(CF_3)_2$. R' = 2,6-$C_6H_3Me_2$.



3.8 Solid state structure of zirconium complexes 20, 21, 23 and 24

The solid state X-ray structures of four zirconium complexes **20**, **21**, **23** and **24** have been determined. The molecular structures are shown in Figures 3.14 and 3.17, with selected distances and angles listed in Tables 3.9 – 3.12.

Figure 3.14. Top: displacement ellipsoid plots of $[Zr(N_3{}^{Ts}N)(CH_2SiMe_3)]_2$ (**20**) and bottom: $[Zr(N_3{}^{TArF})(CH_2SiMe_3)]_2$ (**21**). C-bound H atoms, solvent of crystallisation and minor CF_3 disorder are omitted for clarity. Ellipsoids are drawn at the 25% probability level.

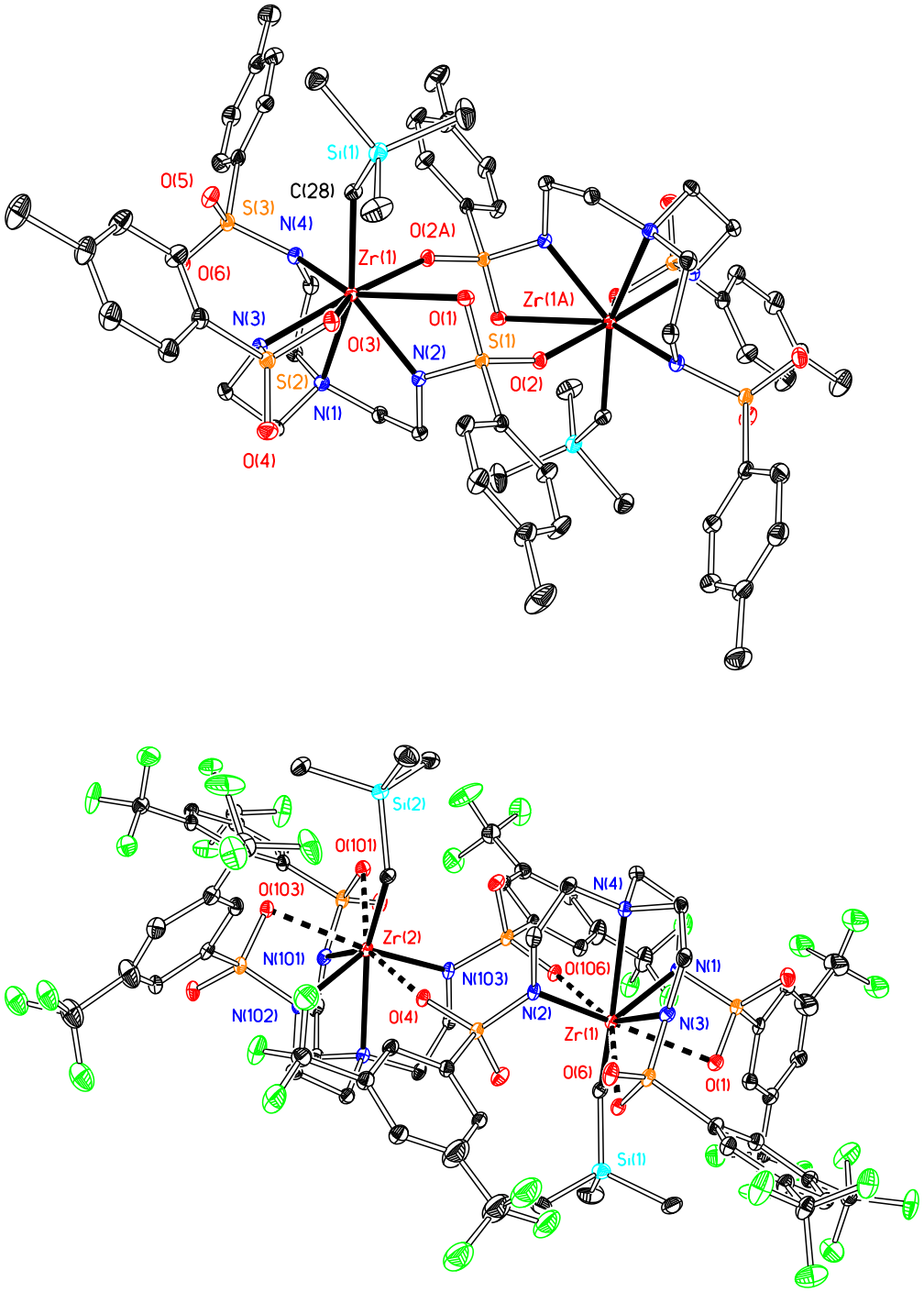


Table 3.9. Selected bond distances (Å) and angles (°) for $[Zr(N_3^{Ts}N)(CH_2SiMe_3)]_2$ (**20**).

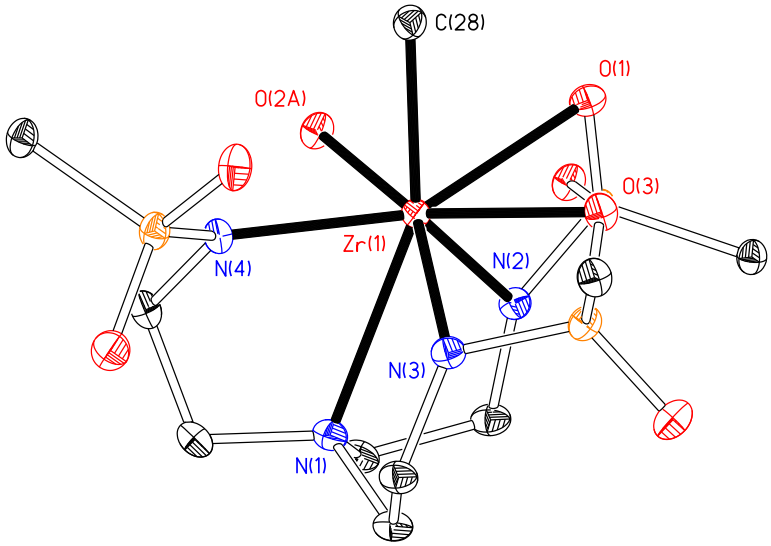
Zr(1)-O(2A)	2.272(2)	Zr(1)-N(1)	2.670(2)
Zr(1)-N(2)	2.232(2)	Zr(1)-N(3)	2.201(2)
Zr(1)-N(4)	2.238(2)	Zr(1)-O(1)	2.672(2)
Zr(1)-O(3)	2.292(2)	Zr(1)-C(28)	2.251(2)
S(1)-O(1)	1.452(2)	S(1)-O(2)	1.468(2)
S(1)-C(3)	1.755(2)	S(2)-O(3)	1.486(2)
S(2)-O(4)	1.4333(16)	S(2)-C(12)	1.765(2)
S(3)-O(5)	1.4396(18)	S(3)-O(6)	1.446(2)
O(2A) -Zr(1)-N(1)	89.93(6)	O(2A) -Zr(1)-N(2)	78.90(6)
N(1)-Zr(1)-N(2)	65.47(6)	O(2A) -Zr(1)-N(3)	154.9(1)
N(1)-Zr(1)-N(3)	67.01(7)	N(2)-Zr(1)-N(3)	99.02(7)
O(2A) -Zr(1)-N(4)	77.78(6)	N(1)-Zr(1)-N(4)	68.08(6)
N(2)-Zr(1)-N(4)	127.42(7)	N(3)-Zr(1)-N(4)	84.17(7)
O(2A) -Zr(1)-O(1)	73.60(6)	N(1)-Zr(1)-O(1)	121.7(1)
N(2)-Zr(1)-O(1)	56.69(6)	N(3)-Zr(1)-O(1)	126.3(1)
N(4)-Zr(1)-O(1)	149.4(1)	O(2A) -Zr(1)-O(3)	142.1(1)
N(1)-Zr(1)-O(3)	115.65(6)	N(2)-Zr(1)-O(3)	86.73(6)
N(3)-Zr(1)-O(3)	61.67(7)	N(4)-Zr(1)-O(3)	136.3(1)
O(2A) -Zr(1)-C(28)	85.35(8)	N(1)-Zr(1)-C(28)	156.7(1)
N(2)-Zr(1)-C(28)	135.2(1)	N(3)-Zr(1)-C(28)	111.7(1)
N(4)-Zr(1)-C(28)	88.64(7)	O(1)-Zr(1)-O(3)	69.23(5)
O(1)-Zr(1)-C(28)	78.69(7)	O(3)-Zr(1)-C(28)	80.57(7)
Zr(1)-N(2)-S(1)	107.62(9)	Zr(1)-N(2)-C(2)	130.6(1)
S(1)-N(2)-C(2)	119.9(1)	Zr(1)-N(3)-S(2)	100.6(9)
Zr(1)-N(3)-C(11)	127.8(1)	S(2)-N(3)-C(11)	121.9(2)
Zr(1)-N(4)-S(3)	129.8(1)	Zr(1)-N(4)-C(20)	113.9(1)
S(3)-N(4)-C(20)	112.14(14)		

Table 3.10. Selected bond distances (Å) and angles (°) for $[Zr(N_3^{TArF})(CH_2SiMe_3)]_2$ (**21**).

Zr(1)-O(1)	2.549(3)	Zr(1)-O(3)	2.762(4)
Zr(1)-O(5)	2.327(3)	Zr(1)-O(106)	2.262(3)
Zr(1)-N(1)	2.231(4)	Zr(1)-N(2)	2.252(4)
Zr(1)-N(3)	2.264(4)	Zr(1)-N(4)	2.623(4)
Zr(1)-C(1)	2.287(5)	Zr(2)-O(4)	2.277(3)
Zr(2)-O(101)	2.334(3)	Zr(2)-O(103)	2.458(3)
Zr(2)-N(101)	2.237(4)	Zr(2)-N(102)	2.217(4)
Zr(2)-N(103)	2.272(4)	Zr(2)-N(104)	2.578(4)
Zr(2)-C(101)	2.270(4)	S(1)-O(1)	1.459(3)
S(1)-O(2)	1.436(3)	S(2)-O(3)	1.446(3)
S(2)-O(4)	1.464(3)	S(3)-O(5)	1.487(3)
S(3)-O(6)	1.434(3)	S(101)-O(101)	1.483(3)
S(101)-O(102)	1.435(4)	S(102)-O(103)	1.467(3)
S(102)-O(104)	1.438(3)	S(103)-O(105)	1.439(3)
S(103)-O(106)	1.475(3)		
N(1)-Zr(1)-N(2)	130.6(1)	N(1)-Zr(1)-N(3)	92.3(1)
N(1)-Zr(1)-N(4)	65.5(1)	N(1)-Zr(1)-C(1)	94.3(2)
N(2)-Zr(1)-N(3)	82.2(1)	N(2)-Zr(1)-N(4)	67.5(1)
N(3)-Zr(1)-N(4)	66.5(1)	N(2)-Zr(1)-C(1)	123.1(2)
N(3)-Zr(1)-C(1)	136.2(2)	N(4)-Zr(1)-C(1)	152.4(2)
N(101)-Zr(2)-N(102)	94.0(1)	N(101)-Zr(2)-N(103)	84.2(1)
N(102)-Zr(2)-N(103)	133.3(1)	N(101)-Zr(2)-N(104)	67.8(1)
N(102)-Zr(2)-N(104)	66.2(1)	N(103)-Zr(2)-N(104)	70.1(1)
N(101)-Zr(2)-C(101)	138.4(2)	N(102)-Zr(2)-C(101)	103.0(2)
N(103)-Zr(2)-C(101)	109.0(2)	N(104)-Zr(2)-C(101)	153.7(2)

Both alkyl complexes **20** and **21** have approximately the same geometry, featuring eight coordinate zirconium centres with bridging sulfonamide groups. This similarity in geometry can be evidenced by the bond angles around the zirconium centre (av. 99.6° for **20**, range 56.69(6) – 156.71(7)° vs. av. 99.3° for **21**, range 54.6(1) – 154.4(1)°). The only major difference between the structures is that **20** features $\kappa^2(N,O)$ sulfonamide bonding of one terminal and one bridging sulfonamide, whereas **21** has $\kappa^2(N,O)$ sulfonamide bonding of both the terminal sulfonamides and not for the bridging group. The geometry around the zirconium centre is best described as a highly distorted square antiprism and Figure 3.15 provides a view of the coordination environment. The square faces are at an angle to each other instead of being parallel as expected for an ideal square antiprism.

Figure 3.15. Displacement ellipsoid plot of the metal coordination environment in $[Zr(N_3{}^{Ts}N)(CH_2SiMe_3)]_2$ (**20**). Ellipsoids are drawn at the 25% probability level.



The structures of **20** and **21** also bear a similarity to $Ti(N_2{}^{Ts}N^{Ph})Cl_2$ (**19**) and the previously reported zirconium complex bearing a bidentate sulfonamide ligand **1.45** (Figure 3.16) in that two of the sulfonamides, the amine and the alkyl form a five-membered plane. The arrangement resembles the equatorial plane in the pentagonal bipyramidal geometry of the previous two structures. The extra donor in the tren ligands takes up an axial position giving two bonds on one side of the plane described by the pentagon rather than one.

Figure 3.16. Previously reported zirconium sulfonamide complex (**1.45**).[25]

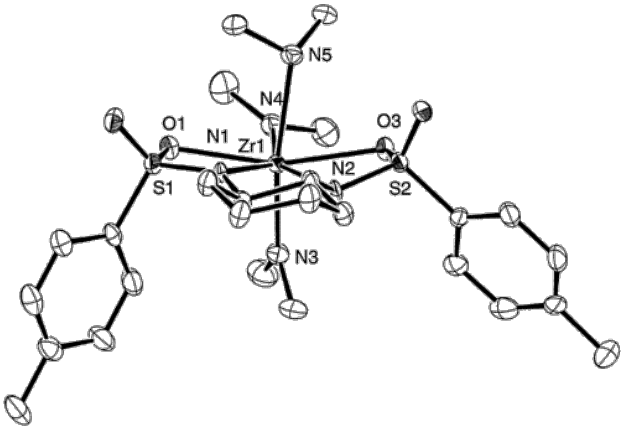


Figure 3.17. Top: displacement ellipsoid plots of $Zr(N_3^{TArF})(NMe_2)$ (**23**) and top: $\{Zr(N_3^{TArF}N)\}_2(\mu\text{-}O)$ (**24**). C-bound H atoms, solvent of crystallisation and minor CF_3 disorder are omitted for clarity. Ellipsoids are drawn at the 25% probability level.

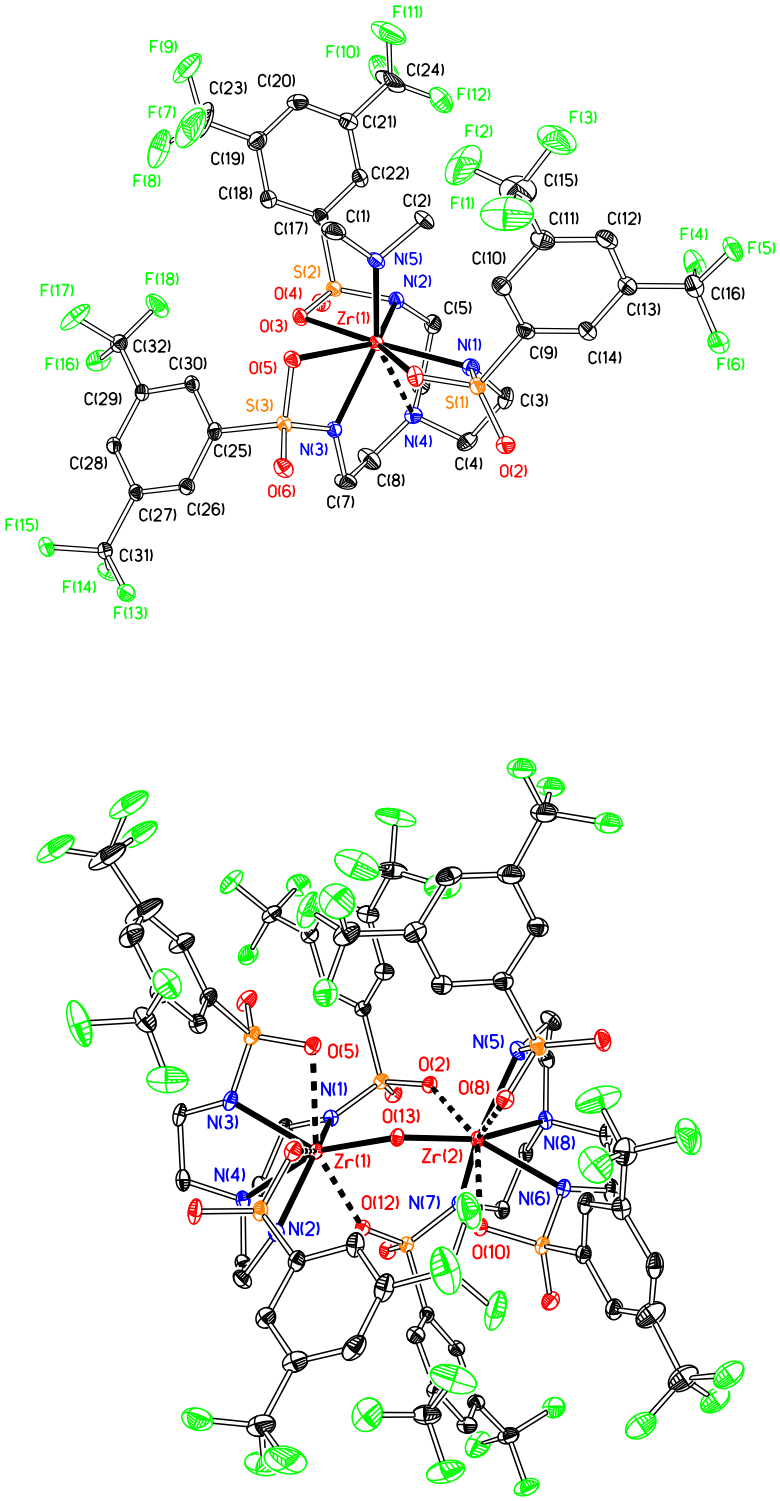


Table 3.11. Selected bond distances (Å) and angles (°) for $Zr(N_3^{TArF})(NMe_2)$ (**23**).

Zr(1)-N(1)	2.231(5)	Zr(1)-N(2)	2.280(5)
Zr(1)-N(3)	2.198(4)	Zr(1)-N(4)	2.725(4)
Zr(1)-N(5)	2.038(5)	Zr(1)-O(1)	2.471(4)
Zr(1)-O(3)	2.322(4)	Zr(1)-O(5)	2.365(4)
S(1)-O(1)	1.467(4)	S(1)-O(2)	1.441(4)
S(2)-O(3)	1.481(4)	S(2)-O(4)	1.437(4)
S(2)-C(17)	1.772(6)	S(3)-O(5)	1.482(4)
S(3)-O(6)	1.430(4)		
N(1)-Zr(1)-N(2)	90.1(2)	N(1)-Zr(1)-N(3)	101.4(2)
N(2)-Zr(1)-N(3)	119.9(2)	N(1)-Zr(1)-N(4)	66.7(2)
N(2)-Zr(1)-N(4)	66.4(2)	N(3)-Zr(1)-N(4)	65.2(2)
N(1)-Zr(1)-N(5)	100.7(2)	N(2)-Zr(1)-N(5)	88.3(2)
N(3)-Zr(1)-N(5)	143.7(2)	N(4)-Zr(1)-N(5)	150.9(2)
Zr(1)-N(1)-S(1)	101.9(2)	Zr(1)-N(1)-C(3)	127.3(4)
S(1)-N(1)-C(3)	119.3(4)	Zr(1)-N(2)-S(2)	96.3(2)
Zr(1)-N(2)-C(5)	124.6(4)	S(2)-N(2)-C(5)	117.8(4)
Zr(1)-N(3)-S(3)	102.4(2)	Zr(1)-N(3)-C(7)	132.7(4)
S(3)-N(3)-C(7)	124.8(4)	Zr(1)-N(5)-C(1)	131.3(4)
Zr(1)-N(5)-C(2)	119.2(4)	C(1)-N(5)-C(2)	109.5(5)

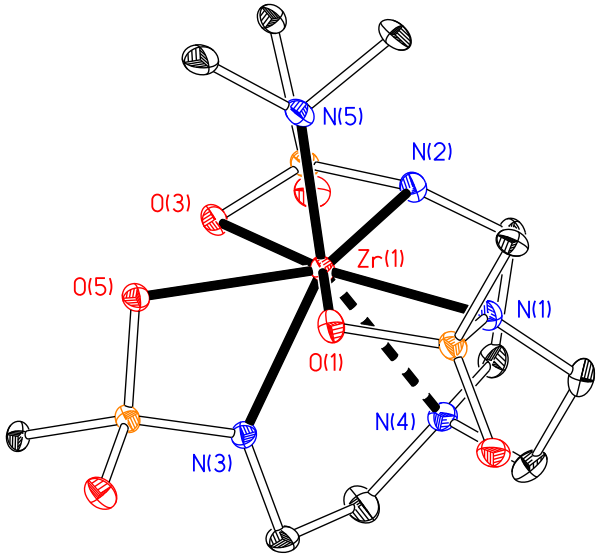
Table 3.12. Selected bond distances (Å) and angles (°) for $\{Zr(N_3^{TArF})\}_2O$ (**24**).

Zr(1)-N(1)	2.249(3)	Zr(1)-N(2)	2.221(4)
Zr(1)-N(3)	2.252(3)	Zr(1)-N(4)	2.510(4)
Zr(1)-O(3)	2.406(3)	Zr(1)-O(5)	2.421(3)
Zr(1)-O(12)	2.290(3)	Zr(1)-O(13)	1.934(3)
Zr(2)-N(5)	2.216(4)	Zr(2)-N(6)	2.256(3)
Zr(2)-N(7)	2.261(3)	Zr(2)-N(8)	2.500(3)
Zr(2)-O(2)	2.285(3)	Zr(2)-O(8)	2.387(3)
Zr(2)-O(10)	2.390(3)	Zr(2)-O(13)	1.951(3)
S(1)-O(1)	1.438(3)	S(1)-O(2)	1.456(3)
S(2)-O(3)	1.476(3)	S(2)-O(4)	1.437(3)
S(3)-O(5)	1.478(3)	S(3)-O(6)	1.436(3)
S(4)-O(7)	1.437(3)	S(4)-O(8)	1.472(3)
S(5)-O(9)	1.436(3)	S(5)-O(10)	1.477(3)
S(6)-O(11)	1.439(3)	S(6)-O(12)	1.462(3)
N(1)-Zr(1)-N(2)	137.2(1)	N(1)-Zr(1)-N(3)	85.0(1)
N(2)-Zr(1)-N(3)	95.3(1)	N(1)-Zr(1)-N(4)	73.7(1)
N(2)-Zr(1)-N(4)	67.1(1)	N(3)-Zr(1)-N(4)	67.6(1)
N(1)-Zr(1)-O(13)	94.3(1)	N(2)-Zr(1)-O(13)	112.1(1)
N(3)-Zr(1)-O(13)	138.2(1)	N(4)-Zr(1)-O(13)	151.7(1)
N(5)-Zr(2)-N(6)	94.3(1)	N(5)-Zr(2)-N(7)	136.8(1)
N(6)-Zr(2)-N(7)	86.1(1)	N(5)-Zr(2)-N(8)	67.6(1)
N(6)-Zr(2)-N(8)	68.88(12)	N(7)-Zr(2)-N(8)	72.5(1)
N(5)-Zr(2)-O(13)	109.97(13)	N(6)-Zr(2)-O(13)	138.3(1)
N(7)-Zr(2)-O(13)	97.23(12)	N(8)-Zr(2)-O(13)	151.5(1)
Zr(2)-O(13)-Zr(1)	141.76(15)		

The dimethylamido complex **23** possesses a monomeric eight coordinate zirconium atom with three $\kappa^2(N,O)$ sulfonamide bonds, based around a highly distorted square antiprism as had been observed for the alkyl analogues. However, the neutral tripodal

nitrogen to metal distance is relatively long when compared to the alkyl complexes **20** and **21,** indicative of a weak interaction (2.725(4) Å vs. av. 2.62 Å, range 2.578(4) – 2.670(2) Å). This suggests that the structure is described better in terms of a highly distorted pentagonal bipyramidal structure as has been observed for $Ti(N_2{}^{Ts}N^{Ph})Cl_2$ (**19**) and **1.45** (Figure 3.18).

Figure 3.18. Displacement ellipsoid plot of the metal coordination environment in $Zr(N_3{}^{TArF}N)(NMe_2)$ (**23**). Ellipsoids are drawn at the 25% probability level.



The oxo-bridged dimer **24** displays a dimeric eight coordinate zirconium complex with three $\kappa^2(N,O)$ sulfonamide bonds, based around a highly distorted square antiprism similar to that observed for the alkyl analogues.

Unexpectedly, some of the sulfonamide nitrogens in complex **23** deviate away from the planarity expected to maximize $2p_\pi$-$4d_\pi$ bonding interactions (all other Group 4 sulfonamide complexes reported to date contain planar sulfonamides). For instance, the sum of the angles around the nitrogens in the dimethylamide complex **23** are 339, 348, 360 and 360°, where for an ideal planar amide complex the angles add up to 360° and for a trigonal pyramid the add to 328°. The deviation away from planarity in the sulfonamide amides N(1) and N(2) is probably a result of competition for $2p_\pi$-$4d_\pi$ bonding orbitals. Supporting this, the sulfonamides that deviate from planar geometries are accompanied by longer metal to nitrogen distances, as would be expected for reduced π-bonding interactions (2.280(5) Å for N(2) (biggest deviation), 2.231(5) Å for N(1) (intermediate), and 2.198(4) Å for N(3) (planar nitrogen)). The

build up of electron density on the sulfonamide nitrogens could also help account for the extreme air and moisture sensitivity of this complex as compared to the alkyls.

This feature is most significant in the bis(dimethylamide) complex **23**, where it is reasonable to expect the greatest competition for $2p_{\pi}$-$4d_{\pi}$ bonding, but is also present in the alkyl and oxo complexes **20**, **21** and **24** (sum of the sulfonamide bond angles, range 350-360°). However, the bond distances do not show the expected variation with diminished planarity being very similar across all three complexes (av. 2.24 Å, range 2.201(2)-2.272(4) Å).

In general the Zr-N_{Ts} distances are slightly shorter than the Zr-N_{TArF} distances for the alkyl complexes (2.223 Å, range 2.201(2)-2.237(2) Å vs. 2.245 Å, range 2.217(4)-2.272(4) Å), showing that the electron withdrawing CF_3 groups have an influence on the sulfonamide bonding. As had been seen in Chapter 2, the $\kappa^2(N,O)$ bound sulfonamide groups feature longer bridging than terminal S-O distances (av. 0.040 Å, range 1.432(1)-1.487(3)), although this effect is less pronounced then had previously been observed (av. difference 0.05 Å).

3.9 Polymerisation studies: ROP of ε-caprolactone

The principal aim of this work of this Chapter was to evaluate the effect of structural variations of sulfonamide-supported Group 4 complexes on the catalytic ROP of ε-CL and *rac*-LA. The titanium amide and alkoxide complexes **12** - **18**, **3.4** and **3.5**, the zirconium alkyl and amide complexes **20** - **23**, as well as the corresponding *in situ* generated zirconium isopropoxide complexes were investigated. *In situ* generation of alkoxide catalysts from stable alkyl or bis(trimethylsilyl)amide intermediates has been widely employed in the literature.[28-36] Polymerisations were performed in toluene at 100 °C so as to allow direct comparison with the catalysts investigated in Chapter 2. The progress of each reaction was monitored by regular sampling and the results summarised in Table 3.13 correspond to the point at which the polymerisations eventually reached *ca*. 100% conversion. The molecular weights and PDIs were determined by GPC using the appropriate Mark-Houwink corrections[37-39] and the yield refers to the amount of poly(ε-CL) isolated. The M_n(calcd) values are those expected for two polymer chain growing per initiator group (i.e. one chain per M-NMe_2 or M-O^{i}Pr bond in the starting complex) at 100% conversion of monomer.

Table 3.13. Solution polymerisation of ε-CL by Ti($N_2^{Ts}N^{Ph}$)(NMe_2)$_2$ (**12**), Ti($N_2^{Ms}N^{Ph}$)(NMe_2)$_2$ (**14**), Ti($N_2^{Ms}N^{OMe}$)(NMe_2)$_2$ (**16**), Ti($N_2^{Ms}N^{Ph}$)(NMe_2)(O^iPr) (**18**), Ti($N_2^{Ts}N^{Ph}$)(O^iPr)$_2$ (**13**), Ti($N_2^{Ms}N^{Ph}$)(O^iPr)$_2$ (**15**), Ti($N_2^{Ms}N^{OMe}$)(O^iPr)$_2$ (**17**), Ti(CyN_2^{Ts})(O^iPr)$_2$ (**3.4**), Ti($CyN_2^{SO_2Mes}$)(O^iPr)$_2$ (**3.5**).[a]

Entry	Catalyst	Yield (%)[b]	Time (h)	$k_{app.}$ (min^{-1})	M_n (GPC)[c]	M_n (calcd)[d]	M_w/M_n
1	Ti($N_2^{Ts}N^{Ph}$)(NMe_2)$_2$ (**12**)	90	6	*e*	12,010	5,710	1.35
2	Ti($N_2^{Ms}N^{Ph}$)(NMe_2)$_2$ (**14**)	94	4	0.0053(3)	11,050	5,710	1.39
3	Ti($N_2^{Ms}N^{OMe}$)(NMe_2)$_2$ (**16**)	83	8	*e*	12,650	5,710	1.46
4	Ti($N_2^{Ms}N^{Ph}$)(NMe_2)(O^iPr) (**18**)	90	4	0.0130(4)	12,370	5,710	2.08
5	Ti($N_2^{Ts}N^{Ph}$)(O^iPr)$_2$ (**13**)	96	1.5	0.042(2)	6,370	5,710	1.73
6	Ti($N_2^{Ms}N^{Ph}$)(O^iPr)$_2$ (**15**)	94	0.5	0.105(8)	6,500	5,710	1.41
7	Ti($N_2^{Ms}N^{OMe}$)(O^iPr)$_2$ (**17**)	89	3	0.023(1)	7,390	5,710	1.57
8	Ti(CyN_2^{Ts})(O^iPr)$_2$ (**3.4**)	96	0.2	0.51(3)	5,080	5,710	1.28
9	Ti($CyN_2^{SO_2Mes}$)(O^iPr)$_2$ (**3.5**)	91	1	0.039(2)	12,640	5,710	1.87

[a] Conditions: [ε-CL]/[catalyst] = 100:1, 6.8 mL toluene at 100 °C. See Experimental section for other details. [b] Isolated yield at 100 % NMR conversion. [c] Molecular weights (g mol^{-1}) determined from GPC using the appropriate Mark-Houwink corrections. [d] Expected M_n (g mol^{-1}) for 2 chains growing per initiator at 100% conversion. [e] not determined.

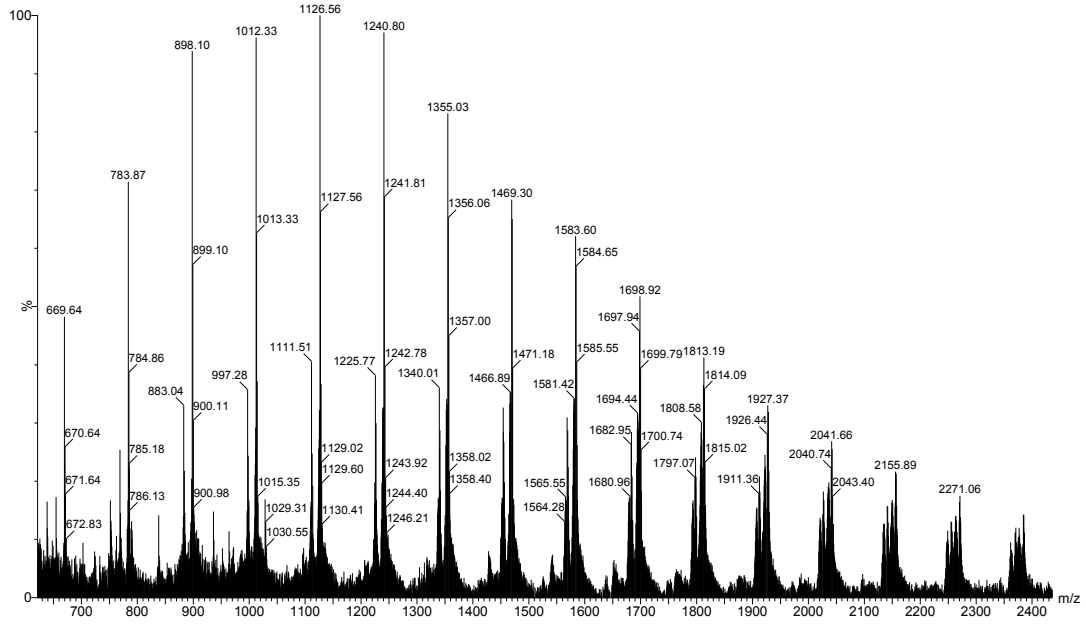
3.9.1 Polymerisation studies: ROP of ε-caprolactone, titanium catalysts

As expected of the titanium catalysts studied, the bis(dimethylamide) catalysts Ti($N_2^{SO_2R}N^{R'}$)(NMe_2)$_2$ (**12**, **14** and **16**) were the slowest of the nine evaluated (entries 1-3, Table 3.13). The GPC data are consistent with only one poly(ε-CL) chain forming per metal on average (M_n(GPC) av. = 11,900 g mol^{-1} *vs*. M_n(calcd) = 11,420 g mol^{-1}), in agreement with the 6-coordinate bis(dimethylamide) complexes studied in Chapter 2. The polymerisation is relatively well controlled with moderate PDIs (~1.4) and good agreement between M_n(calcd) and M_n(GPC), comparing favourably with the amide complexes investigated in Chapter 2 (**1** and **2**) where broad PDIs were observed (1.6-2.0) over longer reaction times. In order to evaluate further the polymerisation process and probe living characteristics, the most efficient catalyst in terms of activity and control (**14**) was monitored throughout the progress of polymerisation. The polymerisation shows a first order dependence on monomer concentration and a reasonably linear M_n(GPC) vs. % conversion (see the Appendix), both of which are characteristic of a living type process. There is also an induction period of around 60 minutes as has been seen previously[1,35,40] and as expected for slow initiation into the Ti-NMe_2 bond. The k_{app} is an order of magnitude slower than the closest bis(isopropoxide) catalyst and further highlights the unfavourable nature of insertion into the Ti-NMe_2 bond (entry 2 and 6, Table 3.13).

The 5-coordinate catalysts are more active than the 6-coordinate analogues. For example, Ti($N_2^{Ms}N^{Ph}$)(NMe_2)$_2$ (**14**) reaches 100% conversion after 4 hours, compared to Ti($N_2^{Ms}N^{OMe}$)(NMe_2)$_2$ (**16**) which requires 8 hours for the same degree of polymerisation. (Ti($N_2^{Ts}N^{Ph}$)(NMe_2)$_2$ (**12**) compared to Ti($N_2^{Ts}N^{py}$)(NMe_2)$_2$ (**1**) or Ti($N_2^{Ts}N^{OMe}$)(NMe_2)$_2$ (**2**) shows the same behaviour (Chapter 2)). There also appears to be a marked effect of the sulfone group for each ligand; those bearing a mesyl rather than tosyl group are more active (e.g. Ti($N_2^{Ts}N^{Ph}$)(NMe_2)$_2$ (**12**) *vs*. Ti($N_2^{Ms}N^{Ph}$)(NMe_2)$_2$ (**14**) or Ti($N_2^{Ts}N^{OMe}$)(NMe_2)$_2$ (**2**, Chapter 2) *vs*. Ti($N_2^{Ms}N^{OMe}$)(NMe_2)$_2$ (**16**)). These effects are interpreted in terms of easier access to the metal, centre since 6-coordinate species are more sterically congested than 5-coordinate ones and the tosly group is bulkier than mesyl.

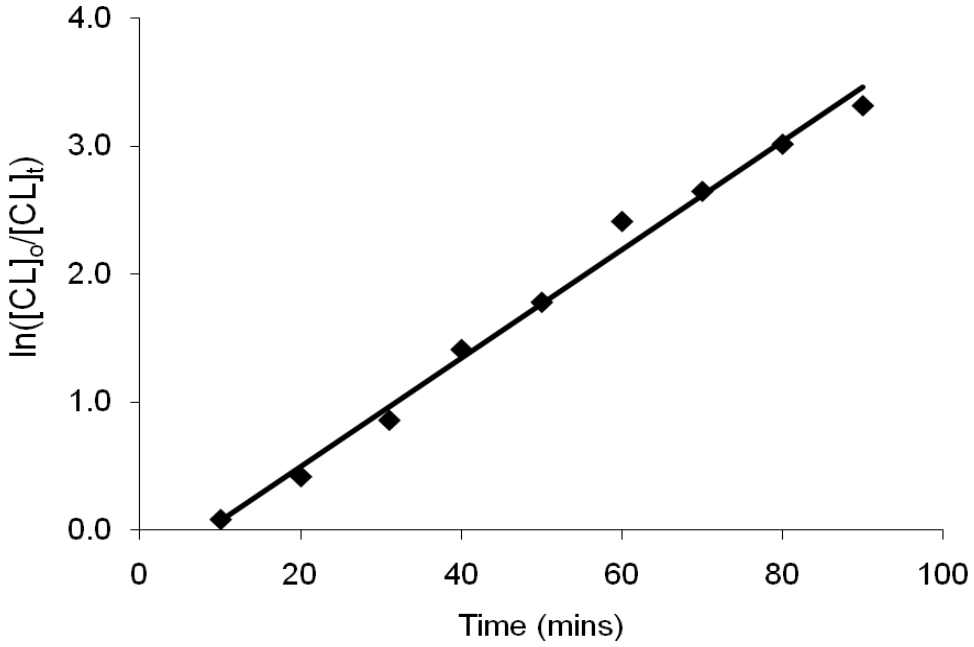
It was also of interest to perform polymerisations utilising the mixed isopropoxide bis(dimethylamide) complex Ti($N_2^{Ms}N^{Ph}$)(NMe_2)(O^iPr) (**18**) to provide a competitive

study between amide and alkoxide initiators. In line with literature precedent,[2,21] the amide is a poor initiator when compared to the isopropoxide group, yielding a polymer with M_n(GPC) in close agreement with one chain growing per metal centre and broad PDI. The NMR spectra of polymers synthesised utilising this catalyst are consistent with alkoxide initiation, which provides the end group of the majority of the chains. However, there are low intensity peaks that are indicative of amide initiation in the MALDI-ToF MS spectra (as well as those expected for the O^{i}Pr end group, Figure 3.19). Initiation from the amide group once propagation is already occurring is probably the source of the broad molecular weight distribution observed (PDI ~2.1). initiated with Ti($N_2^{Ms}N^{Ph}$)(NMe_2)(O^{i}Pr) (**18**). Major peaks correspond to O^{i}Pr terminated polymers, minor peaks correspond to NMe_2 terminated polymers.



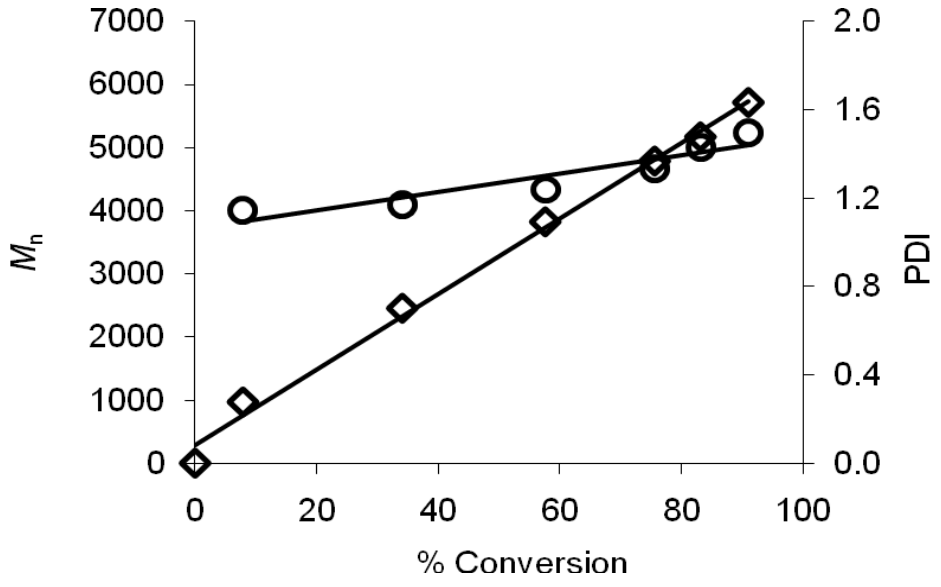
As had been observed previously in Chapter 2, changing from the amide initiators (**12**, **14** and **16**) to the corresponding alkoxides (**13**, **15**, **17** and **3.4**) gives a clear switch from *ca*. one to *ca*. two poly(ε-CL) chains per metal centre and also a significant increase in activity. To investigate fully the isopropoxide initiators, the kinetic behaviour was determined. First order rates of propagation were observed, in addition to a linear increase in M_n with conversion (see Figure 3.20 for representative plots and the Appendix for remaining plots, $k_{app.}$ are given in Table 3.13).

Figure 3.20. First order plot for ε-CL consumption using Ti($N_2^{Ts}N^{Ph}$)(O^iPr)$_2$ (**13**).[a]



[a] Conditions: [ε-CL_0]/[**13**] = 100:1, 6.8 mL toluene, 100 °C, 0.1 mL aliquots taken at the given intervals. See Experimental section for other details. Linear fit (r^2 = 0.995) shown is for the first order region after the induction period.

Figure 3.21. Plots of M_n and PDI (determined by GPC) *vs* conversion for the polymerisation of ε-CL using Ti($N_2^{Ts}N^{Ph}$)(O^iPr)$_2$ (**13**).[a]



[a] Conditions: [ε-CL_0]/[**13**] = 100:1, 6.8 mL toluene, 100 °C, 0.1 mL aliquots taken at the given intervals. Hollow diamonds correspond to M_n and hollow circles to PDI.

All the catalysts showed a short induction period followed by a polymerisation process that was first order with respect to ε-CL concentration (Figure 3.20). Similar

induction periods were observed with titanium isopropoxides (Chapter 2) and have been observed for main group and transition metal isopropoxide catalysts.[1,35,40] The k_p values (Table 3.13) exhibit two main features which were also seen with the bis(dimethylamide) catalyst above. Firstly, for a given sulfone group, sterically less demanding groups provide a higher polymerisation rate. For example Ti(CyN_2^{Ts})(O^iPr)$_2$ (**3.4**) has a much larger k_p than Ti($CyN_2^{SO_2Mes}$)(O^iPr)$_2$ (**3.5**), the latter bearing a mesityl rather than a tolyl group. Secondly, there is a marked coordination number effect for catalysts with the same sulfone group. The general order of k_p values follows the trend 4- > 5- > 6-coordinate. These effects can be interpreted in terms of easier access to the metal centre since smaller sulfonamide R groups and low coordination numbers increases activity; for example, catalyst Ti(CyN_2^{Ts})(O^iPr)$_2$ (**3.4**) provides an extremely rapid polymerisation with good agreement of M_n(GPC) and M_n(calcd) and moderately narrow PDI (1.28).

3.9.2 Polymerisation studies: ROP of ε-caprolactone, zirconium catalysts

The zirconium complexes **20 - 23** were also investigated for the ROP of ε-CL with the aim of evaluating structure to activity relationships within the catalyst families. These complexes allow comparison of different sulfonamide groups and the effect of 5-coordinate *vs*. the 6-coordinate species reported in Chapter 2. *In situ* generation of zirconium alkoxides was performed by reaction of Zr($N_3^{SO_2R}N$)(CH_2SiMe_3) with HO^iPr immediately prior to monomer addition.

Table 3.14. Solution polymerisation of ε-CL by $Zr(N_3^{Ts}N)(CH_2SiMe_3)$ (**20**), $Zr(N_3^{TArF}N)(CH_2SiMe_3)$ (**21**), $Zr(N_3^{Ms}N)(CH_2SiMe_3)$ (**22**) and $Zr(N_3^{TArF}N)(NMe_2)$ (**23**).[a]

Entry	Catalyst	Yield (%)[b]	Time (h)	$k_{app.}$ (min^{-1})	M_n (GPC)[c]	M_n (calcd)[d]	M_w/M_n
1	$Zr(N_3^{Ts}N)(CH_2SiMe_3)$ (**20**)	91	1	0.11(1)	22,270	11,410	1.39
2	$Zr(N_3^{TArF}N)(CH_2SiMe_3)$ (**21**)	93	1.5	[g]	17,600	11,410	1.19
3	$Zr(N_3^{Ms}N)(CH_2SiMe_3)$ (**22**)	96	1	0.057(1)	15,090	11,410	1.33
4	$Zr(N_3^{TArF}N)(NMe_2)$ (**23**)	92	1.4	0.069(1)	13,720	11,410	1.45
5	$Zr(N_3^{Ts}N)(CH_2SiMe_3)$ (**20**)[e]	96	0.9	0.071(1)	11,630	11,410	1.17
6	$Zr(N_3^{Ms}N)(CH_2SiMe_3)$ (**21**)[e]	96	0.7	0.093(2)	10,850	11,410	1.16
7	$Zr(N_3^{TArF}N)(CH_2SiMe_3)$ (**22**)[e]	89	0.6	[g]	11,280	11,410	1.18
8	$Zr(N_3^{TArF}N)(NMe_2)$ (**23**)[f]	94	2	0.029(1)	20,860	11,410	2.12

[a] Conditions: [ε-CL]/[catalyst] = 100:1, 6.8 mL toluene at 100 °C. See Experimental section for other details. [b] Isolated yield at 100 % NMR conversion. [c] Molecular weights (g mol^{-1}) determined from GPC using the appropriate Mark-Houwink corrections. [d] Expected M_n (g mol^{-1}) for 1 chain growing per initiator at 100% conversion. [e] 1 equivalent of HO^iPr. [f] 1 equivalent of HO-2,6-$C_6H_3Me_2$. [g] Neither 1st nor 2nd order in ε-CL.

In agreement with literature precedent[5,11] the zirconium catalysts provide a generally more active catalytic system (for 5-coordinate O^{i}Pr initiators av. k_p (Zr) = 0.085 min^{-1} *vs*. av. k_p (Ti) = 0.057 min^{-1}, Table 3.14), although the most active system was in fact the titanium complex **3.4**. As Kol observed when employing salophan ligands, the activity towards ROP of cyclic esters in the Group 4 triad is highly dependent on the ancillary ligands employed.[41]

As has been previously established with titanium amide initiators (**1**, **2**, **12**, **14** and **16**) Zr($N_3^{TArF}N$)(NMe_2) (**23**) provides a relatively poor polymerisation process with broader PDI (1.45) than both the corresponding alkoxide and alkyl complexes (1.18 and 1.19) although the M_n(GPC) is in closer agreement with M_n(calcd) than for the alkyl **21**. The zirconium amide and alkyl generally quite perform well, yielding polymers with moderate PDIs (1.4 – 1.5) and linear M_n(GPC) *vs*. % conversion plots (see Appendix). They all have higher than expected M_n values but linear M_n(GPC) *vs*. % conversion plots. This indicates that there is some instability of the pre-catalysts, but once the complexes enter the catalytic cycle the polymerisation proceeds in a living fashion. MALDI-ToF mass spectroscopy shows the presence of the expected NMe_2 or CH_2SiMe_3 end-groups for each polymer. For the alkyl complex bearing $N_3^{TArF}N$ (**21**) an interesting kinetic dependence upon ε-CL is observed which is neither first nor second order (see the Appendix).

Preliminary results utilising *in situ* generation of catalysts in the presence of an alcohol (1 equivalent) with the amide complex **23** suffers from initiation of polymer chains with both NMe_2 and OR end-groups, the former possibly through an activated monomer mechanism.[42] For example, polymerisations in the presence of one equivalent HO(2,6-$C_6H_3Me_2$) yields polymers with both amide and ester end-groups. Similar results were observed with HO^{i}Pr, and so Zr($N_3^{TArF}N$)(NMe_2) (**23**) in the presence of co-initiators was not investigated further. Polymerisations utilising the HO(2,6-$C_6H_3Me_2$)/Zr($N_3^{TArF}N$)(NMe_2) (**23**) system (entry 8, Table 3.14) showed non-living characteristics with broad PDI and a non linear M_n(GPC) *vs*. % conversion graph (see the Appendix).

In situ generation of isopropoxide catalysts from the alkyls **20** - **22** gave an extremely well controlled polymerisation as evidenced by linear M_n(GPC) *vs*. % conversion plots, and narrow PDIs (<1.2). The gradients of the M_n(GPC) *vs*. % conversion graphs are in close agreement with that predicted for one chain per metal

centre (av. 111, range 118(5) – 105(4) , expected 114 g mol^{-1} (% conversion)$^{-1}$). The systems **21** and **22** with one equivalent of ^{i}PrOH (entries 6 and 7) are the most active zirconium species of the six systems investigated, giving 100% conversion after 35 min with excellent control. The 6-coordinate isopropoxide catalysts $Zr(N_2{}^{Ts}N^{py})(O^{i}Pr)_2$ (**4**) and $Zr(N_2{}^{Ts}N^{OMe})(O^{i}Pr)_2$ (**6**) both have higher k_p rate constants than the tren systems investigated here (av. k_p = 0.115 *vs*. k_p = 0.082 min^{-1}). The octahedral species are more able to support monomeric and presumably more active (L)Zr-OR (R = poly(*rac*-LA) chain) catalysts, whereas the tren ligands ($N_3{}^{SO_2R}N$) might lead to a higher equilibrium concentration of dormant binuclear complexes with, for example, bridging sulfonyl groups (*cf*. the bridging SO groups in **20** or **21**).

3.10 Polymerisation studies: ROP of *rac*-lactide

Initial investigations centred around the titanium isopropoxide complexes **13**, **15**, **18** and **19** which had demonstrated enhanced activity compared to analogous 6-coordinate species when employed for the ROP of ε-CL. The results are summarised in Table 3.15. Disappointingly, these complexes are unable to polymerise *rac*-LA to completion, with five coordinate **13** giving the highest conversion to polymer of 71% after 11 hours (entry 1, Table 3.15). Higher conversions were obtained with bulkier sulfonamide catalysts bearing the same ligand backbone (entry 1 *vs*. 2, and 4 *vs*. 3) and the 6-coordinate analogues investigated in Chapter 2 (Table 2.10). This is perhaps indicative of dimerisation in solution deactivating the catalysts. All polymers produced were predominantly atactic ($P_r \sim 0.5$).

Table 3.15. Solution polymerisation of *rac*-lactide by $Ti(N_2^{Ts}N^{Ph})(O^iPr)_2$ (**13**), $Ti(N_2^{Ms}N^{Ph})(O^iPr)_2$ (**15**), $Ti(CyN_2^{Ts})(O^iPr)_2$ (**3.4**), $Ti(CyN_2^{SO_2Mes})(O^iPr)_2$ (**3.5**), $Zr(N_3^{Ts}N)(CH_2SiMe_3)$ (**20**), $Zr(N_3^{TArF}N)(CH_2SiMe_3)$ (**21**), $Zr(N_3^{Ms}N)(CH_2SiMe_3)$ (**22**) and $Zr(N_3^{TArF}N)(NMe_2)$ (**23**).[a]

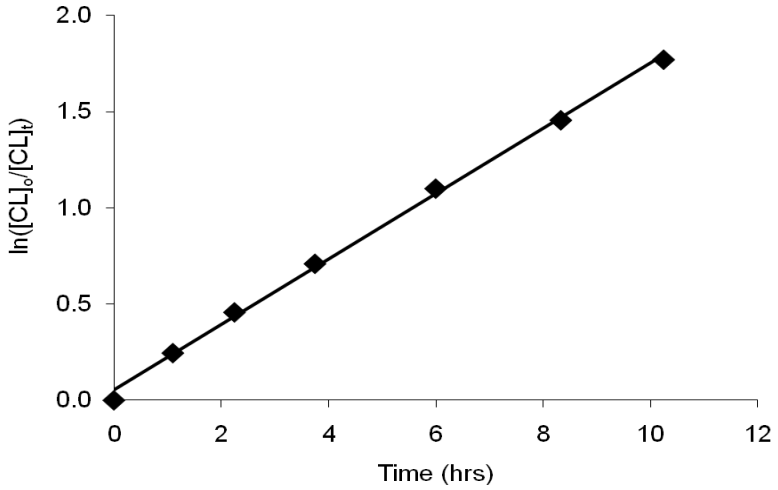
Entry	Catalyst	Conversion (%)[b]	Time (h)	$k_{app.}$ (min^{-1})	M_n (GPC)[c]	M_n (calcd)[d]	M_w/M_n
1	$Ti(N_2^{Ts}N^{Ph})(O^iPr)_2$ (**13**)	71	11	0.119(4)	7,900	5,120	1.13
2	$Ti(N_2^{Ms}N^{Ph})(O^iPr)_2$ (**15**)	44	2	0.29(2)	3,980	3,320	1.09
3	$Ti(CyN_2^{Ts})(O^iPr)_2$ (**3.4**)	32	4	0.111(8)	3,620	2,310	1.16
4	$Ti(CyN_2^{SO_2Mes})(O^iPr)_2$ (**3.5**)	46	4	0.15(1)	4,880	3,320	1.22
5	$Zr(N_3^{Ts}N)(CH_2SiMe_3)$ (**20**)	84	61	0.033(2)	23,690	12,110	1.19
6	$Zr(N_3^{Ms}N)(CH_2SiMe_3)$ (**21**)	83	65	0.021(1)	18,920	11,960	1.38
7	$Zr(N_3^{TArF}N)(NMe_2)$ (**23**)	66	66	0.018(1)	29,260	9,510	1.19
8	$Zr(N_3^{Ts}N)(CH_2SiMe_3)$ (**20**)[e]	96	20	0.154(2)	14,340	13,840	1.08
9	$Zr(N_3^{Ms}N)(CH_2SiMe_3)$ (**22**)[e]	95	24	0.170(3)	15,600	13,690	1.11
10	$Zr(N_3^{TArF}N)(CH_2SiMe_3)$ (**21**)[e]	89	24	0.134(4)	13,005	12,830	1.08

[a] Conditions: [*rac*-LA]/[catalyst] = 100:1, 6.8 mL toluene at 100 °C. See Experimental section for other details. [b] Isolated yield at 100 % NMR conversion. [c] Molecular weights (g mol^{-1}) determined from GPC using the appropriate Mark-Houwink corrections. [d] Expected M_n (g mol^{-1}) for 2 chains growing per initiator at 100% conversion. [e] With 1 equivalent of ^iPrOH.

Attention then focused on the zirconium complexes **20**, **21** and **23** (entries 5 – 10, Table 3.15). As with the ε-CL study, the alkyl complexes **20**, **21** and the amide **23** were found to be active for ROP of *rac*-LA. The polymerisation proceeds slowly for both the alkyl species with higher than expected M_n values, although with linear M_n(GPC) *vs*. % conversion plots. This perhaps indicates there is some instability of the pre-catalysts but once the complexes enter the catalytic cycle the polymerisation proceeds in a living fashion as had been observed for ε-CL. Likewise, **23** shows a relatively controlled polymerisation process with narrow PDIs (1.1-1.2) throughout the polymerisation, but again a much higher than expected M_n is recorded, perhaps indicative of pre-catalyst instability. The MALDI-ToF mass spectroscopy of low molecular weight polyesters showed the expected NMe_2 or CH_2SiMe_3 end groups, as well as evidence of extensive transesterification, with peak envelopes 72 *m*/*z* apart.

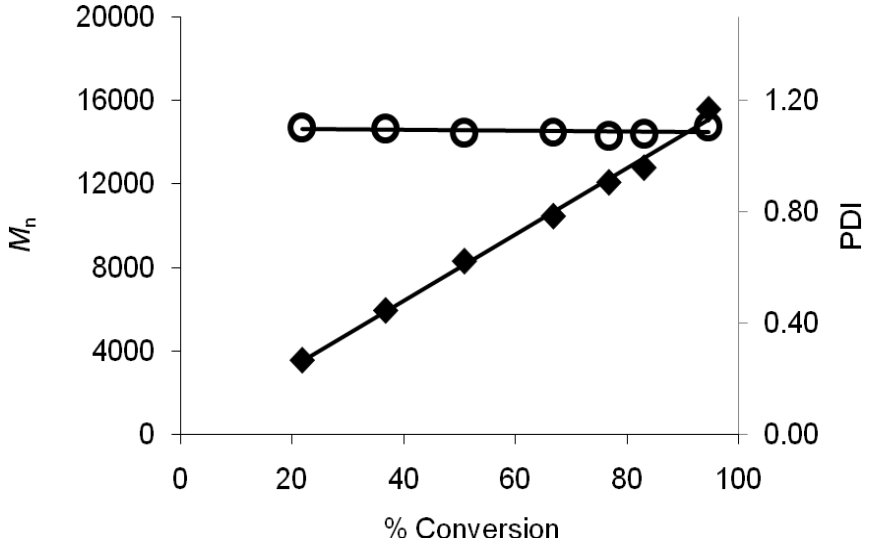
In situ generation of alkoxide catalysts (Entries 8-10, Table 3.15) gave a much better controlled polymerisation process. Catalysts gave linear plots of M_n *vs* % conversion (Figures 3.22 and 3.23 and the Appendix) with extremely narrow PDIs (1.05 – 1.10) which remained effectively constant throughout the reaction. The gradients of the M_n *vs*. % conversion plots were 151(2), 159(4) and 144(2) g mol^{-1} (% conversion)$^{-1}$ (av. 152 g mol^{-1} (% conversion)$^{-1}$) which is close to that expected (144.1 g mol^{-1} (% conversion)$^{-1}$) for one poly(*rac*-LA) chain growing per metal centre. The MALDI-ToF mass spectroscopy shows exclusively isopropoxide end groups with peaks 72 *m*/*z* apart (Figure 3.24). All of these data are consistent with these species acting as living catalysts for the ROP of *rac*-lactide. The k_p values show a dependence on the sulfonamide group with the general order of Ms (**22**) > Ts (**20**) > TArF (**21**). This trend is interpreted as arising from easier access of the monomer to metal centre. All polymer produced with these catalysts are atactic ($P_r \sim 0.5$), as has been observed for all previous polydentate sulfonamide Group 4 ROP catalysts.

Figure 3.22. First order plot for *rac*-LA consumption using $Zr(N_3^{Ms}N)(CH_2SiMe_3)$ (**22**) with ^{i}PrOH co-catalyst.[a]



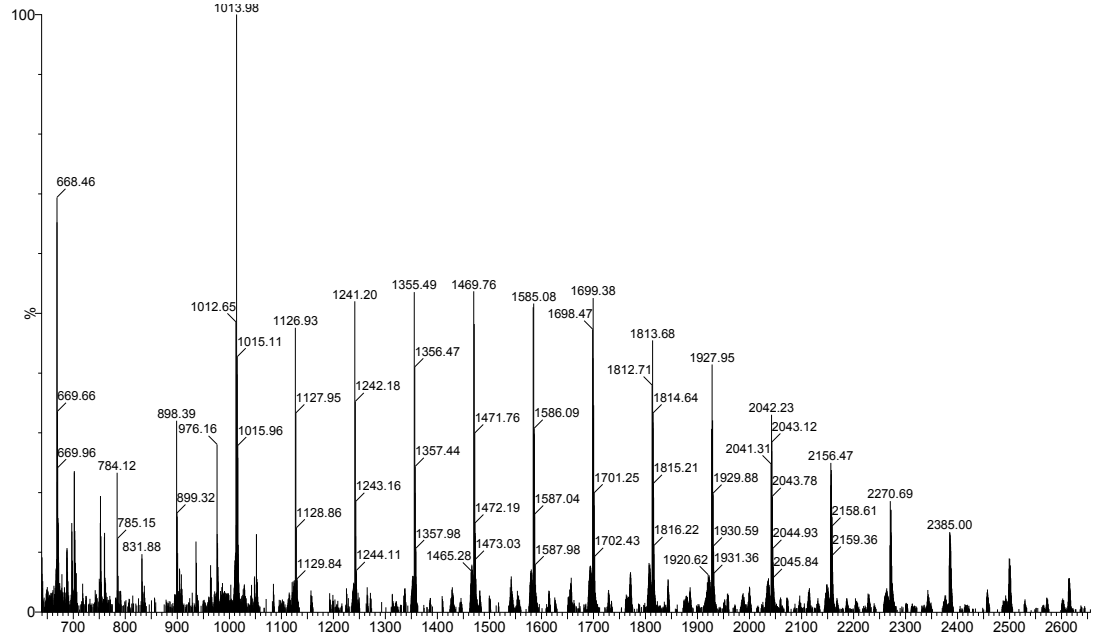
[a] Conditions [*rac*-LA_0]/[**22**]/$HO^{i}Pr$ = 100:1:1, 6 mL toluene, 70 °C, 0.1 mL aliquots taken at the given intervals. See Experimental section for other details. Linear fit (r^2 = 0.998) shown is for the first order region after the induction period.

Figure 3.23. Plots of M_n and PDI (determined by GPC) *vs* conversion for the solution polymerisation of *rac*-LA using $Zr(N_3^{Ms}N)(CH_2SiMe_3)$ (**22**) with $HO^{i}Pr$ co-catalyst.[a]



[a] Conditions: [*rac*-LA_0]/[**22**]/$HO^{i}Pr$ = 100:1:1, 6.0 mL toluene, 70 °C, 0.1 mL aliquots taken at the given intervals. Hollow diamonds correspond to M_n and hollow circles to PDI.

Figure 3.24. MALDI-ToF MS of poly(rac-LA) synthesised using $Zr(N_3^{Ms}N)(O^iPr)$ (**22**). M_n by GPC analysis was 1470 g mol^{-1}.



3.11 Summary and Conclusion

This Chapter has developed systematic sulfonamide ligand variation with the aim of establishing relationships between catalyst structure and ROP activity and control. The new bis(amide) complexes $Ti(N_2^{Ts}N^{ph})(NMe_2)_2$ (**12**), $Ti(N_2^{Ms}N^{Ph})(NMe_2)_2$ (**14**) or $Ti(N_2^{Ms}N^{OMe})(NMe_2)_2$ (**16**) were easily prepared under mild conditions from $Ti(NMe_2)_4$. Similarly, the bis(isopropoxide) complexes $Ti(N_2^{Ts}N^{Ph})(O^iPr)_2$ (**13**), $Ti(N_2^{Ms}N^{Ph})(O^iPr)_2$ (**15**) and $Ti(N_2^{Ms}N^{OMe})(O^iPr)_2$ (**17**) could be synthesised from $Ti(O^iPr)_2(NMe_2)_2$ and the appropriate protio-ligand. A redistribution reaction occurred between $Ti(N_2^{Ts}N^{Ph})(O^iPr)_2$ (**13**) and $Ti(N_2^{Ts}N^{ph})(NMe_2)_2$ (**12**) to give $Ti(N_2^{Ts}N^{Ph})(NMe_2)(O^iPr)$ (**18**). However this product was more conveniently prepared by reaction of the protio-ligand and 3 equivalents of $Ti(O^iPr)_2(NMe_2)_2$. Reaction of Me_3SiCl and $Ti(N_2^{Ts}N^{Ph})(NMe_2)_2$ (**12**) yielded $Ti(N_2^{Ts}N^{Ph})Cl_2$ (**19**) under mild conditions. The X-ray structures of four titanium sulfonamide complexes were determined and showed a variety of 5-, 6- and 7-coordinate structures depending on the sulfonamide ligand and/or additional ligand (amide, alkoxide or chloride). In accordance with the results reported in Chapter 2, the amides were poorer catalysts than the alkoxides towards the ROP of ε-CL. Clear structure-activity relationships were observed with titanium, with lower coordination number and less sterically

encumbered ligands giving the most active and best controlled catalysts. The previously reported Ti(CyN_2^{Ts})(O^iPr)$_2$ (**3.4**) was the most active catalyst of those surveyed for the ROP of ε-CL. All of the titanium complexes were poor catalysts for the ROP of *rac*-lactide, giving poor conversions (30-70%), although bulkier groups on a given ligand backbone gave higher conversions.

C_3 symmetric zirconium catalysts were also investigated. Both the previously-reported and new protio-ligands reported herein reacted readily with Zr(CH_2SiMe_3)$_4$ to form Zr($N_3^{SO_2R}N$)(CH_2SiMe_3) (R = Tol, Me or 2,6-$C_6H_3(CF_3)_2$). Reaction of Zr(NMe_2)$_4$ with $H_3N_3^{TArF}N$ gave the corresponding amide complex Zr($N_3^{TArF}N$)(NMe_2) (**23**), which was found to be highly air and moisture sensitive giving the oxo species {Zr($N_3^{TArF}N$)}$_2$(μ-O) (**24**) in the presence of trace amounts of water. It was possible to conduct *in situ* protonolysis reactions with Zr($N_3^{Ts}N$)(CH_2SiMe_3) (**20**) or Zr($N_3^{TArF}N$)(NMe_2) (**23**) to yield the corresponding alkoxide or aryloxide complexes. Four zirconium sulfonamide complexes were analysed by single crystal X-ray diffraction and showed complex 7- and 8-coordinate structures depending on the sulfonamide ligand and/or additional ligand (amide, alkyl or μ-oxo). As had been observed elsewhere, the zirconium complexes generally provided more active ROP catalysts than the titanium analogues, although Ti(CyN_2^{Ts})(O^iPr)$_2$ was the most active catalyst of all those surveyed for ε-CL. *In situ* generation of alkoxide catalysts from the zirconium alkyl complexes gave well-controlled catalysts with narrow polymer PDIs and predictable M_n. Of these catalysts, the least bulky sulfone substituents yielded the most active catalyst for *rac*-lactide. However, these catalysts were generally found to be less active than the 6-coordinate zirconium complexes investigated in Chapter 2.

3.12 References

(1) Chmura, A. J.; Davidson, M. G.; Jones, M. D.; Lunn, M. D.; Mahon, M. F. *Dalton Trans*. 2006, 887-889.

(2) Takashima, Y.; Nakayama, Y.; Hirao, T.; Yasuda, H.; Harada, A. *J. Organomet. Chem*. 2004, *689*, 612-619.

(3) Takashima, Y.; Nakayama, Y.; Watanabe, K.; Itono, T.; Ueyama, N.; Nakamura, A.; Yasuda, H.; Harada, A.; Okuda, J. *Macromol*. 2002, *35*, 7538-7544.

(4) Takeuchi, D.; Nakamura, T.; Aida, T. *Macromol*. 2000, *33*, 725-729.

(5) Chmura, A. J.; Davidson, M. G.; Jones, M. D.; Lunn, M. D.; Mahon, M. F.; Johnson, A. F.; Khunkamchoo, P.; Roberts, S. L.; Wong, S. S. F. *Macromol*. 2006, *39*, 7250-7257.

(6) Nakayama, Y.; Watanabe, K.; Ueyama, N.; Nakamura, A.; Harada, A.; Okuda, J. *Organometallics* 2000, *19*, 2498-2503.

(7) Kim, Y.; Jnaneshwara, G. K.; Verkade, J. G. *Inorg*. *Chem*. 2003, *42*, 1437-1447.

(8) Kim, Y.; Verkade, J. G. *Macromol*. *Rapid Commun*. 2002, *23*, 917-921.

(9) Kim, Y.; Verkade, J. G. *Organometallics* 2002, *21*, 2395-2399.

(10) Chmura, A. J.; Davidson, M. G.; Frankis, C. J.; Jones, M. D.; Lunn, M. D. *Chem*. *Commun*. 2008, 1293-1295.

(11) Gendler, S.; Segal, S.; Goldberg, I.; Goldschmidt, Z.; Kol, M. *Inorg*. *Chem*. 2006, *45*, 4783-4790.

(12) Kim, Y.; Verkade, J. G. *Macromol*. *Symp*. 2005, *224*, 105-118.

(13) Kim, Y.; Verkade, J. G. *Inorg*. *Chem*. 2003, *42*, 4804-4806.

(14) Kim, Y.; Kapoor, P. N.; Verkade, J. G. *Inorg*. *Chem*. 2002, *41*, 4834-4838.

(15) Chmura, A. J.; Chuck, C. J.; Davidson, M. G.; Jones, M. D.; Lunn, M. D.; Bull, S. D.; Mahon, M. F. *Angew*. *Chem*. *Int*. *Ed*. 2007, *46*, 2280-2283.

(16) Motekaitis, R. J.; Martell, A. E.; Muraset, I. *Inorg*. *Chem*. 1986, 938-944.

(17) Kitagawa, O.; Yotsumoto, K.; Kohriyama, M.; Dobashi, Y.; Taguchi, T. *Org*. *Lett*. 2004, *6*, 3605-3607.

(18) Takahashi, H.; Kawakita, T.; Ohno, M.; Yoshioka, M.; Kobayashi, S. *Tetrahedron* 1992, *48*, 5691-5700.

(19) Nieger, M.; Josten, W.; Vogtle, F. *University of Edinburgh* 2004.

(20) Pritchett, S.; Gantzel, P.; Walsh, P. J. *Organomet*. 1999, *18*, 823-831.

(21) Schwarz, A. D.; Thompson, A. L.; Mountford, P. *Inorg*. *Chem*. 2009, *48*, 10442-10454.

(22) Skinner, M. E. G.; Li, Y.; Mountford, P. *Inorg*. *Chem*. 2002, *41*, 1110-1119.

(23) Fletcher, D. A.; McMeeking, R. F.; Parkin, D. *J*. *Chem*. *Inf*. *Comput*. *Sci*. 1996, *36*, 746 (The United Kingdom Chemical Database Service).

(24) Pritchett, S.; Woodmansee, D. H.; Gantzel, P.; Walsh, P. J. *J*. *Am*. *Chem*. *Soc*. 1998, *120*, 6423-6424.

(25) Ackermann, L.; Bergman, R. G.; Loy, R. N. *J*. *Am*. *Chem*. *Soc*. 2003, *125*, 11956-11963.

(26) Costa, A. M.; García, C.; Carroll, P. J.; Walsh, P. J. *Tetrahedron* 2005, *61*, 6442-6446.

(27) Pritchett, S.; Gantzel, P.; Walsh, P. J. *Organometallics* 1997, *16*, 5130-5132.

(28) Poirier, V.; Roisnel, T.; Carpentier, J.-F.; Sarazin, Y. *Dalton Trans*. 2009, 9820-9827.

(29) Pietrangelo, A.; Hillmyer, M. A.; Tolman, W. B. *Chem*. *Commun*. 2009, 2736-2737.

(30) Du, H.; Velders, A. H.; Dijkstra, P. J.; Zhong, Z.; Chen, X.; Feijen, J. *Macromolecules* 2009, *42*, 1058-1066.

(31) Nomura, N.; Ishii, R.; Yamamoto, Y.; Kondo, T. *Chem*. *Eur*. *J*. 2007, *13*, 4433-4451.

(32) Gamer, M. T.; Roesky, P. W.; Palard, I.; LeHellaye, M.; Guillaume, S. M. *Organometallics* 2007, *26*, 651-657.

(33) Amgoune, A.; Thomas, C. M.; Roisnel, T.; Carpentier, J.-F. *Chem*. - *.Euro*. *J*. 2006, *12*, 169-179.

(34) Ma, H.; Okuda, J. *Macromolecules* 2005, *38*, 2665-2673.

(35) Zhong, Z.; Dijkstra, P. J.; Birg, C.; Westerhausen, M.; Feijen, J. *Macromol*. 2001, *34*, 3863-3868.

(36) Martin, E.; Dubois, P.; Jerome, R. *Macromolecules* 2000, *33*, 1530-1535.

(37) Rudin, A.; Hoegy, H. L. W. *J*. *Polym*. *Sci*. *Part A: Polym*. *Chem*. 1972, *10*, 217-235.

(38) Barakat, I.; Ph, D.; Jérôme, R.; Ph, T. *J*. *Polym*. *Sci*. *Part A: Polym*. *Chem*. 1993, *31*, 505-514.

(39) Dorgan, J. R.; Janzen, J.; Knauss, D. M.; Hait, S. B.; Limoges, B. R.; Hutchinson, M. H. *J*. *Polym*. *Sci*. *Part B: Polym*. *Phys*. 2005, *43*, 3100-3111.

(40) Duda, A.; Penczek, S. *Macromol*. 1995, *28*, 5981-5992.

(41) Zelikoff, A. L.; Kopilov, J.; Goldberg, I.; Coates, G. W.; Kol, M. *Chem*. *Commun*. 2009, 6804-6806.

(42) Clark, L.; Cushion, M. G.; Dyer, H. E.; Schwarz, A. D.; Duchateau, R.; Mountford, P. *Chem*. *Commun*. 2010, *46*, 273-275.

Chapter Four

Sulfonamide-Supported Aluminium Catalysts for the Ring-Opening Polymerisation of *rac*-Lactide

4.1 Overview

Chapter 4 provides an introduction of aluminium catalysed ROP and an overview of the synthesis and characterisation of aluminium alkoxide and alkyl complexes supported by dianionic, tri- and tetradentate sulfonamide ligands. Solution state behaviour and solid state structures will be presented and discussed. These complexes were also assessed for the ROP of *rac*-lactide and the results are presented. This work has recently been published.[1]

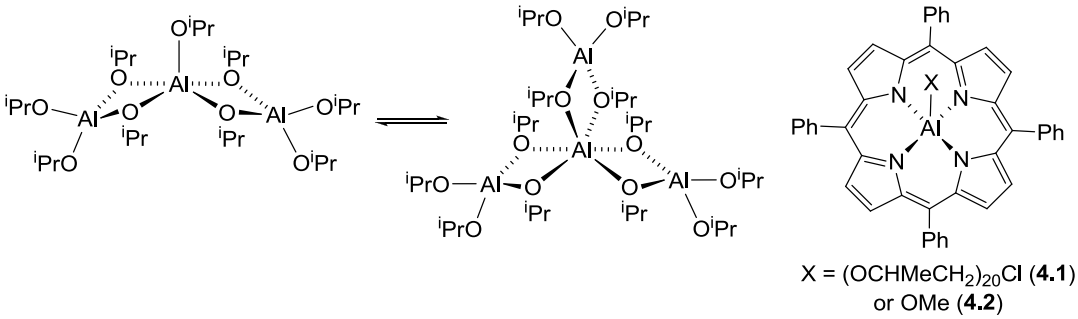
4.2 Introduction

Aluminium catalysts have been extensively exploited for the ROP of *rac*-LA with many examples of predictable molecular weights, narrow polydispersities (PDIs) and either heterotactic or isotactic enrichment being achieved. A brief overview of the area is given below.

$Al(O^iPr)_3$ has been exhaustively studied as an initiator for the ROP of ε-Cl[2-4] and lactide.[5,6] Typically, ε-CL gives polymer of narrow PDI (~1.1) in toluene at room temperature, and LA shows a well behaved polymerisation up to high M_n (90,000 g mol^{-1}) with narrow PDI (~1.2) and on average three chains growing per metal centre. These results are in agreement with $Al(O^iPr)_3$ acting as a well controlled 'living' ROP catalyst.[7] However, at higher monomer:initiator ratios and/or higher temperatures broadened PDIs (~1.5) are obtained, indicative of both inter- and intramolecular transesterification occurring.[8] It has been reported that the rate of polymerisation of ε-CL at 25 °C is 4×10^2 times greater than *L*-LA at 70 °C, due to the favourable release of 7-membered ring strain for ε-CL, and by the coordination of the nearest inserted carbonyl of the poly(LA) chain to the aluminium centre, leading to stable 5-membered chelates which hinder monomer uptake.[9] At 70 °C $Al(O^iPr)_3$ polymerises lactide with all three O^iPr initiators. However, only one chain per metal centre was observed for ε-CL at 25 °C. This is a consequence of $Al(O^iPr)_3$ existing as a mixture of trimeric and tetrameric species in solution.[10-13] Of these, the trimeric form is much more active towards ROP (Figure 4.1).[14-16] At higher temperatures, the trimeric and tetrameric forms are in rapid equilibrium allowing activation of all the aluminium centres. At room temperature the rate of polymerisation is found to be much higher than the rate of inter-conversion. Therefore, the apparent concentration is lower than expected as the bulk of polymerisation proceeds though the trimeric form. The trimer

is postulated to be more active due to facile conversion into a non-aggregated six-coordinate mononuclear species, $Al(O^iPr)_3(monomer)_3$.[17,18] An induction period prior to initiation (40 minutes at 70 °C for LA, 4 minutes at 0 °C for ε-CL)[19] arises from de-aggregation. Convincingly, when the pure trimeric form is employed M_n is consistent with each initiating group being active.[15,19,20]

Figure 4.1 $Al(O^iPr)_3$ and aluminium complexes employing TPP ligands.[10-13,21,22]



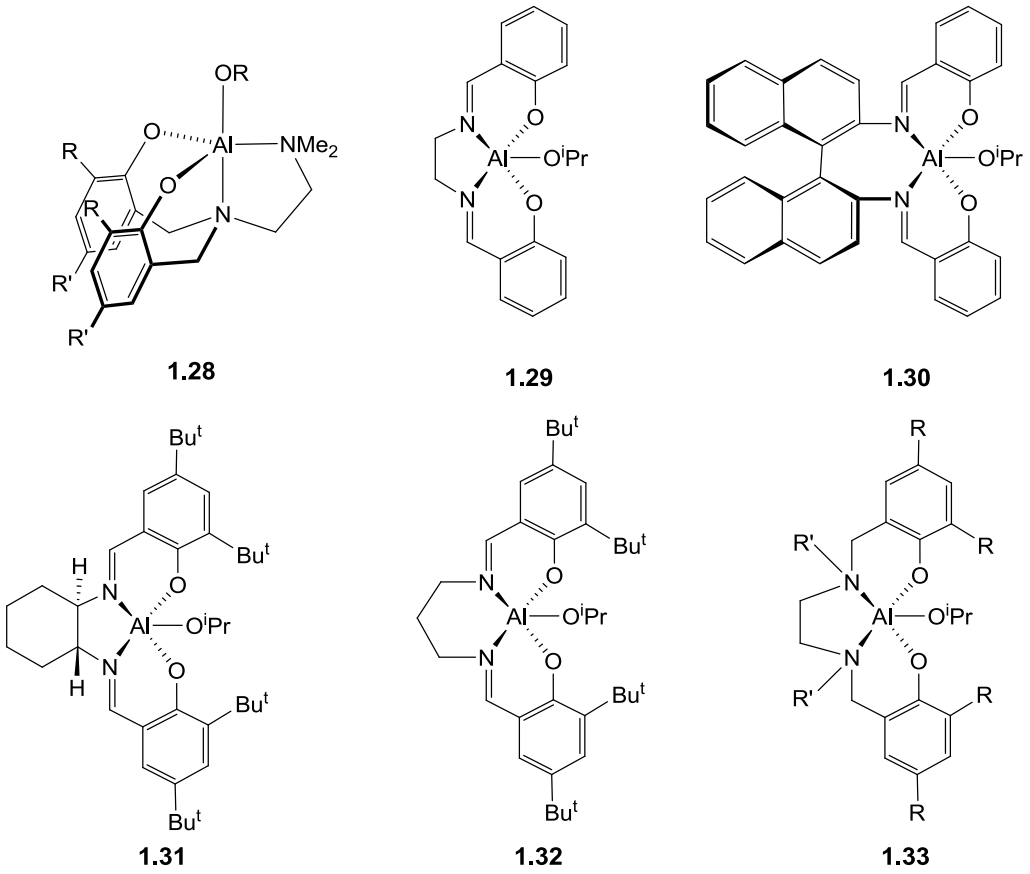
Although the rate of ε-CL homo-polymerisation is much greater than that of lactide, when a mixture of LA and ε-CL are co-polymerised, LA is incorporated preferentially.[23] Indeed the propagating species derived from LA were found to be 2.5 × 10^5 less reactive to ε-CL than ε-CL-derived species towards LA.[9,24] Consequently, diblock copolymers have only been prepared by polymerising ε-CL first.

Simple dialkylaluminium alkoxides have also been shown to initiate the well controlled polymerisation of ε-CL and LA, yielding polymers with narrow PDI and predictable M_n.[25-28] However, as these species still suffer from aggregation behaviour, multidentate ancillary ligands were therefore applied to achieve monomeric single site catalysts.

Some of the earliest examples of single-site initiators for ε-caprolactone and lactide polymerisation were reported by Inoue using tetraphenylporphyrin (TPP) aluminium initiators (Figure 4.1).[21,22] The polymerisations are generally slow but well controlled, forming polymers with narrow PDIs and giving a linear increase of M_n with conversion, typical of 'living' behaviour. For example, **4.1** polymerises 94 equivalents of *D*-LA over 94 hours at 100 °C to give a polymer with a predicable M_n and narrow PDI (1.12).[29] The corresponding alkoxide **4.2** displays similar activity and control and was also shown to exclusively ring-open at the acyl-oxygen bond. Alternative potential initiators such as chlorides, alkyls and carboxylates were found to be inactive for the ROP of LA and ε-CL.[30] TPP-based initiators such as **4.2** can also be used (in

the presence of MeOH) to effect the immortal polymerisation of LA and ε-CL, yielding narrow PDI (>1.15) and predictable M_n.[31] Systematic variation of the tetraphenylporphyrin ligands by substitution with ortho-Cl and ortho-OMe groups has been undertaken and shown to give higher activites.[32]

Figure 4.2. Examples of phenolate-supported aluminium catalysts for the ROP of cyclic esters.[33-47]

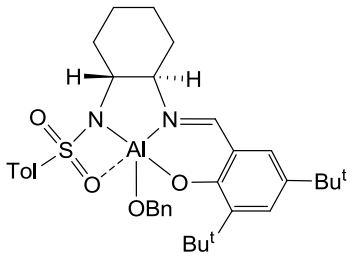


Notable examples of aluminium-based catalysts are the salen[33-46] and salan[47] complexes with which highly isotactic, syndiotactic or tapered isotactic block copolymers can be formed, depending on the stereoisomer of the LA and salen ligands employed (**1.29**–**1.33**, Figure 4.2). Complexes of polydentate phenoxy-amine ligands (**1.28**, Figure 4.2) have also been investigated for the ROP of both *rac*-LA and ε-caprolactone.[48-52] Interesting, although at times contradictory, steric and electronic effects of ligand variation upon catalysis have been observed for these systems. A prime example is the system studied by Hillmyer and Tolman[50] (**1.28**) in which substituting the *tert*-butyl substituent in the 5-position of the phenolate ring for bromine significantly decreases activity. This is in stark contrast to the corresponding

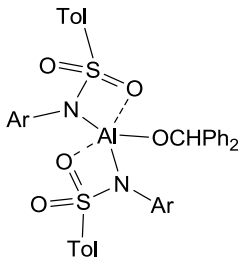
salen ligands for which Gibson showed halide substituents on the phenolate ring *enhanced* activity.[53]

As described in Chapter 1, there have been only two examples of sulfonamide-supported aluminium ROP catalysts, namely **1.22** and **1.41** in Figure 4.3.[54,55] Compound **1.41** gave poor control of the polymerisation process with a much lower than expected M_n and a moderately broad PDI under melt conditions. In contrast, **1.22** showed excellent control in the polymerisation of *L*-LA yielding predominantly isotactic polymer with narrow PDI and predictable M_n.[55]

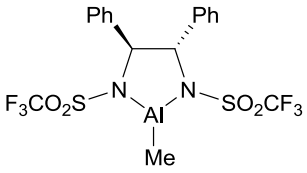
Figure 4.3. Previously reported examples of aluminium sulfonamide complexes.[54-57]



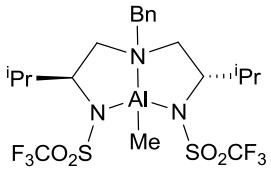
1.22



1.41



1.42



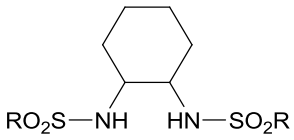
1.43

4.3 Aims

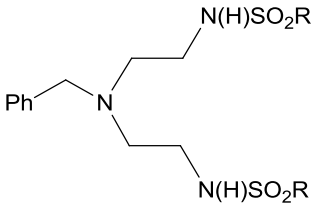
The success with sulfonamide-supported Group 4 ROP catalysts (Chapters 2 and 3), and the promising results recently reported for **1.22**, prompted the development and evaluation of a series of aluminium based ROP catalysts using sulfonamide ligands. This Chapter reports the synthesis and structures of a series of new aluminium complexes derived from the N_2-donor sulfonamides 1,2-$C_6H_{10}(NHSO_2R)_2$ (R = Tol (**3.2**, $H_2CyN_2^{Ts}$) or Mes (**3.3**, $H_2CyN_2^{SO_2Mes}$)), the N_3-donor sulfonamides $PhCH_2N(CH_2CH_2NHSO_2Tol)_2$ (**7**, $H_2N_2^{Ts}N^{Ph}$) and $PhCH_2N(CH_2CH_2NHSO_2Me)_2$ (**8**, $H_2N_2^{Ms}N^{Ph}$), the N_4-donor sulfonamide ligand (2-NC_5H_4)$CH_2N(CH_2CH_2NHSO_2Tol)_2$ (**2.7**, $H_2N_2^{Ts}N^{py}$) or the related N_3O-donor $MeOCH_2CH_2N(CH_2CH_2NHSO_2Tol)_2$ (**2.8**, $H_2N_2^{Ts}N^{OMe}$). The performance of these complexes as ROP catalysts for *rac*-LA is also presented.

4.4 Synthesis of protio-ligand precursors

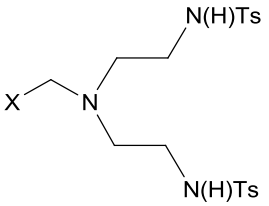
The protio-ligands $H_2CyN_2^{Ts}$ (**3.2**)[58] and $H_2CyN_2^{SO_2Mes}$ (**3.3**),[59] $H_2N_2^{Ts}N^{py}$ (**2.7**)[60] and $H_2N_2^{Ts}N^{OMe}$ (**2.8**)[61] were synthesised according to literature methods. Synthesis of protio-ligands $H_2N_2^{Ts}N^{Ph}$ (**7**) and $H_2N_2^{Ms}N^{Ph}$ (**8**) are described in Chapter 3.



R = Tol (**3.2**) or Mes (**3.3**)



R = Tol (**7**) or Me (**8**)

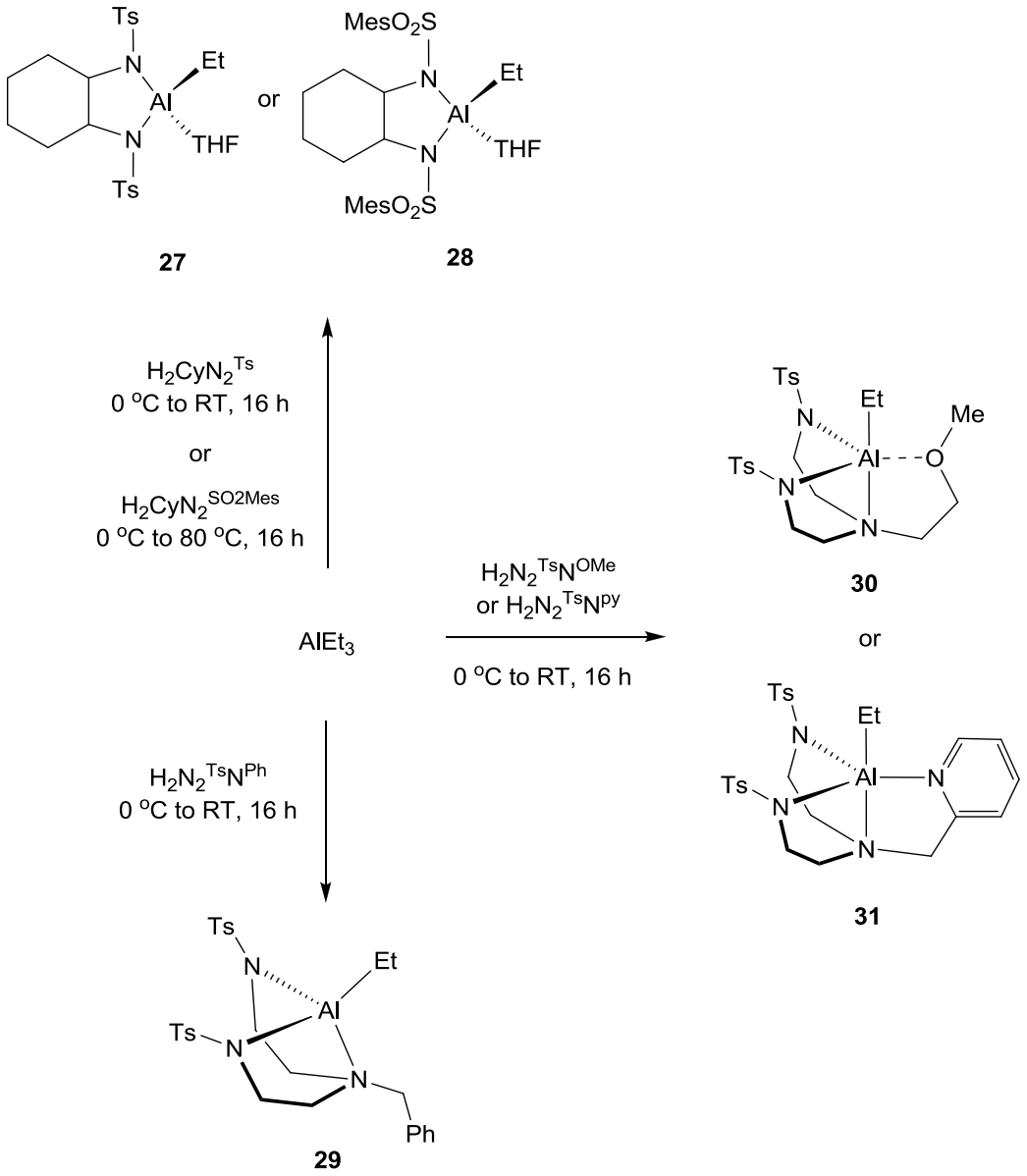


X = 2-NC_5H_4 (**2.7**) or CH_2OMe (**2.8**)

4.5 Synthesis of aluminium alkyl complexes

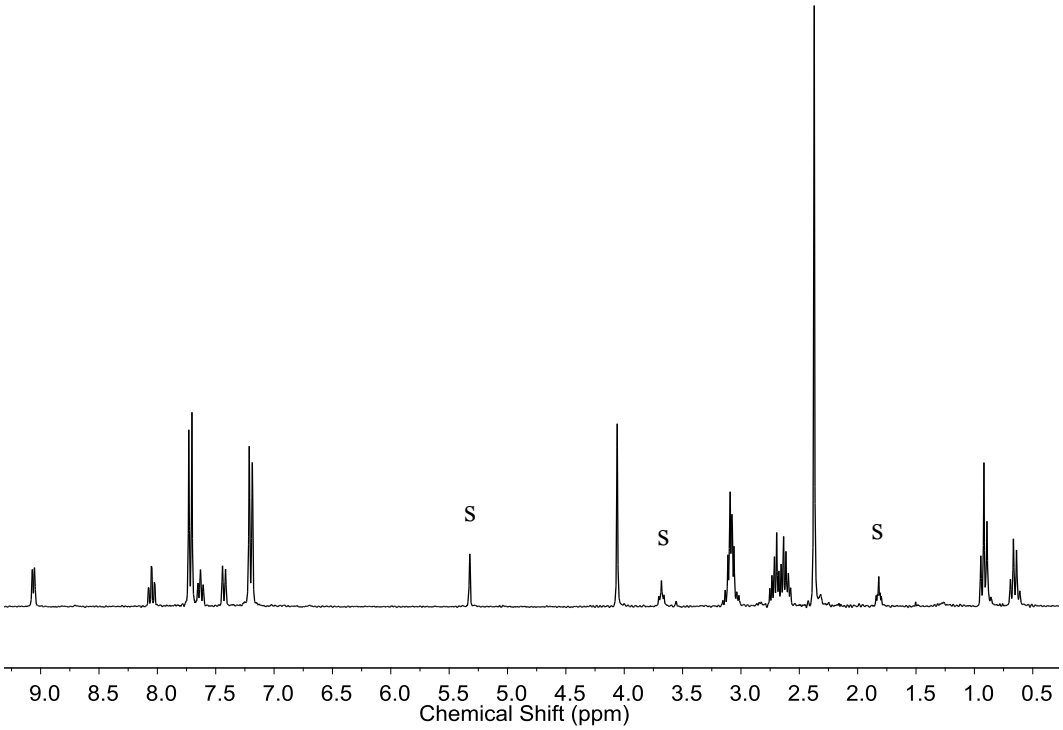
Initial complexation studies (Scheme 4.1) focused on alkyl complexes as intermediates en route to the more desirable alkoxide initiators *via* protonolysis reactions with alcohols, according to literature precedent.[62] Reactions of $AlEt_3$ with $H_2CyN_2^{Ts}$ (**3.2**) or $H_2CyN_2^{SO_2Mes}$ (**3.3**) in THF gave the 4-coordinate Lewis base adducts $Al(CyN_2^{Ts})Et(THF)$ (**27**) and $Al(CyN_2^{SO_2Mes})Et(THF)$ (**28**), the latter reaction requiring heating at 80 ^oC. Reaction with $H_2N_2^{Ts}N^{Ph}$ (**7**) at ambient temperature in the same solvent gave the 4-coordinate, THF-free $Al(N_2^{Ts}N^{Ph})Et$ (**29**) containing a tridentate bis(sulfonamide)amine ligand. Finally, reaction of $AlEt_3$ with $H_2N_2^{Ts}N^{OMe}$ (**2.8**) and $H_2N_2^{Ts}N^{py}$ (**2.7**) gave THF-free complexes $Al(N_2^{Ts}N^{OMe})Et$ (**30**) and $Al(N_2^{Ts}N^{py})Et$ (**31**), respectively.

Scheme 4.1. Synthesis of the new aluminium ethyl complexes **27 - 31**.



The ^{1}H NMR shift of the 2-position hydrogen atom of the pyridyl donor of **31** (δ = 9.05 ppm, Figure 4.4) in CD_2Cl_2 is significantly shifted from that in the free ligand (δ = 8.58 ppm in the same solvent). This is consistent with coordination to Al, giving the 5-coordinate geometry illustrated in Scheme 4.1. The isolated yields for **27-31** were in the range 55-70% after recrystallisation. NMR tube scale monitoring of these reactions in C_6D_6 showed quantitative formation of the complexes.

Figure 4.4. ^{1}H NMR spectrum (299.9 MHz) of **31** in CD_2Cl_2 at 298 K ('s' denotes residual protio-solvent).



4.6 Solid state structures of aluminium alkyl complexes 27, 29 - 31

The X-ray structures of compounds **27**, **29 - 31** have been determined and are compared in Figure 4.5. Selected distances and angles are listed in Tables 4.1–4.4. The solid state structures are consistent with those proposed in Scheme 4.1 on the basis of solution NMR and other analytical data.

Figure 4.5. Displacement ellipsoid plots of Al(CyN_2^{Ts})Et(THF) (**27**, top left), Al($N_2^{Ts}N^{Ph}$)Et (**29**, top right), Al($N_2^{Ts}N^{OMe}$)Et (**30**, bottom left) and Al($N_2^{Ts}N^{py}$)Et (**31**, bottom right). H atoms omitted for clarity. Ellipsoids are drawn at the 20% probability level.

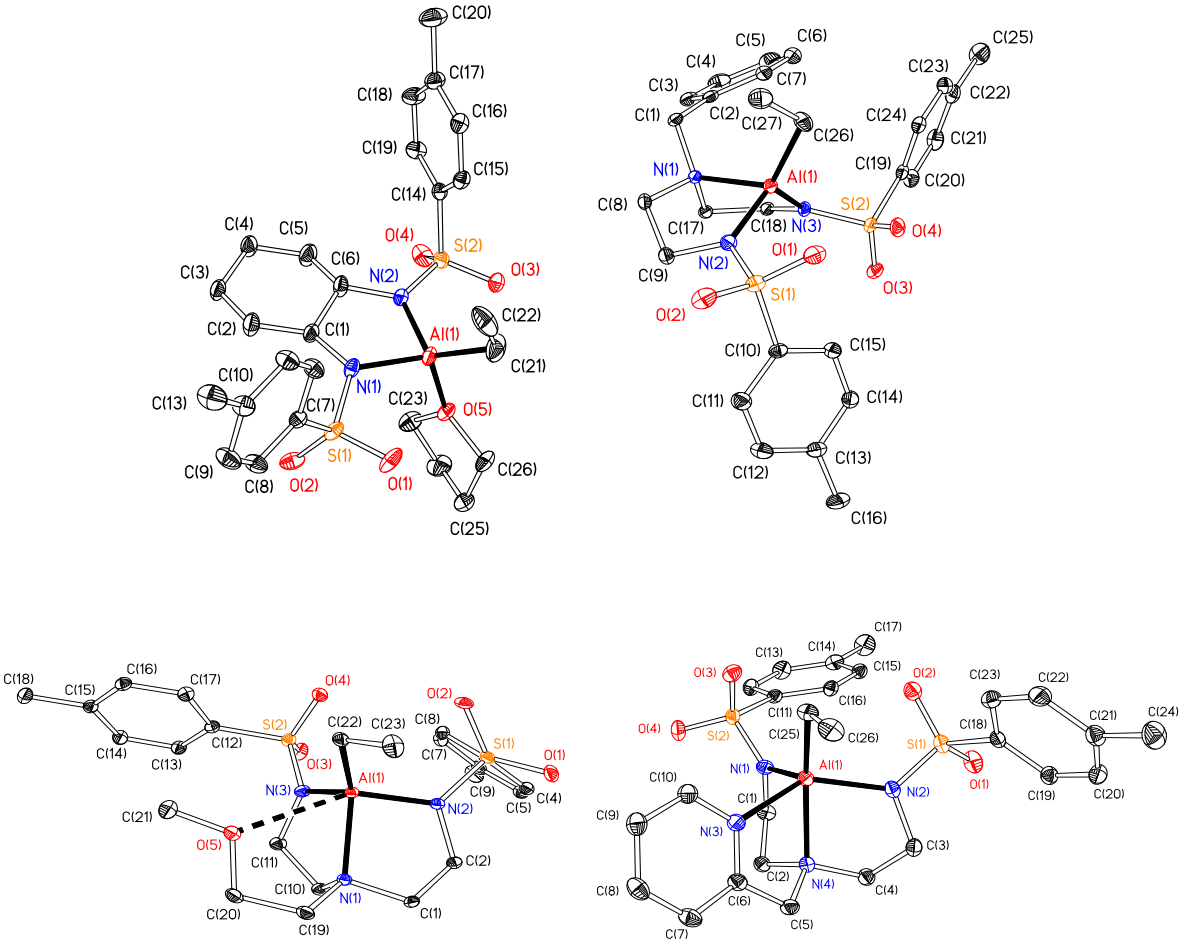


Table 4.1. Selected bond distances (Å) and angles (°) for Al(CyN_2^{Ts})Et(THF) (**27**).

Al(1)-N(1)	1.867(3)	Al(1)-O(5)	1.858(2)
Al(1)-N(2)	1.872(3)	Al(1)-C(21)	1.949(4)
N(1)-Al(1)-N(2)	85.95(11)	N(1)-Al(1)-O(5)	106.7(1)
N(2)-Al(1)-O(5)	103.54(13)	N(1)-Al(1)-C(21)	123.6(2)
N(2)-Al(1)-C(21)	124.1(2)	O(5)-Al(1)-C(21)	109.5(2)

Table 4.2. Selected bond distances (Å) and angles (°) for Al($N_2^{Ts}N^{Ph}$)Et (**29**).

Al(1)-N(1)	2.023(2)	Al(1)-N(3)	1.858(2)
Al(1)-N(2)	1.864(2)	Al(1)-C(26)	1.940(3)
N(1)-Al(1)-N(2)	87.15(9)	N(1)-Al(1)-N(3)	86.37(9)
N(2)-Al(1)-N(3)	116.3(1)	N(1)-Al(1)-C(26)	120.6(1)
N(2)-Al(1)-C(26)	114.6(1)	N(3)-Al(1)-C(26)	122.8(1)

Table 4.3. Selected bond distances (Å) and angles (°) for Al($N_2^{Ts}N^{OMe}$)Et (**30**).

Al(1)-N(1)	2.035(1)	Al(1)-C(22)	1.949(2)
Al(1)-N(2)	1.895(2)	Al(1)···O(5)	2.830(1)
Al(1)-N(3)	1.860(2)		
N(1)-Al(1)-N(2)	86.06(6)	N(1)-Al(1)-N(3)	88.00(6)
N(2)-Al(1)-N(3)	112.3(1)	N(1)-Al(1)-C(22)	126.8(1)
N(2)-Al(1)-C(22)	112.1(1)	N(3)-Al(1)-C(22)	124.2(1)
N(1)-Al(1)···O(5)	67.38(5)	N(2)-Al(1)···O(5)	151.0(1)
N(3)-Al(1)···O(5)	79.54(6)	O(5)···Al(1)-C(22)	77.72(6)

Table 4.4. Selected bond distances (Å) and angles (°) for Al($N_2^{Ts}N^{py}$)Et (**31**).

Al(1)-N(1)	1.911(2)	Al(1)-N(4)	2.185(2)
Al(1)-N(2)	1.952(2)	Al(1)-C(25)	1.986(2)
Al(1)-N(3)	2.107(2)		
N(1)-Al(1)-N(2)	111.65(8)	N(1)-Al(1)-N(3)	102.0(1)
N(1)-Al(1)-N(4)	82.92(7)	N(2)-Al(1)-N(3)	133.8(1)
N(2)-Al(1)-N(4)	79.20(7)	N(3)-Al(1)-N(4)	74.31(7)
N(1)-Al(1)-C(25)	118.0(1)	N(2)-Al(1)-C(25)	100.3(1)
N(3)-Al(1)-C(25)	90.47(8)	N(4)-Al(1)-C(25)	156.7(1)

Compounds **27** and **29** have approximately tetrahedral aluminium centres. Each Al is bonded to two tosyl amide nitrogens and one ethyl ligand, with no significant difference between the Al-N_{Ts} and Al-C distances for the two compounds. In **27** the fourth coordination site is occupied by a THF ligand whereas in **29** the tertiary nitrogen (N_{am}) of $N_2^{Ts}N^{Ph}$ fulfils this role. The aluminium in **30** is also approximately tetrahedral, with an additional long Al···O distance of 2.8305(14) to the pendant arm methoxy donor. The Al···O interaction barely perturbs the coordination sphere around Al as judged by comparison with the $N_2^{Ts}N^{Ph}$ analogue **29** bearing a non-interacting CH_2Ph arm (**29**: Al-C = 1.940(3) Å, N_{am}-Al-C = 120.56(12)°; **30**: Al-C = 1.949(2) Å, N_{am}-Al-C = 126.84(8)°). In contrast, Al($N_2^{Ts}N^{py}$)Et (**31**), featuring an additional pyridyl donor, has a distorted trigonal bipyramidal geometry with an Al-N_{py} distance (2.107(2) Å) within the expected range for a dative bond,[63] consistent with the solution ^{1}H NMR data mentioned above. The N_{am}-Al-C angle has opened up to 156.74(8)° to accommodate the additional donor, and the Al-C (1.986(2) Å) and Al-N_{Ts} (av. 1.932(1) Å) distances are significantly longer than those in **27**, **29** and **30** (range 1.940(3)–1.949(4) and 1.858(2)–1.895(2) Å).

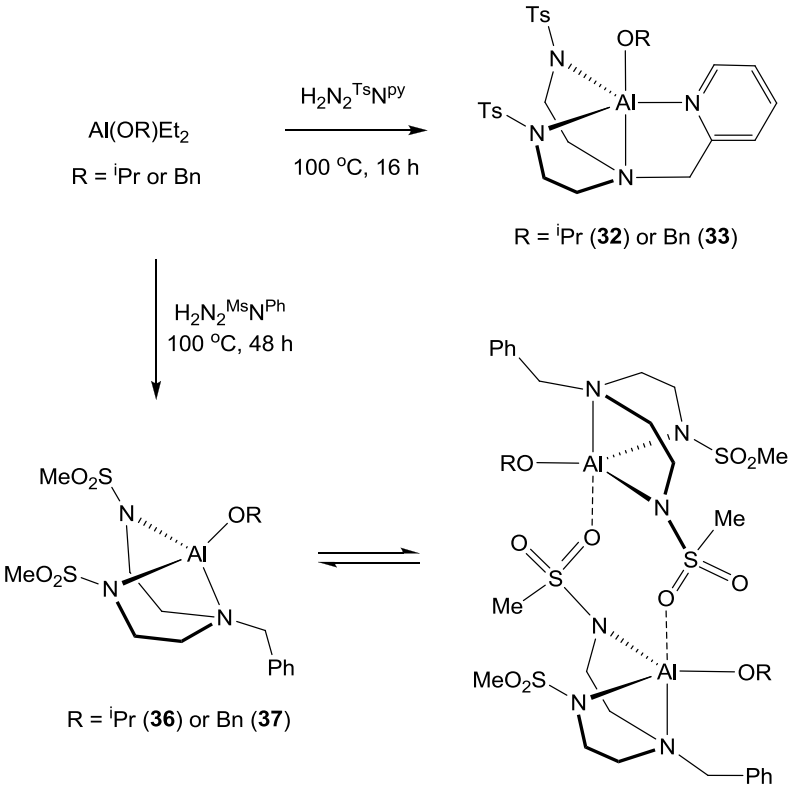
Only two crystallographically characterised aluminium tosyl sulfonamide compounds have been reported previously, namely **1.22** (Figure 4.3)[55] and *S*,*S*,*S*-Al{N(CH(Me)CH_2NTs)$_3$}.[64] Both have additional intramolecular S=O···Al interactions (as shown in Figure 4.3 for **1.22**) which are absent in **27**–**31**. There have also been a number of structures reported for aluminium complexes containing

$N(R)SO_2CF_3$ donors, including the 4-coordinate alkyl complex **1.43** in Figure 4.3 which has a comparable geometry to **27**, **29** and **30**.[56,57,65,66]

4.7 Synthesis of aluminium alkoxide complexes

As mentioned, it was hoped that the new aluminium alkyls would serve as entry points to the corresponding alkoxide complexes which are usually superior initiators for ROP. Unfortunately, reaction of **27 - 31** with either isopropyl or benzyl alcohol yielded mixtures of protio-ligand, residual metal alkyl and $Al(OR)_3$ species in benzene at room temperature. Performing the reactions at low temperature in alternative solvents and/or at high dilution gave similar mixtures. Therefore, a different route to alkoxide complexes was sought. Drawing upon the previous work on titanium complexes where sulfonamide ligand protonolysis was also an issue (Chapter 2),[67] the focus was shifted to reactions with mixed alkyl-alkoxide aluminium precursors of the type $Al(OR)Et_2$ (R = ^{i}Pr or Bn).[68,69]

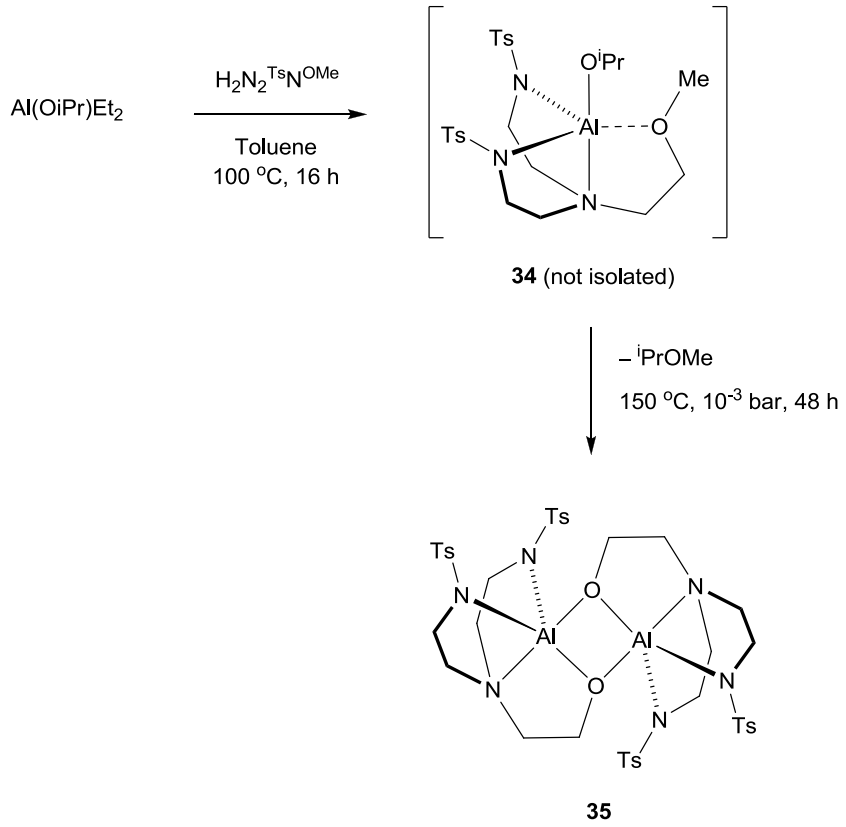
Scheme 4.2. Synthesis of the new aluminium alkoxide complexes **32**, **33**, **36** and **37**.



Reaction of $H_2CyN_2^{Ts}$ (**3.2**) or $H_2N_2^{Ts}N^{Ph}$ (**7**) with $Al(OR)Et_2$ (R = ^{i}Pr or Bn) led to complicated product mixtures from which no single product could be isolated. The corresponding reaction for $H_2CyN_2^{SO_2Mes}$ (**3.3**) also gave a mixture of products, among

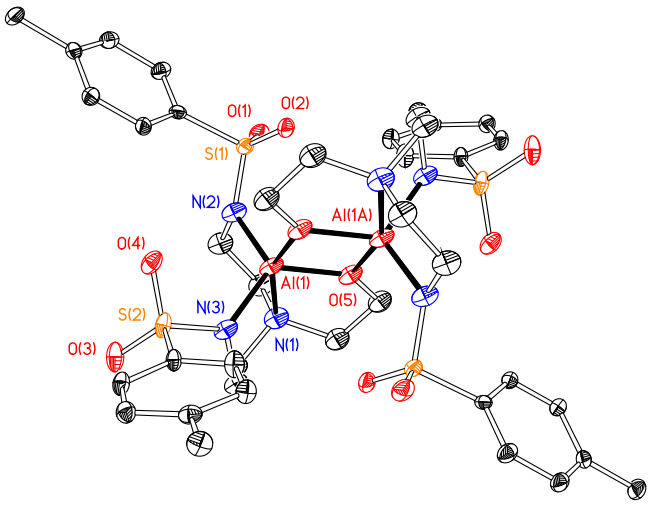
which was Al($CyN_2^{SO_2Mes}$)Et(THF) (**28**), indicative of redistribution reactions. However, reaction of $H_2N_2^{Ts}N^{py}$ with Al(OR)Et_2 proceeded smoothly at 100 °C to give Al($N_2^{Ts}N^{py}$)(O^iPr) (**32**) and Al($N_2^{Ts}N^{py}$)(OBn) (**33**) in *ca*. 65% isolated yield (Scheme 4.2). The NMR data for these compounds are in agreement with 5-coordinate, C_s symmetric aluminium compounds as confirmed crystallographically for Al($N_2^{Ts}N^{py}$)Et (**31**).

Scheme 4.3. Ligand demethylation leading to [Al($N_2^{Ts}N^{O}$)]$_2$ (**35**).



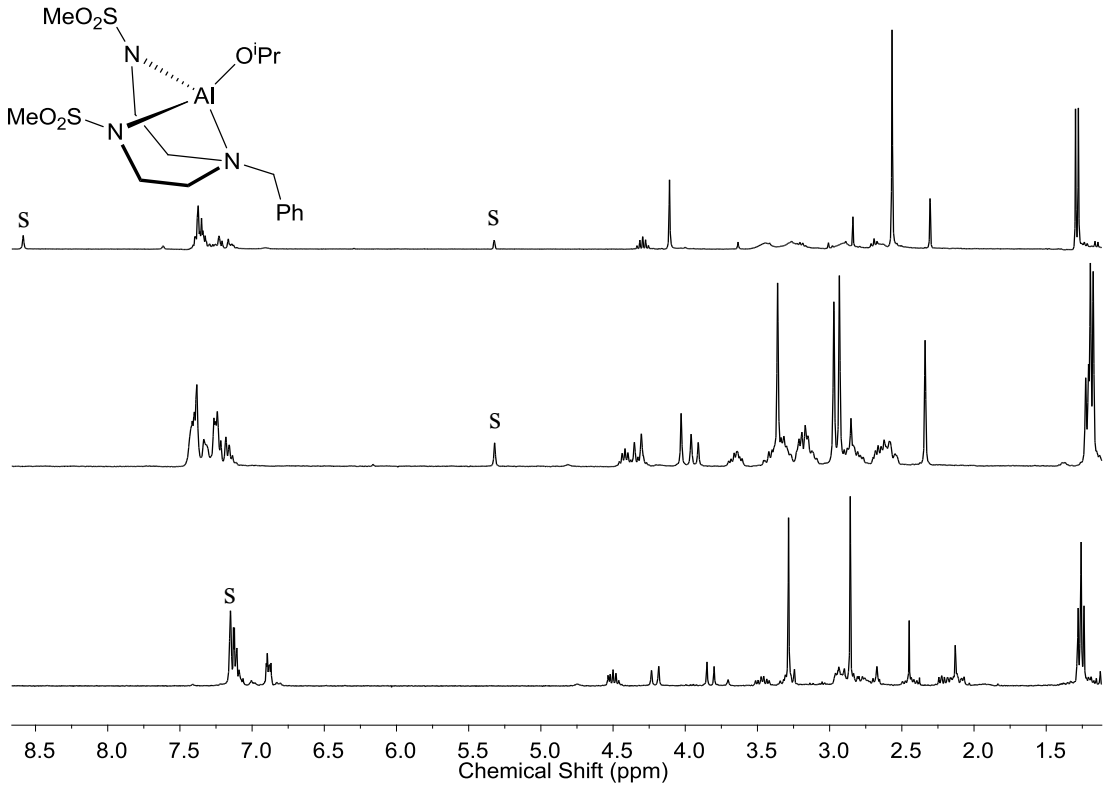
Surprisingly, reaction of $H_2N_2^{Ts}N^{OMe}$ (**2.8**) with Al(O^iPr)Et_2 gave a mixture of products, among which appeared to be the desired alkoxide Al($N_2^{Ts}N^{OMe}$)O^iPr (**34**, Scheme 4.3). However, attempted purification by crystallisation afforded only the ligand-demethylated dimer [Al($N_2^{Ts}N^{O}$)]$_2$ (**35**, $N_2^{Ts}N^{O}$ = $OCH_2CH_2N(CH_2CH_2NTs)_2$) as colourless crystals. The ^{1}H and ^{13}C-{^{1}H} NMR data and a preliminary X-ray structure determination (Figure 4.6) are consistent with the structure illustrated in Scheme 4.3. The molecular structure features a distorted trigonal bipyramidal aluminium centre with bridging methoxy groups. Compound **35** could be reproducibly synthesised in 49 % overall yield by heating the crude initial mixture containing **34** at 150 °C under reduced pressure for 48h.

Figure 4.6. Preliminary structure determination of $[Al(N_2{}^{Ts}N^{O})]_2$ (**35**). The data were of insufficient quality to permit a complete refinement.



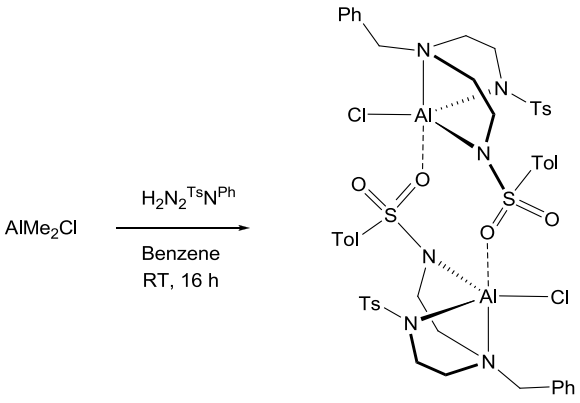
In contrast to the mixtures formed with the tosylated protio-ligand **7**, reaction of $H_2N_2{}^{Ms}N^{Ph}$ (**8**, -NSO_2Me substituted) with $Al(OR)Et_2$ gave $Al(N_2{}^{Ms}N^{Ph})(O^{i}Pr)$ (**36**) and $Al(N_2{}^{Ms}N^{Ph})(OBn)$ (**37**) in good yield (Scheme 4.2). NMR investigations of analytically pure samples in various solvents showed a mixture of monomeric and dimeric species in solution. For example, in C_6D_6 the compounds exist as C_2-symmetric dimers with the PhC$\underline{H}_2$N protons appearing as two mutually-coupled doublets, consistent with S=O···Al bridging sulfone groups in a manner analogous to that for $[Al(N_2{}^{Ts}N^{Ph})Cl]_2$ (**36**, see below). In CD_2Cl_2, the spectra show a *ca*. 1:2 mixture of both dimeric and monomeric (C_s symmetric, akin to $Al(N_2{}^{Ts}N^{Ph})Et$ (**29**)) species, the latter being represented by a singlet for the PhC$\underline{H}_2$N protons. Addition of a few drops of pyridine-d_5 to the CD_2Cl_2 solution significantly simplified the spectrum, consistent with the formation of Lewis base adducts $Al(N_2{}^{Ms}N^{Ph})(OR)$(pyridine-d_5) (Figure 4.7).

Figure 4.7. ^{1}H NMR spectrum (299.9 MHz) of **36** in CD_2Cl_2 with d_5-pyridine (top), CD_2Cl_2 (middle) and C_6D_6 (bottom) at 298 K ('s' denotes residual protio-solvent).



4.8 Synthesis of an aluminium chloride complex

Since reactions between $H_2N_2{}^{Ts}N^{Ph}$ and $Al(OR)Et_2$ gave intractable mixtures, alternative routes to the target alkoxides *via* the corresponding chloride complex were investigated. Reaction of $AlMe_2Cl$ with $H_2N_2{}^{Ts}N^{Ph}$ (**7**) gave $[Al(N^{Ts}{}_2N^{Ph})Cl]_2$ (**38**, Equation 4.1) in 58% yield after recrystallisation.



38

Equation 4.1

The molecular structure is shown in Figure 4.8 and selected bond lengths and angles are given in Table 4.5. Compound **38** is an approximately C_2-symmetric, dimeric species formed though two bridging S=O···Al interactions (Al(1)-O(8) = 1.874(3) Å; Al(2)-O(4) = 1.854(2) Å) as has been observed previously,[56,66] Each Al has an approximately trigonal bipyramidal geometry with the Cl ligands and N_{Ts} donors occupying the equatorial positions. The Al-N_{Ts} distances in **38** (av. 1.904(2) Å, range 1.892(3)–1.916(3) Å) in general lie within the ranges mentioned above. However, the Al-N_{Ts} distances associated with the bridging SO_2Tol groups (av. 1.914(2) Å) are significantly longer than those for the non-bridging ones (av. 1.894(2) Å). Similarly, the S=O···Al interactions significantly lengthen the tosyl S=O bonds (S(2,4)=O = 1.477(2) Å for the bridging oxygens *vs* av. S(2,4)=O = 1.434(2) Å for the terminal ones).

It is interesting to contrast the monomeric nature of 4-coordinate Al($N_2^{Ts}N^{Ph}$)Et (**29**) with the dimeric one found for [Al($N^{Ts}{}_2N^{Ph}$)Cl]$_2$. The difference can be attributed to differences in electronegativity of the ligands, Et and Cl. The solution ^{1}H and ^{13}C-{^{1}H} NMR data for **38** are consistent with this structure being retained in solution, and the spectra are similar to those of the dimeric forms of the alkoxide analogues **36** and **37** (Scheme 4.2). Unfortunately, attempts to make alkoxide complexes analogous to **36** and **37** from **38** using LiOR (R = ^{i}Pr or Bn) were unsuccessful, again giving intractable mixtures of products.

Figure 4.8. Displacement ellipsoid plot of [Al($N^{Ts}{}_2N^{Ph}$)Cl]$_2$ (**38**). H atoms omitted for clarity. Ellipsoids are drawn at the 20% probability level.

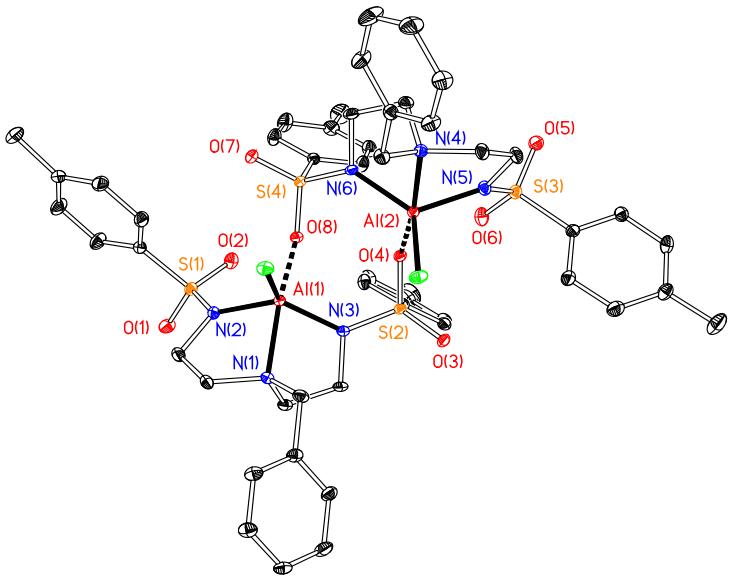


Table 4.5. Selected bond distances (Å) and angles (°) for $[Al(N^{Ts}{}_2N^{Ph})Cl]_2$ (**38**).

Al(1)-N(1)	2.085(3)	Al(2)-N(4)	2.100(3)
Al(1)-N(2)	1.895(3)	Al(2)-N(5)	1.892(3)
Al(1)-N(3)	1.912(3)	Al(2)-N(6)	1.916(3)
Al(1)-O(8)	1.874(3)	Al(2)-O(4)	1.854(2)
Al(1)-Cl(1)	2.178(1)	Al(2)-Cl(2)	2.181(1)
S(2)-O(3)	1.435(3)	S(4)-O(7)	1.434(2)
S(2)-O(4)	1.477(2)	S(4)-O(8)	1.477(2)
N(1)-Al(1)-N(2)	81.68(13)	N(1)-Al(1)-N(3)	80.1(1)
N(1)-Al(1)-N(3)	118.95(13)	N(1)-Al(1)-O(8)	171.7(1)
N(2)-Al(1)-O(8)	99.63(12)	N(3)-Al(1)-O(8)	92.2(1)
N(1)-Al(1)-Cl(1)	93.1(1)	N(2)-Al(1)-Cl(1)	110.9(1)
N(3)-Al(1)-Cl(1)	127.78(10)	O(8)-Al(1)-Cl(1)	94.10(9)
N(4)-Al(2)-N(5)	82.15(13)	N(4)-Al(2)-N(6)	80.7(1)
N(5)-Al(2)-N(6)	118.79(14)	N(4)-Al(2)-O(4)	171.5(1)
N(5)-Al(2)-O(4)	100.28(13)	N(6)-Al(2)-O(4)	91.0(1)
N(4)-Al(2)-Cl(2)	92.57(9)	N(5)-Al(2)-Cl(2)	110.3(1)
N(6)-Al(2)-Cl(2)	128.72(10)	N(6)-Al(2)-Cl(2)	94.21(9)

4.9 Synthesis of aluminium sulfonamide complexes bearing ethoxyamine ligands

In a further effort to stabilise well-defined monomeric alkoxide ROP initiators, reactions were undertaken using $Al(OCH_2CH_2NH_2)Et_2$.[70] This contains a potentially chelating amine functional group which may confer additional stability on the target complexes. A similar strategy was employed by Coates to stabilise yttrium analogues of **1.30** (Figure 4.2).[37] This known compound was structurally characterised and further details are given in Figure 4.9 and Table 4.6. The molecular structure of $Al(OCH_2CH_2NH_2)Et_2$ features a distorted trigonal bipyramidal geometry with bridging methoxy arms, reminiscent of partial structure observed for $[Al(N_2{}^{Ts}N^{O})]_2$ (**35**) (Figure 4.6).

Figure 4.9. Displacement ellipsoid plot of $Al(OCH_2CH_2NH_2)Et_2$. C-bound H atoms omitted for clarity, H(1) and H(2) drawn as spheres of arbitrary radius. Ellipsoids are drawn at the 20% probability level.

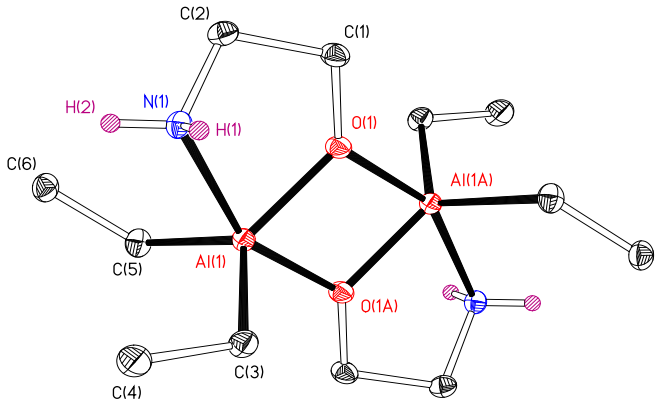


Table 4.6. Selected bond distances (Å) and angles (°) for $Al(OCH_2CH_2NH_2)Et_2$.

Al(1)-O(1)	1.8502(11)	Al(1)-O(1A)	1.933(1)
Al(1)-N(1)	2.151(1)	Al(1)-C(3)	1.993(2)
Al(1)-C(5)	1.9987(16)	N(1)-H(1)	0.89(2)
N(1)-H(2)	0.86(2)		
O(1A)-Al(1)-N(1)	153.81(5)	O(1A)-Al(1)-C(3)	98.38(6)
N(1)-Al(1)-C(3)	93.43(6)	O(1A)-Al(1)-C(5)	97.19(6)
N(1)-Al(1)-C(5)	97.74(6)	C(3)-Al(1)-C(5)	118.0(1)
O(1A)-Al(1)-O(1)	74.76(5)	N(1)-Al(1)-O(1)	79.28(5)
C(3)-Al(1)-O(1)	124.65(6)	C(5)-Al(1)-O(1)	117.3(1)

As summarized in Scheme 4.4, heating toluene solutions of $Al(OCH_2CH_2NH_2)Et_2$ with $H_2N_2{}^{Ts}N^{Ph}$, $H_2N_2{}^{Ts}N^{OMe}$ or $H_2N_2{}^{Ts}N^{py}$ successfully gave the corresponding 2-aminoethoxide complexes $Al(N_2{}^{Ts}N^{Ph})(OCH_2CH_2NH_2)$ (**39**), $Al(N_2{}^{Ts}N^{OMe})(OCH_2CH_2NH_2)$ (**40**) and $Al(N_2{}^{Ts}N^{py})(OCH_2CH_2NH_2)$ (**41**), respectively, in isolated yields of 68–79%. The products of the corresponding reaction with $H_2CyN_2{}^{Ts}$ (**3.2**) gave broad and complicated spectra for which it was not possible to confidently assign. The solid state structure of **40** has been determined and is shown in Figure 4.10. Selected bond distances and angles are given in Table 4.7.

Scheme 4.4. Synthesis of aluminium sulfonamide complexes bearing a 2-aminoethoxide ligand.

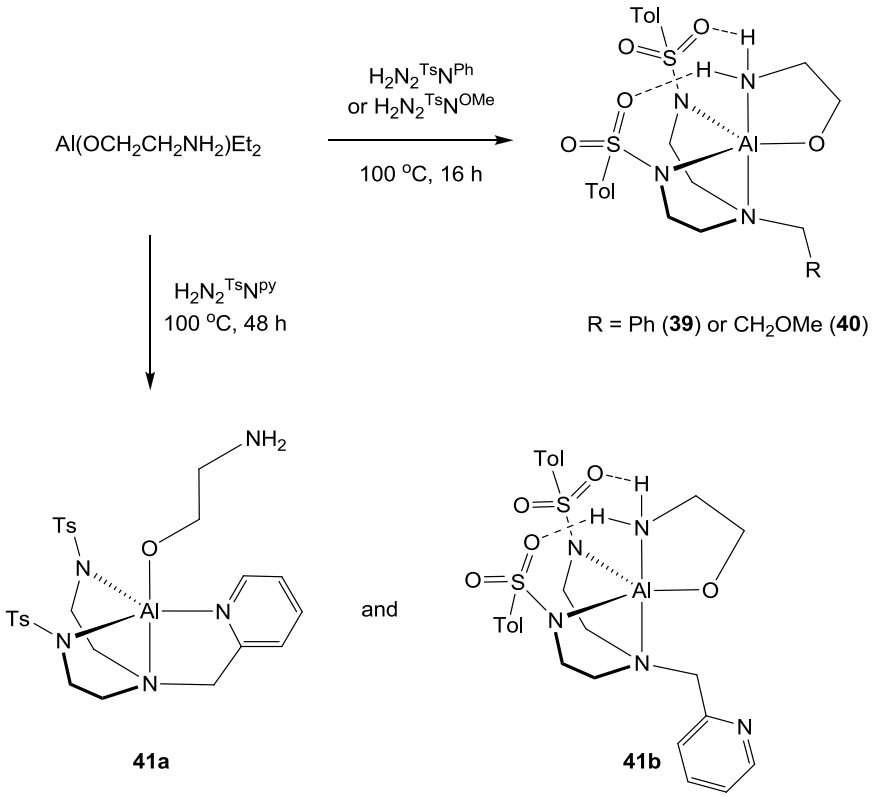


Figure 4.10. Displacement ellipsoid plot of $Al(N_2^{Ts}N^{OMe})(OCH_2CH_2NH_2)$ (**40**). C-bound H atoms omitted for clarity. H(1) and H(2) are drawn as spheres of arbitrary radius. Ellipsoids are drawn at the 20% probability level.

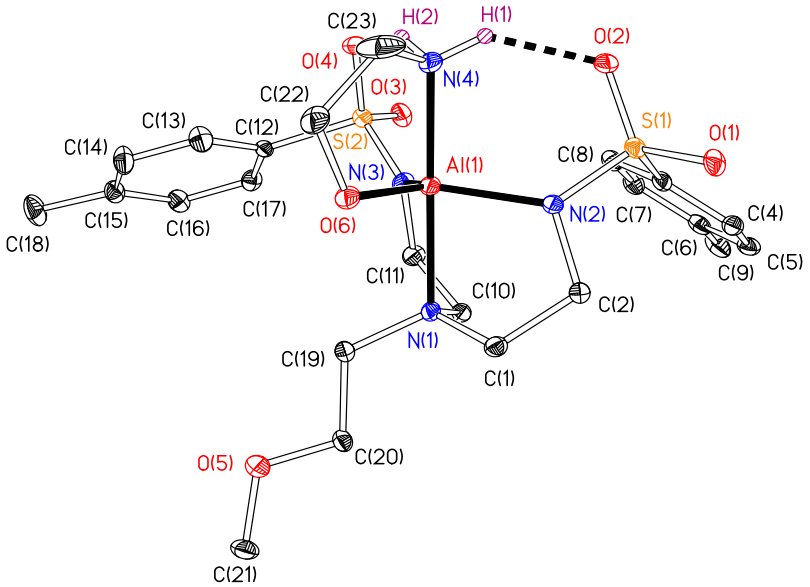


Table 4.7. Selected bond distances (Å) and angles (°) for $Al(N_2^{Ts}N^{OMe})(OCH_2CH_2NH_2)$ (**40**).

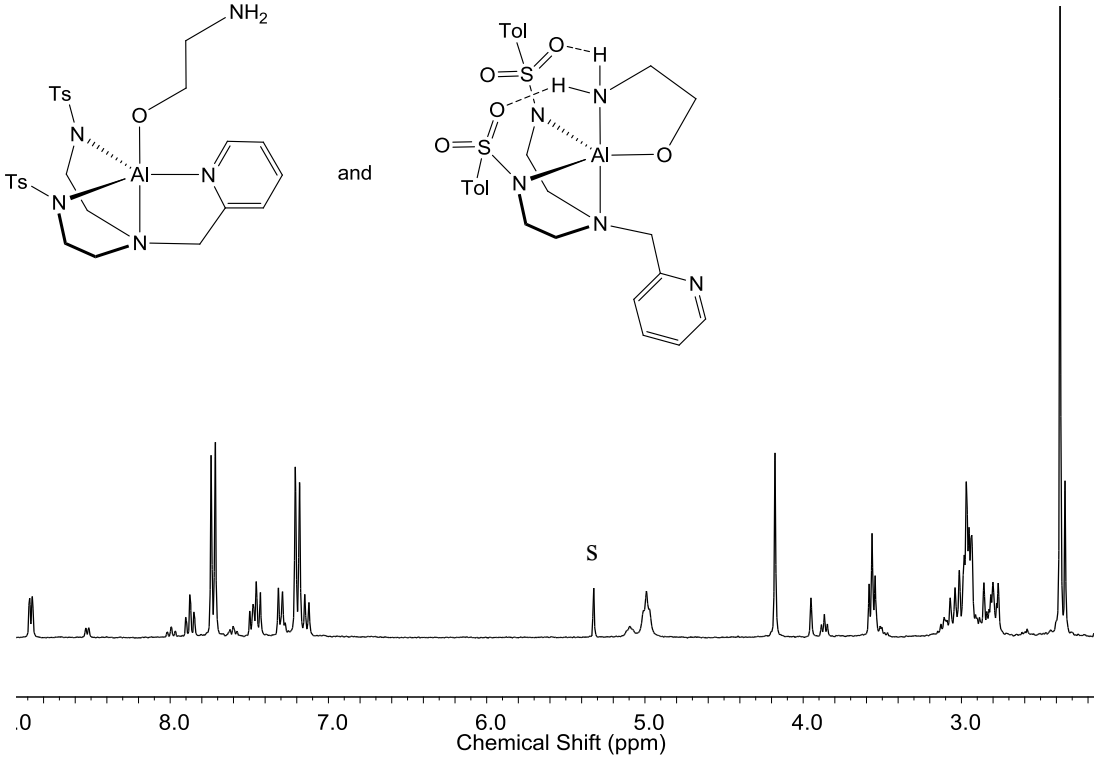
Al(1)-N(1)	2.078(4)	O(2)···H(1)	1.95(7)
Al(1)-N(2)	1.917(4)	O(4)···H(2)	2.06(7)
Al(1)-N(3)	1.915(4)	S(1)-O(1)	1.448(4)
Al(1)-N(4)	2.006(5)	S(1)-O(2)	1.439(4)
Al(1)-O(6)	1.759(4)	S(2)-O(3)	1.441(4)
N(4)-H(1)	0.94(7)	S(3)-O(4)	1.443(4)
N(4)-H(2)	0.81(7)		
N(1)-Al(1)-N(2)	82.68(17)	N(1)-Al(1)-N(3)	83.3(1)
N(2)-Al(1)-N(3)	114.82(19)	N(1)-Al(1)-N(4)	175.4(2)
N(2)-Al(1)-N(4)	95.8(2)	N(3)-Al(1)-N(4)	101.3(2)
N(1)-Al(1)-O(6)	90.71(17)	N(2)-Al(1)-O(6)	120.7(2)
N(3)-Al(1)-O(6)	122.83(19)	N(4)-Al(1)-O(6)	86.3(2)

$Al(N_2^{Ts}N^{OMe})(OCH_2CH_2NH_2)$ (**40**) has a distorted trigonal bipyramidal geometry and approximate C_s molecular symmetry. The anionic sulfonamide nitrogen and alkoxide oxygen donors occupy the equatorial positions, and the tertiary N_{am} of $N_2^{Ts}N^{OMe}$ and the NH_2 of the aminoethoxide take up the axial positions, the latter having comparable bond lengths (Al–N_{am} = 2.078(4); Al–NH_2 = 2.006(5) Å). The OMe donor of the pendant arm is not coordinated, displaced in preference for NH_2 coordination (the primary amine being the more effective Lewis base). In addition, amine coordination is supplemented by intramolecular hydrogen bonding between the NH_2 hydrogens and two adjacent sulfonamide oxygen atoms. The NH···O_{Ts} distances of 1.95(7) and 2.06(7) Å are within the expected ranges for such interactions.[63,71] The IR spectrum of **40** shows ν(N-H) bands at 3306 and 3268 cm^{-1} which are shifted to lower frequency compared to those in the starting compound $Al(OCH_2CH_2NH_2)Et_2$ (ν(N-H) = 3356 and 3287 cm^{-1}) which has a chelating $OCH_2CH_2NH_2$ ligand but no NH···O hydrogen bonds (Figure 4.9). There are no significant differences in length between the S=O bonds engaged in hydrogen bonding (S(1)-O(2), S(2)-O(4)) and those which are not. The Al-N_{Ts} distances (1.917(4) and 1.915(4) Å) are slightly shorter than those in

Al($N_2^{Ts}N^{py}$)Et (**31**, av. 1.932(1) Å) and very similar to those for [Al($N^{Ts}_2N^{Ph}$)Cl]$_2$ (**38**) (av. 1.904(2) Å).

The IR spectrum of Al($N_2^{Ts}N^{Ph}$)($OCH_2CH_2NH_2$) (**39**) has similar ν(N-H) bands (3308 and 3262 cm^{-1}) to those of **40** and a similar structure is proposed (Scheme 4.4). Note that in the otherwise identical Al($N_2^{Ts}N^{Ph}$)($OCH_2CH_2NMe_2$) (**42**, see below), which has an NMe_2 donor in place of NH_2, these bands are absent. The ^{1}H and ^{13}C-{^{1}H} NMR spectra of **39** and **40** are comparable and relatively simple, and consistent with the presence of one 5-coordinate, C_s symmetric isomer in solution in each case.

Figure 4.11. ^{1}H NMR spectrum (299.9 MHz) of **41** in CD_2Cl_2 at 298 K ('s' denotes residual protio-solvent).



In contrast, the IR spectrum of Al($N_2^{Ts}N^{py}$)($OCH_2CH_2NH_2$) (**41**) shows at least four ν(N-H) bands in the range 3320-3160 cm^{-1}, and the solution ^{1}H and ^{13}C-{^{1}H} NMR spectra suggest a mixture of two isomers, **41a** (major) and **41b** (minor) in a *ca*. 2:1 ratio. Both isomers have C_s symmetry and the same composition "Al($N_2^{Ts}N^{py}$)($OCH_2CH_2NH_2$)" according to integration, consistent with the satisfactory elemental analysis for bulk samples of **41**. The ^{1}H NMR shift of the 2-position hydrogen atom of the pyridyl donor in the major isomer appears at δ = 8.87 ppm, consistent with coordination to Al,[67] whereas the shift of δ = 8.52 ppm for the

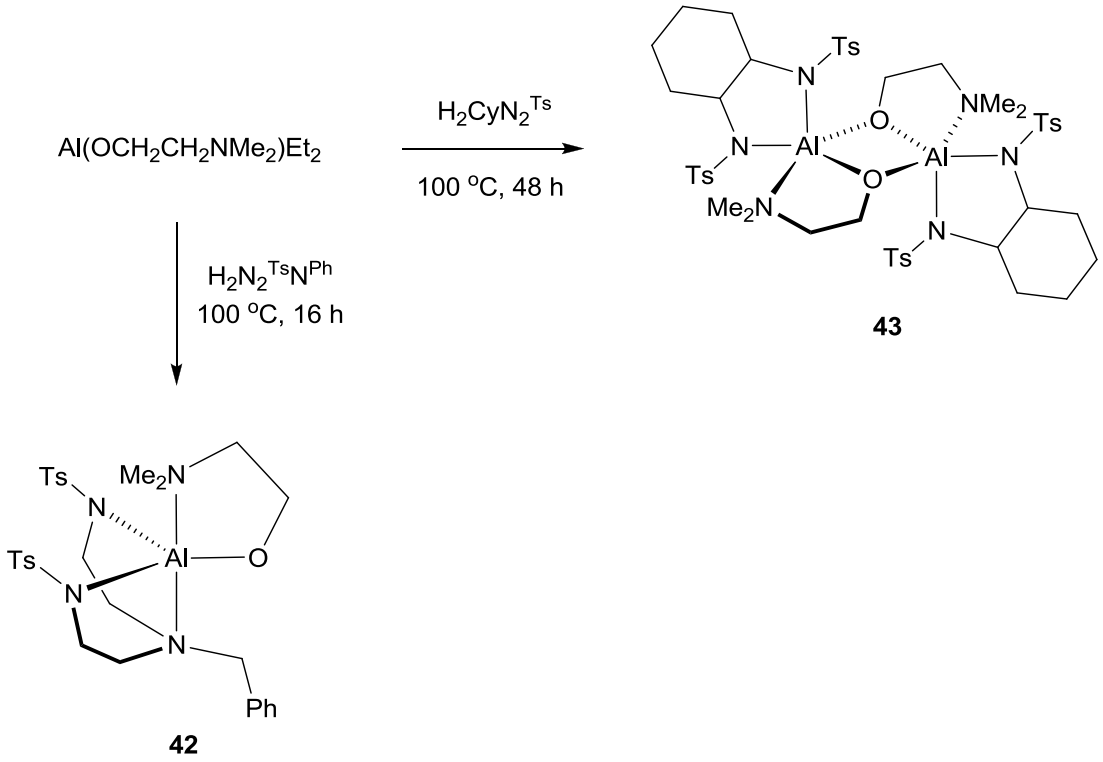
minor isomer is very close to that of the free $H_2N_2^{Ts}N^{py}$ itself in CD_2Cl_2 (δ = 8.58 ppm). These NMR data are interpreted in terms of the structures proposed in Scheme 4.4, with the pendant pyridyl and NH_2 donors competing for the vacant coordination site at Al.

4.10 Synthesis of aluminium sulfonamide complexes bearing a 2-*N*,*N*-dimethylaminoethoxide ligand

As described below, the use of an aminoethoxide ligand in **39**–**41** appeared to lead to poor performance with regard to the controlled ROP of *rac*-LA. To probe these aspects we prepared some representative complexes containing a 2-*N*,*N*-dimethylaminoethoxide ligand (Scheme 4.5), in effect replacing NH_2 with NMe_2. Reaction of $H_2N_2^{Ts}N^{Ph}$ with $Al(OCH_2CH_2NMe_2)Et_2$[70] gave monomeric $Al(N_2^{Ts}N^{Ph})(OCH_2CH_2NMe_2)$ (**42**). The NMR spectra for **42** were consistent with the 5-coordinate structure proposed in Scheme 4.5, which is analogous to those of **39**, **40** and **41b**, but without the intramolecular hydrogen bonding. The spectra indicated molecular C_s symmetry (e.g., equivalent SO_2Tol substituents and NMe_2 methyl groups), and nOe (nuclear Overhauser effect) experiments confirmed the *trans* arrangement of the tertiary N_{am} and NMe_2 donors, together with coordination of NMe_2 to Al.

Whereas reaction of $H_2CyN_2^{Ts}$ with $Al(OCH_2CH_2NH_2)Et_2$ gave rather ill-defined materials (see above), reaction with $Al(OCH_2CH_2NMe_2)Et_2$ formed "$Al(CyN_2^{Ts})(OCH_2CH_2NMe_2)$" (**43**) in 85% isolated yield. The NMR spectra for **43** are more complicated than would be expected for a C_s-symmetric, 4-coordinate monomer analogous to $Al(CyN_2^{Ts})Et(THF)$ and $Al(CyN_2^{SO_2Mes})Et(THF)$ (Scheme 4.1), showing, for example, inequivalent SO_2Tol substituents and NMe_2 methyl groups. As such it is proposed that **43** possesses the dimeric structure shown in Scheme 4.5. A number of related dimeric aluminium complexes containing a $OCH_2CH_2NMe_2$ or related 2-aminoethoxide ligand in the arrangement shown for **43** have been structurally authenticated,[63] including $Al(OCH_2CH_2NH_2)Et_2$ (Figure 4.9).

Scheme 4.5. Synthesis of aluminium sulfonamide complexes bearing an $OCH_2CH_2NMe_2$ ligand.



4.11 Polymerisation studies: solution ROP of *rac*-LA

The series of complexes $Al(N_2^{Ts}N^{R})Et$ (R = Ph (**49**) or py (**31**)), $Al(N_2^{Ts}N^{py})(OR')$ (R′ = ^{i}Pr (**32**) or Bn (**33**)), $Al(N_2^{Ms}N^{Ph})(OR')$ (R′ = ^{i}Pr (**36**) or Bn (**37**)), $Al(N_2^{Ts}N^{R})(OCH_2CH_2NH_2)$ (R = Ph (**39**), OMe (**40**) or py (**41**)), $Al(N_2^{Ts}N^{Ph})(OCH_2CH_2NMe_2)$ (**42**) and $Al(CyN_2^{Ts})(OCH_2CH_2NMe_2)$ (**43**) allowed the systematic evaluation of the effects of sulfonamide ligand coordination number and N-substituents, and initiating group type (Et, "simple" alkoxide or 2-aminoethoxide). Each was assessed for its ROP performance for *rac*-LA. ROP experiments were performed in toluene at 70 °C ($[rac\text{-LA}]_0$:[Al] = 100:1) and under these conditions all the complexes were found to be active. The progress of each was monitored by regular sampling, and the results summarized in Table 4.8 correspond to 72 hours reaction time (see the Appendix for other data). The molecular weights and PDIs were determined by GPC using the appropriate Mark-Houwink corrections for PLA.[72-74] Polymerisation using these aluminium complexes required extended reaction times compared to the sulfonamide-supported zirconium analogues reported in Chapter 2.[67] For example the zirconium alkoxide catalyst based upon $N_2^{Ts}N^{OMe}$ achieved 94 %

conversion of 100 equivalents of *rac*-LA after *ca*. 6 h, (Chapter 2) while **40** reached 96% conversion only after 72 h. This observation is in agreement with literature precedent, for example, bis(phenolate) complexes of zirconium demonstrate enhanced activity compared to similar aluminium species.[51,75,76] This is due to the smaller radius of aluminium and formation of stable 5-membered lactide chelates which hinder monomer uptake.

Table 4.8. Solution polymerisation of *rac*-LA by Al($N_2^{Ts}N^{Ph}$)Et (**29**), Al($N_2^{Ts}N^{py}$)Et (**31**), Al($N_2^{Ts}N^{py}$)(O^iPr) (**32**), Al($N_2^{Ts}N^{py}$)(OBn) (**33**), Al($N_2^{Ms}N^{Ph}$)(O^iPr) (**36**), Al($N_2^{Ms}N^{Ph}$)(OBn) (**37**), Al($N_2^{Ts}N^{Ph}$)($OCH_2CH_2NH_2$) (**39**), Al($N_2^{Ts}N^{OMe}$)($OCH_2CH_2NH_2$) (**40**), Al($N_2^{Ts}N^{py}$)($OCH_2CH_2NH_2$) (**41**), Al($N_2^{Ts}N^{Ph}$)($OCH_2CH_2NMe_2$) (**42**) and Al(CyN_2^{Ts})($OCH_2CH_2NMe_2$) (**43**).[a]

Entry	Catalyst	Conversion (%)[b]	$k_{app.}$ (h^{-1})	M_n (GPC)[c]	M_n (calcd)[d]	M_w/M_n
1	Al($N_2^{Ts}N^{Ph}$)Et (**29**)	20	n.d.	18,320	2,910	1.47
2	Al($N_2^{Ts}N^{py}$)Et (**31**)	48	n.d.	13,060	8,870	1.73
3	Al($N_2^{Ts}N^{py}$)(O^iPr) (**32**)	83	0.0245(5)	19,480	12,010	1.11
4	Al($N_2^{Ts}N^{py}$)(OBn) (**33**)	87	0.0280(8)	14,270	12,610	1.14
5	Al($N_2^{Ms}N^{Ph}$)(O^iPr) (**36**)	81	0.0230(4)	16,040	11,690	1.12
6	Al($N_2^{Ms}N^{Ph}$)(OBn) (**37**)	76	0.0203(7)	16,340	11,690	1.12
7[e]	Al($N_2^{Ts}N^{py}$)(OBn) (**33**)	75	0.0185(6)	2,160	1,900	1.11
8	Al($N_2^{Ts}N^{Ph}$)($OCH_2CH_2NH_2$) (**39**)	96	n.d.	27,150	13,790	1.44
9	Al($N_2^{Ts}N^{OMe}$)($OCH_2CH_2NH_2$) (**40**)	96	n.d.	25,060	13,860	1.45
10	Al($N_2^{Ts}N^{py}$)($OCH_2CH_2NH_2$) (**41**)	93	n.d.	24,770	13,400	1.44
11	Al($N_2^{Ts}N^{Ph}$)($OCH_2CH_2NMe_2$) (**42**)	82	0.0235(11)	16,960	11,890	1.12
12	Al(CyN_2^{Ts})($OCH_2CH_2NMe_2$) (**43**)	76	0.0202(8)	30,460	10,740	1.22

[a] Conditions: [*rac*-LA]:[catalyst] = 100:1, 4.0 mL toluene at 70 °C. See Experimental section for other details. [b] % conversion by NMR at 72 h reaction time. [c] Molecular weights (g mol^{-1}) determined from GPC using the appropriate Mark-Houwink corrections. [d] Expected M_n (g mol^{-1}) for 1 chain growing per metal centre. [e] 5 equiv. $BnNH_2$ co-initiator. All polymer produced is predominantly atactic.

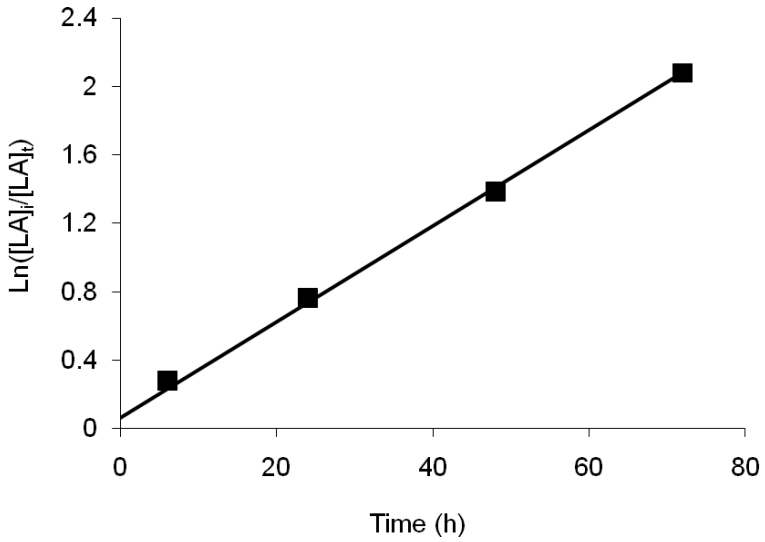
The ethyl complexes **29** and **31** (entries 1 and 2, Table 4.8) were found to be active but with relatively low conversions and poor control. Only *ca* 20–50 % of the *rac*-LA had been polymerized after 72 h, and the polymers formed had broad PDIs (*ca* 1.5–1.7) indicative of a poorly controlled process. The MALDI-ToF mass spectra of the polymers were complex and showed the presence of both cyclic poly(*rac*-LA) and linear chains terminated by EtC(O)CH(Me)O- end groups, the latter forming as a result of insertion of *rac*-LA into the Al-Et of the initiator. The M_n values measured by GPC were substantially higher than predicted based on conversion (judged by ^{1}H NMR analysis of the reaction mixtures) and assuming each aluminium centre is catalytically active. This deviation is consistent with poor rates of initiation (LA insertion into the Al–Et bond) compared to propagation (insertion into The Al–O bond of the so-formed Al–{OCH(Me)C(O)}$_n$–Et growing chains), which is a well-established feature of metal alkyl initiators.[77]

In contrast to **29** and **31**, the alkoxides complexes **32–37** were considerably better behaved (entries 3–6, Table 4.8). The polymerisation experiments were monitored at 6, 24, 48, and 72 h intervals and representative plots concerning the kinetic aspects and control of M_n and PDI are given in Figures 4.12 and 4.13 (see the Appendix for other plots). All gave first order consumption of *rac*-LA and a well-controlled polymerisation process as evidenced by narrow PDIs and a linear relationship between experimental M_n and % conversion. The gradients of the M_n *vs* % conversion plots were 237(13), 161(8), 208(10), and 220(6) g mol^{-1} (% conversion)$^{-1}$, respectively, which are higher than that expected (144.1 g mol^{-1} (% conversion)$^{-1}$ for [*rac*-LA]$_0$:[Al] = 100:1) for one poly(*rac*-LA) chain growing per metal centre. This suggests that not all of the initiating (L)AlOR´ species have entered the catalytic cycle, perhaps due to some instability of the pre-catalysts (initiators) under the reaction conditions. Once polymerisation is underway, the linear first order kinetic plots (e.g. Figure 4.12) and linear M_n *vs*. conversion (e.g. Figure 4.13) all suggest a stable catalyst system. Among these four catalysts, **33** gave the closest agreement between experimental M_n and that expected. The PDI of 1.14 and the linear relationship between M_n and % conversion (Figure 4.13, gradient 161(8) g mol^{-1} (% conversion)$^{-1}$) are also indicative of a well-controlled living-type behaviour.

The apparent propagation rate constants (k_{app}) for pairs of initiators supported by the same ancillary ligand ($N_2^{Ts}N^{py}$ for **32** and **33**; $N_2^{Ms}N^{Ph}$ for **36** and **37**) had very similar

values as would be expected since they lead to the same propagating catalyst. Surprisingly, the values of k_{app} for catalysts based on tetradentate $N_2^{Ts}N^{py}$ (**32** and **33**, av. 0.0263 h^{-1}) are slightly larger than those containing the tridentate $N_2^{Ms}N^{Ph}$ (**36** and **37**, av. 0.0217 h^{-1}). A higher rate might have been expected for the $N_2^{Ms}N^{Ph}$-supported systems since access of *rac*-LA to the metal should be more facile. One explanation could be that the tetradentate homologue is more able to support a monomeric (and presumably more active) active species (L)Al-OR (R = poly(*rac*-LA) chain), whereas the tridentate $N_2^{Ms}N^{Ph}$ might lead to a higher equilibrium concentration of dormant binuclear complexes with, for example, bridging sulfonyl groups (as in **36**, **37** or **4.30**) or a poly(*rac*-LA) chain (*cf*. the bridging OR group in **35** or **43**).

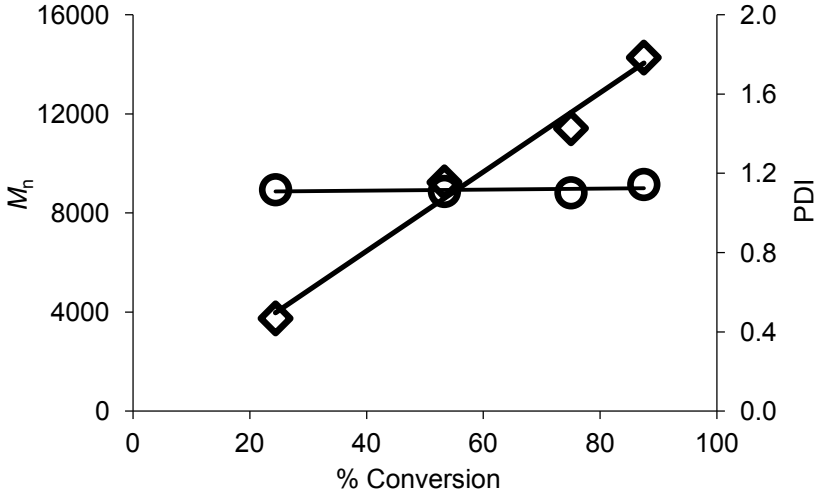
Figure 4.12. First order plot for *rac*-LA consumption using Al($N_2^{Ts}N^{py}$)(OBn) (**33**).[a]



[a] Conditions: [*rac*-LA_0]:[**33**] = 100:1, 4 mL toluene, 70 °C, 0.1 mL aliquots taken at the given intervals. See Experimental section for other details. Linear fit (r^2 = 0.997). See the Appendix for corresponding plots for **32**, **36, 37, 42** and **43**.

The ^{1}H NMR and MALDI-ToF mass spectra confirmed the presence of alkoxide-terminated poly(*rac*-LA). Disappointingly, all of the polymers produced were atactic (P_r ~ 0.5) according to the selectively homonuclear-decoupled NMR spectra. Examination of the MALDI-ToF mass spectra showed a $\Delta(m/z)$ separation of 72 between the polymer chains (i.e. one half of a LA unit, 144.1 amu) consistent with extensive transesterification during the polymerisation process. This, and the high temperatures required for polymerisation (which would be detrimental to any chain-end control of monomer insertion), are possible contributors to the lack of control of polymer tacticity in these systems.

Figure 4.13. Plots of M_n and PDI (determined by GPC) *vs* conversion for the polymerisation of *rac*-LA using Al($N_2^{Ts}N^{py}$)(OBn) (**33**).[a]



[a] Conditions: [*rac*-LA_0]:[**33**] = 100:1, 4 mL toluene, 70 °C, 0.1 mL aliquots taken at the given intervals. Hollow diamonds correspond to M_n and hollow circles to PDI. See the Appendix for corresponding plots for **32**, **36, 37,** and **39, 41** - **43**.

Whereas the alkoxides **32**–**37** led to well-behaved ROP, analogous experiments using the 2-aminoalkoxide analogues Al($N_2^{Ts}N^{R}$)($OCH_2CH_2NH_2$) (**39**–**41**; entries 8–10, Table 4.8) all gave higher than predicted M_n values, larger PDIs and, ultimately, gel formation after *ca*. 18 h reaction time. In contrast, use of the 2-*N*,*N*-dimethylaminoethoxide Al($N_2^{Ts}N^{Ph}$)($OCH_2CH_2NMe_2$) (**42**, entry 11, Table 4.8) once again gave reasonably well controlled ROP as judged by a better agreement between experimental and predicted M_n, a narrow PDI and linear increase of M_n with conversion (Appendix). The k_{app} for **42** (0.0235(11) h^{-1}) was experimentally the same as those of the related Al($N_2^{Ts}N^{Ph}$)(OR´) systems **36** and **37** (0.0230(4) and 0.0203(7) h^{-1}) as expected for virtually identical propagating species. The MALDI-ToF mass spectrum of the polymer obtained using **42** confirmed the presence of the $OCH_2CH_2NMe_2$ end groups. The spectrum again showed a $\Delta(m/z)$ separation of 72 between the polymer chains, consistent with extensive transesterification.

It is possible to propose two explanations for the unusual behaviour of **39**–**41**, both based on the presence of the terminal $–NH_2$ group. Firstly, as seen in the structures (Scheme 4.4), the aminoethoxide ligand is strongly chelating to the aluminium centre, augmented by two NH···O=S hydrogen bonds. Conceivably this could lead to sluggish initiation compared to the "normal" alkoxides **32**–**37** and **42**, the latter having a less Lewis basic $–NMe_2$ donor and no supporting hydrogen bonds. Secondly,

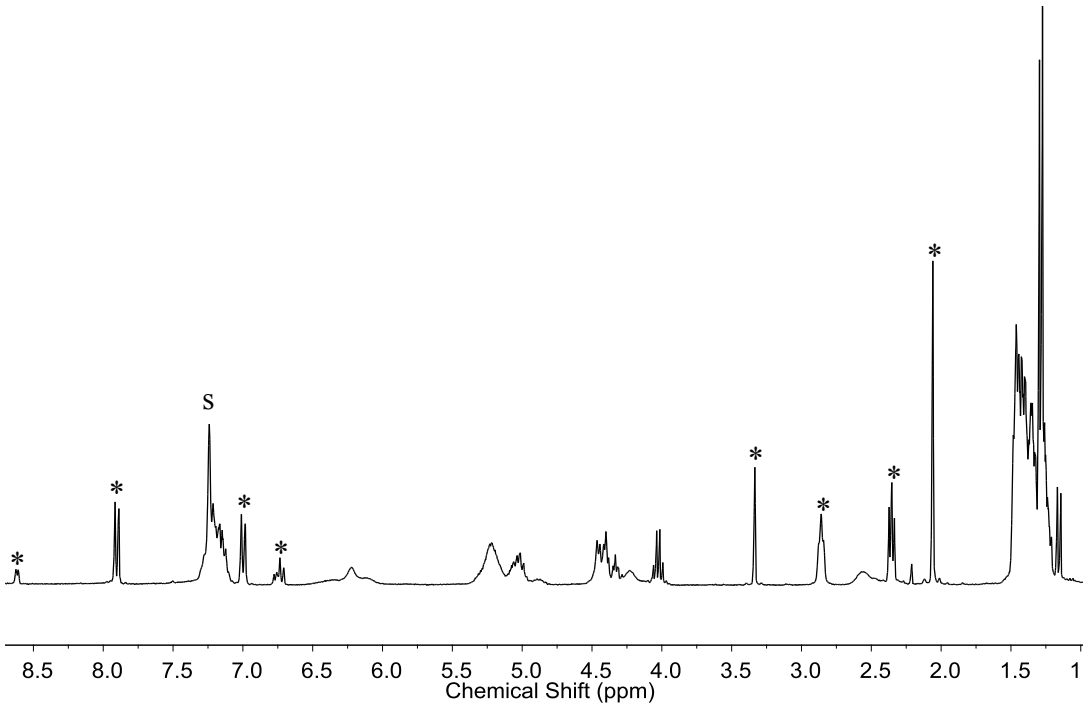
the terminal –NH_2 group of the growing polymeric chain in Al($N_2^{Ts}N^R$){poly(*rac*-LA)}-$OCH_2CH_2NH_2$ may also be able to co-initiate the ROP of another *rac*-LA through an activated monomer process.[78] Such a process could lead to cross-linking and gel formation.

In order to investigate the effects of the amine groups in catalysts **28 - 30**, polymerisation reactions of **33** in the presence of H_2NBn co-initiator were undertaken. NMR scale reactions undertaken in C_6D_6 between H_2NBn and catalyst **33** did not proceed at any appreciable rate, even after heating the reaction mixtures at 70 °C for up to 7 days. However during full scale polymerisation reactions, a clear effect of the benzyl amine co-initiator is evidenced (Entry 7, Table 4.8). Linear plots of M_n *vs.* conversion and narrow PDIs (<1.20) are observed throughout the polymerisation process (see the Appendix) indicative of a well controlled 'living' type catalyst, and also close agreement is observed between M_n recorded by GPC and that expected from the % conversion for 6 chains per metal centre (gradient = 27(2) g mol^{-1} (% conversion)$^{-1}$, (24 g mol^{-1} (% conversion)$^{-1}$). MALDI-ToF MS confirmed the presence of both benzyl amide and benzyl ester end groups. These results clearly demonstrate the benzyl amine is able to act as a co-initiator and the resulting polymerisation has immortal characteristics, yielding uniform polymer of narrow PDIs.

Concurrent work in our group has examined rare earth catalysts with various amine co-initiators for the catalytic behaviour towards the ROP of *rac*-LA. It is postulated that the reaction proceeds via an activated monomer mechanism to form amine terminated alcohol oligomers in the initial step. These oligomers are then in a dynamic equilibrium with bound alkoxide groups on the metal centre and so initiate an 'immortal' type polymerisation.[78] However, reactions between alkyl complex **31** and ROH (R = ^{i}Pr or Bn) protonate the sulfonamide ligands from the metal centre. Therefore, NMR tube scale polymerisations were undertaken to ascertain the nature of the catalyst in these reactions. In accordance with the aforementioned mechanism the sulfonamide ligand is quantitatively protonated from the metal centre to yield a mixture of protio ligand, poly(LA) oligomers and active tris(alkoxide) catalyst (Figure 4.14). GPC analysis of the resulting poly(LA) gave M_n of 388 $gmol^{-1}$ (PDI of 1.15), which is close to the expected value of 400 g mol^{-1} for 6 chains per metal centre. MALDI-ToF MS shows peaks 72 *m/z* apart corresponding to 107.1 *m/z* indicative of transesterification and a benzyl amine end group (see the Appendix and Chapter 5 for

further details). Interestingly, it appears that the sulfonamide protio-ligand itself is incapable of initiating this type of catalysis in contrast to benzyl amine or the secondary amine piperidine,[78] which is probably a consequence of the electron withdrawing nature of the sulfone substituent.

Figure 4.14. ^{1}H NMR spectrum (299.9 MHz) of *rac*-lactide polymerisation initiated by **32** with 5 equivalents benzyl amine co-initiator in $CDCl_3$ at 298 K ('s' denotes residual protio-solvent; * donates protio-ligand).



Catalyst **43** gives a linear relationship between M_n and monomer conversion with narrow PDIs (~1.2) throughout the polymerisation. Disappointingly, it was again observed that the experimental M_n was much higher than predicted, possibly consistent with sluggish initiation compared to propagation. The dimeric nature proposed for **43**, with a bridged-chelating $Al(\mu\text{-}OCH_2CH_2NMe_2)_2Al$ core, could likely account for this.

Table 4.9. Solvent-free (melt) polymerisation of *rac*-LA by Al($N_2^{Ts}N^{Ph}$)Et (**29**), Al($N_2^{Ts}N^{py}$)Et (**31**), Al($N_2^{Ts}N^{py}$)(O^iPr) (**32**), Al($N_2^{Ts}N^{py}$)(OBn) (**33**), Al($N_2^{Ms}N^{Ph}$)(O^iPr) (**36**), Al($N_2^{Ms}N^{Ph}$)(OBn) (**37**), Al($N_2^{Ts}N^{Ph}$)($OCH_2CH_2NH_2$) (**39**), Al($N_2^{Ts}N^{OMe}$)($OCH_2CH_2NH_2$) (**40**), Al($N_2^{Ts}N^{py}$)($OCH_2CH_2NH_2$) (**41**) and Al($N_2^{Ts}N^{Ph}$)($OCH_2CH_2NMe_2$) (**42**).[a]

Entry	Catalyst	Yield (%)[b]	M_n (GPC)[c]	M_n (calcd)[d]	M_w/M_n
1	Al($N_2^{Ts}N^{Ph}$)Et (**29**)	80	41,430	34,600	1.44
2	Al($N_2^{Ts}N^{py}$)Et (**31**)	75	37,390	32,540	1.47
3	Al($N_2^{Ts}N^{py}$)(O^iPr) (**32**)	83	41,150	35,900	1.21
4	Al($N_2^{Ts}N^{py}$)(OBn) (**33**)	79	34,310	34,160	1.20
5	Al($N_2^{Ms}N^{Ph}$)(O^iPr) (**36**)	94	35,480	40,490	1.60
6	Al($N_2^{Ms}N^{Ph}$)(OBn) (**37**)	95	36,710	40,920	1.53
7	Al($N_2^{Ts}N^{Ph}$)($OCH_2CH_2NH_2$) (**39**)	91	36,540	31,100	1.30
8	Al($N_2^{Ts}N^{OMe}$)($OCH_2CH_2NH_2$) (**40**)	81	35,000	34,870	1.52
9	Al($N_2^{Ts}N^{py}$)($OCH_2CH_2NH_2$) (**41**)	87	29,640	29,650	1.45
10	Al($N_2^{Ts}N^{Ph}$)($OCH_2CH_2NMe_2$) (**42**)	46	16,440	19,700	1.37

[a] Conditions: [*rac*-LA]$_0$:[Al] = 300:1 at 130 °C. See Experimental section for other details. [b] % conversion by NMR at 2 h reaction time. [c] Molecular weights (g mol^{-1}) determined by GPC in THF at 30 °C using the appropriate Mark-Houwink corrections. [d] Expected M_n (g mol^{-1}) for 1 chain growing per metal centre.

4.12 Polymerisation studies: ROP of *rac*-LA under solvent-free (melt) conditions

Catalysts **29**, **31**–**33**, **36**, **37** and **39**–**42**, were also assessed for their capabilities towards the ROP of *rac*-LA at 130 °C for 2 h ([*rac*-LA]$_0$:[Al] = 300:1) under industrially-relevant solvent-free (melt) conditions. The results are summarized in Table 4.9.

The best-performing initiators from the solution state studies, namely the non-chelating alkoxides **32**, **33**, **36** and **37** (entries 3–6), performed well under the more demanding, higher temperature melt conditions. Conversions of between *ca*. 80 and 95% with good agreements between found and calculated M_n values, and reasonable PDIs were found (PDIs under melt conditions are typically broader than for the corresponding solution phase studies[67]). In particular the initiators supported by the tetradentate $N_2^{Ts}N^{py}$ ligand (**32** and **33**) gave poly(*rac*-LA) with a narrow PDI of *ca*. 1.2. The agreement between found and calculated M_n was especially good for **33**, mirroring the excellent performance of this complex in the solution phase (Table 4.8). Good M_n control and a reasonable PDI were also achieved with the 2-*N*,*N*-dimethylaminoethoxide species Al($N_2^{Ts}N^{Ph}$)($OCH_2CH_2NMe_2$) (**42**, entry 10).

Surprisingly, both of the ethyl aluminium complexes **29** and **31** (entries 1 and 2) gave significantly improved ROP in the melt compared to the solution. The extents of conversion and PDIs of the poly(*rac*-LA) were comparable to those achieved with the alkoxides after 2 h, and there was reasonable agreement between the experimental and calculated M_n data. Similarly, catalysts **39**–**41** also gave much-improved performance in terms of molecular weight control and molecular weight distributions, with the $N_2^{Ts}N^{py}$-supported system **41** providing the best agreement between measured and calculated M_n. The origins of this difference are not fully clear. Perhaps the more forcing conditions and higher lactide concentration under melt conditions may help overcome the kinetic limitations associated with insertion into the Al-Et bonds of **29** and **31**, or opening up the chelating aminoethoxide-aluminium chelate rings of **39**–**41**. Further work on other aluminium alkyl catalysts under melt conditions would be required to confirm this hypothesis, but time prevented a more detailed study here.

4.13 Summary and Conclusions

Chapter 4 has reported the first comprehensive study of the synthesis, structures and *rac*-LA ROP capability of sulfonamide-supported aluminium complexes. Protio-ligands reacted readily with $AlEt_3$ to form $Al(CyN_2^{R})Et(THF)$ (R = Ts or SO_2Mes) and $Al(N_2^{Ts}N^{R})Et$ (R = Ph, OMe, or py). Corresponding reactions with $Al(OR')Et_2$ (R′ = ^{i}Pr, Bn, $CH_2CH_2NH_2$ or $CH_2CH_2NMe_2$) gave $Al(N_2^{Ts}N^{py})(OR')$, $Al(N_2^{Ms}N^{Ph})(OR')$, $Al(N_2^{Ts}N^{R})(OCH_2CH_2NH_2)$ (R = Ph, OMe, or py), $Al(N_2^{Ts}N^{Ph})(OCH_2CH_2NMe_2)$ and $Al(CyN_2^{Ts})(OCH_2CH_2NMe_2)$. In general all of the above syntheses were straightforward, although reaction of $Al(OR)Et_2$ with $H_2N_2^{Ts}N^{OMe}$ led to O-demethylation of the sulfonamide ligand. The X-ray structures of eight sulfonamide complexes showed a variety of 4- and 5-coordinate structures dependent upon the sulfonamide ligand and/or additional ligand (ethyl, chloride, 2-aminoethoxide).

Detailed comparison of solution ROP results with those in the literature should be undertaken with caution because of differences in experimental conditions such as temperature, solvent type, monomer:initiator ratio and concentration. Generally speaking, however, the activity and molecular weight control achieved by the sulfonamide-supported catalysts compare well with literature results in the solution phase.[49]

Since most melt ROP experiments are usually carried out in the range 120–150 °C in very similar ways, this allow a more precise comparison of our results with those reported previously. Feijen's complex **1.31** (Figure 4.2) polymerizes 400 equiv. of *rac*-LA to 95 % conversion in the melt over 2 days at 130 °C.[40] The κ^2 bound sulfonamide complex **1.41** (Figure 4.3) is also active under melt conditions, although still requires fairly long reaction times (90 % conversion after 10 h at 130 °C). The isotactic poly(lactide) formed has modest PDI values of *ca*. 1.5 but there is poor control of molecular weight.[54] Carpentier's aluminium complexes of salen-like ligands polymerize 400 equiv. of *rac*-LA at 120 °C to 87 % conversion after 0.5 h. The so-formed isotactic poly(lactide) had moderate to broad PDIs (1.4–1.9), but poor agreement between found and expected molecular weight.[79] The results described herein (Table 4.9) compare favourably with these examples. High conversions of up to 95% within 2 h reaction time were achieved, along with excellent control in the case of catalyst **33** as judged by with close agreement between experimental and calculated

M_n and narrow PDI. However, further iterations of ligand design will be required to find catalysts capable of achieving stereochemical control (e.g., high levels of heterotactic enrichment) either under solution or melt ROP conditions.

4.14 References

(1) Schwarz, A. D.; Chu, Z.; Mountford, P. *Organometallics* **2010**, *29*, 1246-1260.

(2) Ouhadi, T.; Stevens, C.; Teyssie, P. *Makromol. Chem. Suppl.* **1975**, *1*, 191.

(3) Dubois, P.; Jerome, R.; Teyssie, P. *Polym. Bull.* **1989**, *22*, 475-482.

(4) Tian, D.; Dubois, P.; Jerome, R. *Macromolecules* **1997**, *30*, 2575-2581.

(5) Dubois, P.; Jacobs, C.; Jerome, R.; Teyssie, P. *Macromolecules* **1991**, *24*, 2266-2270.

(6) Yui, N.; Dijkstra, P. J.; Feijen, J. *Mackromol. Chem.* **1990**, 481.

(7) Mecerreyes, D.; Jerome, R. *Macromol. Chem. Phys.* **1999**, *200*, 2581-2590.

(8) Dubois, P.; Barakat, I.; Jerome, R.; Teyssie, P. *Macromolecules* **1993**, *26*, 4407-4412.

(9) Vanhoorne, P.; Dubois, P.; Jerome, R.; Teyssie, P. *Macromolecules* **1992**, *25*, 37-44.

(10) Shiner, V. J.; Whittaker, D.; Fernandez, V. P. *J. Am. Chem. Soc.* **1963**, *85*, 2318-2322.

(11) Oliver, J. G.; Phillips, P. K.; Worrall, I. J. *Inorg. Nucl. Chem.* **1969**, *31*, 1609-1613.

(12) Turova, N. Y.; Kozunov, V. A.; Yanovskii, A. I.; Bokii, N. G.; Struchkov, Y. T.; Tarnopol'skii, B. L. *Inorg. Nucl. Chem.* **1979**, *41*, 5-11.

(13) Folting, K.; Streib, W. E.; Caulton, K. G.; Poncelet, O.; Hubert-Pfalzgraf, L. G. *Polyhedron* **1991**, *10*, 1639-1646.

(14) Duda, A.; Penczek, S. *Macromol. Rapid Commun.* **1995**, *16*, 67-76.

(15) Duda, A.; Penczek, S. *Macromolecules* **1995**, *28*, 5981-5992.

(16) Duda, A. *Macromolecules* **1996**, *29*, 1399-1406.

(17) Ropson, N.; Dubois, P.; Jerome, R.; Teyssie, P. *Macromolecules* **1993**, *26*, 6378-6385.

(18) Ropson, N.; Dubois, P.; Jerome, R.; Teyssie, P. *Macromolecules* **1994**, *27*, 5950-5956.

(19) Ropson, N.; Dubois, P.; Jerome, R.; Teyssie, P. *Macromolecules* **1995**, *28*, 7589-7598.

(20) Kowalski, A.; Duda, A.; Penczek, S. *Macromol*. **1998**, *31*, 2114-2122.

(21) Aida, T.; Inoue, S. *Acc*. *Chem*. *Res*. **1996**, *29*, 39-48.

(22) Shohei, I. *J*. *Polym*. *Sci*. *Polym*. *Chem*. **2000**, *38*, 2861-2871.

(23) Vion, J. M.; Jerome, R.; Teyssie, P.; Aubin, M.; Prudhomme, R. E. *Macromolecules* **1986**, *19*, 1828-1838.

(24) Jacobs, C.; Dubois, P.; Jerome, R.; Teyssie, P. *Macromolecules* **1991**, *24*, 3027-3034.

(25) Duda, A.; Florjanczyk, Z.; Hofman, A.; Slomkowski, S.; Penczek, S. *Macromolecules* **1990**, *23*, 1640-1646.

(26) Duda, A.; Penczek, S. *Macromol*. *Rapid Commun*. **1994**, *15*, 559-566.

(27) Tian, D.; Dubois, P.; Jerome, R.; Teyssie, P. *Macromolecules* **1994**, *27*, 4134-4144.

(28) Reeve, M. S.; McCarthy, S. P.; Gross, R. A. *Macromolecules* **1993**, *26*, 888-894.

(29) Trofimoff, L.; Aida, T.; Inoue, S. *Chem*. *Lett*. **1987**, 991-994.

(30) Yasuda, T.; Aida, T.; Inoue, S. *Bull*. *Chem*. *Soc*. *Jpn*. **1986**, 3931.

(31) Endo, M.; Aida, T.; Inoue, S. *Macromolecules* **1987**, *20*, 2982-2988.

(32) Sugimoto, H.; Aida, T.; Inoue, S. *Macromolecules* **1990**, *23*, 2869-2875.

(33) Tang, Z.; Chen, X.; Pang, X.; Yang, Y.; Zhang, X.; Jing, X. *Biomacromol*. **2004**, *5*, 965-970.

(34) Zhaohui, T.; Xuesi, C.; Yongkun, Y.; Xuan, P.; Jingru, S.; Xuefei, Z.; Xiabin, J. *J*. *Polym*. *Sci*. *Part A: Polym*. *Chem*. **2004**, *42*, 5974-5982.

(35) Wisniewski, M.; Borgne, A. L.; Spassky, N. *Macromol*. *Chem*. *Phys*. **1997**, *198*, 1227-1238.

(36) Spassky, N.; Wisniewski, M.; Pluta, C.; LeBorgne, A. *Macromol*. *Chem*. *Phys*. **1996**, *197*, 2627.

(37) Ovitt, T. M.; Coates, G. W. *J*. *Am*. *Chem*. *Soc*. **2002**, *124*, 1316-1326.

(38) Ovitt, T. M.; Coates, G. W. *J*. *Polym*. *Sci*. *Part A: Polym*. *Chem*. **2000**, *38*, 4686-4692.

(39) Radano, C. P.; Baker, G. L.; Smith, M. R. *J*. *Am*. *Chem*. *Soc*. **2000**, *122*, 1552.

(40) Zhong, Z.; Dijkstra, P. J.; Feijen, J. *Angew*. *Chem*. *Int*. *Ed*. **2002**, *41*, 4510-4513.

(41) Zhong, Z.; Dijkstra, P. J.; Feijen, J. *J. Am. Chem. Soc.* **2003**, *125*, 11291-11298.

(42) Nomura, N.; Ishii, R.; Akakura, M.; Aoi, K. *J. Am. Chem. Soc.* **2002**, *124*, 5938-5939.

(43) Chisholm, M. H.; Gallucci, J. C.; Quisenberry, K. T.; Zhou, Z. *Inorg. Chem.* **2008**, *47*, 2613-2624.

(44) Nomura, N.; Ishii, R.; Yamamoto, Y.; Kondo, T. *Chem. Eur. J.* **2007**, *13*, 4433-4451.

(45) Du, H. Z.; Pang, X.; Yu, H. Y.; Zhuang, X. L.; Chen, X. S.; Cui, D. M.; Wang, X. H.; Jing, X. B. *Macromolecules* **2007**, *40*, 1904-1913.

(46) Jing, Y.; Qiaobo, L.; Yang, L.; Lin, J.; Qiang, F.; Amin, C. *J. Polym. Sci. Part A: Polym. Chem.* **2006**, *44*, 2045-2058.

(47) Hormnirun, P.; Marshall, E. L.; Gibson, V. C.; White, A. J. P.; Williams, D. J. *J. Am. Chem. Soc.* **2004**, *126*, 2688-2689.

(48) Johnson, A. L.; Davidson, M. G.; Perez, Y.; Jones, M. D.; Merle, N.; Raithby, P. R.; Richards, S. P. *Dalton Trans.* **2009**, 5551-5558.

(49) Tang, Z.; Gibson, V. C. *E. Polym. J.* **2007**, *43*, 150-155.

(50) Alcazar-Roman, L. M.; O'Keefe, B. J.; Hillmyer, M. A.; Tolman, W. B. *Dalton Trans.* **2003**, 3082-3087.

(51) Chen, C.-T.; Huang, C.-A.; Huang, B.-H. *Dalton Trans.* **2003**, 3799-3803.

(52) Chen, C.-T.; Huang, C.-A.; Huang, B.-H. *Macromol.* **2004**, *37*, 7968-7973.

(53) Cameron, P. A.; Jhurry, D.; Gibson, V. C.; White, A. J. P.; Williams, D. J.; Williams, S. *Macromol. Rapid Commun.* **1999**, *20*, 616-618.

(54) Zhao, J.; Song, H.; Cui, C. *Organomet.* **2007**, *26*, 1947-1954.

(55) Wu, J.; Pan, X.; Tang, N.; Lin, C.-C. *E. Polym. J.* **2007**, *43*, 5040-5046.

(56) Corey, E. J.; Sarshar, S.; Lee, D.-H. *J. Am. Chem. Soc.* **1994**, *116*, 12089-12090.

(57) Nelson, S. G.; Kim, B.-K.; Peelen, T. J. *J. Am. Chem. Soc.* **2000**, *122*, 9318-9319.

(58) Kitagawa, O.; Yotsumoto, K.; Kohriyama, M.; Dobashi, Y.; Taguchi, T. *Org. Lett.* **2004**, *6*, 3605-3607.

(59) Takahashi, H.; Kawakita, T.; Ohno, M.; Yoshioka, M.; Kobayashi, S. *Tetrahedron* **1992**, *48*, 5691-5700.

(60) Skinner, M. E. G.; Li, Y.; Mountford, P. *Inorg. Chem.* **2002**, *41*, 1110-1119.

(61) Bailey, N. A.; Fenton, D. E.; Hellier, P. C.; Hempstead, P. D.; Casellatob, U.; Vigatob, P. A. *Dalton Trans*. **1992**, 2809-2816.

(62) Peng, K.-F.; Chen, C.-T. *Dalton Trans*. **2009**, 9800-9806.

(63) Fletcher, D. A.; McMeeking, R. F.; Parkin, D. *J*. *Chem*. *Inf*. *Comput*. *Sci*. **1996**, *36*, 746 (The United Kingdom Chemical Database Service).

(64) Forcato, M.; Lake, F.; Blazquez, M. M.; Renner, P.; Crisma, M.; Gade, L. H.; Licini, G.; Moberg, C. *Eur*. *J*. *Inorg*. *Chem*. **2006**, 1032-1040.

(65) Takashi, O.; Hayato, I.; Keiji, M. *Angew*. *Chem*. *Int*. *Ed*. **2001**, *40*, 3610-3612.

(66) Corey, E. J.; Sarshar, S.; Bordner, J. *J*. *Am*. *Chem*. *Soc*. **1992**, *114*, 7938-7939.

(67) Schwarz, A. D.; Thompson, A. L.; Mountford, P. *Inorg*. *Chem*. **2009**, *48*, 10442-10454.

(68) Kunicki, A. R.; Pasynkiewicz, S.; Jankowski, J.; Mank, B. *Pol*. *J*. *Chem*. **2004**, *78*, 1857-1864.

(69) Hirabayashi, T.; Sakakibara, T.; Ishii, Y. *J*. *Organomet*. *Chem*. **1972**, *35*, 19-25.

(70) Hurley, T. J.; Robinson, M. A.; Scruggs, J. A.; Trotz, S. I. *Inorg*. *Chem*., **1967**, *3*, 1310-1315.

(71) Aullón, G.; Bellamy, D.; Orpen, A. G.; Brammer, L.; Bruton, E. A. *Chem*. *Commun*. **1998**, 653 - 654.

(72) Rudin, A.; Hoegy, H. L. W. *J*. *Polym*. *Sci*. *Part A: Polym*. *Chem*. **1972**, *10*, 217-235.

(73) Barakat, I.; Ph, D.; Jérôme, R.; Ph, T. *J*. *Polym*. *Sci*. *Part A: Polym*. *Chem*. **1993**, *31*, 505-514.

(74) Dorgan, J. R.; Janzen, J.; Knauss, D. M.; Hait, S. B.; Limoges, B. R.; Hutchinson, M. H. *J*. *Polym*. *Sci*. *Part B: Polym*. *Phys*. **2005**, *43*, 3100-3111.

(75) Chmura, A. J.; Davidson, M. G.; Jones, M. D.; Lunn, M. D.; Mahon, M. F.; Johnson, A. F.; Khunkamchoo, P.; Roberts, S. L.; Wong, S. S. F. *Macromol*. **2006**, *39*, 7250-7257.

(76) Liu, X.; Shang, X.; Tang, T.; Hu, N.; Pei, F.; Cui, D.; Chen, X.; Jing, X. *Organometallics* **2007**, *26*, 2747-2757.

(77) Gong, S.; Ma, H. *Dalton Trans*. **2008**, 3345-3357.

(78) Clark, L.; Cushion, M. G.; Dyer, H. E.; Schwarz, A. D.; Duchateau, R.; Mountford, P. *Chem*. *Commun*. **2010**, *46*, 273-275.

(79) Bouyahyi, M.; Grunova, E.; Marquet, N.; Kirillov, E.; Thomas, C. M.; Roisnel, T.; Carpentier, J.-F. o. *Organomet*. **2008**, *27*, 5815-5825.

Chapter Five

Experimental details and characterising data

Experimental Section

5.1. General methods and instrumentation. All manipulations were carried out using standard Schlenk line or dry-box techniques under an atmosphere of argon or dinitrogen. Solvents were degassed by sparging with dinitrogen and dried by passing through a column of the appropriate drying agent. Toluene was refluxed over sodium and distilled. Deuterated solvents were dried over sodium (C_6H_6) or P_2O_5 ($CDCl_3$ and CD_2Cl_2), distilled under reduced pressure and stored under dinitrogen in Teflon valve ampoules. NMR samples were prepared under dinitrogen in 5 mm Wilmad 507-PP tubes fitted with J. Young Teflon valves. ^1H and ^{13}C-{^1H} NMR spectra were recorded on Varian Mercury-VX 300 and Varian Unity Plus 500 spectrometers at ambient temperature unless stated otherwise and referenced internally to residual protio-solvent (^1H) or solvent (^{13}C) resonances, and are reported relative to tetramethylsilane ($\delta = 0$ ppm). Assignments were confirmed using two dimensional ^1H-^1H and ^{13}C-^1H NMR correlation experiments. Chemical shifts are quoted in δ (ppm) and coupling constants in Hz. IR spectra were recorded on a Nicolet Magna 560 E.S.P. FTIR spectrometer. Samples were prepared in a dry-box as Nujol mulls between NaCl plates, and the data are quoted in wavenumbers (cm^{-1}). Elemental analyses were carried out by the Elemental Analysis Service at the London Metropolitan University.

MALDI-ToF-MS analysis was performed on a Waters MALDI micro equipped with a 337 nm nitrogen laser. An accelerating voltage of 25 kV was applied. The polymer samples were dissolved in THF at a concentration of 1 mg mL^{-1}. The cationization agent used was potassium trifluoroacetate (Fluka, >99%) dissolved in THF at a concentration of 5 mg mL^{-1}. The matrix used was *trans*-2-[3-(4-*tert*-butylphenyl)-2-methyl-2-propenylidene]malononitrile (DCTB) (Fluka) and was dissolved in THF at a concentration of 40 mg mL^{-1}. Solutions of matrix, salt and polymer were mixed in a volume ratio of 4:1:4, respectively. The mixed solution was hand-spotted on a stainless steel MALDI target and left to dry. The spectra were recorded in the refectron mode.

Polymer molecular weights (M_n, M_w) were determined by GPC using a Polymer Laboratories Plgel Mixed-D column (300 mm length, 7.5 mm diameter) and a Polymer Laboratories PL-GPC50 Plus instrument equipped with a refractive index detector. THF (HPLC grade) was used as an eluent at 30 °C with a rate of 1 mL min^{-1}. Linear polystyrenes were used as primary calibration standards, and Mark-Houwink

corrections for poly(ε-CL) or poly(*rac*-LA) in THF were applied for the experimental samples.[1-3]

5.2. Literature Preparations.

$Ti(NMe_2)_4$,[4-6] $Ti(NMe_2)_2(O^iPr)_2$,[7,8] $Zr(CH_2SiMe_3)_4$,[9] $Zr(NMe_2)_4$,[6] $H_2N_2^{Ts}N^{py}$,[10] $H_2N_2^{Ts}N^{OMe}$,[11] $H_2CyN_2^{Ts}$,[12] $H_2CyN_2^{SO_2Mes}$,[13] $H_3N_3^{Ts}N$,[14] N-mesyl aziridine,[15] N-tosyl aziridine,[10] $Al(O^iPr)Et_2$,[16,17] $Al(OBn)Et_2$,[16,17] $Al(OCH_2CH_2NH_2)Et_2$,[18] and $Al(OCH_2CH_2NMe_2)Et_2$[18] were synthesised according to published procedures. ε-CL was dried over freshly ground CaH_2 and distilled before use. *Rac*-LA was recrystallised twice from toluene and then sublimed twice prior to use. Other reagents were purchased from Sigma-Aldrich and used without further purification.

5.3. Experimental details and characterising data for Chapter Two

$Ti(N_2^{Ts}N^{py})(NMe_2)_2$ (1). A slurry of $H_2N_2^{Ts}N^{py}$ (0.25 g, 0.50 mmol) in benzene (30 mL) was added to a solution of $Ti(NMe_2)_4$ (0.12 mL, 0.50 mmol) in benzene (10 mL). The mixture was stirred for 19 h, resulting in a dark red solution with brown percipitate. The solid was filtered off and washed with pentane (3 × 30 mL). Recrystallisation from a saturated benzene solution yielded **1** as a brick-red solid that was washed with pentane (3 × 20 mL) and dried *in vacuo*. Yield: 0.17 g (55%). ^{1}H NMR (CD_2Cl_2, 299.9 MHz, 303 K): δ 8.91 (1H, m, 2-NC_5H_4), 8.31 (1H, m, 4-NC_5H_4), 7.78 (1H, app. t, ^3J = 6.9 Hz, 3-NC_5H_4), 7.52 (1H, d, ^3J = 4.3 Hz, 2-$C_6\underline{H}_4Me$), 7.20 (1H, m, 5-NC_5H_4), 7.12 (1H, d, ^3J = 4.5 Hz, 3-$C_6\underline{H}_4Me$), 3.79 (6H, s, NMe_2 *cis* to py), 3.59 (4H, br. m, overlapping py$C\underline{H}_2$ and Ts$NC\underline{H}_2$), 3.44 (6H, br. s, NMe_2 *trans* to py), 3.21 (2H, br. m, Ts$NC\underline{H}_2C\underline{H}_2$), 2.87 (4H, br. m, Ts$NC\underline{H}_2C\underline{H}_2$), 2.37 (6H, s, $C_6H_4\underline{Me}$) ppm. A satisfactory ^{13}C NMR spectrum could not be obtained due to the fluxional nature of the compound. IR: 3464 (w), 1255 (w), 1143 (m), 1088 (m), 947 (m), 665 (m), 511 (w) cm^{-1}. Anal. found (calcd. for $C_{28}H_{40}N_6O_4S_2Ti$): C, 52.85 (52.82); H, 6.33 (6.26); N, 13.15 (13.20) %.

$Ti(N_2^{Ts}N^{OMe})(NMe_2)_2$ (2). A slurry of $H_2N_2^{Ts}N^{OMe}$ (0.16 g, 0.34 mmol) in benzene (60 mL) was added to a solution of $Ti(NMe_2)_4$ (0.6 mL, 2.54 mmol) in benzene (20 mL). The mixture was heated at 70 ºC for 16 h, resulting in a dark red solution. Removal of the volatiles under reduced pressure yielded a dark red solid that was recrystallised from a concentrated benzene solution to yield **2** as a red solid which was washed with pentane (3 × 20 mL) and dried *in vacuo*. Yield: 0.11 g (51%). ^{1}H NMR (CD_2Cl_2, 299.9

MHz): δ 7.72 (4H, d, ^3J = 6.1 Hz, 2-$C_6\underline{H}_4Me$) 7.29 (4H, d, ^3J = 6.1 Hz, 3-$C_6\underline{H}_4Me$), 3.54 (6H, s, NMe_2 *cis* to OMe), 3.43 – 3.34 (9H, m, overlapping OMe, OCH_2 and $TsNCH_2$), 3.20 (6H, s, NMe_2 *trans* to OMe) 2.82 (6H, m, overlapping $OCH_2\underline{CH}_2$ and $TsNCH_2\underline{CH}_2$) 2.40 (6H, s, $C_6H_4\underline{Me}$). ^{13}C-{^1H} NMR (CD_2Cl_2, 75.4 MHz): δ 141.8 (1-C_6H_4Me), 140.4 (4-C_6H_4Me), 130.4 (3-C_6H_4Me), 127.9 (2-C_6H_4Me), 69.7 ($TsNCH_2$), 61.3 (OCH_2), 55.7 ($TsNCH_2\underline{C}H_2$), 51.4 ($OCH_2\underline{C}H_2$), 49.6 (*cis* to OMe NMe_2), 49.5 ($TsNCH_2$), 49.3 (NMe_2 *trans* to OMe), 21.6 ($C_6H_4\underline{Me}$). IR: 3446 (w) 1302 (m), 1295 (w), 1284 (m), 1139 (m), 1020 (s), 943 (s), 864 (m), 666 (m), 554 (w) cm^{-1}. Anal. found (calcd. for $C_{25}H_{41}N_5O_5S_2Ti$); C, 49.60 (49.74); H, 6.94 (6.85); N, 11.48 (11.60) %.

Ti($N_2^{Ts}N^{py}$)(O^iPr)$_2$ (3). A slurry of $H_2N_2{}^{Ts}N^{py}$ (0.75 g, 1.50 mmol) in toluene (50 mL) was added to a solution of Ti(O^iPr)$_4$ (2.2 mL, 7.5 mmol) in toluene (20 mL). The mixture was heated at 100 ºC for 16 h, resulting in an off-white slurry. The solid was filtered off and washed with pentane (3 × 30 mL). Recrystallisation from a saturated dichloromethane solution layered with pentane yielded **3** as a beige solid that was washed with hexanes (3 × 20 mL) and dried *in vacuo*. Yield: 0.62 g (62%). ^1H NMR (CD_2Cl_2, 299.9 MHz): δ 8.76 (1H, dd, ^3J = 4.7 Hz, ^4J = 6.0 Hz, 2-NC_5H_4), 7.66 (1H, dt, ^3J = 4.7 Hz, ^3J = 9.0 Hz, 4-NC_5H_4), 7.46 (4H, d, ^3J = 7.9 Hz, 2-$C_6\underline{H}_4Me$), 7.12 (6H, d, ^3J = 7.9 Hz, overlapping 3-$C_6\underline{H}_4Me$, 3- and 5-NC_5H_4), 5.32 (1H, sept., ^3J = 6.1 Hz, $OC\underline{H}Me_2$ *cis* to py), 5.16 (1H, sept., ^3J = 6.1 Hz, $OC\underline{H}Me_2$ *trans* to py) 3.94 (2H, s, $pyC\underline{H}_2N$), 3.40 (4H, m, $TsNCH_2\underline{CH}_2N$), 3.10 (2H, m, $TsNC\underline{H}_2CH_2N$) 2.88 (2H, m, $TsNCH_2C\underline{H}_2N$) 2.35 (6H, s, $C_6H_4\underline{Me}$) 1.51 (6H, d, ^3J = 6.1 Hz, $OCH\underline{Me}_2$ *cis* to py) 1.37 (6H, d, ^3J = 6.1 Hz, $OCH\underline{Me}_2$ *trans* to py) ppm. ^{13}C-{^1H} NMR (CD_2Cl_2, 75.4 MHz): δ 158.8 (6-NC_5H_4), 152.2 (2-NC_5H_4), 143.4 (1-C_6H_4Me), 143.2 (4-C_6H_4Me), 140 (3-NC_5H_4), 131.4 (3-C_6H_4Me), 128.1 (2-C_6H_4Me), 125.6 (4-NC_5H_4), 121.6 (5-NC_5H_4), 85.4 ($O\underline{C}HMe_2$ *cis* to py), 81.7 ($O\underline{C}HMe_2$ *trans* to py), 62.9 ($py\underline{C}H_2N$), 61.8 ($TsNCH_2\underline{C}H_2N$), 50.9 ($TsN\underline{C}H_2CH_2N$), 28.6 ($OCH\underline{Me}_2$ *cis* to py), 28.3 ($OCH\underline{Me}_2$ *trans* to py), 23.4 ($C_6H_4\underline{Me}$) ppm. IR: 3435 (w), 1607 (s), 1290 (m), 1280 (m), 1141 (s), 1088 (s), 1018 (s), 969 (m), 942 (m), 920 (m), 854.5 (w), 832 (m), 774 (w), 665 (m), 600 (m), 554 (m), 508 (m) cm^{-1}. Anal. found (calcd. for $C_{30}H_{42}N_4O_6S_2Ti$); C, 54.05 (54.05); H, 6.45 (6.35); N, 8.28 (8.40) %.

Alternative NMR tube scale synthesis of Ti($N_2^{Ts}N^{py}$)(O^iPr)$_2$ (3). To a solution of Ti(NMe_2)$_2$(O^iPr)$_2$ (6.1 mg, 23.8 μmol) in CD_2Cl_2 (0.2 mL) was added a solution of

$H_2N_2^{Ts}N^{py}$ (12 mg, 23.8 μmol) in CD_2Cl_2 (0.2 mL). A colour change of the initially light brown to light yellow was observed. After 1 h analysis by ^{1}H NMR indicated that **3** had been formed quantitatively.

Zr($N_2^{Ts}N^{py}$)(O^iPr)$_2$ (4). A slurry of $H_2N_2^{Ts}N^{py}$ (1.00 g, 2.00 mmol) in toluene (50 mL) was added to a solution of $Zr(O^iPr)_4{\cdot}HO^iPr$ (3.00 g, 7.80 mmol) in toluene (20 mL). The mixture was heated at 100 ºC for 16 h, resulting in an off-white slurry. The solid was filtered off and washed with pentane (3 × 30 mL). Recrystallisation from a saturated benzene solution layered with hexanes yielded **4** as a white solid that was washed with pentane (3 × 20 mL) and dried *in vacuo*. Yield: 0.60 g (42%). ^{1}H NMR (C_6D_6, 299.9 MHz, 343 K): δ 9.47 (1H, br. m, 2-NC_5H_4), 8.25 (4H, br. d, ^{3}J = 6.0 Hz, 2-$C_6\underline{H}_4Me$), 6.95 (5H, br. d, ^{3}J = 6.0 Hz, overlapping 3-$C_6\underline{H}_4Me$ and 4-NC_5H_4), 6.68 (1H, br. m, 3-NC_5H_4), 6.42 (1H, br. d, ^{3}J = 6.1 Hz, 5-NC_5H_4), 5.16 (1H, br. sept, ^{3}J = 6.0 Hz, $OC\underline{H}Me_2$ *cis* to py), 4.62 (1H, br. sept, ^{3}J = 6.1 Hz, $OC\underline{H}Me_2$ *trans* to py), 3.62 (2H, br. s, $pyC\underline{H}_2$), 3.17, (4H, br. m, $TsNC\underline{H}_2C\underline{H}_2$), 2.54 (4H, $TsNC\underline{H}_2C\underline{H}_2$), 1.97 (6H, s, $C_6H_4\underline{Me}$), 1.58 (6H, br. d, ^{3}J = 6.1 Hz, $CH\underline{Me}_2$ *cis* to py), 1.20 (6H, br. d, ^{3}J = 6.1 Hz, $CH\underline{Me}_2$ *trans* to py). A satisfactory ^{13}C NMR spectrum could not be obtained due to the fluxional nature of the compound. IR: 3431 (w), 1605 (w), 1164 (m), 1016 (m), 961 (w), 815 (m), 723 (w), 666 (m), 557 (w) cm^{-1}. Anal. found (calcd. for $C_{30}H_{42}N_4O_6S_2Zr$); C, 50.85 (50.75); H, 5.92 (5.96); N, 7.89 (7.89) %.

Ti($N_2^{Ts}N^{OMe}$)(O^iPr)$_2$ (5). A mixture of $H_2N_2^{Ts}N^{OMe}$ (0.15 g, 0.32 mmol) and $Ti(O^iPr)_4$ (2.0 mL, 6.76 mmol) was heated and stirred at 130 ºC under dynamic vacuum (70 mbar) for 4 hours. The mixture was cooled to RT resulting in a yellow solid which was recrystallised from saturated dichloromethane solution layered with pentane to yield **5** as a yellow solid that was washed with pentane (3 × 20 mL) and dried *in vacuo*. Yield: 0.10 g (47%). ^{1}H NMR (CD_2Cl_2, 299.9 MHz): δ 7.74 (4H, d, ^{3}J = 9.0 Hz, 2-$C_6\underline{H}_4Me$), 7.25 (4H, d, ^{3}J = 9.0 Hz, 3-$C_6\underline{H}_4Me$), 5.16 (1H, sept., ^{3}J = 6.5 Hz, $OC\underline{H}Me_2$ *cis* to OMe), 4.93 (1H, sept., ^{2}J = 6.5 Hz, $OC\underline{H}Me_2$ *trans* to OMe), 3.91 (3H, s, OMe), 3.80 (2H, t, ^{3}J = 6.5 Hz, $MeOC\underline{H}_2$), 3.42 - 3.12 (6H, m, overlapping $TsNC\underline{H}_2$ and $TsNCH_2C\underline{H}_2$), 2.74 (4H, m, overlapping $MeOCH_2C\underline{H}_2$ and $TsNCH_2C\underline{H}_2$), 2.37 (6H, s, $C_6H_4\underline{Me}$), 1.41 (4H, d, ^{3}J = 6.5 Hz, $OCH\underline{Me}_2$ *cis* to OMe), 1.14 (4H, d, ^{3}J = 6.5 Hz, $OCH\underline{Me}_2$ *trans* to OMe) ppm. ^{13}C-{^{1}H} NMR (CD_2Cl_2, 75.4 MHz) δ 141.6 (1-C_6H_4Me), 141.5 (4-C_6H_4Me), 129.4 (3-C_6H_4Me), 127.3 (2-C_6H_4Me), 84.5 ($O\underline{C}HMe_2$ *cis* to OMe), 81.5 ($O\underline{C}HMe_2$ *trans* to OMe), 71.6 ($MeO\underline{C}H_2$), 63.9 (OMe),

58.1 (TsN$\underline{C}H_2$), 54.6 (MeO$CH_2\underline{C}H_2$), 48.7 (TsN$CH_2\underline{C}H_2$), 26.1 (OCH$\underline{Me}_2$ *trans* to OMe), 25.9 (OCH$\underline{Me}_2$ *cis* to OMe), 21.6 ($C_6H_4\underline{Me}$) ppm. IR: 3428 (w), 1297 (m), 1284 (s), 1145 (s), 1090 (s), 959 (m), 855 (m), 829 (s), 758 (w), 602 (m), 506 (w) cm^{-1}. Anal. found (calcd. for $C_{27}H_{43}N_3O_7S_2Ti$); C, 51.08 (51.18); H, 6.88 (6.84); N, 6.61 (6.63) %.

Alternative synthesis of Ti($N_2^{Ts}N^{OMe}$)(O^iPr)$_2$ (5). A solution of $H_2N_2{}^{Ts}N^{OMe}$ (0.50 g, 1.1 mmol) in dichloromethane (30 mL) was added to a solution of Ti(NMe_2)$_2$(O^iPr)$_2$ (0.30 g, 1.2 mmol) in dichloromethane (30 mL). The mixture was stirred for 2 h, resulting in a yellow solution. Removal of the volatiles under reduced pressure afforded a yellow solid that was recrystallised from a concentrated dichloromethane solution layered with pentane to give **5** as a yellow solid that was washed with pentane (3 × 20 mL) and dried *in vacuo*. Yield: 0.52 g (78%).

Zr($N_2^{Ts}N^{OMe}$)(O^iPr)$_2$ (6). A mixture of $H_2N_2{}^{Ts}N^{OMe}$ (0.11 g, 0.23 mmol) and Zr(O^iPr)$_4$·HO^iPr (0.50 g, 1.29 mmol) was heated with stirring at 125 ºC under dynamic vacuum (75 mbar) for 5 h. The mixture was cooled to RT resulting in a yellow solid which was crystallised from saturated dichloromethane solution layered with pentane to yield **6** as a pale yellow solid that was washed with pentane (3 × 20 mL) and dried *in vacuo*. Yield: 0.07 g (41%). ^{1}H NMR (CD_2Cl_2, 499.9 MHz, 273 K): δ 7.82 (4H, br. d, ^{3}J = 7.0 Hz, 2-C_6H_4Me), 7.26 (4H, br. d, ^{3}J = 7.0 Hz, 3-C_6H_4Me), 4.52 (1H, br. sept. ^{3}J = 5.8 Hz, OC$\underline{H}Me_2$ *cis* to OMe), 4.41 (1H, br. sept. ^{3}J = 5.8 Hz, OC$\underline{H}Me_2$ *trans* to OMe), 3.93 (2H, s, C$\underline{H}_2$py), 3.24 – 2.81 (8H, br. m), 2.37 (6H, s, $C_6H_4\underline{Me}$), 1.21 (6H, br. d, ^{3}J = 6.1 Hz, OCH$\underline{Me}_2$ *cis* to OMe), 1.11 (6H, br. d, ^{3}J = 6.0 Hz, OCH$\underline{Me}_2$ *trans* to OMe). A satisfactory ^{13}C NMR spectrum could not be obtained due to the fluxional nature of the compound. IR: 3453 (w), 1599 (w), 1299 (m), 1143 (w), 1105 (m), 1060 (m), 1024. (w), 962 (w), 939 (m), 829 (w), 669 (w) cm^{-1}. cm^{-1}. Anal. found (calcd. for $C_{27}H_{43}N_3O_7S_2Zr$); C, 47.87 (47.90); H, 6.31 (6.40); N, 6.17 (6.21) %.

5.4. Experimental details and characterising data for Chapter Three

$H_2N_2{}^{Ts}N^{Ph}$ (7). To a slurry of N-tosyl aziridine (4.93 g, 0.025 mol) in EtOH (250 mL) was added dropwise benzyl amine (1.4 mL, 0.013 mol). The reaction mixture was stirred for 24 h at 35 °C after which time volatiles of the resulting brown mixture were removed under reduced pressure yielding a thick brown oil. The oil was purified by column chromatography (silica gel, eluent EtOAc and Et_3N (100: 1)) to give **7** as a light brown oil which crystallised on standing. Yield: 4.31 g (69 %). Light brown single crystals suitable for X-ray diffraction were obtained from a saturated diethyl

ether solution at 4 °C. ^{1}H NMR ($CDCl_3$, 299.9 MHz): 7.78 (4H, d, ^{3}J = 9.0 Hz, 2-$C_6\underline{H}_4Me$), 7.33 (4H, d, ^{3}J = 9.0 Hz, 3-$C_6\underline{H}_4Me$), 7.20 – 7.00 (5H, m, overlapping Ph), 5.43 (2H, app. t, ^{3}J = 6.2 Hz, NH), 3.46 (2H, s, $C\underline{H}_2Ph$), 2.94 (4H, app. q, ^{3}J = 6.2 Hz, $C\underline{H}_2NHS$), 2.54 (4H, t, ^{3}J = 3.8 Hz, $C\underline{H}_2CH_2NHS$), 2.45 (6H, s, $C_6H_4\underline{Me}$). ^{13}C-{^{1}H} ($CDCl_3$, 75.4 MHz): 143.3 (1-C_6H_4Me), 137.7 (4-C_6H_4Me), 136.6 (1-C_6H_5), 129.7 (2-C_6H_4Me), 128.9 (2-C_6H_5), 128.5 (3-C_6H_5), 127.1 (3-C_6H_4Me), 58.4 ($\underline{C}H_2Ph$), 53.1 ($\underline{C}H_2NHS$), 40.6 ($\underline{C}H_2NHS$), 21.5 ($C_6H_4\underline{Me}$). ES-MS: $[M+H]^+$ 502.1834 (calcd. for $C_{25}H_{32}N_3O_4S_2$, 502.1834). IR (NaCl plates, Nujol mull, cm^{-1}): 3283 (m), 1924 (w), 1812 (w), 1494 (s), 1261 (s), 1093 (s), 1028 (s), 1020 (m) 997 (m), 847 (w), 769 (w). Anal. found (calcd. for $C_{25}H_{31}N_3O_4S_2$); C, 59.41 (59.85); H, 6.22 (6.23); N, 8.04 (8.38) %.

$H_2N_2^{Ms}N^{Ph}$ (8). To a solution of 1-(methylsulfonyl)aziridine (2.77 g, 0.022 mol) in EtOH (100 mL) was added benzylamine (1.14 mL , 0.010 mol) dropwise. After stirring at 40 °C for 16 h the resulting yellow solution was concentrated under reduced pressure and purified using column chromatography (eluent ethyl acetate: pentane: NH_4OH, 50:10:1) to give **8** as a light yellow powder. Yield: 3.30 g (95 %). Diffraction-quality crystals were grown from a concentrated benzene solution. ^{1}H NMR ($CDCl_3$, 299.9 MHz): 7.25-7.00 (5H, m, overlapping Ph), 5.20 (2H, broad t, ^{3}J = 5.54 Hz, NH), 3.56 (2H, s, $C\underline{H}_2Ph$), 3.10 (4H, app. q, ^{3}J = 5.21 Hz, ^{3}J = 5.54 Hz, $C\underline{H}_2NHS$), 2.84 (6H, s, $SO_2\underline{Me}$), 2.62 (4H, t, ^{3}J = 5.21 Hz, $C\underline{H}_2CH_2NHS$). ^{13}C-{^{1}H} ($CDCl_3$, 75.4 MHz): 138.1 (1-C_6H_5), 129.9 (2-C_6H_5), 129.2 (3-C_6H_5), 128.2 (4-C_6H_5), 59.1 ($\underline{C}H_2Ph$), 53.7 ($\underline{C}H_2CH_2NHMs$), 40.9 ($\underline{C}H_2NHMs$), 39.4 ($S\underline{Me}$). ES-MS: $[M+1]^+$ 350.1195 (calcd for $C_{13}H_{24}N_3O_4S_2$, 350.1208). IR (NaCl plates, Nujol mull, cm^{-1}): 3277 (m), 1496 (s), 1466 (s), 1378 (s), 1332 (s), 1279 (w), 1233 (w), 1161 (s), 1136 (m), 1089 (m), 1048 (w), 993 (m), 978 (m), 940 (vw), 926 (w), 907 (w), 820 (m), 783 (s), 750 (s), 731 (m), 700 (m), 668 (w), 615 (w), 600 (w), 524 (w). Anal. found (calcd. for $C_{13}H_{23}N_3O_4S_2$): C, 44.18 (44.68); H, 6.68 (6.63); N, 11.60 (12.02) %.

$H_2N_2^{Ms}N^{OMe}$ (9). To a solution 1-(methylsulfonyl)aziridine (4.42 g, 0.036 mol) in EtOH (200 mL) at room temperature, was added 2-methoxyethylamine (1.44 g, 0.017 mol) dropwise. The resulting orange solution was stirred at 40 °C for 16 h, filtered and concentrated under reduced pressure. An analytically pure sample was obtained by column chromatography (SiO_2, elutent system ethyl acetate: pentane: NH_4OH (aq), 50:10:1) to give a light orange oil. Yield: 5.64 g, (50%). ^{1}H NMR ($CDCl_3$, 293 K,

300.7 MHz): 3.40 (2H, t, ^3J = 4.9 Hz, C$\underline{H_2}$OMe), 3.10 (4H, t, ^3J = 5.4 Hz, C$\underline{H_2}$NHS), 3.36 (3H, s, OMe), 2.90 (6H, s, SO_2Me), 2.68 (4H, t, ^3J = 5.4 Hz, C$\underline{H_2}CH_2$NHS), 2.60 (2H, t, ^3J = 4.9 Hz, C$\underline{H_2}CH_2$OMe). ^{13}C-{^1H} NMR ($CDCl_3$, 293 K, 75.4 MHz) 70.8 (C$\underline{H_2}CH_2$OMe), 59.0 (OMe), 54.0 (C$\underline{H_2}CH_2$NS), 52.8 (SO_2Me), 42.0 (C$\underline{H_2}$NHS), 40.0 (C$\underline{H_2}$OMe). IR (KBr plates, Nujol mull cm^{-1}): 3285 (m), 3015 (w), 2847 (s), 2361 (w), 2340 (w), 1736 (w), 1718 (w), 1700 (w), 1684 (w), 1653 (m), 1645 (m), 1636 (m), 1559 (w), 1378 (s), 1199 (w), 1057 (m), 1012 (w), 973 (m), 769 (m), 668 (w), 523 (w). ES-HRMS: *m/z* = 318.1142 ($[M+1]^+$; calcd. for $C_9H_{23}N_3O_5S_2$: 318.1157).

$H_3N_3^{Ms}N$ (10). To a solution of Tris(2-aminoethyl)amine (25.20 g, 26.0 ml, 0.17 mol) and NaOH (22.00 g, 0.55 mol) in H_2O (100 ml) was added dropwise a solution of Methanesulfonyl chloride (59.24 g, 40.0 ml, 0.52 mol) in diethyl ether (300 ml) and stirred at RT for 2 h. The resulting solution was evaporated under reduced pressure and the resulting white solid recrystallised from H_2O (30 ml) at 100 °C. The resulting white crystalline solid was filtered and dried *in vacuo*. Yield 12.01 g (18%). ^1H NMR ($(CD_3)_2SO$, 299.8 MHz, 298 K): δ 7.00 (3H, br. s, NH), 3.15 (6H, br. s, SNC$\underline{H_2}CH_2$N), 3.07 (9H, s, SO_2Me), 2.65 (6H, br. s, $SNCH_2C\underline{H_2}N$) ppm. ^{13}C-{^1H} NMR ($(CD_3)_2SO$, 75.4 MHz, 298 K): 67.8 ($SNCH_2\underline{C}H_2N$), 65.5 ($SN\underline{C}H_2CH_2N$), 54.7 (SO_2Me) ppm. IR: 3301 (m), 3242 (s), 3224 (s), 2725 (w), 1419 (w), 1348 (w), 1305 (s), 1261 (m), 1234 (w), 1224 (m), 1162 (s), 1137 (s), 1091 (m), 1068 (w), 1046 (w), 1026 (w), 1000 (w), 986 (m), 962 (s), 926 (m), 909 (w), 807 (m), 772 (s), 721 (w), 668 (w). ES-MS: $[M+H]^+$ 381.0926 (calcd. for $C_9H_{25}N_4O_6S_3$, 381.0936). Anal. found (calcd. for $C_9H_{24}N_4O_6S_3$); C, 28.41 (28.41); H, 6.43 (6.36); N, 14.65 (14.72) %.

$H_3N_3^{TArF}N$ (11). To a solution of Tris(2-aminoethyl)amine (2.34 g, 2.4 ml, 16.0 mmol) and NaOH (2.00 g, 34.2 mmol) in H_2O (105 ml) was added dropwise a solution of 3,5-bis(trifluoromethyl)benzene sulfonyl chloride (15.00 g, 48.1 mmol) in diethyl ether (210 ml) and stirred at RT for 2 h. After which time the white solid formed filtered and washed with H_2O (3 × 15 ml) and diethyl ether (3 × 20 ml). Product was recrystallised from acetonitrile (40 ml) and methanol (50ml). Yield 12.37 g (79%). ^1H NMR ($(CD_3)_2SO$, 299.8 MHz, 298 K): δ 8.43 (3H, s, 4-$C_6H_3(CF_3)_2$), 8.31 (6H, s, 2-$C_6H_3(CF_3)_2$), 7.90 (3H, br. s, NH), 2.76 (6H, t, ^3J = 6.1 Hz, SNC$\underline{H_2}CH_2$N), 2.29 (6H, t, ^3J = 6.1 Hz, $SNCH_2C\underline{H_2}N$) ppm. ^{13}C-{^1H} NMR ($(CD_3)_2SO$, 75.4 MHz, 298 K): 143.5 (1-$C_6H_3(CF_3)_2$), 131.4 (CF_3, ^1J = 33.2 Hz), 127.0 (2-$C_6H_3(CF_3)_2$), 124.4 (3-$C_6H_3(CF_3)_2$), 120.8 (4-$C_6H_3(CF_3)_2$), 53.2 ($SNCH_2\underline{C}H_2N$), 40.4 ($SN\underline{C}H_2CH_2N$) ppm.

^{19}F NMR ((CD$_3$)$_2$SO, 282.1 MHz, 298 K) -61.7 (18F, s, CF$_3$) ppm. IR: 3292 (s), 3227 (m), 3091 (w), 1627 (w), 1408 (w), 1336 (m), 1298 (s), 1282 (s), 1268 (w), 1195 (m), 1139 (s), 1111 (m), 1089 (w), 1046 (w), 1018 (w), 959 (w), 950 (w), 906 (s), 947 (m), 838 (w), 794 (w), 726 (w), 697 (m), 682 (m), 629 (w). Anal. found (calcd. for $C_{30}H_{24}F_{18}N_4O_6S_3$); C, 37.03 (36.97); H, 2.48 (2.50); N, 5.84 (5.75) %.

Ti($N_2^{Ts}N^{Ph}$)(NMe_2)$_2$ (12). To a solution of $H_2N_2{}^{Ts}N^{Ph}$ (2.00 g, 4.0 mmol) in benzene (50 mL) was added to a solution of Ti(NMe$_2$)$_4$ (0.94 ml, 12.0 mmol) in benzene (30 mL). The mixture was stirred for 2 h, resulting in a red solution. The solution was concentrated under reduced pressure to yield a yellow solid that was recrystallised from a concentrated benzene solution (20 ml) layered with pentane (30 ml) to yield **12** as a red solid that was washed with pentane (3 × 20 mL) and dried *in vacuo*. Yield: 2.18 g (86%). The recrystallised product yielded crystals suitable for an x-ray diffraction study. ^{1}H NMR (CD$_2$Cl$_2$, 499.9 MHz, 248 k): δ 7.73 (4H, d, ^{3}J = 10.0 Hz, 2-C$_6$H$_4$Me), 7.36 – 7.32 (3H, m, overlapping 3-C$_6$H$_5$ and 4-C$_6$H$_5$) 7.29 (4H, d, ^{3}J = 10.0 Hz, 3-C$_6$H$_4$Me) 7.06 (2H, d, ^{3}J = 9.5 Hz, 2-C$_6$H$_5$), 3.72 (2H, s, C$\underline{H}_2$C$_6$H$_5$), 3.57 (8H, s, overlapping NMe$_2$ and TsNC$\underline{H}_2$CH$_2$N), 3.31 (8H, s, overlapping NMe$_2$ and TsNC$\underline{H}_2$CH$_2$N) 2.68 (2H, m, TsNCH$_2$C$\underline{H}_2$N), 2.57 (2H, m, TsNCH$_2$C$\underline{H}_2$N) 2.37 (6H, s, C$_6$H$_4\underline{Me}$) ppm. ^{13}C-{^{1}H} NMR (CD$_2$Cl$_2$, 248 K, 75.4 MHz) 142.0 (1-C$_6$H$_4$Me), 139.0 (4-C$_6$H$_4$Me), 131.3 (4-C$_6$H$_5$), 130.0 (1-C$_6$H$_5$), 129.3 (3-C$_6$H$_4$Me), 128.7 (4-C$_6$H$_5$), 128.5 (3-C$_6$H$_5$), 127.1 (2-C$_6$H$_4$Me), 54.6 (C$\underline{H}_2$C$_6$H$_5$), 50.9 (NMe$_2$), 47.8 (TsNCH$_2\underline{C}$H$_2$N), 47.7 (NMe$_2$), 45.6 (TsN$\underline{C}$H$_2$CH$_2$N), 21.3 (C$_6$H$_4\underline{Me}$) ppm. IR: 2774 (w), 1342 (w), 1294 (m), 1280 (s), 1268 (m), 1249 (m), 1205 (w), 1144 (s), 1082 (s), 909 (m), 868 (w), 813 (m), 797 (w), 773 (w), 730 (w), 712 (w), 703 (w), 676 (m), 663 (m), 650 (w). Anal. found (calcd. for $C_{29}H_{41}N_5O_4S_2Ti$); C, 55.18 (54.79); H, 6.56 (6.50); N, 11.02 (10.70) %.

Ti($N_2^{Ts}N^{Ph}$)(O^iPr)$_2$ (13). To a solution of $H_2N_2{}^{Ts}N^{Ph}$ (0.50 g, 1.0 mmol) in chlorobenzene (30 mL) was added Ti(NMe$_2$)$_2$(O^iPr)$_2$ (254 mg, 1.0 mmol) in chlorobenzene (30 mL). The resulting light yellow solution mixture was stirred for 2 h concentrated under reduced pressure to yield a yellow solid that was recrystallised from a concentrated dichloromethane (10 ml) solution layered with pentane (30 ml) to yield **13** as a light yellow solid that was washed with pentane (3 × 20 mL) and dried *in vacuo*. Yield: 0.31 g (47 %). ^{1}H NMR (CD$_2$Cl$_2$, 299.9 MHz, 246 K): δ 8.16 (4H, d, ^{3}J = 9.2 Hz, 2-C$_6$H$_4$Me), 6.98 (4H, m, overlapping 3-C$_6$H$_5$ and 4-C$_6$H$_5$) 6.95 (4H, d, ^{3}J = 9.2

Hz, 3-C_6H_4Me), 6.70 (2H, d, ^3J = 8.5 Hz, 2-C_6H_5), 5.51 (1H, sept., ^3J = 6.2 Hz, OC<u>H</u>Me_2), 5.31 (1H, sept., ^3J = 5.9 Hz, OC<u>H</u>Me_2), 4.15 (2H, s, $CH_2C_6H_5$), 3.34 (4H, app. t, ^3J = 6.3 Hz, TsNC<u>H</u>$_2CH_2N$), 2.22 (4H, app. t, ^3J = 6.3 Hz, $TsNCH_2C$<u>H</u>$_2N$), 1.98 (6H, s, C_6H_4<u>Me</u>), 1.61 (12H, two overlapping d, ^3J = 6.2 and 5.9 Hz, OCH<u>Me</u>$_2$) ppm. ^{13}C-{^1H} NMR (CD_2Cl_2, 246 K, 75.4 MHz) 142.5 (1-C_6H_4Me), 139.0 (4-C_6H_4Me), 131.5 (4-C_6H_5), 131.0 (1-C_6H_5), 129.5 (3-C_6H_4Me), 129.0 (4-C_6H_5), 128.8 (3-C_6H_5), 127.4 (2-C_6H_4Me), 84.4 (O<u>C</u>HMe_2), 83.4 (O<u>C</u>HMe_2), 57.1 (<u>C</u>$H_2C_6H_5$), 50.8 ($TsNCH_2$<u>C</u>H_2N), 47.7 (TsN<u>C</u>H_2CH_2N), 25.4 (OCH<u>Me</u>$_2$), 24.9 (OCH<u>Me</u>$_2$), 21.3 (C_6H_4<u>Me</u>) ppm. IR: 2723 (w), 1298 (m), 1152 (s), 1109 (m), 1086 (m), 1028 (w), 997 (w), 946 (m), 906 (w), 814 (m), 772 (w), 732 (m), 667 (m). Anal. found (calcd. for $C_{31}H_{43}N_3O_6S_2Ti$); C, 55.63 (55.29); H, 6.39 (6.34); N, 6.19 (6.45) %.

Ti($N_2^{Ms}N^{Ph}$)(NMe_2)$_2$ (14). A solution of $H_2N_2^{Ms}N^{Ph}$ (0.50 g, 1.43 mmol) in benzene (50 ml) was added dropwise to a solution of Ti(NMe_2)$_4$ (0.231 g, 1.43 mmol) in benzene (30 ml) and stirred for 2.5 hrs. The volatiles were removed under reduced pressure and the residue dissolved toluene and cooled to -80 °C for 18 hours, yielding red crystals, which were filtered and dried *in vacuo*. Yield: 0.30g, (45%). ^1H NMR (CD_2Cl_2, 213 K, 499.9 MHz): δ 7.16 (2H, s, 3-C_6H_5), 7.08 (1H, s, 4-C_6H_5), 6.58 (2H, d, ^3J = 8.3 Hz, 2-C_6H_5), 3.79 (2H, s, C<u>H</u>$_2C_6H_5$), 3.73 (2H, t, ^3J = 6.1 Hz, C<u>H</u>$_2$NS), 3.36 (6H, s, N<u>Me</u>$_2$), 3.32 (6H, s, N<u>Me</u>$_2$), 2.63 (2H, t, ^3J = 6.1 Hz, C<u>H</u>$_2$NS), 2.47 (6H, s, SO_2<u>Me</u>), 1.95 (2H, t, ^3J = 6.0 Hz, NC<u>H</u>$_2CH_2$NS), 1.68 (2H, t, ^3J = 6.0 Hz, NC<u>H</u>$_2CH_2$NS) ppm.^{13}C-{^1H} data (CD_2Cl_2, 213 K, 75.5 MHz): δ 131.9 (2-C_6H_5), 131.4 (1-C_6H_5), 130.0 (4-C_6H_5), 129.0 (3-C_6H_5), 57.3 (<u>C</u>$H_2C_6H_5$), 51.4 (N<u>Me</u>$_2$), 48.9 (N<u>C</u>H_2CH_2NS), 44.1 (SO_2Me), 40.5 (<u>C</u>H_2NS). IR data (KBr plates, Njol mull, cm^{-1}) ν 2924 (s), 2361 (m), 2338 (w), 1734 (w), 1684 (w), 1636 (m), 1559 (w), 1540 (w), 1521 (w), 1507 (m), 1377(m), 1260 (m), 805 (w), 666 (w), 477 (s). Elemental Analysis: Anal. Found (calcd. for $C_{17}H_{33}N_5O_4S_2Ti$) C, 42.18 (42.23); H, 6.91 (6.88); N, 14.39 (14.49) %.

Ti($N_2^{Ms}N^{Ph}$)(O^iPr)$_2$ (15). A soultion of $H_2N_2^{Ms}N^{Ph}$ (0.37 g, 1.073 mmol) in benzene (50 ml) was added dropwise to a solution of Ti(NMe_2)$_2$(O^iPr)$_2$ (0.30 g, 1.18 mmol) in benzene (20 ml). The resulting solution was stirred for 2 hrs and volatiles removed under reduced pressure. The residue was extracted into benzene, and volatiles removed under reduced pressure, the resulting red solid was washed with hexane (3 × 15 ml), and dried *en vacuo* yielding **15** as a red powder. Yield: 0.30 g, (56%). ^1H NMR

(CD_2Cl_2, 223 K, 449.9 MHz): δ 7.16 (2H, m, 3-C_6H_5), 7.10 (1H, s, 4-C_6H_5), 6.77 (2H, d, ^3J = 7.0 Hz, 2-C_6H_5), 5.38 (1H, q,^3J = 5.4 Hz, OC<u>H</u>Me_2), 4.11 (2H, s, C<u>H_2</u>C_6H_5), 3.72 (2H, q, ^3J = 5.6 Hz, C<u>H_2</u>NS), 2.93 (2H, t, ^3J = 6.9 Hz, NC<u>H_2</u>CH_2NS), 2.64 (6H, s, SO_2<u>Me</u>), 2.21 (2H, t, ^3J=5.39 Hz, C<u>H_2</u>NS), 1.93 (2H, t, ^3J = 6.16 Hz, NC<u>H_2</u>CH_2NS), 1.61 (6H, d, ^3J = 6.3 Hz, OCH<u>Me_2</u>) ppm. ^{13}C-{^{1}H} (CD_2Cl_2, 293 K, 75.5 MHz): δ 132.4 (1-C_6H_5). 132.0 (2-C_6H_5), 129.0 (4-C_6H_5) , 128.9, (3-C_6H_5), 83.5 (O<u>C</u>HMe_2), 58.6 (<u>C</u>$H_2C_6H_5$), 51.5 (N<u>C</u>H_2CH_2NS), 48.7 (SO_2Me), 39.4 (<u>C</u>H_2NS), 26.1 (OCH<u>Me_2</u>), IR data (KBr plates, Njol mull, cm^{-1}) ν: 3853 (m), 3838 (w), 3821 (s), 3801 (w), 3751 (m), 3745 (w), 3735 (m), 3676 (w), 3649 (m), 3629 (m), 3583 (w), 2361 (s), 2341 (m), 2275 (s), 2120 (m), 2050 (m), 1772 (w), 1740 (w), 1717 (w), 1700 (w), 1684 (w), 1670 (w), 1653 (w), 1636 (w), 1617 (w), 1570 (m) 1559 (w), 1541 (w), 1521 (s), 1507 (m), 1377 (s), 1260 (s), 1019 (s), 802 (m), 721 (w), 666 (s), 542 (s), 446 (s), EI-MS: m/z = 453.0570, ([M-O$_i$Pr]$^+$, calc for $C_{19}H_{35}N_3O_6S_2Ti$ = 453.0570), m/z = 348.0798 ([L]$^+$, calcd. for $C_{19}H_{35}N_3O_6S_2Ti$ = 348.1130). Elemental Analysis: Found (calcd. for ($C_{19}H_{35}N_3O_6S_2Ti$): C, 44.35 (44.44); H, 6.91 (6.87); N, 8.14 (8.18) %.

Ti($N_2^{Ms}N^{OMe}$)(NMe_2)$_2$ (16). A solution of $H_2N_2^{Ms}N^{OMe}$ (0.50 g, 0.002 mol) in benzene (20 mL) was added dropwise to Ti(NMe_2)$_4$ (1.06 g, 0.005 mol) in benzene (20 mL) and stirred for 4 hrs . The resulting red solution was filtered and volatiles removed under reduced pressure to give **16** as a red solid. Further solid was obtained by recrystallisation from toluene (50 mL) at -80 °C, combined and dried *in vacuo*. Yield: 0.11 g (40%). ^{1}H NMR (C_6D_6, 298 K, 300.7 MHz): δ 3.40 (12H, s, N<u>Me_2</u>) 3.40 (2H, m, C<u>H_2</u>NS), 2.90 (3H, s, OMe), 2.80 (2H, t, ^3J = 4.3 Hz, C<u>H_2</u>OMe), 2.50 (6H, s, SO_2<u>Me</u>), 2.40 (2H, t, ^3J = 7.2 Hz, NC<u>H_2</u>CH_2OMe), 2.20 (4H, t, ^3J = 6.4 Hz, NC<u>H_2</u>CH_2NS). ^{13}C-{^{1}H} (C_6D_6, 298 K, 75.4 MHz): δ 68.0 (NMe_2), 60.0 (CH_2O<u>Me</u>), 53.0 (<u>C</u>H_2CH_2NS), 52.0 (CH_2<u>C</u>H_2O),49.0 (CH_2<u>C</u>H_2NS). IR data (KBr plates, Nujol mull, cm^{-1}): 1734 (w), 1717 (w), 1700 (w), 1684 (w), 1653 (w), 1646 (w), 1636 (w), 1616 (w), 1576 (w), 1559 (w), 1540 (w),1521 (w), 1507 (w), 1418 (m), 1376 (m), 1259 (s), 1181 (w), 1154 (s), 1118 (m), 1020 (m), 949 (s), 788 (s), 667 (w), 593 (m), 502 (s). EI-HRMS: *m/z* = 407.0904 ([*M* - NMe_2]$^+$; calcd. for $C_{13}H_{33}N_5O_5S_2Ti$: 407.0902). Anal. found (calcd. for $C_{13}H_{33}N_5O_5S_2Ti$): C, 34.47 (34.59); H, 7.19 (7.37); N, 15.64 (15.51) %.

Ti($N_2^{Ms}N^{OMe}$)(O^iPr)$_2$ (17). A solution of $H_2N_2^{Ms}N^{OMe}$ (0.340 g, 0.0011 mol) in benzene (20 mL) was added dropwise to a solution of Ti(NMe_2)$_2$(O^iPr)$_2$ (0.550 g,

0.0022 mol) in benzene (20 mL). The resulting bright orange solution was stirred for 2 hrs at room temperature, and volatiles were removed under reduced pressure. The residue was extracted into toluene (50 mL) and cooled to -80 °C for 16 hrs. The resulting orange solution was filtered and dried *in vacuo* to yield **17** as an orange powder. Yield: 0.23 g (44%). Red single crystals suitable for an X-ray diffraction study were obtained by recrystalisation from a concentrated toluene/hexane solution (1:3) at -80 °C. ^{1}H NMR (C_6D_6, 353 K, 499.2 MHz): δ 5.01 (2H, sep, ^{3}J = 6.1 Hz, OC<u>H</u>Me$_2$), 3.19 (3H, s, O<u>Me</u>), 3.05 (2H, t, ^{3}J = 5.1 Hz, C<u>H</u>$_2$NS), 2.77 (4H, app. q, ^{3}J = 5.7 Hz, overlapping NC<u>H</u>$_2$CH$_2$NS and CH$_2$C<u>H</u>$_2$OMe), 2.54 (6H, s, SO$_2$<u>Me</u>), 2.18 (2H, t, ^{3}J = 5.5 Hz, C<u>H</u>$_2$CH$_2$OMe), 1.27 (12H, d, ^{3}J = 6.1 Hz, OCH<u>Me</u>$_2$) ppm. ^{13}C-{^{1}H} ($C_6D_5CD_3$, 353 K, 75.5 MHz): δ 70.5 (O<u>C</u>HMe$_2$), 63.0 (O<u>Me</u>), 59.0 (<u>C</u>H$_2$CH$_2$NS), 58.0 (<u>C</u>H$_2$CH$_2$OMe), 54 (<u>C</u>H$_2$OMe), 49.5 (SO$_2$<u>Me</u>), 39.5 (<u>C</u>H$_2$NS), 26.0 (OCH<u>Me</u>$_2$) ppm. IR (KBr plates, Nujol mull, cm^{-1}) 1653 (w), 1559 (w), 1321 (s), 1363 (m), 1261 (w), 1162 (s), 1007 (m), 851 (w), 805 (w), 666 (w), 617 (w), 488 (m). EI-HRMS *m*/*z* = 422.0889 ([*M* - OiPr]$^{+}$; calcd. for $C_{21}H_{29}N_3O_7S_2Ti$: 422.0899). Anal. found (calcd. for $C_{21}H_{29}N_3O_7S_2Ti$): C, 37.51 (37.42); H, 7.27 (7.25); N, 8.69 (8.73) %.

Ti(N$_2^{Ts}$N^{Ph})(O^{i}Pr)(NMe$_2$) (18). To a solution of Ti(O^{i}Pr)$_2$(NMe$_2$)$_2$ (0.84 g, 3.30 mmol) in dichloromethane (30 mL) was added to a solution of H$_2$N$_2^{Ts}$N^{Ph} (0.50 g, 1.00 mmol) in dichloromethane (30 mL). The mixture was stirred for 16 h, resulting in an orange solution. The solution was concentrated to *ca*. 15 ml and hexane (40 ml) added to precipitate the product, which was filtered. The orange solid was recrystallised from a concentrated dichloromethane solution layered with pentane to yield **18** as an orange solid that was washed with pentane (3 × 20 mL) and dried *in vacuo*. The recrystallised product yielded crystals suitable for an x-ray diffraction study. Yield: 0.48 g (74%).^{1}H NMR (CD_2Cl_2, 299.9 MHz, 248 K): δ 7.73 (4H, d, ^{3}J = 9.0 Hz, 2-C$_6$H$_4$Me), 7.38 (2H, m, 2-C$_6$H$_5$) 7.29 (4H, d, ^{3}J = 9.0 Hz, 3-C$_6$H$_4$Me), 7.00 (3H, m,overlapping 3-C$_6$H$_5$ and 4-C$_6$H$_5$), 5.16 (1H, sept., ^{3}J = 6.1 Hz, OC<u>H</u>Me$_2$), 3.73 (2H, s, CH$_2$C$_6$H$_5$), 3.43 (10H, s, overlapping NMe$_2$ and TsNC<u>H</u>$_2$CH$_2$N), 2.74 (4H, m, TsNCH$_2$C<u>H</u>$_2$N), 2.37 (6H, s, C$_6$H$_4$<u>Me</u>), 1.61 (6H, d, ^{3}J = 6.1 Hz, OCH<u>Me</u>$_2$) ppm. ^{13}C-{^{1}H} NMR (CD_2Cl_2, 248 K, 75.4 MHz) 141.9 (1-C$_6$H$_4$Me), 139.6 (4-C$_6$H$_4$Me), 131.4 (4-C$_6$H$_5$), 129.8 (1-C$_6$H$_5$), 129.2 (3-C$_6$H$_4$Me), 128.9 (4-C$_6$H$_5$), 128.5 (3-C$_6$H$_5$), 126.9 (2-C$_6$H$_4$Me), 83.1 (O<u>C</u>HMe$_2$), 54.7 (<u>C</u>H$_2$C$_6$H$_5$), 52.7 (NMe$_2$), 47.6 (TsNCH$_2$<u>C</u>H$_2$N), 47.5 (TsN<u>C</u>H$_2$CH$_2$N), 25.8 (OCH<u>Me</u>$_2$), 21.3 (C$_6$H$_4$<u>Me</u>) ppm. IR: 2723 (w), 1297 (s), 1168 (w), 1143 (m), 1085 (m), 1022 (m), 952 (s), 903 (w), 820 (w), 771 (w), 723 (m), 668

(m). Anal. found (calcd. for $C_{30}H_{42}N_4O_5S_2Ti$); C, 55.68 (55.92); H, 6.51 (6.58); N, 8.61 (8.44) %.

Alternative NMR tube scale synthesis of Ti($N_2^{Ts}N^{Ph}$)(O^iPr)(NMe_2) (18). To a solution of Ti($N_2^{Ts}N^{Ph}$)(NMe_2)$_2$ (10 mg, 15.7 μmol) in C_6D_6 (0.2 mL) was added a solution of Ti($N_2^{Ts}N^{Ph}$)(O^iPr)$_2$ (10.5 mg, 15.7 μmol) in C_6D_6 (0.2 mL). Initial ^{1}H NMR indicated that no reaction had taken place. The reaction mixture was then heated at 80 °C for 4 days. A colour change of the initially dark orange to light orange was observed. Analysis by ^{1}H NMR indicated that **18** had been formed quantitatively.

Ti($N_2^{Ts}N^{Ph}$)Cl_2 (19). To a solution of Ti($N_2^{Ts}N^{Ph}$)(NMe_2)$_2$ (0.3 g, 0.47 mmol) in benzene (30 ml) was added Me_3SiCl (0.13 ml, 1.04 mmol) and the resulting yellow solution stirred at RT for 48 h. At which time a yellow solid formed which was filtered, washed with pentane (3 × 15 ml) and dried *in vacuo*. Yield: 0.13 g (46 %). Single crystals suitable for x-ray diffraction studies were grown from a concentrated dichloromethane solution layered with hexane. ^{1}H NMR (CD_2Cl_2, 499.9 MHz, 263 K): δ 8.16 (4H, d, ^{3}J = 10.1 Hz, 2-C_6H_4Me), 7.44 (4H, br. d, ^{3}J = 10.1 Hz, overlapping 3-C_6H_4Me, 3-$CH_2C_6H_5$, and 4-$CH_2C_6H_5$), 7.29 (2H, m, 2-$CH_2C_6H_5$), 4.57 (2H, s, $\underline{CH_2}C_6H_5$), 4.50 (2H, dt, ^{3}J = 4.9 Hz, ^{3}J = 15.3 Hz, NC$\underline{H_2}CH_2$), 4.31 (2H, dd, ^{3}J = 15.3 Hz, ^{3}J = 4.9 Hz, $NCH_2C\underline{H_2}$), 3.76 (4H, dt, ^{3}J = 15.3 Hz, ^{3}J = 4.9 Hz, $NCH_2C\underline{H_2}$), 3.38 (4H, dd, ^{3}J = 15.3 Hz, ^{3}J = 4.9 Hz, $NCH_2C\underline{H_2}$), 2.45 (6H, s, MeC_6H_4). ^{13}C-{^{1}H} NMR (CD_2Cl_2, 75.4 MHz) 145.7 (1-C_6H_4Me), 136.5 (1-C_6H_5), 132.5 (4-C_6H_4Me), 130.9 (3-C_6H_4Me), 130.1 (4-C_6H_5), 129.8 (3-C_6H_5), 129.3 (2-C_6H_5), 128.5 (2-C_6H_4Me), 58.5 (Ph$\underline{C}H_2$N), 57.5 (TsNCH$_2\underline{C}H_2$N), 50.6 (TsN$\underline{C}H_2CH_2$N), 21.8 ($C_6H_4\underline{Me}$) ppm. IR: 2723 (w), 1301 (s), 1261 (m), 1156 (s), 1092 (w), 1017 (w), 965 (w), 941 (m), 891 (w), 803 (m), 773 (m), 668 (m) cm^{-1}. Anal. found (calcd. For $C_{25}H_{29}Cl_2N_3O_4S_2Ti$); C, 48.85 (49.23); H, 4.73 (4.78); N, 6.79 (6.66) %.

Zr($N_3^{Ts}N$)(CH_2SiMe_3) (20). To a solution of Zr(CH_2SiMe_3)$_4$ (0.52 g, 1.2 mmol) in THF (15 ml) was added a solution of $H_3N_3^{Ts}N$ (0.71 g, 1.2 mmol) in THF (15 ml). The reaction was stirred at RT for 16 h after which time the resulting light yellow solution was concentrated to *ca*. half the original volume and cooled to -78 °C. The resulting white crystalline solid was filtered, washed with pentane (3 × 15 ml) and dried *in vacuo*. Yield 0.63 g (67%). Crystals suitable for X-ray diffraction studies were obtained from slow evaporation of a THF solution at RT. ^{1}H NMR (CD_2Cl_2, 299.9 MHz, 298 K): δ 7.90 (6H, d, ^{3}J = 6.4 Hz, 2-C_6H_4Me), 7.31 (6H, d, ^{3}J = 6.4 Hz,

3-C_6H_4Me), 3.53 (6H, m, TsNC$\underline{H_2}CH_2N$), 2.82 (6H, m, TsNCH$_2$C$\underline{H_2}$N), 2.41 (9H, s, $C_6H_4\underline{Me}$), 0.26 (2H, br. s, C$\underline{H_2}$Si), -0.30 (9H, s, Si$\underline{Me_3}$) ppm. ^{13}C-{^{1}H} NMR (CD_2Cl_2, 75.4 MHz, 298 K) 141.9 (1-C_6H_4Me), 139.1 (4-C_6H_4Me), 129.8 (3-C_6H_4Me), 127.5 (2-C_6H_4Me), 60.8 (TsNCH$_2\underline{C}$H$_2$N), 47.6 (TsN$\underline{C}$H$_2$CH$_2$N), 21.5 ($C_6H_4\underline{Me}$), 3.8 ($\underline{C}H_2Si$), 2.4 (Si$\underline{Me_3}$) ppm. IR: 1262 (s), 1161 (m), 1110 (m), 1019 (w), 968 (w), 814 (s), 668 (m), 635 (w). Anal. found (calcd. for $C_{29}H_{41}N_5O_4S_2Ti$); C, 47.42 (47.48); H, 5.76 (5.66); N, 7.09 (7.14) %.

Zr($N_3^{TArF}N$)(CH_2SiMe_3) (21). To a solution of $Zr(CH_2SiMe_3)_4$ (0.19 g, 0.2 mmol) in toluene (5 ml) was added a slurry of $H_3N_3^{TArF}N$ (0.40 g, 0.2 mmol) in toluene (15 ml) and heated to 100 °C for 2 h. After which time the light yellow solution was cooled to 0 °C. White crystalline product was isolated by filtration and dried *in vacuo*. Yield 0.21 g (89%). Crystals suitable for X-ray diffraction studies were obtained from a concentrated benzene solution. ^{1}H NMR (CD_2Cl_2, 299.9 MHz, 313 K): δ 8.52 (6H, s, 2-$C_6H_3(CF_3)_2$), 8.14 (3H, s, 4-$C_6H_3(CF_3)_2$), 3.69 (6H, br. s, SNC$\underline{H_2}$CH$_2$N), 2.98 (6H, br. s, SNCH$_2$C$\underline{H_2}$N), 0.34 (2H, br. s, C$\underline{H_2}$Si), 0.36 (9H, s, Si$\underline{Me_3}$) ppm. ^{13}C-{^{1}H} NMR (CD_2Cl_2, 75.4 MHz, 313 K) 145.8 (1-$C_6H_3(CF_3)_2$), 133.5 (CF_3, ^1J = 34.3 Hz), 127.8 (3-$C_6H_3(CF_3)_2$), 127.0 (2-$C_6H_3(CF_3)_2$), 125.0 (4-$C_6H_3(CF_3)_2$), 61.0 (SNCH$_2\underline{C}$H$_2$N), 58.0 (SN$\underline{C}$H$_2$CH$_2$N), 1.8 (Si$\underline{Me_3}$) ppm. ^{19}F NMR (CD_2Cl_2, 282.1 MHz, 313 K) -61.5 (18F, s, CF_3) ppm. IR: 3102 (w), 2726 (w), 1624 (w), 1365 (s), 1282 (s), 1193 (s), 1141 (s), 1084 (m), 1044 (w), 1007 (w), 994 (w), 970 (m), 937 (m), 908 (s), 845 (s), 823 (m), 808 (m), 747 (w), 720 (w), 698 (m), 682 (s), 651 (w), 644 (m). Anal. found (calcd. for $C_{34}H_{32}F_{18}N_4O_6S_3Zr$); C, 35.47 (35.51); H, 2.79 (2.80); N, 4.78 (4.87) %.

Zr($N_3^{Ms}N$)(CH_2SiMe_3) (22). To a solution of $Zr(CH_2SiMe_3)_4$ (0.50 g, 0.1 mmol) in toluene (10 ml) was added a slurry of $H_3N_3^{Ms}N$ (0.44 g, 0.1 mmol) in toluene (15 ml) and heated to 100 °C for 3 h. After which time the solution was cooled to RT and filtered. The resulting light yellow solution was concentrated to *ca*. 5 ml. The resulting white crystalline solid was filtered, washed with pentane (3 × 15 ml) and dried *in vacuo*. Yield 0.35 g (60%) ^{1}H NMR (CD_2Cl_2, 299.9 MHz, 298 K): δ 3.47 (6H, t, ^3J = 6.0 Hz, SNC$\underline{H_2}$CH$_2$N), 3.08 (9H, s, SO_2Me) 2.74 (6H, t, ^3J = 6.0 Hz, SNCH$_2$C$\underline{H_2}$N), 0.29 (2H, br. s, C$\underline{H_2}$Si), -0.30 (9H, s, Si$\underline{Me_3}$) ppm. ^{13}C-{^{1}H} NMR (CD_2Cl_2, 75.4 MHz, 298 K) 60.8 (SNCH$_2\underline{C}$H$_2$N), 46.8 (SO_2Me), 40.7 (SN$\underline{C}$H$_2$CH$_2$N), 3.1 ($\underline{C}H_2SiMe_3$), 2.8 (Si$\underline{Me_3}$) ppm. IR: 2723 (w), 1324 (w), 1249 (s), 1150 (w), 1075 (m), 982 (s), 863 (m),

936 (m), 761 (w), 722 (w), 697 (w), 668 (w). Anal. found (calcd. for $C_{13}H_{32}N_4O_6S_3SiZr$); C, 27.96 (28.09); H, 5.82 (5.80); N, 9.99 (10.08) %.

Zr($N_3^{TArF}N$)(NMe_2) (23). To a solution of $Zr(NMe_2)_4$ (0.11 g, 0.4 mmol) in THF (15 ml) was added a solution of $H_3N_3^{TArF}N$ (0.40 g, 0.41 mmol) in THF (15 ml) and stirred at RT for 16 h. After which time the light yellow solution was concentrated to *ca*. half its original volume and cooled to -78 °C. White crystalline product was isolated by filtration and dried *in vacuo*. Yield 0.37 g (82%). Crystals suitable for X-ray diffraction studies were obtained from a concentrated THF solution. ^{1}H NMR (C_6D_6, 499.9 MHz, 298 K): δ 8.50 (6H, s, 2-$C_6H_3(CF_3)_2$), 7.63 (3H, s, 4-$C_6H_3(CF_3)_2$), 2.99 (6H, br. s, SNC$\underline{H}_2$CH_2N), 2.86 (6H, s, NMe_2), 2.22 (6H, br. s, SNCH_2C$\underline{H}_2$N) ppm. ^{13}C-{^{1}H} NMR (CD_2Cl_2, 75.4 MHz, 298 K) 145.35 (1-$C_6H_3(CF_3)_2$), 133.1 (CF_3, ^1J = 33.9 Hz), 126.2 (3-$C_6H_3(CF_3)_2$), 125.2 (2-$C_6H_3(CF_3)_2$), 121.6 (4-$C_6H_3(CF_3)_2$), 60.45 (SNC$H_2\underline{C}H_2$N), 46.2 (SN$\underline{C}H_2$CH_2N), 44.1 (NMe_2) ppm. ^{19}F NMR (CD_2Cl_2, 282.1 MHz, 298 K) -62.7 (18F, s, CF_3) ppm. IR: 2724 (w), 1365 (m), 1280 (s), 1191 (m), 1125 (s), 1053 (w), 1016 (w), 956 (w), 937 (m), 924 (m), 901 (m), 780 (s), 738 (w), 720 (w), 698 (m), 682 (m), 644 w). Anal. found (calcd. for $C_{32}H_{27}F_{18}N_5O_6S_3Zr$); C, 34.66 (34.72); H, 2.42 (2.46); N, 6.38 (6.33) %.

{Zr($N_3^{TArF}N$)}$_2$(μ-O) (24). Zr($N_3^{TArF}N$)(NMe_2) (**23**) (0.10 g, 0.1 mmol) was washed with ether (5 × 15 ml) and dried *in vacuo* to yield **24** as a white solid. Yield 0.12 g (61%) Crystals suitable for X-ray diffraction studies were obtained from slow evaporation of a concentrated diethyl ether solution at RT. ^{1}H NMR (C_6D_6, 499.9 MHz, 298 K): δ 8.79 (2H, s, 2-$C_6H_3(CF_3)_2$), 8.60 (2H, s, 2-$C_6H_3(CF_3)_2$), 8.38 (2H, s, 2-$C_6H_3(CF_3)_2$), 7.90 (1H, s, 4-$C_6H_3(CF_3)_2$), 7.82 (1H, s, 4-$C_6H_3(CF_3)_2$), 7.56 (1H, s, 4-$C_6H_3(CF_3)_2$), 3.80 (1H, m, SNCH_2CH_2N), 3.20 (2H, m, SNCH_2CH_2N), 2.77 (1H, m, SNCH_2CH_2N), 2.67 (1H, m, SNCH_2CH_2N), 2.53 (1H, m, SNCH_2CH_2N), 2.28 (1H, m, SNCH_2CH_2N), 2.06 (1H, m, SNCH_2CH_2N), 1.87 (1H, m, SNCH_2CH_2N), 1.52 (1H, m, SNCH_2CH_2N), 1.36 (1H, m, SNCH_2CH_2N), 0.95 (1H, m, SNCH_2CH_2N) ppm. A satisfactory ^{13}C NMR could not be obtained due to the insoluble nature of this compound. ^{19}F NMR (C_6D_6, 125.8 MHz, 298 K) -128.2 (6F, s, CF_3), -128.1 (6F, s, CF_3), -127.9 (6F, s, CF_3) ppm IR: 2725 (w), 1281 (s), 1139 (s), 1006 (w), 992 (w), 966 (w), 905 (m), 844 (m), 808 (w), 722 (m), 698 (m), 682 (m), 648 (w). Anal. found (calcd. for $C_{60}H_{42}F_{36}N_8O_{13}S_6Zr$); C, 35.50 (35.14); H, 1.93 (2.06); N, 5.19 (5.46) %.

NMR tube scale synthesis of Zr(N_3^{Ts}N)(O^iPr) (25). To a solution of Zr(N_3^{Ts}N)(CH_2SiMe_3) (**20**) (10 mg, 12.8 μmol) in CD_2Cl_2 (0.2 mL) was added a solution of HO^{i}Pr (0.77 mg, 1.0 μl, 12.8 μmol) in CD_2Cl_2 (0.2 mL). After 1 h analysis by ^{1}H NMR indicated that **25** had been formed quantitatively. ^{1}H NMR (CD_2Cl_2, 299.9 MHz, 298 K): δ 9.97 (6H, d, ^{3}J = 9.0 Hz, 2-C_6H_4Me), 7.29 (6H, d, ^{3}J = 9.0 Hz, 3-C_6H_4Me), 4.40 (1H, sept., ^{3}J = 6.0, OC<u>H</u>Me_2) 3.39 (6H, t, ^{3}J = 5.8, TsNC<u>H_2</u>CH_2N), 2.89 (6H, t, ^{3}J = 5.8, TsNCH_2C<u>H_2</u>N), 2.42 (9H, s, C_6H_4<u>Me</u>), 0.98 (1H, sept., ^{3}J = 6.0, OC<u>H</u>Me_2) ppm.

NMR tube scale synthesis of Zr(N_3^{TArF}N)(O(2,6-$C_6H_3Me_2$) (26). To a solution of Zr(N_3^{TArF}N)(NMe_2) (**23**) (10 mg, 8.7 μmol) in CD_2Cl_2 (0.2 mL) was added a solution of HO(2,6($Me_2C_6H_3$) (1.1 mg, 8.7 μmol) in CD_2Cl_2 (0.2 mL). After 1 h analysis by ^{1}H NMR indicated that **26** had been formed quantitatively. ^{1}H NMR (CD_2Cl_2, 299.9 MHz, 298 K): δ 8.34 (6H, s, 2-$C_6H_3(CF_3)_2$), 7.51 (6H, s, 4-$C_6H_3(CF_3)_2$), 6.64 (2H, d, ^{3}J = 9.0 Hz, 4-$C_6H_3Me_2$), 6.48 (2H, d, ^{3}J = 9.0 Hz, 3-$C_6H_3Me_2$), 2.97 (6H, br. s, SNC<u>H_2</u>CH_2N), 2.21 (6H, br. s, SNCH_2C<u>H_2</u>N), 2.14 (2H, s, C_6H_3<u>Me_2</u>) ppm.

5.5. Experimental details and characterising data for Chapter Four

Al(CyN_2^{Ts})Et(THF) (27). To a solution of $H_2CyN_2^{Ts}$ (2.00 g, 4.73 mmol) in THF (30 mL) cooled to 0 °C was added dropwise a solution of $AlEt_3$ in hexanes (1.0 M, 5.68 mL, 5.68 mmol). The mixture was allowed to warm to room temperature and stirred for 16 h. The orange solution was concentrated to half its volume under reduced pressure and hexanes (30 mL) was added. The resulting white solid was filtered, washed with hexanes (3 × 15 mL) and dried *in vacuo*, giving **27** as a white solid. Yield: 1.80 g (70%). Diffraction-quality crystals were grown from a saturated solution of THF and hexanes at room temperature. ^{1}H NMR (C_6D_6, 299.9 MHz, 303 K): δ 7.94 (4H, d, ^{3}J = 8.1 Hz, 2-C_6<u>H_4</u>Me), 6.84 (4H, d, ^{3}J = 8.1 Hz, 3-C_6<u>H_4</u>Me), 3.56 (4H, m, THF), 3.34 (2H, d, ^{3}J=8.7Hz, 1,6-C_6<u>$H_{10}N_2$</u>), 2.36 (2H, m, C_6<u>$H_{10}N_2$</u>), 1.92 (6H, s, C_6H_4<u>Me</u>), 1.78 (3H, t, ^{3}J=8.1Hz, $AlCH_2$<u>Me</u>), 1.42 (4H, m, THF), 1.15 (6H, br. m, overlapping C_6<u>$H_{10}N_2$</u>, C<u>H_2</u>Me, and C_6<u>$H_{10}N_2$</u>), 0.82 (2H, br. m, C_6<u>$H_{10}N_2$</u>) ppm. A satisfactory ^{13}C NMR spectrum could not be obtained due to the insolubility and fluxional nature of the compound. IR (NaCl plates, Nujol mull, cm^{-1}): 1597 (w), 1495 (w), 1209 (w), 1147 (m), 1108 (m), 1088 (m), 1050 (m), 1021 (w), 983 (m), 958 (m), 903 (m), 865 (m), 842 (m), 824 (m), 816 (w), 798 (w), 733 (m), 720 (w), 678 (m), 670 (m), 615 (m), 583 (m),

553 (s). Anal. found (calcd. for $C_{26}H_{37}AlN_2O_5S_2$): C, 56.82 (56.91); H, 6.84 (6.80); N, 5.07 (5.11) %.

Al($CyN_2^{SO_2Mes}$)Et(THF) (28). To a solution of $H_2CyN_2^{SO_2Mes}$ (1.0 g, 2.04 mmol) in THF (10 mL) was added a solution of $AlEt_3$ in hexanes (1.0 M, 2.24 mL, 2.24 mmol). The mixture was heated up to 80 °C for 16 h. The volatiles of the resulting orange solution were removed under reduced pressure and the white solid was dissolved in a minimum volume of THF and layered with hexanes (40 mL). The resulting white solid was filtered, washed with hexanes (3 × 15 mL) and dried *in vacuo*, giving **28** as a white solid. Yield: 0.81 g (66%). ^{1}H NMR (C_6D_6, 299.9 MHz, 303 K): δ 6.67 (4H, s, $C_6\underline{H}_2Me_3$), 3.54 (4H, m, THF), 3.40 (2H, br. s, 1,6-$C_6\underline{H}_{10}N_2$), 2.70 (12H, br. s, 2,6-$NC_6H_2\underline{Me}_3$), 1.94 (6H, s, 4-$NC_6H_2\underline{Me}_3$), 1.94 (2H, m, $C_6\underline{H}_{10}N_2$), 1.71 (3H, t, ^{3}J=8.1Hz, $CH_2\underline{Me}$), 1.42 (4H, m, THF), 1.07 (4H, br. m, overlapping $C_6\underline{H}_{10}N_2$ and $C\underline{H}_2Me$), 0.97 (4H, br. m, $C_6\underline{H}_{10}N_2$) ppm. A satisfactory ^{13}C NMR spectrum could not be obtained due to the fluxional nature of the compound. IR (NaCl plates, Nujol mull, cm^{-1}): 1602 (w), 1565 (w), 1402 (w), 1292 (m), 1253 (m), 1211 (w), 1132 (m), 1115 (m), 1098 (m), 1074 (m), 1054 (m), 982 (m), 932 (w), 898 (m), 865 (w), 847 (w), 833 (m), 796 (w), 732 (w), 703 (m), 689 (m), 674 (m), 660 (m), 619 (m), 591 (m). Anal. found (calcd. for $C_{30}H_{45}AlN_2O_5S_2$): C, 59.69 (59.58); H, 7.39 (7.50); N, 4.69 (4.63) %. ES MS m/z = 503 [*M*-Et, THF + H]$^+$ 25%.

Al($N_2^{Ts}N^{Ph}$)Et (29). $AlEt_3$ (2.2 mL, 1 M in hexanes) was added to a solution of a solution of $H_2N_2^{Ts}N^{Ph}$ (1.00 g, 2.0 mmol) in THF (30 mL) at 0 °C. The mixture was stirred at RT for 4 h, resulting in a colourless solution. Removal of the volatiles under reduced pressure yielded **29** as a white solid that was washed with pentane (3 × 20 mL) and dried *in vacuo*. Yield: 0.70 g (63%). Diffraction-quality crystals were grown from a concentrated dichloromethane solution layered with hexanes. ^{1}H NMR (CD_2Cl_2, 299.9 MHz): δ 7.83 (4H, d, ^{3}J = 8.0 Hz, 2-$C_6\underline{H}_4Me$), 7.41 (3H, m, overlapping 3- and 4-C_6H_5), 7.28 (4H, d, ^{3}J = 8.0 Hz, 3-$C_6\underline{H}_4Me$), 7.41 (2H, m, 2-C_6H_5), 3.97 (2H, s, $C\underline{H}_2C_6H_5$), 3.23 (2H, m, $TsNC\underline{H}_2CH_2$), 3.00 (2H, m, $TsNC\underline{H}_2CH_2$), 2.83 (2H, m, $TsNCH_2C\underline{H}_2$), 2.62 (2H, m, $TsNCH_2C\underline{H}_2$), 2.42 (6H, s, $C_6H_4\underline{Me}$), 1.26 (3H, t, ^{3}J = 8.0 Hz, $AlCH_2\underline{Me}$), 0.42 (2H, q, ^{3}J = 8.0 Hz, $AlC\underline{H}_2Me$) ppm. ^{13}C-{^{1}H} NMR (CD_2Cl_2, 75.4 MHz): δ 142.7 (1-C_6H_4Me), 137.6 (4-C_6H_4Me), 131.3 (4-C_6H_5), 129.7 (1-C_6H_5), 129.4 (3-C_6H_4Me), 129.3 (2-C_6H_5), 128.3 (3- C_6H_5), 127.3 (2-C_6H_4Me), 55.0 ($N\underline{C}H_2C_6H_5$), 48.9 ($TsNCH_2\underline{C}H_2$), 39.7 ($TsN\underline{C}H_2CH_2$), 21.2 ($C_6H_4\underline{Me}$), 8.7

($AlCH_2\underline{Me}$), -1.5 ($Al\underline{C}H_2Me$). IR (NaCl plates, Nujol mull, cm^{-1}): 3066 (w), 1495 (w), 1310 (s), 1303 (s), 1286 (w), 1267 (w), 1244 (w), 1152 (s), 1126 (m), 1097 (m), 1053 (w), 1043 (w), 1022 (w), 998 (m), 970 (w), 940 (w), 889 (w), 845 (w), 815 (w), 799 (w), 742 (w), 711 (w), 702 (w), 683 (w), 652 (w),630 (w). Anal. found (calcd. for $C_{27}H_{34}AlN_3O_4S_2$): C, 58.30 (58.36); H, 6.28 (6.17); N, 7.56 (7.46) %.

Al($N_2^{Ts}N^{OMe}$)Et (30). $AlEt_3$ (2.34 mL, 1 M in hexanes) was added to a solution of $H_2N_2{}^{Ts}N^{OMe}$ (1.00 g, 2.13 mmol) in THF (30 mL) at 0 °C. The mixture was stirred at RT for 3 h, resulting in a colourless solution. Removal of the volatiles under reduced pressure yielded a white solid that was recrystallized from a concentrated toluene solution at 100 °C to yield **30** as a white solid which was washed with pentane (3 × 20 mL) and dried *in vacuo*. Yield: 0.60 g (54%). Diffraction-quality crystals were grown from a concentrated dichloromethane solution layered with hexanes. ^{1}H NMR (CD_2Cl_2, 299.9 MHz): δ 7.78 (4H, d, ^{3}J = 6.0 Hz, 2-$C_6\underline{H}_4Me$), 7.26 (4H, d, ^{3}J = 6.0 Hz, 3-$C_6\underline{H}_4Me$), 3.57 (6H, app. t, ^{3}J = 6.0 Hz, $OCH_2\underline{CH_2}$), 3.25 (3H, s, OMe), 3.01 – 2.92 (10H, m, overlapping CH_2), 2.40 (6H, s, $C_6H_4\underline{Me}$), 1.15 (3H, t, ^{3}J = 9.0 Hz, $AlCH_2\underline{Me}$), 0.28 (2H, q, ^{3}J = 9.0 Hz, $Al\underline{CH_2}Me$) ppm . ^{13}C-{^{1}H} NMR (CD_2Cl_2, 75.4 MHz): δ 142.9 (1-C_6H_4Me), 138.0 (4-C_6H_4Me), 129.6 (3-C_6H_4Me), 127.6 (2-C_6H_4Me), 67.4 (MeO), 58.7 ($O\underline{C}H_2CH_2$), 51.7 ($TsN\underline{C}H_2CH_2$), 51.0 ($TsNCH_2\underline{C}H_2$), 40.3 ($OCH_2\underline{C}H_2$), 21.5 ($C_6H_4\underline{Me}$), 8.9 ($AlCH_2\underline{Me}$), -2.1 ($Al\underline{C}H_2Me$). IR (NaCl plates, Nujol mull, cm^{-1}): 1598 (w), 1350 (w), 1304 (s), 1285 (m), 1245 (m), 1227 (w), 1203 (w), 1146 (s), 1095 (s), 1067 (w), 1035 (m), 1023 (w), 991 (s), 931 (w), 912 (w), 899 (w), 846 (m), 818 (m), 800 (w), 748 (w), 728 (w), 712 (w), 679 (m), 652 (w), 630 (w), 618 (w). Anal. found (calcd. for $C_{23}H_{34}AlN_3O_5S_2$): C, 52.59 (52.75); H, 6.40 (6.54); N, 7.86 (8.02) %.

Al($N_2^{Ts}N^{py}$)Et (31). $AlEt_3$ (2.2 mL, 1 M in hexanes) was added to a solution of a solution of $H_2N_2{}^{Ts}N^{py}$ (1.00 g, 2.00 mmol) in THF (30 mL) at 0 °C. The mixture was stirred at RT for 16 h, resulting in a colourless solution with a white precipitate. Removal of the volatiles under reduced pressure yielded a white solid, that was recrystallized from a concentrated THF and dichloromethane (1:1) solution to yield **31** as a white solid which was washed with pentane (3 × 20 mL) and dried *in vacuo*. Yield: 0.69 g (63%). Diffraction-quality crystals were grown from a concentrated dichloromethane solution layered with hexanes. ^{1}H NMR (CD_2Cl_2, 299.9 MHz): δ 9.05 (1H, dd, ^{3}J = 7.6 Hz, ^{4}J = 1.5 Hz, 2-NC_5H_4), 8.04 (1H, dt, ^{3}J = 7.6 Hz, ^{3}J = 7.0 Hz, 3-NC_5H_4), 7.71 (4H, d, ^{3}J = 8.2 Hz, 2-C_6H_4Me), 7.63 (1H, dd, ^{3}J = 7.0 Hz, ^{3}J = 7.6 Hz,

4-NC_5H_4), 7.43 (1H, d, ^3J = 7.0 Hz, 5-NC_5H_4), 7.19 (4H, d, ^3J = 8.2 Hz, 3-C_6H_4Me), 4.06 (2H, s, py$C\underline{H}_2$N), 3.09 (4H, m, overlapping Ts$NC\underline{H}_2C\underline{H}_2$N), 2.75-2.45 (4H, m, Ts$NC\underline{H}_2C\underline{H}_2$N), 2.37 (6H, s, $C_6H_4\underline{Me}$), 0.91 (3H, t, ^3J = 7.6 Hz, $AlCH_2\underline{Me}$), 0.65 (2H, q, ^3J = 7.6 Hz, $AlC\underline{H}_2Me$) ppm. ^{13}C-{^1H} NMR (CD_2Cl_2, 75.4 MHz): δ 154.5 (6-NC_5H_4), 150.1 (1-C_6H_4Me), 142.0 (2-NC_5H_4), 140.9 (4-C_6H_4Me), 140 (3-NC_5H_4), 129.5 (3-C_6H_4Me), 127.5 (2-C_6H_4Me), 125.5 (4-NC_5H_4), 124.1 (5-NC_5H_4), 68.3 (py$\underline{C}H_2$N), 57.11 (Ts$NCH_2\underline{C}H_2$N), 42.4 (Ts$N\underline{C}H_2CH_2$N), 26.1 ($AlCH_2\underline{Me}$), 21.6 ($C_6H_4\underline{Me}$), 10.1 ($Al\underline{C}H_2Me$) ppm. IR (NaCl plates, Nujol mull, cm^{-1}): 1653 (w), 1306 (m), 1281 (m), 1281 (m), 1261 (m), 1162 (w), 1141 (m), 1095 (w), 1022 (w), 980 (m), 957 (w), 813 (w), 799 (w), 723 (w), 672 (w). Anal. found (calcd. for $C_{26}H_{33}AlN_4O_4S_2$): C, 55.98 (56.10); H, 5.86 (5.98); N, 9.98 (10.06) %.

Al($N_2^{Ts}N^{py}$)(O^iPr) (32). A solution of Al(O^iPr)Et_2 (0.29 g, 2.0 mmol), $H_2N_2^{Ts}N^{py}$ (1.0 g, 2.00 mmol) and toluene (30 mL) were heated at 100 °C for 16 h. Removal of the volatiles under reduced pressure yielded a brown solid which was washed with Et_2O (3 × 20 mL) and dried *in vacuo*. Yield: 0.77 g (66%). ^1H NMR (CD_2Cl_2, 499.9 MHz): δ 9.73 (1H, d, ^3J = 6.3 Hz, 2-NC_5H_4), 8.04 (1H, dt, ^3J = 7.8 Hz, ^4J = 1.5 Hz, 4-NC_5H_4), 7.78 (4H, d, ^3J = 7.8 Hz, 2-$C_6\underline{H}_4Me$), 7.63 (1H, t, ^3J = 6.3 Hz, 3-NC_5H_4), 7.41 (1H, d, ^3J = 7.8 Hz, 5-NC_5H_4), 7.20 (4H, d, ^3J = 7.8 Hz, 3-$C_6\underline{H}_4Me$), 4.50 (1H, sept., ^3J = 6.0 Hz, $C\underline{H}Me_2$), 4.06 (2H, s, py$C\underline{H}_2$N), 3.16 (2H, m, Ts$NC\underline{H}_2CH_2$N), 3.08 (2H, m, Ts$NC\underline{H}_2CH_2$N), 2.79 (2H, m, Ts$NCH_2C\underline{H}_2$N), 2.60 (2H, m, Ts$NCH_2C\underline{H}_2$N), 2.37 (6H, s, $C_6H_4\underline{Me}$), 1.13 (6H, d, ^3J = 6.0 Hz, $CH\underline{Me}_2$) ppm. ^{13}C-{^1H} NMR (CD_2Cl_2, 75.4 MHz): δ 155.4 (6-NC_5H_4), 152.1(2-NC_5H_4), 142.4 (4-NC_5H_4), 141.7 (1-C_6H_4Me), 141.1 (4-C_6H_4Me), 129.2 (3-C_6H_4Me), 127.2 (2-C_6H_4Me), 124.8 (3-NC_5H_4), 123.5 (5-NC_5H_4), 63.8 ($\underline{C}HMe_2$) 57.1 (py$\underline{C}H_2$N), 54.6 (Ts$NCH_2\underline{C}H_2$N), 42.6 (Ts$N\underline{C}H_2CH_2$N), 27.6 ($CH\underline{Me}_2$), 21.4 ($C_6H_4\underline{Me}$) ppm. IR (NaCl plates, Nujol mull, cm^{-1}): 3050 (w), 1734 (w), 1559 (w), 1298 (s), 1144 (m), 1093 (m), 1025 (w), 971 (w), 816 (w), 722 (w), 668 (w). Anal. found (calcd. for $C_{27}H_{35}AlN_4O_5S_2$): C, 55.10 (55.27); H, 6.05 (6.01); N, 9.60 (9.55) %.

Al($N_2^{Ts}N^{py}$)(OBn) (33). A solution of Al(OBn)Et_2 (0.19 g, 1.0 mmol), $H_2N_2^{Ts}N^{py}$ (0.5 g, 1.00 mmol) in toluene (30 mL) was heated at 100 °C for 16 h. Removal of the volatiles under reduced pressure yielded a brown solid, that was recrystallized from a concentrated THF and pentane (1:1) solution to yield **33** as a white solid which was washed with pentane (3 × 20 mL) and dried *in vacuo*. Yield: 0.38 g (61%). ^1H NMR

(CD_2Cl_2, 499.9 MHz): δ 9.35 (1H, d, ^3J = 4.5 Hz, 2-NC_5H_4), 7.96 (1H, dt, ^3J = 7.8 Hz, ^4J = 1.2 Hz, 4-NC_5H_4), 7.80 (4H, d, ^3J = 8.1 Hz, 2-$C_6\underline{H}_4Me$), 7.39 (4H, d, ^3J = 7.5 Hz, overlapping 2-C_6H_5, 3- NC_5H_4 and 5-NC_5H_4), 7.28 (2H, t, ^3J = 7.5 Hz, 3-C_6H_5) 7.15 (5H, d, ^3J = 8.1 Hz, overlapping 3-$C_6\underline{H}_4Me$ and 4-C_6H_5), 5.18 (2H, s, $OC\underline{H}_2C_6H_5$), 4.00 (2H, s, $pyC\underline{H}_2N$), 3.25 (2H, m, $TsNC\underline{H}_2CH_2N$), 3.12 (2H, m, $TsNC\underline{H}_2CH_2N$), 2.86 (2H, m, $TsNCH_2C\underline{H}_2N$), 2.61 (2H, m, $TsNCH_2C\underline{H}_2N$), 2.36 (6H, s, $C_6H_4\underline{Me}$) ppm. ^{13}C-{^1H} NMR (CD_2Cl_2, 75.4 MHz): δ 155.1 (6-NC_5H_4), 152.1(2-NC_5H_4), 147.0 (1-C_6H_5), 142.7 (4-NC_5H_4), 141.7 (1-C_6H_4Me), 141.0 (4-C_6H_4Me), 129.2 (3-C_6H_4Me), 128.0 (3-C_6H_5), 127.4 (2-C_6H_5), 127.0 (2-C_6H_4Me), 125.8 (4-C_6H_5), 124.9 (3- NC_5H_4), 123.9 (5-C_6H_5), 66.2 ($O\underline{C}H_2C_6H_5$), 55.8 ($py\underline{C}H_2N$), 52.7 ($TsNCH_2\underline{C}H_2N$), 42.4 ($TsN\underline{C}H_2CH_2N$), 21.4 ($C_6H_4\underline{Me}$) ppm. IR (NaCl plates, Nujol mull, cm^{-1}): 1559 (w), 1334 (m), 1261 (s), 1183 (m), 1104 (s), 1012 (s), 801 (m), 722 (m), 689 (w). Anal. found (calcd. for $C_{31}H_{35}AlN_4O_5S_2$): C, 58.75 (58.66); H, 5.61 (5.56); N, 8.81 (8.83) %.

Al($N_2^{Ms}N^{Ph}$)(O^iPr) (36). A mixture of Al(O^iPr)Et_2 (0.12 g, 0.86 mmol) and $H_2N_2^{Tm}N^{Ph}$ (0.30 g, 0.86 mmol) in toluene (30 mL) was heated at 100 °C for 48 h resulting in a colourless solution with a white precipitate. This was filtered and washed with pentane (3 × 20 mL) and dried *in vacuo* to give **36** as a light brown solid. Yield: 0.19 g (51%). ^1H NMR (CD_2Cl_2 + NC_5D_5, 299.9 MHz): δ 7.20 – 7.05 (5H, m, overlapping $NCH_2(2\text{-}C_6H_5)$, $NCH_2(3\text{-}C_6H_5)$ and $NCH_2(4\text{-}C_6H_5)$), 4.31 (1H, sept., ^3J = 6 H_z, $OC\underline{H}Me_2$), 4.16 (2H, s, $NC\underline{H}_2C_6H_5$), 3.43 (2H, m, $TsNC\underline{H}_2CH_2N$), 3.26 (2H, m, $TsNC\underline{H}_2CH_2N$), 2.95 (2H, m, $TsNCH_2C\underline{H}_2N$), 2.68 (2H, m, $TsNCH_2C\underline{H}_2N$), 2.57 (6H, s, SO_2Me), 1.28 (6H, d, ^3J = 6 H_z, $OCHMe_2$) ppm. . ^{13}C-{^1H} NMR (CD_2Cl_2 + NC_5D_5, 75.4 MHz): δ 131.8 (1-C_6H_5), 131.5 (3-C_6H_5), 128.6 (2-C_6H_5), 128.5 (4-C_6H_5), 63.8 ($O\underline{C}HMe_2$), 57.4 ($N\underline{C}H_2C_6H_5$), 50.9 ($MsNCH_2\underline{C}H_2N$), 42.4 ($MsN\underline{C}H_2CH_2N$), 39.6 (SO_2Me), 27.6 ($O\underline{C}HMe_2$) ppm. IR (NaCl plates, Nujol mull, cm^{-1}): 1496 (w), 1328 (w), 1291 (s), 1264 (s), 1230 (w), 1180 (m), 1120 (s), 1104 (m), 1079 (w), 1064 (w), 1019 (s), 982 (m), 898 (w), 776 (m), 738 (m), 706 (m), 669 (w), 652 (w). Anal. found (calcd. for $C_{16}H_{28}AlN_3O_5S_2$): C, 44.36 (44.33); H, 6.46 (6.51); N, 9.69 (9.66) %.

Al($N_2^{Ms}N^{Ph}$)(OBn) (37). A mixture of Al(OBn)Et_2 (0.17 g, 0.86 mmol) and $H_2N_2^{Tm}N^{Ph}$ (0.30 g, 0.86 mmol) in toluene (30 mL) was heated at 100 °C for 48 h resulting in a colourless solution with a white precipitate. This was then filtered and washed with pentane (3 × 20 mL) and dried *in vacuo* to give **37** as a cream solid. Yield: 0.27 g (65%).^1H NMR (CD_2Cl_2 + NC_5D_5, 299.9 MHz): δ 7.53 (2H, d, ^3J = 8.3 Hz,

$OCH_2(2\text{-}C_6H_5)$), 7.20 – 7.08 (8H, m, overlapping $OCH_2(3\text{-}C_6H_5)$, $OCH_2(4\text{-}C_6H_5)$, $NCH_2(2\text{-}C_6H_5)$, $NCH_2(3\text{-}C_6H_5)$ and $NCH_2(4\text{-}C_6H_5)$), 5.11 (2H, s, $OC\underline{H}_2C_6H_5$), 3.97 (2H, s, $NC\underline{H}_2C_6H_5$), 3.57 (2H, m, $TsNC\underline{H}_2CH_2N$), 3.31 (2H, m, $TsNC\underline{H}_2CH_2N$), 2.95 (2H, m, $TsNCH_2C\underline{H}_2N$), 2.71 (2H, m, $TsNCH_2C\underline{H}_2N$), 2.59 (6H, s, SO_2Me) ppm. $^{13}C\text{-}\{^1H\}$ NMR (CD_2Cl_2 + NC_5D_5, 75.4 MHz): δ 145.5 ($OCH_2(1\text{-}C_6H_5)$), 132.9 ($NCH_2(1\text{-}C_6H_5)$), 131.5 ($OCH_2(2\text{-}C_6H_5)$), 128.9 ($NCH_2(6\text{-}C_6H_5)$), 128.8 ($OCH_2(3\text{-}C_6H_5)$), 128.6 ($NCH_2(3\text{-}C_6H_5)$), 126.9 ($OCH_2(4\text{-}C_6H_5)$), 126.5 ($NCH_2(4\text{-}C_6H_5)$), 65.6 ($O\underline{C}H_2C_6H_5$), 56.9 ($N\underline{C}H_2C_6H_5$), 50.8 (SO_2Me), 42.7 ($TsNCH_2\underline{C}H_2N$), 39.9 ($TsN\underline{C}H_2CH_2N$) ppm. IR (NaCl plates, Nujol mull, cm^{-1}): 3039 (w), 1296 (s), 1273 (m), 1226 (w), 1166 (m), 1149 (w), 1133 (m), 1098 (m), 1080 (w), 1024 (m), 983 (m), 800 (w), 772 (m), 742 (w), 704 (w), 668 (w), 656 (w). Anal. found (calcd. for $C_{20}H_{28}AlN_3O_5S_2$): C, 49.92 (49.88); H, 5.85 (5.86); N, 8.70 (8.73) %.

$[Al(N_2{}^{Ts}N^{O})]_2$ (35). A mixture of $Al(O^iPr)Et_2$ (0.31 g, 2.13 mmol) and $H_2N_2{}^{Ts}N^{OMe}$ (1.00 g, 2.13 mmol) in toluene (30 mL) was heated at 100 °C for 16 h. Removal of the volatiles under reduced pressure yielded crude $Al(N_2{}^{Ts}N^{OMe})(O^iPr)$ a light yellow solid. This was heated at 150 °C for 48 h under a dynamic vacuum (1 mbar). The resulting white solid (**35**) was washed with pentane (3 × 20 mL) and dried *in vacuo*. Yield: 0.75 g (73%). Diffraction-quality crystals were grown from a saturated solution of dichloromethane at room temperature. ^1H NMR (CD_2Cl_2, 499.9 MHz): δ 7.91 (4H, d, ^3J = 8.2 Hz, $2\text{-}C_6\underline{H}_4Me$), 7.37 (4H, d, ^3J = 8.2 Hz, $3\text{-}C_6\underline{H}_4Me$), 4.14 (2H, t, ^3J = 5.7 Hz, OCH_2), 3.29 (2H, m, $TsNC\underline{H}_2CH_2N$), 3.15 (2H, m, $TsNC\underline{H}_2CH_2N$), 2.83 (2H, t, ^3J = 5.7 Hz, $OCH_2C\underline{H}_2$), 2.66 (2H, m, $TsNCH_2C\underline{H}_2N$), 2.62 (2H, m, $TsNCH_2C\underline{H}_2N$), 2.42 (6H, s, $C_6H_4\underline{Me}$) ppm. $^{13}C\text{-}\{^1H\}$ NMR (CD_2Cl_2, 75.4 MHz): δ 142.7 ($1\text{-}C_6H_4Me$), 140.5 ($4\text{-}C_6H_4Me$), 130.2 ($3\text{-}C_6H_4Me$), 127.4 ($2\text{-}C_6H_4Me$), 60.2 (OCH_2), 53.6 ($TsNCH_2\underline{C}H_2N$), 52.9 ($OCH_2\underline{C}H_2$), 42.2 ($TsN\underline{C}H_2CH_2N$), 21.8 ($C_6H_4\underline{Me}$) ppm. IR (NaCl plates, Nujol mull, cm^{-1}): 3029 (w), 1559 (w), 1281 (s), 1158 (w), 1140 (m), 1104 (m), 1066 (w), 1048 (w), 1034 (w), 967 (m), 911 (w), 869 (w), 829 (m), 742 (m), 722 (m), 694 (w), 667 (w). Anal. found (calcd. for $C_{40}H_{52}Al_2N_6O_{10}S_4$): C, 50.14 (50.09); H, 5.56 (5.46); N, 8.88 (8.76) %.

$[Al(N_2{}^{Ts}N^{Ph})Cl]_2$ (38). $AlMe_2Cl$ (2.0 mL, 1 M in hexanes) was added dropwise to a solution of a solution of $H_2N_2{}^{Ts}N^{ph}$ (1.00 g, 2.00 mmol) in C_6H_6 (30 mL). The mixture was stirred at RT for 16 h, resulting in a yellow solution. Removal of the volatiles under reduced pressure yielded a light yellow solid, that was washed with ether (3 × 15

mL) and recrystallized from a concentrated dichloromethane solution (10 mL) layered with hexanes (30 mL) to yield **38** as a light yellow solid. This was washed with pentane (3 × 20 mL) and dried *in vacuo*. Yield: 0.65 g (58%). Diffraction-quality crystals were grown from a saturated solution of dichloromethane layered with hexanes at room temperature. ^{1}H NMR (C_6D_6, 299.9 MHz):): δ 8.72 (2H, d, ^{3}J = 8.1 Hz, bridging 2-$C_6\underline{H}_4$Me), 8.31 (2H, d, ^{3}J = 8.7 Hz, terminal 2-$C_6\underline{H}_4$Me), 7.18 (2H, d, ^{3}J = 8.1 Hz, bridging 3-$C_6\underline{H}_4$Me), 7.00 (1H, m, 4-C_6H_5), 6.90 (2H, t, ^{3}J = 7.5 Hz, 3-C_6H_5), 6.78 (2H, d, ^{3}J = 8.7 Hz, terminal 3-$C_6\underline{H}_4$Me), 6.90 (2H, d, ^{3}J = 7.5 Hz, 2-C_6H_5), 4.55 (1H, d, ^{2}J = 15 Hz, NC$\underline{H}_2C_6H_5$), 4.44 (1H, d, ^{2}J = 15 Hz, NC$\underline{H}_2C_6H_5$), 3.95 (1H, dt, ^{2}J = 6.9 Hz, ^{3}J = 4.8 Hz, TsNC$\underline{H}_2CH_2$N), 3.26 (1H, m, TsNCH$_2$C$\underline{H}_2$N), 2.95-2.55 (4H, m, TsNC$\underline{H}_2$C$\underline{H}_2$N), 1.96 (3H, s, bridging $C_6H_4\underline{Me}$), 1.83 (5H, s, overlapping $C_6H_4\underline{Me}$ and TsNC$\underline{H}_2$C$\underline{H}_2$N) ppm. ^{13}C-{^{1}H} NMR (C_6D_6, 75.4 MHz): δ 142.8 (1-C_6H_4Me), 141.6 (1-C_6H_4Me), 140.5 (4-C_6H_4Me), 136.0 (4-C_6H_4Me), 132.0 (2-C_6H_5), 131.4 (1-C_6H_5), 129.4 (3-C_6H_4Me), 129.1 (3-C_6H_4Me), 128.7 (2-C_6H_4Me), 128.6 (2-C_6H_4Me), 128.5 (4-C_6H_5), 128.4 (4-C_6H_5), 55.6 (NC$\underline{H}_2C_6H_5$) 47.4 (TsNCH$_2\underline{C}$H$_2$N), 42.2 (TsNCH$_2\underline{C}$H$_2$N), 41.8 (overlapping TsN$\underline{C}$H$_2$CH$_2$N), 26.1 (AlCH$_2\underline{Me}$), 21.6 ($C_6H_4\underline{Me}$), 10.1 (Al$\underline{C}$H$_2$Me) ppm. IR (NaCl plates, Nujol mull, cm^{-1}): 2726 (w), 1506 (w), 1304 (m), 1262 (s), 1155 (m), 1062 (s), 1021 (s), 1003 (w), 807 (w), 722 (s), 668 (w). Anal. found (calcd. for $C_{58}H_{58}Al_2Cl_2N_6O_8S_4$): C, 53.47 (53.42); H, 5.32 (5.20); N, 7.44 (7.44) %.

Al($N_2^{Ts}N^{Ph}$)($OCH_2CH_2NH_2$) (39). A mixture of Al($OCH_2CH_2NH_2$)Et$_2$ (0.14 g, 1.0 mmol) and $H_2N_2{}^{Ts}N^{Ph}$ (0.50 g, 1.00 mmol) in toluene (30 mL) was heated at 100 °C for 16 h. Removal of the volatiles under reduced pressure yielded **39** as a cream solid, which was washed with pentane (3 × 20 mL) and dried *in vacuo*. Yield: 0.40 g (68%). ^{1}H NMR (CD_2Cl_2, 299.9 MHz): 7.71 (4H, d, ^{3}J = 7.8 Hz, 2-$C_6\underline{H}_4$Me), 7.29 (3H, m, overlapping 2-C_6H_5 and 4-C_6H_5), 7.23 (4H, d, ^{3}J = 7.8 Hz, 3-$C_6\underline{H}_4$Me), 7.04 (2H, m, 3-C_6H_5), 4.81 (2H, br. t, ^{3}J = 6.0 Hz, NH_2) 3.87 (2H, s, NC$\underline{H}_2C_6H_5$), 3.87 (2H, t, ^{3}J = 6.0 Hz, C$\underline{H}_2$O), 3.20 (2H, m, TsNC$\underline{H}_2$CH$_2$N), 3.01 (2H, m, C$\underline{H}_2$NH$_2$), 2.73 (2H, m, TsNC$\underline{H}_2$CH$_2$N), 2.56 (2H, m, TsNCH$_2$C$\underline{H}_2$N), 2.38 (6H, s, $C_6H_4\underline{Me}$), 2.15 (2H, m, TsNCH$_2$C$\underline{H}_2$N) ppm. ^{13}C-{^{1}H} NMR (C_6D_6, 75.4 MHz): δ 142.8 (1-C_6H_4Me), 138.1 (4-C_6H_4Me), 131.8 (2-C_6H_5), 131.7 (1-C_6H_5), 129.6 (3-C_6H_4Me), 128.9 (4-C_6H_5), 128.8 (3-C_6H_5), 127.4 (2-C_6H_4Me), 60.6 (O$\underline{C}$H$_2$CH$_2$NMe$_2$), 55.2 (N$\underline{C}$H$_2C_6H_5$), 44.8 (TsNCH$_2\underline{C}$H$_2$N), 42.6 (O$\underline{C}$H$_2$), 41.7 (TsN$\underline{C}$H$_2$CH$_2$N), 21.5 ($C_6H_4\underline{Me}$) ppm. IR (NaCl plates, Nujol mull, cm^{-1}): 3308 (m), 3262 (w), 1598 (w), 1299 (s), 1260 (s), 1154 (s),

1091 (s), 1020 (m), 974 (m), 908 (w), 851 (w), 803 (w), 722 (m), 668 (w). Anal. found (calcd. for $C_{27}H_{35}AlN_4O_5S_2$): C, 55.42 (55.27); H, 6.11 (6.01); N, 9.57 (9.55) %.

Al($N_2^{Ts}N^{OMe}$)($OCH_2CH_2NH_2$) (40). A mixture of $Al(OCH_2CH_2NH_2)Et_2$ (0.15 g, 1.00 mmol) and $H_2N_2{}^{Ts}N^{OMe}$ (0.50 g, 1.03 mmol) in toluene (30 mL) was heated at 100 °C for 16 h. Removal of the volatiles under reduced pressure yielded **40** a cream solid, which was washed with pentane (3 × 20 mL) and dried *in vacuo*. Yield: 0.45 g (79%). Diffraction-quality crystals were grown from a saturated solution of dichloromethane layered with hexanes at RT. ^{1}H NMR (CD_2Cl_2, 499.9 MHz): 7.69 (4H, d, ^3J = 8.0 Hz, 2-$C_6\underline{H}_4$Me), 7.25 (4H, d, ^3J = 8.0 Hz, 3-$C_6\underline{H}_4$Me), 4.75 (2H, br. t, ^3J = 7.5 Hz, NH_2), 3.78 (2H, t, ^3J = 7.5 Hz, OCH_2), 3.43 (2H, t, ^3J = 7.5 Hz, $H_2NC\underline{H}_2$), 3.16 (3H, s, OMe), 3.05-2.95 (4H, m, $TsNCH_2$), 2.72 (2H, m, $TsNCH_2\underline{CH}_2N$), 2.43 (2H, m, $TsNCH_2C\underline{H}_2N$), 2.20 (6H, s, $C_6H_4\underline{Me}$) ppm. ^{13}C-{^{1}H} NMR (CD_2Cl_2, 75.4 MHz): δ 142.7 (1-C_6H_4Me), 138.4 (4-C_6H_4Me), 129.6 (3-C_6H_4Me), 127.4 (2-C_6H_4Me), 67.9 ($O\underline{C}H_2CH_2NH_2$), 60.5 ($MeO\underline{C}H_2$), 58.7 (OMe), 50.8 ($TsNCH_2\underline{C}H_2$), 46.2 ($TsN\underline{C}H_2$), 42.5 ($OCH_2\underline{C}H_2N$), 41.9 ($MeOCH_2\underline{C}H_2N$), 21.5 ($C_6H_4\underline{Me}$) ppm. IR (NaCl plates, Nujol mull, cm^{-1}): 3306 (m), 3268 (m), 2688 (w), 1636 (w), 1307 (w), 1296 (w), 1280 (s), 1258 (m), 1193 (w), 1156 (s), 1145 (m), 1087 (s), 1054 (m), 1018 (m), 976 (m), 906 (w), 808 (w), 736 (w), 667 (w). Anal. found (calcd. for $C_{23}H_{35}AlN_4O_6S_2$): C, 49.77 (49.80); H, 6.36 (6.26); N, 10.02 (10.10) %.

Al($N_2^{Ts}N^{py}$)($OCH_2CH_2NH_2$) (41). A mixture of $Al(OCH_2CH_2NH_2)Et_2$ (0.14 g, 1.0 mmol) and $H_2N_2{}^{Ts}N^{py}$ (0.50 g, 1.00 mmol) in toluene (30 mL) was heated at 100 °C for 48 h. Removal of the volatiles under reduced pressure yielded a brown solid, that was recrystallized from a concentrated THF (10 mL) solution layered with pentane (30 mL). The resulting light brown solid (**41**) was washed with pentane (3 × 20 mL) and dried *in vacuo*. Yield: 0.44 g (75%).

Major isomer **41a**; ^{1}H NMR (CD_2Cl_2, 499.9 MHz): δ 8.87 (1H, d, ^3J = 5.1 Hz, 2-NC_5H_4), 7.86 (1H, dt, ^3J = 7.7 Hz, ^4J = 1.3 Hz, 3-NC_5H_4), 7.72 (5H, d, ^3J = 8.2 Hz, overlapping 2-$C_6\underline{H}_4$Me and 4-NC_5H_4), 7.45 (1H, d, ^3J = 7.7 Hz, 5- NC_5H_4), 7.20 (4H, d, ^3J = 8.2 Hz, 3-$C_6\underline{H}_4$Me), 4.98 (2H, br. t, ^3J = 5.5 Hz, NH_2), 4.17 (2H, s, $pyC\underline{H}_2N$), 3.56 (2H, t, ^3J = 5.5 Hz, OCH_2), 3.25 – 2.75 (10H, m, overlapping $TsNC\underline{H}_2C\underline{H}_2N$ and $C\underline{H}_2NH_2$), 2.37 (6H, s, $C_6H_4\underline{Me}$) ppm. ^{13}C-{^{1}H} NMR (CD_2Cl_2, 75.4 MHz): δ 152.7 (6-NC_5H_4), 147.6 (2-NC_5H_4), 141.9 (1-C_6H_4Me), 140.7 (4-NC_5H_4), 139.1 (4-C_6H_4Me), 130.1 (5-NC_5H_4), 129.6 (3-C_6H_4Me), 127.7 (2-C_6H_4Me), 127.1

(3-NC_5H_4), 61.8 (py$\underline{C}H_2N$), 59.9 ($\underline{C}H_2O$) 57.3 (TsNCH$_2\underline{C}H_2$N), 43.7 ($\underline{C}H_2NH_2$), 43.2 (TsN$\underline{C}H_2CH_2N$), 21.6 ($C_6H_4\underline{Me}$) ppm.

Minor isomer **41b**; ^{1}H NMR (CD_2Cl_2, 499.9 MHz): δ 8.52 (1H, d, ^{3}J = 5.5 Hz, 2-NC_5H_4), 7.98 (1H, dt, ^{3}J = 7.9 Hz, ^{4}J = 1.3 Hz, 3-NC_5H_4), 7.59 (1H, d, ^{3}J = 7.9 Hz, 5-NC_5H_4), 7.28 (4H, d, ^{3}J = 7.8 Hz, 2-$C_6\underline{H}_4$Me), 7.23 (1H, d, ^{3}J = 7.9 Hz, 5- NC_5H_4), 7.13 (4H, d, ^{3}J = 8.2 Hz, 3-$C_6\underline{H}_4$Me), 5.14 (2H, br. t, ^{3}J = 5.7 Hz, NH_2), 3.95 (2H, s, py$C\underline{H}_2$N), 3.88 (2H, t, ^{3}J = 5.7 Hz, OCH_2), 3.11 (2H, t, ^{3}J = 5.7 Hz, NH_2CH_2), 3.25 – 2.75 (8H, m, overlapping TsNC$\underline{H}_2C\underline{H}_2$N), 2.29 (6H, s, $C_6H_4\underline{Me}$) ppm. ^{13}C-{^{1}H} NMR (CD_2Cl_2, 75.4 MHz): δ 152.3 (6-NC_5H_4), 145.3 (2-NC_5H_4), 141.6 (1-C_6H_4Me), 140.6 (4-NC_5H_4), 140.1 (4-C_6H_4Me), 137.5 (5-NC_5H_4), 129.5 (3-C_6H_4Me), 127.5 (2-C_6H_4Me), 124.2 (3-NC_5H_4), 59.7 ($\underline{C}H_2O$), 66.9 (py$\underline{C}H_2$N), 54.5 (TsNCH$_2\underline{C}H_2$N), 43.8 ($\underline{C}H_2NH_2$), 42.4 (TsN$\underline{C}H_2CH_2$N), 21.4 ($C_6H_4\underline{Me}$) ppm.

IR (NaCl plates, Nujol mull, cm^{-1}): 3318 (w), 3310 (w), 3202 (w), 3159 (w), 1612 (m), 1266 (s), 1134 (s), 1103 (s), 1085 (s), 1029 (m), 996 (m), 974 (m), 933 (w), 879 (w), 801 (w), 725 (w), 672 (w), 662 (w), 626 (w). Anal. found (calcd. for $C_{26}H_{34}AlN_5O_5S_2$): C, 53.23 (53.14); H, 5.90 (5.83); N, 11.82 (11.92) %.

Al($N_2^{Ts}N^{Ph}$)($OCH_2CH_2NMe_2$) (42). A mixture of Al($OCH_2CH_2NMe_2$)Et_2 (0.17 g, 1.0 mmol) and $H_2N_2^{Ts}N^{py}$ (0.50 g, 1.00 mmol) in toluene (30 mL) was heated at 100 °C for 16 h. Removal of the volatiles under reduced pressure yielded a cream solid. Recrystallization from a concentrated dichloromethane solution layered with pentane (30 mL) gave **42** as a cream solid which was washed with pentane (3 × 20 mL) and dried *in vacuo*. Yield: 0.52 g (85%). ^{1}H NMR (C_6D_6, 299.9 MHz): 8.10 (4H, d, ^{3}J = 8.1 Hz, 2-$C_6\underline{H}_4$Me), 7.03 (3H, m, overlapping 3-C_6H_5 and 4-C_6H_5), 7.15 (4H, d, ^{3}J = 8.1 Hz, 3-$C_6\underline{H}_4$Me), 6.83 (2H, dd, ^{3}J = 7.8 Hz, ^{4}J = 2.1 Hz, 2-C_6H_5), 4.08 (2H, s, N$\underline{H}_2C_6H_5$), 3.77 (2H, t, ^{3}J = 6.0 Hz, O$\underline{H}_2$), 3.15 – 3.10 (4H, m, TsNC$\underline{H}_2CH_2$N), 2.98 (2H, br. t, ^{3}J = 6 Hz, $OCH_2C\underline{H}_2NMe_2$), 2.69 (6H, s, $OCH_2CH_2N\underline{Me}_2$), 2.65 (4H, m, TsNCH$_2C\underline{H}_2$N), 1.92 (6H, s, $C_6H_4\underline{Me}$) ppm. ^{13}C-{^{1}H} NMR (C_6D_6, 75.4 MHz): δ 141.5 (1-C_6H_4Me), 140.9 (4-C_6H_4Me), 134.3 (1-C_6H_5), 131.8 (2-C_6H_5), 129.5 (3-C_6H_4Me), 128.5 (3-C_6H_5), 128.4 (4-C_6H_5), 127.5 (2-C_6H_4Me), 62.6 ($OCH_2\underline{C}H_2NMe_2$), 58.8 (N$\underline{C}H_2C_6H_5$), 57.8 (O$\underline{C}H_2$), 51.3 (TsNCH$_2\underline{C}H_2$N), 46.3 ($OCH_2CH_2N\underline{Me}_2$), 43.0 (TsN$\underline{C}H_2CH_2$N), 21.0 ($C_6H_4\underline{Me}$) ppm. IR (NaCl plates, Nujol mull, cm^{-1}): 2730 (w), 1700 (w), 1301 (m), 1261 (m), 1143 (m), 1092 (s), 1019 (s), 800

(s), 723 (s), 667 (s). Anal. found (calcd. for $C_{29}H_{39}AlN_4O_5S_2$): C, 56.62 (56.66); H, 6.39 (6.39); N, 9.10 (9.11) %.

Al(CyN_2^{Ts})($OCH_2CH_2NMe_2$) (43). A mixture of $H_2CyN_2^{Ts}$ (1.00 g, 2.37 mmol) and $Al(OCH_2CH_2NMe_2)Et_2$ (0.450 g, 2.60 mmol) in toluene (30 mL) was heated to 100 °C and stirred at this temperature for 16 h. The volatiles were removed under reduced pressure to give white solid. The solid was re-dissolved in minimal volume of dichloromethane and layered 4-fold hexanes to give needle-like crystals. The crystals was filtered, washed with hexanes (3 × 15 mL) and dried under vacuum to give **43** as a white solid. Yield: 0.99g (78%). Diffraction-quality crystals were grown from a saturated solution of dichloromethane and hexanes at room temperature. ^{1}H NMR (CD_2Cl_2, 299.9 MHz, 303 K): δ 7.78 (4H, d, ^{3}J = 8.1 Hz, 2-$C_6\underline{H}_4Me$), 7.73 (4H, d, ^{3}J = 8.1 Hz, 2-$C_6\underline{H}_4Me$), δ 7.24 (4H, d, ^{3}J = 8.1 Hz, 3-$C_6\underline{H}_4Me$), 6.84 (4H, d, ^{3}J = 8.1Hz, 3-$C_6\underline{H}_4Me$), 4.91 (2H, m, $C_6\underline{H}_{10}N_2$), 4.30 (2H, m, $C_6\underline{H}_{10}N_2$), 4.00 (2H, t, ^{3}J=8.4 Hz, $OC\underline{H}_2CH_2NMe_2$), 3.19 (2H, m, $OCH_2C\underline{H}_2NMe_2$), 3.00 (3H, s, $OCH_2CH_2NMe_2$), 2.74 (3H, s, $OCH_2CH_2NMe_2$), 2.59 (2H, m, $C_6\underline{H}_{10}N_2$), 2.38 (3H, s, $C_6H_4\underline{Me}$), 2.14 (3H, s, $C_6H_4\underline{Me}$), 1.40 (2H, m, $C_6\underline{H}_{10}N_2$), 1.00 (4H, m, $C_6\underline{H}_{10}N_2$), 0.84 (2H, m, $C_6\underline{H}_{10}N_2$) ppm. ^{13}C-{^{1}H} NMR (C_6D_6, 75.4 MHz): δ 144.2 (4-$\underline{C}_6H_4Me$), 142.9 (4-$\underline{C}_6H_4Me$), 141.8 (1-$\underline{C}_6H_4Me$), 141.1 (1-$\underline{C}_6H_4Me$), 129.3 (3-$\underline{C}_6H_4Me$), 128.4 (3-$\underline{C}_6H_4Me$), 127.4 (2-$\underline{C}_6H_4Me$), 126.1 (2-$\underline{C}_6H_4Me$), 62.3 ($\underline{C}_6H_{10}N_2$), 61.9 ($OCH_2\underline{C}H_2NMe_2$), 58.6 ($\underline{C}_6H_{10}N_2$), 55.7 ($O\underline{C}H_2CH_2NMe_2$), 47.3 ($OCH_2CH_2NMe_2$), 47.0 ($OCH_2CH_2NMe_2$), 32.1 ($\underline{C}_6H_{10}N_2$), 31.9 ($\underline{C}_6H_{10}N_2$), 25.2 ($\underline{C}_6H_{10}N_2$), 21.4 ($C_6H_4\underline{Me}$), 21.2 ($C_6H_4\underline{Me}$) ppm. IR (NaCl plates, Nujol mull, cm^{-1}): 1598 (w), 1277 (m), 1245 (w), 1212 (w), 1144 (m), 1088 (m), 1070 (m), 1052 (m), 1019 (w), 983 (m), 950.2 (m), 902.2 (m), 838 (m), 817 (w), 799 (w), 730 (m), 676 (m), 588 (m), 558 (m). Anal. found (calcd. for $C_{24}H_{34}AlN_3O_5S_2$): C, 53.68 (53.81); H, 6.36 (6.40); N, 7.74 (7.84) %.

NMR scale polymerisation of *rac*-LA with H_2NBn and 33. To a solution of **33** (4.4 mg, 6.8 μmol) and H_2NBn (3.8 μL, 1.36 μmol) in C_6D_6 (0.2 mL) was added a slurry of *rac*-LA (20 mg, 0.139 mmol) in C_6D_6 (0.2 mL). After heating at 80 °C for 48 h analysis by ^{1}H NMR spectroscopy showed that a mixture of products was present in which protio-ligand ($H_2N_2^{Ts}N^{py}$) had been formed quantitatively.

5.6 Polymerisation procedures for Chapters 2, 3 and 4

All Polymerisations were performed with a Heidolph MR Hei-Standard stirrer plate and an EKT Hei-Con stainless steel temperature sensor immursed in a silicon oil bath

of *ca*. 1 L volume. The temperature quoted below should be regarded as being accurate to +/- 1 °C of the value stated below. The reaction flasks were all stirred utilising a magnetic stirrer flea in a manner described below.

General procedure for polymerisation of ε-CL. Parallel duplicate experiments were carried out in each of which a solution of ε-CL (6.6 mmol) in toluene (3.0 mL) was heated to 100 ^{o}C and added to a solution of catalyst (0.066 mmol) in toluene (3.8 mL) also at 100 ^{o}C. For one sample aliquots were taken at the respective time. Upon completion the reaction was quenched by addition of wet THF (10 mL) and the solution evaporated to dryness to give the crude polymer. Isolated yields were obtained from the parallel experiment for which the polymer was quenched by wet THF (10 mL) and precipitated by addition to ethanol (250 mL) with vigorous stirring, filtered and dried to constant weight *in vacuo*.

Procedure for polymerisation of ε-CL in the presence alcohol co-initators (Chapter 3). Parallel duplicate experiments were carried out in each of which, to catalyst (0.066 mmol) was added a solution of HOR (0.066 mmol) in toluene (3.8 mL). This solution was stirred for 15 mins at room temperature then heated to 100 ^{o}C and a solution of ε-CL (6.6 mmol) in toluene (3.0 mL) also at 100 ^{o}C was added. For one sample aliquots were taken at the respective time. Upon completion the reaction was quenched by addition of wet THF (10 mL) and the solution evaporated to dryness to give the crude polymer. Isolated yields were obtained from the parallel experiment for which the polymer was quenched by wet THF (10 mL) and precipitated by addition to ethanol (250 mL) with vigorous stirring, filtered and dried to constant weight *in vacuo*.

General procedure for solution polymerisation of *rac*-LA. *Rac*-LA (6.00 mmol) and catalyst (0.06 mmol) were added to a Schlenk flask and heated to 70 °C. To this, hot (70 ^{o}C) toluene (6.0 mL) was added, rapidly disolving both solids. The resultant solution heated at 70 ^{o}C and aliquots were taken at the respective time. Upon completion of the reaction wet THF (10 mL) was added and the solution evaporated to dryness to give the poly(*rac*-LA). Conversions were determined by ^{1}H NMR integration of the OC<u>H</u>Me resonance relative intensities of the residual *rac*-LA and poly(*rac*-LA).

Procedure for solution polymerisation of *rac*-LA in the presence of alcohol co-initiators (Chapter 3). *Rac*-LA (6.00 mmol) and catalyst (0.06 mmol) were added to a Schlenk flask and heated to 70 °C. To this, a hot (70 °C) solution of HOR (0.06

mmol) in toluene (6.0 mL) was added, rapidly disolving both solids. The resultant solution heated at 70 ^{o}C and aliquots were taken at the respective time. Upon completion of the reaction wet THF (10 mL) was added and the solution evaporated to dryness to give the poly(*rac*-LA). Conversions were determined by ^{1}H NMR integration of the OCHMe resonance relative intensities of the residual *rac*-LA and poly(*rac*-LA).

General procedure for solventless (melt) polymerisation of *rac*-LA. A Schlenk flask was charged with catalyst and *rac*-LA at the desired ratio and heated at 130 ^{o}C for 30 mins with stirring. The mixture was cooled to RT, and wet THF (10 ml) was then added and the resulting solution evaporated to dryness to give the crude polymer.

5.7 X-ray data collection and processing parameters for Chapter 2

Crystal structure determinations of $H_2N_2^{Ts}N^{OMe}$ (2.7), $Ti(N_2^{Ts}N^{py})(NMe_2)_2$ (1), $Ti(N_2^{Ts}N^{OMe})(NMe_2)_2$ (2), $Ti(N_2^{Ts}N^{py})(O^iPr)_2$ (3), $Zr(N_2^{Ts}N^{py})(O^iPr)_2$ (4), $Ti(N_2^{Ts}N^{OMe})(O^iPr)_2$ (5) and $Zr(N_2^{Ts}N^{OMe})(O^iPr)_2$ (6). Crystal data collection and processing parameters are given in Table 5.1. Crystals were mounted on glass fibers using perfluoropolyether oil and cooled rapidly in a stream of cold N_2 using an Oxford Cryosystems Cryostream unit. Diffraction data were measured using an Enraf-Nonius KappaCCD diffractometer. As appropriate, absorption and decay corrections were applied to the data and equivalent reflections merged.[19] The structures were solved with SIR92[20] or SHELXS-97[21] and further refinements and all other crystallographic calculations were performed using either the CRYSTALS program suite[22] or SHELXS-97.[23] Other details of the structure solution and refinements are given in the Supporting Information (CIF data). A full listing of atomic coordinates, bond lengths and angles and displacement parameters for all the structures have been deposited at the Cambridge Crystallographic Data Centre. See Notice to Authors, Issue No. 1.

Table 5.1. X-ray data collection and processing parameters for $H_2N_2^{Ts}N^{OMe}$ (**2.7**), $Ti(N_2^{Ts}N^{py})(NMe_2)_2$ (**1**), $Ti(N_2^{Ts}N^{OMe})(NMe_2)_2 \cdot 2(C_6H_6)$ (**2·2(C$_6$H$_6$)**), $Ti(N_2^{Ts}N^{py})(O^iPr)_2$ (**3**), $Ti(N_2^{Ts}N^{OMe})(O^iPr)_2$ (**5**), $Zr(N_2^{Ts}N^{py})(O^iPr)_2$ (**4**) and $Zr(N_2^{Ts}N^{OMe})(O^iPr)_2$ (**6**).

compound		**2.7**	**1**	**2·2(C$_6$H$_6$)**	**3**
empirical formula		$C_{21}H_{31}N_3O_5S_2$	$C_{28}H_{40}N_6O_4S_2Ti$	$C_{25}H_{41}N_5O_5S_2Ti \cdot 2(C_6H_6)$	$C_{30}H_{42}N_4O_6S_2Ti$
fw		469.63	636.70	759.89	666.70
temp / K		150	150	150	150
wavelength / Å		0.71073	0.71073	0.71073	0.71073
space group		$P\,2_12_12_1$	$P\,2_1/c$	$C\,2/c$	$P\,2_1/c$
a / Å		7.34540(10)	9.7433(3)	13.9610(5)	8.9177(18)
b / Å		13.02980(10)	18.4302(5)	12.7787(5)	9.6354(19)
c / Å		24.3794(3)	17.1845(5)	21.6251(10)	36.811(7)
α / deg		90	90	90	90
β / deg		90	90.163(1)	93.0481(12)	90.00(3)
γ / deg		90	90	90	90
V / Å^3		2333.33(5)	3085.8(2)	3852.5(3)	3163.0(11)
Z		4	4	4	4
d (calcd) / Mg·m^{-3}		1.337	1.370	1.310	1.400
abs coeff / mm^{-1}		0.265	0.456	0.378	0.451
R indices:[a]	R_1 =	0.0298[b]	0.0380[b]	0.0672[b]	0.0788[c]
	R_w =	0.0341[b]	0.0379[b]	0.0670[b]	-
	wR_2 =	-	-	-	0.2026

Table 5.1 (contd).

compound	**5**	**4**	**6**
empirical formula	$C_{27}H_{43}N_3O_7S_2Ti$	$C_{30}H_{42}N_4O_6S_2Zr$	$C_{27}H_{43}N_3O_7S_2Zr$
fw	633.66	710.04	677.01
temp / K	150	150	150
wavelength / Å	0.71073	0.71073	0.71073
space group	$P\,2_1/c$	$P\,\bar{1}$	$P\,2_1/c$
a / Å	9.9927(1)	9.2206(2)	10.01950(10)
b / Å	9.6963(1)	9.6331(2)	9.89890(10)
c / Å	31.4855(4)	18.7269(5)	31.5596(4)
α / deg	90	85.4348(14)	90
β / deg	92.733(1)	78.1548(15)	92.7258(6)
γ / deg	90	84.6582(16)	90
V / Å^3	3047.23(6)	1617.76(7)	3126.60(6)
Z	4	2	4
d (calcd) / Mg·m^{-3}	1.381	1.458	1.438
abs coeff / mm^{-1}	0.466	0.517	0.532
R indices:[a] R_1 =	0.0400[c]	0.0326[b]	0.0376[b]
R_w =	-	0.0370[b]	0.0355[b]
wR_2 =	0.0980[d]	-	-

[a] $R_1 = \Sigma||F_o|-|F_c|| / \Sigma|F_o|$; $R_w = \sqrt{\{\Sigma w\,(|F_o|-|F_c|)^2 / \Sigma w|F_o|^2\}}$; w$R2 = \sqrt{\{\Sigma w\,(F_o^2-F_c^2)^2/ \Sigma w(F_o^2)^2\}}$;

[b] For data wih I $> 3\sigma$(I); [c] For data with I $> 2\sigma$(I); [d] For all data.

5.8 X-ray data collection and processing parameters for Chapter 3

Crystal structure determinations of $H_2N_2^{Ts}N^{Ph}$ (7), $H_2N_2^{Ms}N^{Ph}$ (8), $H_3N_3^{Ms}N$ (10), $H_2CyN_2^{SO_2Mes}$ (3.3), $Ti(N_2^{Ms}N^{OMe})(O^iPr)_2$ (17), $Ti(N_2^{Ts}N^{Ph})(NMe_2)_2$ (12), $Ti(N_2^{Ts}N^{Ph})(O^iPr)(NMe_2)$ (18), $Ti(N_2^{Ts}N^{Ph})Cl_2$ (19), $Zr(N_3^{Ts}N)(CH_2SiMe_3)$ (20), $Zr(N_3^{TArF})(CH_2SiMe_3)$ (21), $Zr(N_3^{TArF})(NMe_2)$ (23) and $\{Zr(N_3^{TArF}N)\}_2(\mu$-O) (24). Crystal data collection and processing parameters are given in Table 5.2. Crystals were mounted on glass fibers using perfluoropolyether oil and cooled rapidly in a stream of cold N_2 using an Oxford Cryosystems Cryostream unit. Diffraction data were measured using an Enraf-Nonius KappaCCD diffractometer. As appropriate, absorption and decay corrections were applied to the data and equivalent reflections merged.[19] The structures were solved with SIR92[20] or SHELXS-97[21] and further refinements and all other crystallographic calculations were performed using either the CRYSTALS program suite[22] or SHELXS-97.[23] Other details of the structure solution and refinements are given in the Supporting Information (CIF data). A full listing of atomic coordinates, bond lengths and angles and displacement parameters for all the structures have been deposited at the Cambridge Crystallographic Data Centre. See Notice to Authors, Issue No. 1.

Table 5.2. X-ray data collection and processing parameters for $H_2N_2^{Ts}N^{Ph}$ (**7**), $H_2N_2^{Ms}N^{Ph}$ (**8**), $H_3N_3^{Ms}N$ (**10**), $H_2CyN_2^{SO_2Mes}$ (**3.3**), $Ti(N_2^{Ms}N^{OMe})(O^iPr)_2$ (**17**), $Ti(N_2^{Ts}N^{Ph})(NMe_2)_2$ (**12**), $Ti(N_2^{Ts}N^{Ph})(O^iPr)(NMe_2)$ (**18**), $Ti(N_2^{Ts}N^{Ph})Cl_2$ (**19**), $Zr(N_3^{Ts}N)(CH_2SiMe_3)$ (**20**), $Zr(N_3^{TArF}N)(CH_2SiMe_3)$ (**21**), $Zr(N_3^{TArF}N)(NMe_2)$ (**23**) and $\{Zr(N_3^{TArF}N)\}_2(\mu\text{-}O)$ (**24**).

compound	**7**	**8**	**10**	**3.3**
empirical formula	$C_{25}H_{31}N_3O_4S_2$	$C_{13}H_{23}N_3O_4S_2$	$C_9H_{24}N_4O_6S_3$	$C_{24}H_{34}N_2O_4S_2$
fw	501.67	349.48	380.51	478.68
temp / K	150	150	150	150
wavelength / Å	0.71073	0.71073	0.71073	0.71073
space group	$P\,2_1/c$	$P\,2_1/n$	$P\,2_1/c$	$P\,\bar{1}$
a / Å	11.8932(2)	9.3901(2)	15.802(3)	7.8913(3)
b / Å	10.8548(3)	15.3139(3)	8.1846(16)	8.2462(4)
c / Å	19.8155(5)	11.9953(3)	14.456(3)	19.0435(9)
α / deg	90	90	90	88.423(2)
β / deg	97.2262(14)	108.4426(9)	115.82(3)	89.411(2)
γ / deg	90	90	90	75.9003(18)
V / Å^3	2537.83(10)	1636.32(6)	1683.0(7)	1201.43(9)
Z	4	4	4	2
d (calcd) / Mg·m^{-3}	1.313	1.419	1.502	1.323
abs coeff / mm^{-1}	0.246	0.346	0.472	0.255
R indices:[a] R_1 =	0.0388[b]	0.0358[b]	0.0362[b]	0.0478[b]
R_w =	0.0404[b]	0.0363[b]	0.0372[b]	0.0567[b]

Table 5.2 (contd).

compound	**17**	**12**	**18**	**19**
empirical formula	$C_{15}H_{35}N_3O_7S_2Ti$	$C_{29}H_{41}N_5O_4S_2Ti$	$C_{30}H_{42}N_4O_5S_2Zr$	$C_{25}H_{29}Cl_2N_3O_4S_2Ti$
fw	481.49	713.82	650.72	618.46
temp / K	150	150	150	150
wavelength / Å	0.71073	0.71073	0.71073	0.71073
space group	*P* $2_1/c$	*P* $2_1/n$	*P* 2_1	*P* $2_1/c$
a / Å	14.7911(4)	8.3514(2)	8.38760(10)	14.2061(3)
b / Å	9.5434(3)	28.2936(5)	18.7925(3)	16.215(3)
c / Å	17.0501(6)	15.3443(3)	10.4541(2)	12.466(3)
α / deg	90	90	90	90
β / deg	110.5083(12)	94.2902(8)	102.4530(10)	111.87(3)
γ / deg	90	90	90	90
V / $Å^3$	2254.21(12)	3615.56(13)	1609.05(4)	2664.8(9)
Z	4	4	2	4
d (calcd) / $Mg \cdot m^{-3}$	1.419	1.311	1.343	1.541
abs coeff / mm^{-1}	0.604	0.396	0.440	0.717
R indices:[a] R_1 =	0.0788[b]	0.0398[b]	0.0328[b]	0.0366[b]
R_w =	0.0860[b]	0.0292[b]	0.0358[b]	0.0413[b]

[a] $R_1 = \Sigma||F_o|-|F_c|| / \Sigma|F_o|$; $R_w = \sqrt{\{\Sigma w (|F_o|-|F_c|)^2 / \Sigma w|F_o|^2\}}$; $wR2 = \sqrt{\{\Sigma w (F_o^2-F_c^2)^2 / \Sigma w(F_o^2)^2\}}$;

[b] For data wih I $> 3\sigma(I)$; [c] For data with I $> 2\sigma(I)$; [d] For all data.

Table 5.2 (contd).

compound	**20**	**21**	**23**	**24**
empirical formula	$C_{62}H_{88}N_8O_{12}S_6Si_2Zr_2$	$C_{64}H_{62}F_{18}N_4O_6S_3SiZr$	$C_{32}H_{27}F_{18}N_5O_6S_3Zr$	$C_{71}H_{60}F_{36}N_8O_{14}S_6Zr_2$
fw	1724.66	1315.85	1106.98	2308.07
temp / K	150	150	150	150
wavelength / Å	0.71073	0.71073	0.71073	0.71073
space group	*P* $2_1/n$	*P* $\bar{1}$	*C* 2/*c*	*P* $2_1/c$
a / Å	11.120(2)	17.7133(2)	39.3524(6)	16.34020(10)
b / Å	32.411(7)	18.3479(2)	13.9389(2)	24.5787(2)
c / Å	12.042(2)	18.5380(2)	15.1909(3)	22.9231(2)
α / deg	90	64.3587(5)	90	90
β / deg	112.08(3)	88.4433(5)	96.7558(6)	102.6647(4)
γ / deg	90	84.7710(5)	90	90
V / $Å^3$	4021.7(16)	5408.45(11)	8274.8(2)	8982.40(12)
Z	4	2	8	4
d (calcd) / $Mg·m^{-3}$	1.424	1.616	1.777	1.707
abs coeff / mm^{-1}	0.508	0.455	0.548	0.510
R indices:[a] R_1 =	0.0303[b]	0.0547[b]	0.0595[b]	0.0540[b]
R_w =	0.0338[b]	0.0568[b]	0.0656[b]	0.0595[b]

[a] $R_1 = \Sigma||F_o|-|F_c|| / \Sigma|F_o|$; $R_w = \sqrt{\{\Sigma w (|F_o|-|F_c|)^2 / \Sigma w|F_o|^2\}}$; $wR2 = \sqrt{\{\Sigma w (F_o^2-F_c^2)^2 / \Sigma w(F_o^2)^2\}}$;

[b] For data wih I > 3σ(I); [c] For data with I > 2σ(I); [d] For all data.

5.9 X-ray data collection and processing parameters for Chapter 4

Crystal structure determinations of Al(CyN_2^{Ts})Et(THF) (27), Al($N_2^{Ts}N^{Ph}$)Et (29), Al($N_2^{Ts}N^{OMe}$)Et (30), Al($N_2^{Ts}N^{py}$)Et (31), [Al($N^{Ts}{}_2N^{Ph}$)Cl]$_2$ (38) and Al($N_2^{Ts}N^{OMe}$)($OCH_2CH_2NH_2$) (40). X-ray data collection and processing parameters are given in Table 5.3. Crystals were mounted on glass fibers using perfluoropolyether oil and cooled rapidly in a stream of cold N_2 using an Oxford Cryosystems Cryostream unit. Diffraction data were measured using an Enraf-Nonius KappaCCD diffractometer. As appropriate, absorption and decay corrections were applied to the data and equivalent reflections merged.[19] The structures were solved with SIR92[20] or SHELXS-97[21] and further refinements and all other crystallographic calculations were performed using either the CRYSTALS program suite[22] or SHELXS-97.[23] Other details of the structure solution and refinements are given in the Supporting Information (CIF data). A full listing of atomic coordinates, bond lengths and angles and displacement parameters for all the structures have been deposited at the Cambridge Crystallographic Data Centre. See Notice to Authors, Issue No. 1.

Table 5.3. X-ray data collection and processing parameters for Al(CyN$_2^{Ts}$)Et(THF) (**27**), Al(N$_2^{Ts}$N^{Ph})Et (**29**), Al(N$_2^{Ts}$N^{OMe})Et (**30**), Al(N$_2^{Ts}$N^{py})Et (**31**), [Al(N$^{Ts}_2$N^{Ph})Cl]$_2$ (**38**), Al(OCH$_2$CH$_2$NH$_2$)Et$_2$ and Al(N$_2^{Ts}$N^{OMe})(OCH$_2$CH$_2$NH$_2$) (**40**).

compound	**27**	**29·CH$_2$Cl$_2$**	**30**	**Al(OCH$_2$CH$_2$NH$_2$)Et$_2$**
empirical formula	$C_{26}H_{37}AlN_2O_5S_2$	$C_{26}H_{32}AlN_3O_4S_2{\cdot}CH_2Cl_2$	$C_{23}H_{34}AlN_3O_5S_2$	$C_{12}H_{32}Al_2N_2O_2$
fw	548.70	641.62	523.65	290.36
temp / K	150	150	150	150
wavelength / Å	0.71073	0.71073	0.71073	0.71073
space group	*P* 2$_1$/*c*	*P* 2$_1$/*c*	*P* n	*P* 2$_1$/*n*
a / Å	10.61030(10)	12.66370(10)	7.85910(10)	6.56090(10)
b / Å	16.4039(2)	15.0088(2)	12.9952(2)	9.9473(2)
c / Å	16.3028(2)	15.4108(2)	12.7598(2)	13.1716(3)
α / deg	90	90	90	90
β / deg	92.3235(6)	108.6423(5)	99.7066(7)	95.2425(8)
γ / deg	90	90	90	90
V / Å^3	2835.17(6)	2775.40(6)	1284.51(3)	856.03(3)
Z	4	4	2	4
d (calcd) / Mg·m^{-3}	1.285	1.330	1.354	1.126
abs coeff / mm^{-1}	0.256	0.261	0.280	0.168
R indices:[a] R_1 =	0.0599	0.0450	0.0277	0.0373
R_w =	0.0611	0.0466	0.0287	0.0394

Table 5.3 (contd).

compound	**31·CH_2Cl_2**	**38·1.25(CH_2Cl_2)**	**40·C_7H_8**
empirical formula	$C_{26}H_{33}AlN_4O_4S_2 \cdot CH_2Cl_2$	$C_{25}H_{29}AlClN_3O_4S_2 \cdot 1.25(CH_2Cl_2)$	$C_{23}H_{35}AlN_4O_6S_2 \cdot C_7H_8$
fw	641.62	668.26	646.81
temp / K	150	150	150
wavelength / Å	0.71073	0.71073	0.71073
space group	*P* $2_1/n$	*P* $2_1/n$	*P* $2_1/c$
a / Å	8.20760(10)	9.68870(10)	8.24890(10)
b / Å	38.2977(4)	24.7319(2)	40.6884(6)
c / Å	9.67340(10)	25.5491(3)	10.2827(2)
α / deg	90	90	90
β / deg	96.4865(5)	90.8599(4)	109.7782(6)
γ / deg	90	90	90
V / $Å^3$	3021.20(6)	6121.38(11)	3247.64(9)
Z	4	4	4
d (calcd) / $Mg \cdot m^{-3}$	1.411	1.450	1.323
abs coeff / mm^{-1}	0.422	0.546	0.239
R indices:[a] R_1 =	0.0460	0.0557	0.0577
R_w =	0.0490	0.0605	0.0602

[a] $R_1 = \Sigma||F_o|-|F_c|| / \Sigma|F_o|$; $R_w = \sqrt{\{\Sigma w (|F_o|-|F_c|)^2 / \Sigma w|F_o|^2\}}$ for data with $I > 3\sigma(I)$.

5.10 References

(1) Rudin, A.; Hoegy, H. L. W. *J. Polym. Sci. Part A: Polym. Chem.* **1972**, *10*, 217-235.

(2) Barakat, I.; Ph, D.; Jérôme, R.; Ph, T. *J. Polym. Sci. Part A: Polym. Chem.* **1993**, *31*, 505-514.

(3) Dorgan, J. R.; Janzen, J.; Knauss, D. M.; Hait, S. B.; Limoges, B. R.; Hutchinson, M. H. *J. Polym. Sci. Part B: Polym. Phys.* **2005**, *43*, 3100-3111.

(4) Bradley, D. C.; Thomas, I. M. *J. Chem. Soc.* **1960**, 3857.

(5) Diamond, G. M.; Jordan, R. F.; Petersen, J. L. *Organometallics* **1996**, *15*, 4030-4037.

(6) Bradley, D. C.; Thomas, I. M. *J. Chem. Soc.* **1960**, 3857 - 3861.

(7) Benzing, E.; Kornicker, W. *Chem. Ber.* **1961**, 2263-2267.

(8) Kempe, R.; Arndt, P. *Inorg. Chem.* **1996**, *35*, 2644-2649.

(9) Collier, M. R.; Lappert, M. F.; Pearce, R. *J. Chem. Soc., Dalton Trans.* **1973**, 445 - 451.

(10) Skinner, M. E. G.; Li, Y.; Mountford, P. *Inorg. Chem.* **2002**, *41*, 1110-1119.

(11) Bailey, N. A.; Fenton, D. E.; Hellier, P. C.; Hempstead, P. D.; Casellatob, U.; Vigatob, P. A. *Dalton Trans.* **1992**, 2809-2816.

(12) Kitagawa, O.; Yotsumoto, K.; Kohriyama, M.; Dobashi, Y.; Taguchi, T. *Org. Lett.* **2004**, *6*, 3605-3607.

(13) Takahashi, H.; Kawakita, T.; Ohno, M.; Yoshioka, M.; Kobayashi, S. *Tetrahedron* **1992**, *48*, 5691-5700.

(14) Motekaitis, R. J.; Martell, A. E.; Muraset, I. *Inorg. Chem.* **1986**, 938-944.

(15) Herbert, B. *Jus. Lie. Annal. d. Chem.* **1950**, *566*, 210-244.

(16) Kunicki, A. R.; Pasynkiewicz, S.; Jankowski, J.; Mank, B. *Pol. J. Chem.* **2004**, *78*, 1857-1864.

(17) Hirabayashi, T.; Sakakibara, T.; Ishii, Y. *J. Organomet. Chem.* **1972**, *35*, 19-25.

(18) Hurley, T. J.; Robinson, M. A.; Scruggs, J. A.; Trotz, S. I. *Inorg*. *Chem*., **1967**, *3*, 1310-1315.

(19) Otwinowski, Z.; Minor, W. *Processing of X-ray Diffraction Data Collected in Oscillation Mode*; Academic press: New York, 1997.

(20) Altomare, A.; Cascarano, G.; Giacovazzo, G.; Guagliardi, A.; Burla, M. C.; Polidori, G.; Camalli, M. *J*. *Appl*. *Crystallogr*. **1994**, *27*, 435.

(21) Sheldrick, G. M. *Acta Crystallogr*., *Section A* **1990**, *46*, 467.

(22) Betteridge, P. W.; Cooper, J. R.; Cooper, R. I.; Prout, K.; Watkin, D. J. *J*. *Appl*. *Cryst*. **2003**, *36*, 1487.

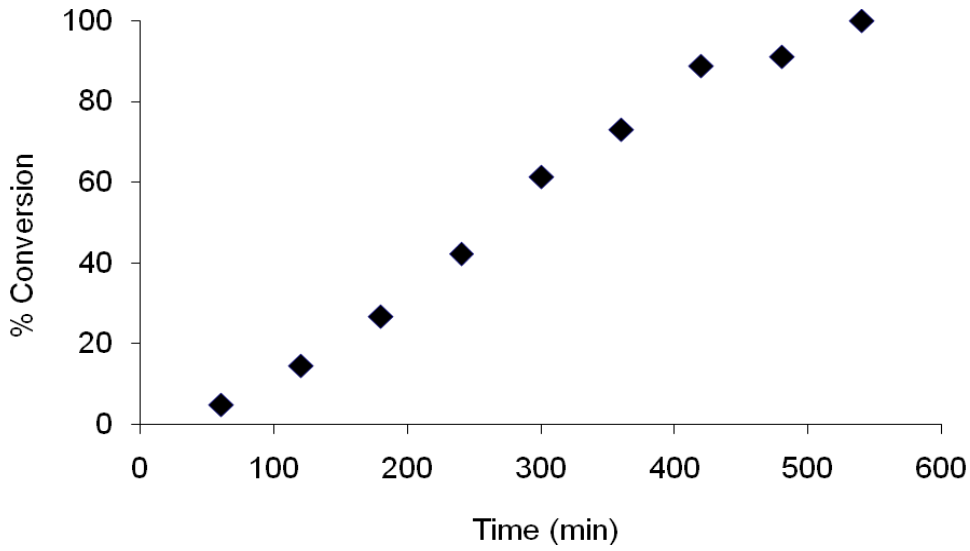
(23) Sheldrick, G. M.; Schneider, T. R. *Methods Enzymol*. **1997**, *277*, 319-343.

Sulfonamide-supported Catalysts for the Ring-Opening Polymerization of ε-Caprolactone and *rac*-lactide

---

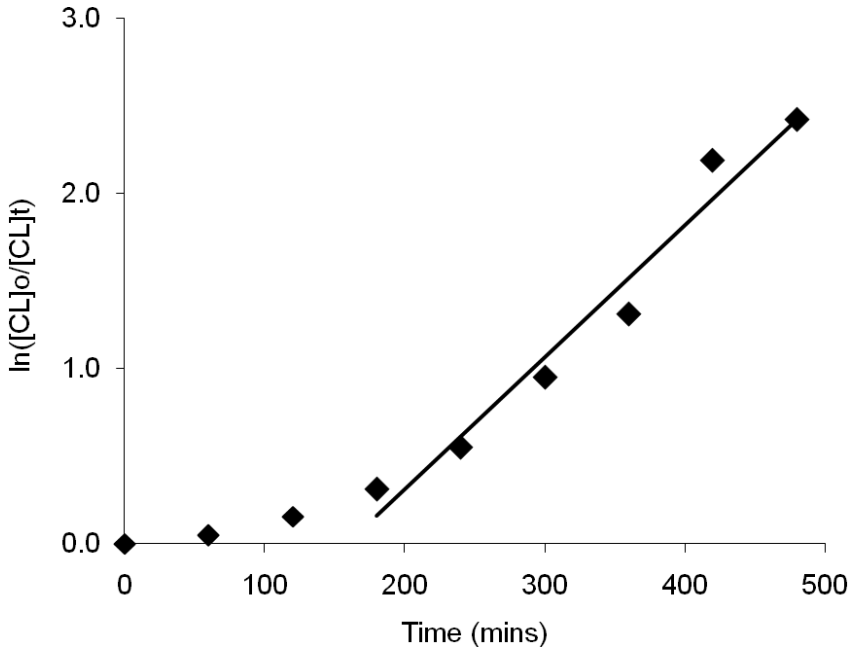
Supporting Information for Chapter 2

Figure S2.1. Plot for ε-CL consumption *vs* time using Ti($N_2^{Ts}N^{py}$)(O^iPr)$_2$ (**£c3£**).[a]



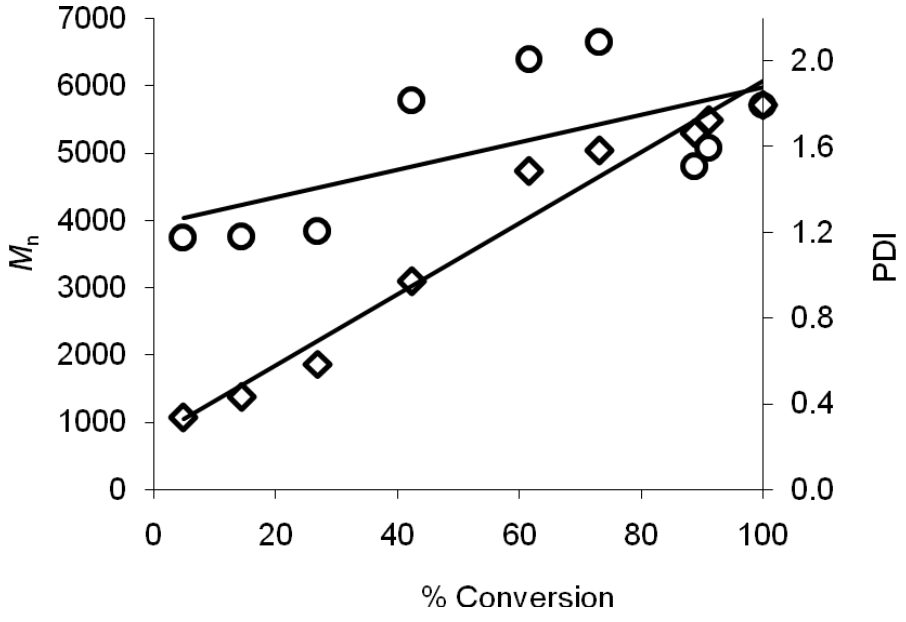
[a] Conditions: [ε-CL_0]/[**£c3£**] = 100:1, 6.8 mL toluene, 100 °C, 0.1 mL aliquots taken at the given intervals. See Experimental section for other details.

Figure S2.2. First order plot for ε-CL consumption using Ti($N_2^{Ts}N^{py}$)(O^iPr)$_2$ (**£c3£**).[a]



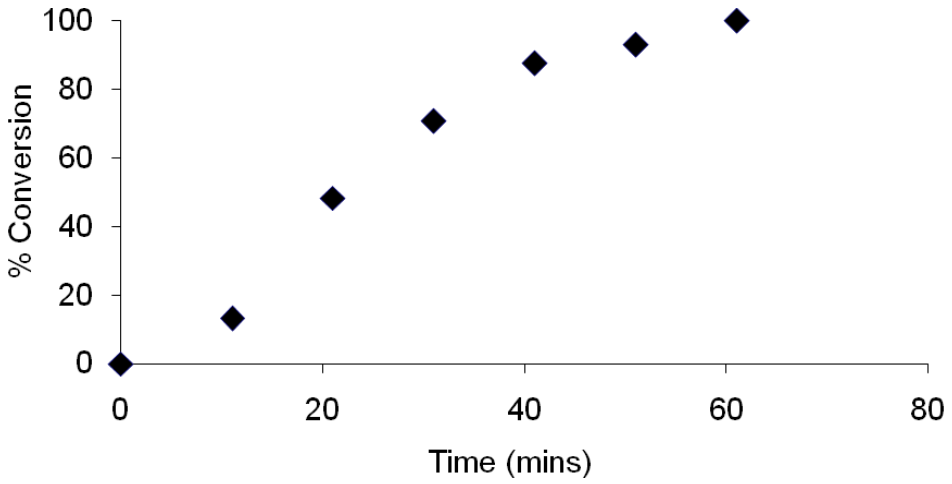
[a] Conditions: [ε-CL_0]/[**£c3£**] = 100:1, 6.8 mL toluene, 100 °C, 0.1 mL aliquots taken at the given intervals. See Experimental section for other details. Linear fit (r^2 = 0.964) shown is for the first order region after the induction period.

Figure S2.3. Plots of M_n and PDI (determined by GPC) *vs* conversion for the polymerization of ε-CL using Ti($N_2^{Ts}N^{py}$)(O^iPr)$_2$ (**£c3£**).[a]



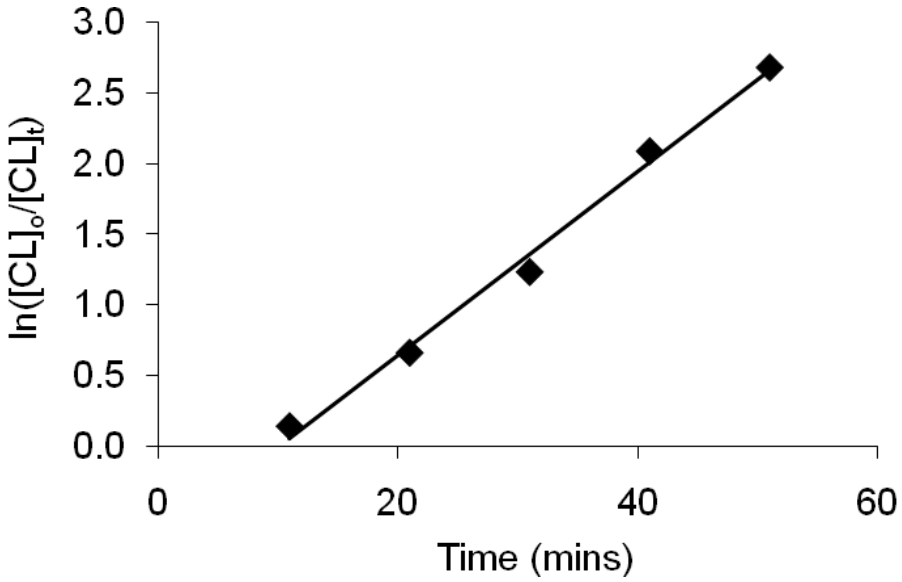
[a] Conditions: [ε-CL_0]/[**£c3£**] = 100:1, 6.8 mL toluene, 100 °C, 0.1 mL aliquots taken at the given intervals. Hollow diamonds correspond to M_n and hollow circles to PDI.

Figure S2.4. Plot for ε-CL consumption *vs* time using Ti($N_2^{Ts}N^{OMe}$)(O^iPr)$_2$ (**£c5£**).[a]



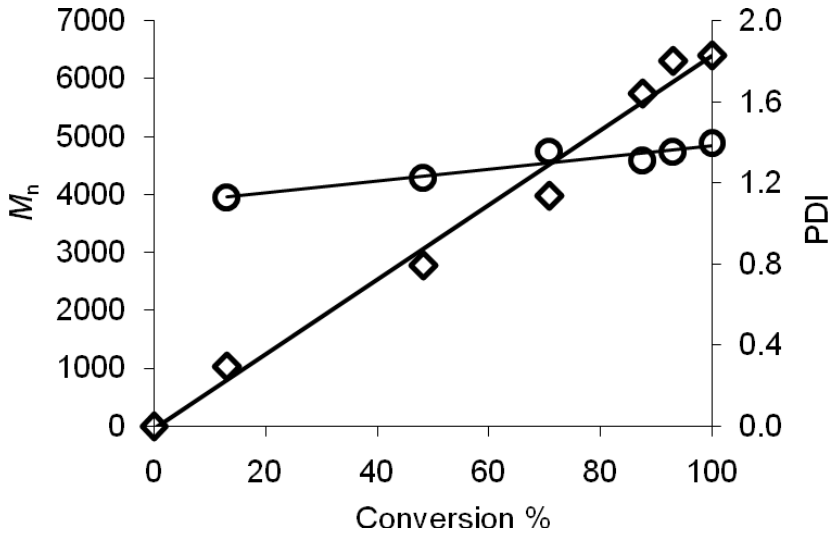
[a] Conditions: [ε-CL_0]/[**£c5£**] = 100:1, 6.8 mL toluene, 100 °C, 0.1 mL aliquots taken at the given intervals. See Experimental section for other details.

Figure S2.5. First order plot for ε-CL consumption using Ti($N_2^{Ts}N^{OMe}$)(O^iPr)$_2$ (**£c5£**).[a]



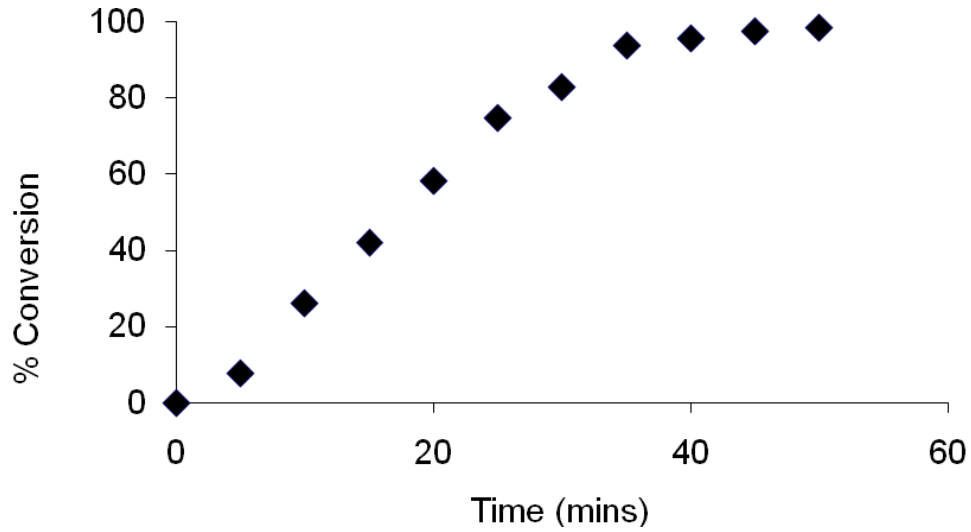
[a] Conditions: [ε-CL_0]/[**£c5£**] = 100:1, 6.8 mL toluene, 100 °C, 0.1 mL aliquots taken at the given intervals. See Experimental section for other details. Linear fit (r^2 = 0.992) shown is for the first order region after the induction period.

Figure S2.6. Plots of M_n and PDI (determined by GPC) *vs* conversion for the polymerization of ε-CL using $Ti(N_2^{Ts}N^{OMe})(O^iPr)_2$ (**£c5£**).[a]



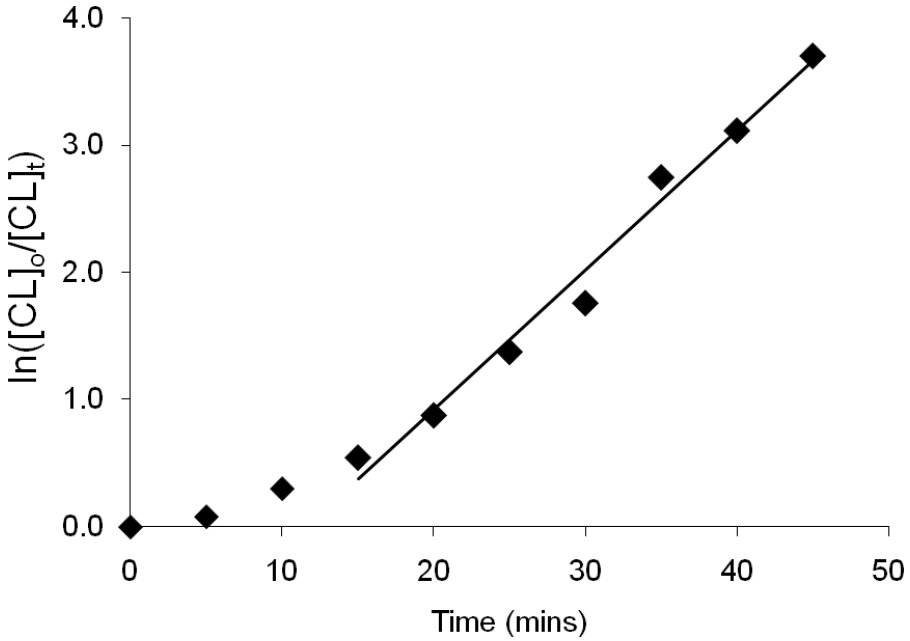
[a] Conditions: [ε-CL_0]/[**£c5£**] = 100:1, 6.8 mL toluene, 100 °C, 0.1 mL aliquots taken at the given intervals. Hollow diamonds correspond to M_n and hollow circles to PDI.

Figure S2.7. Plot for ε-CL consumption *vs* time using $Zr(N_2^{Ts}N^{py})(O^iPr)_2$ (**£c4£**).[a]



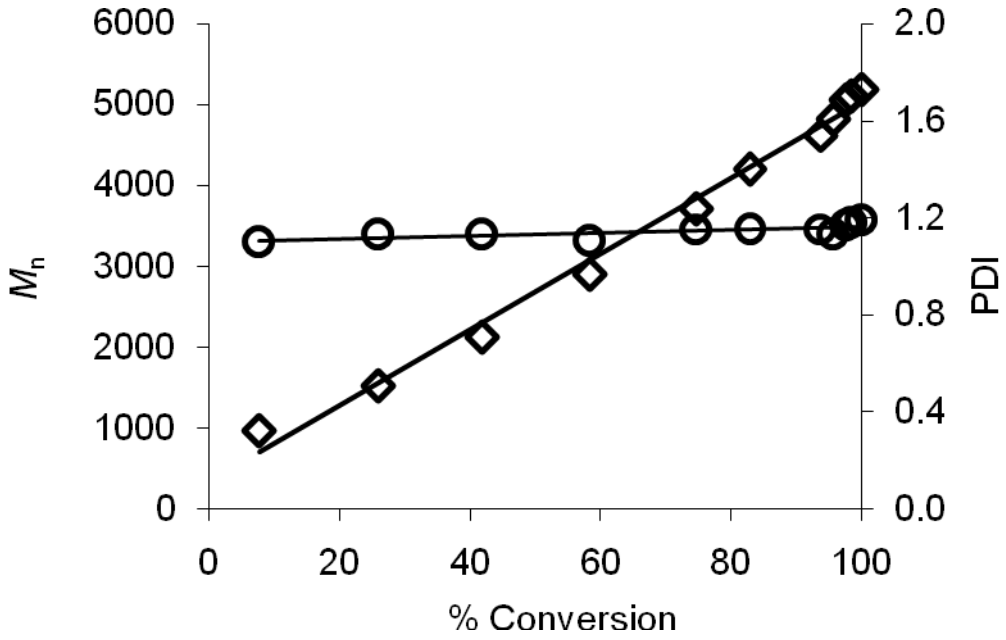
[a] Conditions: [ε-CL_0]/[**£c4£**] = 100:1, 6.8 mL toluene, 100 °C, 0.1 mL aliquots taken at the given intervals. See Experimental section for other details.

Figure S2.8. First order plot for ε-CL consumption using $Zr(N_2{}^{Ts}N^{py})(O^iPr)_2$ (**£c4£**).[a]



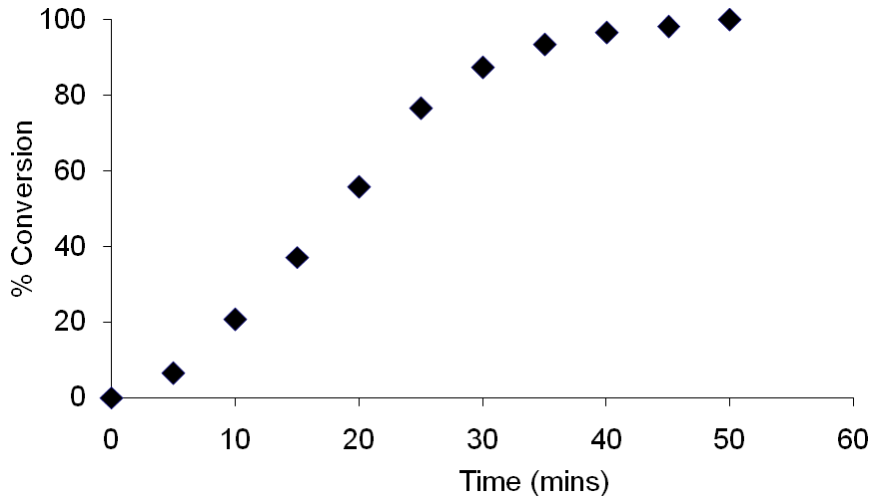
[a] Conditions: [ε-CL_0]/[**£c4£**] = 100:1, 6.8 mL toluene, 100 °C, 0.1 mL aliquots taken at the given intervals. See Experimental section for other details. Linear fit (r^2 = 0.983) shown is for the first order region after the induction period.

Figure S2.9. Plots of M_n and PDI (determined by GPC) *vs* conversion for the polymerization of ε-CL using $Zr(N_2{}^{Ts}N^{py})(O^iPr)_2$ (**£c4£**).[a]



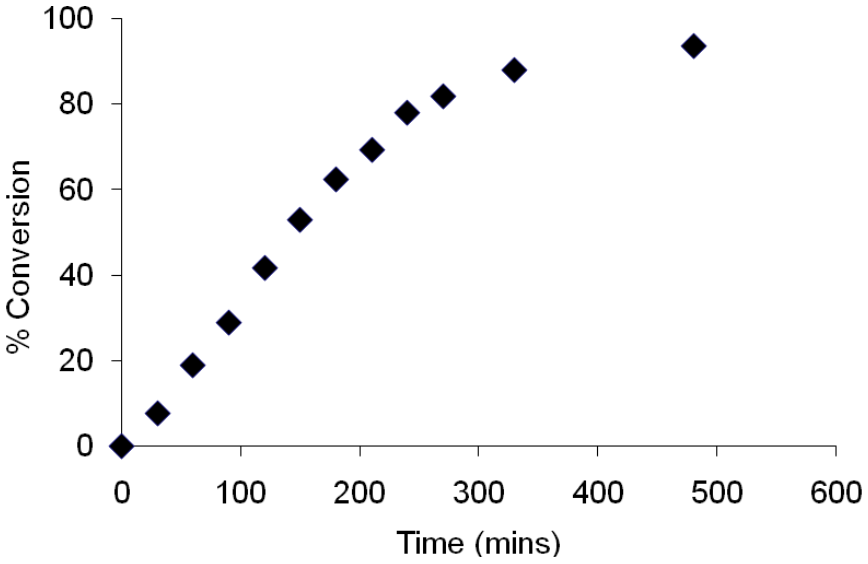
[a] Conditions: [ε-CL_0]/[**£c4£**] = 100:1, 6.8 mL toluene, 100 °C, 0.1 mL aliquots taken at the given intervals. Hollow diamonds correspond to M_n and hollow circles to PDI.

Figure S2.10. Plot for ε-CL consumption *vs* time using $Zr(N_2{}^{Ts}N^{OMe})(O^iPr)_2$ (**£c6£**).[a]



[a] Conditions: $[\varepsilon\text{-}CL_0]/[$**£c6£**$]$ = 100:1, 6.8 mL toluene, 100 °C, 0.1 mL aliquots taken at the given intervals. See Experimental section for other details.

Figure S2.11. Plot for rac-LA consumption *vs* time using $Zr(N_2{}^{Ts}N^{OMe})(O^iPr)_2$ (**£c6£**).[a]



[a] Conditions: $[\text{rac-}LA_0]/[$**£c6£**$]$ = 100:1, 6.8 mL toluene, 70 °C, 0.1 mL aliquots taken at the given intervals. See Experimental section for other details.

Figure S2.12. ^{1}H NMR spectra of poly(ε-CL) synthesised using $Zr(N_2{}^{Ts}N^{OMe})(O^{i}Pr)_2$ (**£c6£**).

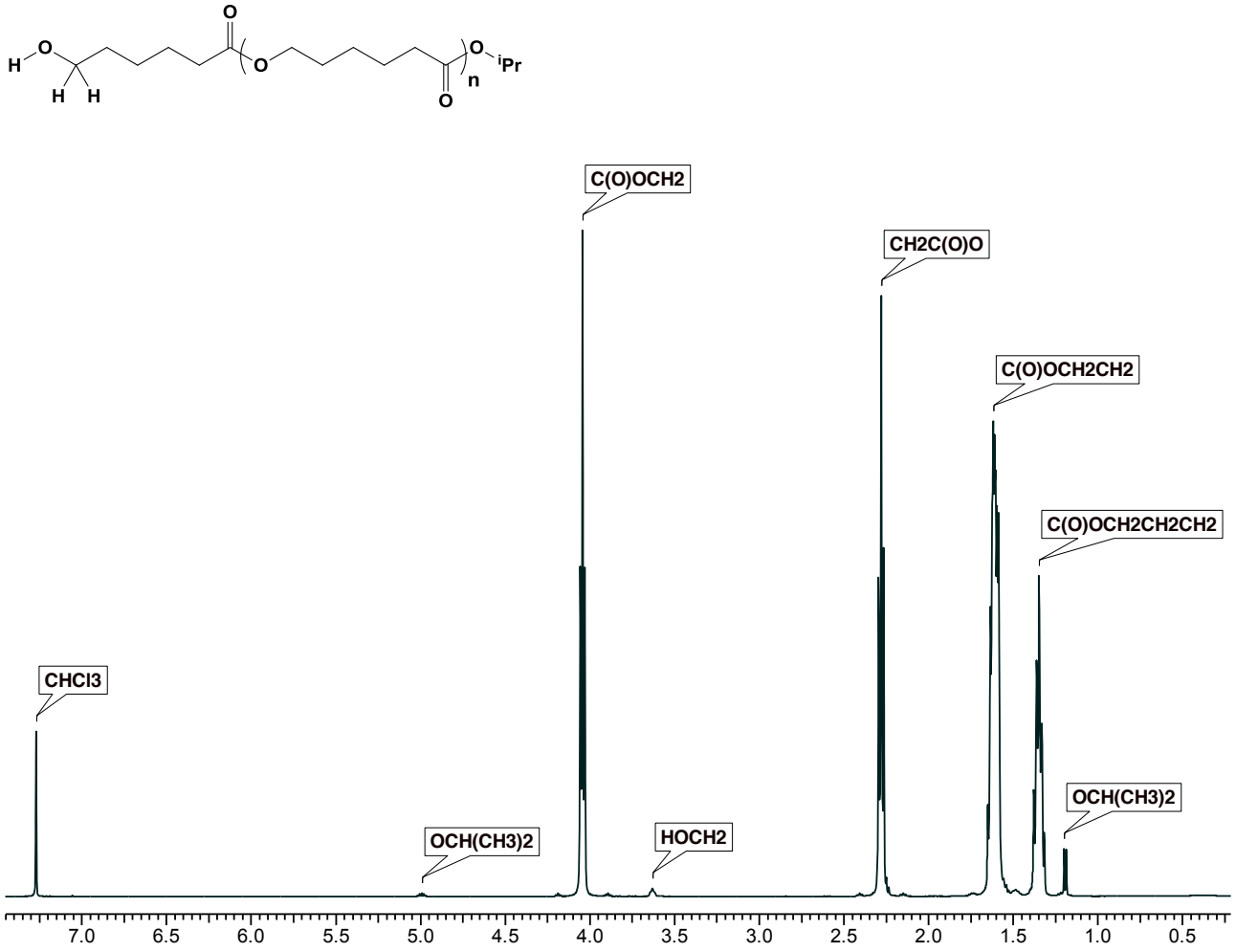


Figure S2.13. MALDI-ToF MS of poly(ε-CL) synthesised using $Ti(N_2{}^{Ts}N^{py})(O^iPr)_2$ (**£c3£**). M_n by GPC analysis was 3740 g mol^{-1}.

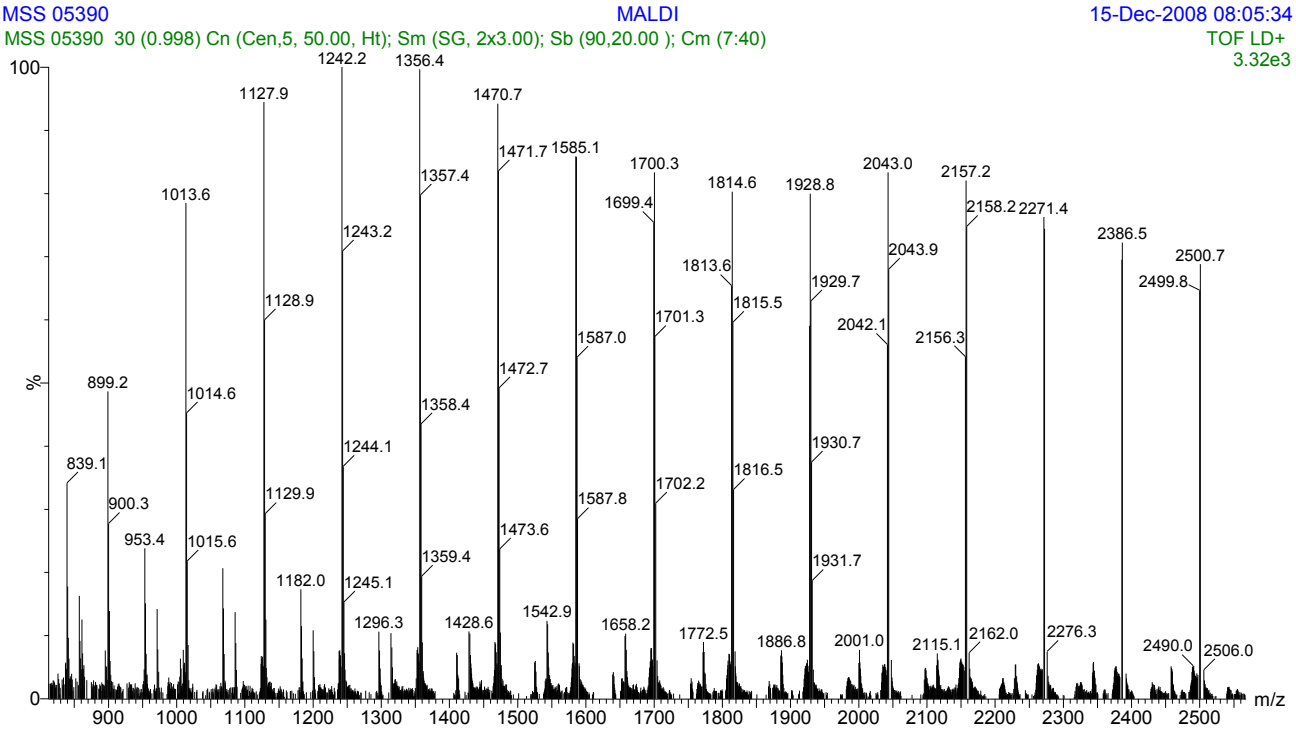
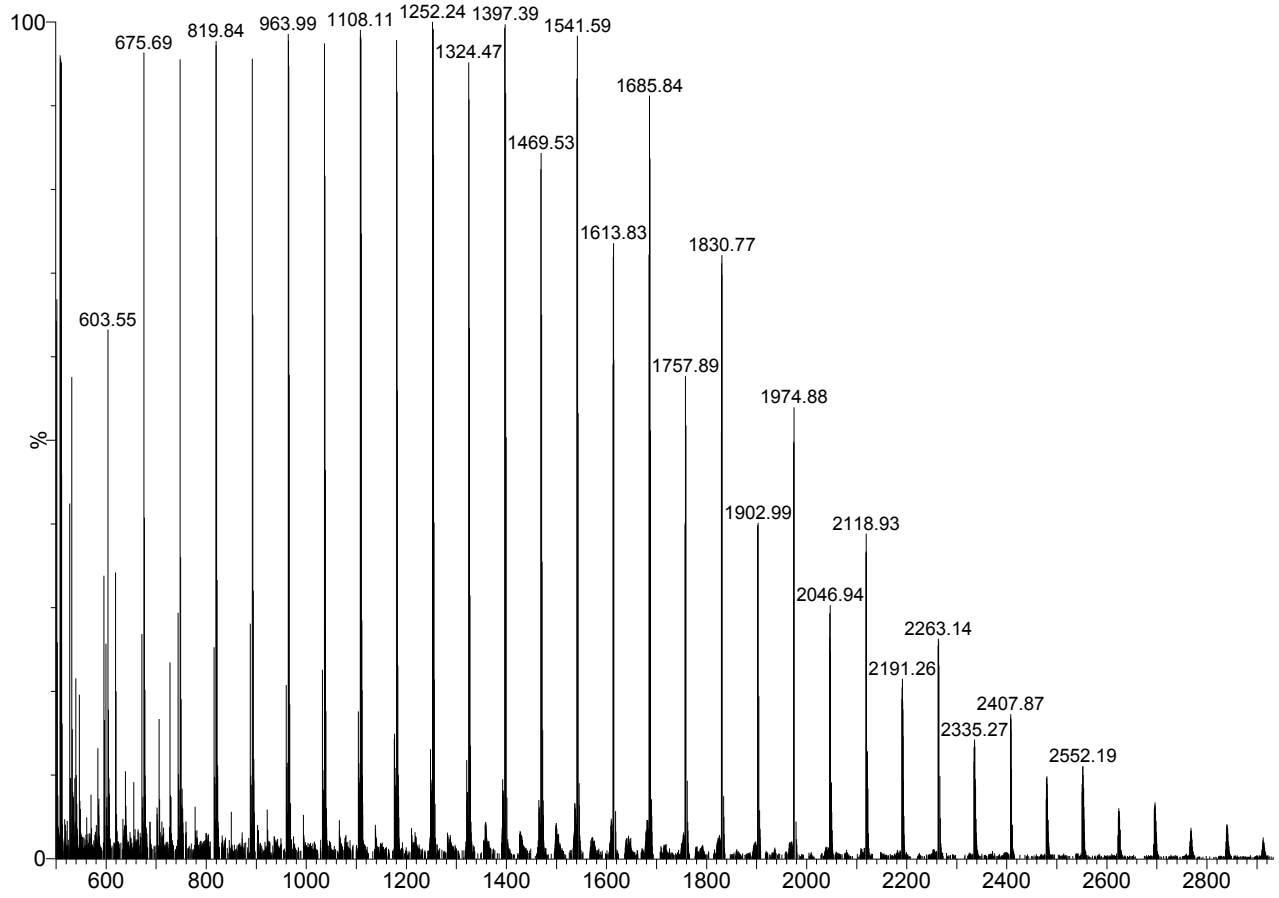
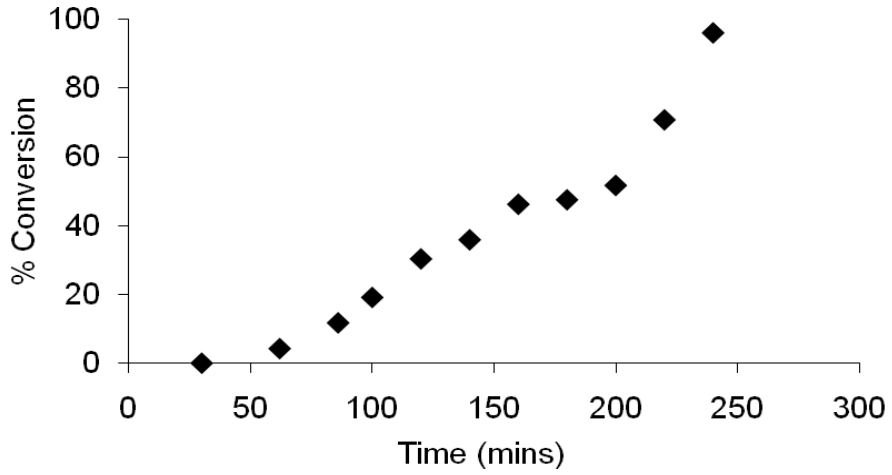


Figure S2.14. MALDI-ToF MS of poly(*rac*-LA) synthesised using $Zr(N_2{}^{Ts}N^{OMe})(O^iPr)_2$ (**£c6£**). M_n by GPC analysis was 1470 g mol^{-1}.



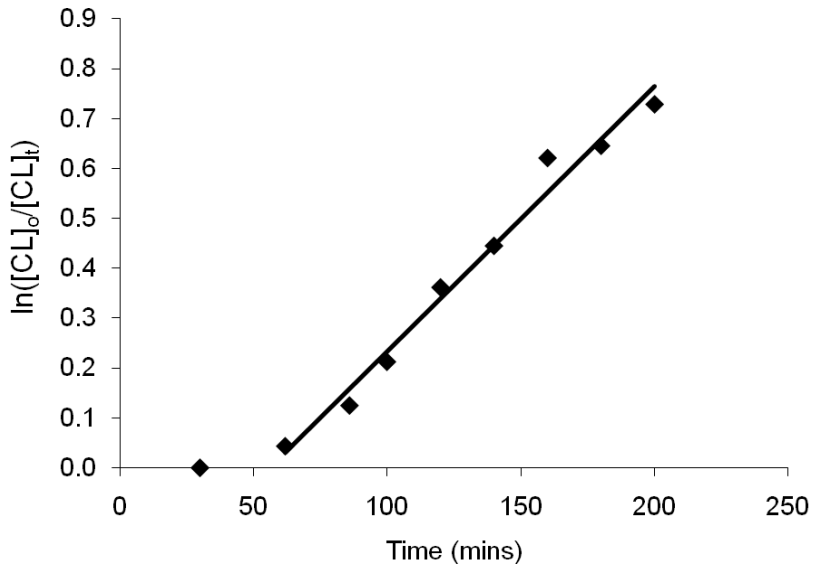
Supporting Information for Chapter 3

Figure S3.1. Plot for ε-CL consumption *vs* time using Ti($N_2^{Ms}N^{Ph}$)(O^iPr)$_2$ (**£c15£**).[a]



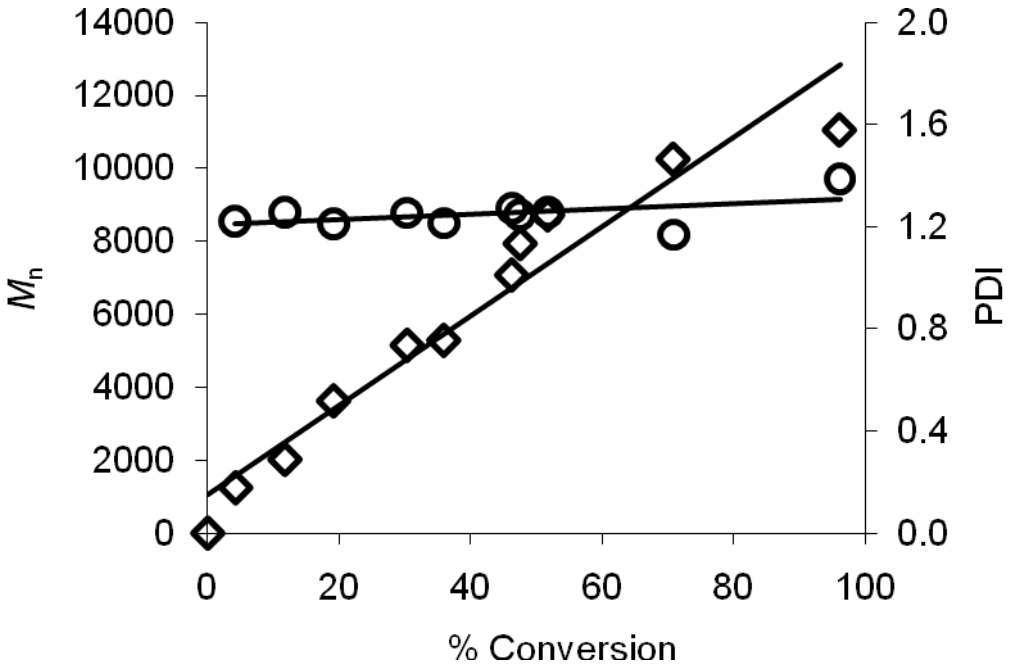
[a] Conditions: [ε-CL_0]/[**£c15£**] = 100:1, 6.8 mL toluene, 100 °C, 0.1 mL aliquots taken at the given intervals. See Experimental section for other details.

Figure S3.2. First order plot for ε-CL consumption using Ti($N_2^{Ms}N^{Ph}$)(O^iPr)$_2$ (**£c15£**).[a]



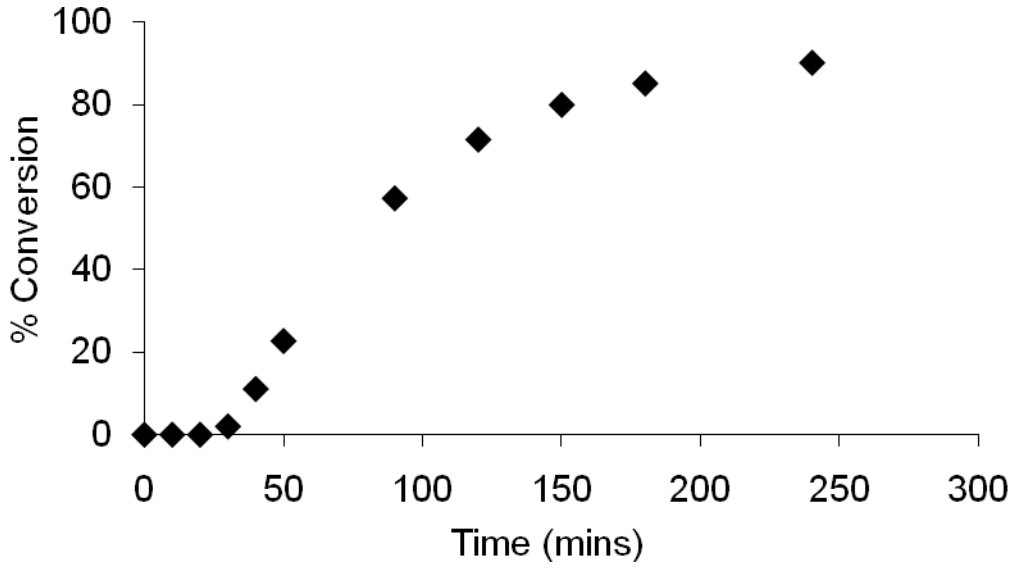
[a] Conditions: [ε-CL_0]/[**£c15£**] = 100:1, 6.8 mL toluene, 100 °C, 0.1 mL aliquots taken at the given intervals. See Experimental section for other details. Linear fit (r^2 = 0.982) shown is for the first order region after the induction period.

Figure S3.3. Plots of M_n and PDI (determined by GPC) *vs* conversion for the polymerization of ε-CL using $Ti(N_2^{Ms}N^{Ph})(O^iPr)_2$ (**£c15£**).[a]



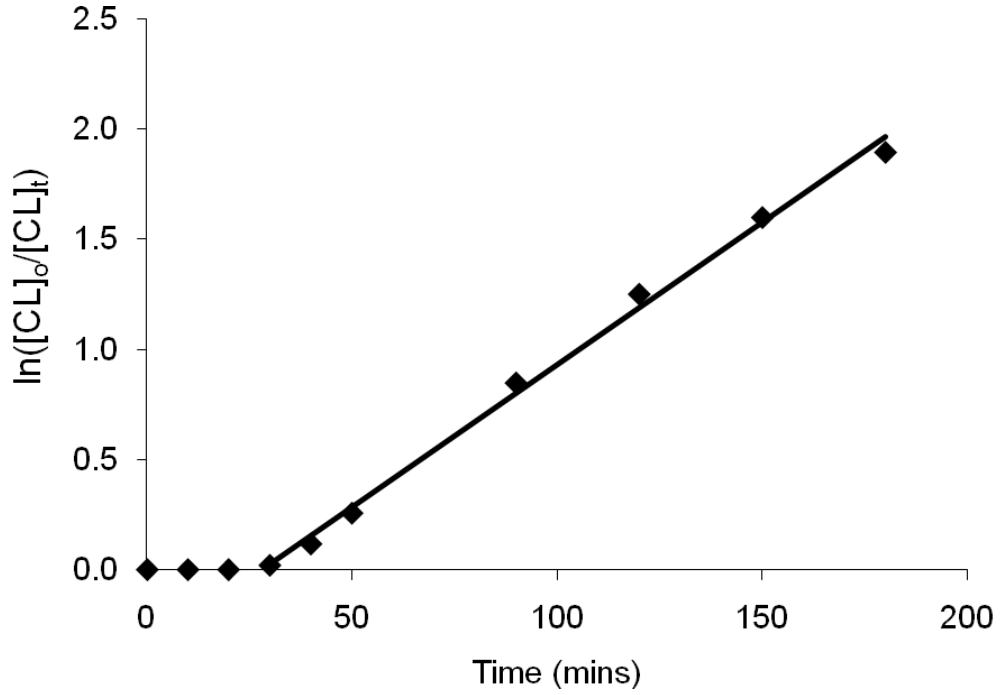
[a] Conditions: [ε-CL_0]/[**£c15£**] = 100:1, 6.8 mL toluene, 100 °C, 0.1 mL aliquots taken at the given intervals. Hollow diamonds correspond to M_n and hollow circles to PDI.

Figure S3.4. Plot for ε-CL consumption *vs* time using $Ti(N_2^{Ts}N^{Ph})(NMe_2)(O^iPr)$ (**£c18£**).[a]



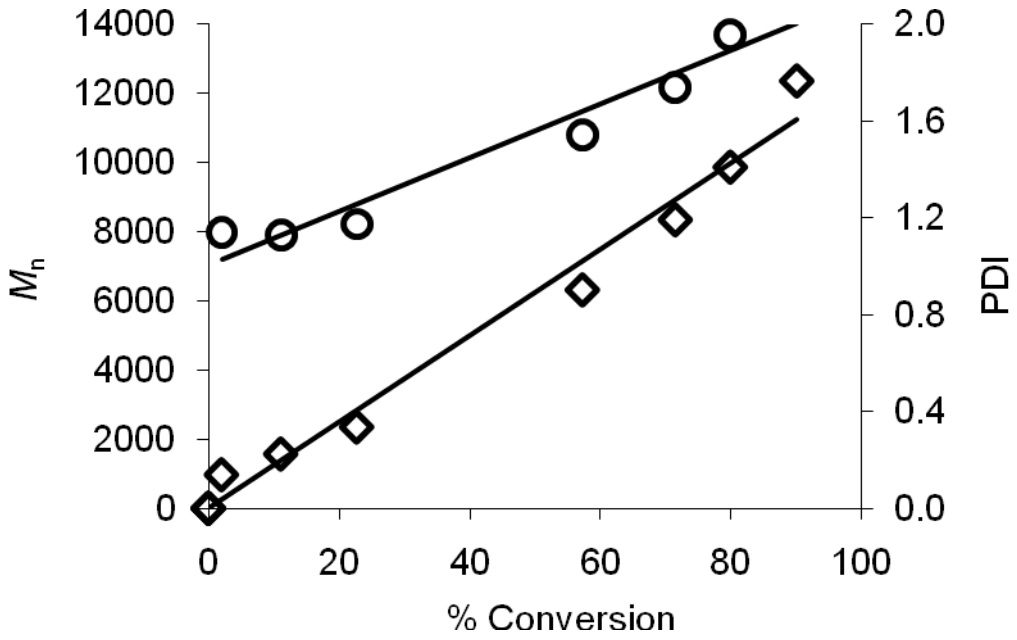
[a] Conditions: [ε-CL_0]/[**£c18£**] = 100:1, 6.8 mL toluene, 100 °C, 0.1 mL aliquots taken at the given intervals. See Experimental section for other details.

Figure S3.5. First order plot for ε-CL consumption using Ti($N_2^{Ts}N^{Ph}$)(NMe_2)(O^iPr) (**£c18£**).[a]



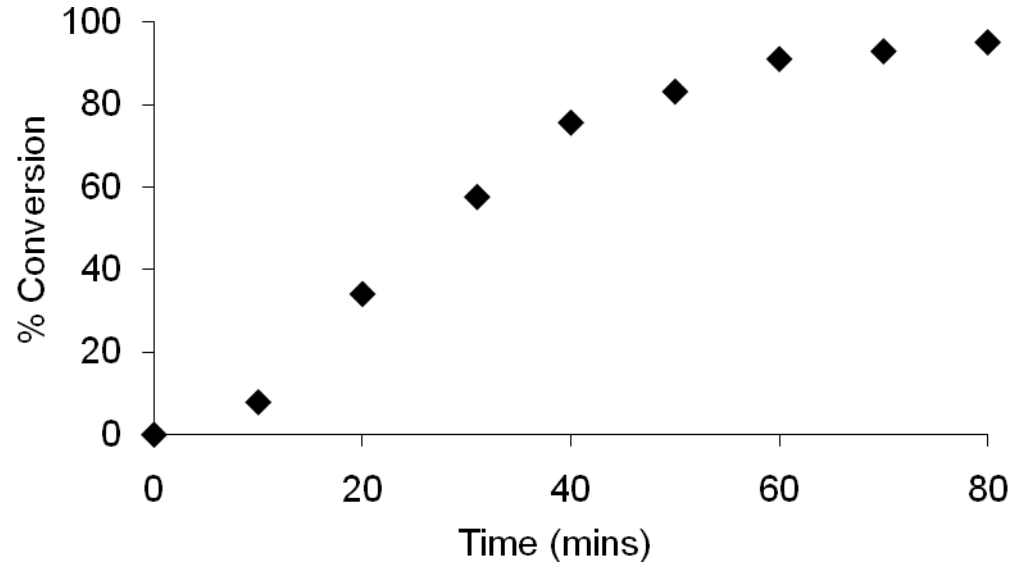
[a] Conditions: [ε-CL_0]/[**£c18£**] = 100:1, 6.8 mL toluene, 100 °C, 0.1 mL aliquots taken at the given intervals. See Experimental section for other details. Linear fit (r^2 = 0.996) shown is for the first order region after the induction period.

Figure S3.6. Plots of M_n and PDI (determined by GPC) *vs* conversion for the polymerization of ε-CL using Ti($N_2^{Ts}N^{Ph}$)(NMe_2)(O^iPr) (**£c18£**).[a]



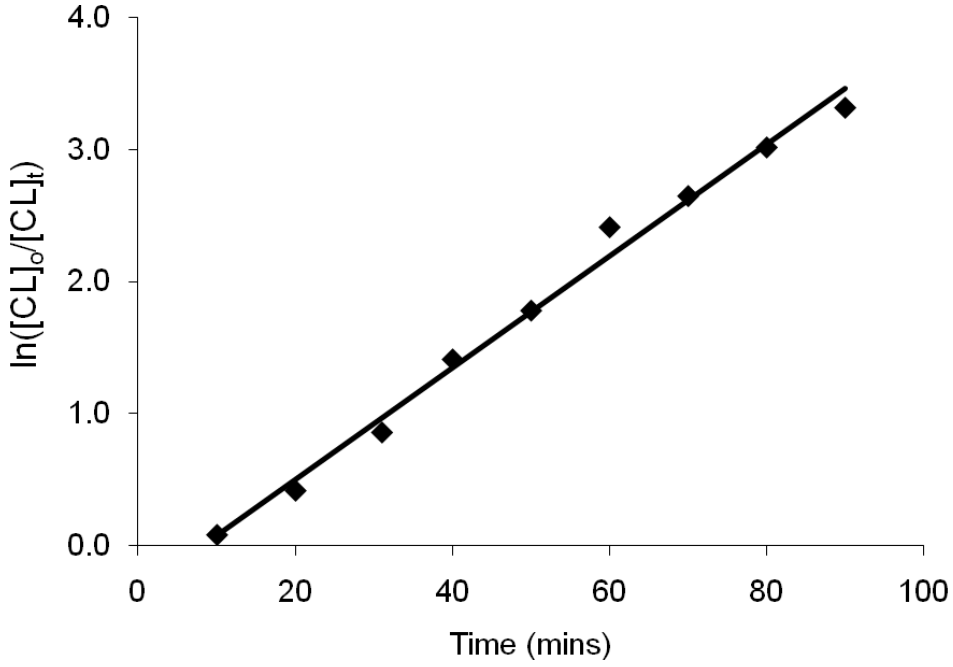
[a] Conditions: [ε-CL_0]/[**£c18£**] = 100:1, 6.8 mL toluene, 100 °C, 0.1 mL aliquots taken at the given intervals. Hollow diamonds correspond to M_n and hollow circles to PDI.

Figure S3.7. Plot for ε-CL consumption *vs* time using $Ti(N_2^{Ts}N^{Ph})(O^iPr)_2$ (**£c13£**).[a]



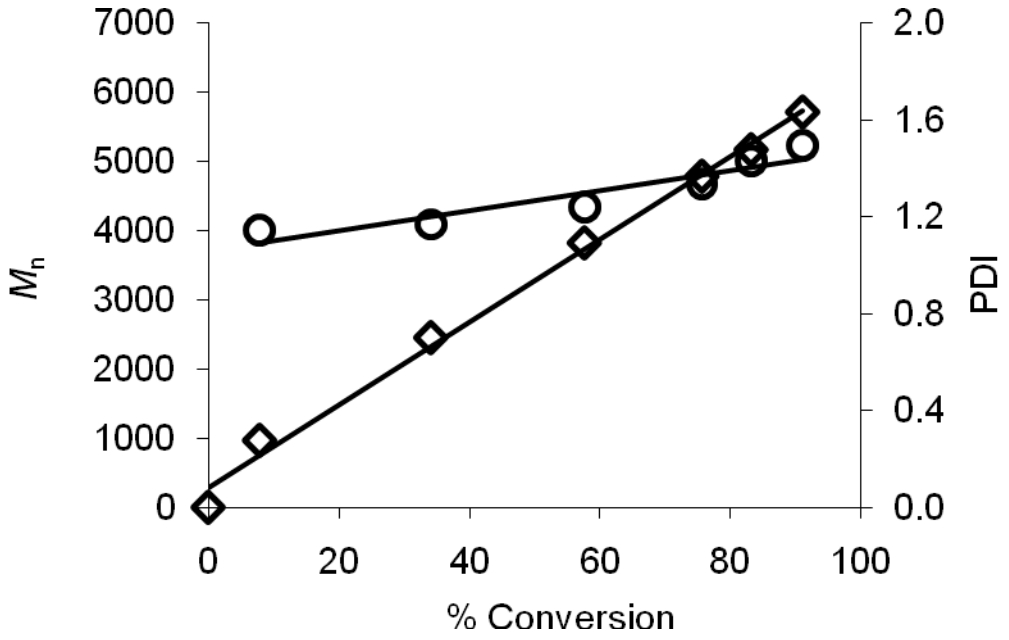
[a] Conditions: [ε-CL_0]/[**£c13£**] = 100:1, 6.8 mL toluene, 100 °C, 0.1 mL aliquots taken at the given intervals. See Experimental section for other details.

Figure S3.8. First order plot for ε-CL consumption using $Ti(N_2^{Ts}N^{Ph})(O^iPr)_2$ (**£c13£**).[a]



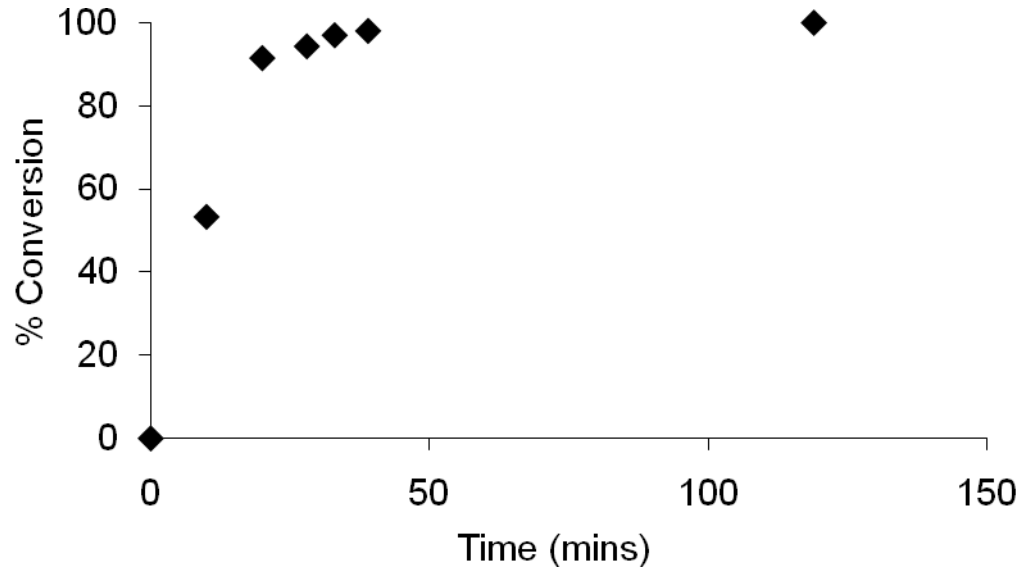
[a] Conditions: [ε-CL_0]/[**£c13£**] = 100:1, 6.8 mL toluene, 100 °C, 0.1 mL aliquots taken at the given intervals. See Experimental section for other details. Linear fit (r^2 = 0.991) shown is for the first order region after the induction period.

Figure S3.9. Plots of M_n and PDI (determined by GPC) *vs* conversion for the polymerization of ε-CL using Ti($N_2^{Ts}N^{Ph}$)(O^iPr)$_2$ (**£c13£**).[a]



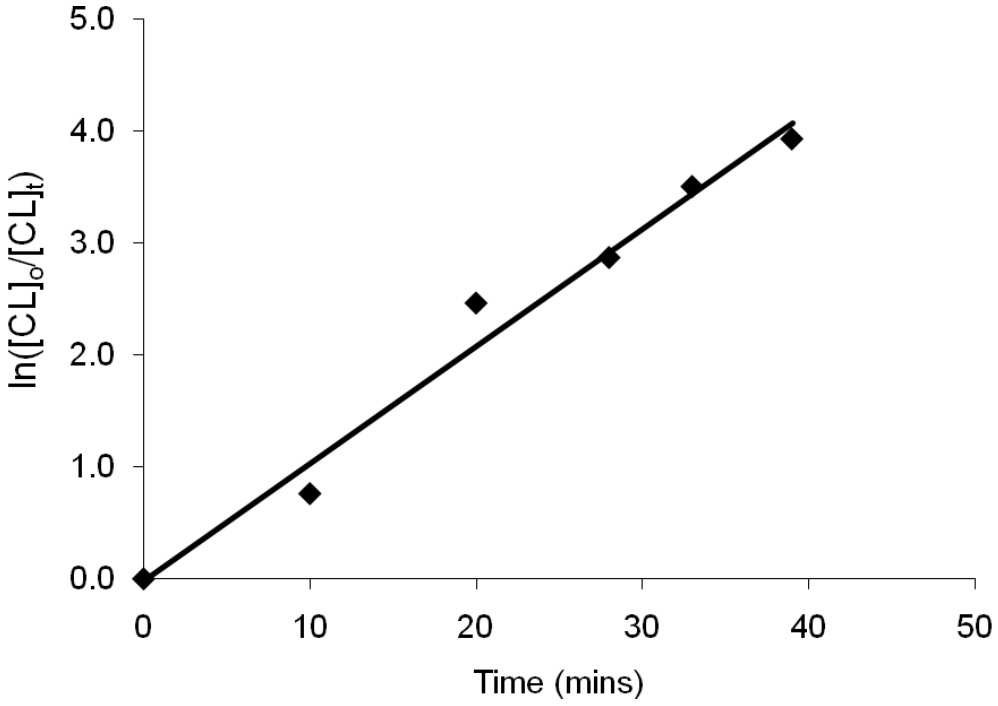
[a] Conditions: [ε-CL_0]/[**£c13£**] = 100:1, 6.8 mL toluene, 100 °C, 0.1 mL aliquots taken at the given intervals. Hollow diamonds correspond to M_n and hollow circles to PDI.

Figure S3.10. Plot for ε-CL consumption *vs* time using Ti($N_2^{Ms}N^{Ph}$)(O^iPr)$_2$ (**£c15£**).[a]



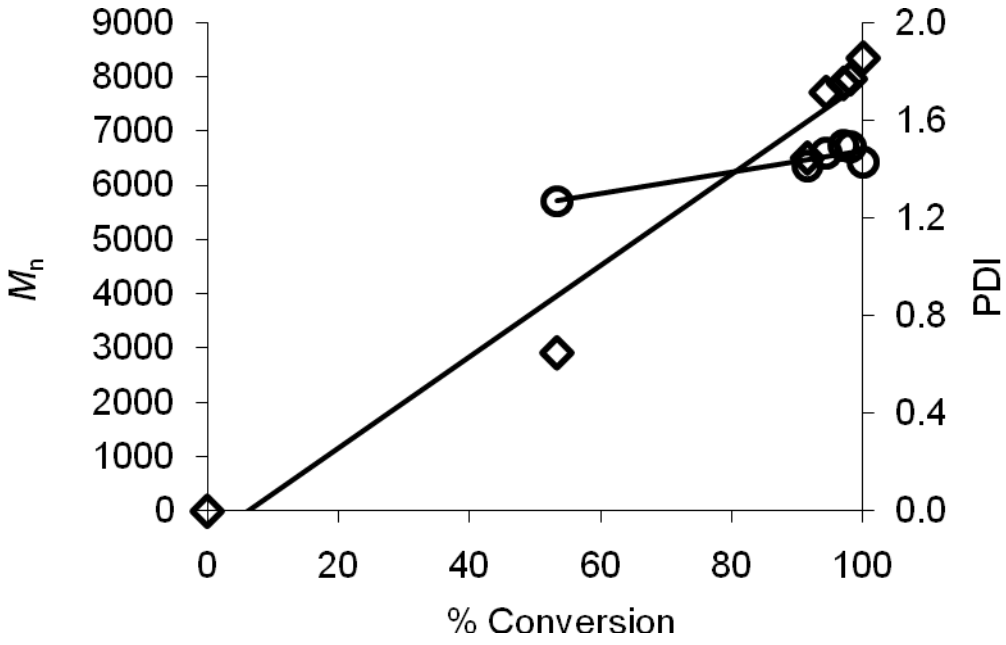
[a] Conditions: [ε-CL_0]/[**£c15£**] = 100:1, 6.8 mL toluene, 100 °C, 0.1 mL aliquots taken at the given intervals. See Experimental section for other details.

Figure S3.11. First order plot for ε-CL consumption using Ti($N_2^{Ms}N^{Ph}$)(O^iPr)$_2$ (**£c15£**).[a]



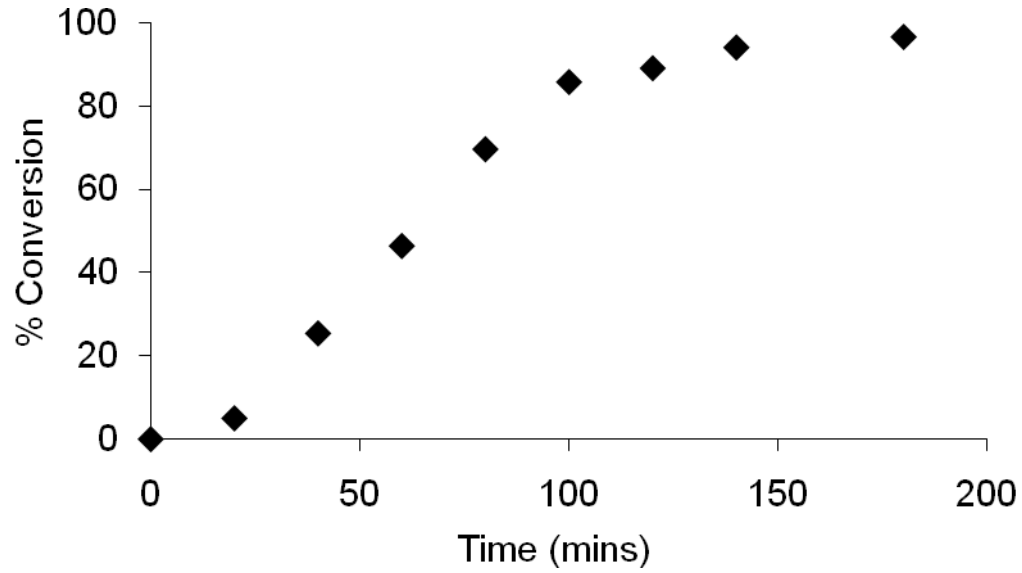
[a] Conditions: [ε-CL_0]/[**£c15£**] = 100:1, 6.8 mL toluene, 100 °C, 0.1 mL aliquots taken at the given intervals. See Experimental section for other details. Linear fit (r^2 = 0.980) shown is for the first order region after the induction period.

Figure S3.12. Plots of M_n and PDI (determined by GPC) *vs* conversion for the polymerization of ε-CL using Ti($N_2^{Ms}N^{Ph}$)(O^iPr)$_2$ (**£c15£**).[a]



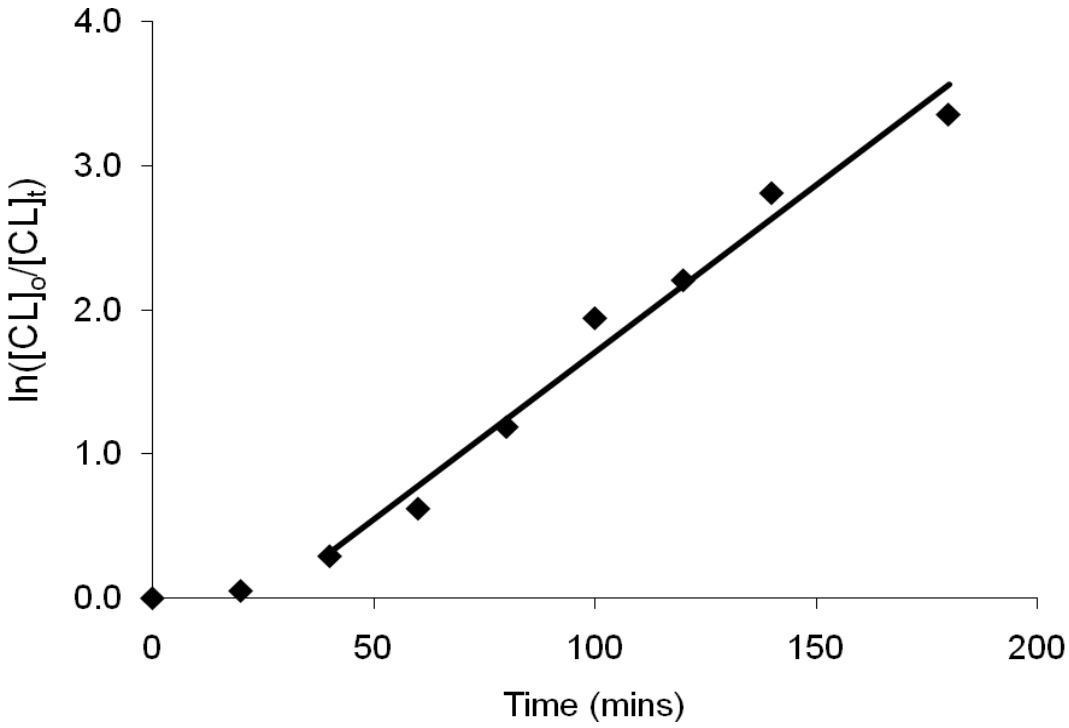
[a] Conditions: [ε-CL_0]/[**£c15£**] = 100:1, 6.8 mL toluene, 100 °C, 0.1 mL aliquots taken at the given intervals. Hollow diamonds correspond to M_n and hollow circles to PDI.

Figure S3.13. Plot for ε-CL consumption *vs* time using Ti($N_2^{Ms}N^{OMe}$)(O^iPr)$_2$ (**£c17£**).[a]



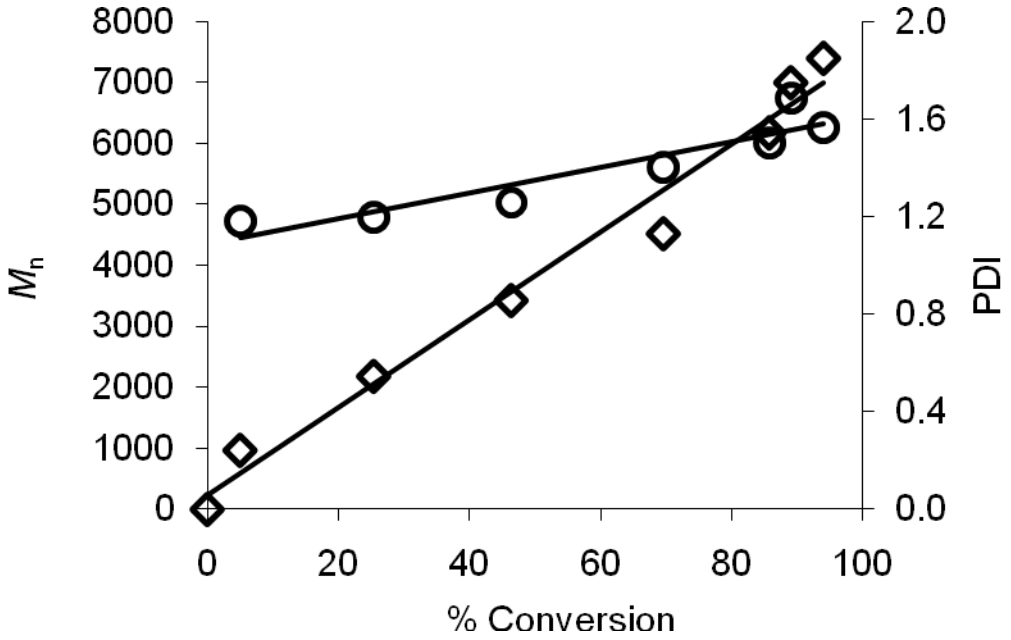
[a] Conditions: [ε-CL_0]/[**£c17£**] = 100:1, 6.8 mL toluene, 100 °C, 0.1 mL aliquots taken at the given intervals. See Experimental section for other details.

Figure S3.14. First order plot for ε-CL consumption using Ti($N_2^{Ms}N^{OMe}$)(O^iPr)$_2$ (**£c17£**).[a]



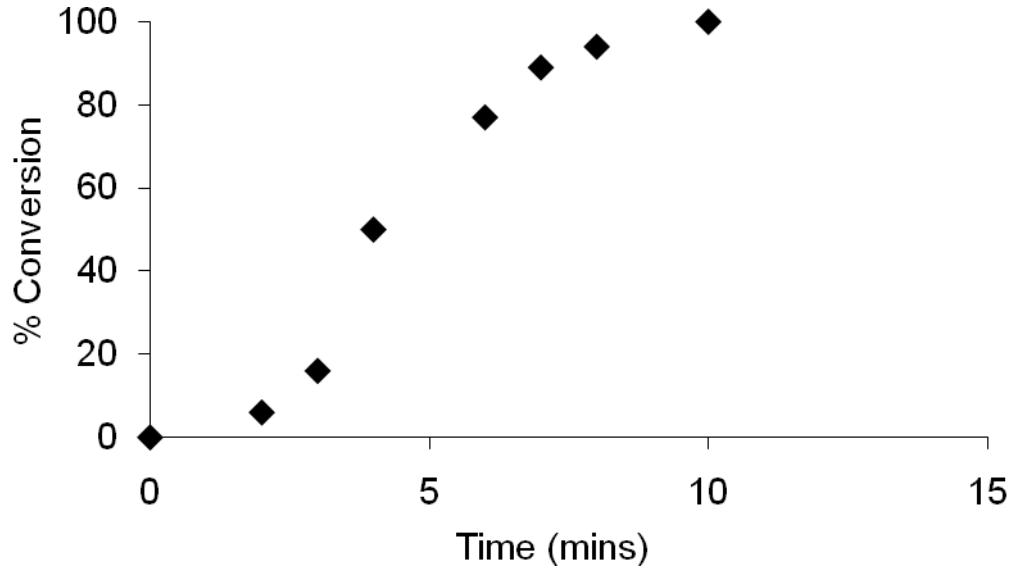
[a] Conditions: [ε-CL_0]/[**£c17£**] = 100:1, 6.8 mL toluene, 100 °C, 0.1 mL aliquots taken at the given intervals. See Experimental section for other details. Linear fit (r^2 = 0.979) shown is for the first order region after the induction period.

Figure S3.15. Plots of M_n and PDI (determined by GPC) *vs* conversion for the polymerization of ε-CL using Ti($N_2^{Ms}N^{OMe}$)(O^iPr)$_2$ (**£c17£**).[a]



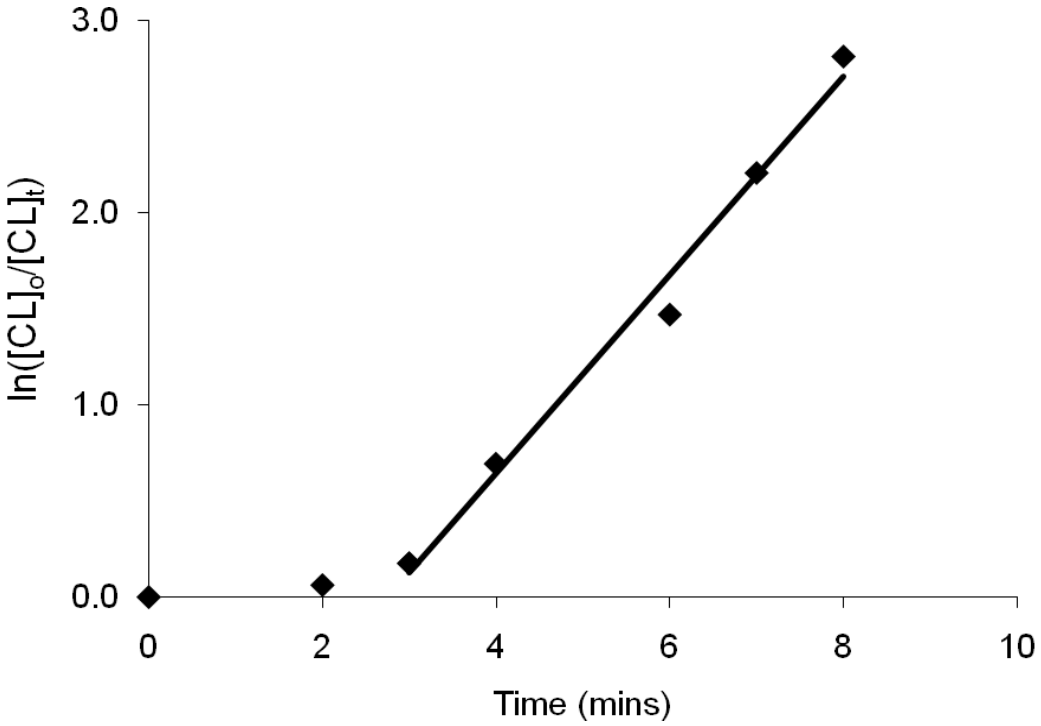
[a] Conditions: [ε-CL_0]/[**£c17£**] = 100:1, 6.8 mL toluene, 100 °C, 0.1 mL aliquots taken at the given intervals. Hollow diamonds correspond to M_n and hollow circles to PDI.

Figure S3.16. Plot for ε-CL consumption *vs* time using Ti(CyN_2^{Ts})(O^iPr)$_2$ (**£c3.4£**).[a]



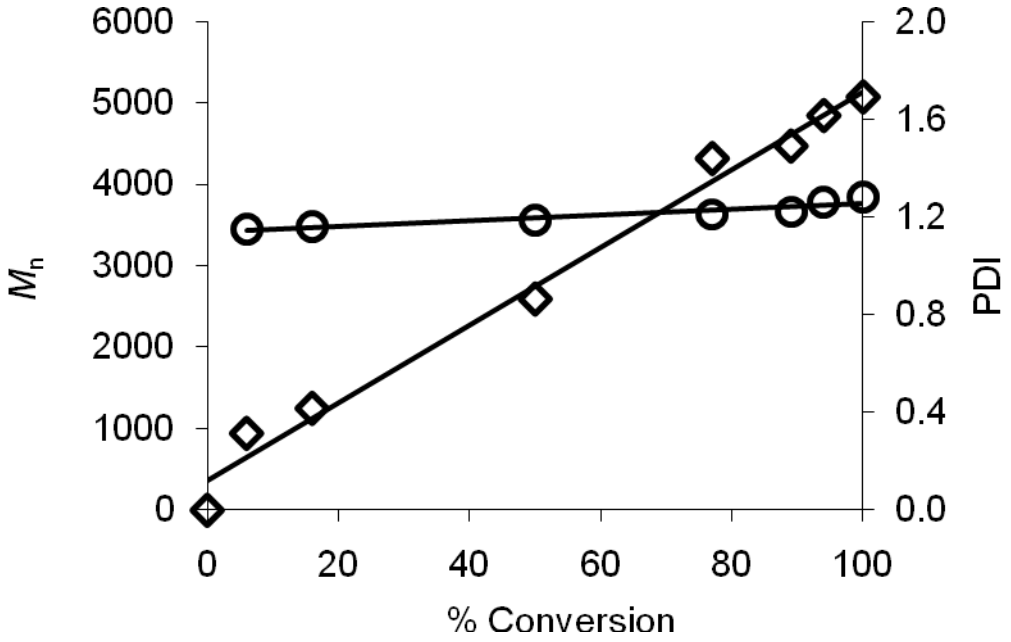
[a] Conditions: [ε-CL_0]/[**£c3.4£**] = 100:1, 6.8 mL toluene, 100 °C, 0.1 mL aliquots taken at the given intervals. See Experimental section for other details.

Figure S3.17. First order plot for ε-CL consumption using Ti(CyN_2^{Ts})(O^iPr)$_2$ (**£c3.4£**).[a]



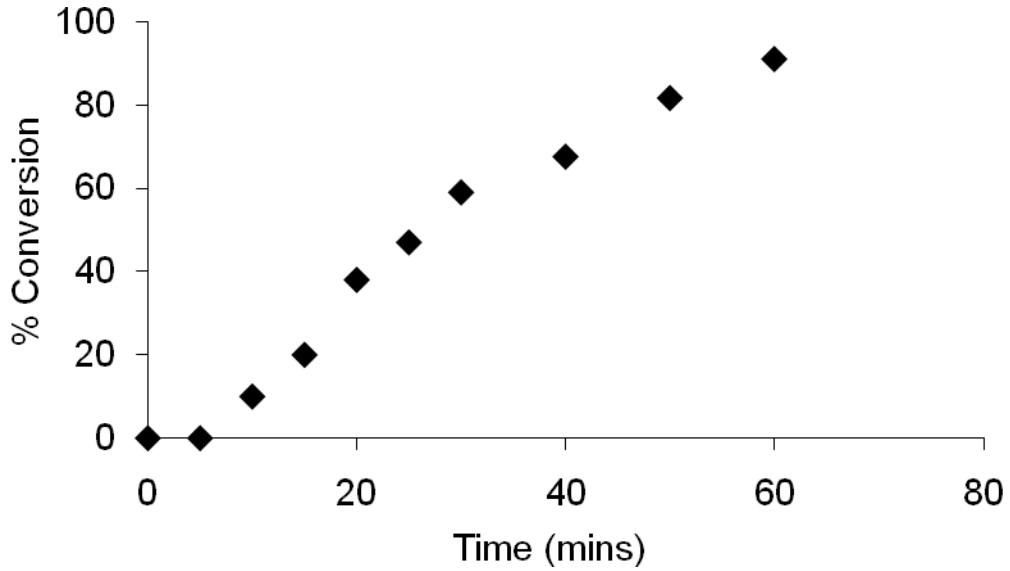
[a] Conditions: [ε-CL_0]/[**£c3.4£**] = 100:1, 6.8 mL toluene, 100 °C, 0.1 mL aliquots taken at the given intervals. See Experimental section for other details. Linear fit (r^2 = 0.987) shown is for the first order region after the induction period.

Figure S3.18. Plots of M_n and PDI (determined by GPC) *vs* conversion for the polymerization of ε-CL using Ti(CyN_2^{Ts})(O^iPr)$_2$ (**£c3.4£**).[a]



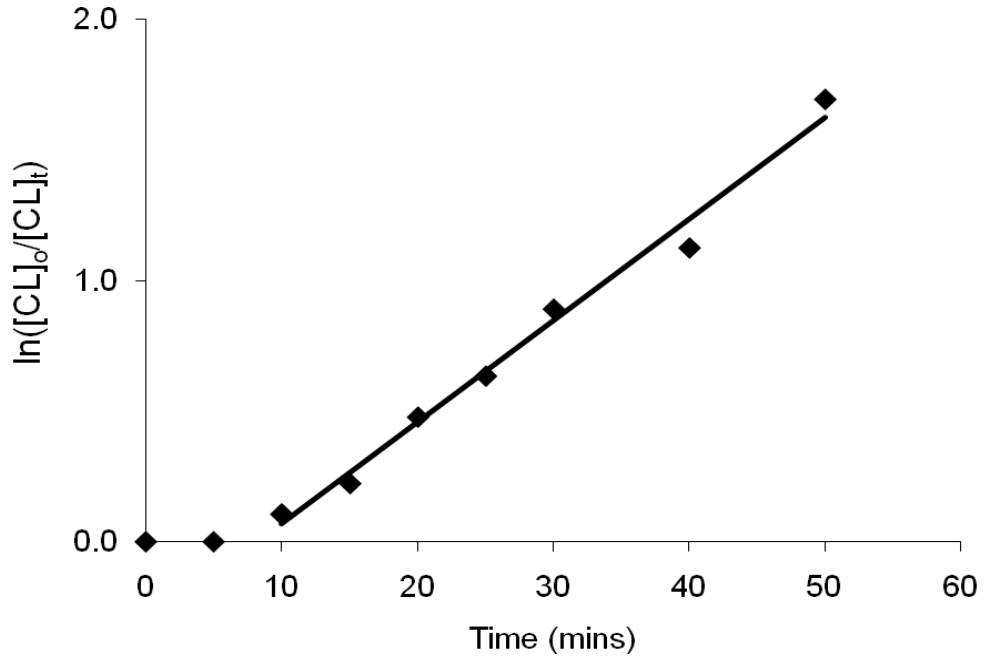
[a] Conditions: [ε-CL_0]/[**£c3.4£**] = 100:1, 6.8 mL toluene, 100 °C, 0.1 mL aliquots taken at the given intervals. Hollow diamonds correspond to M_n and hollow circles to PDI.

Figure S3.19. Plot for ε-CL consumption *vs* time using Ti($CyN_2^{SO_2Mes}$)(O^iPr)$_2$ (**£c3.5£**).[a]



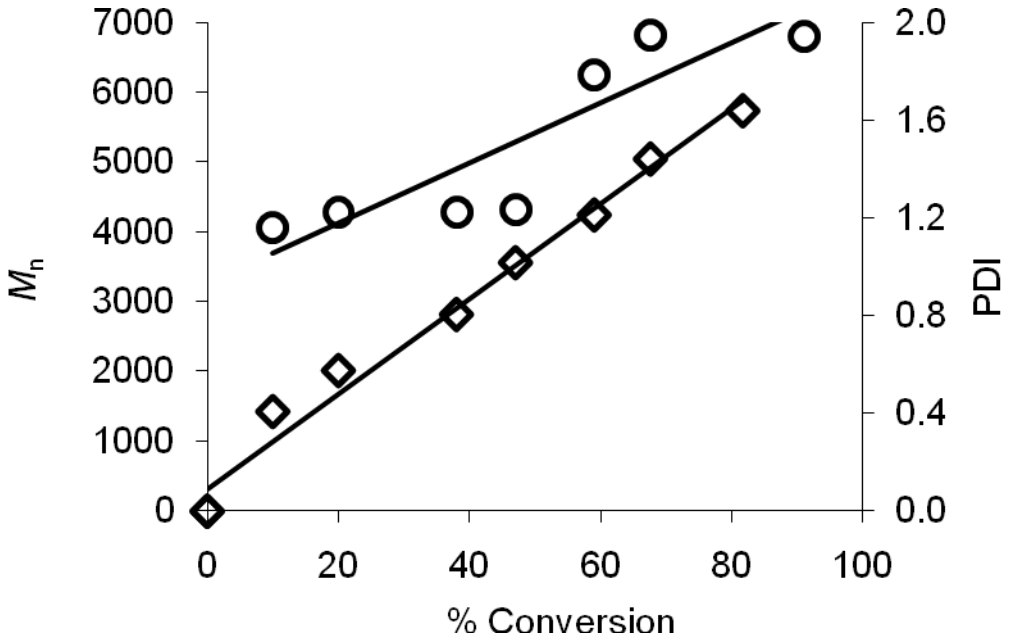
[a] Conditions: [ε-CL_0]/[**£c3.5£**] = 100:1, 6.8 mL toluene, 100 °C, 0.1 mL aliquots taken at the given intervals. See Experimental section for other details.

Figure S3.20. First order plot for ε-CL consumption using Ti($CyN_2^{SO_2Mes}$)(O^iPr)$_2$ (**£c3.5£**).[a]



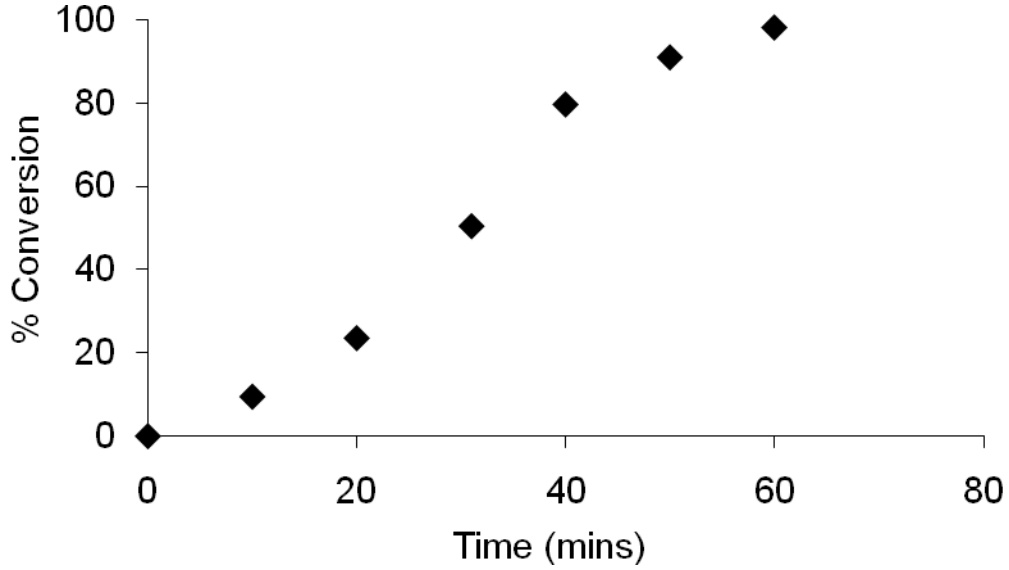
[a] Conditions: [ε-CL_0]/[**£c3.5£**] = 100:1, 6.8 mL toluene, 100 °C, 0.1 mL aliquots taken at the given intervals. See Experimental section for other details. Linear fit (r^2 = 0.988) shown is for the first order region after the induction period.

Figure S3.21. Plots of M_n and PDI (determined by GPC) *vs* conversion for the polymerization of ε-CL using $Ti(CyN_2^{SO_2Mes})(O^iPr)_2$ (**£c3.5£**).[a]



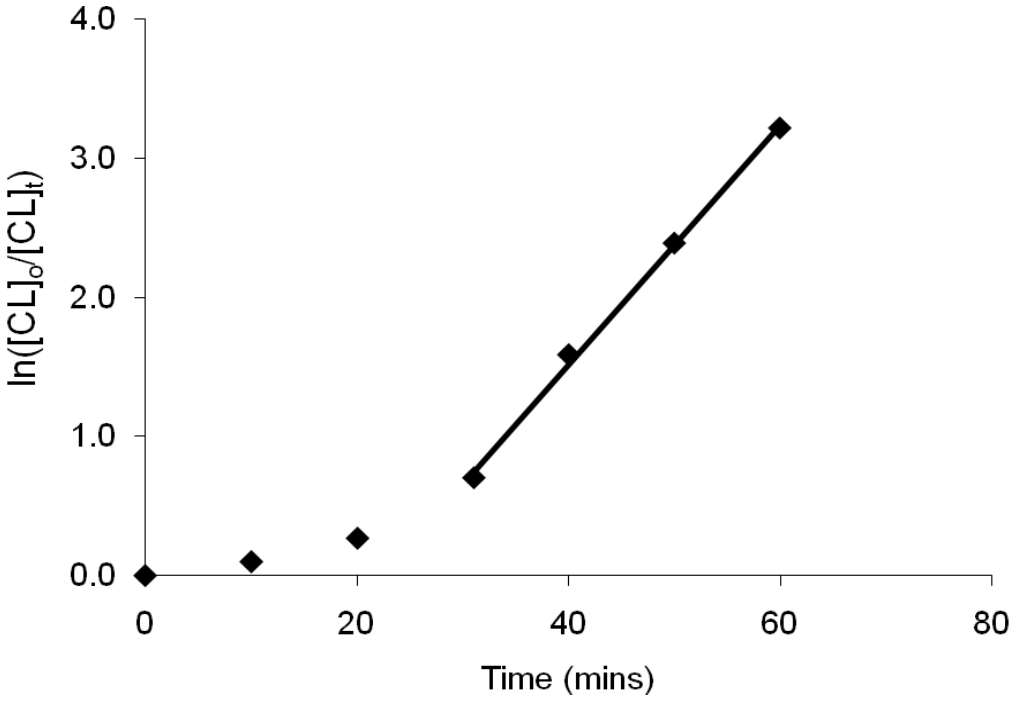
[a] Conditions: [ε-CL_0]/[**£c3.5£**] = 100:1, 6.8 mL toluene, 100 °C, 0.1 mL aliquots taken at the given intervals. Hollow diamonds correspond to M_n and hollow circles to PDI.

Figure S3.22. Plot for ε-CL consumption *vs* time using $Zr(N_3^{Ts}N)(CH_2SiMe_3)$ (**£c20£**).[a]



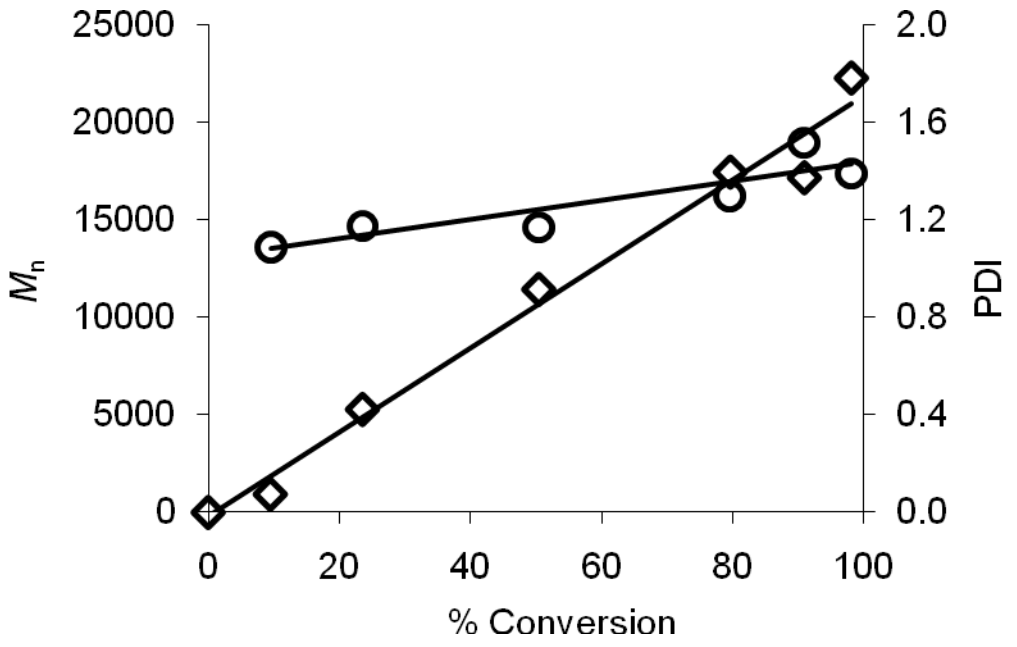
[a] Conditions: [ε-CL_0]/[**£c20£**] = 100:1, 6.8 mL toluene, 100 °C, 0.1 mL aliquots taken at the given intervals. See Experimental section for other details.

Figure S3.23. First order plot for ε-CL consumption using $Zr(N_3^{Ts}N)(CH_2SiMe_3)$ (**£c20£**).[a]



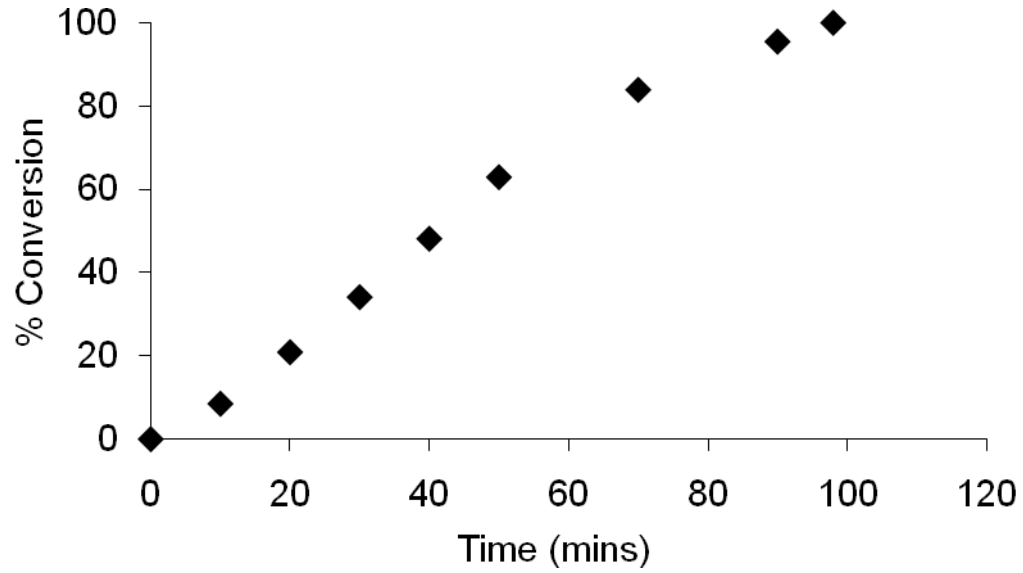
[a] Conditions: [ε-CL_0]/[**£c20£**] = 100:1, 6.8 mL toluene, 100 °C, 0.1 mL aliquots taken at the given intervals. See Experimental section for other details. Linear fit (r^2 = 0.998) shown is for the first order region after the induction period.

Figure S3.24. Plots of M_n and PDI (determined by GPC) *vs* conversion for the polymerization of ε-CL using $Zr(N_3^{Ts}N)(CH_2SiMe_3)$ (**£c20£**).[a]



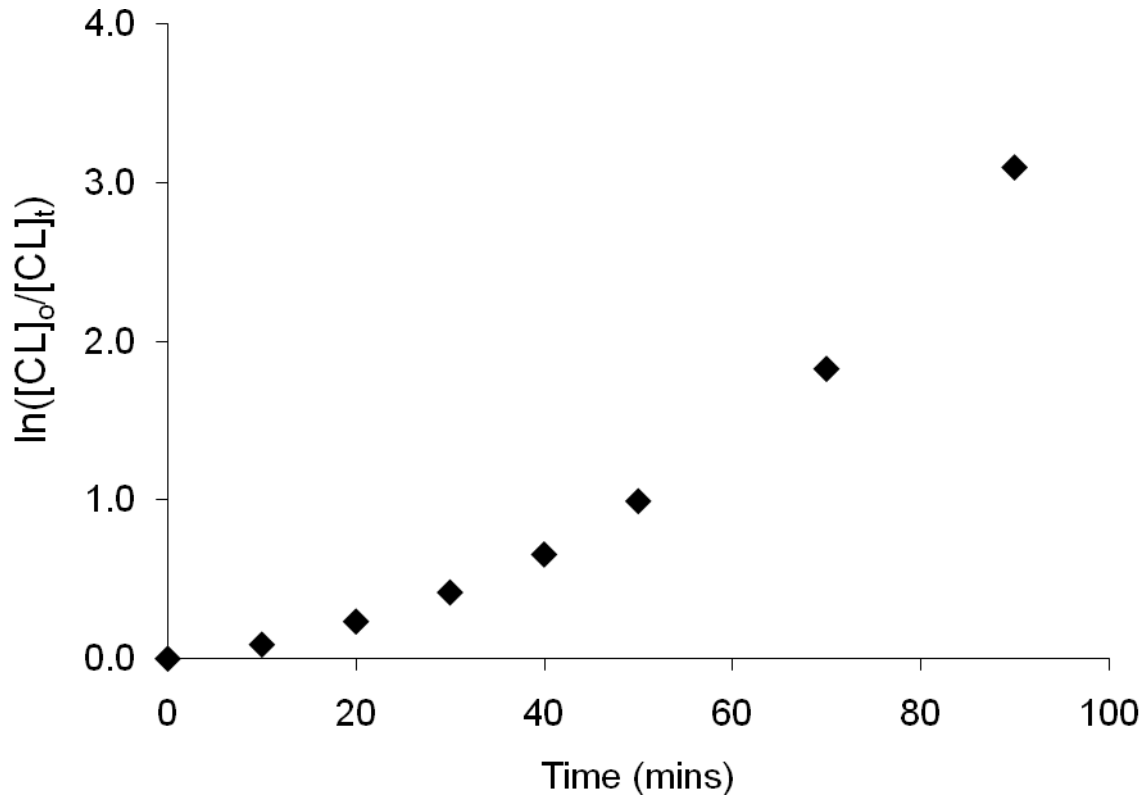
[a] Conditions: [ε-CL_0]/[**£c20£**] = 100:1, 6.8 mL toluene, 100 °C, 0.1 mL aliquots taken at the given intervals. Hollow diamonds correspond to M_n and hollow circles to PDI.

Figure S3.25. Plot for ε-CL consumption *vs* time using $Zr(N_3^{TArF}N)(CH_2SiMe_3)$ (**£c21£**).[a]



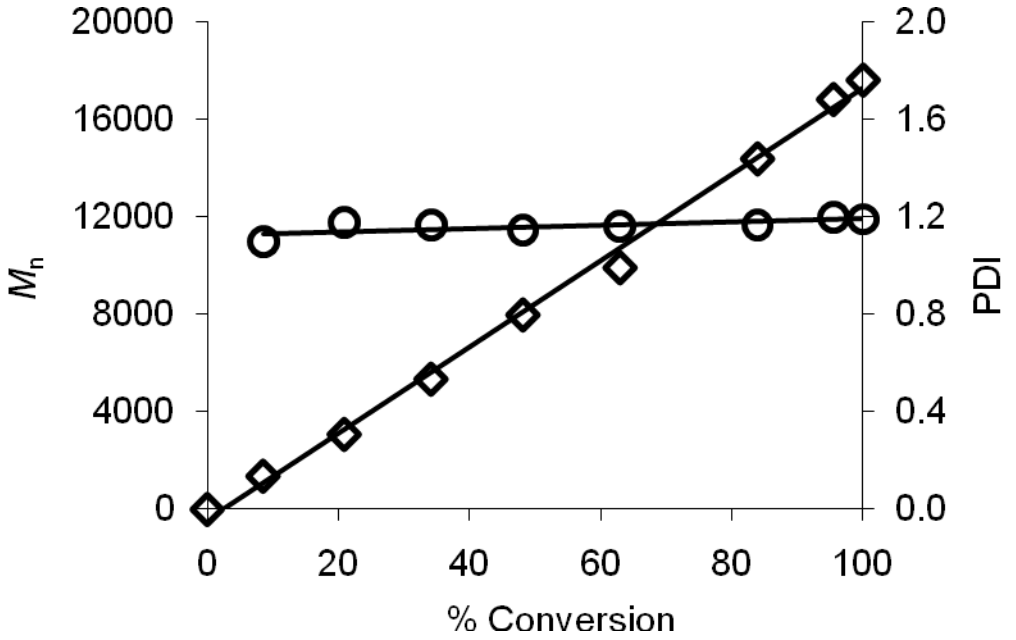
[a] Conditions: $[\varepsilon\text{-}CL_0]/[$**£c21£**$]$ = 100:1, 6.8 mL toluene, 100 °C, 0.1 mL aliquots taken at the given intervals. See Experimental section for other details.

Figure S3.26. First order plot for ε-CL consumption using $Zr(N_3^{TArF}N)(CH_2SiMe_3)$ (**£c21£**).[a]



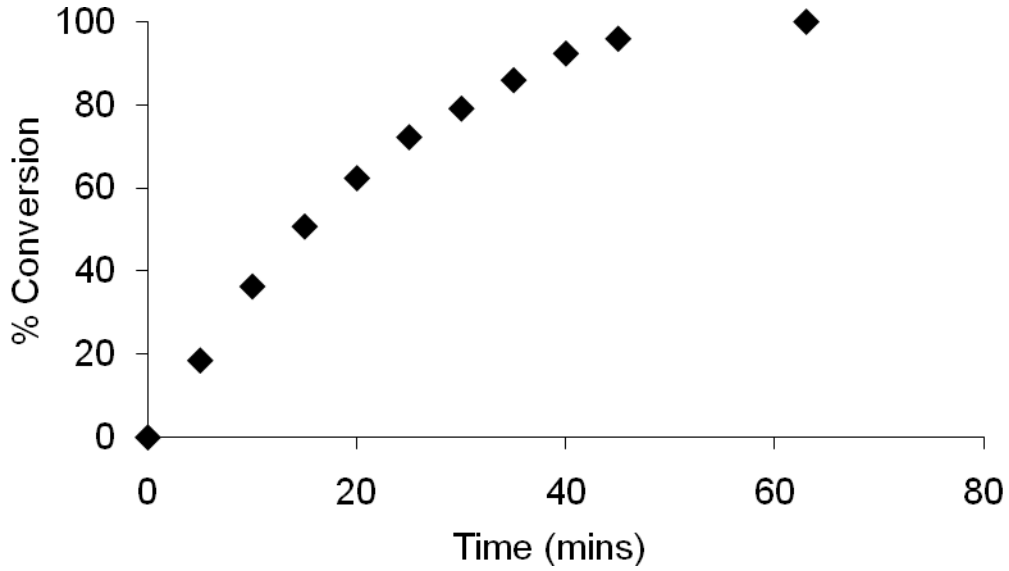
[a] Conditions: $[\varepsilon\text{-}CL_0]/[$**£c21£**$]$ = 100:1, 6.8 mL toluene, 100 °C, 0.1 mL aliquots taken at the given intervals. See Experimental section for other details. No Linear fit was possible.

Figure S3.27. Plots of M_n and PDI (determined by GPC) *vs* conversion for the polymerization of ε-CL using $Zr(N_3^{TArF}N)(CH_2SiMe_3)$ (**£c21£**).[a]



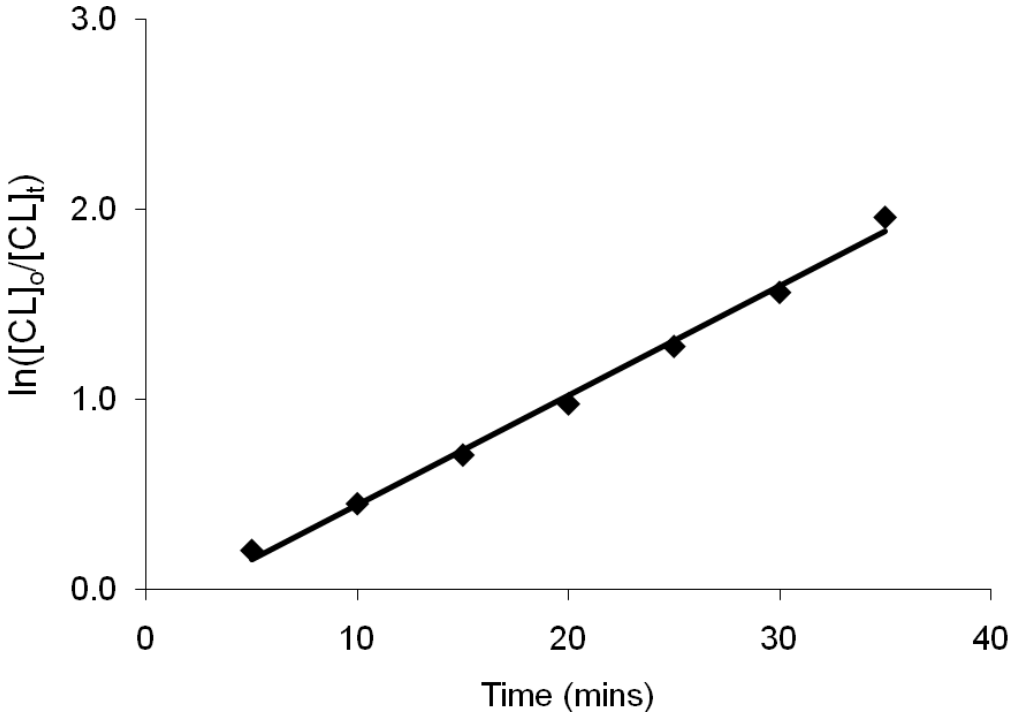
[a] Conditions: [ε-CL_0]/[**£c21£**] = 100:1, 6.8 mL toluene, 100 °C, 0.1 mL aliquots taken at the given intervals. Hollow diamonds correspond to M_n and hollow circles to PDI.

Figure S3.28. Plot for ε-CL consumption *vs* time using $Zr(N_3^{Ms}N)(CH_2SiMe_3)$ (**£c22£**).[a]



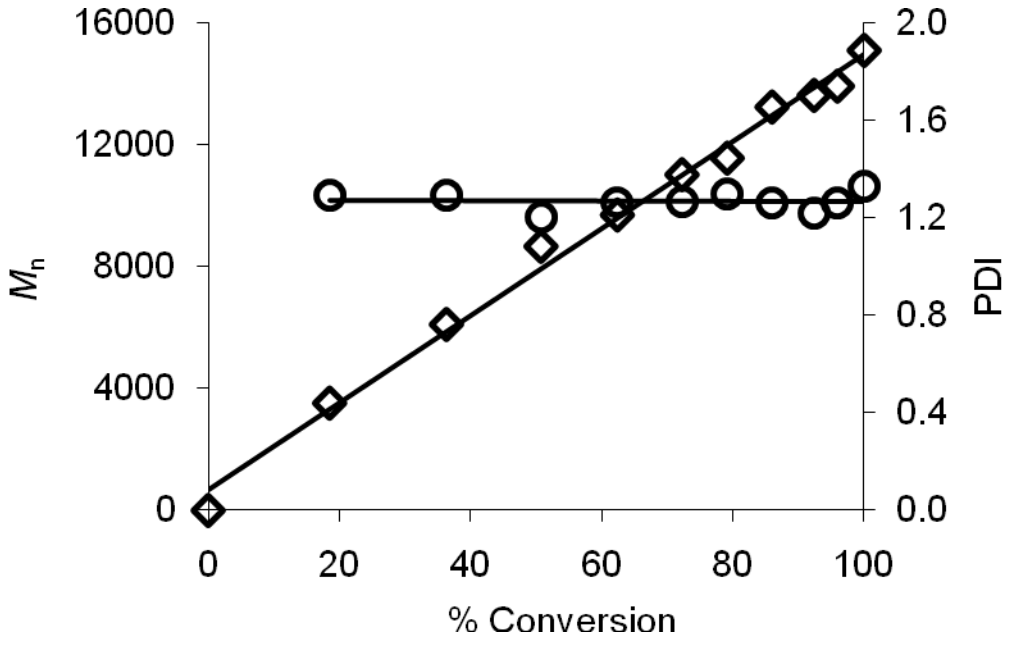
[a] Conditions: [ε-CL_0]/[**£c22£**] = 100:1, 6.8 mL toluene, 100 °C, 0.1 mL aliquots taken at the given intervals. See Experimental section for other details.

Figure S3.29. First order plot for ε-CL consumption using $Zr(N_3^{Ms}N)(CH_2SiMe_3)$ (**£c22£**).[a]



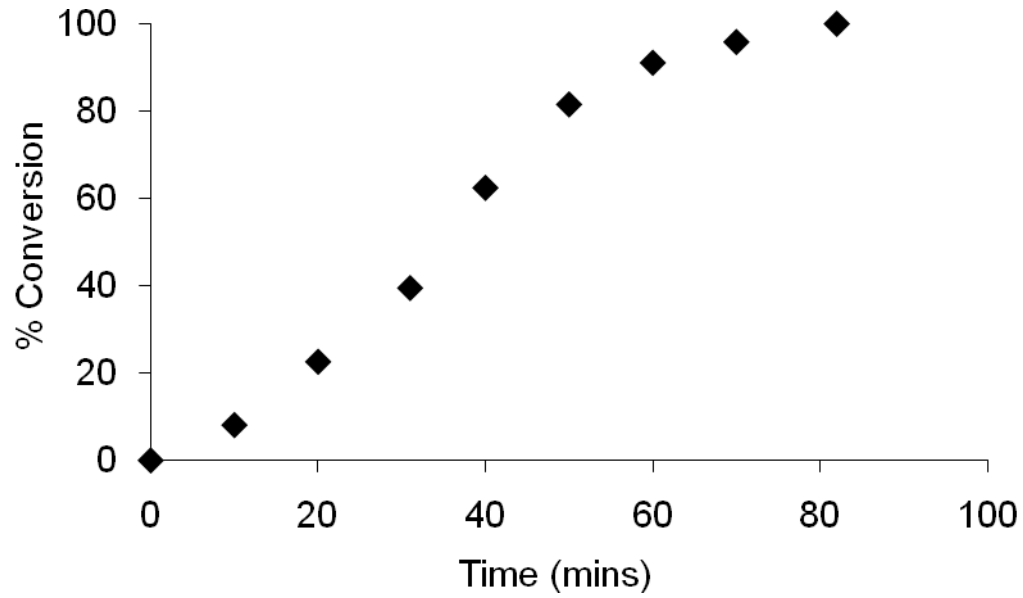
[a] Conditions: [ε-CL_0]/[**£c22£**] = 100:1, 6.8 mL toluene, 100 °C, 0.1 mL aliquots taken at the given intervals. See Experimental section for other details. Linear fit (r^2 = 0.995) shown is for the first order region after the induction period.

Figure S3.30. Plots of M_n and PDI (determined by GPC) *vs* conversion for the polymerization of ε-CL using $Zr(N_3^{Ms}N)(CH_2SiMe_3)$ (**£c22£**).[a]



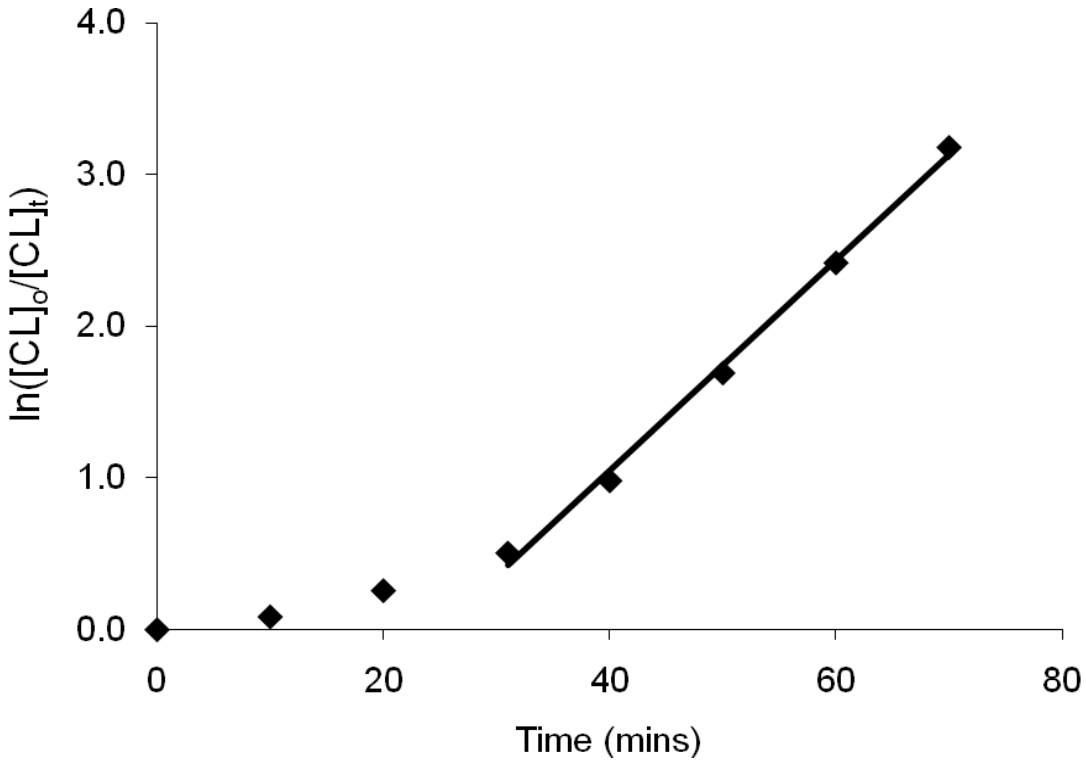
[a] Conditions: [ε-CL_0]/[**£c22£**] = 100:1, 6.8 mL toluene, 100 °C, 0.1 mL aliquots taken at the given intervals. Hollow diamonds correspond to M_n and hollow circles to PDI.

Figure S3.31. Plot for ε-CL consumption *vs* time using $Zr(N_3^{TArF}N)(NMe_2)$ (**£c23£**).[a]



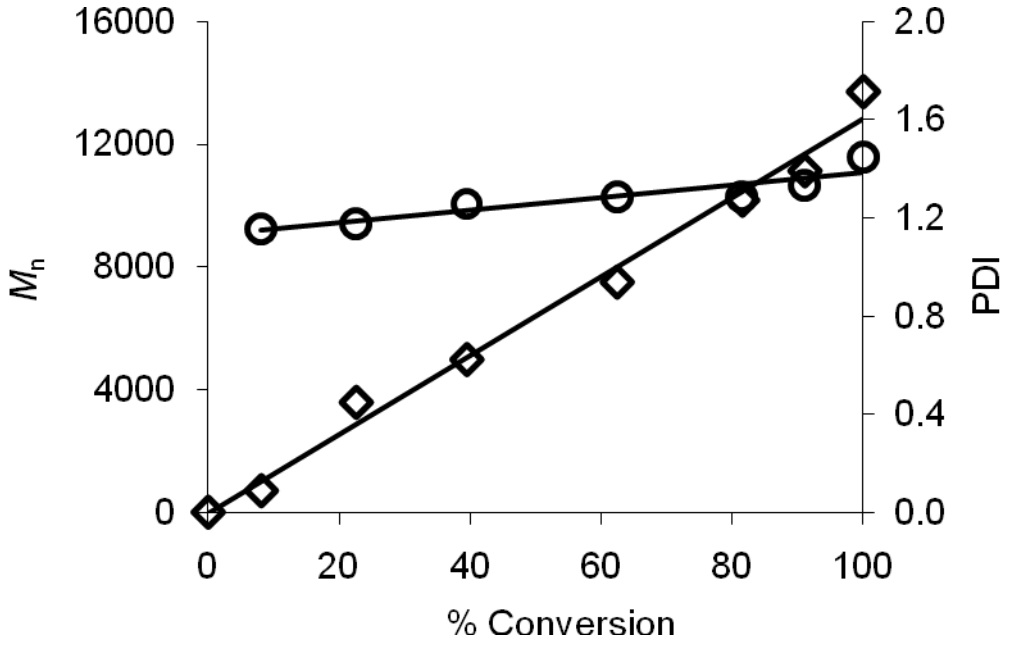
[a] Conditions: [ε-CL_0]/[**£c23£**] = 100:1, 6.8 mL toluene, 100 °C, 0.1 mL aliquots taken at the given intervals. See Experimental section for other details.

Figure S3.32. First order plot for ε-CL consumption using $Zr(N_3^{TArF}N)(NMe_2)$ (**£c23£**).[a]



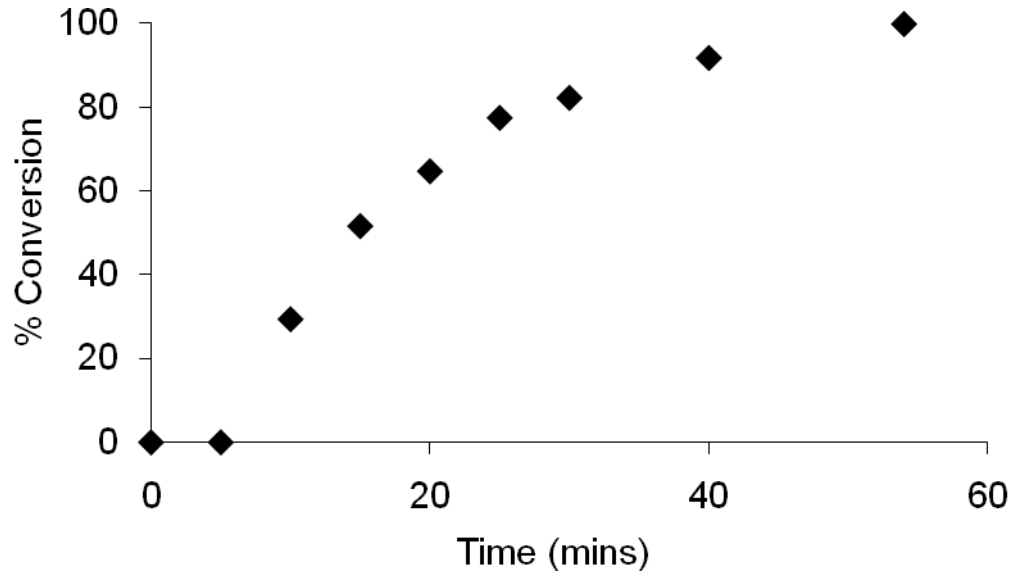
[a] Conditions: [ε-CL_0]/[**£c23£**] = 100:1, 6.8 mL toluene, 100 °C, 0.1 mL aliquots taken at the given intervals. See Experimental section for other details. Linear fit (r^2 = 0.997) shown is for the first order region after the induction period.

Figure S3.33. Plots of M_n and PDI (determined by GPC) *vs* conversion for the polymerization of ε-CL using Zr(N_3^{TArF}N)(NMe_2) (**£c23£**).[a]



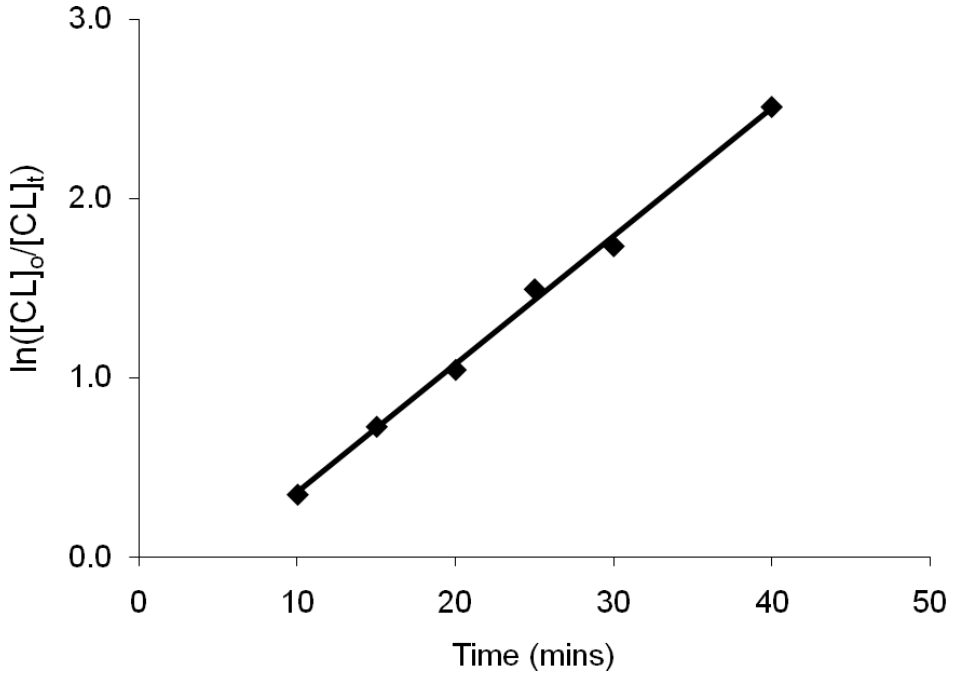
[a] Conditions: [ε-CL_0]/[**£c23£**] = 100:1, 6.8 mL toluene, 100 °C, 0.1 mL aliquots taken at the given intervals. Hollow diamonds correspond to M_n and hollow circles to PDI.

Figure S3.34. Plot for ε-CL consumption *vs* time using Zr(N_3^{Ts}N)(CH_2SiMe_3) (**£c20£**) and HO^iPr.[a]



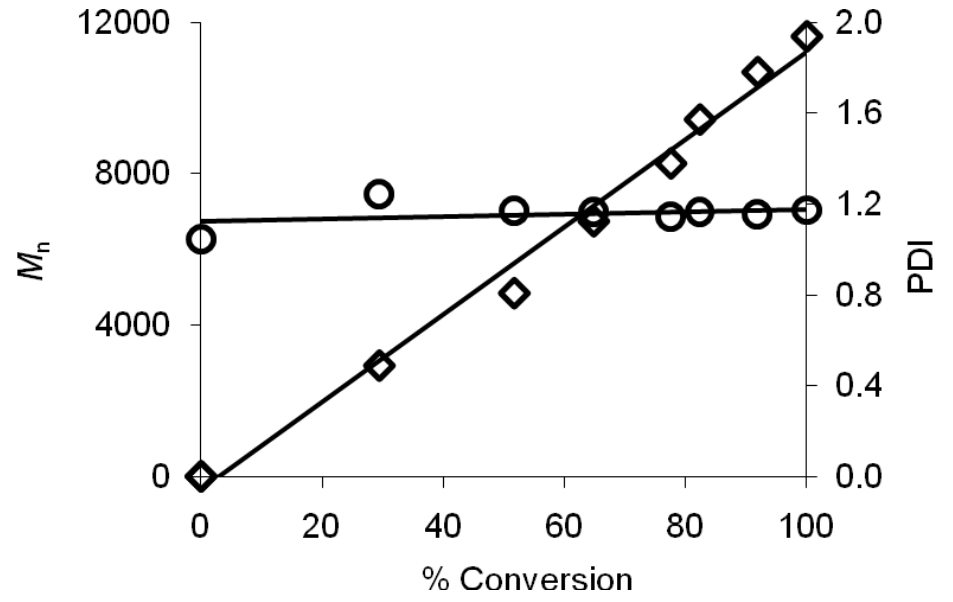
[a] Conditions: [ε-CL_0]/[**£c20£**]/[HO^iPr] = 100:1:1, 6.8 mL toluene, 100 °C, 0.1 mL aliquots taken at the given intervals. See Experimental section for other details.

Figure S3.35. First order plot for ε-CL consumption using $Zr(N_3^{Ts}N)(CH_2SiMe_3)$ (**£c20£**) and HO^iPr.[a]



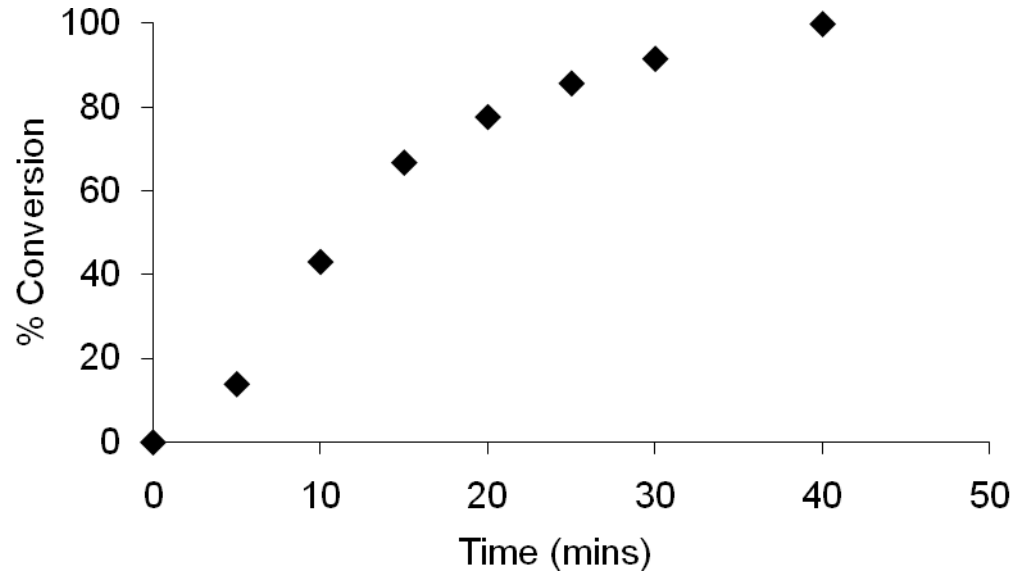
[a] Conditions: [ε-CL_0]/[**£c20£**]/[HO^iPr] = 100:1:1, 6.8 mL toluene, 100 °C, 0.1 mL aliquots taken at the given intervals. See Experimental section for other details. Linear fit (r^2 = 0.997) shown is for the first order region after the induction period.

Figure S3.36. Plots of M_n and PDI (determined by GPC) *vs* conversion for the polymerization of ε-CL using $Zr(N_3^{Ts}N)(CH_2SiMe_3)$ (**£c20£**) and HO^iPr.[a]



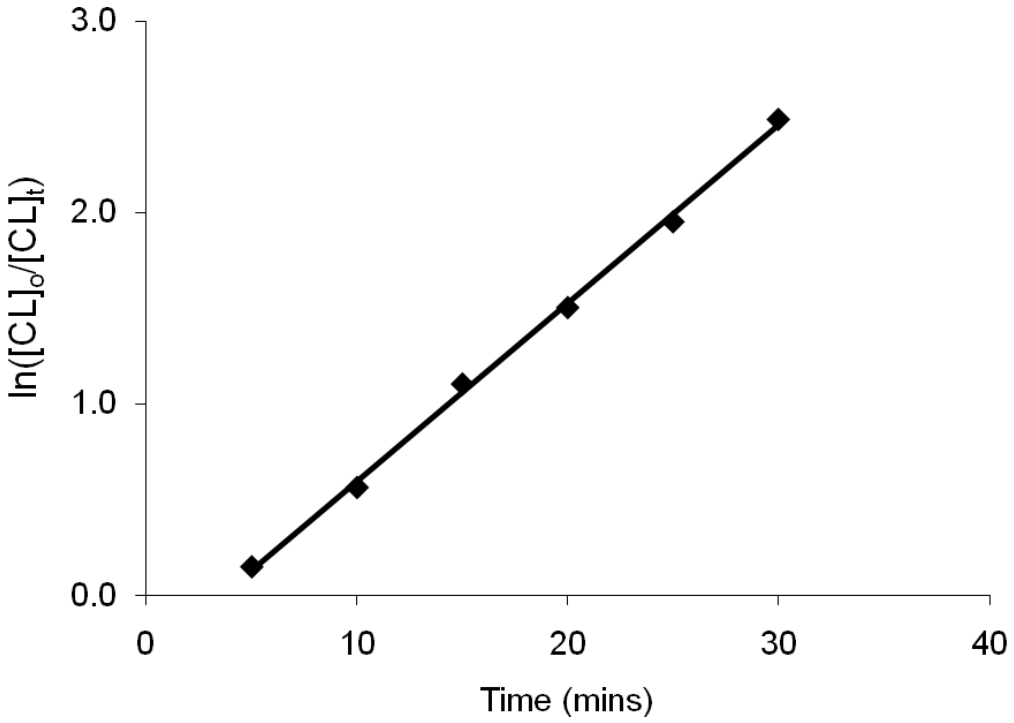
[a] Conditions: [ε-CL_0]/[**£c20£**]/[HO^iPr] = 100:1:1, 6.8 mL toluene, 100 °C, 0.1 mL aliquots taken at the given intervals. Hollow diamonds correspond to M_n and hollow circles to PDI.

Figure S3.37. Plot for ε-CL consumption *vs* time using $Zr(N_3^{Ms}N)(CH_2SiMe_3)$ (**£c21£**) and HO^iPr.[a]



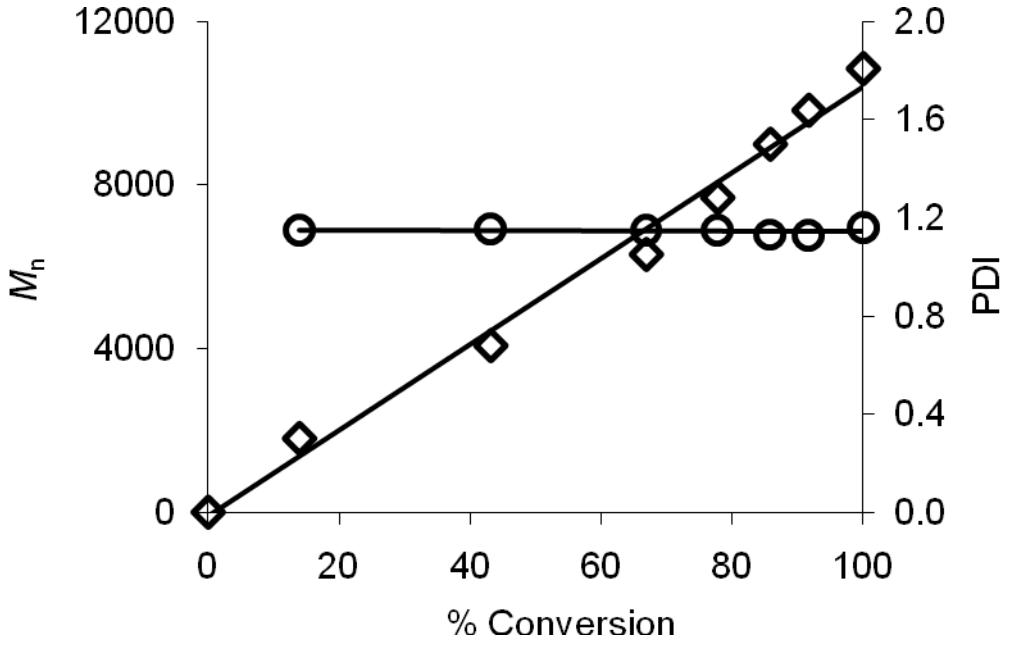
[a] Conditions: [ε-CL_0]/[**£c21£**]/[HO^iPr] = 100:1:1, 6.8 mL toluene, 100 °C, 0.1 mL aliquots taken at the given intervals. See Experimental section for other details.

Figure S3.38. First order plot for ε-CL consumption using $Zr(N_3^{Ms}N)(CH_2SiMe_3)$ (**£c21£**) and HO^iPr.[a]



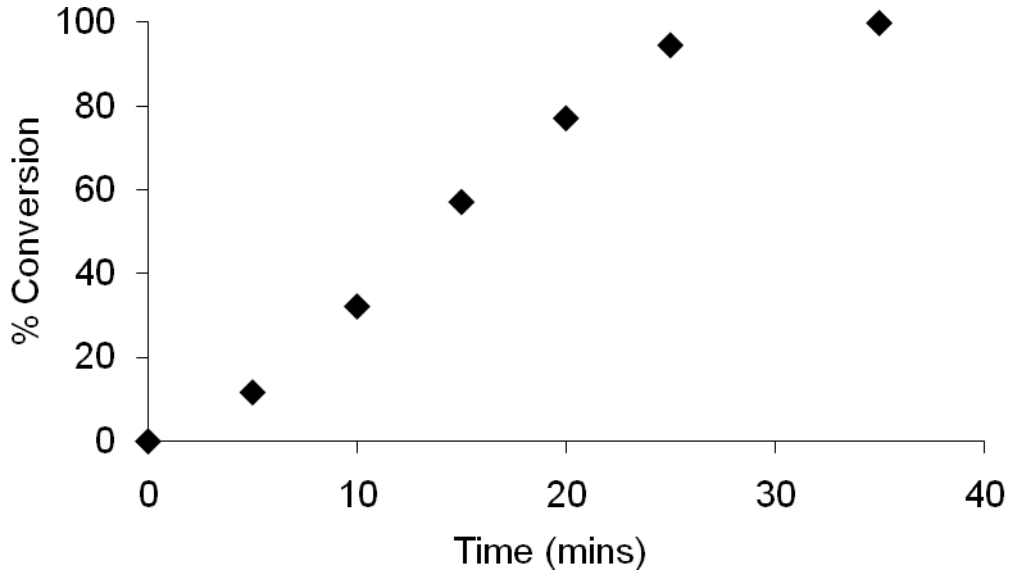
[a] Conditions: [ε-CL_0]/[**£c21£**]/[HO^iPr] = 100:1:1, 6.8 mL toluene, 100 °C, 0.1 mL aliquots taken at the given intervals. See Experimental section for other details. Linear fit (r^2 = 0.998) shown is for the first order region after the induction period.

Figure S3.39. Plots of M_n and PDI (determined by GPC) *vs* conversion for the polymerization of ε-CL using $Zr(N_3^{Ms}N)(CH_2SiMe_3)$ (**£c21£**) and HO^iPr.[a]



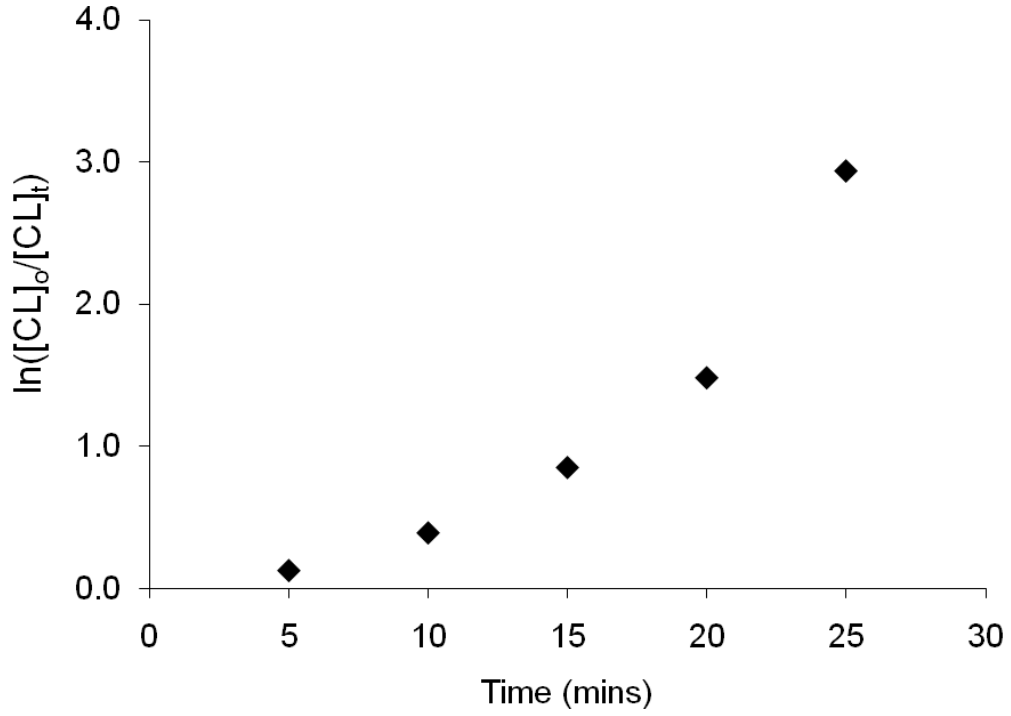
[a] Conditions: [ε-CL_0]/[**£c21£**]/[HO^iPr] = 100:1:1, 6.8 mL toluene, 100 °C, 0.1 mL aliquots taken at the given intervals. Hollow diamonds correspond to M_n and hollow circles to PDI.

Figure S3.40. Plot for ε-CL consumption *vs* time using $Zr(N_3^{TArF}N)(CH_2SiMe_3)$ (**£c22£**) and HO^iPr.[a]



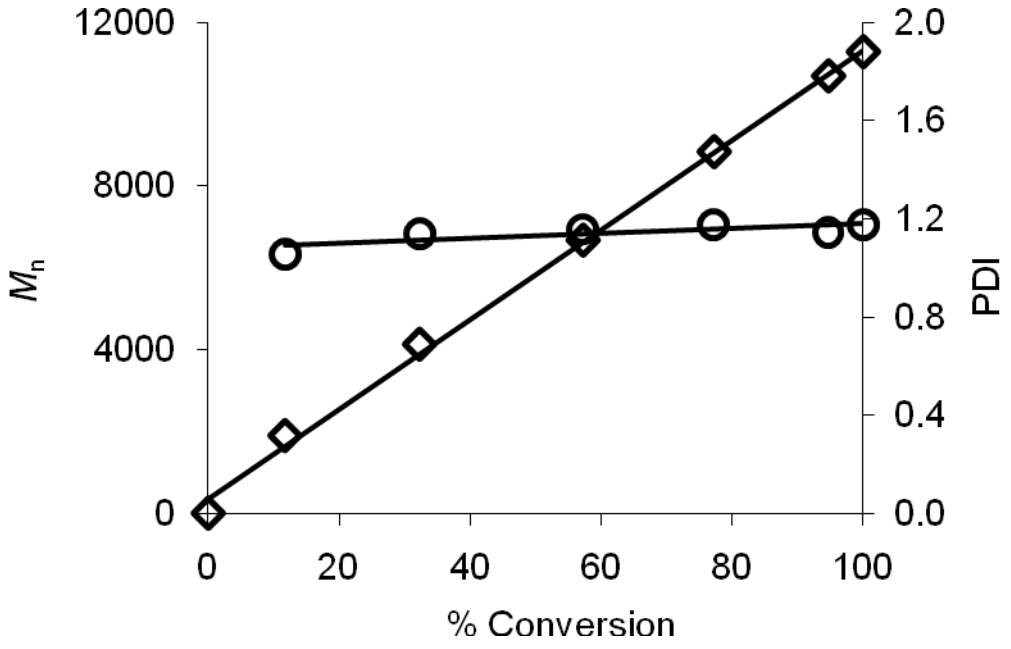
[a] Conditions: [ε-CL_0]/[**£c22£**]/[HO^iPr] = 100:1:1, 6.8 mL toluene, 100 °C, 0.1 mL aliquots taken at the given intervals. See Experimental section for other details.

Figure S3.41. First order plot for ε-CL consumption using $Zr(N_3^{TArF}N)(CH_2SiMe_3)$ (**£c22£**) and HO^iPr.[a]



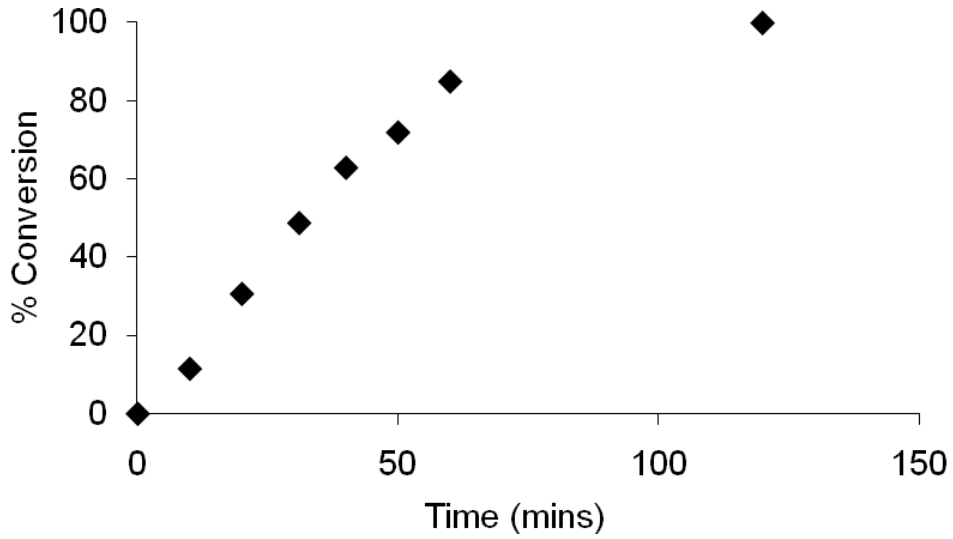
[a] Conditions: [ε-CL_0]/[**£c22£**]/[HO^iPr] = 100:1:1, 6.8 mL toluene, 100 °C, 0.1 mL aliquots taken at the given intervals. See Experimental section for other details. No Linear fit was possible.

Figure S3.42. Plots of M_n and PDI (determined by GPC) *vs* conversion for the polymerization of ε-CL using $Zr(N_3^{TArF}N)(CH_2SiMe_3)$ (**£c22£**) and HO^iPr.[a]



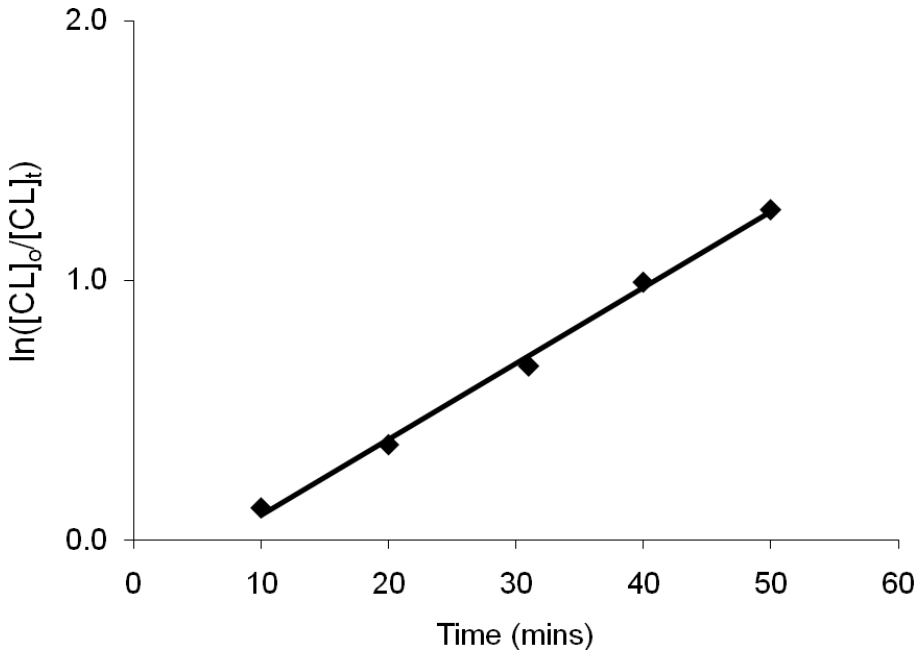
[a] Conditions: [ε-CL_0]/[**£c22£**]/[HO^iPr] = 100:1:1, 6.8 mL toluene, 100 °C, 0.1 mL aliquots taken at the given intervals. Hollow diamonds correspond to M_n and hollow circles to PDI.

Figure S3.43. Plot for ε-CL consumption *vs* time using Zr(N_3^{TArF}N)(NMe_2) (**£c23£**) and HO(2,6-($C_6H_3Me_2$).[a]



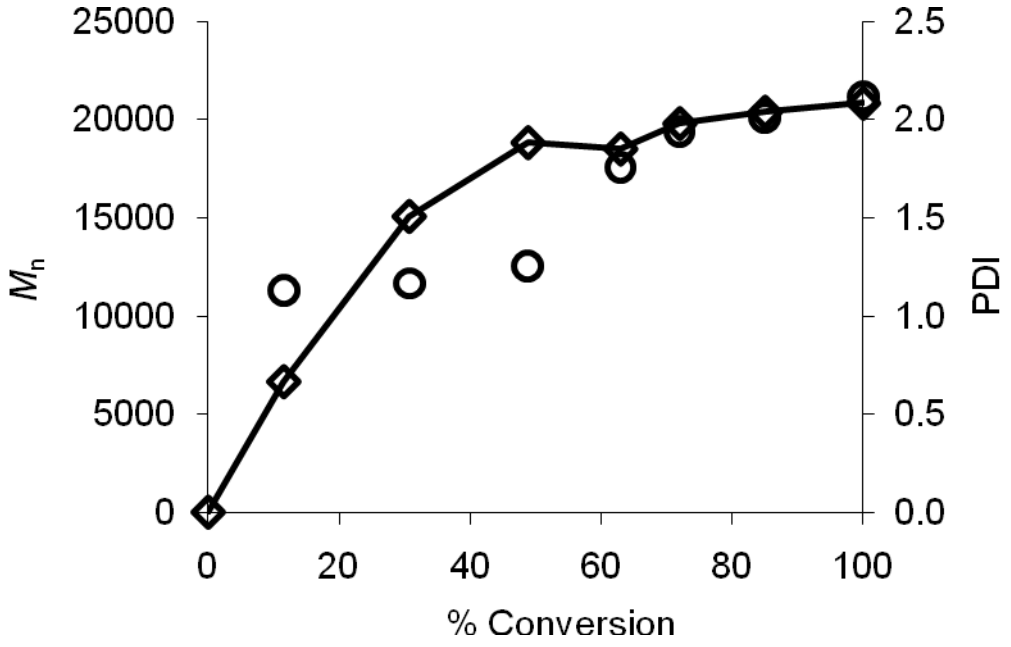
[a] Conditions: [ε-CL_0]/[**£c23£**]/[HO(2,6-($C_6H_3Me_2$)] = 100:1:1, 6.8 mL toluene, 100 °C, 0.1 mL aliquots taken at the given intervals. See Experimental section for other details.

Figure S3.44. First order plot for ε-CL consumption using Zr(N_3^{TArF}N)(NMe_2) (**£c23£**) and HO(2,6-($C_6H_3Me_2$).[a]



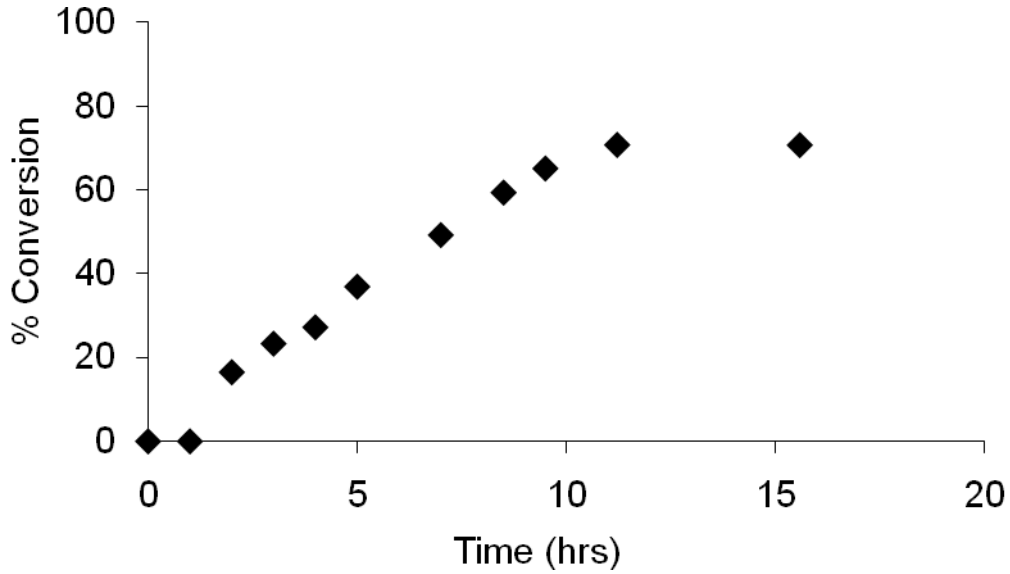
[a] Conditions: [ε-CL_0]/[**£c23£**]/[HO(2,6-($C_6H_3Me_2$)] = 100:1:1, 6.8 mL toluene, 100 °C, 0.1 mL aliquots taken at the given intervals. See Experimental section for other details. Linear fit (r^2 = 0.996) shown is for the first order region after the induction period.

Figure S3.45. Plots of M_n and PDI (determined by GPC) *vs* conversion for the polymerization of ε-CL using Zr($N_3^{TArF}N$)(NMe_2) (**£c23£**) and HO(2,6-($C_6H_3Me_2$).[a]



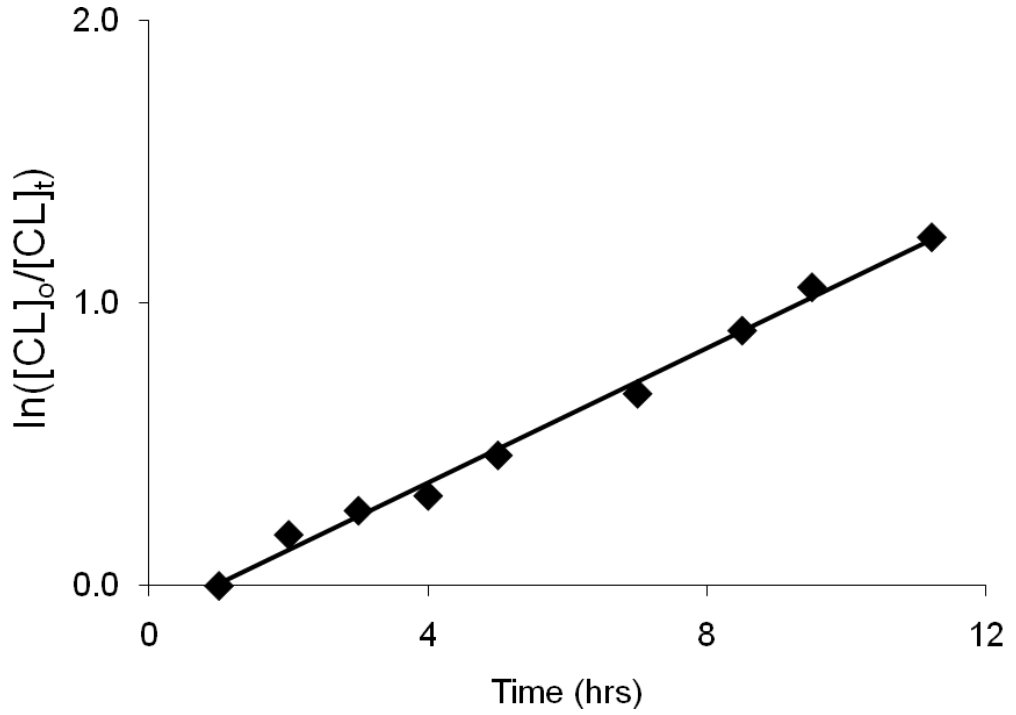
[a] Conditions: [ε-CL_0]/[**£c23£**]/[HO(2,6-($C_6H_3Me_2$)] = 100:1:1, 6.8 mL toluene, 100 °C, 0.1 mL aliquots taken at the given intervals. Hollow diamonds correspond to M_n and hollow circles to PDI.

Figure S3.46. Plot for rac-LA consumption *vs* time using Ti($N_2^{Ts}N^{Ph}$)(O^iPr)$_2$ (**£c13£**).[a]



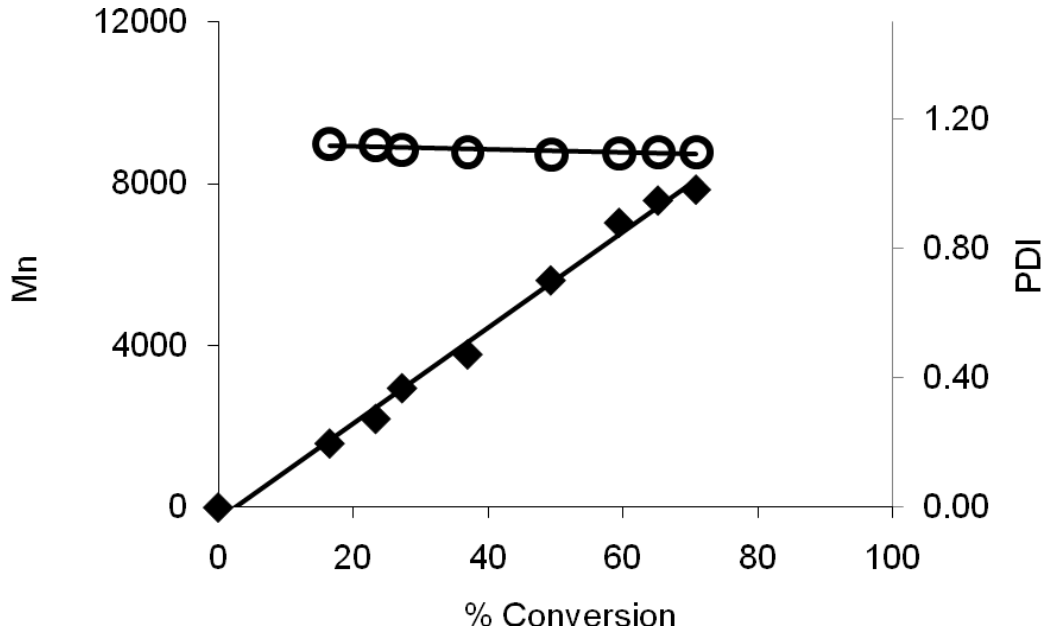
[a] Conditions: [rac-LA_0]/[**£c13£**] = 100:1, 6.8 mL toluene, 70 °C, 0.1 mL aliquots taken at the given intervals. See Experimental section for other details.

Figure S3.47. First order plot for *rac*-LA consumption using Ti($N_2^{Ts}N^{Ph}$)(O^iPr)$_2$ (**£c13£**).[a]



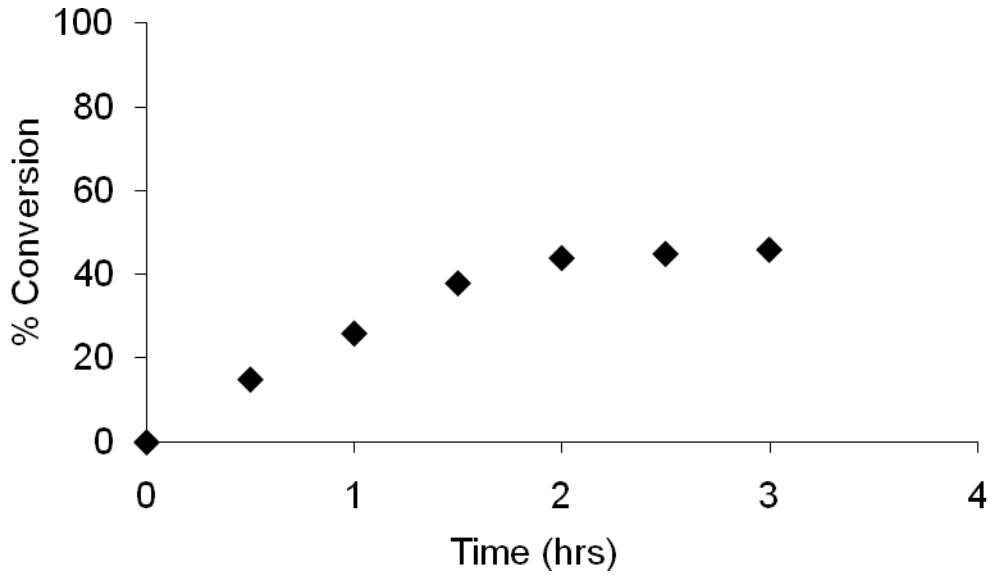
[a.] Conditions [*rac*-LA_0]/[**£c13£**] = 100:1, 6 mL toluene, 70 °C, 0.1 mL aliquots taken at the given intervals. See Experimental section for other details. Linear fit (r^2 = 0.994) shown is for the first order region after the induction period.

Figure S3.48. Plots of M_n and PDI (determined by GPC) *vs* conversion for the solution polymerisation of *rac*-LA using Ti($N_2^{Ts}N^{Ph}$)(O^iPr)$_2$ (**£c13£**).[a]



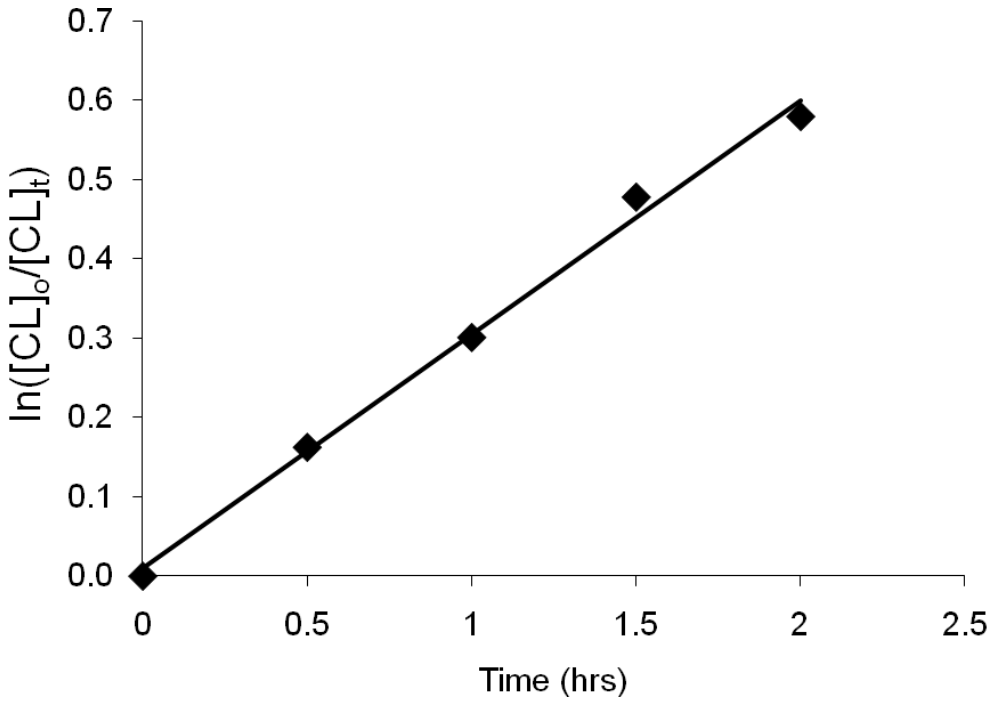
[a] Conditions: [*rac*-LA_0]/[**£c13£**] = 100:1, 6.0 mL toluene, 70 °C, 0.1 mL aliquots taken at the given intervals. Hollow diamonds correspond to M_n and hollow circles to PDI.

Figure S3.49. Plot for rac-LA consumption *vs* time using Ti($N_2^{Ms}N^{Ph}$)(O^iPr)$_2$ (**£c15£**).[a]



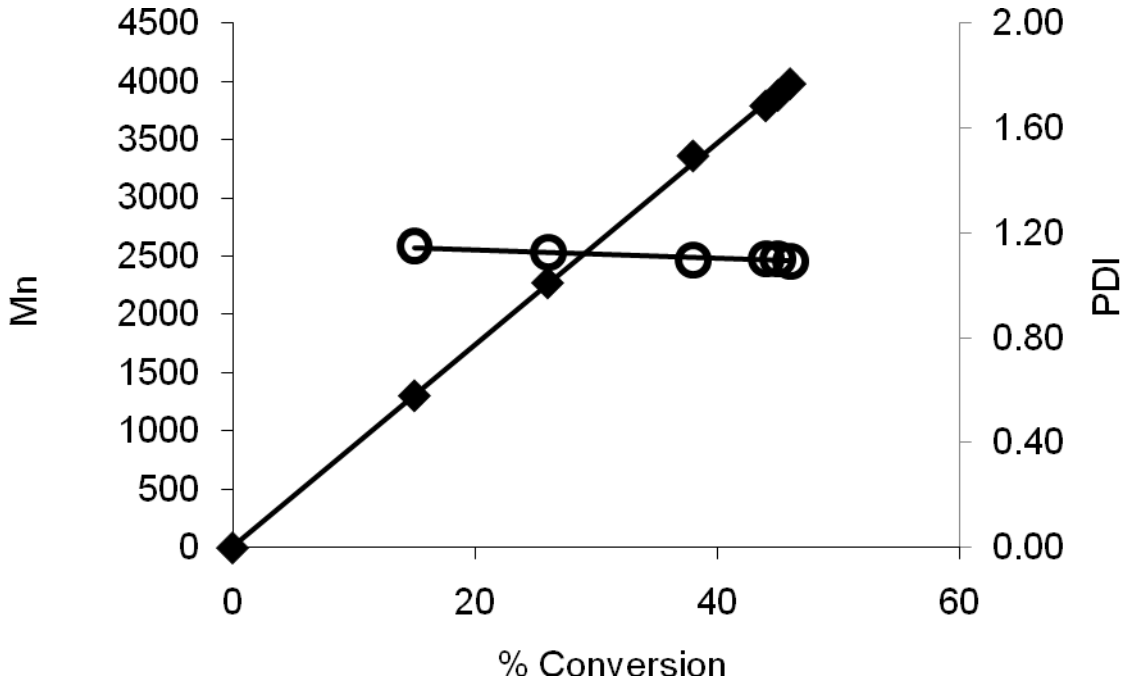
[a] Conditions: [rac-LA_0]/[**£c15£**] = 100:1, 6.8 mL toluene, 70 °C, 0.1 mL aliquots taken at the given intervals. See Experimental section for other details.

Figure S3.50. First order plot for *rac*-LA consumption using Ti($N_2^{Ms}N^{Ph}$)(O^iPr)$_2$ (**£c15£**).[a]



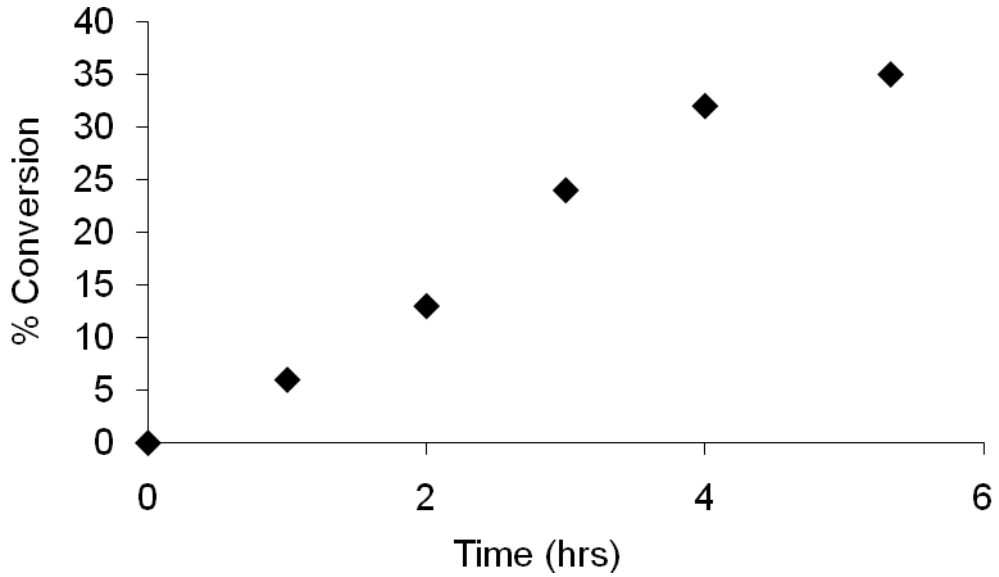
[a.] Conditions [*rac*-LA_0]/[**£c15£**] = 100:1, 6 mL toluene, 70 °C, 0.1 mL aliquots taken at the given intervals. See Experimental section for other details. Linear fit (r^2 = 0.994) shown is for the first order region after the induction period.

Figure S3.51. Plots of M_n and PDI (determined by GPC) *vs* conversion for the solution polymerisation of *rac*-LA using Ti($N_2^{Ms}N^{Ph}$)(O^iPr)$_2$ (**£c15£**).[a]



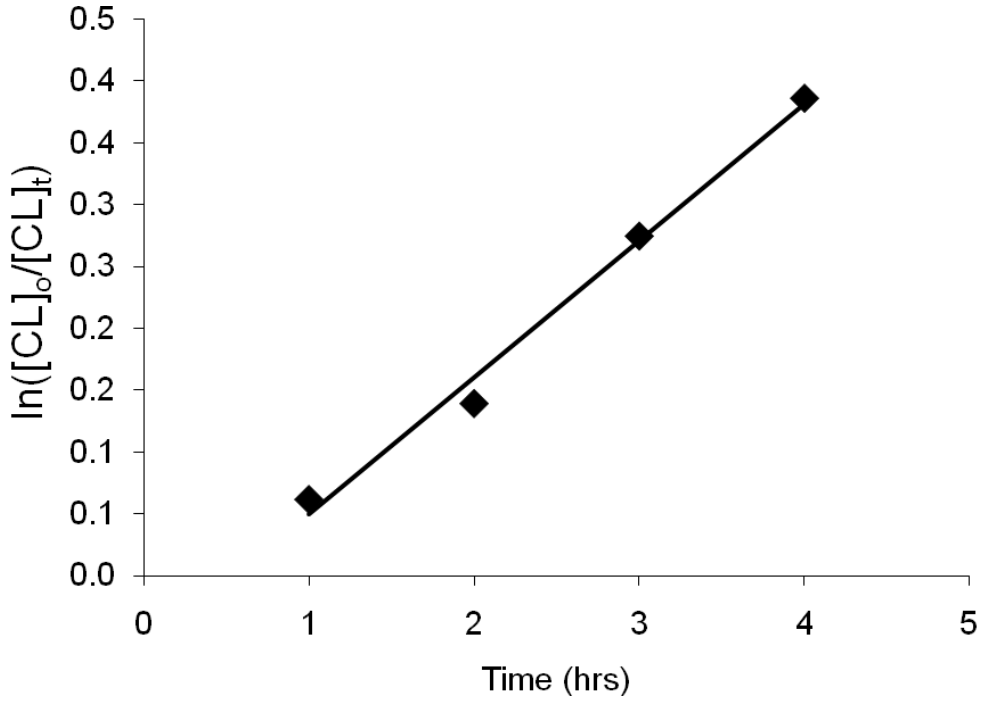
[a] Conditions: [*rac*-LA_0]/[**£c15£**] = 100:1, 6.0 mL toluene, 70 °C, 0.1 mL aliquots taken at the given intervals. Hollow diamonds correspond to M_n and hollow circles to PDI.

Figure S3.52. Plot for rac-LA consumption *vs* time using Ti(CyN_2^{Ts})(O^iPr)$_2$ (**£c3.4£**).[a]



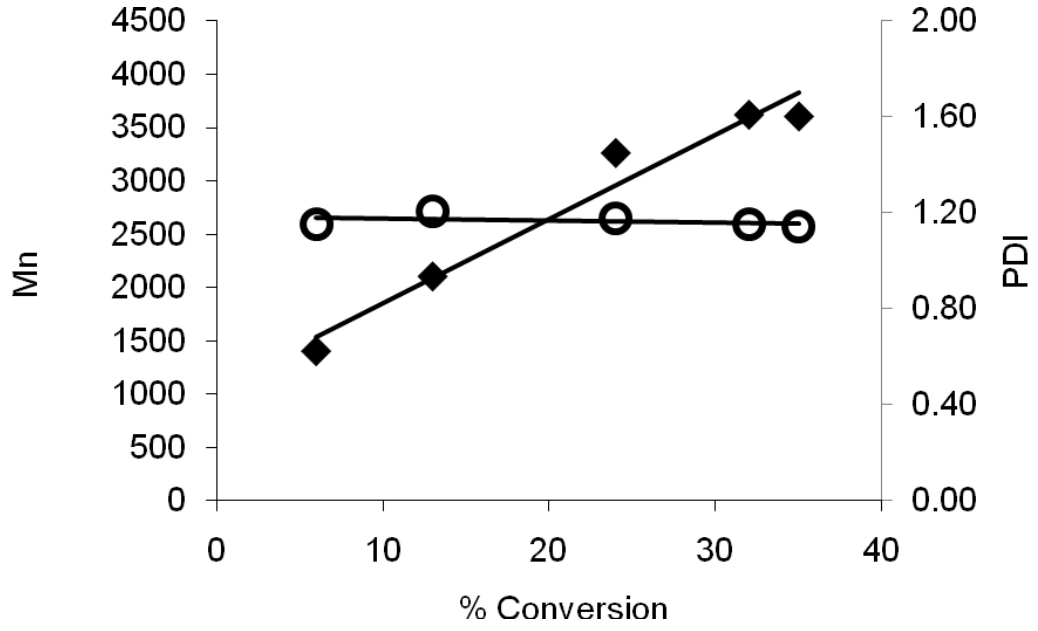
[a] Conditions: [rac-LA_0]/[**£c3.4£**] = 100:1, 6.8 mL toluene, 70 °C, 0.1 mL aliquots taken at the given intervals. See Experimental section for other details.

Figure S3.53. First order plot for *rac*-LA consumption using Ti(CyN$_2^{Ts}$)(O^{i}Pr)$_2$ (**£c3.4£**).[a]



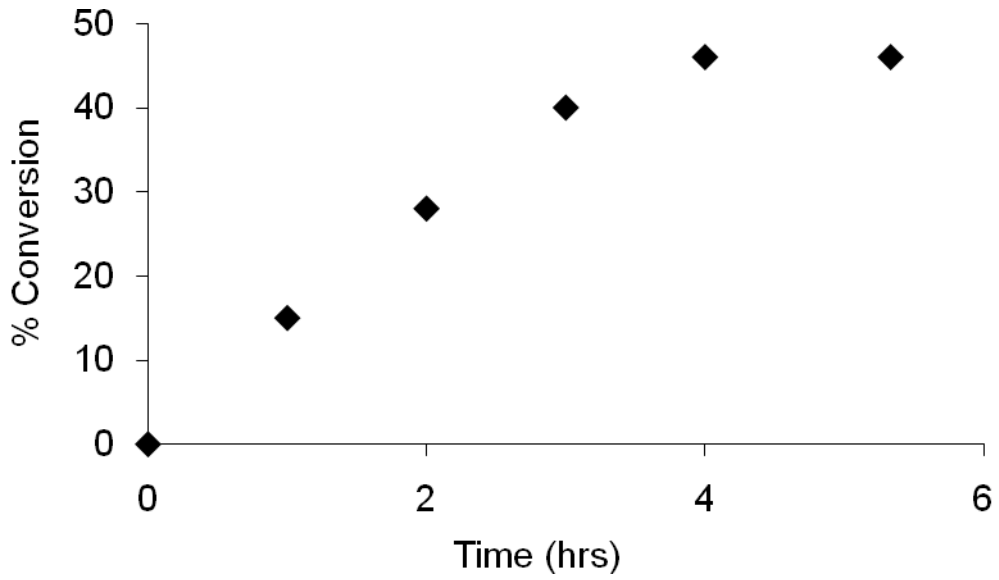
[a.] Conditions [*rac*-LA$_0$]/[**£c3.4£**] = 100:1, 6 mL toluene, 70 °C, 0.1 mL aliquots taken at the given intervals. See Experimental section for other details. Linear fit (r^2 = 0.994) shown is for the first order region after the induction period.

Figure S3.54. Plots of M_n and PDI (determined by GPC) *vs* conversion for the solution polymerisation of *rac*-LA using Ti(CyN$_2^{Ts}$)(O^{i}Pr)$_2$ (**£c3.4£**).[a]



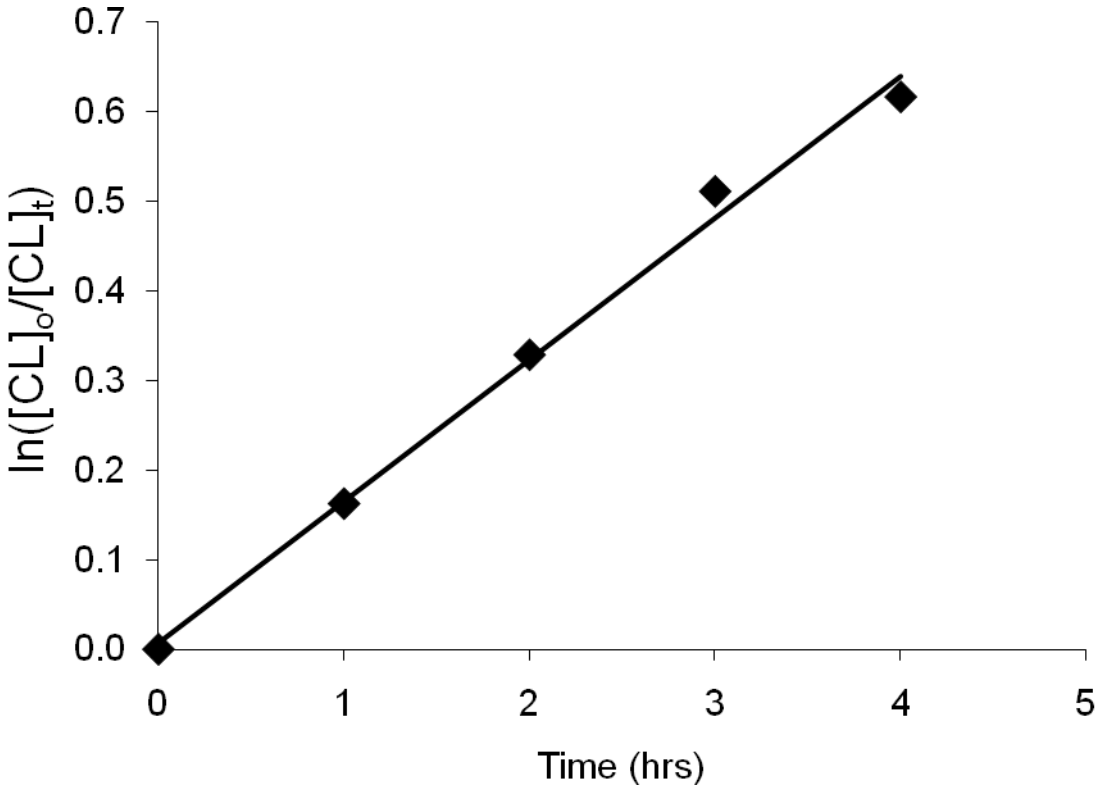
[a] Conditions: [*rac*-LA$_0$]/[**£c3.4£**] = 100:1, 6.0 mL toluene, 70 °C, 0.1 mL aliquots taken at the given intervals. Hollow diamonds correspond to M_n and hollow circles to PDI.

Figure S3.55. Plot for rac-LA consumption *vs* time using Ti($CyN_2^{SO_2Mes}$)(O^iPr)$_2$ (**£c3.5£**).[a]



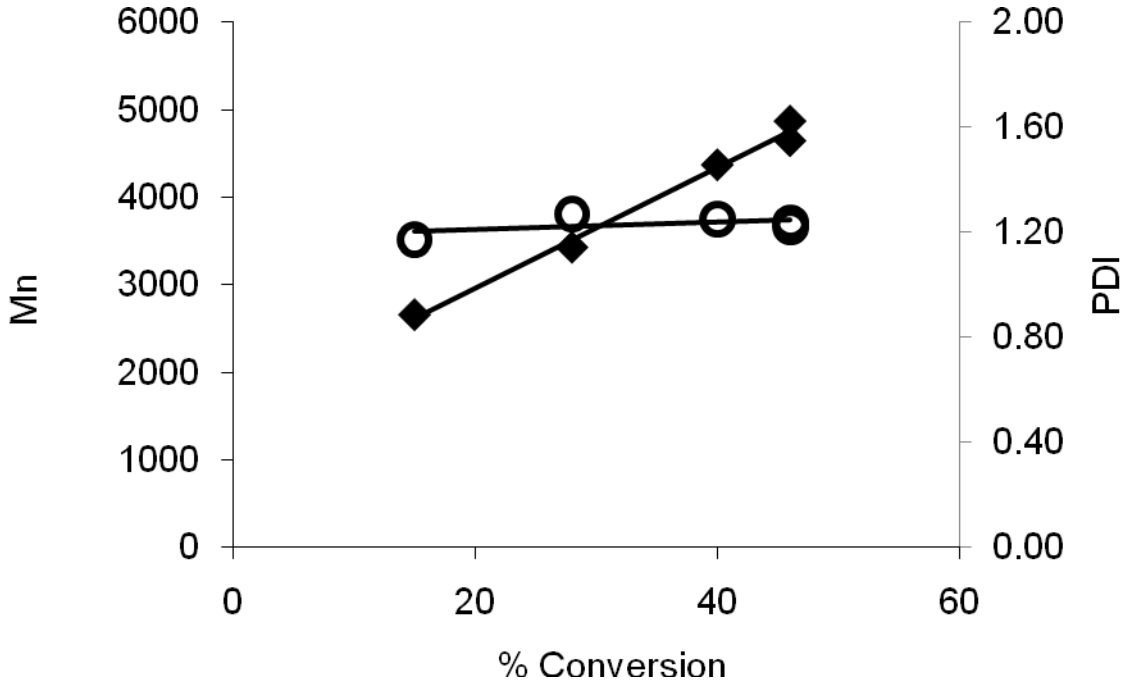
[a] Conditions: [rac-LA_0]/[**£c3.5£**] = 100:1, 6.8 mL toluene, 70 °C, 0.1 mL aliquots taken at the given intervals. See Experimental section for other details.

Figure S3.56. First order plot for *rac*-LA consumption using Ti($CyN_2^{SO_2Mes}$)(O^iPr)$_2$ (**£c3.5£**).[a]



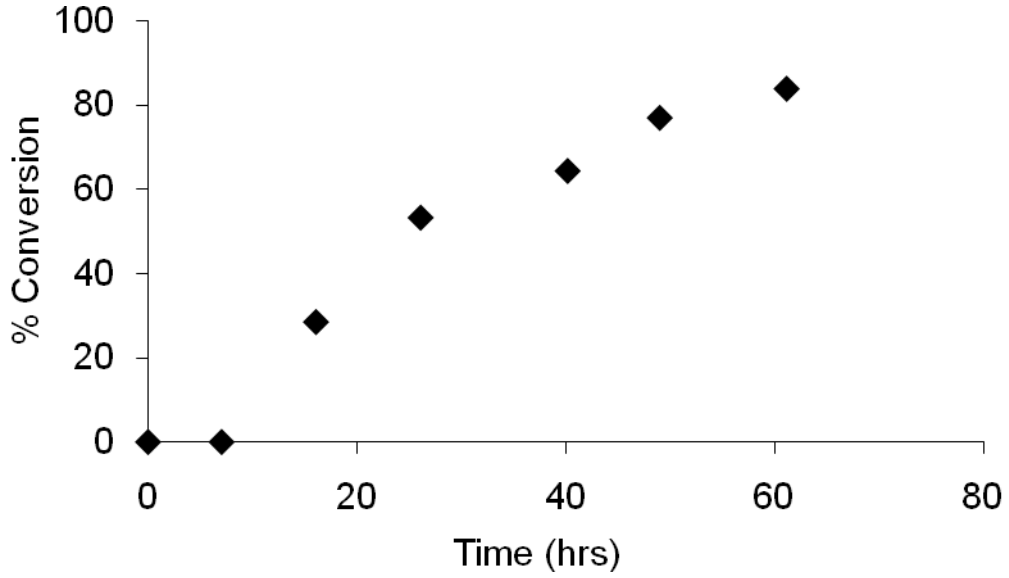
[a.] Conditions [*rac*-LA_0]/[**£c3.5£**] = 100:1, 6 mL toluene, 70 °C, 0.1 mL aliquots taken at the given intervals. See Experimental section for other details. Linear fit (r^2 = 0.994) shown is for the first order region after the induction period.

Figure S3.57. Plots of M_n and PDI (determined by GPC) *vs* conversion for the solution polymerisation of *rac*-LA using $Ti(CyN_2^{SO_2Mes})(O^iPr)_2$ (**£c3.5£**).[a]



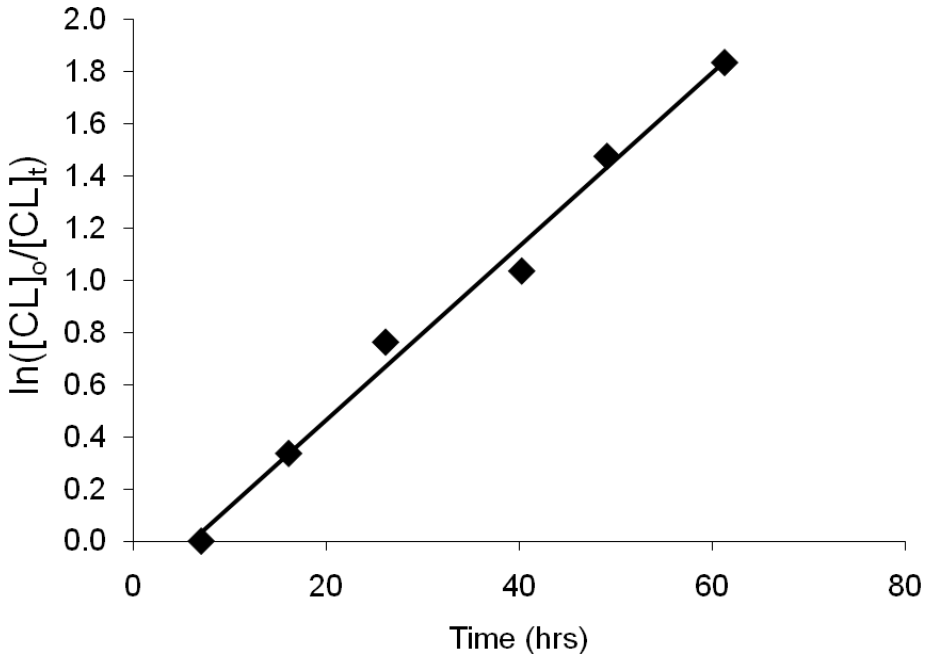
[a] Conditions: [*rac*-LA_0]/[**£c3.5£**] = 100:1, 6.0 mL toluene, 70 °C, 0.1 mL aliquots taken at the given intervals. Hollow diamonds correspond to M_n and hollow circles to PDI.

Figure S3.58. Plot for rac-LA consumption *vs* time using $Zr(N_3^{Ts}N)(CH_2SiMe_3)$ (**£c20£**).[a]



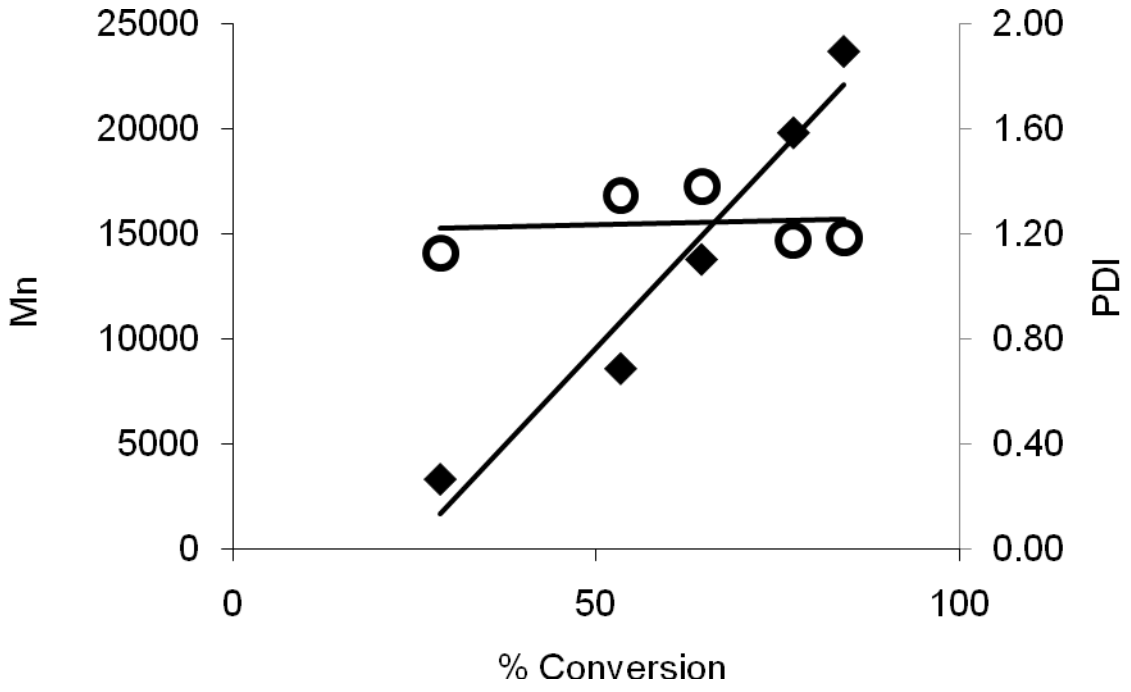
[a] Conditions: [rac-LA_0]/[**£c20£**] = 100:1, 6.8 mL toluene, 70 °C, 0.1 mL aliquots taken at the given intervals. See Experimental section for other details.

Figure S3.59. First order plot for *rac*-LA consumption using $Zr(N_3^{Ts}N)(CH_2SiMe_3)$ (**£c20£**).[a]



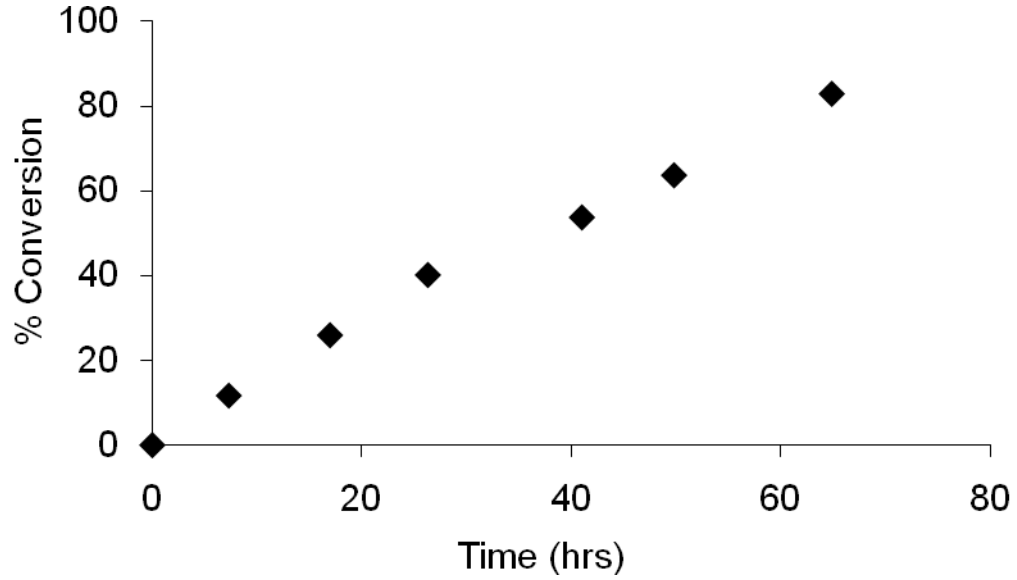
[a.] Conditions [*rac*-LA_0]/[**£c20£**] = 100:1, 6 mL toluene, 70 °C, 0.1 mL aliquots taken at the given intervals. See Experimental section for other details. Linear fit (r^2 = 0.994) shown is for the first order region after the induction period.

Figure S3.60. Plots of M_n and PDI (determined by GPC) *vs* conversion for the solution polymerisation of *rac*-LA using $Zr(N_3^{Ts}N)(CH_2SiMe_3)$ (**£c20£**).[a]



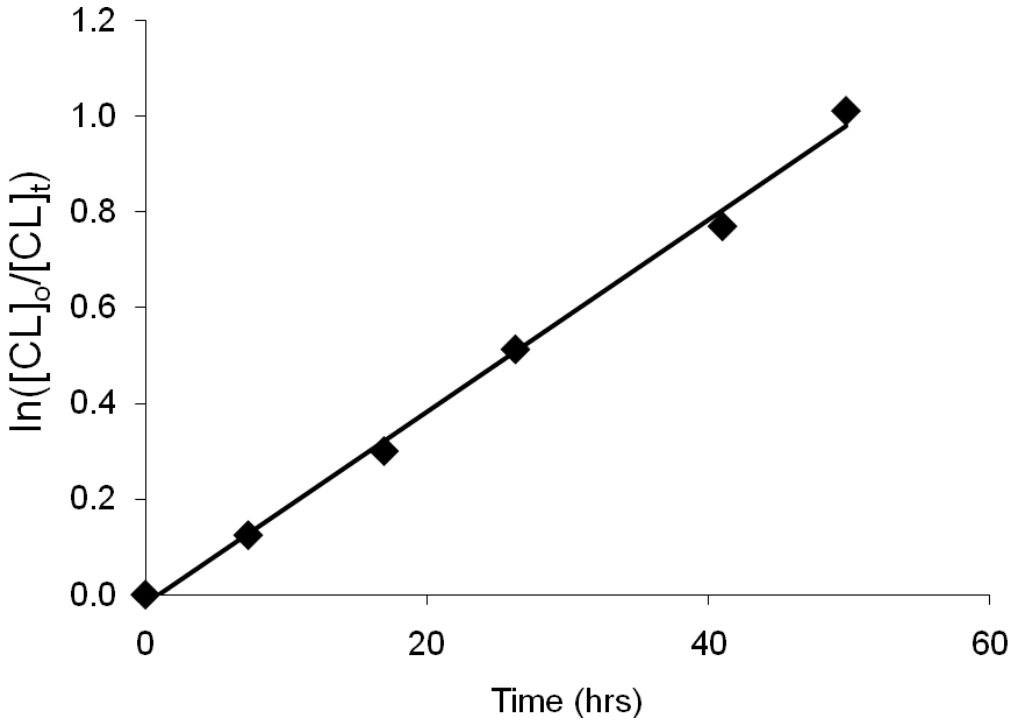
[a] Conditions: [*rac*-LA_0]/[**£c20£**] = 100:1, 6.0 mL toluene, 70 °C, 0.1 mL aliquots taken at the given intervals. Hollow diamonds correspond to M_n and hollow circles to PDI.

Figure S3.61. Plot for rac-LA consumption *vs* time using $Zr(N_3^{Ms}N)(CH_2SiMe_3)$ (**£c21£**).[a]



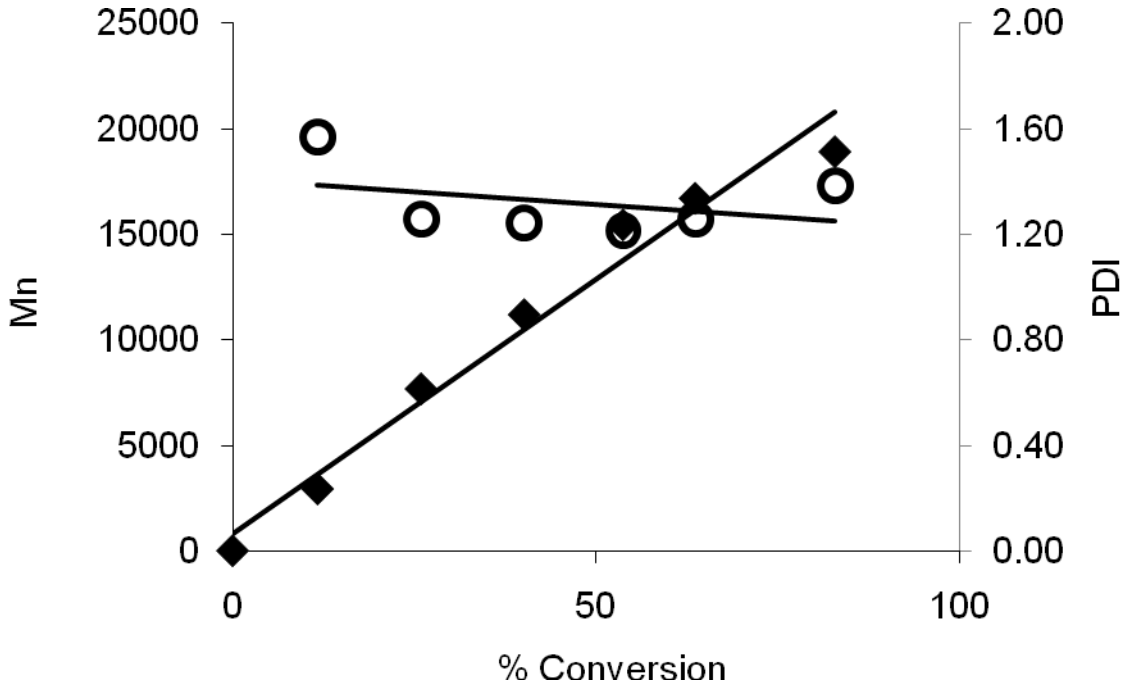
[a] Conditions: [rac-LA_0]/[**£c21£**] = 100:1, 6.8 mL toluene, 70 °C, 0.1 mL aliquots taken at the given intervals. See Experimental section for other details.

Figure S3.62. First order plot for *rac*-LA consumption using $Zr(N_3^{Ms}N)(CH_2SiMe_3)$ (**£c21£**).[a]



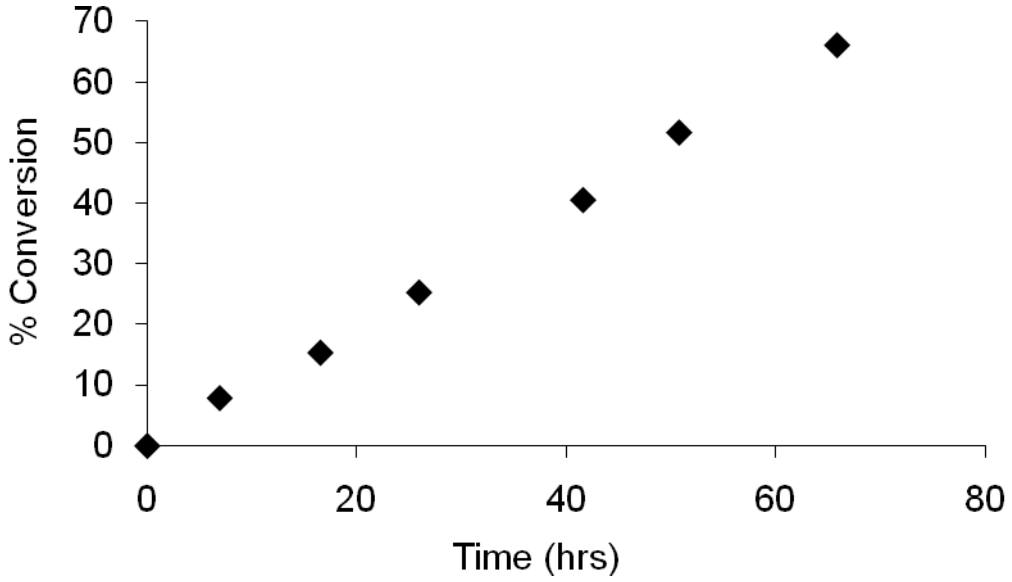
[a.] Conditions [*rac*-LA_0]/[**£c21£**] = 100:1, 6 mL toluene, 70 °C, 0.1 mL aliquots taken at the given intervals. See Experimental section for other details. Linear fit (r^2 = 0.996) shown is for the first order region after the induction period.

Figure S3.63. Plots of M_n and PDI (determined by GPC) *vs* conversion for the solution polymerisation of *rac*-LA using Zr(N_3^{Ms}N)(CH_2SiMe_3) (**£c21£**).[a]



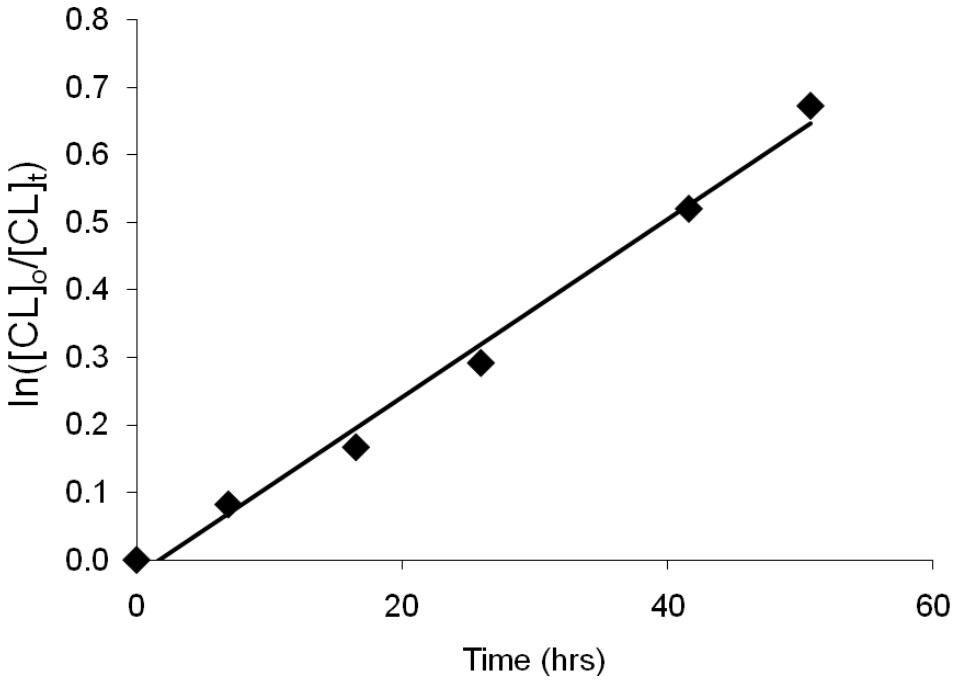
[a] Conditions: [*rac*-LA_0]/[**£c21£**] = 100:1, 6.0 mL toluene, 70 °C, 0.1 mL aliquots taken at the given intervals. Hollow diamonds correspond to M_n and hollow circles to PDI.

Figure S3.64. Plot for rac-LA consumption *vs* time using Zr(N_3^{TArF}N)(NMe_2) (**£c23£**).[a]



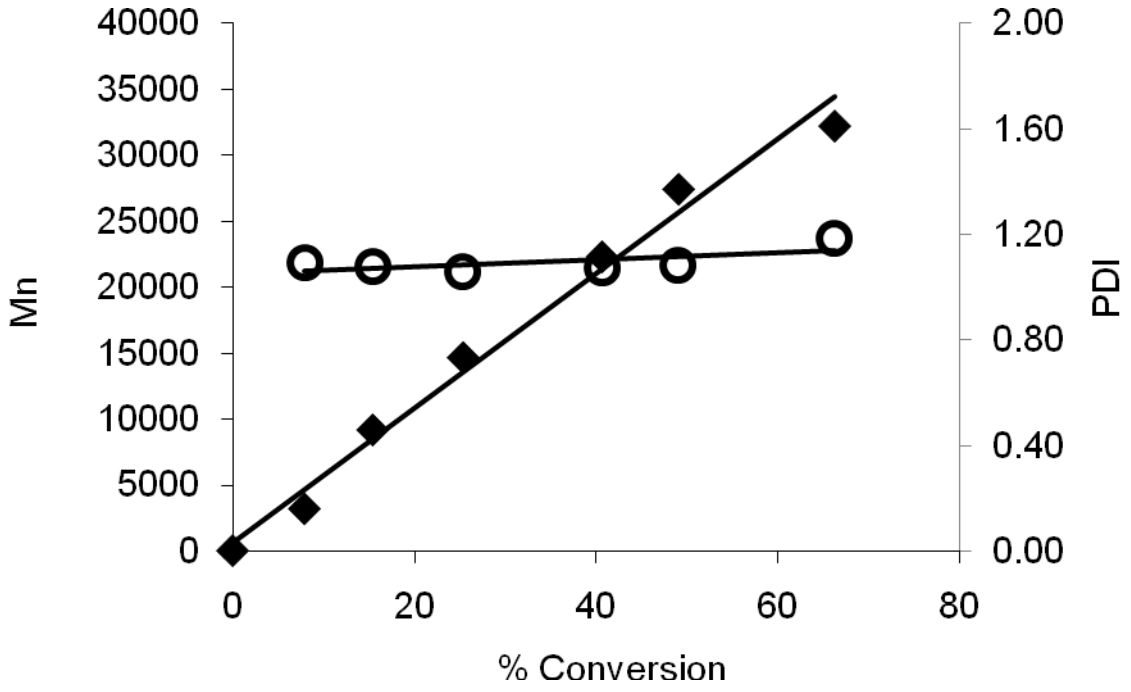
[a] Conditions: [rac-LA_0]/[**£c23£**] = 100:1, 6.8 mL toluene, 70 °C, 0.1 mL aliquots taken at the given intervals. See Experimental section for other details.

Figure S3.65. First order plot for *rac*-LA consumption using Zr($N_3^{TArF}N$)(NMe_2) (**£c23£**).[a]



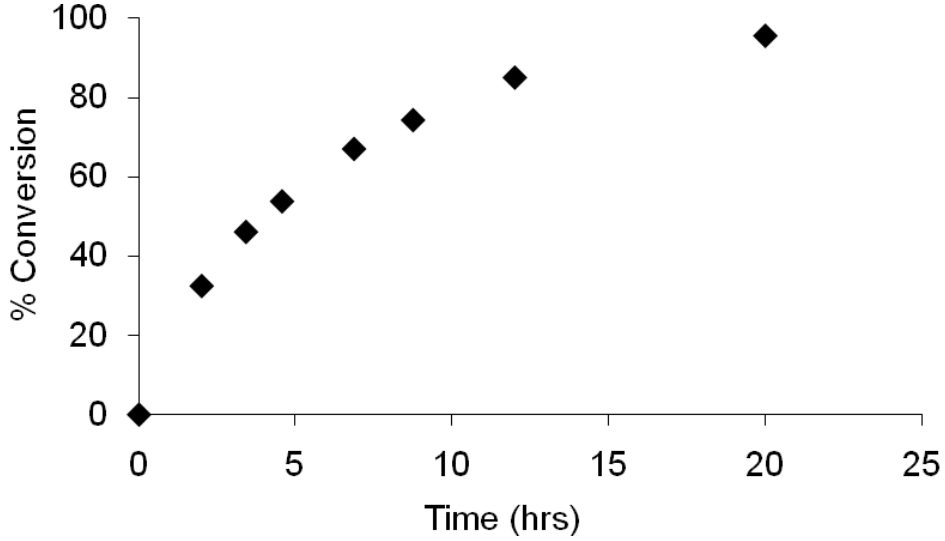
[a.] Conditions [*rac*-LA_0]/[**£c23£**] = 100:1, 6 mL toluene, 70 °C, 0.1 mL aliquots taken at the given intervals. See Experimental section for other details. Linear fit (r^2 = 0.991) shown is for the first order region after the induction period.

Figure S3.66. Plots of M_n and PDI (determined by GPC) *vs* conversion for the solution polymerisation of *rac*-LA using Zr($N_3^{TArF}N$)(NMe_2) (**£c23£**).[a]



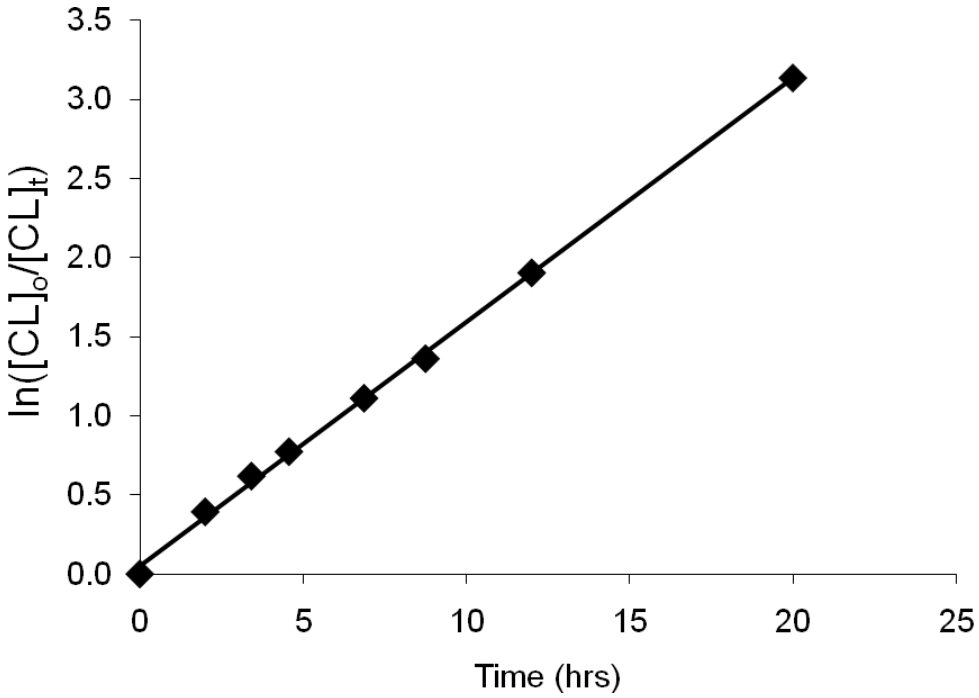
[a] Conditions: [*rac*-LA_0]/[**£c23£**] = 100:1, 6.0 mL toluene, 70 °C, 0.1 mL aliquots taken at the given intervals. Hollow diamonds correspond to M_n and hollow circles to PDI.

Figure S3.67. Plot for rac-LA consumption *vs* time using $Zr(N_3^{Ts}N)(CH_2SiMe_3)$ (**£c20£**) with HO^iPr co-catalyst.[a]



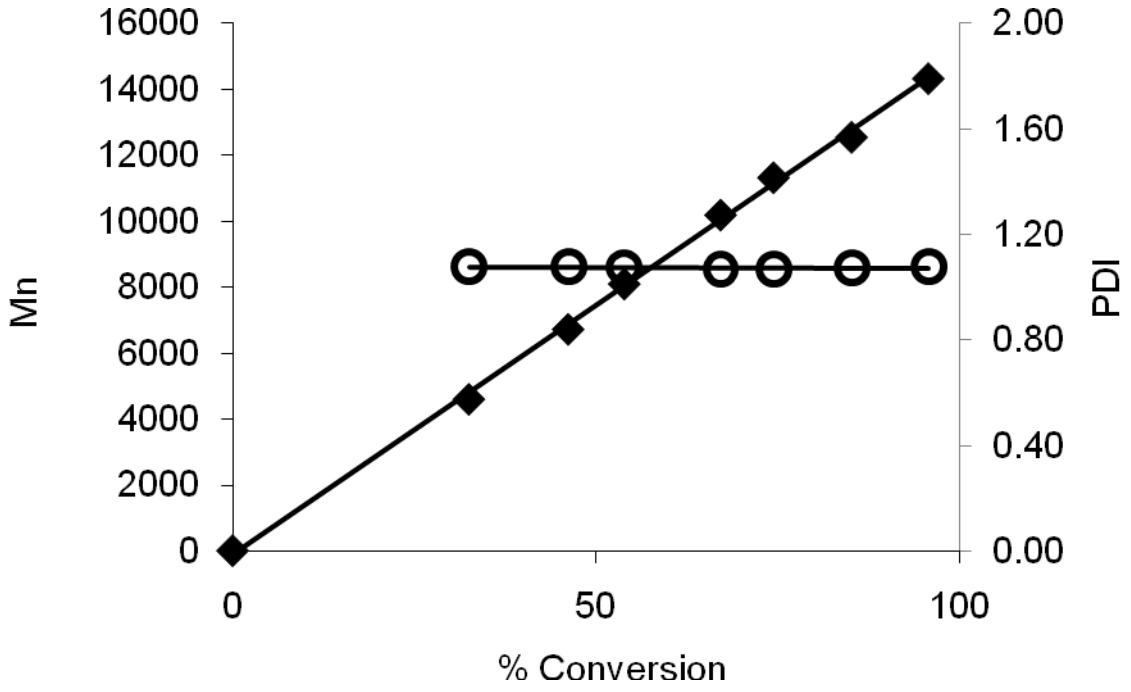
[a] Conditions: $[rac\text{-}LA_0]/[$**£c20£**$]/HO^iPr$ = 100:1:1, 6.8 mL toluene, 70 °C, 0.1 mL aliquots taken at the given intervals. See Experimental section for other details.

Figure S3.68. First order plot for *rac*-LA consumption using $Zr(N_3^{Ts}N)(CH_2SiMe_3)$ (**£c20£**) with HO^iPr co-catalyst.[a]



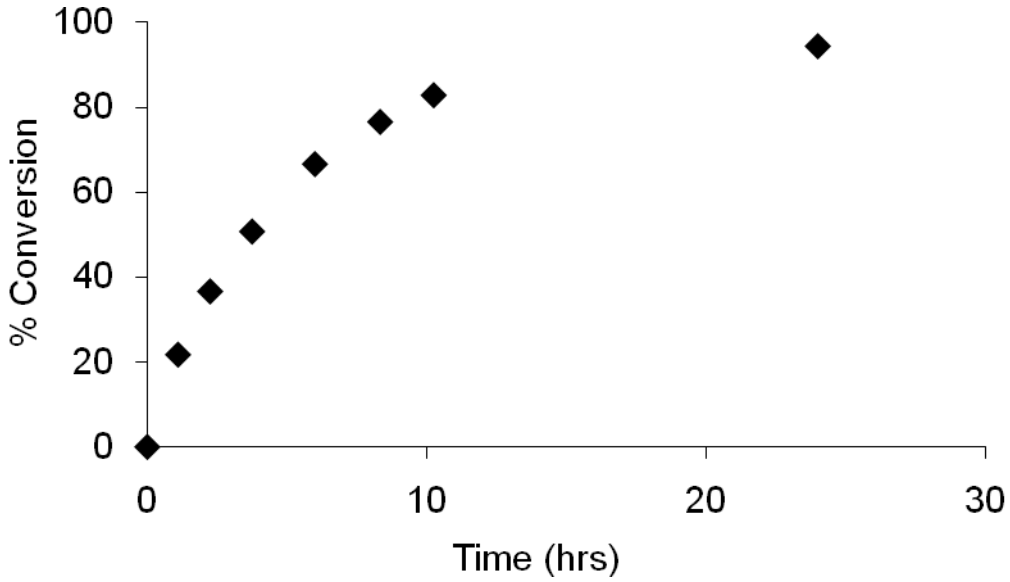
[a] Conditions $[rac\text{-}LA_0]/[$**£c20£**$]/HO^iPr$ = 100:1:1, 6 mL toluene, 70 °C, 0.1 mL aliquots taken at the given intervals. See Experimental section for other details. Linear fit (r^2 = 0.991) shown is for the first order region after the induction period.

Figure S3.69. Plots of M_n and PDI (determined by GPC) *vs* conversion for the solution polymerisation of *rac*-LA using $Zr(N_3^{Ts}N)(CH_2SiMe_3)$ (**£c20£**) with HO^iPr co-catalyst.[a]



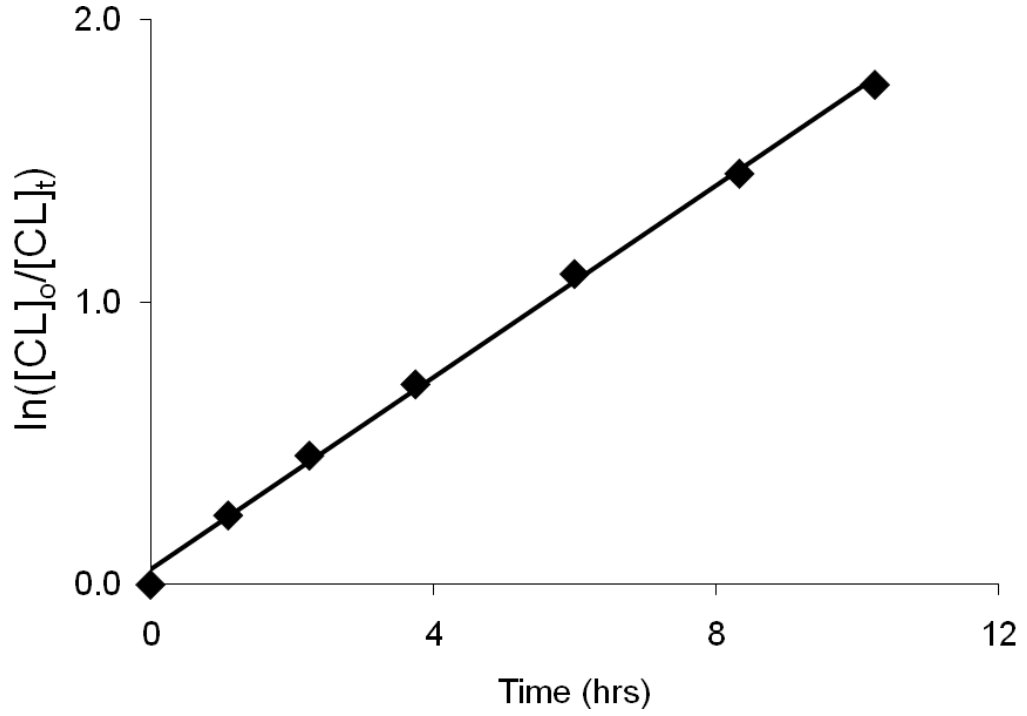
[a] Conditions: [rac-LA_0]/[**£c20£**]/HO^iPr = 100:1:1, 6.0 mL toluene, 70 °C, 0.1 mL aliquots taken at the given intervals. Hollow diamonds correspond to M_n and hollow circles to PDI.

Figure S3.70. Plot for rac-LA consumption *vs* time using $Zr(N_3^{Ms}N)(CH_2SiMe_3)$ (**£c22£**) with HO^iPr co-catalyst.[a]



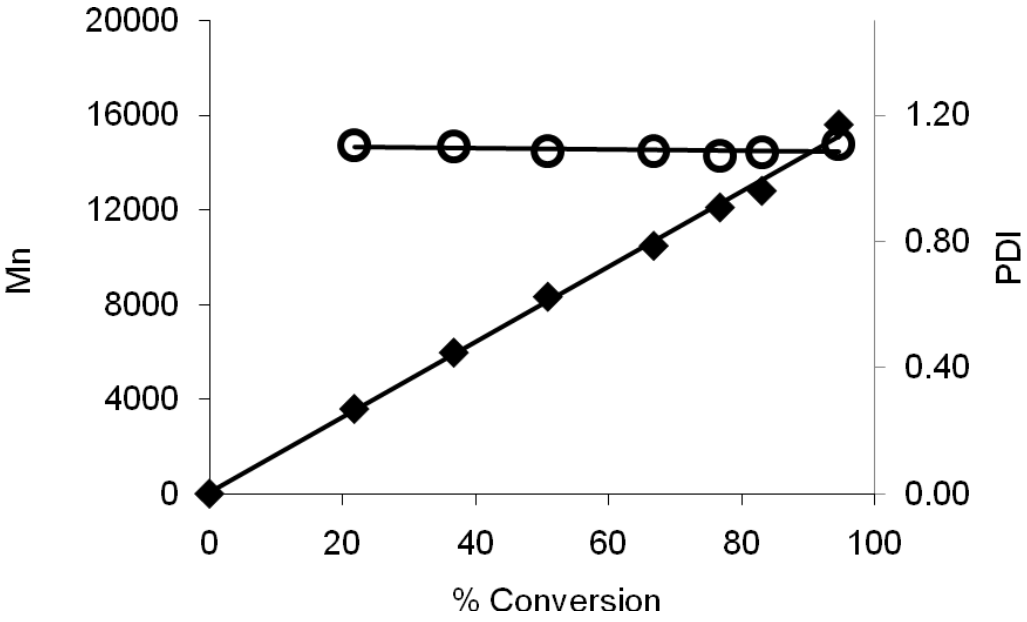
[a] Conditions: [rac-LA_0]/[**£c22£**]/HO^iPr = 100:1:1, 6.8 mL toluene, 70 °C, 0.1 mL aliquots taken at the given intervals. See Experimental section for other details.

Figure S3.71. First order plot for *rac*-LA consumption using $Zr(N_3^{Ms}N)(CH_2SiMe_3)$ (**£c22£**) with HO^iPr co-catalyst.[a]



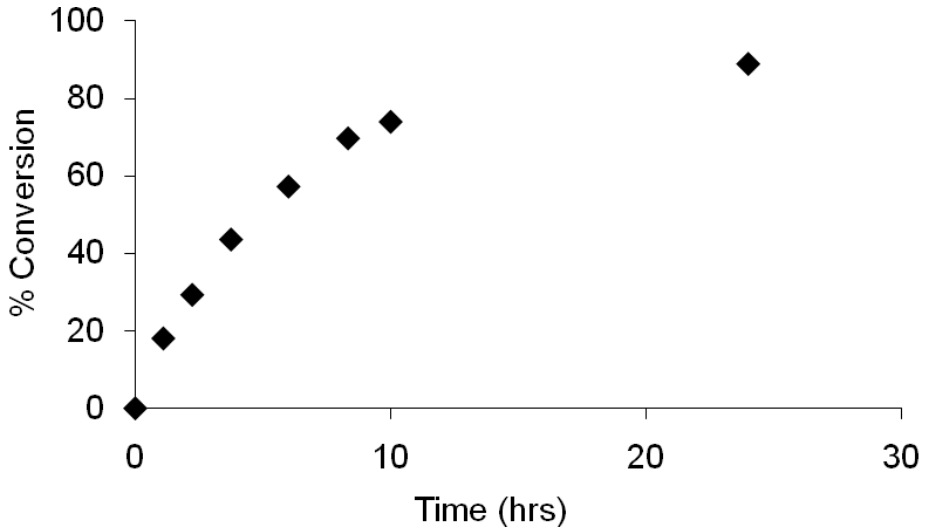
[a] Conditions [rac-LA_0]/[**£c22£**]/HO^iPr = 100:1:1, 6 mL toluene, 70 °C, 0.1 mL aliquots taken at the given intervals. See Experimental section for other details. Linear fit (r^2 = 0.998) shown is for the first order region after the induction period.

Figure S3.72. Plots of M_n and PDI (determined by GPC) *vs* conversion for the solution polymerisation of *rac*-LA using $Zr(N_3^{Ms}N)(CH_2SiMe_3)$ (**£c22£**) with HO^iPr co-catalyst.[a]



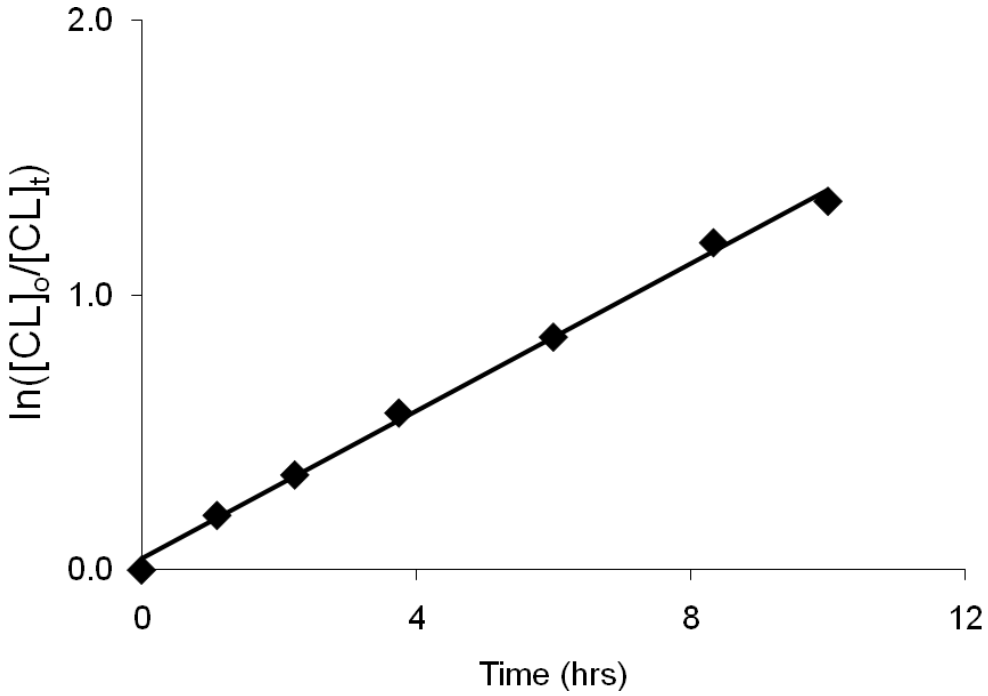
[a] Conditions: [rac-LA_0]/[**£c22£**]/HO^iPr = 100:1:1, 6.0 mL toluene, 70 °C, 0.1 mL aliquots taken at the given intervals. Hollow diamonds correspond to M_n and hollow circles to PDI.

Figure S3.73. Plot for rac-LA consumption *vs* time using $Zr(N_3^{TArF}N)(CH_2SiMe_3)$ (**£c21£**) with HO^iPr co-catalyst.[a]



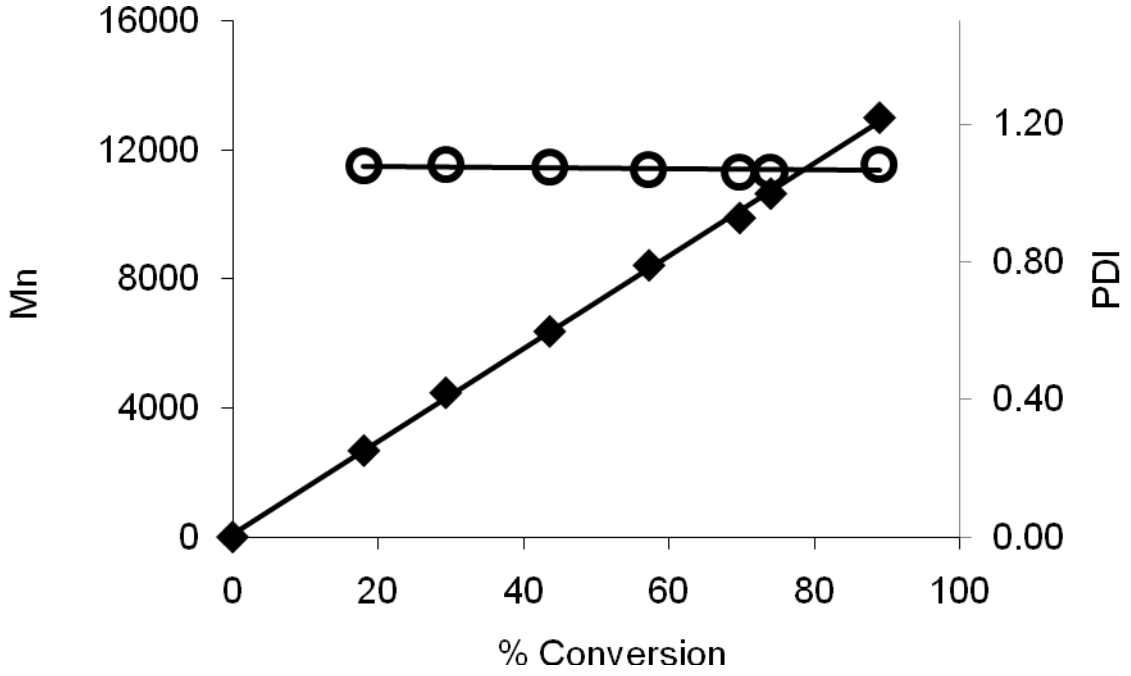
[a] Conditions: [rac-LA_0]/[**£c21£**]/HO^iPr = 100:1:1, 6.8 mL toluene, 70 °C, 0.1 mL aliquots taken at the given intervals. See Experimental section for other details.

Figure S3.74. First order plot for *rac*-LA consumption using $Zr(N_3^{TArF}N)(CH_2SiMe_3)$ (**£c21£**) with HO^iPr co-catalyst.[a]



[a.] Conditions [rac-LA_0]/[**£c21£**]/HO^iPr = 100:1:1, 6 mL toluene, 70 °C, 0.1 mL aliquots taken at the given intervals. See Experimental section for other details. Linear fit (r^2 = 0.997) shown is for the first order region after the induction period.

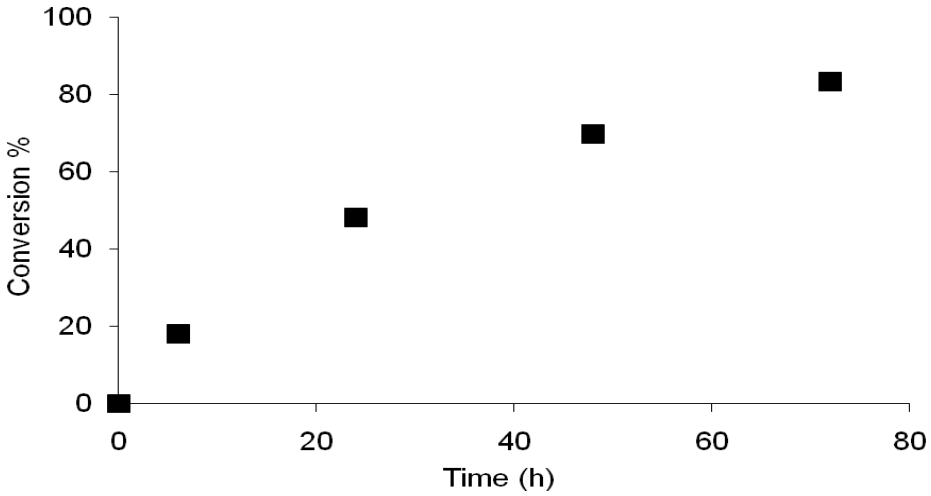
Figure S3.75. Plots of M_n and PDI (determined by GPC) *vs* conversion for the solution polymerisation of *rac*-LA using Zr($N_3^{TArF}N$)(CH_2SiMe_3) (**£c21£**) with HO^{i}Pr co-catalyst.[a]



[a] Conditions: [rac-LA_0]/[**£c21£**]/HO^{i}Pr = 100:1:1, 6.0 mL toluene, 70 °C, 0.1 mL aliquots taken at the given intervals. Hollow diamonds correspond to M_n and hollow circles to PDI.

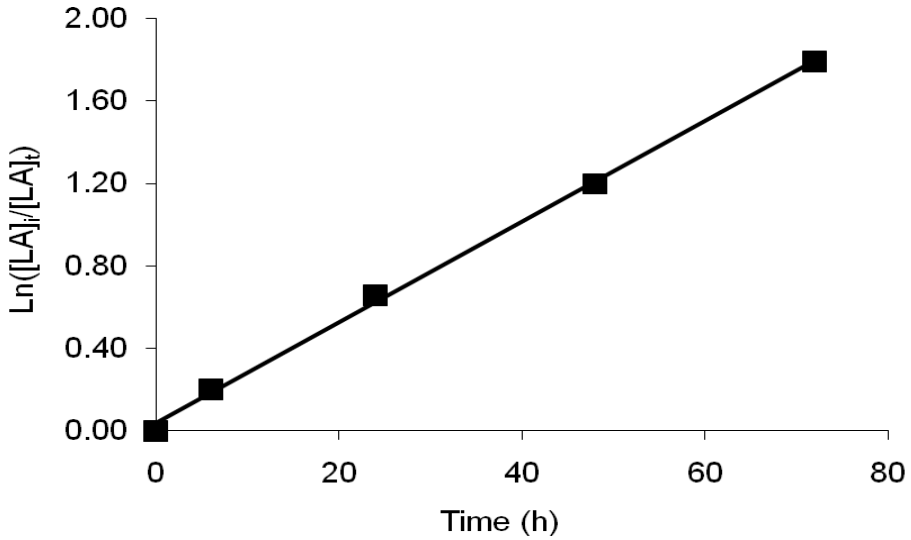
Supporting Information for Chapter 4

Figure S4.1. Plot for *rac*-LA consumption *vs* time using Al($N_2^{Ts}N^{py}$)(O^iPr) (**32**).[a]



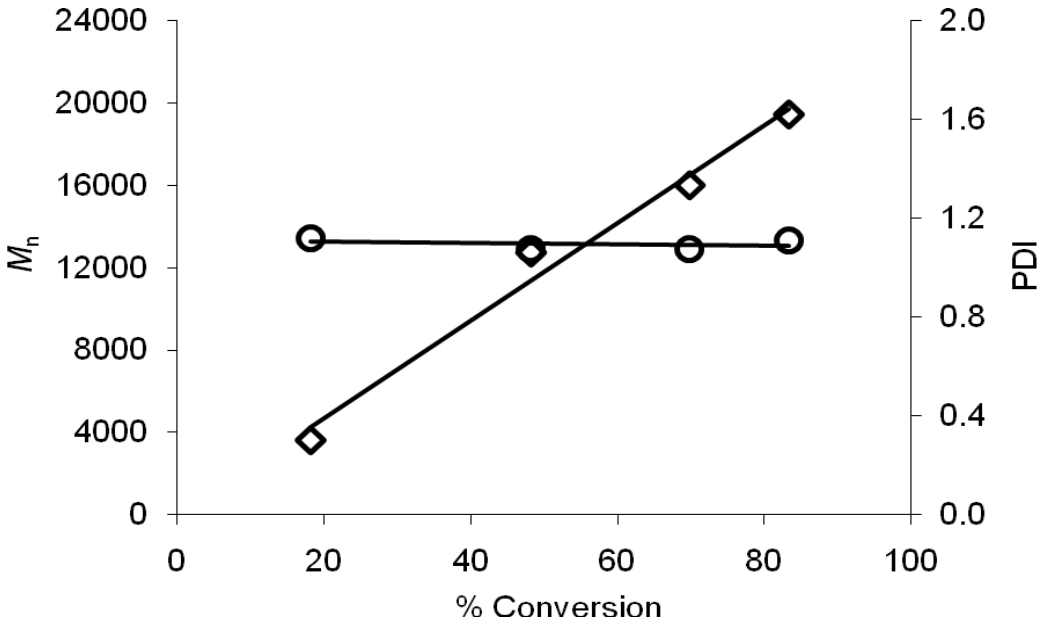
[a] Conditions: [*rac*-LA_0]:[**32**] = 100:1, 6.0 mL toluene, 70 °C, 0.1 mL aliquots taken at the given intervals. See Experimental section for other details.

Figure S4.2. First order plot *rac*-LA consumption using Al($N_2^{Ts}N^{py}$)(O^iPr) (**32**).[a]



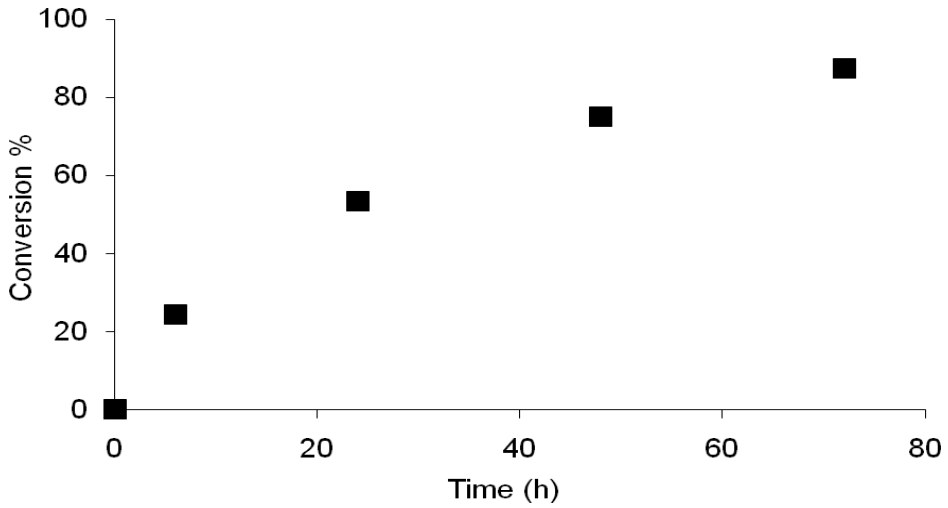
[a] Conditions: [*rac*-LA_0]:[**32**] = 100:1, 6.0 mL toluene, 70 °C, 0.1 mL aliquots taken at the given intervals. See Experimental section for other details. Linear fit (r^2 = 0.999).

Figure S4.3. Plots of M_n and PDI (determined by GPC) *vs* conversion for the polymerization of *rac*-LA using Al($N_2^{Ts}N^{py}$)(O^iPr) (**32**).[a]



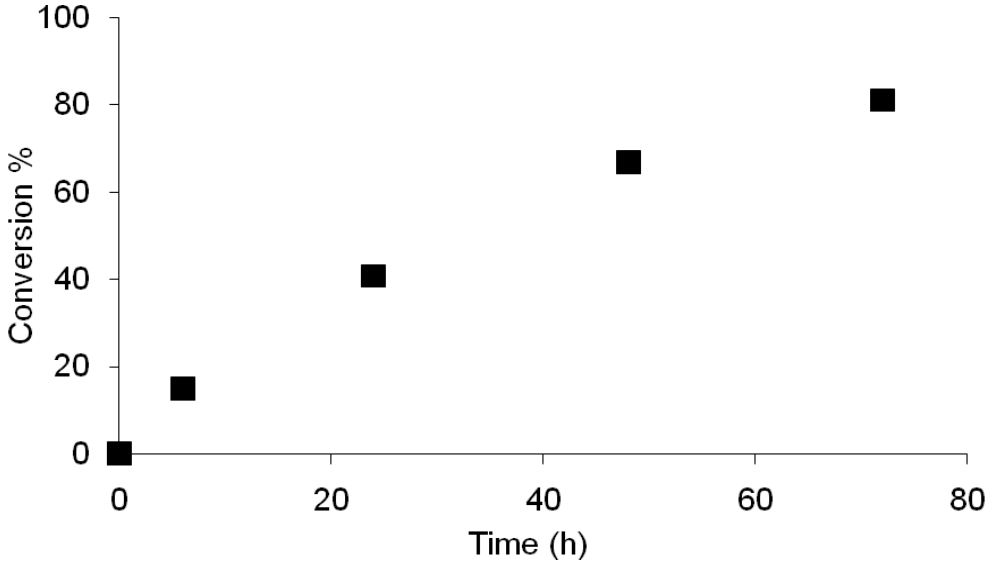
[a] Conditions: [*rac*-LA_0]:[**32**] = 100:1, 6.0 mL toluene, 70 °C, 0.1 mL aliquots taken at the given intervals. Hollow diamonds correspond to M_n and hollow circles to PDI.

Figure S4.4. Plot for *rac*-LA consumption *vs* time using Al($N_2^{Ts}N^{py}$)(OBn) (**33**).[a]



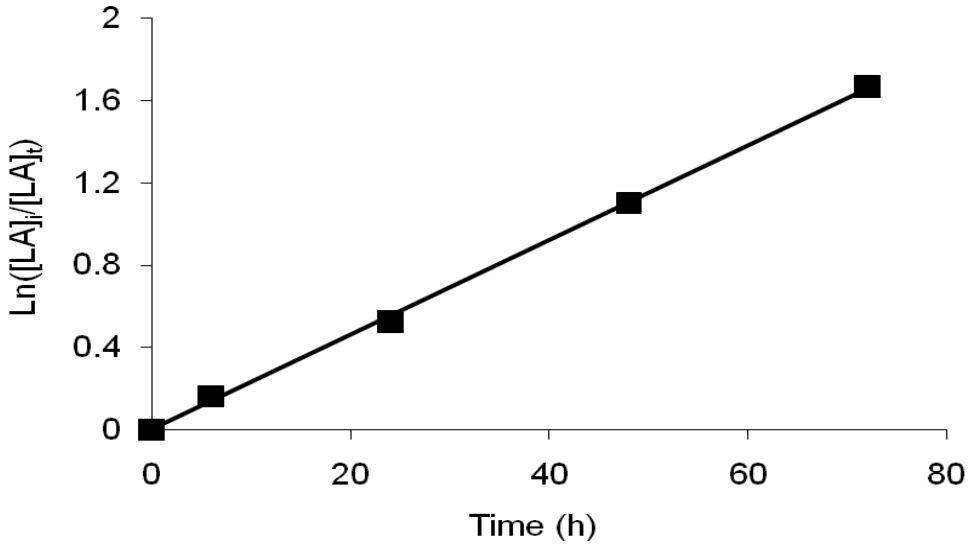
[a] Conditions: [*rac*-LA_0]:[**33**] = 100:1, 6.0 mL toluene, 70 °C, 0.1 mL aliquots taken at the given intervals. See Experimental section for other details.

Figure S4.5. Plot for *rac*-LA consumption *vs* time using Al($N_2^{Ms}N^{Ph}$)(O^iPr) (**36**).[a]



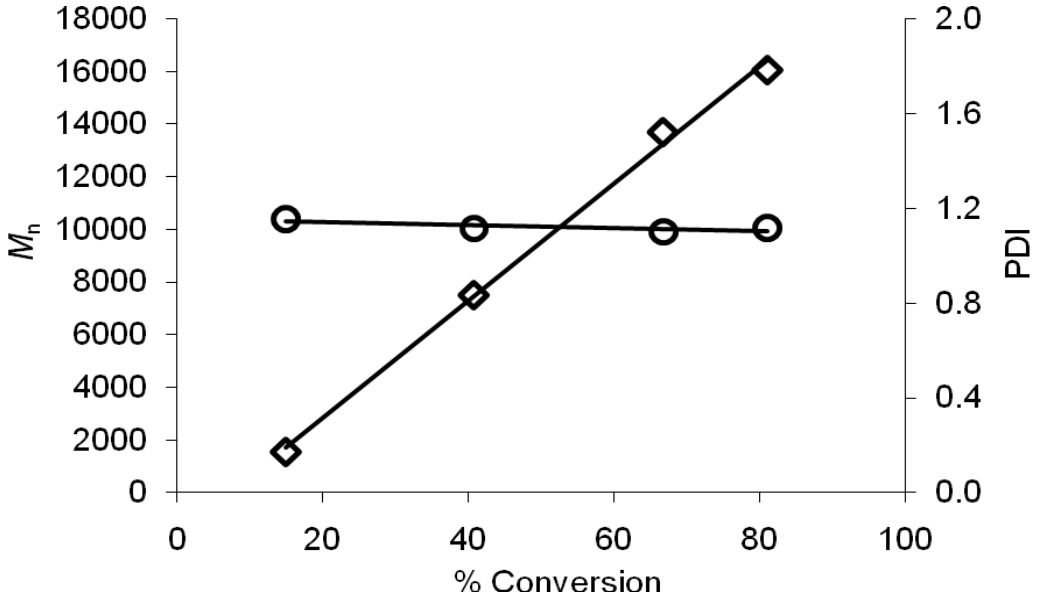
[a] Conditions: [*rac*-LA_0]:[**36**] = 100:1, 6.0 mL toluene, 70 °C, 0.1 mL aliquots taken at the given intervals. See Experimental section for other details.

Figure S4.6. First order plot *rac*-LA consumption using Al($N_2^{Ms}N^{Ph}$)(O^iPr) (**36**).[a]



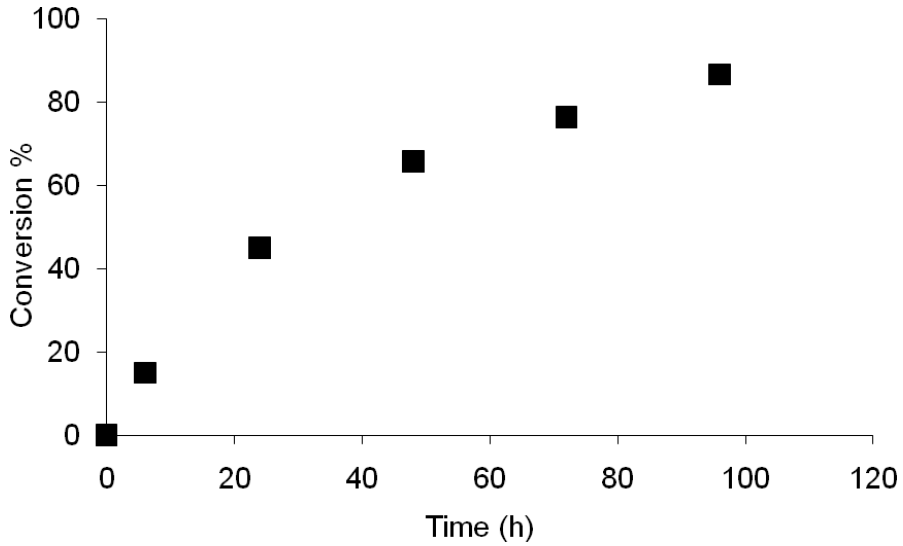
[a] Conditions: [*rac*-LA_0]:[**36**] = 100:1, 6.0 mL toluene, 70 °C, 0.1 mL aliquots taken at the given intervals. See Experimental section for other details. Linear fit (r^2 = 0.997).

Figure S4.7. Plots of M_n and PDI (determined by GPC) *vs* conversion for the polymerization of *rac*-LA using Al($N_2^{Ms}N^{Ph}$)(O^iPr) (**36**).[a]



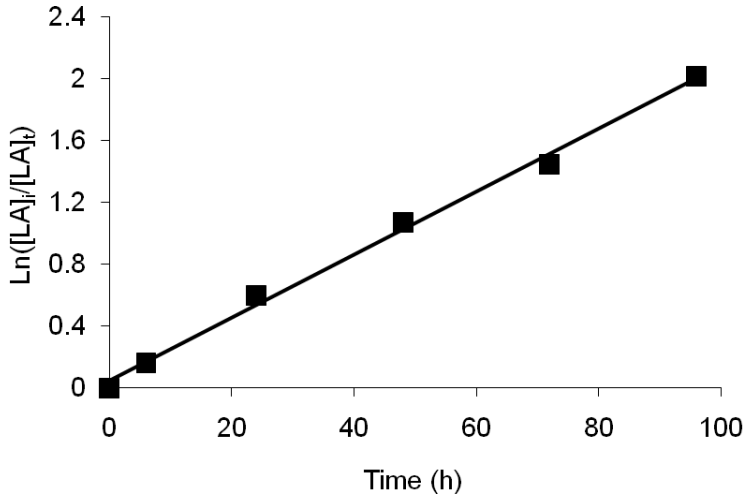
[a] Conditions: [*rac*-LA_0]:[**36**] = 100:1, 6.0 mL toluene, 70 °C, 0.1 mL aliquots taken at the given intervals. Hollow diamonds correspond to M_n and hollow circles to PDI.

Figure S4.8. Plot for *rac*-LA consumption *vs* time using Al($N_2^{Ms}N^{Ph}$)(OBn) (**37**).[a]



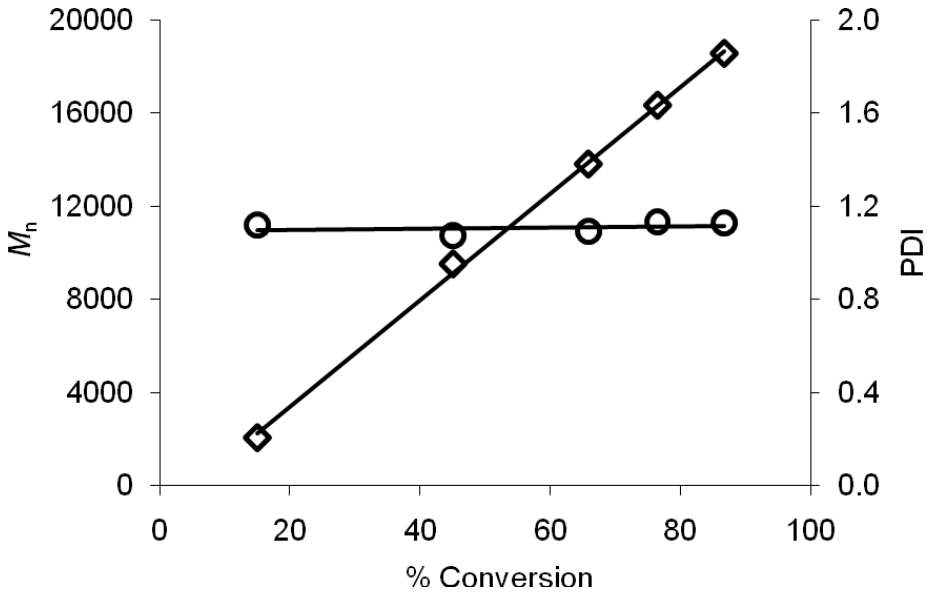
[a] Conditions: [*rac*-LA_0]:[**37**] = 100:1, 6.0 mL toluene, 70 °C, 0.1 mL aliquots taken at the given intervals. See Experimental section for other details.

Figure S4.9. First order plot *rac*-LA consumption using Al($N_2^{Ms}N^{Ph}$)(OBn) (**37**).[a]



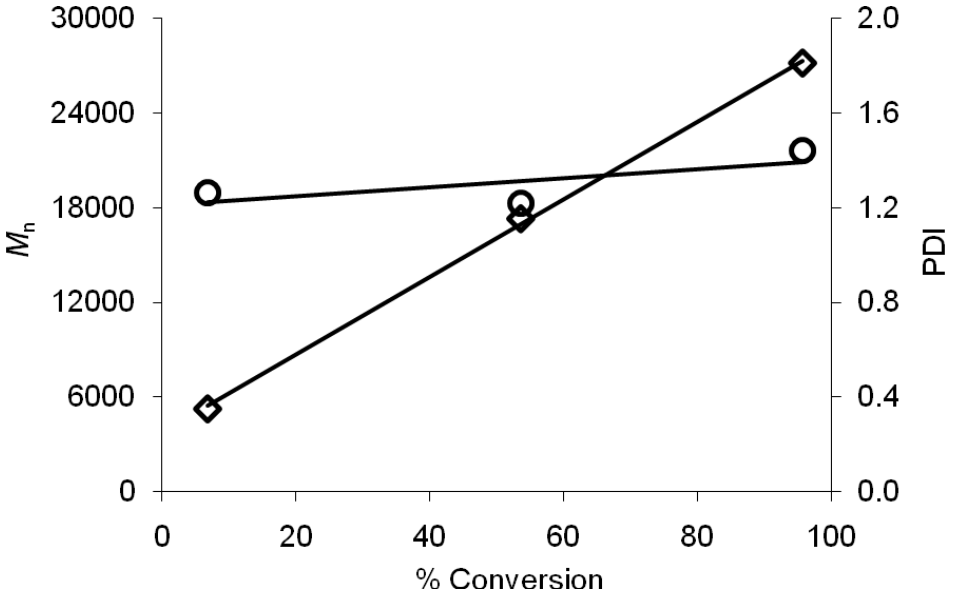
[a] Conditions: [*rac*-LA_0]:[**37**] = 100:1, 6.0 mL toluene, 70 °C, 0.1 mL aliquots taken at the given intervals. See Experimental section for other details. Linear fit (r^2 = 0.996).

Figure S4.10. Plots of M_n and PDI (determined by GPC) *vs* conversion for the polymerization of *rac*-LA using Al($N_2^{Ms}N^{Ph}$)(OBn) (**37**).[a]



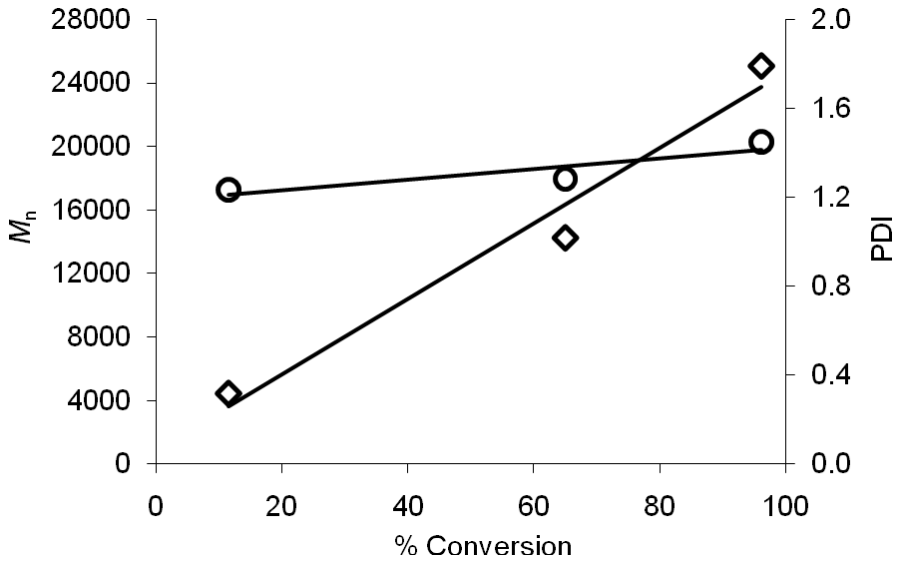
[a] Conditions: [*rac*-LA_0]:[**37**] = 100:1, 6.0 mL toluene, 70 °C, 0.1 mL aliquots taken at the given intervals. Hollow diamonds correspond to M_n and hollow circles to PDI.

Figure S4.11. Plots of M_n and PDI (determined by GPC) *vs* conversion for the polymerization of *rac*-LA using Al($N_2^{Ts}N^{Ph}$)($OCH_2CH_2NH_2$) (**39**).[a]



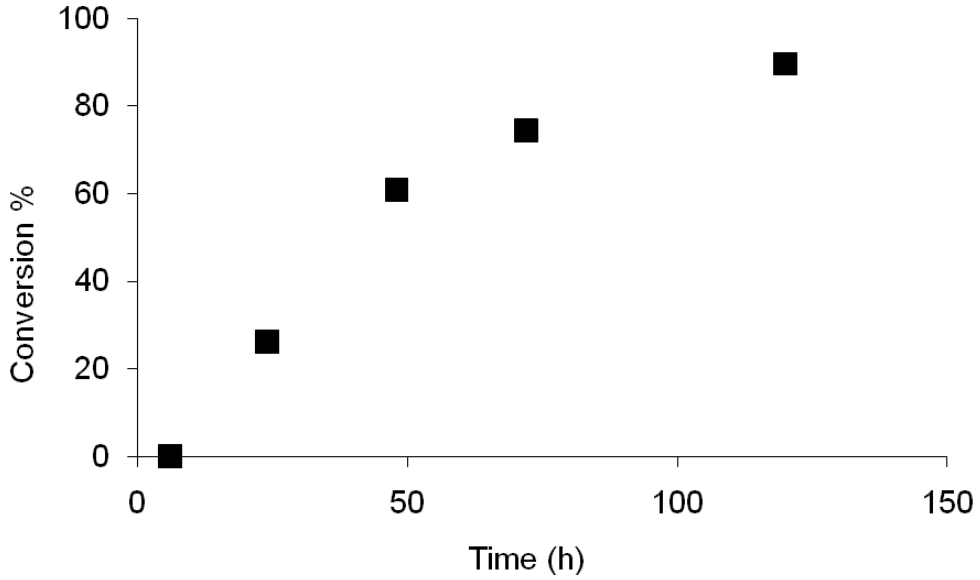
[a] Conditions: [*rac*-LA_0]:[**39**] = 100:1, 6.0 mL toluene, 70 °C, 0.1 mL aliquots taken at the given intervals. Hollow diamonds correspond to M_n and hollow circles to PDI.

Figure S4.12. Plots of M_n and PDI (determined by GPC) *vs* conversion for the polymerization of *rac*-LA using Al($N_2^{Ts}N^{py}$)($OCH_2CH_2NH_2$) (**41**).[a]



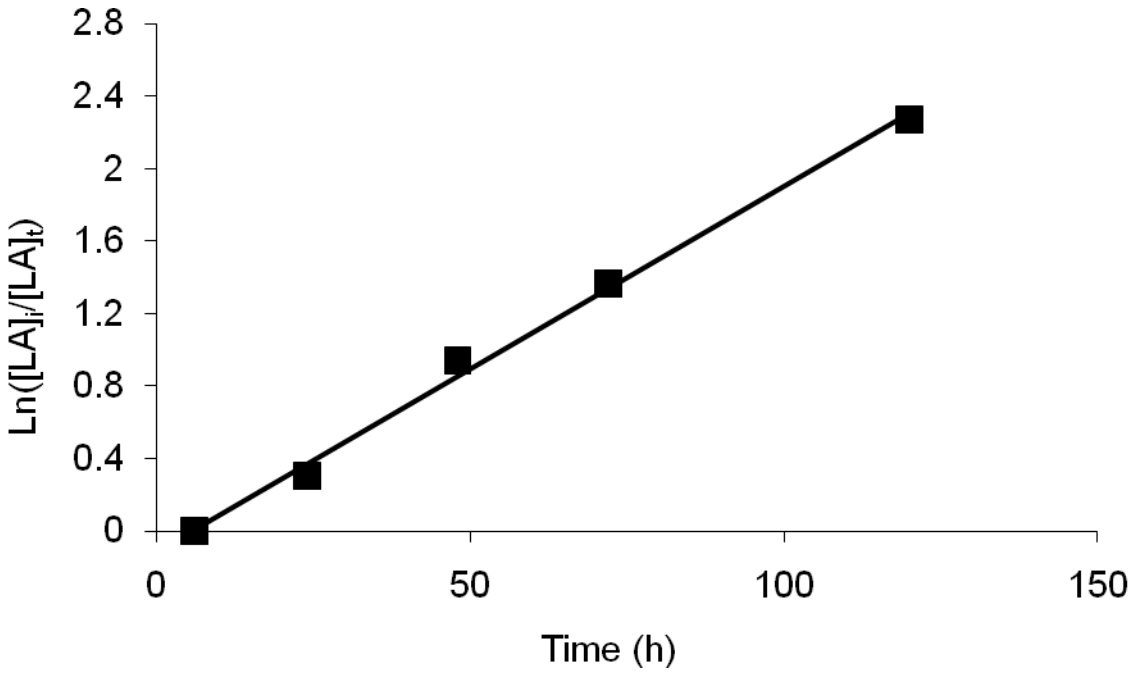
[a] Conditions: [*rac*-LA_0]:[**41**] = 100:1, 6.0 mL toluene, 70 °C, 0.1 mL aliquots taken at the given intervals. Hollow diamonds correspond to M_n and hollow circles to PDI.

Figure S4.13. Plot for *rac*-LA consumption *vs* time using Al(CyN_2^{Ts})($OCH_2CH_2NMe_2$) (**43**).[a]



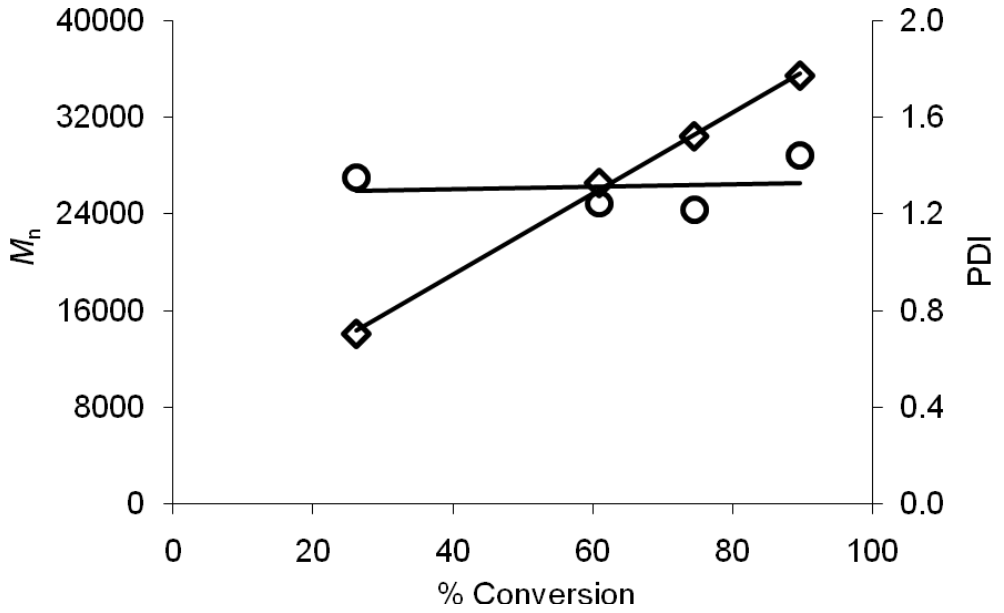
[a] Conditions: [*rac*-LA_0]:[**43**] = 100:1, 6.0 mL toluene, 70 °C, 0.1 mL aliquots taken at the given intervals. See Experimental section for other details.

Figure S4.14. First order plot *rac*-LA consumption using Al(CyN_2^{Ts})($OCH_2CH_2NMe_2$) (**43**).[a]



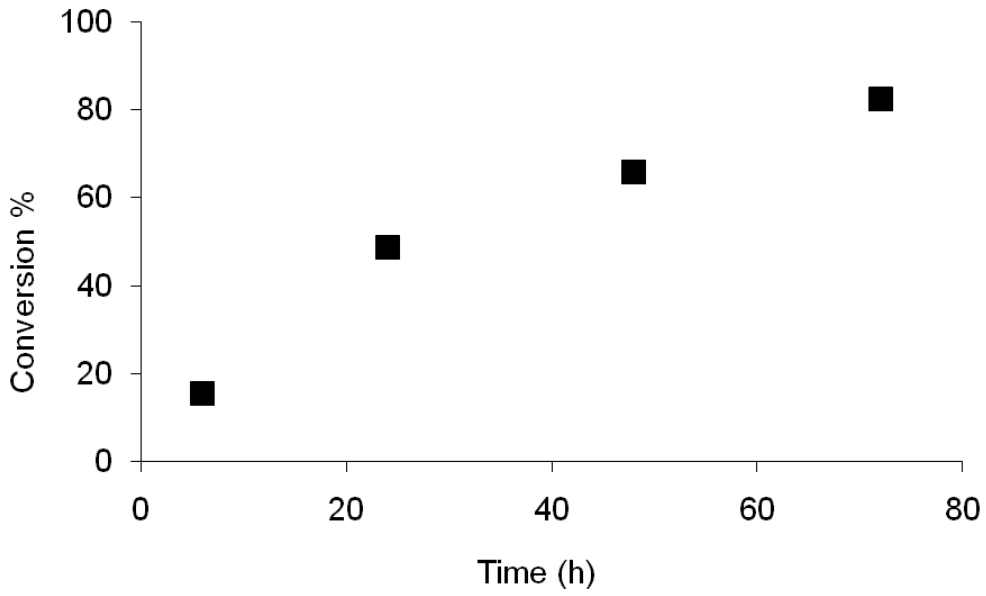
[a] Conditions: [*rac*-LA_0]:[**43**] = 100:1, 6.0 mL toluene, 70 °C, 0.1 mL aliquots taken at the given intervals. See Experimental section for other details. Linear fit (r^2 = 0.996).

Figure S4.15. Plots of M_n and PDI (determined by GPC) *vs* conversion for the polymerization of *rac*-LA using Al(CyN$_2^{Ts}$)(OCH$_2$CH$_2$NMe$_2$) (**43**).[a]



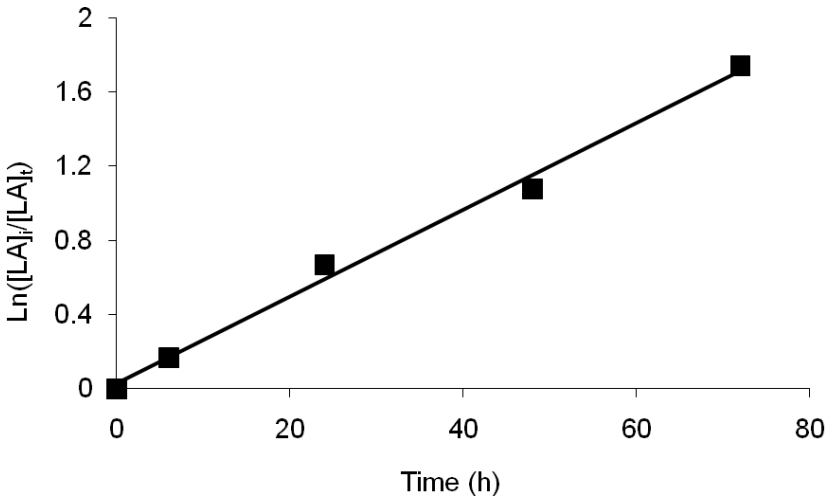
[a] Conditions: [*rac*-LA$_0$]:[**43**] = 100:1, 6.0 mL toluene, 70 °C, 0.1 mL aliquots taken at the given intervals. Hollow diamonds correspond to M_n and hollow circles to PDI.

Figure S4.16. Plot for *rac*-LA consumption *vs* time using Al(N$_2^{Ts}$N^{Ph})(OCH$_2$CH$_2$NMe$_2$) (**42**).[a]



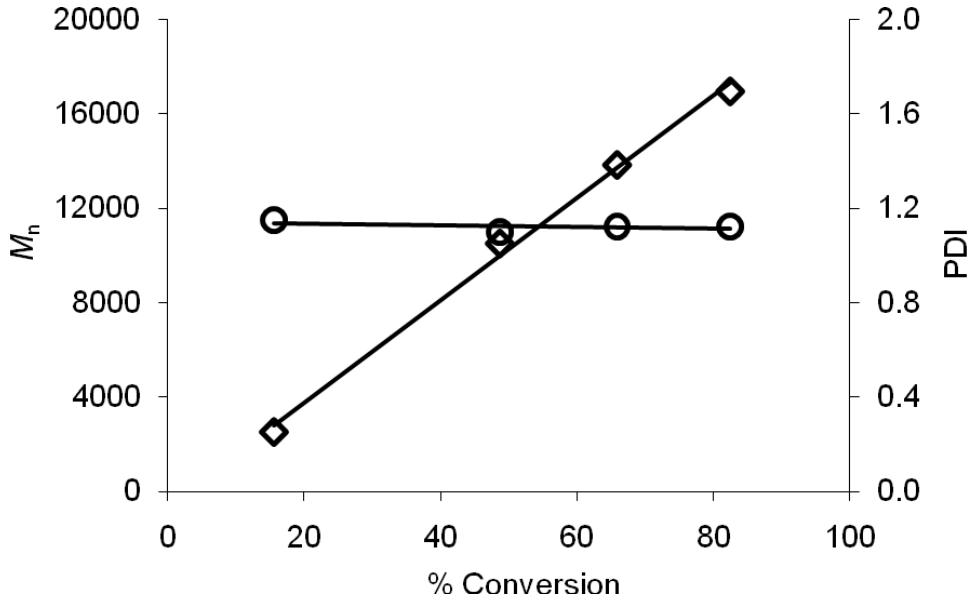
[a] Conditions: [*rac*-LA$_0$]:[**42**] = 100:1, 6.0 mL toluene, 70 °C, 0.1 mL aliquots taken at the given intervals. See Experimental section for other details.

Figure S4.17. First order plot *rac*-LA consumption using Al($N_2^{Ts}N^{Ph}$)($OCH_2CH_2NMe_2$) (**42**).[a]



[a] Conditions: [*rac*-LA_0]:[**42**] = 100:1, 6.0 mL toluene, 70 °C, 0.1 mL aliquots taken at the given intervals. See Experimental section for other details. Linear fit (r^2 = 0.993).

Figure S4.18. Plots of M_n and PDI (determined by GPC) *vs* conversion for the polymerization of *rac*-LA using Al($N_2^{Ts}N^{Ph}$)($OCH_2CH_2NMe_2$) (**42**).[a]



[a] Conditions: [*rac*-LA_0]:[**42**] = 100:1, 6.0 mL toluene, 70 °C, 0.1 mL aliquots taken at the given intervals. Hollow diamonds correspond to M_n and hollow circles to PDI.

Figure S4.19. Detail of MALDI-ToF MS of the poly(*rac*-LA) synthesised using Al($N_2^{Ts}N^{py}$)(OBn) (**33**). M_n by GPC analysis was 3740 g mol^{-1}.

